Biological transformations involved in the deterioration of the cementitious linings in sewer-networks : Application for the definition of a biodeterioration resistance test

Matthieu Peyre-Lavigne

Université de Toulouse

THÈSE

En vue de l'obtention du

DOCTORAT DE L'UNIVERSITÉ DE TOULOUSE

Délivré par :
Institut National des Sciences Appliquées de Toulouse (INSA de Toulouse)

Cotutelle internationale avec :

Présentée et soutenue par :
Matthieu PEYRE LAVIGNE

Le mardi 11 février 2014

Titre :
Transformations biologiques impliquées dans la dégradation des revêtements cimentaires en réseau d'assainissement :
Application à la définition d'un test de résistance à la biodétérioration

---

ED MEGEP : Génie des procédés et de l'Environnement

Unité de recherche :
Laboratoire d'Ingéniérie des Systèmes Biologiques et des Procédés (UMR 5504/792)

Directeur(s) de Thèse :

Etienne PAUL (Professeur des Universités, INSA-Toulouse)
Arnaud COCKX (Maitre de Conférences, INSA-Toulouse)

Rapporteurs :

Thierry CHAUSSADENT (Directeur de Recherche, IFSTTAR)
Pierre BUFFIERE (Professeur des Universités, INSA-Lyon)

Autre(s) membre(s) du jury :

Alexandra BERTRON (Maitre de Conférences, IUT-GC Toulouse III)
Alain TOURNIER (Directeur du Centre de Recherche de Saint-Gobain PAM)
Oriol GUTIERREZ (Researcher, Institut Catalan de Recherche sur l'Eau - ICRA, Girona)
Jean-Noël FOUSSARD (Maitre de Conférences, INSA-Toulouse)

Résumé

La fonction première des réseaux d'assainissement, en vue de la protection sanitaire des populations, est la collecte des eaux usées et leur acheminement vers les installations de traitement. Dans des conditions d'exploitations particulières conduisant à la production de sulfure d'hydrogène (H_2S), des détériorations majeures des infrastructures en béton sont observées dans les phases aériennes de ces mêmes réseaux. En effet, des études ont montré qu'un environement H_2S entrainait la sélection au contact des parois cimentaires de bactéries capables d'oxyder les composés soufrés réduits (bactéries sulfo-oxydantes), oxydation biologique conduisant à la production d'acide et de sulfate. Cette production d'un milieu agressif particulier entraine donc la détérioration locale des ouvrages et à terme fragilise les installations, par la dissolution des matrices cimentaires et leur recomposition minéralogique, participant ainsi à la perturbation de la collecte des eaux-usées, imposant donc des travaux de rehabilitations couteux.

Dans un contexte normatif « NF EN 598 » concernant les canalisations en fonte ductile et « NF EN 14647 » imposant la validation des revêtements utilisables dans de telles conditions par des tests uniquement chimiques peu représentatifs de la réalité, le LISBP en partenariat avec l'entreprise Saint-Gobain PAM, ont mené ce travail de thèse avec pour objectif industriel le dévelopment d'un test de biodétérioration des revêtements cimentaires.

Pour répondre à cet objectif ce projet de recherche s'est articulé autour d'une analyse bibliographique des phénomènes participant à la biodétérioration des matériaux cimentaires en réseau d'assainissement et ce afin de proposer un dispositif expérimental modèle permettant, à l'échelle d'une section de canalisation industrielle, l'étude couplée des transformations biologiques et chimiques déterminant le devenir des revêtements cimentaires utilisés. Deux hypohtèses de travail ont alors été proposées puis validées, (i) la possibilité de travailler sans H_2S par l'utilisation de composés soufrés réduits, tel que le thiosulfate, afin d'optimiser les flux matières dédiées aux transformations biologiques, (ii) le travail à partir d'un consortium microbien non sélectionné issu de l'assainissement. La sélection d'une activité sulfo-oxydante étant ainsi conjointement assurée, à travers le dispositif expérimental, par la maîtrise des conditions opératoires et le revêtement testé.

Afin d'évaluer ces deux hypothèses, cette étude s'est alors appuyée dans un premier temps, par un suivi des bilans matières, via des expériences en laboratoire à l'échelle de la

canalisation. Par la suite, hors revêtement cimentaire, le découplage des processus chimiques et biologiques, via des expériences ciblées associée à une modélisation des transformations chimiques et biologiques des thiosulfates en fonction des conditions opératoires (pH, aération et concentrations), a assuré la sélection, la description et la quantification de la production d'acide biogénique. Finalement, le travail sur deux types de revêtements cimentaires (ciment aux laitiers de haut-fourneau (CEM III) et ciment alumineux (CAC)), aux comportements contrastés face à ce type d'environnement, a permis d'évaluer la représentativité du système proposé par rapport aux transformations rencontrés en réseaux d'assainissement et d'assurer la discrimination en 15 semaines entre deux types de matériaux. Ce travail final a été réalisé par le couplage d'une analyse temporelle des transformations par bilan matières et d'une analyse des évolutions chimiques, minéralogiques et microstructurelles des revêtements testés.

Ainsi un système modèle, définissant un dispositif expérimental (techniques analytiques associées) et les méthodes d'exploitation des mesures, a été proposé. Celui-ci est basé sur la sélection au contact de revêtements cimentaires de bactéries sulfo-oxydantes à partir de consortia réels issus de l'assainissement, et ce via le contrôle des conditions opératoires (substrat soufré, charges en nutriments, température).

Par cette approche, un nouveau protocole d'essai est proposé, participant à l'évaluation de la résistance des revêtements cimentaires utilisés en réseau d'assainissement face à des attaques d'acide biogénique. Ce protocole d'essais d'une durée de trois mois assurera à terme une aide à la décision dans la gestion des réseaux d'assainissement existants et la conception des réseaux futurs.

<u>Mots clefs</u> : Réseau d'assainissement, Biodétériorations, Matériaux cimentaires, Oxydations biologiques des composés soufrés.

Abstract

The main function of the sewer-networks is the collection of the wastewaters to ensure their treatment for the health protection of the populations. Under specific conditions of the wastewater collection leading to the production of hydrogen sulfide (H_2S), major deteriorations of the concrete infrastructures are observed in the headspace of the sewer-networks. Indeed, studies showed that an H_2S environment involved the selection in contact with the cementitious walls of bacteria able to oxidize the reduced sulfur compounds (sulfur-oxidizing bacteria: SOB). These biological oxidations lead to a local production of acid and sulfate in contact with the cementitious materials, and then are involved in the local deterioration of the collection system by the dissolution of the cementitious matrices and their mineralogical transformations. These deteriorations disturb the wastewater collection by the exfiltrations of the effluents to the ground and/or by the intrusion of parasitic clear water, leading to expensive works of rehabilitation, associated to disturbances for the residents (odorous pollutions, disturbances of the road traffic etc…).

In a normative context "NF EN 598" for cast-iron pipe and "NF EN 14647" imposing the validation of the cementitious usable under such conditions by only chemical tests not very representative of the reality, the LISBP in partnership with the company Saint-Gobain PAM, undertook this research work with an industrial objective to develop a biodeterioration test of the cementitious linings.

To achieve this aim this research project is based around a literature review of the phenomena involved in the biodeterioration of cementitious materials in sewer-networks. Then, an experimental device is proposed. At the level of a section of industrial sewer-pipe, this experimental device allows the coupled study of the biological and chemical transformations determining the becoming of a cementitious lining under controlled conditions. Two major asumptions were made, (i) the work without H_2S as sulfur source, by the use of reduced sulfur compounds, such as thiosulfate, in order to optimize flows matters, aiming the SOB activity, (ii) the work start from a microbial consortium not selected resulting from wastewater treatment plant. The selection of a sufur-oxidizng activity is ensured jointly, through the experimental device, by the control of the operating conditions and the cementitious lining tested.

In order to evaluate these two assumptions, firstly the system was tested via experiments in laboratory at the level of a sewer-pipe, by a mass balances approach. Thereafter, the chemical and the biological transformations of the thiosulfate were studied. For that specific decoupled experiments linked to the development of a dynamical model ensured the selection, the description and the quantification of the biogenic production of acid according to the conditions of pH, aeration and thiosulfate concentrations. Finally, work on two types of cementitious lining (blast furnace slag cement (BFSC) and aluminate cement (CAC)), with contrasted behavior against biogenic acid environment, allowed the evaluation of the system representativeness and ensured the discrimentation in 15 weeks between two linings. This final work was achieved by dynamical analyses and mass balances, and the analyses of the chemical, mineralogical and microstructural evaluation of the linings tested.

Thus a system, defining an experimental device (associated analytical techniques) and the evaluation methods of analytical measurements, was proposed. This experimental device is based on the selection in contact with cementitious lining of SOB activity from wastewater treatment plant consortium, and this through the control of the operating conditions (sulfur substrate, loads in nutrients, temperature).

By this approach, a new essay is proposed. It enables the evaluation of the resistance of the cementitious linings used in sewer-networks against biogenic acid attacks, by the association of physicochemical resitance of the material and the influence of the material on the microbial activity. This new protocol, of three months duration, will ensure a help decision for the management of the rehabilitation of the existing sewer-networks and the design of the future networks.

Key words: Sewer-networks, Biodeteriorations, Cementitious materials, Biological Oxidations of sulfur compounds.

Remerciements

Le travail présenté dans ce document est la vision personnelle d'un travail qui fut celui d'une équipe. Par ces quelques mots je souhaite remercier les personnes qui ont participé de prés ou de loin à l'aboutissement de ce travail et sans qui rien n'aurait été possible.

Tout l'intérêt de ce document leur est du, le reste m'appartient seulement.

Je souhaite tout d'abord remercier Jean-Noël FOUSSARD, Arnaud COCKX et Etienne PAUL qui ont encadré ce projet de thèse et ont permis son aboutissement, et qui par leurs conseils et leur confiance m'ont accompagné au cours de ces années et m'ont permis d'élargir bien au-delà du domaine traité mes connaissances et mes compétences.

Je remercie Alain TOURNIER et Alzbeta HUTLOVA et à travers eux le centre de recherche et de développement de l'entreprise Saint-Gobain PAM, pour avoir soutenu ce projet, ainsi que moi-même, au fil des années et ce à travers différents contrats réalisés avec le LISBP.

Je souhaite tout particulièrement remercier l'équipe SYMBIOSE du LISBP dans son ensemble, pour ce qu'elle est en tant qu'équipe. Je souhaite remercier à travers elle, Mathieu SPERANDIO à qui je dois mon entrée à l'INSA et la possibilité qui m'a été offerte par la suite. Je tiens à remercier Evrard MENGELLE sans qui rien n'aurait pu être fait et qui tout au long de ces années m'a appris bien plus que mon métier. Avec lui, je remercie Mansour BOUNOUBA et Delphine DELAGNES qui d'un point de vue du travail ont permis d'assurer le suivi et le contrôle des expériences pilote et à qui je dois bien plus. Je remercie Gérard CANCEL, pour son accueil et ses conseils, qui m'ont permis par son absolue disponibilité d'élargir le panel d'analyses réalisées et ainsi de renforcer l'étude. Je remercie les membres de l'équipe qui était là à mon arrivée et qui m'ont accueilli à bras ouverts, Yolaine BESSIERE, Elizabeth NEUHAUSER, Isabelle QUEINNEC, Xavier LEFEVBRE, Sébastien POMMIER et Michel MAURET, je les remercie pour ceux qu'ils sont tous ensembles et séparément, pour leur présence, leurs conseils et leur absolue bienveillance, avec le regret de ne pas avoir eu la chance de pouvoir directement travailler avec eux. Je remercie Guillermina HERNANDEZ-RAQUET pour ses observations et ses conseils, et avec elle Myriam MERCADE-LOUBIERE et Catherine BOTANCH pour leur apport et leur implication en cours de projet sur les aspects d'écologie environnementale.

Je tiens à remercier Clarisse CONFORTIN, Cédric HAMON, Danielle CORRADI et Nathalie VETTORI qui ont assuré le suivi administratif de ce projet et m'ont accompagné durant ces années avec leur bienveillance. Je tiens à exprimer mes profonds remerciements à

Maïté ROSSATO qui durant ma formation par son dévouement et sa persévérance assura ma réussite et celle de bon nombre de mes collègues.

Je remercie Mohamed-Arezki CHEKROUN qui durant un stage de master recherche participa à ce projet, et lui apporta pendant 6 mois ses qualités scientifiques et techniques, son sérieux et sa persévérance. A travers lui je remercie tous les stagiaires qui ont participé durant ces années à la recherche et à la vie de l'équipe.

Ce travail de thèse, première sur cette thématique au sein du LISBP, a fait appel aux conseils et à l'expérience de bon nombre de personnes au sein du laboratoire. Je tiens ici à remercier, pour leur accueil, pour leurs conseils, pour le temps pris, Stéphane MATHE, Alain LINE, Gille HEBRARD et César ACEVES-LARA.

Ce projet de recherche porte sur une thématique profondément pluridisciplinaire, et il n'aurait pu être ce qu'il est sans l'intérêt, l'expertise et l'engagement de personnes extérieures au laboratoire. Je souhaite donc remercier, toutes les personnes qui ont participé à l'analyse des matériaux et qui ont accueilli le projet et moi-même et m'ont permis de suivre et de participer à cette étape finale. Je tiens à remercier Marlène FOURRE et Pierre NICOT de la « Division transfert de technologie » du LMDC, Vanessa MAZARS, Maude SCHIETTEKATTE, Guillaume LAMBARE. Je tiens à remercier Gilles ESCADEILLAS qui a participé aux réunions de travail durant la dernière année du projet et dont l'intérêt et les conseils ont été d'un grand soutien. Je tiens également à remercier tout particulièrement Alexandra BERTRON, dont l'expertise, l'enthousiasme et l'engagement absolu ont permis au projet d'être ce qu'il est aujourd'hui et dont les encouragements et l'intérêt furent essentiels à mes yeux.

Ce projet de recherche, d'un point de vue personnel a été associé à un projet d'enseignement. Je tiens ici tout d'abord à remercier à nouveau mes encadrants dont la confiance et les propositions ont été la première marche essentielle à cette partie de ma formation et à sa diversité. Dans ce cadre, je tiens à nouveau à remercier Mansour BOUNOUBA qui m'a formé, conseillé et accompagné sur certains TP. Je tiens à remercier Nathalie CLERGERIE et Aude DIDI pour leur accueil, leur disponibilité et leur formation. Je remercie également Dominique AUBAN qui me forma et participa à une part de mes enseignements. Je remercie également, Jean-Stéphane PIC, Stéphane MATHE, Jérôme MORCHAIN et Maria Aurora FERNANDEZ pour mon intégration au sein d'un département d'enseignement. Je remercie également Christelle CAUSSERAND du LGC pour une semaine Franco-chinoise qui aurait été plus difficile sans sa bienveillance. Cette part essentielle de ma

formation, m'a permis de rencontrer ou de prolonger la rencontre d'autres collègues. Je tiens tout particulièrement à remercier ici Mélanie JIMENEZ pour son apport, son aide et son soutien qui ont largement dépassé le cadre du travail, et Patrick LOULERGUE pour tout, tout simplement.

Outre les collaborateurs directs, un travail de recherche ne peut exister sans l'apport quasi invisible et pourtant si essentiel des collègues de bureau. Rien n'aurait été pareil sans eux. Leur présence, leurs conseils, leurs engagements, leur simplicité, leurs qualités humaines et professionnelles ont permis la réalisation de ce projet. Les anciennes tout d'abord, Ahlem FILALI, Angelas MANAS-LLAMAS, Irène MOZO, au près de qui j'ai appris énormément et dont les projets de recherches, si éloignés qu'ils étaient en apparence, ont nourri celui-ci par bien des aspects. Au-dela du travail, je les remercie tout simplement pour les années passées en leur compagnie. Je remercie aussi les nouveaux, Anil SHEWANI, Adèle LAZUKA, Lucas AUER, Mourad BENNEOUALA, Zhen-Ju WU, pour leur rencontre et les derniers mois passés parmi eux, et Sandrine PAISSE, partie pour d'autres horizons mais dont la rencontre fut un plaisir et une ouverture supplémentaire dans ma formation.

Et puis, il y a le petit bureau au sens élargi. Mathieu POCQUET et Laetitia CAVAILLE d'abord, indissociables jusqu'ici, dont la rencontre d'un point de vue personnelle fut une joie et d'un soutien sans faille et qui participa grandement au simple plaisir de venir au labo, et dont les qualités professionnelles furent d'un grand apport pour ce projet de recherche. Bien des choses leur appartiennent dans ce manuscrit. Je remercie profondément Hélène HAUDUC pour tout ce qu'elle m'a apporté en et hors du travail, pour le plaisir de sa compagnie, l'inspiration de ces engagements et l'excellence de ses compétences. Avec elle je remercie Jan GUNTHER, Yannick MALBERT et Peter MIKHAILENKO pour le bout de route fait ensemble, leur soutien en et hors des chemins du laboratoire. Pour finir, je tiens à exprimer ma profonde gratitude envers Sophie DECREMPS et Yoan PECHAUD. Je les remercie de ce qu'ils sont, de leur rencontre. Je les remercie pour tout ce qu'ils m'ont apporté.

Merci à Yoan, Sophie, Laetitia, Mathieu, Hélène, Evrard, Mansour, Delphine, Sandrine, Ahlem, Irène, Angela, Mélanie, Patrick, Alexandra, Arnaud et Jean-Noel. Merci à Etienne, pour tout.

Sommaire

Production scientifique

Conférences

Conférences Internationales

Peyre Lavigne, M., Bertron, A., Cockx, A., Foussard, J.N., Escadeillas, G., and Paul, E., (2014). A new test method to evaluate the resistance of cementitious materials exposed to biogenic attack in sewer network. 13th International Conference on Durability of Building Materials and Components. 2-5 Sept. 2014. Sao Paulo, Brazil. *(Accepted abstract)*

Peyre Lavigne, M., Bertron, A., Cockx, A., Foussard, J.N., Escadeillas, G., and Paul, E., (2014). A new method for the evaluation of cement-based material resistance against biogenic attacks in sewer-like environment: comparison between CAC and BFSC lining. International Conference on Calcium Aluminates. 18-21st May 2014. Avignon, France. *(Accepted abstract)*

Poster

Peyre Lavigne, M., Cockx, A., Foussard, J.N., Hernandez-Raquet, G., and Paul, E., (2013). Biofilm role in concrete deterioration in sewers: biotic and abiotic comparison for two sulfur substrate (Poster). 9th International Conference on Biofilm Reactors. 28-31 May 2013. Paris, France.

Conférences en France

Peyre Lavigne, M., Bertron, A., Hernandez-Raquet, G., Cockx, A., Foussard, J.N., Escadeillas, G., and Paul, E., (2013). Etude de l'interaction biofilm/matériau dans la biodétérioration des matrices cimentaires en réseaux d'assainissement. Réseau National Biofilm, 19-20 novembre 2013. Pau, France.

Pechaud, Y., Peyre Lavigne, M., Bessiere, Y., Queinnec, I. et Paul, E., (2013). Analyse et optimisation de l'élimination de biofilms développés dans les réseaux d'eau industriels. Réseau National Biofilm, 19-20 novembre 2013. Pau, France.

Pechaud, Y., Peyre Lavigne, M., Bessiere, Y., Queinnec, I. et Paul, E., (2013). Analyse de l'influence des conditions de croissance sur la compétition entre différents morphotypes microbiens. Réseau National Biofilm, 19-20 novembre 2013. Pau, France.

Peyre Lavigne, M., Mercade, M., Hernandez-Raquet, G., Cockx, A., Foussard, J.N., et Paul, E., (2013). Test alternatif pour l'évaluation de la résistance des matrices cimentaires face à la biodétérioration en réseau d'assainissement. XIV^{e} Congrès SFGP, 8 au 10 octobre 2013. Lyon, France.

Peyre Lavigne, M., Cockx, A., Foussard, J.N., and Paul, E., (2011). Biodétérioration des ciments en assainissement : rôles des acides gras volatils. XIII^{e} Congrès SFGP, du 29 novembre au 1 décembre 2011. Lille, France.

Poster

Peyre Lavigne, M., Cockx, A., Foussard, J.N., and Paul, E., (2012). Pilotes pour l'étude de la biodétérioration des matrices cimentaires en réseau d'assainissement (Poster). Cinquième journées du Réseau National Biofilm, 24-26 janvier 2012. Narbonne, France.

Liste des tables

Liste des figures

Liste des symboles

Symboles	Définitions	Unités
(i)	Activité d'un composé i en solution	
[i]	Concentration molaire d'un composé i en solution	$[M_i.L^{-3}]$
$[i]^{(0)}$	Concentration du composé i à t = 0	$[M_i.L^{-3}]$
$[O_2^{sat}]\ (T)$	Concentration de saturation en dioxygène dissous en fonction de la température	$[M.L^{-3}]$
$\Delta G°$	Energie libre de Gibbs	$[M.L^2.T^{-2}.M_S]$
μ	Force ionique	
μ^{max}_{SOB}	Taux spécifique maximum de croissance pour les bactéries sulfo-oxydantes	$[T^{-1}]$
μ^{obs}_{SOB}	Taux spécifique de croissance observé pour les bactéries sulfo-oxydantes	$[T^{-1}]$
$\mu_{SOB}(T)$	Taux spécifique de croissance pour les bactéries sulfo-oxydantes en fonction de la temparature	$[T^{-1}]$
A	Température dépendance des coefficients d'activité	
a	Aire interfaciale volumétrique	$[L^2.L^{-3}]$
A_c	Surface interne de la canalisation	$[L^2]$
AGV	Acides gras volatils	
AH_3	Hydroxide d'aluminium	
AS 1	Activated-Sludge from the city of Muret as inoculum	
AS 2	Activated-Sludge from the city of Villefranche as inoculum	
ASOM	Microorganismes sulfo-oxydants acidophiles	
ATP	Adénosine Tri-phosphate	
BFSC	Blast-Furnace Slag Cement = CEM III	
BOD	Demande biologique en oxygène	$[M_{BOD}.L^{-3}]$
BSE mode	Mode d'analyse par électron secondaire (pour SEM)	
Ca^{2+}_{tot}	Cumul total de calcium lixivié	$[M_{Ca2+}]$
CAC	Ciments alumineux	
CAH	Aluminates de calcium hydraté	
CEM I	Ciments portland	
CEM III	Ciments portland avec ajout de laitier de haut-fourneau	
CH	Portlandite = $Ca(OH)_2$	
CO	Carbone organique	
CO_2	Dioxyde de carbone	
CO_3^{2-}	Ion carbonate	
COD	Demande chimique en oxygène	$[M_{COD}.L^{-3}]$
CODp	Demande chimique en oxygène de la fraction particulaire	$[M.L^{-3}]$
COV	Composés organiques volatils	

CSH	Silicates de calcium hydraté	
D	Diamètre de la canalisation	[L]
d	Diamètre hydraulique de la canalisation	[L]
d[S]/dt	Taux de production de sulfide (pomeroy model)	$[M_S.L^{-3}.T^{-1}]$
Dev_O_2	Facteur de déviation entre valeurs expérimentales et valeurs simulées pour la concentration en oxygène dissous, évaluation réalisée par la méthode des moindres carrés pour une expérience	
Dev_O_2	Moyenne des facteurs de déviation concernant la concentration en oxygène dissous pour toutes les expériences	
Dev_pH	Facteur de déviation entre les valeurs expérimentales et valeurs simulées pour le pH, évaluation réalisée par la méthode des moindres carrés pour une expérience	
Dev_pH	Moyenne des facteurs de déviation concernant le pH de la solution pour toutes les expériences	
$Dev\_S_2O_3$	Facteur de déviation entre valeurs expérimentales et valeurs simulée pour la concentration en thiosulfate, évaluation réalisée par la méthode des moindres carrés pour une expérience	
Dev_SO_4	Facteur de déviation entre valeurs expérimentales et valeurs simulée pour la concentration en sulfate, évaluation réalisée par la méthode des moindres carrés pour une expérience	
Dev_SO_4	Moyenne des facteurs de déviation concernant la concentration en sulfate pour toutes les expériences	
d_m	Hauteur d'eau moyenne dans la canalisation	[L]
ECO2	Facteur d'accélération du transfert gaz-liquide du dioxyde de carbone	
EDS	Spectrométrie à Energie Dispersive	
EO2	Facteur d'accélération du transfert gaz-liquide de l'oxygène	
EPMA	Sonde à électron pour micro-analyses	
F	Nombre de Froude = $u.(g.d_m)^{-0,5}$	
fd	Coefficient d'activité des ions divalents	
fm	Coefficient d'activité des ions monovalents	
g	Accélération gravitationnelle	$[L.T^{-2}]$
H^+_{tot}	Cumul total de protons produits	$[M_{H+}]$
H_2CO_3	Dioxyde de carbone hydraté	
H_2S	Sulfure d'hydrogène	
$H_2S_2O_3$	Acide thiosulfurique	
H_2SO_3	Acide sulfureux	
H_{AH}	Constante de Henry d'un acide gras volatil dans l'eau	$[M.L^{-1}.T^{-2}]$
Hatta	Nombre de Hatta	
$H_{CO2/water}\ (T)$	Constante de Henry du dioxyde de carbone dans l'eau	$[M.L^{-1}.T^{-2}]$

HCO_3^-	Ion bicarbonate	
H_{H2S}	Constante de Henry de l'H_2S dans l'eau	$[M.L^{-1}.T^{-2}]$
H_{NH3}	Constante de Henry de l'ammoniac dans l'eau	$[M.L^{-1}.T^{-2}]$
HRT	Temps de séjour hydraulique	[T]
HS^-	Ion bisulfure	
$HS_2O_3^-$	Ion bithiosulfate	
$H_{SO2/water}$	Constante de Henry du dioxyde de soufre dans l'eau	$[M.L^{-1}.T^{-2}]$
HSO_3^-	Ion bisulfite	
i	Composé i	
IC	Carbone inorganiques ($CO_2 + HCO_3^- + CO_3^{2-}$)	
Ka_1	Constante d'équilibre $H_2S + H_2O = HS^- + H_3O^+$	
Ka_2	Constante d'équilibre $HS^- + H_2O = S^{2-} + H_3O^+$	
Ka_3	Constante d'équilibre $AH + H_2O = A^- + H_3O^+$	
Ka_4	Constante d'équilibre $NH_4^+ + H_2O = NH_3 + H_3O^+$	
Ka_{C1}	Constante d'équilibre $H_2CO_3 + H_2O = HCO_3^- + H_3O^+$	
Ka_{C2}	Constante d'équilibre $HCO_3^- + H_2O = CO_3^{2-} + H_3O^+$	
$Ka_{S(IV)1}$	Constante d'équilibre $H_2SO_3 + H_2O = HSO_3^- + H_3O^+$	
$Ka_{S(IV)2}$	Constante d'équilibre $HSO_3^- + H_2O = SO_3^{2-} + H_3O^+$	
$Ka_{S(VI)1}$	Constante d'équilibre $H_2SO_4 + H_2O = HSO_4^- + H_3O^+$	
$Ka_{S(VI)2}$	Constante d'équilibre $HSO_4^- + H_2O = SO_4^{2-} + H_3O^+$	
Ka_{T1}	Constante d'équilibre $H_2S_2O_3 + H_2O = HS_2O_3^- + H_3O^+$	
Ka_{T2}	Constante d'équilibre $HS_2O_3^- + H_2O = S_2O_3^{2-} + H_3O^+$	
kC1	Constante de vitesse de l'équilibre du dioxyde de carbone	[1]
kC2	Constante de vitesse de l'équilibre du bicarbonate	[1]
K_{CO2}	Constante de demi-saturation par rapport au dioxyde de carbone en fonction de microorganismes concernés	$[M_{CO2}.L^{-3}]$
kdis	Constante de vitesse de la dismutation des thiosulfates	[1]
k_{HSO3}	Constante dde vitesse de l'oxydation des bisulfites en présence d'oxygène	
$Ki_{S2O3(2-)}$	Constante d'inhibition par rapport au thiosulfate en fonction de microorganismes concernés	$[M_{S2O3(2-)}.L^{-3}]$
$Ki_{S4O6(2-)}$	Constante d'inhibition par rapport au tetrathionate en fonction de microorganismes concernés	$[M_{S4O6(2-)}.L^{-3}]$
$kl.a_{H2S}$	Coefficient de transfert volumique de l'H_2S	$[T^{-1}]$
$kl.a_{O2}$	Coefficient de transfert volumique de l'O_2	$[T^{-1}]$
KlaCO2	Coefficient de transfert volumique du dioxyde de carbone	$[T^{-1}]$
KlaSO2/KlaO2	Rapport entre le coefficient de transfert volumique du dioxyde de soufre et le coefficient de transfert volumique de l'oxygène	

klO2	Coefficient de transfert de l'oxygène	$[L.T^{-1}]$
K_{O2}	Constante de demi-saturation par rapport à l'oxygène en fonction de microorganismes concernés	$[M_{O2}.L^{-3}]$
k_{obs}	Constante de vitesse de la réaction la consommation d'oxygène durant l'oxydation des bisulfites (Connick and Zhang, 1996)	
kS(IV)1	Constante de vitesse de l'équilibre de l'acide sulfureux	1
kS(IV)2	Constante de vitesse de l'équilibre du bisulfite	1
kS(VI)1	Constante de vitesse de l'équilibre de l'acide sulfurique	1
kS(VI)2	Constante de vitesse de l'équilibre du bisulfate	1
$K_{S2O3(2-)}$	Constante de demi-saturation par rapport au thiosulfate en fonction de microorganismes concernés	$[M_{S2O3(2-)}.L^{-3}]$
$K_{S4O6(2-)}$	Constante de demi-saturation par rapport au tetrathionate en fonction de microorganismes concernés	$[M_{S4O6(2-)}.L^{-3}]$
$Ks_{Ca(OH)2}$	Constante d'équilibre de la solubilité de la portlandite ($Ca(OH)_2$)	
Ks_{CaSO4}	Constante de solubilité des sels de sulfate de calcium	
k_{SO3}	Constante de vitesse de l'oxydation des sulfites en présence d'oxygène	
K_{Sub}	Constante de demi-saturation par rapport au substrat en fonction de microorganismes concernés	$[M_{Sub}.L^{-3}]$
kT1	Constante de vitesse de l'équilibre de l'acide thiosulfurique	1
kT2	Constante de vitesse de l'équilibre du bithiosulfate	1
k_u	Constante de vitesse de la réaction l'oxydation des bisulfites en présence d'oxygène (Lancia et al., 1999)	
Kw	Constante d'ionisation de l'eau $2H_2O = H_3O+ + OH^-$	
kw	Constante de vitesse de la réaction d'ionisation de l'eau	1
m	Coefficient de maintenance des microorganismes oxydant en fonction du substrat	$[M_{Sub}.M_X^{-1}.T^{-1}]$
mean(Dev_S_2O_3)	Moyenne des facteurs de déviation concernant la concentration en thiosulfate pour toutes les expériences	
M_h	Concentration en microorganimses hétérothrophes	$[M_X.L^{-3}]$
MICC	Microbial Induced Concrete Corrosion	
Model evaluation	Pondération des facteurs de déviation à la moyenne des facteurs de déviation pour chaque expérience pour une expérience	
N_{air}	Débit molaire d'air au sein d'une canalisation	$[M.T^{-1}]$
NSOM	Microorganismes sulfo-oxydants neutrophiles	
o	Ordre partiel sur les bisulfites lors de l'oxydation des bisulfites en présence d'oxygène	
O_2	Dioxygène dissous	
OPC	Ordinary porland cement	
$OUR^{(0)}_{max}$	Vitesse de consommation maximum de l'oxygène pour le pulse de thiosulfate à t = 0	$[M.L^{-3}.T^{-1}]$

OUR(t)	Vitesse de consommation de l'oxygène en fonction du temps	$[M.L^{-3}.T^{-1}]$
OUR_{max}	Vitesse de consommation maximum de l'oxygène pour un pulse de thiosulfate	$[M.L^{-3}.T^{-1}]$
p	Ordre partiel sur l'oxygène lors de l'oxydation des bisulfites en présence d'oxygène	
P_{atm}	Pression atmosphérique	$[M.L^{-1}.T^{-2}]$
$P^{sat}_{(T°cond)}$	Pression de vapeur saturante à la température ($T°_{cond}$)	$[M.L^{-1}.T^{-2}]$
$P^{sat}_{(T°vap)}$	Pression de vapeur saturante à la température ($T°_{vap}$)	$[M.L^{-1}.T^{-2}]$
q	Ordre partiel sur l'acide sulfureux lors de l'oxydation de l'acide sulfureux en présence d'oxygène	
Q_{air}	Débit volumique d'air au sein d'une canalisation	$[L^3.T^{-1}]$
Q_{cond}	Débit volumique d'eau condensée	$[L^3.T^{-1}]$
Q_{SBR}	Débit en entrée du réacteur batch séquencé	$[L^3.T^{-1}]$
r	Rayon hydraulique de la canalisation	[L]
R	Constante des gaz parfait	$[M.L^2.T^{-2}.K^{-1}.M^{-1}]$
r	Ordre partiel sur oxygène lors de l'oxydation de l'acide sulfureux en présence d'oxygène	
rCa	Vitesse de lixiviation du calcium	$[M_{Ca}.T^{-1}]$
Re	Nombre de Reynolds	
s	Ordre partiel sur les thiosulfates lors de la dismutation des thiosulfates	
s	Pente de la canalisation	[L/L]
S(IV)-oxides	Oxydes de soufre au degrés d'oxydation IV, correspondant aux composés H_2SO_3, HSO_3^-, SO_3^{2-}	
S(VI)-oxides	Oxydes de soufre au degrés d'oxydation VI, correspondant aux composés H_2SO_4, HSO_4^-, SO_4^{2-}	
S^0	Soufre élémentaire	
S^{2-}	Ion sulfure	
$S_2O_3^{2-}$	Thiosulfate	
$S_2O_3^{2-}$	Ion thiosulfate	
$S_2O_6^{2-}$	Dithionate	
$S_3O_6^{2-}$	Trithionate	
$S_4O_6^{2-}$	Tetrathionate	
$S_5O_6^{2-}$	Pentathionate	
S_8	Soufre élémentaire précipité sous la forme de cycle	
Sat_O2aq (T)	Concentration en oxygène dissous à saturation	$[M_{O2}.L^{-3}]$
SBR	Réacteur Batch Séquencé	
SEM	Microscope Electronique à Balayage	
SI	Index de saturation	

SO_2	Dioxyde de soufre	
SO_3^{2-}	Ion sulfite	
SO4	Concentration en sulfate dans les eaux usées	$[M_S.L^{-3}]$
SOB	Bactérie sulfo-oxydantes	
SRT	Temps de séjour des solides	[T]
T	Température	[K]
t	Ordre partiel sur les bithiosulfates lors de la dismutation des thiosulfates	
t	Temps	[T]
$T°_{cond}$	Température appliquée pour la condensation de l'eau	[K]
$T°_{vap}$	Température appliquée pour la vaporisation de l'eau	[K]
$T°_{wall}$	Température appliquée à la paroi de la canalisation	[K]
u	Vitesse moyenne d'écoulement des eaux usées	$[L.T^{-1}]$
V	Volume de la canalisation	$[L^3]$
$X^{(0)}_{SOB}$	Concentration en bactéries sulfo-oxydantes à t = 0	$[M_X.L^{-3}]$
x_i	Fraction molaire du composé i dans la phase liquide	
X^{in}_{SOB}	Concentration en bactéries sulfo-oxydantes en entrée de réacteur	$[M_X.L^{-3}]$
X^{out}_{SOB}	Concentration en bactéries sulfo-oxydantes en sortie de réacteur	$[M_X.L^{-3}]$
XRD	Diffraction des rayons X	
X_{SOB}	Concentration en microorganismes sulfo-oxydants	$[M_X.L^{-3}]$
X_{SOB}	Concentration en bactéries sulfo-oxydantes au cours du temps	$[M_X.L^{-3}]$
y_i	Fraction molaire du composé i dans la phase gaz	
$Y^{obs}_{XSOB/S2O32-}$	Rendement de biomasse observable	$[M_X.M_S^{-1}]$
$Y_{X/S}$	Rendement de biomasse en fonction du soufre oxydé	$[M_X.M_S^{-1}]$
$Y_{X/Sub}$	Rendement de biomasse en fonction du substrat oxydé	$[M_X.M_{Sub}^{-1}]$
Zi	Valence du composé i	
α_r	Coefficient de température pour la ré-aération = 1,024.T	

[1] *: unités dépendantes des ordres partiels de la réaction*

Introduction Générale

1. Contexte général

Un rapport publié par l'Institut français de l'environnement (Ifen, 2006) fait état pour la France d'un réseau d'assainissement collectif de 250 000 km et de 16 100 stations d'épuration publiques traitant 5,6 milliards de m^3 d'effluents. En l'absence de nouvelle enquête publique, ces données sont toujours citées à ce jour (COL, 2008). La valeur patrimoniale de ce réseau d'assainissement est estimée à 65-75 milliards d'euros et celle des stations d'épuration à 14 milliards d'euros (Berland and Juery, 2003) en 2002 (en se basant sur une valeur du linéaire de 305 euros – Agence de l'Eau Seine-Normandie). Compte tenu de l'âge des structures qui, pour une grande partie, est proche de 40-50 ans, le coût estimé des réhabilitations représentent alors 1 milliards d'euros par an

Par ailleurs, les investissements correspondant au développement de l'urbanisation ont quelquefois conduit à négliger la maitrise du vieillissement de ces infrastructures urbaines. En France, l'enquête menée par le CSTB et l'AGHTM (CSTB-AGHTM, 1989) auprès de 1106 gestionnaires pour un linéaire test de 49281 km a permis de recenser la nature et le type des défauts observés sur les réseaux d'assainissement. Il a été estimé qu'environ 20% des réseaux devaient faire l'objet d'une réhabilitation. Les dégradations liées aux matériaux (tous types confondus) comme la corrosion, l'abrasion et la fissuration représentent près de 25% des défauts recensés. Ces nombreux défauts entraînent des perturbations significatives de la collecte, pouvant à terme pénaliser fortement les traitements mis en place.

Au niveau international, l'assemblée générale des Nations Unis a déclaré l'année 2008 Année internationale de l'assainissement. Dans le cadre des objectifs du millénaire pour le développement, les Nations Unis se sont engagées à réduire de moitié le nombre de personnes n'ayant pas accès à l'eau potable et à un assainissement convenable d'ici 2015. Cet enjeu d'améliorer et de sauver des vies nécessite toutefois des moyens financiers importants et des technologies innovantes et pérennes qui doivent répondre à des conditions locales souvent très particulières (Herisson, 2012).

Plus proche de nous, les obligations que doivent remplir les communes en matière d'assainissement suite à la directive européenne du 21 mai 1991 relative au traitement des eaux résiduaires urbaines, conduisent à des décisions de construction et de développement de nouveaux réseaux d'assainissement et de stations d'épuration qu'il est nécessaire de définir *a priori* comme durables. L'un des points faibles majeurs identifiés est le manque de solutions justifiées concernant la nature des matériaux utilisés notamment en ce qui concerne leur durabilité vis-à-vis des attaques biologiques.

2. Les réseaux d'assainissement et la biodétérioration

La fonction première des réseaux d'assainissement, en vue de la protection sanitaire des populations, est la collecte des eaux usées et leur acheminement vers les installations de traitement. De par le type d'effluents collectés, la longueur des réseaux, leur mode de fonctionnement, de nombreux processus physiques, chimiques et biologiques interviennent au sein de ces mêmes réseaux, transformant ainsi au cours de la collecte la matière organique et la matière minérale (Hvitved-Jacobsen, 2002). A ce niveau, dans des conditions d'exploitations particulières, certaines configurations peuvent conduire à la production biologique de sulfure d'hydrogène (H_2S) (stagnation des effluents : poste de refoulement, contre-pentes ou faibles pentes) (Pomeroy and Boon, 1990). En France il est estimé entre 40 à 50% des postes de refoulements présentant des dégagements d'H_2S important et problématique pour les exploitants. En zone rurale, il est avancé que 70% de ce type d'ouvrages serait concerné. De nombreuses études ont montré que la détérioration des matériaux cimentaires était directement liée à cette production intempestive d'H_2S, en particulier par la sélection et le développement sur les parois des canalisations de différents types de microorganismes chimio-lithotrophes de l'espèce *Thiobacillus* (Parker, 1945b) (Milde et al., 1983) (Islander et al., 1991). Cette détérioration à terme fragilise les installations, participant ainsi aux phénomènes d'exfiltrations des effluents au niveau des sols et/ou à l'intrusion d'eaux claires parasites au sein du réseau.

Dans les pays industrialisés, en présence de réseaux d'assainissement ancien, afin d'assurer la protection des populations et de l'environnement, ces détériorations appellent la mise en place de programmes de réhabilitions coûteux. Par exemple, en 1996 dans le comté de Los-Angeles, environ 10% des canalisations d'assainissement étaient concernés par ce type de détérioration. Le coût de réhabilitation à l'époque a été estimé à 400 millions de dollars (Sydney et al., 1996) (Zhang et al., 2008). En Allemagne le coût total de la réhabilitation de l'ensemble du réseau a été estimé en 1999 à 100 milliards de dollars, pour un pourcentage de défauts imputables à la biodétérioration des matériaux du même ordre que celui évalué sur le réseau de Los-Angeles (Kaempfer and Berndt, 1999). A coté de ces estimations, Vincke en 2002 (Vincke et al., 2002) évalue également que 10% des détériorations rencontrées sur les réseaux en Belgique sont directement liées à la production de sulfure d'hydrogène.

Ainsi, le besoin de proposer de nouvelles solutions en termes de revêtements cimentaires, aussi bien pour la réhabilitation de l'important patrimoine que constitue les réseaux

d'assainissement existant, que pour la conception de nouveaux réseaux, appelle une évaluation raisonnée des revêtements des canalisations.

3. Objectifs généraux et organisation de l'étude

Ce travail de recherche a pour objectif scientifique la compréhension des mécanismes conduisant à la détérioration des matériaux cimentaires en réseaux d'assainissement, avec un focus sur les interactions entre les activités biologiques se développant à la surface des matériaux et l'évolution de ces mêmes matériaux au cours du temps. Une maitrise des transformations clés intervenant dans le phénomène globale est visée. En termes d'enjeu industriel, il sera alors possible de proposer un système modèle permettant d'évaluer à l'échelle d'un essai de laboratoire, dans des conditions contrôlées, la résistance de revêtements industriels face aux attaques d'acide biogénique intervenant en réseau d'assainissement.

Ce document propose en chapitre I l'étude bibliographique de la biodétérioration des matrices cimentaires en réseau d'assainissement. Le chapitre II, basé sur l'étude bibliographique, détaille le cadre de l'étude et les approches scientifiques et techniques choisies. Suite à un chaptire III détaillant le matériel et les méthodes utilisés, les résultats de l'étude sont alors rassemblés dans quatre chapitres, deux chapitres (chapitre IV et VII) portant sur le système activités biologiques / matériaux, deux chapitres intermédiaires (chapitre V et VI) portant sur les transformations chimiques et biologiques participant à la sélection et à l'intensification d'une production d'acide sulfurique biogénique. De plus, le chapitre VII à partir du dispositif expérimental développé dans cette étude sur deux revêtements industriels différents, propose un protocole d'essai pour l'évaluation de la résistance des revêtements cimentaires dans les réseaux d'assainissement face aux attaques d'acide biogénique.

Chapitre I

Bibliographie : biodétérioration des matrices cimentaires en réseau d'assainissement

1. La biodétérioration des matrices cimentaires en réseau d'assainissement

Au sein des réseaux d'assainissement, les processus de dégradation des matériaux cimentaires liées à l'activité biologique sont uniquement observés dans les phases aériennes des réseaux (Hvitved-Jacobsen, 2002). Ces détériorations sont localisées sur le réseau et associées à la production biologique de sulfure d'hydrogène (H_2S), à la volatilisation de ce composé et à sa conversion par voie biologique en acide biogénique au niveau des parois aériennes des réseaux d'assainissement (Islander et al., 1991). Ces différents processus sont liés à des conditions particulières de collecte. Pour autant, même si la production d'H_2S est un facteur clé dans la dégradation des matrices cimentaires, sa production et son action découlent de nombreux phénomènes qu'ils soient physiques, chimiques et biologiques liés au devenir d'autres composés (Hvitved-Jacobsen, 2002).

La détérioration des matériaux cimentaires en réseaux d'assainissement est en premier lieu la résultante de la création aux parois des canalisations d'un milieu favorable à l'implantation et au développement de communautés microbiennes dont l'activité biologique produit un milieu agressif pour les matériaux considérés (Roberts et al., 2002).

Les paragraphes suivant s'attachent à décrire les phénomènes clés participant à ces détériorations biologiques des infrastructures, en partant d'une description à l'échelle du réseau pour par la suite, étape par étape réduire l'échelle d'observation et permettre de décrire et de proposer un schéma simplifié d'interactions communauté microbienne / revêtement cimentaire dans les conditions d'assainissement.

Les objectifs de ce chapitre sont (i) la description des phénomènes impliqués dans la biodéterioration des matériaux cimentaires en réseaux d'assainissement et (ii) la représentation des processus clés, et ce dans l'objectif industriel de proposer à terme un protocole d'essai permettant d'évaluer la résistance de revêtements cimentaires à l'échelle d'une canalisation et ce face à une attaque d'acide biogénique produit au contact des matériaux par un consortium microbien sélectionné.

1.1. La production d'une phase atmosphérique conduisant à la détérioration des matrices cimentaires

1.1.1. Localisation liées à la diversité de typologie des réseaux d'assainissement

La collecte des eaux-usées est principalement assurée via des canalisations dites gravitaires. Cependant, durant la collecte des contraintes géographiques (pentes, obstacles) imposent l'emploi de poste de refoulement[1] ou de poste de relevage[2] afin d'assurer l'acheminement des eaux usées jusqu'à la station d'épuration (STEP). La production d'H_2S est liée à la création de zones de stagnation durant la collecte : (i) soit au sein des postes de refoulement et/ou poste de relevage, dont le fonctionnement intermittent induit une immobilisation des effluents dans le poste lui-même (accentué en période de nuit) et au sein des canalisations sous pression permettant le refoulement des effluents, (ii) soit durant la collecte gravitaire elle-même de part la création de bouchon ou de dépôt entrainant une accumulation locale d'effluent, ou de part le mauvais dimensionnement du réseau et la création de contre pente lors de la pose des canalisations. La figure 1 illustre sur un réseau rural ces différentes situations pouvant être rencontrées lors de la collecte des eaux usées.

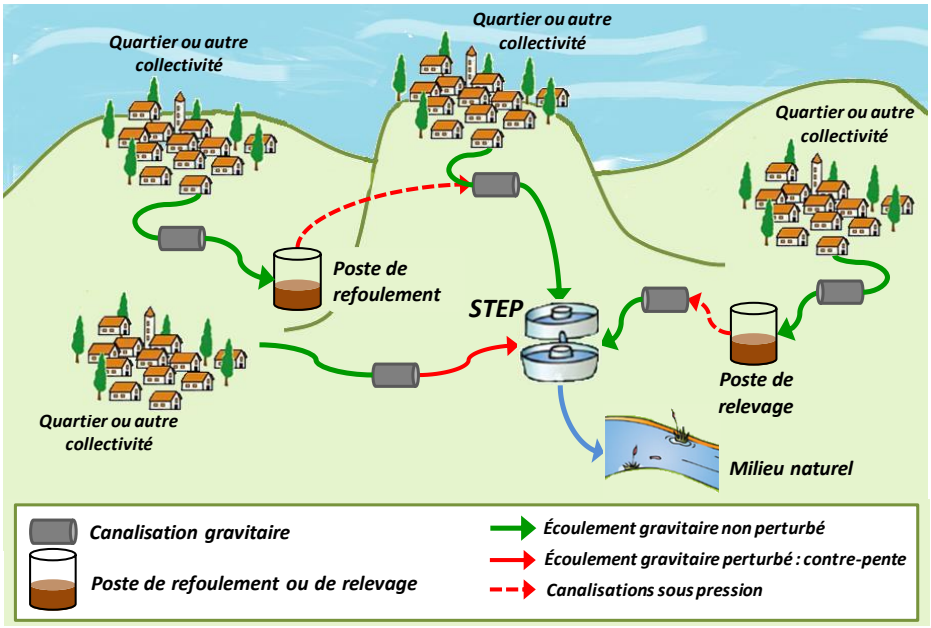

Figure 1 : Illustration de différentes situations de collecte des eaux usées, avec signalisation des zones potentiellement productrice d'H_2S.

[1] : un poste de refoulement assure le franchissement d'un obstacle type rivière ou dénivelé via l'utilisation de pompe afin d'acheminer les eaux usées vers une zone gravitaire du réseau.
[2] : un poste de relevage est utilisé le long d'un réseau gravitaire pour limiter les profondeurs de creuse lors de la pose des canalisations quand les faibles pentes naturelles et les distances à parcourir le nécessitent.

1.1.2. Phases de stagnation

1.1.2.1. Production du sulfure d'hydrogène en phase liquide

Les schémas présentés page suivante (figure 3 et figure 2) illustrent la reprise d'un effluent dans un réseau gravitaire après la collecte de celui-ci par un poste de refoulement (figure 3) ainsi que le cycle du soufre au sein d'une canalisation gravitaire avec stagnation d'effluent (figure 2, adaptée de Islander et al., 1991)).

La stagnation des effluents, aussi bien au niveau des postes de refoulement que des canalisations gravitaires, conduit à la création d'une zone anaérobie (figure 2(A) et figure 3(A)). Au niveau des postes de refoulement l'effluent « septique » séjourne de plus dans une canalisation de refoulement (sous pression) qui est strictement anaérobie. La combinaison de ces deux séjours en phase anaérobie (poste de refoulement et canalisation de refoulement) favorise une forte production d'H_2S par voie biologique (processus 1 figure 3).

L'absence d'oxygène dissous (O_2) combinée à une absence de nitrates (NO_3^-) conduit certaines populations bactériennes capables de réduire les sulfates (sulfate reducing bacteria : SRB), devenus alors l'accepteur d'électrons prioritaire, à oxyder la matière organique disponible en produisant de l'H_2S (Hvitved-Jacobsen, 2002) (Eq 1).

Eq 1 : $SO_4^{2-} + matière\ organique \overset{SRB}{\rightarrow} S^{2-} + H_2O + CO_2$

Une fois produit dans les zones anaérobies l'H_2S diffuse au sein de la phase liquide (figure 2 (B) et figure 3(B)). En phase liquide l'H_2S est un diacide en équilibre avec l'ion HS^- (Eq 2), lui-même en équilibre avec l'ion S^{2-} (Eq 3).

Eq 2 : $H_2S_{(aq)} + H_2O \overset{Ka_1}{=} HS^- + H_3O^+ \ avec\ Ka_1 = 3{,}64.10^{-3} \times exp^{(-3331/T)}$

Eq 3 : $HS^- + H_2O \overset{Ka_2}{=} S^{2-} + H_3O^+ \quad avec\ Ka_2 = 6{,}37.10^{-5} \times exp^{(-5990/T)}$

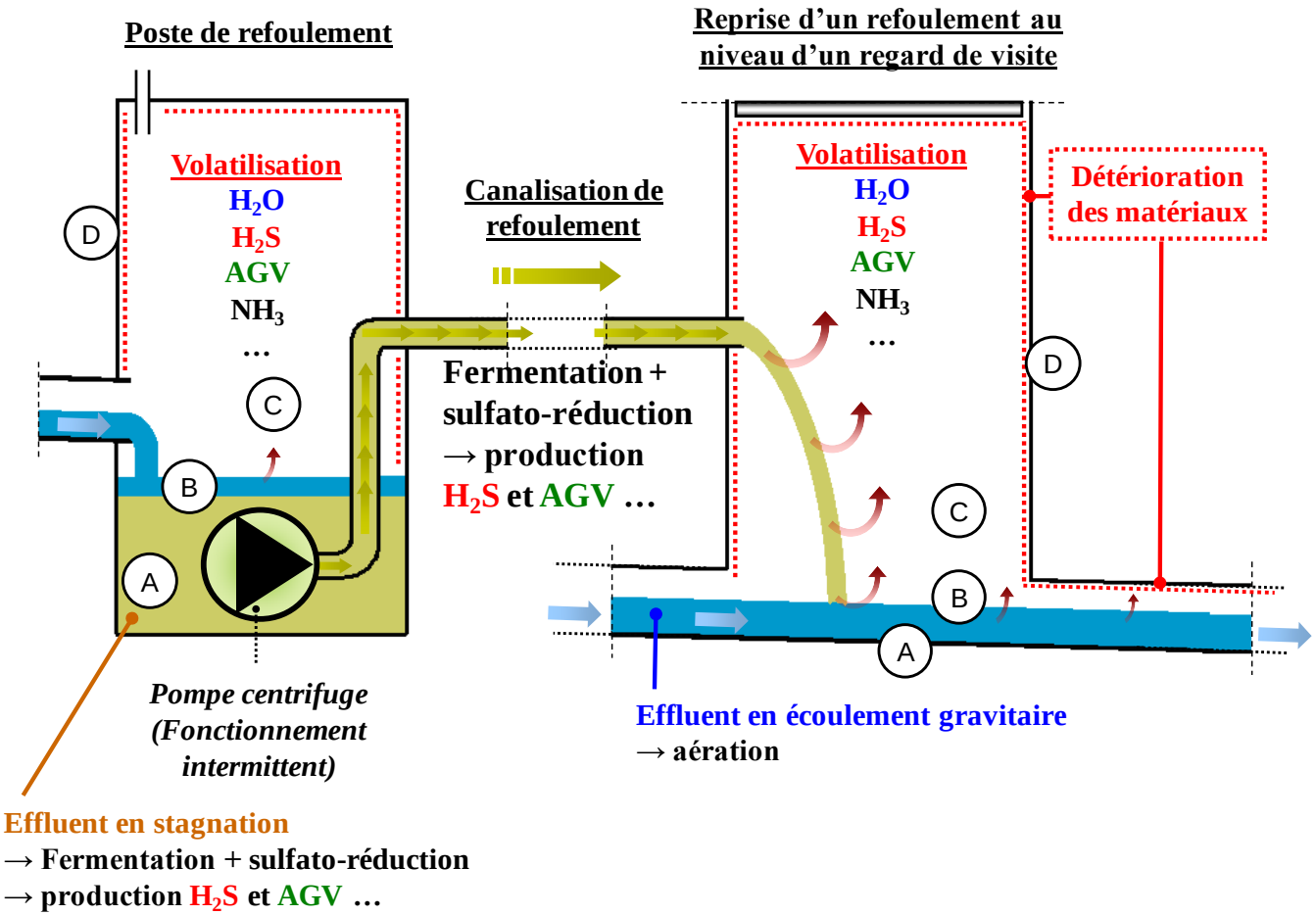

Figure 3: Schéma d'un poste de refoulement et du regard de visite associé au refoulement sur un réseau d'assainissement. Production d'une phase gaz particulières. Les marques (A) à (D) correspondent aux zones décrites dans la figure 3 ci-contre. Les détériorations majeures des matériaux cimentaires (·····), sont observées au sein des réseaux d'assainissement au niveau des regards de visites en reprise de refoulement, ainsi qu'au niveau des canalisations situées en aval de ces regards de visites.

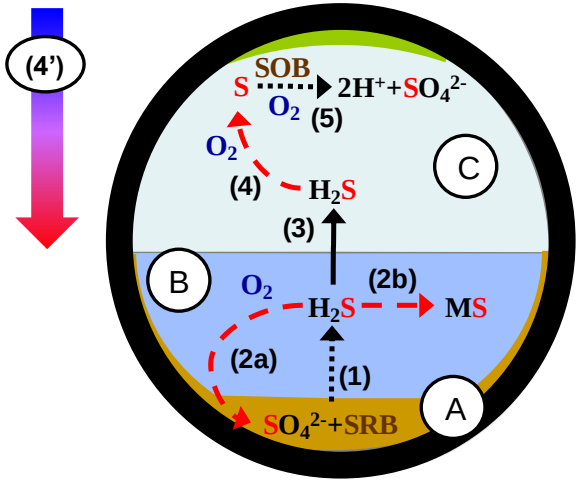

Figure 2 : Cycle du soufre dans une canalisation d'assainissement. Quatre zones particulières sont identifiées ; A : sédiment et biofilm immergé) (1) production d'H_2S par des bactéries sulfato-réductrice (SRB) ; B : phase liquide dans la zone aérobie oxidation d'H_2S avec O_2 (2a) et précipitation S^{2-} avec cation divalent (Fe^{2+} …) (2b); C: Phase atmosphérique (zone aérobie) volatilisation de l'H_2S, flux matière dirigé vers le haut de la canalisation (conditionné par le gradient de température entre la paroi de la canalisation enterrée et les eaux usées collectées ; D : Paroi canalisation (revêtement cimentaire) 5 : Zone humide → développement Biofilm ; 6 : Gradient de température ; SOB: bactéries sulfo-oxydantes; S(X) : Composés soufrés. Adapted from (Hitvited-Jacobsen, 2002)

L'évolution de la concentration en sulfures totaux (H_2S_{aq} + HS^- + S^{2-}) produit dans la phase liquide des réseaux d'assainissement et la résultante d'une phase de production biologique via la réduction des sulfates et de la compétition avec des phénomènes chimiques issus du transfert d'oxygène (reaction d'oxydation 2a de la figure 2 (Busiman et al., 1990) (Nielsen et al., 2004) (Nielsen et al., 2006b) (Sharma and Yuan 2010)), donc de la géométrie locale (hydraulique), et de la composition de l'effluent (affinité des ions sulfures en particulier (S^{2-}) pour certain cation métallique tel que l'ion ferrique (Fe^{2+}) par exemple (réaction 2b de la figure 2) avec précipitation de pyrite (FeS)) (Hivtved-Jacobsen, 2002).

Différentes corrélations ont été proposées dans la littérature pour évaluer l'évolution de la concentration en sulfures dans la phase liquide. Le tableau 1 en présente certaines en fonction des dimensions et des conditions de collecte (canalisations de refoulement et gravitaires).

D'autres approches couplant transformations biologiques et physicochimiques ont proposé des modèles intégrants la production de sulfures (Sharma et al., 2008) via le développement de biofilms (Hivtved-Jacobsen, 2002) (Jiang et al., 2009).

Tableau 1 : Corrélations proposées dans la littérature pour décrire l'évolution de la concentration en sulfides totaux dans la phase liquide de canalisations sous pression et de canalisations gravitaires.

Equation	**Ref**
Cas des canalisations sous pression (refoulement ou relevage)	
Eq 4: $d[S]/dt = 0.228 \times 10^{-3} [COD]\, 1.07^{T-20} r^{-1} (1 + 0.37D)$	*Boon & Lister (1975)*
Eq 5: $d[S]/dt = 1.0 \times 10^{-3} [BOD]\, 1.07^{T-20} r^{-1} (1 + 0.37D)$	*Pomeroy & Parkhurst (1977)*
Eq 6: $d[S]/dt = k^* ([COD]_S - 50)^{0.5}\, 1.07^{T-20} A_c / V$	*Hvitved-Jacobsen et al. (1988)*
Eq 7: $d[S]/dt = a^{**} ([COD]_S - 50)^{0.5}\, 1.03^{T-20} A_c / V$	*Nielsen (1998)*
Cas des canalisations gravitaires	
Eq 8: $d[S]/dt = 0.50 \times 10^{-3} . u . [BOD]^{0.8} [SO_4]^{0.4}\, 1.14^{T-20} r^{-1}$	*Thistlethwayte (1972)*
Eq 9: $d[S]/dt = 0.32 \times 10^{-3} [BOD] (1.07)^{T-20} r^{-1} - 0.96 (s.u)^{3/8} d^{-1} [S]$	*Pomeroy & Boon (1990)*
Eq 10: $d[S]/dt = 0.073 \times 10^{-3} [COD] (1.07)^{T-20} r^{-1} - 0.96 (s.u)^{3/8} d^{-1} [S]$	

d[S]/dt : taux de production de sulfures ($mgS.l^{-1}.h^{-1}$)
BOD : demande biologique en oxygène ($gBOD/m^3$)
COD : demande chimique en oxygène ($gCOD/m^3$)
SO4 : concentration en sulfate (gS/m^3)
T : température (°C)
D : diamètre de la canalisation (m)
u : vitesse d'écoulement (m/s)
s : pente de la canalisation (m/100m)
d : diamètre hydraulique (m)
r : rayon hydraulique de la canalisation (m)
A_c : surface de la canalisation (m^2)
V : volume de la canalisation (m^3)
k : paramètre à ajuster*
*a** : paramètre à ajuster*

1.1.2.2. Volatilisation et formation d'une phase atmosphérique favorable aux détériorations des matrices cimentaires

La volatilisation du sulfur d'hydrogène (H_2S) est décrite par l'équation d'équilibre gaz-liquide (Eq 11). La détermination des fractions molaires à l'équilibre est fixée par la constante de Henry à 20°C de l'H_2S dans l'eau qui est H_{H2S} = 4,98.10^7 Pa (la théorie sur les équilibres gaz liquides est présentée en annexes du chaptire III).

Eq 11 : $H_2S_{(g)} \overset{H_{H2S}}{=} H_2S_{(aq)}$ *Equilibre Gaz / Liquide*

En phase liquide, en particulier dans la gamme de pH des eaux usées (6 < pH < 8) (Pomeroy and Boon, 1990), l'H_2S a tendance naturellement à se volatiliser de la phase liquide vers la phase atmosphérique. Cependant l'intensité de cette volatilisation est fortement dépendante du pH, comme le montre la figure suivante (figure 4) (Nielsen et al., 2008b), où la concentration en H_2S en phase gaz d'un regard de visite est mesurée en parallèle du pH de l'effluent, et où une diminution de 0.4 point de pH (7.6 à 7.2) induit une concentration en H_2S dans la phase gaz passant de 2 ppm à environ 10 ppm.

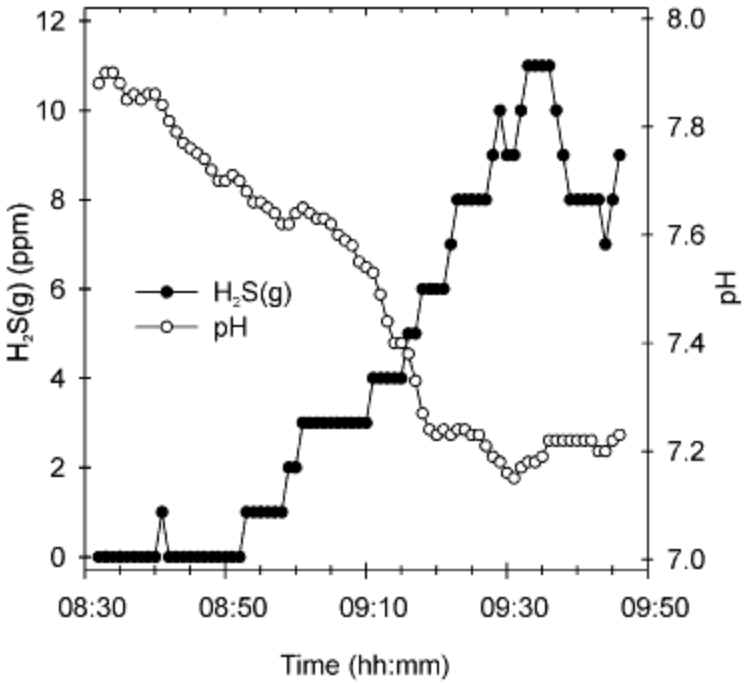

Figure 4 : concentration en H_2S mesurée au niveau d'un regard d'un visite, confrontée à la mesure de l'effluent collecté (Nielsen et al., 2008b).

Pour autant, comme décrit précédemment (Hivtved-Jacobsen, 2002), la quantité d'H_2S volatilisée est sans doute inférieure à la quantité d'H_2S produit par voie biologique dans les

zones anaérobies des réseaux d'assainissement. En effet cette quantité d'H_2S volatilisée est la résultante d'une compétition entre la volatilisation (dépendante des conditions de transfert, des processus d'aération) et les réactions chimiques décrites précédemment intervenant dans la phase liquide (figure 2).

De plus, la production d'H_2S est associée à la production d'acide gras volatil (AGV) lors de la fermentation des effluents stagnants (majoritairement acide acétique, acide propionique et acide butyrique) (Hvitved-Jacobsen, 2002), qui de part leur caractères volatils, peuvent participer à la composition de la phase gazeuse produite au niveau des zones de stagnation (figure 2(C)).

La décomposition de l'urée en particulier, durant la collecte des eaux usées va également conduire à la production d'ammonium au sein de la phase liquide (figure 3 (A) (B)) conduisant à la volatilisation d'une fraction d'ammoniaque.

Les équations décrivant les équilibres acido-basiques et gaz-liquides régissant les concentrations des composés entre la phase liquide et la phase gaz sont décrites en suivant :

- Pour l'acide acétique en tant que composé modèle pour les AGV

L'équilibre acido-basique

Eq 12 : $AH_{(aq)} + H_2O \overset{Ka_3}{=} A^- + H_3O^+$ *avec* $Ka_3 = 1{,}78.10^{-5}$ *pour l'acide acétique*

L'équilibre Gaz/liquide (constante de Henry pour l'acide acétique à 20°C, H_{AH}= 6,42.10^3 Pa)

Eq 13 : $AH_{(g)} \overset{H_{AH}}{=} AH_{(aq)}$

- Pour l'ammonium

L'équilibre acido-basique

Eq 14 : $NH_4^+ + H_2O \overset{Ka_4}{=} NH_{3(aq)} + H_3O^+$ *avec* $Ka_4 = 5.01.10^{-10}$ *pour l'ammonium*

L'équilibre Gaz/liquide (constante de Henry pour l'ammoniaque à 20°C, H_{NH3} = 6,42.10^3 Pa)

Eq 15 : $NH_{3(g)} \overset{H_{NH3}}{=} NH_{3(aq)}$

Au niveau de la reprise d'une canalisation de refoulement en réseau gravitaire par exemple, la création de turbulences (diminution de l'épaisseur de la couche limite de diffusion à l'interface) et d'une aire d'échange augmentée (figure 3), conduit à une intensification des

quantités volatilisées. Concernant l'H_2S, la tendance naturelle de volatilisation due à l'équilibre thermodynamique vers la phase gaz est également favorisée par la température, l'écoulement des eaux usées, les variations de débit, ainsi que les turbulences et les faibles valeurs de pH (Yongsiri et al., 2004a) (Yongsiri et al., 2005). La figure suivante (figure 5) adaptée d'Alexander and Fourie 2011), illustre la variabilité journalière de la volatilisation d'H_2S au niveau d'une zone sensible, ainsi que la variabilité de celle-ci en fonction de la saison de mesure (été ou hiver).

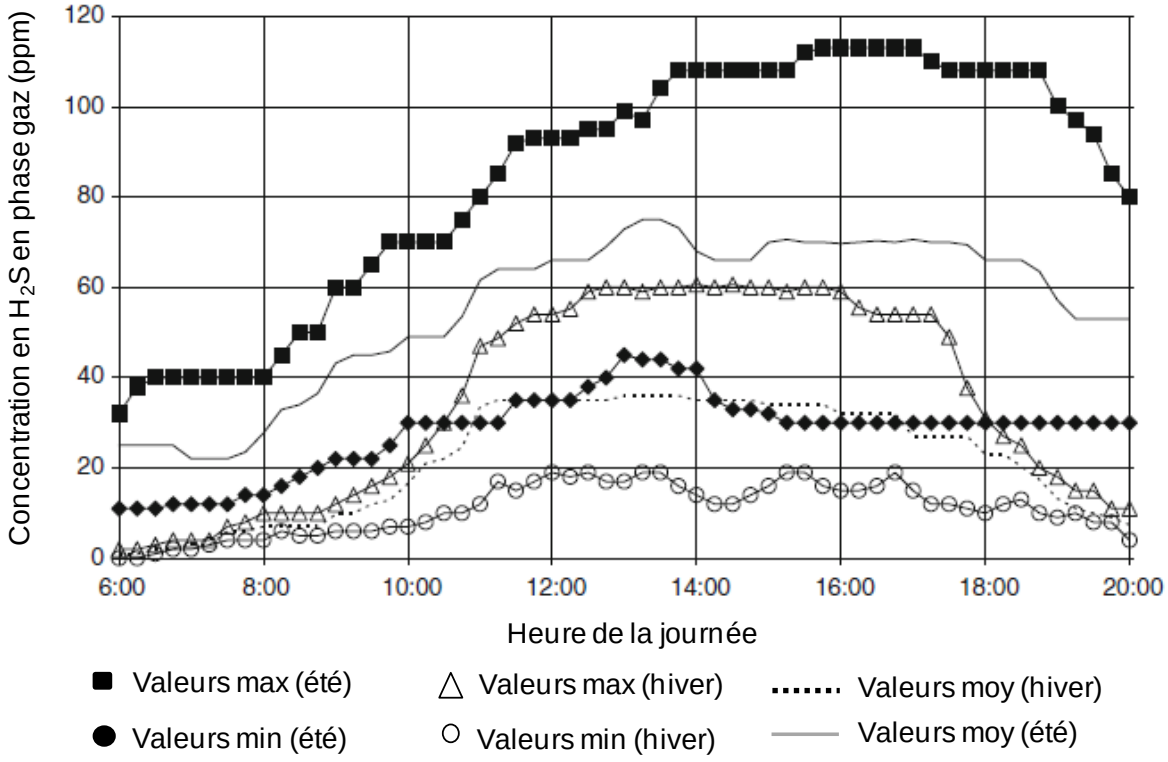

Figure 5 : concentration gaz en H_2S dans un réseau d'assainissement sensible au cours d'une journée moyenne d'été et d'hiver. Valeurs moyennes, maxima et minima (Alexander et Fourie 2011).

Ainsi, basé sur ces différents paramètres, Yongsiri (Yongsiri et al., 2003) a déterminé empiriquement un coefficient de transfert en fonction du pH se rapportant à un coefficient de transfert déterminé dans les mêmes conditions pour l'oxygène :

Eq 16 : $kl.a_{H_2S} = (1{,}736 - 0{,}196.pH) \times kl.a_{O_2}$ *avec* $4{,}5 \leq pH \leq 8{,}0$ *à 20°C*

avec : $kl.a_{H_2S}$: coefficient de transfert de l'H_2S à 20°C (h^{-1})

$kl.a_{O_2}$: coefficient de transfert de l'O_2 à 20°C (h^{-1})

où l'expression du $kl.a_{O_2}$ de façon empirique (Jensen, 1995) prend en compte dans la canalisation le débit des eaux usées, la pente et la hauteur d'eau, ainsi que la température :

Eq 17 : $kl.a_{O_2} = 0{,}86 \times (1 + 0{,}2 \times F^2).(s.u)^{3/8} \times d_m^{-1}.\alpha_r \times (T - 20)$

avec : u : vitesse moyenne des eaux usées ($m.s^{-1}$) ; s : pente de la canalisation ($m.m^{-1}$) ; d_m : hauteur d'eau moyenne dans la canalisation (m) ; F : nombre de Froude = $u.(g.d_m)^{-0,5}$; g : accélération gravitationnelle ($m.s^{-2}$) ; α_r : coefficient de température pour la ré-aération $\alpha_r = 1{,}024.T$ (T en °C)

Tout comme pour la production de sulfures d'autres corrélations mathématiques existent concernant la volatilisation d'H_2S, aussi bien dans le cas des canalisations gravitaires que des reprises en cascade suite au refoulement des eaux usées. Le sujet de ce document n'étant pas d'étudier les transferts d'H_2S au sein des réseaux d'assainissement, nous renvoyons le lecteur au livre dirigé par Hvitved-Jacobsen édité en 2002 et réédité en 2013 « Sewer Processes: Microbial and Chemical Process Engineering of Sewer Networks, Second Edition CRC » pour de plus amples détails.

Les autres composés volatils produits en phase liquide ou initialement présent vont également composer la phase gaz (NH_3, les composées organiques volatils (COV) dont les AGV font parti), et ce en fonction de leur propriétés thermodynamiques (pKa et constante de Henry). Aux pH classiques des eaux usées (entre 6 et 8) (Metcalf and Eddy, 2003), les AGV (acide acétique 50%, acide propionique 20% et acide butyrique 30%) et l'ammoniac (NH_3), sont majoritairement sous une forme ionique non volatile (déproptonée pour les AGV, protonée pour l'ammoniaque). De plus, les AGV ont des propriétés de volatilisation moins importantes que le NH_3, l'H_2S et le CO_2 (voir les constantes de Henry à 20°C présentées au tableau 2).

Tableau 2 : Constante de Henry à 20°C pour certains composés volatils rencontrés en réseaux d'assainissement

Composés	**Constante de Henry à 20°C (Pa)**
Acide acétique (CH_3-COOH)	6.42×10^3
Acide propionique (CH_3-CH_2-COOH)	5.66×10^3
Acide butyrique (CH_3-CH_3-CH_2-COOH)	1.81×10^3
Ammoniaque (NH_3)	7.93×10^4
Sulfure d'hydrogène (H_2S)	4.98×10^7
Dioxyde de carbone (CO_2)	1.47×10^8

La composition d'une phase gaz en réseau d'assainissement est ainsi extrêmement variable et a été en partie décrite par Thistlethwayte et Goleb dans le tableau suivant (tableau 3) en considérant 4 groupes de composés hormis l'ammoniaque (Thistlethwayte et Goleb (1972), issu de Hvitved-Jacobsen, 2002).

Tableau 3 : gammes de valeur de la composition de l'air en réseau d'assainissement correspondant à des conditions de temps sec et des conditions anaérobies (adapté de Hvitved-Jacobsen, 2002).

Groupe de composés	**Gamme de concentration en % de volume**
1. Dioxyde de carbone (CO_2)	0.05 – 1.0 %
2. Hydrocarbures et hydrocarbures chlorées	
a. Hydrocarbures (principalement aliphatique C_6-C_{14} et en majorité C_8-C_{12} issue du pétrole)	0 – 500 ppm
b. Hydrocarbures chlorés	0 – 100 ppm
3. Sulfure d'Hydrogène (H_2S)	0 – 100 ppm
4. Composés organiques odorants	
a. Sulfides et mercaptans (thiols)	0 – 50 ppb
b. Amines	0 – 50 ppb
c. Aldehydes	0 – 50 ppb

En 2001 Sato effectue un travail portant sur l'analyse des odeurs produites au niveau des systèmes d'assainissement. Il a évalué par stripping la part volatile d'échantillons issus d'un réservoir de stockage d'eaux usées urbaines. La phase gaz dont la composition est donnée dans le tableau suivant (tableau 4) correspond, de par les conditions de l'expérience, à la composition maximale de la phase gaz associée aux phénomènes biologiques se déroulant lors de la stagnation des effluents (Sato et al., 2001).

Tableau 4 : composition d'une phase gaz artificiellement volatilisée issue d'un réservoir de stockage d'eau usée urbaine (adapté de Sato et al., 2001).

Composés	**Concentration en phase gaz**
Acide acétique (CH_3-COOH)	40 – 120 ppm
Acide propionique (CH_3-CH_2-COOH)	5.30 – 27 ppm
Acide butyrique (CH_3- CH_3-CH_2-COOH)	1.50 – 9.20 ppm
Sulfure d'hydrogène (H_2S)	19 – 50 ppm
Methyl mercaptan (CH_3-SH)	0.70 - 1.1 ppm
Ammoniaque (NH_3)	18 – 134 ppm

Ainsi en fonction des conditions de collecte (hydraulique), des conditions environnementales (T°C, pH), après des zones de stagnation, la volatilisation de nombreux composés produit une phase gaz spécifique. Celle-ci, basée sur un air enrichi en CO_2, est constituée de composés soufrés (H_2S en majorité), de composé organique (COV et en particulier AGV) et d'azote (NH_3 en majorité).

1.2. Détériorations localisées au niveau d'une canalisation gravitaire

En réseau d'assainissement, si la détérioration des matériaux est due à la production d'une phase particulière liée à la typographie et aux modes de collecte des eaux-usées, la détérioration des matériaux cimentaires n'est pas homogène au niveau des lieux de fortes détériorations. Des zones de détériorations préférentielles sont observées au sommets des canalisations et au niveau des zones de marnages des eaux usées (Sand and Bock, 1984) (Islander et al., 1991) (Mori et al., 1992) (Roberts et al., 2002).

1.2.1. Phénomène de condensation au sommet de la canalisation

La variation de la température des eaux collectées par les réseaux d'assainissement (3°C à 27°C pour les Etats-Unis) (Metcalf and Eddy, 2003) est en moyenne toujours supérieure à la température du sous-sol dans lequel sont enterrées les canalisations. Cette différence crée un gradient de température au sein même de la phase atmosphérique des canalisations. De ce fait, un phénomène de volatilisation des eaux usées dans la phase atmosphérique et de recondensation à la paroi des canalisations est favorisé (Pomeroy and Boon 1990). De plus l'existence du gradient de température au sein des canalisations d'assainissement, par des modifications locales de la masse volumique de la phase atmosphérique, induit des courants préférentiels de circulation d'air (Pomeroy and Boon 1990). Ces courants transportent donc la matière volatilisée vers certaines zones de la paroi, en particulier celles situées au sommet des canalisations. La figure 6.a présente un schéma (adapté de Pomeroy and Boon 1990, lui-même adapté de l'USEPA 1974) représentant la mise en mouvement de la phase gaz dans une canalisation gravitaire avec stagnation des eaux usées. Ce schéma illustre la focalisation des flux matières volatilisés vers le sommet de la canalisation. La figure (6.b) présente les résultats d'une simulation réalisée sous le logiciel COMSOL multiphysics® réprésentant la même structure. Ces résultats de simulations (température de l'eau usée fixée à 20°C, pour

une température à la paroi de la canalisation fixée à 10°C), illustrés par la représentation des champs de vitesse dans la phase gaz (flèches), confirment l'intensification des flux matières volatilisés vers le sommet de la canalisation et ce par la mise en mouvement de la masse d'air due à une simple différence de température entre les eaux usées collectées et la paroi de la canalisation.

a) Schéma représentant la coupe en section d'une canalisation gravitaire avec effluent stagnant et l'influence du gradient de température sur les déplacements de la masse d'air de la phase non-immergée.

b) Résultat de simulation pour la section d'une canalisation gravitaire avec effluent stagnant et l'influence du gradient de température sur les déplacements de la masse d'air de la phase non-immergée.

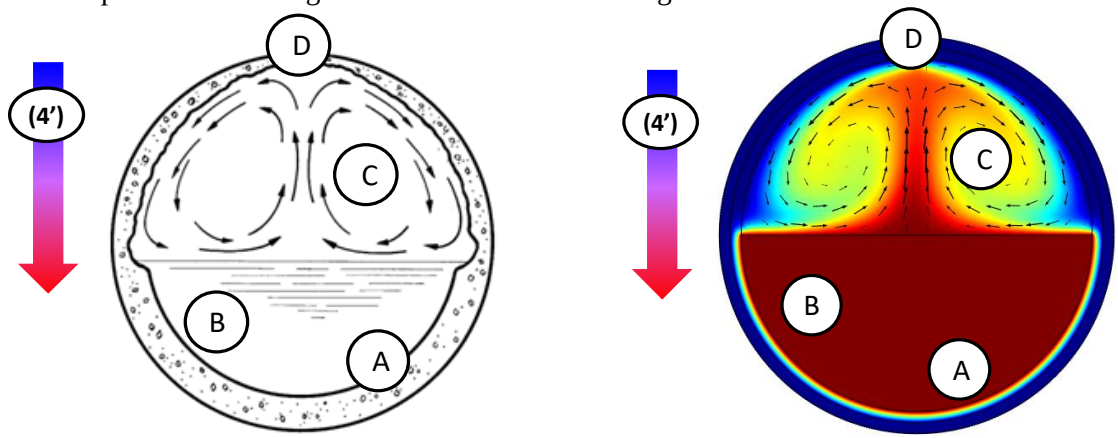

Figure 6: Schéma (adapté de Pomeroy and Boon (1990), lui-même adapté de l'agence de la protection de l'environnement des USA (USEPA, 1974)), et résultat de simulation (COMSOL multiphysics®) illustrant par les phénomènes de convection de l'air dans la canalisation (dus au gradient de température) la focalisation des flux matières dans la phase atmosphérique des canalisations gravitaires vers le sommet de la canalisation.

La température maintenue au niveau de la paroi des canalisations au niveau de la phase aérienne entraine un phénomène de condensation, permettant sur la paroi des canalisations la condensation des composés précédemment volatilisés (H_2S, CO_2, AGV, NH_3) et ainsi la création d'un milieu favorable au développement des microorganismes entrainant localement la production d'acide biogénique.

1.2.2. La zone de marnage des eaux usées

Les fortes détériorations observées au niveau de la zone de marnage des eaux usées sont la résultante de différents phénomènes. Outre la production d'acide biogénique produit localement, ou issu du ruissellement de l'acide produit dans les zones supérieures, des phénomènes de séchage/mouillage et d'abrasion sont à considérer pour expliquer

l'intensification dans cette zone des phénomènes de détérioration (Monteny et al., 2001). Pour autant, l'attaque biologique est première dans la déstructuration des matériaux, cette détérioration localisée étant peu observée au niveau de canalisations exemptes d'H_2S.

Ainsi, même si le rôle des phénomènes physiques est important dans la déstructuration des matériaux, les paragraphes suivant se focalisent sur la description et la compréhension des phénomènes régissant les transformations biologiques se déroulant au niveau du condensat formé au sommet des canalisations détériorées. Une description des différentes transformations (chimiques et biologiques) conduisant à la production d'un milieu agressif est proposée. Par la suite, l'évolution des matériaux cimentaires face à ce type d'environnement sera décrite, permettant de proposer en fin de chapitre un schéma phénoménologique de la biodétérioration indiquant l'interaction entre l'activité biologique et les matériaux. Le schéma sera par la suite simplifié en blocs réactionnels, permettant de proposer une réduction du système à reproduire et ainsi de focaliser l'étude expérimentale sur les interactions spécifiques clés.

1.3. Transformations chimiques et biologiques au niveau du condensat

1.3.1. Processus généraux

La formation d'un condensat au niveau des parois des canalisations, associée à un flux de matière des composés volatilisés focalisé vers le sommet des canalisations, conduit à la création au contact des parois des canalisations d'un milieu réactionnel particulier. Les paragraphes suivants, après une vision générale, se proposent de décrire spécifiquement les devenirs de l'H_2S et des COV (en particulier les AGV). L'ammoniaque, de part son caractère basique n'a que peu d'effet direct sur les matériaux cimentaires. Il intervient uniquement pour l'apport de l'azote nécessaire à la croissance microbienne des différentes populations impliquées dans la détérioration des matériaux.

Les matériaux cimentaires, quelles que soient leurs différentes compositions, possèdent des propriétés basiques, et une valeur de pH de surface, pour un revêtement neuf, comprise généralement entre 11 et 13 (Lea, 1970) (Roberts et al., 2002). Ce pH initial est peu propice à l'implantation et à la croissance de populations microbiennes. Les observations menées sur des milieux détériorés en réseaux d'assainissement font état de pH de surface souvent inférieur à 2 (Islander et al., 1991) (Mori et al., 1992) (Satoh et al., 2009). L'activité

biologique de par les différents composés produits conduit donc au cours du temps à l'abaissement du pH en surface des matériaux. D'un autre coté les populations bactériennes sont généralement très sensibles au pH du milieu dans lequel elles se développent (Bielefeldt et al., 2010). Cet abaissement progressif, est un vecteur de sélection spatiale et temporelle des populations impliquées dans la détérioration. Ainsi, au cours du temps, le pH inhibe certaines populations, favorise l'implantation d'autres qui alimentent ainsi, par leur métabolisme, le processus d'acidification. Une succession bactérienne, liée également à d'autres conditions que le pH de surface (type de composés intermédiaires produits, propriétés de diffusion des différents substrats), est donc responsable, en partie par la production finale d'acide biogénique, des phénomènes de détériorations (Roberts et al., 2002, Cho and Mori, 1995, Islander et al., 1991, Nica et al., 2000, Okabe et al., 2007).

Ainsi, une phase initiale d'abaissement du pH de surface est liée à la dissolution au sein du condensat du dioxyde de carbone CO_2 et de l'H_2S (Islander et al., 1991) et potentiellement dans une moindre mesure des AGV. Le rôle respectif de l'H_2S et du CO_2 sur cette phase initiale est encore discuté, Joseph en 2012 montrait que l'évolution du pH de surface était majoritairement due à la dissolution de l'H_2S comparativement au CO_2, quand Ismail en 1993 (Ismail, 1993) remarque que les bétons au niveau de certaines installations sont détériorés quand ils sont exposés à des atmosphères à faible concentration en H_2S mais avec une forte concentration en CO_2. Il constate également que la carbonatation de la surface des bétons est essentielle à la colonisation par des bactéries (Ismail, 1993).

Cependant, une fois le pH de surface descendu à des valeurs plus favorables pour l'implantation de populations microbiennes, la présence de composé soufré et de COV pour une part plus réduite, en présence d'azote et d'oxygène (phase aérienne des canalisations) va conduire au développement d'une activité microbienne complexe, faisant intervenir : (i) des bactéries capables d'oxyder les composés soufrés (responsable de la production d'acide sulfurique biogénique) via des métabolismes diverses (Parker, 1945b) (Sand and Bock, 1984) (Islander et al., 1991) (Satoh et al., 2009), (ii) des bactéries hétérotrophes oxydant la matière organique (COV) et produisant localement du dioxyde de carbone (Sand and Bock, 1984) (Vincke et al., 2001) (Okabe et al., 2007) et (iii) des champignons capables d'oxyder la matière organique en présence d'oxygène et ayant pour particularité métabolique une importante production d'acides organiques et une large adaptation en terme de pH (Mori et al., 1992) (Gu et al., 1998) (Vincke et al., 2001).

1.3.2. Devenir de l'H_2S

La dissolution de l'H_2S au contact du matériau cimentaire, tirée par les équilibres acido-basiques, due à la présence d'oxygène et de par la réactivité des sulfures (H_2S, HS^- et S^{2-}) conduit à la production de différent composés soufrés (soufre élémentaire (S^0, précipité généralement sous la forme S_8 (Joseph et al., 2012) (Hérisson et al., 2012)) ; thiosulfate ($S_2O_3^{2-}$) et autres polythionates (tetrathionate ($S_4O_6^{2-}$), pentathionate ($S_5O_6^{2-}$)) (Islander et al., 1991) (Okabe et al., 2007). En présence d'oxygène, ces composés soufrés, comme l'H_2S peuvent être oxydés par des bactéries sulfo-oxydantes (SOB). Ces oxydations conduisent à la production finale d'acide et de sulfate au contact des matériaux cimentaires. Avec l'acidification du milieu la réactivité chimique des composés va être modifiée, ainsi que l'activité des bactéries impliquée, réorientant les modes de transformations et les populations impliquées. Parker (Parker, 1945) a noté que sur des ciments neufs les sulfures pouvaient être oxydés en thiosulfate ($S_2O_3^{2-}$) et tetrathionate ($S_4O_6^{2-}$). Sur des ciments détériorés, à pH de surface acide, la précipitation de soufre élémentaire pouvait être observée (Joseph et al., 2012) (Hérisson, 2012). Ainsi, une fois l'H_2S absorbé au niveau du condensat, l'acidification du milieu réactionnel au contact des matériaux cimentaires est due au couplage de différentes réactions chimiques et biologiques dépendantes de l'évolution des conditions locales en termes de voies réactionnelles et de cinétiques. La figure 7 (adaptée de Islander et al., 1991) illustre les principaux intermédiaires réactionnels pouvant intervenir durant l'oxydation de l'H_2S en sulfate, et ce en fonction de conditions de pH du condensat, les voies réactionnelles générales quelles soient chimiques et/ou biologiques, ainsi que la production d'acide pour chaque réaction liée à l'oxydation d'un atome de soufre.

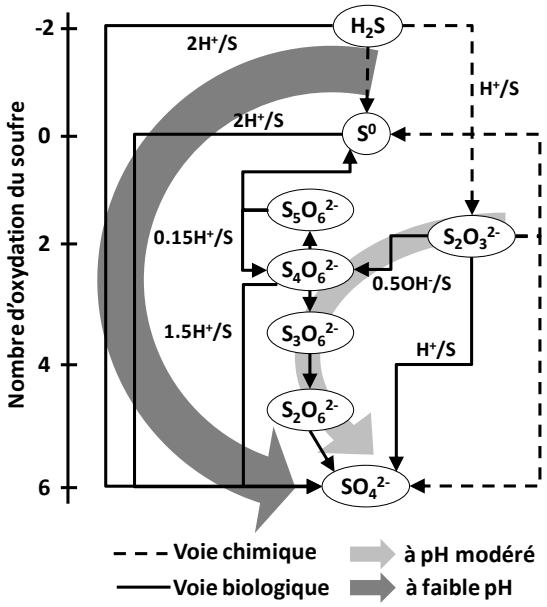

Figure 7: Oxydation des composés soufrés au cours de la succession bactérienne (adapté de Islander et al., 1991).

Des exemples de réactions d'oxydation par des microorganismes sulfo-oxydants, conduisant à la production d'acide biogénique liée à une production de sulfates, sont donnés par les équations suivantes (Eq 18, Eq 19, Eq 20, Eq 21, Eq 22). Les énergies libres de Gibbs associées sont issues d'un article de Kelly paru en 1999 (Kelly 1999).

Production d'acide et de sulfate à partir d'H_2S :

Eq 18 : $H_2S + 2O_2 \rightarrow SO_4^{2-} + 2H^+$ ($\Delta G° = -714.1$ kJ/molS-Substrat)

Production de soufre élémentaire à partir d'H_2S :

Eq 19 : $H_2S + O_2 \rightarrow S + 2H_2O$ ($\Delta G° = -209.3$ kJ/molS-Substrat)

Production d'acide et de sulfates à partir de soufre élémentaire (S^0) :

Eq 20 : $S^0 + H_2O + 1.5O_2 \rightarrow SO_4^{2-} + 2H^+$ ($\Delta G° = -507.4$ kJ/molS-Substrat)

Production d'acide et de sulfate à partir de thiosulfate ($S_2O_3^{2-}$) :

Eq 21 : $S_2O_3^{2-} + 2O_2 + H_2O \rightarrow 2SO_4^{2-} + 2H^+$ ($\Delta G° = -375.05 \pm 8.05$ kJ/molS-Substrat)

Production d'acide et de sulfate à partir de tetrathionate ($S_4O_6^{2-}$) :

Eq 22 : $S_4O_6^{2-} + 3.5O_2 + 3H_2O \rightarrow 4SO_4^{2-} + 6H^+$ ($\Delta G° = -311.15$ kJ/molS-Substrat)

L'énergie libre de Gibbs informe sur le caractère énergétique de l'oxydation de tel ou tel composé soufré. Ainsi pour 1 mole de soufre oxydée l'oxydation d'H_2S devrait permettre aux cellules impliquées de retirer 2 fois plus d'énergie que l'oxydation de thiosulfate. Mais pour cela, il est nécessaire que l'activité microbienne ne soit pas concurrencée par des oxydations chimiques (abiotiques), concurrence qui peut être double puisque en plus d'oxyder totalement ou partiellement la source soufrée d'énergie elles consommeront une part de l'accepteur final d'électron qu'est l'oxygène.

1.3.3.1. Réactivité abiotique des composés soufrés réduits

Le pH à la surface du matériau cimentaire (interface gaz/condensat) varie au cours du temps, lié aux réactions mises en jeu et à l'avancement des phénomènes de détérioration (pH d'un revêtement neuf entre 10 et 13, et pH d'une zone fortement détériorée < 2). Cette

variation du pH influencée au départ par la dissolution de l'H_2S et d'autres gaz acides (CO_2, AGVs) (Islander et al., 1991) (Joseph et al., 2012), puis par l'activité biologique sulfo-oxydante conduit en solution à une spéciation évolutive des sulfures (H_2S, HS^- et S^{2-}).

En présence d'oxygène la réactivité des sulfures dépend des formes en présence, donc du pH au niveau de la zone de réaction, de plus le type de composés produits lors de ces oxydations chimiques va également être influencé par le type de sulfures réagissant (pour exemple les équations suivantes proposées par Chen et Morris (1972) montrent en présence d'oxygène la formation de différents composés soufrés à partir de l'ion HS^-).

Eq 23 : $2HS^- + O_2 + 2H^+ \rightarrow 2H_2O + 2S^0$

Eq 24 : $2HS^- + 2O_2 \rightarrow H_2O + S_2O_3^{2-}$

Eq 25 : $2HS^- + 4O_2 \rightarrow 2SO_4^{2-} + 2H^+$

Ainsi, Chen et Morris, sur des expériences en solutions tamponnées à différents pH, ont estimé une cinétique d'oxydation abiotique des sulfures totaux, dont le taux d'oxydation spécifique (k) est fonction du pH (Chen and Morris, 1972). La figure 8 présente la relation empirique déterminée et les résultats obtenus en termes de valeurs expérimentales de (k) à une température de travail de 25°C, confrontés à la spéciation des sulfures en fonction du pH (spéciation calculée à partir des constantes d'acidité présentées dans les équations précédentes (Eq 2 et Eq 3)).

L'oxydation abiotique des sulfures seraient donc due préférentiellement à la présence commune de l'ion HS^- avec H_2S ou avec S^{2-}. Les résultats semblent indiquer également l'absence d'oxydation de l'H_2S à des pH inférieur à 6, quand l'H_2S est la seule forme de sulfures présente en solution. Ce qui laisserait supposer, à des pH inférieurs à 6, l'absence de réaction abiotique concurrentielle de la biologie. Pourtant, d'autre études ont montré à pH acide, sur des matériaux détériorés (Jospeh et al., 2012) (Herisson, 2012) ou en solution, la formation abiotique de soufre élémentaire (Steudel,1996) (Jensen et al., 2012). Cette production de soufre élémentaire est due à l'oxydation directe des sulfure en soufre élémentaire (Joseph et al., 2012) (Jensen et al., 2012), elle peut aussi être du à des pH acides (< 4) à la dismutation des thiosulfates initialement produits (Johnston and McAmish, 1973) (Harrison, 1984) conduisant à la production de soufre élémentaire et de sulfites (SO_3^{2-}) rapidement oxydés en sulfates (SO_4^{2-}) en présence d'oxygène (Linek and Vacek, 1981).

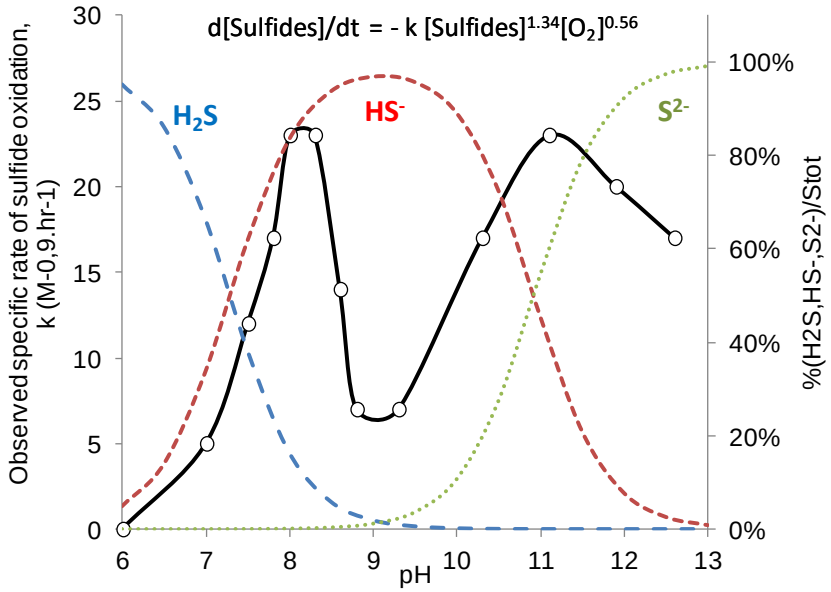

Figure 8: Taux d'oxydation spécifique observé en solution des sulfures en fonction du pH, relation cinétique empirique, comparé à la spéciation des sulfures en solution à 25°C (adaptée de Chen and Morris, 1972). **—○—** **:** évolution en fonction du pH de la valeur expérimentale du taux d'oxydation spécifique observée (k) concernant l'oxydation abiotique des sulfures totaux ; **— — —**: proportion d'H_2S par rapport aux sulfures totaux ; **— — —** : proportion d'HS^- par rapport aux sulfures totaux ; **·····**: proportion d'S^{2-} par rapport aux sulfures totaux.

La précipitation de soufre élémentaire à partir de solution de sulfures est décrite par Steudel (1996) a travers un mécanisme réactionnel dans lequel peuvent intervenir des ions métalliques tel que le vanadium (V^V), le fer (Fe^{III}) ou le cuivre (Cu^{II}). Le mécanisme réactionnel (Steudel, 1996) fait intervenir dans une première étape l'ion HS^- et la formation d'un radical $HS^{\bullet}$ et par la suite via la production d'un radical $S^{\bullet-}$ et la formation de polysulfures (S_x^{2-}) de plus en plus long aboutissant en fin de réaction à la production de cycle de soufre élémentaire (S_8) constituant les premiers précipités soufrés observés en réseau d'assainissement (Joseph et al., 2012) (Hérisson, 2012). Ce mécanisme réactionnel peut être résumé par les deux équations générales suivantes (Eq 26 et Eq 27), ou M représente le cation métallique intervenant dans la réaction et étant par la suite régénéré par la réduction d'oxygène en présence de protons (Steudel, 1996).

Eq 26 : $HS^- + 2M^{n+} \rightarrow S^0 + H^+ + 2M^{(n-1)+}$

Eq 27 : $4M^{(n-1)+} + O_2 + 2H^+ \rightarrow 4M^{n2+} + 2OH^-$

Cependant, Steudel, pour une solution saturée en H_2S, dont le pH est alors de 4.1 (donc concentration en HS^- proche de 0 (cf. figure 8)) a montré l'oxydation rapide de l'H_2S sous une atmosphère d'oxygène pure. Sous des conditions de réseau d'assainissement, Jensen a également montré en 2009, que la consommation de l'H_2S de la phase gaz était due à

l'activité biologique aux parois des canalisations ainsi qu'a des phénomènes physico-chimiques de sorption. Ainsi, concernant les sulfures seuls, une compétition entre l'activité biologique et la réactivité abiotique de ces composés a lieu lors de la dissolution de l'H_2S au niveau du condensat. Des études autres que Jensen ont tenté d'évaluer la part de l'oxydation abiotique par rapport à l'oxydation biologique, mais seulement dans des conditions de solutions aqueuses avec des résultats très disparates, certains montrant que l'oxydation biologique atteint 12 à 56 % de l'oxydation totale de l'H_2S (Wilmot et al., 1988), d'autres obtenant 86% à 99% en participation biologique à pH 8 et 25°C en fonction de la concentration initiale en sulfure (100 mgS/l ou 10 mgS/l respectivement) (Buisman et al., 1990), où 70% de participation biologique a été estimée dans les eaux usées à pH 7 et 25°C (Kotronarou and Hoffman, 1991), mais toujours à partir de bactéries adaptées à la charge en sulfures apportés.

Ainsi, si l'H_2S est la source première de soufre, sa réactivité en fonction des conditions à la paroi des canalisations et de leur évolution implique, spécifiquement dans le cas d'une production intermittente en H_2S telle qu'elle est rencontrée en réseaux d'assainissement, soit une activité biologique intense (ce qui ne peut être le cas dans les premiers temps de la colonisation) soit le passage via des composés qui bien que moins intéressant d'un point de vue énergétique, sont stables dans les conditions rencontrées. A des pH neutres ou légèrement alcalins, en eaux usées, sous des concentrations en oxygène importantes (15 mgO_2/l) Sharma et Yuan ont observé la formation abiotique de thiosulfate en tant que principal produit (Sharma and Yuan, 2010). Par conséquences, les conditions de pH et les conditions d'aération peuvent influencer l'avancement de la réaction d'oxydation. La formation de thiosulfate a également été identifiée sur des bétons frais, en zone humide et en présence d'H_2S (Parker, 1945b). Les thiosulfates, comme d'autres polythionates tels que les tetrathionates sont stables en condition alcaline ou neutre, les tetrathionates étant également stable à pH acide (hormis dans des conditions de fortes concentration en cations métalliques permettant, par catalyse, l'oxydation de ce composé (Druschel et al., 2003a)). A pH acide, la précipitation de soufre élémentaire, qu'elle soit directe ou via la dismutation des thiosulfates, permet d'immobiliser au contact des matériaux cimentaires un substrat potentiel pour certaines bactéries sulfo-oxydantes. Dans un système intermittent de production d'H_2S (cas des réseaux d'assainissement), couplé à la focalisation des flux d'H_2S vers le sommet des canalisations, cette précipitation peut expliquer l'implantation et le maintient de population sulfo-oxydantes au niveau de la paroi de la canalisation.

1.3.3.2. Succession bactérienne à la surface des matériaux cimentaires

L'absorption de l'H_2S au niveau du condensat formé à la paroi des canalisations favorise le développement de microorganismes particuliers et ce par l'apport de composé soufré réduits. La description des phénomènes dans le temps via une succession bactérienne en fonction du pH permet d'illustrer d'une manière qualitative, par la production d'acide et de sulfate produits biologiquement au contact des matériaux, les détériorations observées dans les conditions de réseaux d'assainissement (Parker and Jackson, 1965) (Islander et al., 1991) (Roberts et al., 2002) (Okabe et al., 2007). Cette succession bactérienne théorique peut être décrite en trois étapes (figure 9) liées en particulier à un abaissement progressif du pH en surface des canalisations et donc à la réactivité abiotique des composés mis en jeu.

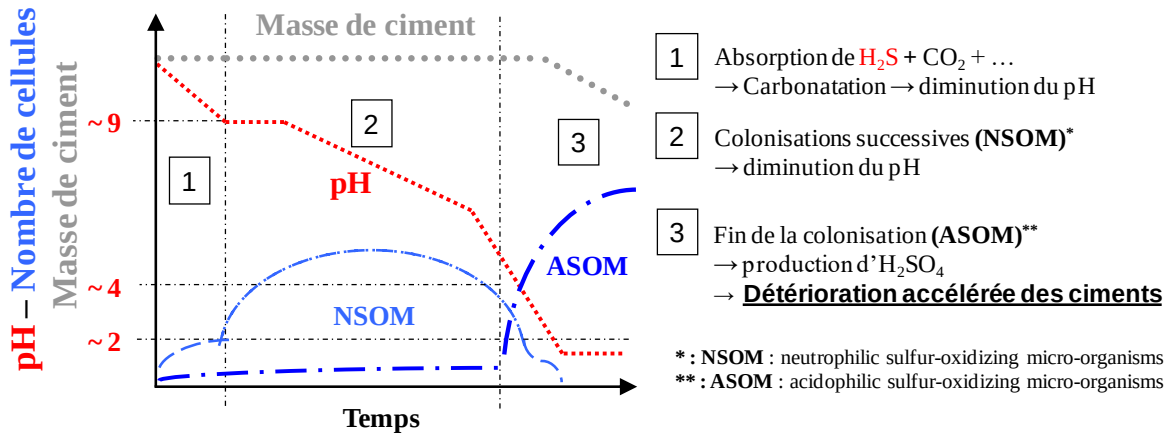

Figure 9: Changements théoriques dans les propriétés biologiques et physiques du ciment au cours du temps. Illustration de la succession bactérienne. Evolution du pH. Influence sur les populations microbiennes, qui par leur métabolismes propres influence également l'évolution du pH à la surface des matériaux, d'où à terme une perte de masse des ciments mis en contact, dans les conditions des réseaux d'assainissement, avec ce type de microorganismes (Islander et al., 1991, Roberts et al., 2002).

L'étape (1) (figure 9) correspondant à la phase d'abaissement du pH par la dissolution au sein du condensat des gaz acides présents dans la phase atmosphérique des réseaux a été décrite précédemment (paragraphe [1.3.1.] de ce chapitre).

Par la suite ((étape (2) figure 9), l'abaissement du pH de surface et l'apport en nutriments via la phase gaz, ou via la projection d'aérosol, permet l'implantation sur la paroi des canalisations de différentes populations dont l'activité biologique via les produits finaux de réactions participe à la diminution progressive du pH de surface (Roberts et al., 2002). L'évolution de la valeur du pH à la surface des parois conditionne le milieu de croissance et sélectionne ainsi les différentes populations susceptibles de croître. On recense ainsi des

populations NSOM (neutrophilic sulfur-oxidizing micoorganisms) se développant à des pH compris entre 9 et 4, et des populations ASOM (acidophilic sulfur-oxidizing microorganism) dont la croissance est favorisée par de faibles pH compris entre 4 et 1 (Islander et al., 1991) (Roberts et al., 2002) (Okabe et al., 2007). Le tableau suivant (tableau 5) présente quelques unes des espèces sulfo-oxydantes observées au niveau des zones sensibles à la détérioration en réseaux d'assainissement (Parker, 1945b) (Sand and Bock, 1984) (Roberts et al., 2002). Le métabolisme général de ces différentes espèces est présenté, qu'il soit autotrophe (croissance liée uniquement à la fixation de carbone inorganique), mixotrophe (croissance pouvant être assurée soit à travers l'utilisation de carbone inorganique, soit par oxydation de matière organique), ainsi que la zone de pH d'activité, et les substrats soufrés consommés et les produits formés.

Tableau 5 : Exemple d'espèces de Thiobacillus identifiés en réseaux d'assainissement adapté de (Roberts et al., 2002)

Espèces	**pH croissance**	**Caractéristiques**	**Substrats soufrés**	**Produits**
T.thioparus	4,5 - 10	Autotrophe	Thiosulfate, H_2S	S^0, acides polythio.
T.novellus	5 – 9,2	Mixotrophe	Thiosulfate	S^0
T.neapolitanus	4 – 9	Autotrophe	H_2S, S^0, Thiosulfate	Acides polythio., $2H^+$, SO_4^{2-}
T.intermedius	1,7 – 9	Mixotrophe	Thiosulfate	Acides polythio., $2H^+$, SO_4^{2-}
A.thiooxydans	0,5 – 4	Autotrophe	Thiosulfate, S^0	S^0, $2H^+$, SO_4^{2-}

La production d'acide biogénique par ce type de populations microbiennes (étape (3)) (cf Eq 18, Eq 19, Eq 20, Eq 21, Eq 22) permet dans un dernier temps d'accentuer en surface les phénomènes de dissolution dus à l'abaissement du pH et donc aux réactions acido-basiques se produisant entre les composés dissous et les matériaux constituants le revêtement des canalisations (Scrivener et al, 1999) (Lamberet, 2005), de plus outre la production d'acide, la production de sulfate va également être essentielle pour expliquer les degrés de détérioration observés (Davis et al, 1998) (Scrivener et al, 1999) (De Belie et al., 2002).

Okabe (2007) a suivi la flore microbienne se développant sur des coupons de béton (composition du matériau non-précisée) installés dans la phase aérienne d'un regard de visite (concentration en H_2S 20-30 ppm). De plus il montre l'évolution des populations en fonction

de l'évolution des matériaux en couplant des mesures de pH de surface et de perte de masse des coupons exposés. Il corrèle ainsi l'implantation de populations acidophiles avec une détérioration accentuée du matériau cimentaire testé. La figure 10 montre, sur une durée de 374 jours, les résultats obtenus en termes d'abaissement du pH de surface des coupons et de la perte de masses.

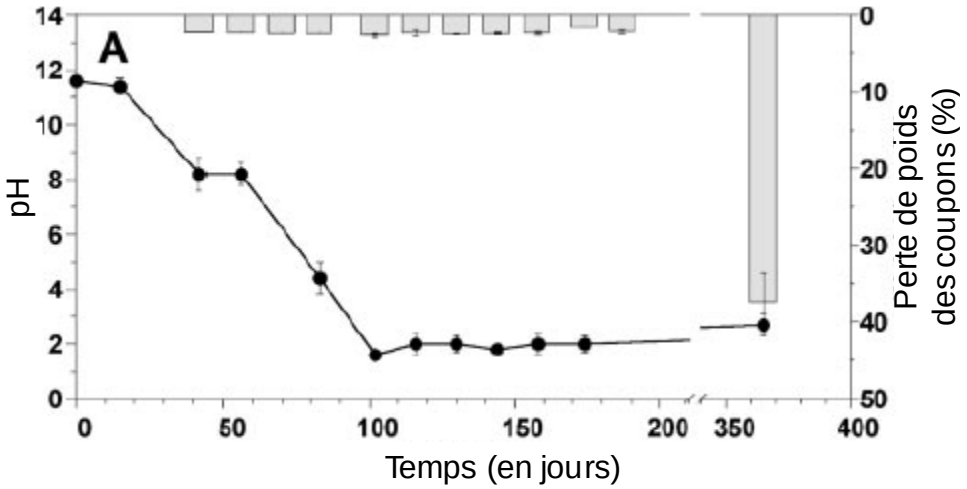

Figure 10: Evolution du pH de surface, de la perte de masse des coupons exposés, ainsi que l'accumulation de sulfate et de soufre élémentaire au sein de la matrice cimentaires (adaptée d'Okabe et al., 2007).

La figure 11 présente les résultats obtenus en termes d'identification des populations par le croisement de méthodes d'extraction, purification de l'ADNr 16S, puis par clonage et séquençage de l'ADNr 16S, et des mesures de caractérisation par FISH (Fluorescent In Situ Hybridization).

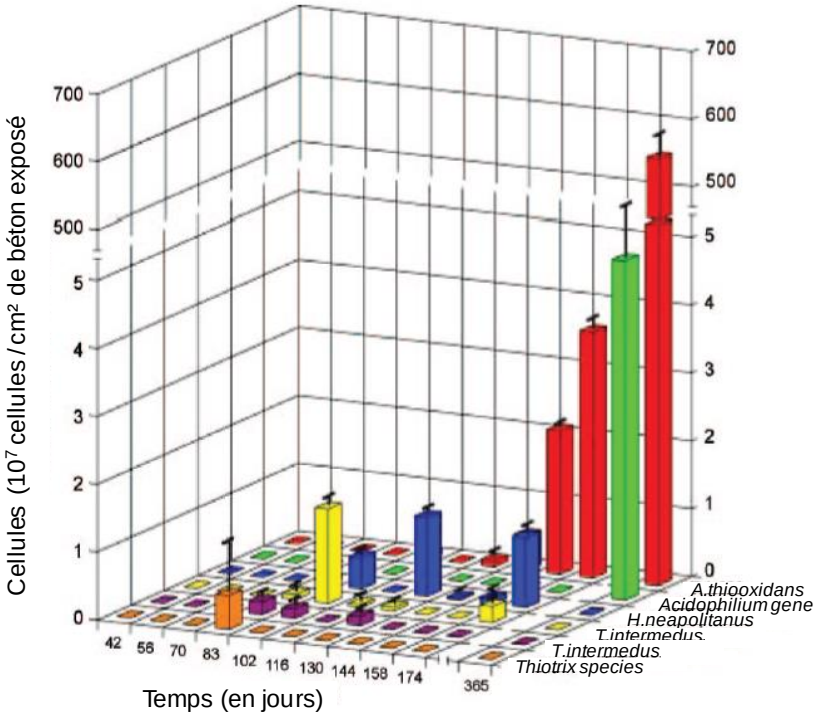

Figure 11: Evolution en nombre du type de cellules sulfo-oxydantes détectées par des analyses FISH réalisées par des sondes d'espèces ou de gènes spécifiques. Les barres d'erreurs représentent l'erreur standard de mesures réalisées en duplicata (Okabe et al., 2007).

L'apparition de l'espèce *Thiobacillus thiooxidans* correspond donc à un pH de surface de 2, et son développement correspond au maintien de ce pH de surface, liée après 374 jours à une perte de masse des coupons exposés de l'ordre de 40%. Après 374 jours l'espèce *Thiobacillus thiooxidans* est devenue l'espèce prédominante concernant les bactéries sulfo-oxydantes implantées (Okabe et al., 2007).

Ainsi, appuyé sur d'autres études antérieures l'espèce *Thiobacillus thiooxidans* apparait comme moteur dans l'oxydation finale et locale des composés soufrés réduit entrainant la production d'acide et de sulfate au contact des matériaux cimentaires (Parker, 1945) (Milde et al., 1983) (Nica et al, 2000) (Vincke et al., 2001). Pour autant les consortiums microbiens analysés au niveau de zones fortement détériorées demeurent complexes. Le tableau 6 (Jensen, 2009) récapitule différentes espèces bactériennes identifiées au niveau de zones fortement détériorées.

Tableau 6 : Exemple de la diversité bactérienne identifiée au niveau de matériaux détériorés au niveau de différents réseaux d'assainissement dans le monde (Jensen, 2009)

Genus	**Species**	**Ref**
Achromobacter	*xylosoxidans*	Okabe et al., 2007
Acidiphilium	*acidophilum*	Nica et al., 2000 ; Okabe et al., 2007
Acidithiobacillus	*thiooxidans*	Nica et al., 2000 ; Vincke et al., 2001 ; Hernandez et al., 2002
Acinetobacter	*junii*	Okabe et al., 2007
Aeromicrobium	*erythreum*	Vincke et al., 2001
Agrobacterium		Vincke et al., 2001
Azonexus	*caeni*	Okabe et al., 2007
Bacillus	*psychrodurans*	Vincke et al., 2001
Cellvibrio		Vincke et al., 2001
Clostridium	*bartletti*	Okabe et al., 2007
Flavobacterium	*aff.*	Vincke et al., 2001
Leptospirillum	*ferrooxidans*	Okabe et al., 2007
Methylobacterium		Vincke et al., 2001
Microbacterium		Nica et al., 2000
Mycobacterium	*sudneyiensis*	Vincke et al., 2001
	florentinum	Okabe et al., 2007
Ochrobactrum	*antrophi*	Nica et al., 2000
	tritici	Okabe et al., 2007
Propionibacterium	*acnes*	Vincke et al., 2001
Pseudomonas	*pseudoalcaligenes*	Vincke et al., 2001
Sphingomonas		Vincke et al., 2001
Stenothrophomonas	*maltophilia*	Vincke et al., 2001 ;Maeda et al., 1999
Thiobacillus	*ferrooxidans*	Yamanaka et al., 2002
Turicibacter	*sanguinis*	Okabe et al., 2007
Xylanivorum		Vincke et al., 2001

La large présence de champignons a également été mise en évidence (environ 50% des populations identifiées) (Parker et Jackson 1965) (Gu et al., 2008) (Vincke et al., 2001). Gu

en 1998 a montré un impact majeur de l'activité microbienne d'un champignon (*Fungus Fusarium*) sur des matériaux cimentaires d'assainissement (Gu et al., 1998), mais peu de données existent sur le rôle direct de ces microorganismes hétérotrophes sur la biodétérioration des matrices cimentaires.

1.3.3. Populations microbiennes hétérogènes et activités spécifiques

L'étude microbiologique du système responsable des détériorations a montré la nécessaire présence de différents microorganismes (type Thiobacilli) capables de consommer différents composés soufrés (Parker, 1945b, Sand, 1987, Islander et al., 1991, Nica et al., 2000). Ces différentes études ont toujours rapporté la présence au sein même du système microbien de populations hétérotrophes (Sand and Bock, 1984) (Islander et al., 1991), ainsi que la présence de champignons (Cho and Mori, 1995) (Gu et al., 1998). Sand et Bock (Sand and Bock, 1984) en particulier ont rapporté pour des prélèvements effectués sur le réseau d'assainissement de la ville de Hambourg en 1984 la présence de microorganismes hétérotrophes à la surface des canalisations d'assainissement dans une gamme de pH allant de 6,2 à 1,5 unité de pH.

La présence de substrats carbonés volatils, tel que les AGV, ou de composés organiques apportés via des aérosols, la présence également d'ammoniaque, crée en présence d'oxygène un milieu favorable au développement d'un consortium microbien *a priori* constitué en un biofilm hétérogène. Différents composés soufrés, à forte concentration, sont toxiques pour les différentes populations microbiennes, même pour les bactéries sulfo-oxydantes (Vollertsen et al., 2008). De même à partir d'une certaine concentration en composés organiques tels que les acides gras volatils (AGV), il est possible d'observer l'inhibition aussi bien des populations hétérotrophes, que des populations chimio-lithotrophes facultatives du genre Thiobacillus. De plus les microorganismes de l'espèce *T. thiooxidans,* de par leur métabolisme, produisent de l'acide pyruvique et de l'acide oxaloacétique, qui à une certaine concentration (2.10^{-5} et 7.10^{-5} mol/L) sont inhibitants pour cette même espèce (Borichewski, 1967, Roberts et al., 2002). Il est donc possible d'envisager une complémentarité des métabolismes expliquant, par la complexité du consortium microbien, la levée des inhibitions. De plus, la production de dioxyde de carbone au contact des matériaux cimentaires, via les métabolismes hétérotrophes peut entrainer une forte carbonatation locale préjudiciable dans le cas d'une forte acidité produite ultérieurement sur cette même zone (Ismaël et al., 1993), le dioxyde de carbone

produit pouvant également être ainsi disponible pour le développement des bactéries autotrophes (tel que *Thiobacillus thiooxidans*) (Ismaël, 1993) (Jaworska and Urbanek, 1997).

De part la faible proportion d'AGV présent dans la phase atmosphérique, l'attaque directe de ces composés par leur dissolution dans le condensat est difficilement envisageable. Pour autant, la production locale d'acide organique, via des métabolismes hétérotrophes (et spécialement via l'activité biologique de champignons) par des mécanismes légèrement différents de l'acide sulfurique biogénique (solubilités disparates des sels de calcium formés en particulier, pour détails voir les paragraphes suivants) peut expliquer les fortes détériorations observées par Gu et al.

La production d'exopolymères assurant l'adhésion et la cohésion des colonies microbiennes peut également jouer un rôle dans la biotérioration, (i) par le simple maintien des populations produisant un milieu agressif en contact avec le matériau, (ii) par un effet direct chélateur (des cations divalents en particuliers tel que Ca^{2+} contenu dans le matériau fortement constituée de composés calciques) déstabilisant un peu plus la matrice cimentaire et donc accentuant potentiellement sa dissolution.

1.4. Devenir des matériaux cimentaire face à l'acide biogénique

1.4.1. Les matériaux considérés

Cette étude est réalisée en partenariat avec l'entreprise Saint-Gobain PAM, producteur de canalisations en fonte ductile (conforme à la norme NF EN 598 concernant les ouvrages à écoulement libre) et munies de revêtements intérieurs en matériaux cimentaires. Ces revêtements servent à protéger la structure en fonte de l'agressivité des eaux usées collectées. Des matériaux cimentaires de différentes compositions peuvent être utilisés en fonction des usages visés. Leurs compositions vont influer sur leur résistance face aux attaques acides (Scrivener et al., 1999) (Bertron, 2004) (Lamberet, 2005), mais également peuvent jouer un rôle vis-à-vis de l'implantation et de la prolifération des microorganismes à la paroi du matériau (Erhrich et al., 1999) (Herisson, 2012).

Historiquement les pâtes cimentaires étaient constituées majoritairement de portlandite ($Ca(OH)_2$), composé extrêmement réactif en milieu acide de part l'équilibre régissant sa solubilité (Eq 28).

Eq 28: $Ca(OH)_2\ (portlandite) = Ca^{2+} + 2OH^-$

avec $Ks_1 = 6.37.10^{-6}$ (issu de minteq database)

D'autres composés tels que des silicates de calcium participent à la composition générale de ces ciments. Ces ciments classés par la norme européenne EN 197-1 en tant CEM I, ne présentent que peu d'intérêt pour les conditions rencontrées en réseau d'assainissement de part la forte teneur en portlandite des pâtes. Mais leur composition initiale permet d'expliquer les choix réalisés durant les décennies passées pour proposer de nouvelles solutions de revêtements cimentaires plus résistants en conditions acides.

La norme européenne EN 197-1 définit cinq types de ciments courants (i) les CEM I correspondant aux ciments Portland classiques, (ii) les CEM II correspondant aux ciments Portland composés, (iii) les CEM III correspondant aux ciments au laitier de haut fourneau, (iv) les CEM IV correspondant aux ciments pouzzolaniques et (v) les CEM V correspondant aux ciments composés.

La norme NF EN 206-1 défini trois classes d'exposition correspondants à trois niveaux d'agressivité chimique croissante (XA1, XA2 et XA3) correspondant à des gammes de concentration en H_2S en phase gaz (Herisson, 2012).

Dans les conditions d'exposition les plus agressives (XA3) le fascicule FD P 18-011 publiée par l'AFNOR préconise l'utilisation de CEM III, IV et V.

L'étude présentée dans ce document se focalisera sur des mortiers basés sur des pâtes de ciments au laitier de haut fourneau (CEM III) et des pâtes de ciments alumineux (CAC identifiés en termes de ciments spéciaux).

Concernant les CEM III (dont il existe différentes catégories en fonction des proportions des constituants), l'ajout de laitier de haut fourneau réduit la part de portlandite au sein de la matrice cimentaire, induisant ainsi une réactivité moindre face aux attaques acides. Concernant les ciments alumineux (il en existe plusieurs catégories en fonction des proportions en alumine (Al_2O_3) constituant le ciment final), leur résistance vis-à-vis des environnements acides est due à l'absence de libération d'hydroxyde de calcium ($Ca(OH)_2$) durant leur hydratation (Herisson, 2012), à la formation de composé alumineux moins solubles que la portlandite (Eq 29 et Eq 30) et à un gain en pouvoir tampon lors de leur dissolution (Scrivener et al., 1999).

Eq 29: $Al(OH)_3\,(amorphe) = Al^{3+} + 3OH^-$

avec $Ks_2 = 6.31.10^{-32}$ (issu de minteq database)

Eq 30: $Al(OH)_3\,(gibbsite) = Al^{3+} + 3OH^-$

avec $Ks_3 = 1.95.10^{-34}$ (issu de minteq database)

Différentes études ont montré l'intérêt des revêtements CAC face aux attaques acides, comparativement au CEM III (Scrivener et al., 1999) (Erich et al.1999) (Alexander and Fourie, 2011). Dans un premier temps, les paragraphes suivant décrivent la réactivité générale des pâtes de ciments à base de ciment portland, le comportement particulier des ciments alumineux comparativement sera décrit ultérieurement.

1.4.2. Attaque acide sur les matériaux cimentaires

1.4.2.1. Généralités : les matériaux cimentaires en présence d'acide sulfurique biogénique

Les matériaux cimentaires sont sensibles aux interactions avec leur environnement qui sont à l'origine de leur vieillissement. Les facteurs influençant le vieillissement des matériaux cimentaires en réseaux d'assainissement sont d'origines physiques et/ou chimiques et/ou biologiques. Le facteur biologique est souvent négligé (Nica et al., 2000) (Tulliani et al., 2002). Les phénomènes de biodégradation mettent en jeu trois éléments : matériau – milieu – microorganismes. Comme décrit précédemment, en présence de composés soufrés volatils, différentes réactions chimiques et biologiques (dues à différentes espèces microbiennes) conduisent à la production d'acide biogénique et de sulfate, en contact avec la surface des matériaux cimentaires utilisées en réseaux d'assainissement. Ce milieu agressif pour les matériaux cimentaires réagit avec les différents composés alcalins constituant le matériau (portlandite : $Ca(OH)_2$, silicates de calcium hydraté : $Ca\text{-}SiO_2\text{-}H_2O$ principalement, aluminate de calcium : $CaO.Al_2O_3$ secondairement dans le cas de pate cimentaire à base de ciment portland (CEM I, CEM II, CEM III), provoquant ainsi leur dissolution et la formation de différents composés minéraux peu cohésifs et/ou expansifs tel que le gypse $(CaSO_4.2H_2O)$ et l'ettringite ($3CaO, Al_2O_3, 3CaSO_4, 32\ H_2O$) majoritairement (Tazaki et al., 1992, Sand and Bock, 1984, Davis et al., 1998, Islander et al., 1991). Ces transformations sont décrites par les équations suivantes :

Eq 31 : $Ca(OH)_2\,(portlandite) + H_2SO_4 \rightarrow CaSO_4.2H_2O\,(gypse)$

Eq 32 : $CaO.SiO_2.2H_2O + H_2SO_4 \rightarrow CaSO_4\,(gypse) + Si(OH)_4 + H_2O$

Eq 33 : $3CaO.Al_2O_3. + 3CaSO_4.2H_2O + 26H_2O \rightarrow 3CaO.Al_2O_3.3CaSO_4.32H_2O$

De manière surprenante, Schmidt (Schmidt et al., 1997) a rapporté que même si les bétons possédaient une certaine résistance à l'acide sulfurique, cela n'impliquait pas toujours une résistance équivalente face à ce que l'on peut appeler l'acide sulfurique « biogénique » (Sand and Bock, 1991) (Ehrich et al., 1999). Les raisons de ces différences d'action impliquant des degrés variables de détérioration restent encore à déterminer (rôle et impact de la biologie dans toute sa diversité (bacteries sulfo-oxydantes, bactéries hétérotrophes, champignons), interactions biologie/matériaux, événements hydrauliques, etc.).

Dans cette dynamique, la calcite formée lors de la carbonatation induite par la dissolution du dioxyde de carbone réagit également avec l'acide sulfurique produit dans les étapes ultérieures (2) et (3) de la succession microbienne (figure 9). L'attaque par l'acide sulfurique de la calcite superficielle néoformée suite à la carbonatation est régie par l'équation suivante :

Eq 34 : $CaCO_3\,(calcite) + H_2SO_4 + H_2O \rightarrow CaSO_4.2H_2O\,(gypse) + CO_2$

Pour représenter une attaque d'acide biogénique l'acide sulfurique est souvent employé en tant qu'acide modèle, car son utilisation apporte au milieu aussi bien une forte acidité que des sulfates.

La mise en contact d'acide sulfurique et du béton entraîne la dissolution de certains composés constituants le matériau, ainsi que la formation de produits issus de cette détérioration. Dans le cas de la réaction de l'acide sulfurique sur les bétons, la formation de gypse ($CaSO_4, 2H_2O$) (Eq 31, Eq 32 et Eq 34) est communément admise (Tazaki et al., 1992) (Davis et al., 1998), et même observée en réseau d'assainissement (Sand and Bock, 1984) (Davis et al., 1998) (Monteny et al., 2000) (Okabe et al., 2007). Pourtant, la formation d'un tel composé et son impact sur le revêtement cimentaire est encore discuté (Tian and Cohen, 2000). De plus, l'étude de la formation d'ettringite ($3CaO, Al_2O_3, 3CaSO_4, 32\ H_2O$) (Eq 32) demande encore un approfondissement. En particulier, la question de la stabilité d'un tel composé dans les conditions étudiées et de son rôle dans les détériorations observées est régulièrement posée (Israel et al., 1997) (Davis et al., 1998) (Aviam et al., 2004).

1.4.2.2. Impact d'un milieu acide complexe sur les matériaux cimentaires

Un acide est identifié par sa capacité à céder un ou plusieurs protons lorsqu'il est mis en solution. C'est un composé que l'on peut schématiquement dissocier en ions H^+ et en un contre ion particulier (Exemple H^+ et NO_3^- pour l'acide nitrique HNO_3, ou H^+ et CH_3COO^- pour l'acide acétique, ou encore $2H^+$ et SO_4^{2-} pour l'acide sulfurique). Les différents composés basiques constituant les bétons, donnant ses propriétés alcalines à la surface du matériau, conduisent généralement, dans une première approche de la détérioration, à la simple explication d'une réaction acido-basique entre les protons en solution et les composés basiques constituant le matériau. En conséquence, plus l'acide est fort, plus le pH des solutions mises en contact avec les matériaux est bas, et plus les détériorations observées devraient être importantes. Pourtant, ce résultat n'est pas systématiquement observé. En effet, un acide faible tel que l'acide acétique peut être plus agressif vis-à-vis des bétons que certains acides forts (Zivica and Bajza, 2002) (Larreur-Cayol et al., 2012). La différence de solubilité des sels de calcium formés explique les résultats obtenus lors de ces études (solubilité de l'acétate de calcium 374 $g.kg^{-1}$, pour 2,4 $g.kg^{-1}$ pour le sulfate de calcium) (Allahverdi and Skvara, 2000b) :

Dissolution de l'acétate de calcium :

Eq 35 : $Ca(CH_3COO)_2 = Ca^{2+} + 2CH_3COO^- \ avec \ Ks_4 = 2.65$

Dissolution du sulfate de calcium (Lide, Handbook of Chemistry 2002)

Eq 36 : $CaSO_4.(nH_2O) = Ca^{2+} + SO_4^{2-} + nH_2O \quad avec \ Ks_5 = 3.14 \, x \, 10^{-5} \ (gypse)$

Il en va de même avec les différents composés formant ce qu'il est commun d'appeler les hydrogels, substances constitués de différents oxydes, qu'ils soient de silicium, d'aluminium ou de fer (Allahverdi and Skvara, 2000b). Donc pour caractériser l'agressivité d'une solution acide vis-à-vis des bétons, la concentration réelle en acide a plus de sens que la simple valeur du pH en surface (Revertegat et al., 1992) et ce afin de pouvoir expliquer, par les composés formés et leur propriétés physico-chimiques (solubilités, volume molaires), les dissolutions observées ainsi que les phénomènes locaux de gonflement et de fissuration.

En même temps, l'implication dans le phénomène de détérioration des matériaux cimentaires de différentes réactions chimiques, contrôlées à l'interface par des échanges

entres différentes phases, rend compte de l'importance de la dynamique des processus et donc des phénomènes de transferts contrôlés par les équilibres chimiques.

1.4.2.3. Rôle des sulfates et des précipitations secondaires

a. A l'extérieur des matrices cimentaire

Il est donc important de noter que dans un milieu statique, l'attaque par l'acide sulfurique, malgré une forte agressivité due au pH de la solution, entraînerait, à cause de la faible solubilité des composés formés, de moindres détériorations que dans d'autres cas. En effet, dans un environnement statique, la faible solubilité des sels de calcium formés conduit, en surface du béton, à la constitution d'une sur-couche de produits issus de la détérioration (Monteny et al., 2000). A terme cette couche peut agir comme une couche de protection (figure 12), en particulier en limitant la diffusion des composés agressifs vers le front de détérioration tout en maintenant d'un autre coté les produits formés lors des premiers temps de la détérioration (Allahverdi and Skvara, 2005) (Allahverdi and Skvara, 2006). En statique la profondeur de la couche détériorée est supérieure pour une exposition à un environnement d'acide sulfurique à pH 2 (figure 12.B), comparativement au même matériau exposé à de l'acide sulfurique à pH 1 (figure 12.A), et ce par la formation à pH 1 de cristaux de gypse au niveau du réseau de fissures, réduisant la porosité, et donc la diffusion de l'acide au sein de la matrice cimentaire.

Zone corrodée, forte fissuration

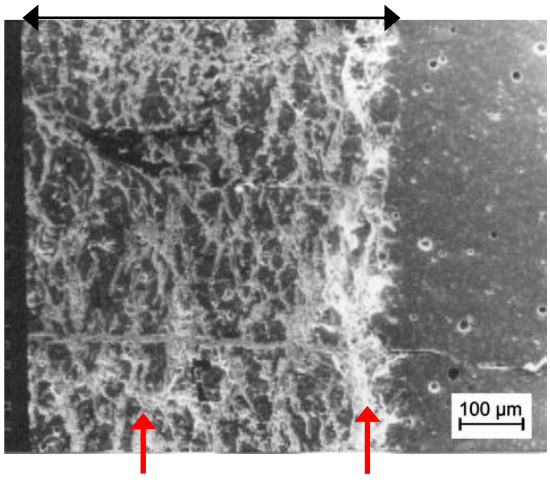

A)

Gypse précipité au sein du réseau de fissuration

Zone corrodée, forte fissuration

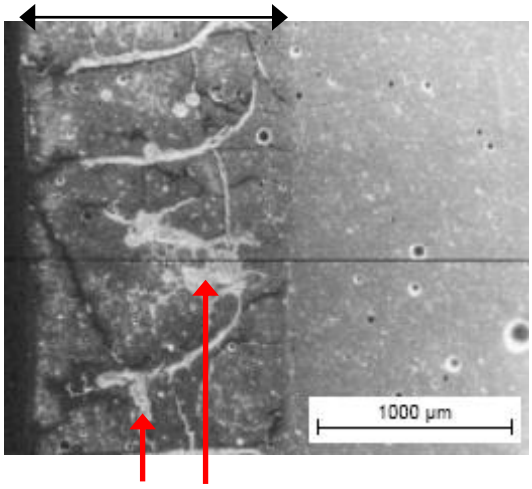

B)

Gypse précipité au sein du réseau de fissuration

Figure 12 : Observation de la couche détériorée d'un échantillon de ciment après une exposition de 60 jours à de l'acide sulfurique à pH 1 (A) (Allahverdi and Skvara, 2005) , à pH 2 (B) (Allahverdi and Skvara, 2006). En milieu statique la profondeur détériorée est supérieure à pH = 2 par rapport à pH = 1.

Dans un environnement statique chimique il y a donc établissement d'un équilibre qui limite la détérioration des matériaux (Allahverdi and Skvara, 2000a). La formation d'une importante couche de gypse est observée en réseau d'assainissement, comme le montre la figure 13 où des coupons (d'une épaisseur initiale de 8 mm) positionnées dans la phase aérienne d'un regard de visite révèlent après 1 an d'exposition à une atmosphère en H_2S entre 20 et 30 ppm, une épaisseur de gypse d'environ 10 mm (figure 13.A), pour un coupon sain réduit à 4 mm d'épaisseur (figure 13.B) (Okabe et al., 2007). Ainsi la zone externe détériorée, de par la formation de gypse aurait subi un gonflement entrainant une augmentation de volume de 2,5 fois.

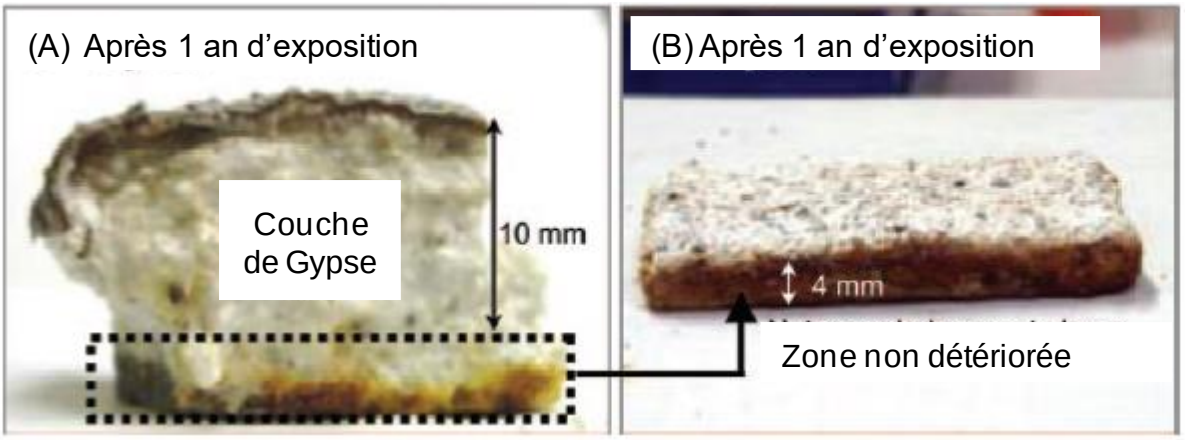

Figure 13 : Observation de la formation d'une couche de gypse en surface d'un coupon positionné dans la phase aérienne d'un regard de visité après 1 an d'exposition à des concentrations en H_2S en phase gaz entre 20 – 30 ppm (A). La photo (B) correspond à la zone non corrodée après lessivage de la surcouche de gypse formée présentée à la photo (A) – les coupons neufs ayant une épaisseur de 8 mm (Okabe et al., 2007).

Si dans le cas de l'acide sulfurique, pour certains auteurs (Grube and Rechenberg, 1989) (Pavlik, 1994), en conditions statiques, l'attaque du béton conduit à la formation d'une couche protectrice limitant la détérioration des matériaux, d'autres auteurs (Tazaki et al., 1992) (Torii and Kawamura, 1994) (Israel et al., 1997) (Roberts et al., 2002) rapportent que la formation de gypse ($CaSO_4$, $2H_2O$) étant expansive, elle ne protège en rien les matériaux mais tend plutôt, par des processus physiques, à l'éclatement des surfaces et donc à l'exposition toujours renouvelée d'une matrice intacte. Cette propriété expansive du gypse est cependant toujours discutée actuellement (Tian and Cohen, 2000). En effet, le tableau suivant (tableau 7, adapté de Chabrelie, 2010), présente pour certaines phases caractérisitiques des pâtes cimentaires, certaines propiétés thermodynamiques telles que les constantes de solubilité, les energies de formation de Gibbs ($\Delta_r G°$) et le volume molaire, comparé aux mêmes propriétés concernant le gypse et l'ettringite.

Tableau 7 : propriétés thermodynamique à 25°C de certaines phases classique rencontrées au sein de pates cimentaires. Les phases en gras étant formées secondairement dans des environnements sulfatiques (d'après Chabrelie, 2010).

Phases	**Constante de solubilité** *- log Ks*	**Energie de formation de Gibbs** $\Delta rG°$ (kJ.mol^{-1})	**Volume molaire** (cm^3.mol^{-1})
Portlandite : $Ca(OH)_2$	- 5,2	- 897,01	33
C_3A : $3CaO.Al_2O_3$	_	- 3382,3	89
Jennite : $(CaO)_{1,67}.SiO_2.(H_2O)_{2,1}$	13,2	- 2480,81	78
Tobermorite : $(CaO)_{0,83}.SiO_2.(H_2O)_{1,3}$	8	- 1744,36	59
Gyspe : $CaSO_4.2H_2O$	4,6	- 1797,76	75
Ettringite : $3CaO.Al_2O_3.3CaSO_4.32H_2O$	44,9	- 15205,94	707

Ainsi, pour d'autres auteurs la réaction de l'acide sulfurique sur les bétons forme en surface une couche de produits issus de la détérioration qui avec le temps pénètre à l'intérieur des bétons, augmentant la dégradation due à l'importante différence de volume molaire (tableau 7) entre les ciments constituants les bétons et les produits issus de la réaction de l'acide sulfurique sur ce type de matériau (Atkins et al., 1992) (Mori et al., 1992). Essentiellement pour ces auteurs, ce nouveau matériau n'a aucune force structurelle (gypse + hydrogels), et peut être arraché par l'augmentation des contraintes mécaniques (phénomènes hydrodynamiques, lessivage des parois).

Dans le cas des réseaux d'assainissement, et donc de la présence de bactéries participant activement à la détérioration des bétons, la formation de gypse change la nature du microenvironnement que rencontre les microorganismes sulfo-oxydants (Roberts et al., 2002). Il retient l'eau et réduit ainsi les effets des périodes de temps sec sur les organismes se développant aussi bien dans la sur-couche issue de la détérioration, qu'à la surface des bétons. Il se comporte également comme une barrière, ralentissant le transport chimique entre la surface et le ciment interne, conduisant à l'hypothèse que la détérioration par de l'acide sulfurique « biogénique » est d'abord un phénomène de surface lié en profondeur à la migration de l'acide, des sulfates (Islander et al., 1991) (Davis et al., 1998). Ce phénomène de propagation peut expliquer l'augmentation des taux de détérioration observés en présence d'un lessivage régulier des parois (cas de la zone de marnage en réseaux d'assainissement (Mori et al., 1992) et dans le cas de la mise en œuvre de certains tests de résistance des matériaux cimentaires (Vincke et al., 1999) (De Belie et al., 2002) (Aviam et al., 2004)).

b. A l'intérieur de la matrice cimentaire

Outre la dissolution des composés par l'abaissement du pH en surface, une autre réaction contribue plus profondément à la détérioration des matériaux. Une réaction qui a lieu par la suite entre les cristaux de gypse nouvellement formés et les aluminates de calcium contenus dans la matrice cimentaire des bétons. Cette réaction conduit à la production d'ettringite ($3CaO.Al_2O_3.3CaSO_4.32H_2O$) (Eq 33), qui participe à la dégradation des ciments en augmentant la pression interne des matériaux, entraînant des éclatements locaux (Aviam et al., 2004), augmentant ainsi la porosité du revêtement et donc exposant une plus large surface de béton au processus de détérioration, tout en accélérant les phénomènes de pénétration de l'acide sulfurique et des microorganismes (Davis et al., 1998). En même temps, ce sel complexe peut être décomposé par des acides carboxyliques et des acides organiques produits par les bactéries, fragilisant d'autant plus la structure des ciments (Monteny et al., 2000).

Cette description générale indique que les mécanismes de dégradation des revêtements cimentaires, comme le montrent les équations (Eq 31, Eq 32et Eq 33), sont dépendants de la composition initiale des matériaux et de leur évolution. Par exemple la composition en portlandite aura une influence sur les phénomènes de dissolution, mais également sur la proportion de gypse formé. D'un autre coté la présence de composé alumineux aura une influence ultérieure sur la possible formation d'ettringite secondaire et donc sur des phénomènes de fissuration et d'accélération des processus de dégradation. Ainsi, un revêtement cimentaire formé à partir d'une pate de ciment CEM III, de part sa faible teneur en portlandite devrait proposer une bonne résistance générale face aux attaques acides. En revanche l'ajout de laitier de haut-fourneaux (augmentation de la teneur en aluminium au sein du matériau), pourrait favoriser la formation à l'intérieur de la matrice de précipités secondaires expansifs tel que l'ettringite entrainant la fragilisation du matériau et contrebalançant potentiellement la dissolution limitée.

1.4.2.4. Cas particuliers des ciments alumineux

Les ciments alumineux sont basés sur un système chimique très différent des pâtes cimentaires à base de ciment portland, où la portlandite et les silicates de calcium hydratés assurent majoritairement l'alcalinité du matériau (Herisson, 2012). Dans le cas des ciments alumineux, l'alcalinité du matériau est assurée par différents aluminates hydratés

($CaO.Al_2O_3.10H_2O$, $(CaO)_2.Al_2O_3.8H_2O$, $(CaO)_3.Al_2O_3.6H_2O$, $Al_2O_3.3H_2O$). Une attaque acide sur ce type de matériaux va entrainer la dissolution de ces hydrates, avec une lixiviation d'ion Ca^{2+} et la néoformation de précipité de type $Al(OH)_3$ (hydroxyde d'aluminium) décrit par les équations suivantes (Eq 37, Eq 38 et Eq 39) (Herisson, 2012) :

Eq 37 : $CaO.Al_2O_3.10H_2O + 2H^+ \rightarrow Ca^{2+} + 2Al(OH)_3(s) + 8H_2O$

Eq 38 : $(CaO)_2.Al_2O_3.8H_2O + 4H^+ \rightarrow 2Ca^{2+} + 2Al(OH)_3(s) + 7H_2O$

Eq 39 : $(CaO)_3.Al_2O_3.6H_2O + 6H^+ \rightarrow 3Ca^{2+} + 2Al(OH)_3(s) + 6H_2O$

Les ciments alumineux sont réputés durables en milieux agressifs et notamment en milieux acides (Bertron, 2004). En 1994, des tests réalisés sur différents types de mortiers, sous contraintes chimiques (H_2SO_4) et en chambre de simulation de biodétérioration (Ehrich et al., 1999) ont montré une meilleure tenue des mortiers à base de ciments alumineux, aussi bien sur la perte de poids des échantillons en fin de test, que sur l'évolution du pH de surface au cours des tests. En 1998, Lemaitre (Lemaître et al., 1998), en vu d'augmenter la durée de vies des ouvrages en béton exposés à l'acidité de certains milieux industriels, préconisait l'utilisation de ciments alumineux, pour l'unique raison qu'ils ne libèrent pas de chaux lors de leur hydratation.

Selon Scrivener (Scrivener et al., 1999), la bonne tenue des ciments alumineux face à des solutions acides est principalement due aux propriétés physico-chimiques de ses hydrates, et particulièrement à la formation d'hydroxyde d'aluminium $Al(OH)_3$, faiblement cristallisé dans les pâtes hydratées de ces ciments, et stable jusqu'à un pH de 3 ou 4 (Bertron, 2004) (Herisson, 2012).

Scrivener (Scrivener et al., 1999) toujours, suggère que la présence de cette phase dans les produits d'hydratation initiaux et sa néoformation dans les pores de la matrice, liée à la dissolution du calcium dans les autres phases, permet d'obtenir des cinétiques de dégradations plus faibles qu'une pâte de ciment Portland ordinaire. De plus, ces auteurs mettent également en avant une capacité de neutralisation d'acidité plus importante de la pâte de ciment alumineux par rapport à une pâte de ciment portland (60 % plus élevée pour la pâte de ciment alumineux) (Scrivener, 2009). La figure 14 illustre les capacités de neutralisation différentes concernant les ciments portland (CEM I) et les ciments CAC dues en particulier à la formation durant l'attaque d'un gel d'$Al(OH)_3$.

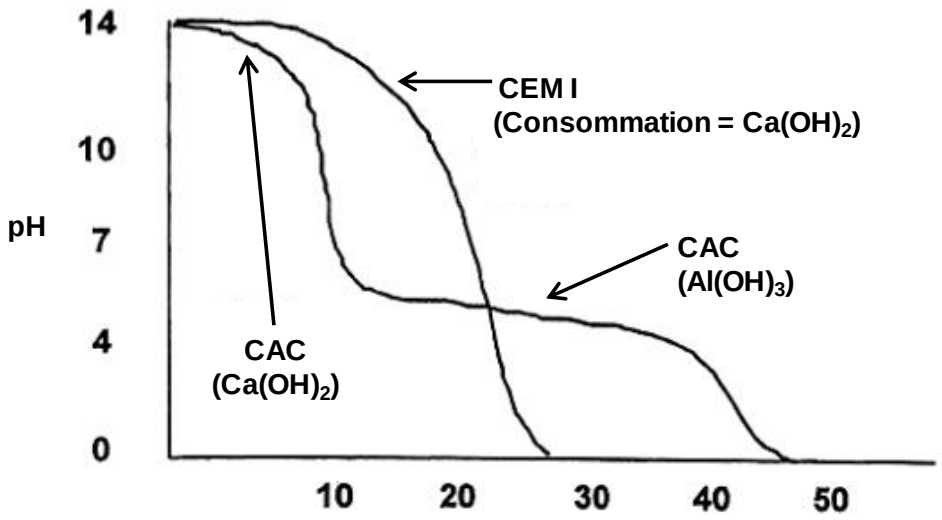

Figure 14 : Capacité de neutralisation des acides par des matériaux cimentaires. Exemple d'un ciment portland (CEM I) et d'un ciment alumineux (CAC) (tirée de Lamberet, 2008, adaptée de Letourneux et Scrivener 1999).

Berndt, en 2011, pour une étude réalisée sur la protection des bétons contre les bactéries sulfo-oxydantes, au niveau de tour de refroidissement, a testé différents types de mortiers, dont certains à base de ciment alumineux (Berndt, 2011). Les tests réalisés en milieu réel (bassin de tour de refroidissement), et en laboratoire sur des cellules Atlas (ASTM C 868 C) ensemencées par des populations de *Thiobacillus ferrooxidans*, confirment la meilleure résistance, pour les attaques acides biologiques, des mortiers à base de ciments alumineux (dans ce cas un mortier constitué de ciment alumineux et d'agrégats d'aluminate de calcium (Alag®) produit par la société Lafarge : SewperCoat®).

Alexander et Fourie, également en 2011, ont réalisé des séries de tests sur différents types de ciments OPC (Ordinary Portland Cement = CEM I) et CAC (Calcium Aluminate Cement), chacun associé, soit à des agrégats solubles en milieu acide, soit à des agrégats insolubles dans les mêmes conditions (Alexander and Fourie, 2011). Ces tests ont été menés soit à partir de solutions acides (HCl ; pH 1), soit par l'installation des échantillons au niveau d'une zone d'un réseau d'assainissement particulièrement sensible à la biodégradation. Les résultats obtenus montrent :

- En solution HCl, les bétons à base de CAC avec des agrégats dolomite ne sont pas plus performants que les bétons préparés dans les mêmes conditions à partir de CEM I. Par contre, en utilisant des agrégats synthétiques type alag (TM), les mortiers

à base de ciments alumineux montrent de très bonnes performances, dues en particulier à la formation d'une microstructure homogène.

- En condition d'assainissement, les performances des CAC sont bien meilleures que les CEM I, car d'autres mécanismes interviennent.

Pour les auteurs (Alexander and Fourie, 2011), cette performance en milieu biologique est à relier avec la capacité des CAC d'influer sur le métabolisme des micro-organismes impliqués dans la biodétérioration, limitant ainsi la génération d'acide sulfurique biogénique. Hypothèse également soutenue par Saucier et Lamberet en 2009, qui supposent un effet « bactériostatique » de l'ion Al^{3+} libéré par la dissolution, ralentissant la croissance bactérienne, et limitant ainsi la production d'acide sulfurique biogénique (Saucier and Lamberet, 2009).

Erich et al en 1999, après une comparaison entre des tests chimiques et des tests biologiques en chambre de simulation (type Hambourg, voir paragraphes suivant pour plus de détail sur les différentes installations expérimentales développées pour étudier la biodétérioration des matrices cimentaires en réseau d'assainissement), avancent également cette hypothèse (Ehrich et al., 1999). Pour plusieurs types de ciments testés, les résultats différents en termes de perte de poids des échantillons entre les tests chimiques, et les tests biologiques, pour le seul CAC, leur fait conclure à un effet de l'aluminium sur les populations bactériennes mise en jeu (*Thiobacillus thiooxidans, T. intermedius, T. novellus, et T. neapolitanus*).

Pour autant, aux vues de la sensibilité des populations impliquées vis-à-vis du pH du milieu (Bielefeldt et al., 2010), la neutralisation (apport de base) plus importante des CAC par rapport aux autres types de ciments, pourrait à elle seule expliquer dans ces conditions la diminution de la production d'acide biogénique, et ce par un impact direct sur les conditions de croissance. Les résultats de Erich et al, en terme de comptages cellulaires après tests, s'ils confirment une limitation de la croissance, ne permettent pourtant pas d'affirmer l'une ou l'autre hypothèse (Ehrich et al., 1999).

Ainsi, les ciments alumineux apparaissent comme plus performants en termes de durée de vie face à des environnements agressifs (type acide biogénique). Cette résistance accrue est due *a priori* à la composition propre des hydrates formés et principalement à la formation, durant l'attaque acide, de l'hydroxyde d'aluminium ($Al(OH)_3$), qui apporte au matériau

attaqué une capacité de neutralisation d'acide plus importante, ainsi qu'un effet de barrière physique limitant la pénétration des composés agressifs (acides et sulfates) au sein du matériau. Le choix des agrégats apparaît également important, pouvant modifier les performances des ciments en jouant sur leur microstructure et la tenue de celle-ci au cours du temps, ainsi que l'apport d'un pouvoir tampon accru par ajout de granulats réactifs (Alexander and Fourie, 2011). Pour autant certaines études avancent également l'idée d'un effet direct d'inhibition des ciments alumineux sur l'activité biologique (Ehrich et al., 1999) (Saucier and Lamberet, 2009) (Alexander and Fourie, 2011).

1.4.3. Influence de l'aluminium sur les populations microbiennes impliquées dans la biodétérioration des matrices cimentaires en réseau d'assainissement.

L'aluminium n'a pas de rôle métabolique connu au sein des organismes vivants, par contre de nombreuses études rapportent ses effets toxiques sur des bactéries, des plantes et les hommes (Macdonald and Martin, 1988).

Les métaux peuvent inhiber l'activité microbienne à travers différents mécanismes (Dopson et al., 2003), incluant :

- La modification de conformation des enzymes
- Le blocage des sites de transport
- La perte d'intégrité de la membrane

1.4.3.1. Influence de l'ion Al^{3+} sur les populations microbiennes impliquées dans la biodétérioration des matrices cimentaires.

En terme de référence, il existe très peu de données quantitatives sur la concentration en ions aluminium (Al^{3+}) observable au niveau du condensat d'une zone détériorée de réseau d'assainissement. Jean Hérisson, durant des expériences réalisées sur site sur des cylindres de différents mortiers, munis d'un manche plastique creux recueillant l'eau condensée, a mesuré une concentration en aluminium pouvant atteindre en stagnation 3,363 gAl/l, mesure réalisée après 375 jours d'exposition d'un mortier à base de ciment alumineux (Herisson, 2012). De plus, Jean Hérisson, sur les mêmes échantillons d'eau condensée a réalisé des mesures

d'ATPmétries afin d'évaluer l'activité biologique. La figure suivante issue de la thèse de Jean Hérisson (figure 15), après 375 jours d'expositions, montre sur sites réels une estimation de l'impact de la concentration en aluminium dans le condensat sur l'activité biologique, où une valeur seuil de 350 mgAl/l a été identifiée.

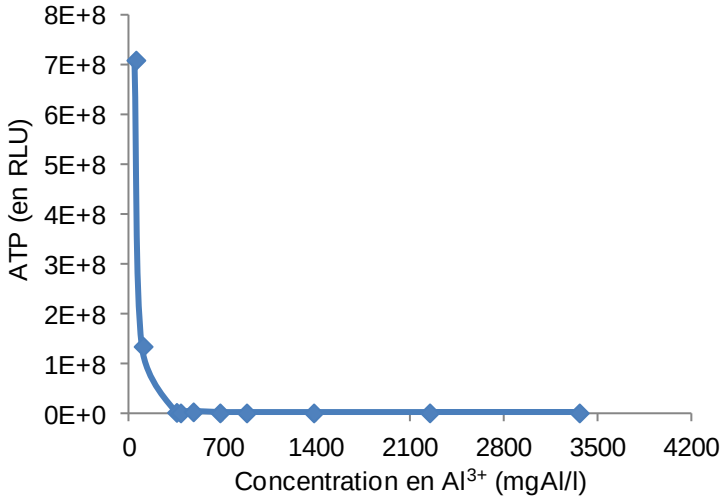

Figure 15 : mesure d'ATP totale en fonction de la concentration en aluminium total mesurée au niveau de manche creux recueillant l'eau condensée associée à des échantillons de différents mortiers disposés sur des sites réels exposés à des biodégradations avérées (Herisson, 2012)

Face aux peu de données exploitables dans la littérature, et même si ces valeurs peuvent être discutées de part leur caractère unique et de possibles pollutions survenues, elles permettent de confronter à des données terrains les résultats de la littérature présentés dans le tableau suivant en terme d'effet sur l'activité de populations bactériennes en présence de différentes concentrations en ion aluminium (tableau 8).

Tableau 8 : revue bibliographique des effets de l'ion aluminium (Al^{3+}) sur l'activité de différentes espèces bactériennes.

Espèces microbiennes	Concentrations en aluminium testées	Effet sur l'activité microbienne	Références
Esherichia colie	~ 0,03 g/l	Inhibition	Guida et al., 1991
Halothiobacillus neapolitnanus	> 0,250 g/l	Inhibition	Ehrich, 1998
Starkeylla novella	> 0,075 g/l	Inhibition	-
Thiomonas intermedia	> 0,050 g/l	Inhibition	-
Acidithiobacillus thiooxidans	> 0,750 g/l	Inhibition	-
-	2,7 – 10,8 g/l	Effet retard de quelques heures sur la croissance	Fisher et al., 2002
Acidiphilum cryptum	2,7 – 10,8 g/l	Effet retard de quelques heures sur la croissance	-
Acidiphilum acidophilum	2,7 – 10,8 g/l	Limitation de la croissance	-
Acidobacterium capsulatum	2,7 – 10,8 g/l	Limitation de la croissance	-
Thiobacillus ferrooxidans	> 6 g/l	Inhibition	Zajic, 1969
-	> 10 g/l	Inhibition	Tuovinen et al., 1971
-	> 2,5 g/l	Inhibition	Malik et al., 2004
-	2,3 g/l	Faible limitation de la cinétique (~ 14 %)	Blight et Raplh, 2008
Acidophiles	2,7 – 5,4 g/l	Limitation de la croissance	Kawai et al., 2000
Consortium microbien en réseaux d'assainissement	> 0,350 g/l	Inhibition	Herisson, 2012

Mise à part les résultats obtenus par Ehrich en 1998 et Jean Herisson en 2012, les concentrations d'expériences pour lesquelles des effets quantifiables ont été relevés, sont extrêmement importantes, bien supérieures (tableau 8), ou dans la gamme supérieure des concentrations observées sur site réel par Jean Hérisson. Il apparait donc difficile de conclure sur un effet marqué de l'ion Al^{3+} sur l'activité bactérienne impliquée dans la détérioration des matrices cimentaires en réseau d'assainissement.

Si une revue bibliographique ne permet pas de conclure sur les effets de l'aluminium en phase soluble auprès de cultures libres, il est pourtant important de ne pas conclure hâtivement sur un faible impact de l'aluminium soluble sur les populations réellement impliquées dans la biodétérioration des matrices cimentaires en réseaux cimentaires. En effet, en réalité il s'agit de consortium complexe ou l'interconnexion des métabolismes est encore très mal connue. De plus, une structuration du consortium microbien sous la forme de biofilm et/ou de colonies microbiennes en contact avec le matériau pourrait être déstabilisé par un

composé connu pour son affinité avec les composés organiques ($AlCl_3$ étant utilisé industriellement en tant que coagulant), tel que les exopolymères produits par les communautés microbiennes lors de leur structuration en agrégats biologiques. De la même manière, il est également possible que les composés alumineux solides aient des propriétés influençant, soit l'implantation, soit l'activité microbienne.

1.4.3.2. Influence de l'Aluminium sous la forme solide sur les populations microbiennes impliquées dans la biodétérioration.

La présence d'aluminium dans les ciments peut ne pas se traduire uniquement, lors de la lixiviation, par un enrichissement du milieu en ions Al^{3+}. Ainsi, des composés alumineux sous forme solide peuvent influencer les populations microbiennes en présence. Cependant, cet aspect est quasi absent de la littérature.

En ne considérant que l'aluminium, Yoshida et al, en 1998, ont testé l'effet de 0,1 g de particules de métaux lourds (Al, Cd, Fe, Pb, Mo, Ni, Zn) sur 3 types de populations microbiennes (*Thiobacillus intermedius 13-1*, *Escherichia coli JM109*, *Agrobacterium radiobacter IFO12665b1*) (Yoshida et al., 1998). Les expériences ont été réalisées sur deux supports, un support solide (type boite de Pétri), et en milieu liquide (type Erlenmeyer agité avec milieu de culture). Pour *Thiobacillus intermedius 13-1*, les résultats ont montré que l'aluminium solide n'a pas d'effet sur la croissance, quand par contre le cadmium et le nickel inhibent totalement le démarrage de la croissance (expériences menées sur 42h). Pour autant ce travail porte sur un matériau métallique, et non sur les hydrates d'aluminium présent dans le ciment alumineux.

Ainsi, s'agissant de l'impact de l'hydroxyde d'aluminium ($Al(OH)_3$) Seidel et al. ont montré qu'un apport de 2 à 10% de ce composé dans le milieu de culture d'*A.thiooxidans* induisait une augmentation du temps de latence mais n'influençait pas la croissance de ces microorganismes (Herisson, 2012). Hérisson, en travaillant sur boite de pétri, à partir de quatre espèces de bactéries sulfo-oxydantes (*S.novella, T.intermedia, H.neapolitanus* et *A.thiooxidans*), avec ou sans ajout en surface de 0,25 g de $Al(OH)_3$ stérile saupoudré avant ensemencement, a montré à 5 jours un effet sur les trois premières espèces *S. novella, T. intermedia, H. neapolitanus* (correspondant à des bactéries intervenant dans la deuxième phase de la colonisation bactérienne décrite sur la figure 9 de ce chapitre). Concernant, la

dernière espèce, la plus acidophile, *A. thiooxidans*, aucun effet de l'hydroxyde d'aluminium sous forme solide n'a pu être observé.

1.4.3.3. Conclusions préliminaires sur l'effet de l'aluminium ou des composés alumineux sur les populations microbiennes impliquées dans la biodétérioration des matrices cimentaires en réseaux d'assainissement.

A l'heure actuelle, d'après les études réalisées et dans les conditions d'expériences observées, il n'est pas permis d'accréditer la thèse d'un rôle inhibiteur majeur des composés alumineux sur les populations impliquées dans la biodétérioration. Car même si certains effets ont pu être observés, les concentrations effectives sont trop disparates pour se prononcer. De plus, dans certains cas seuls des effets retards sont enregistrés, ces effets de quelques heures à l'échelle du processus de détérioration (plusieurs mois à plusieurs années) peuvent en réalité être négligés. Pour autant, les études ne portant pas sur des consortiums microbiens développés sur les surfaces concernés, il est également impossible d'affirmer que l'aluminium, même sous forme ionique n'a pas d'effet, non sur l'activité biologique, mais sur la structuration d'un consortium microbien défavorable (effet sur les champignons, effet sur des bactéries hétérotrophes, participant (i) à la consommation de composés organiques potentiellement toxiques lors de leur accumulation, (ii) à la formation d'agrégats biologiques permettant la définition de niches biologiques particulières.

Cependant, hors de toutes données sur ces aspects, la bonne tenue des ciments alumineux, relativement à des ciments ordinaires de type Portland (CEM I), apparaît principalement due à la formation d'hydroxyde d'aluminium ($Al(OH)_3$), moins soluble en milieu acide que la Portlandite ($K_{s\ Al(OH)3\ amorphe} = 10^{-31.2}$ and $K_{s\ Al(OH)3\ Gibbsite} = 10^{-33.791}$ (Minteq database)) et permettant également une meilleure neutralisation de l'acidité, ainsi qu'un effet protecteur en modifiant favorablement la porosité du matériau.

1.5. Description schématique de la biodétérioration des matrices cimentaires en réseau d'assainissement

Suite à la revue bibliographique présentée dans les précédents paragraphes, une description schématique des principaux phénomènes physico-chimiques et des principales réactions (chimiques et biologiques) intervenant dans la biodétérioration des matrices cimentaires en réseau d'assainissement est proposée à la figure 16. Les phénomènes de lessivage des parois par l'augmentation du débit au sein des canalisations sont considérés secondaires dans la description du phénomène, secondaire non en termes d'intensité, mais en termes d'apparition. Ils ne sont donc pas pris en compte, puisque sans la fragilisation première des matériaux cimentaires par les réactions chimiques et biologiques, l'augmentation des contraintes hydrodynamiques, à l'échelle du réseau, n'aurait que peut d'impact sur les revêtements.

Ainsi, après la recondensation à la paroi des canalisations d'une phase gaz enrichie en H_2S la biodétérioration des matériaux cimentaires en réseau d'assainissement peut être décrite par la conversion des composés soufrés réduits en acide et en sulfate via des réactions chimiques et biologiques. Cette production d'acide est assurée par la succession à la paroi des canalisations de bactéries sulfo-oxydantes. L'abaissement du pH, et donc la création d'un milieu favorable à la colonisation de différentes espèces de bactéries sulfo-oxydantes (X_{SOB}), peut être accentué par l'implantation concomitante de bactéries hétérotrophes et de champignons (M_h), assurant la production de dioxyde de carbone (CO_2) au contact de la paroi, via la consommation et la production de composés organiques. L'apport de dioxyde de carbone (CO_2), par voie biologique ou par voie abiotique (atmosphère des réseaux), va entrainer la carbonatation des matériaux cimentaires. Ainsi carbonatés, ceux-ci vont perdre en pouvoir alcalin, spécifiquement en surface, favorisant l'implantation de colonies microbiennes et fragilisant également les matériaux par rapport aux attaques acides ultérieures. La production d'acides organiques (AO) au contact des parois cimentaires, via des métabolismes fongiques et/ou des métabolismes bactériens peut soit accentuer la dissolution des matériaux calciques, soit déstabiliser ou protéger la matrice cimentaire par la précipitation de composés secondaires (effet favorables ou défavorables dépendant de la solubilité des produits formés ainsi que de leur volume molaire).

Une fois les populations sulfo-oxydantes implantées, la production d'acide et de sulfate au contact des matrices cimentaires va entrainer en premier lieu la dissolution en surface des composés calciques, ouvrant ainsi la porosité du matériau.

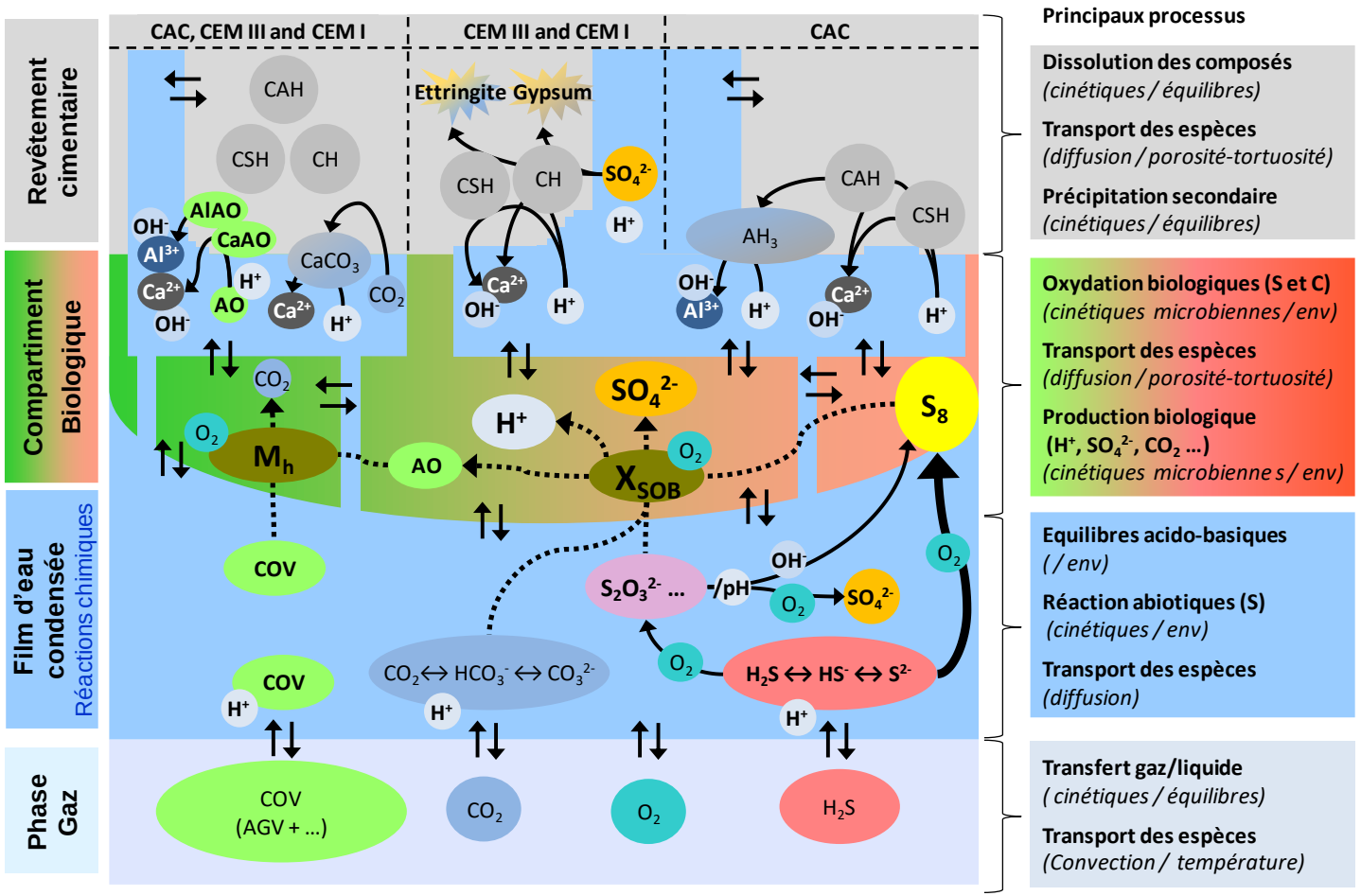

M_h : microorganismes hétérotrophes (bactéries et/ou champignons)

X_{SOB} : bactéries sulfo-oxydantes

AO : acides organiques issus de l'activité biologique (CaAO: sel de calcium associé)

Figure 16 : Schéma décrivant les principaux phénomènes physico-chimiques et les principales réactions chimiques en traits pleins ou biologiques pointillés) intervenant dans la biodétérioration des matrices cimentaires en réseau d'assainissement. Description se focalisant sur le haut des canalisations touchées, dans le cas de trois types généraux de revêtements cimentaires (CEM I, CEM III et CAC).

Dans le cas de pâtes cimentaires à base de ciment portland, en fonction de sa composition (proportion de portlandite en particulier CH et en silicates de calcium hydratés (CSH), puis proportion d'aluminate de calcium CAH), la lixiviation en surface du calcium par acidification va entrainer la formation d'un gel de silice inerte mais peu cohésif à partir des CSH. Par la suite, par la diffusion des sulfates à l'intérieur de la matrice des composés secondaires peu cohésifs et/ou expansifs du type gypse et/ou ettringite vont précipiter, induisant une fragilisation du matériau par gonflement et création d'un important réseau de fissures. Ce phénomène de fissuration va également augmenter les vitesses de transport des composés au sein de la matrice cimentaire et donc accélérer la pénétration de l'acide et des sulfates accentuant ainsi dans le temps l'altération des matériaux.

Dans le cas des ciments alumineux, la formation d'hydroxyde d'aluminium (AH_3) pendant la dissolution des aluminates de calcium hydratés (CAH) va augmenter le pouvoir tampon du matériau, et ainsi augmenter la résistance chimique du revêtement aux attaques acides. De plus la formation de cet hydroxyde en surface, à la différence du gel de silice va réduire la porosité de surface du matériau et ainsi limiter la diffusion des composés agressifs tel que l'acide et les sulfates au sein de la matrice cimentaire, et donc limiter les phénomènes de fissuration induit par la formation de composés secondaires.

Ainsi à partir de cette description phénoménologique et du schéma complexe présenté à la figure 16, il est possible de proposer un schéma simplifié du système, celui-ci décrit uniquement par des blocs couplant processus de transport et réactions (figure 17 ci-dessous).

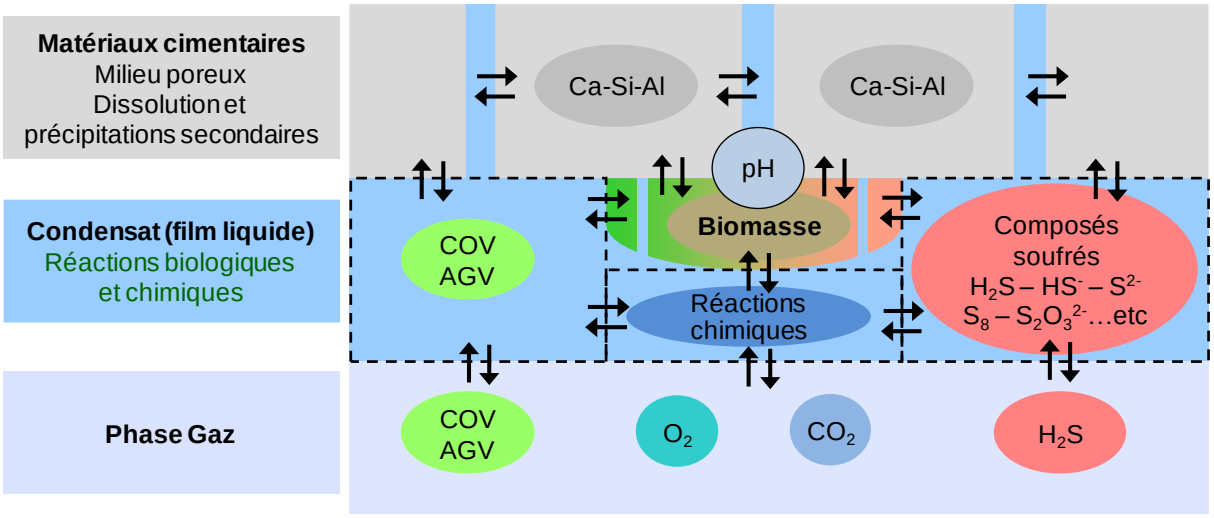

Figure 17 : Schéma simplifié décrivant à la paroi haute d'une canalisation le système de la biodétérioration des revêtements cimentaires en réseaux d'assainissement.

Ce schéma général (figure 17) va servir de base dans les chapitres suivants, afin de positionner chaque partie de l'étude dans le système général de la biodétérioration des matrices cimentaires en réseau d'assainissement. Une première étape va porter sur une simplification du système via une étude bibliographique plus approfondie et ce afin de proposer un système expérimental adapté aux différents objectifs de l'étude : (i) les objectifs scientifiques portants sur la définition d'un système permettant l'étude couplée des interactions activités microbiennes sulfo-oxydantes / revêtements cimentaires ; (ii) les objectifs industriels visant la proposition d'un protocole de test de résistance des revêtements cimentaires à la biodétérioration rencontrée en réseau d'assainissement.

Dans cet objectif, les paragraphes suivants, aux vues des descriptions phénoménologiques réalisées dans cette étude bibliographique, présentent les différents systèmes expérimentaux proposés dans la littérature pour l'étude de la biodétérioration des matrices cimentaires en réseau d'assainissement.

2. Systèmes expérimentaux pour l'étude de la biodétérioration des matrices cimentaires en réseau d'assainissement

De par l'impact des dégradations rencontrées, différentes voies ont été abordées afin de remédier à l'attaque des matériaux cimentaires par l'acide sulfurique « biogénique ». Dans cette optique, deux voies principales ont été identifiées : une voie curative liée à l'exploitation des réseaux, et une voie structurelle visant à adapter les matériaux utilisés en tant que revêtement des canalisations. La voie curative consiste lors de la collecte à minimiser la production d'H_2S par ajout de différents composés (H_2O_2, NO_3^-) (Zhang et al., 2008). La voie structurelle cherche à munir les canalisations de revêtements plus résistants à ce type d'attaques.

Dans ce cas, afin de valider les choix par l'expérience, le développement de tests a été nécessaire. Il existe à ce jour 3 grands types de tests : les tests chimiques, les tests in situ et les tests biologiques (Monteny et al., 2000). Les tests chimiques, malgré leur réponse potentiellement rapide ne sont pas toujours représentatifs de la réalité (Hormann et al., 1997) (Ehrich et al., 1999) (Herisson et al., 2012), alors que les tests menés in situ ont pour contraintes majeures, (i) le temps nécessaire à l'observation des phénomènes mis en jeu, (ii) l'asservissement des résultats obtenues aux conditions locales non-maitrisées.

Seul le test chimique est actuellement imposé par la norme européenne en vigueur [NF EN 598] qui concerne les « Tuyaux et raccords en fonte ductile et leurs assemblages pour l'assainissement ». Il s'étale sur une période de 6 mois et impose en termes de résistance des matériaux aux milieux agressifs un test à pH 3 pour les milieux acides et à pH 10 pour les milieux basiques.

Les conditions environementales permettent l'oxydation des composés soufrés réduits et participant à l'implantation d'une activité sulfo-oxydantes conduisant à la production d'acide sulfurique biogénique, créant les conditions particulières participant aux phénomènes de détérioration des matériaux cimentaires (Monteny et al., 2000). Ce rôle de la biologie est à considérer aussi avec l'aspect dynamique des phénomènes observés. Par ailleurs, comme vue précédemment, certaines conditions hydrauliques (rappels : variation des débits collectés, et donc de la hauteur d'eau au sein des canalisations, déplacement des équilibres chimiques par ruissellement le long de paroi ou par lessivage) rencontrées dans les réseaux d'assainissement participent également aux détériorations observées (Mori et al., 1992) (Vincke et al., 1999) (Aviam et al., 2004). Ce chapitre se propose donc de présenter uniquement les dispositif

expérimentaux développés au cours des dernières décennies et les études sur pilote relatives à la détérioration en présence d'une activité biologique.

Même si leurs mises en œuvre peuvent être extrêmement différentes, la base de tous ces tests ou pilotes est de reproduire les principaux phénomènes impliqués dans la bio-détérioration des matériaux cimentaires en les accélérant si possible. Les conditions opératoires, le type d'inoculum, le type de matériaux testés, le mode d'exposition des matériaux (statique ou dynamique), ainsi que la prise en compte ou non de l'influence de l'hydrodynamique sont les principaux facteurs permettant d'analyser la mise en œuvre de ces différentes études. Il est important de noter qu'actuellement, malgré l'identification des problèmes liés à la bio-détérioration des matériaux cimentaires, aucun test biologique n'est inclus dans la norme européenne régissant les infrastructures propres à l'assainissement.

2.1. Les différents tests biologiques

2.1.1. Chambre de simulation dite de Hamburg (Sand and Bock, 1984, Sand et al., 1987)

Principe de fonctionnement : Des échantillons de mortiers (Ciment alumineux CAC, ciment portland) (Ehrich et al., 1999) préparés à cet effet (cubes prédécoupés de dimensions connues) sont placés dans une chambre de simulation (figure 18) contenant en fond un volume d'eau de 10 cm de hauteur. La température de l'eau au sein de la chambre est maintenue constante (30°C) durant le test, alors que les parois sont maintenues à une température plus froide (2 – 3°C). L'air contenu dans la chambre de simulation, par effet du gradient de température, est alors chargée en humidité (98%) (Ehrich et al., 1999), ce qui permet au contact des échantillons de mortier la formation d'un milieu favorable à la croissance bactérienne. La chambre de simulation est par la suite ensemencée régulièrement durant 90 jours. L'inoculation est réalisée par la pulvérisation d'une solution de culture contenant 4 espèces de Thiobacilli (*Acidithiobacillus thiooxidans, T. intermedius, T. novellus,* et *T.neapolitanus).* Après inoculation, un mélange d'air et d'H_2S (1 à 10 ppm en continu) est injecté sous forme gaz, permettant ainsi aux bactéries inoculées de produire l'acide sulfurique par son oxydation. L'aspect dynamique du test biologique de détérioration est alors assuré par le maintien d'un flux d'apport régulier permis par la mise en mouvement de la phase gaz à l'intérieur de la chambre de test. La mesure du taux de détérioration est réalisée par la mesure d'une différence de masse pour chaque échantillon après brossage, et élimination de la zone

détériorée. La figure suivante (figure 18) présente le schéma de l'installation proposée par Sand et Bock en 1984 (A), et son adaptation par Ehrich et al. en 1999 (B). L'installation de coupelles, complétées d'une solution d'antibiotique et de pyruvate pour éviter toute croissance biologique, en dessous de chaque échantillon (adaptation réalisée par Ehrich et al. en 1999) a permis de récupérer l'eau ayant ruisselé sur la paroi des matériaux. Ainsi en fin d'expérience, le dosage des sulfates couplé au soufre total contenu dans les matériaux exposés et comparé au soufre total des matériaux initiaux a permis une analyse des flux de soufre transformés au contact du matériau et ainsi estimer la quantité totale d'acide produit au contact des matériaux (l'oxydation totale de l'H_2S (Eq 18)).

Les cultures des bacteries sulfo-oxydantes sont réalisées en parallèle, dans des réacteurs stériles. *T. intermedius, T. novellus,* et *T.neapolitanus* sont cultivés dans des milieux thiosulfates, *Acidithiobacillus thiooxidans* est cultivé dans un milieu soufre élémentaire.

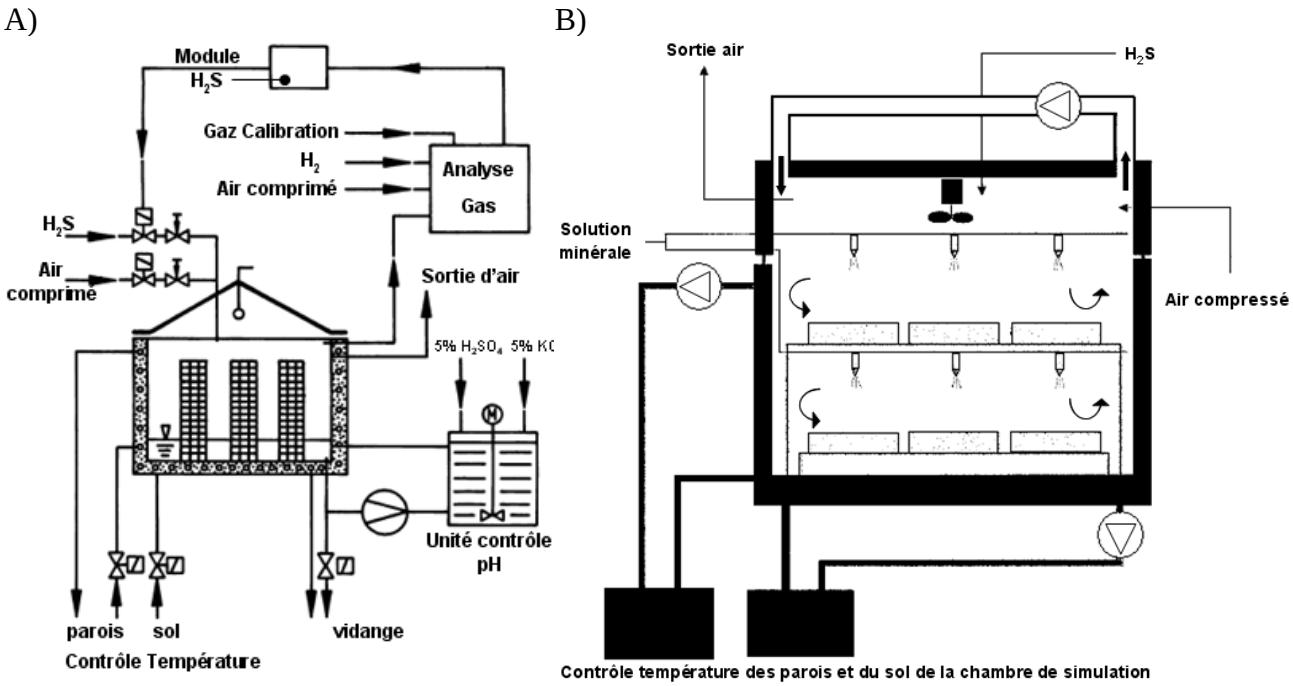

Figure 18: schéma de principe de la chambre de simulation développée par : Sand et Bock (a) (Sand et al., 1987) ; (b) adaptation (Ehrich et al., 1999)

Tests : l'expérience a montré que le taux de détérioration est à corréler avec le nombre de bactérie du type *A.thiooxidans* se développant sur les surfaces des échantillons (Sand and Bock, 1984). Entre 3 types de sources de soufre (sulfur d'hydrogène H_2S, thiosulfate $S_2O_3^{2-}$, methylmercaptan CH_3CS), l'apport par H_2S apparaît comme le plus favorable à l'intensification de la détérioration (Sand, 1987). Une détérioration est observée avec les thiosulfates quand aucune détérioration n'est observée avec le CH_3CS. Comparativement à

des observations réalisées sur le réseau d'assainissement de la ville de Hambourg, avec l'utilisation d'H_2S un taux de détérioration environ 8 fois supérieur a été observé par rapport au terrain. La perte de poids observée a été de 3,3% à 5,8 % en 270 jours (Sand and Bock,1984) (Sand, 1987) (Sand et al., 1987).

Dans le cas d'Ehrich (Ehrich et al., 1999), le test a durée 350 jours. Comparativement les ciments alumineux testés (perte de poids de 20 à 40%) ont montré une plus grande résistance que les ciments classiques de type portland (perte de poids de 100%). De la même manière que précédemment l'accélération des processus a été estimée à 3 fois celle observée par Sand (Sand et al., 1987), soit une accélération de 24 par rapport aux détériorations réelles observées sur le terrain.

Aujourd'hui, basé sur cette installation (Ehrich et al., 1999), l'IFSTTAR, à travers la thèse de Jean Hérisson, a optimisé le procédé, à travers une validation successive de différentes conditions opératoires clés dans le fonctionnement de la chambre de simulation dans le but d'assurer l'accélération et la reproductibilité de l'essai. L'étude étant encore en cours, aucun résultat d'essai n'a aujourd'hui été publié.

2.1.2. Chambre de simulation (Mori et al., 1992)

Principe de fonctionnement : dans une chambre de simulation (44cm x 30cm x 30 cm) (figure 19) des échantillons de mortier (d'une qualité non précisée) trempent dans différents milieux liquides (trois milieux testés : eau distillée – milieu synthétique sans thiosulfate – eaux usées). Une inoculation répétée des échantillons est réalisée à partir de souches pures de bactéries de l'espèce *A.thiooxidans*. L'apport en soufre est assuré par l'injection sous forme gaz d'H_2S après production de celui-ci dans un compartiment particulier par réaction de sulfure de sodium (Na_2S) avec de l'acide chlorhydrique (HCl). Le but de l'étude est d'analyser l'influence du milieu liquide sur la détérioration des matériaux cimentaires. Le test s'est déroulé sur une période de 6 mois. Le sulfure d'hydrogène en sortie de la chambre est alors récupéré par le barbotage de la phase gaz dans une solution d'acétate de zinc ($Zn(CH_3COO)_2$).

L'étude est réalisée par un suivi de l'épaisseur du béton au niveau de la zone eau/air, par une étude de surface par microscopie électronique, et un suivi de la biologie par comptage cellulaire.

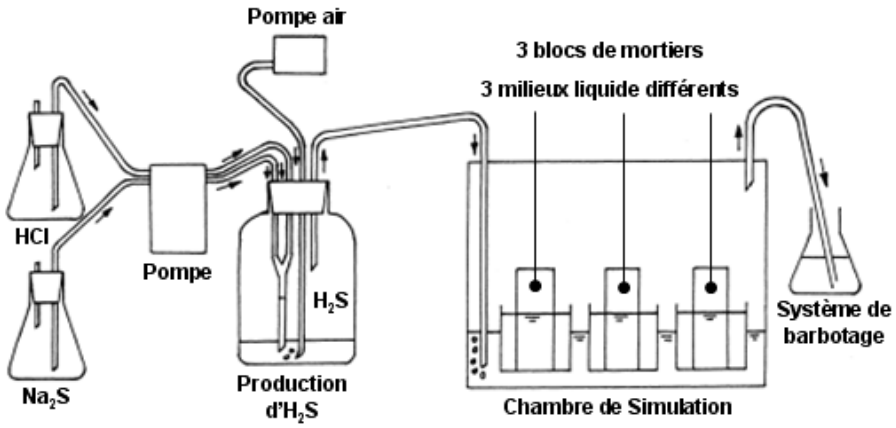

Figure 19 : schéma de principe de la chambre de simulation développée par Mori (Mori et al., 1992)

Tests : sur les trois milieux utilisés, le bloc de mortier trempant dans des eaux usées est celui dont la réduction d'épaisseur est la plus marquée. La perte de matière est plus faible pour le milieu synthétique alors qu'elle est nulle dans le cas de l'eau distillée, ce qui indique que la seule présence d'H_2S dans les mêmes conditions de concentration et d'ensemencement ne suffit pas à expliquer la détérioration des mortiers. La présence de nutriments contenus dans les eaux usées est indispensable à la croissance bactérienne et donc à l'observation des phénomènes de détérioration biologique. En parallèle, sur les échantillons dégradés, une forte détérioration est observée au niveau de la zone liquide/air. Ce qui correspond à la zone de marnage dans les canalisations d'assainissement. Ceci peut s'expliquer par le fait que les blocs de mortiers sont à température ambiante. Aucune condensation n'est alors observable dans la zone atmosphérique.

2.1.3. Pilote de démonstration : étude de la bio-détérioration (Mori et al., 1992)

Principe de fonctionnement : un pilote d'étude (figure 20), reproduit une canalisation d'assainissement. Un écoulement régulier d'eaux usées, auquel est mélangé une solution de Na_2S, permet l'apport de tous les composés assurant en réseau d'assainissement le développement de microorganismes sulfo-oxydants, et donc la détérioration en phase atmosphérique, en particulier au niveau de la zone liquide/air, des matériaux cimentaires. Des échantillons de mortier sont placés régulièrement le long de la canalisation de test. L'inoculation du milieu se fait à partir d'une culture pure de bactéries *A.thiooxidans*. Cette inoculation est réalisée toutes les deux semaines. La concentration en H_2S dans la phase gaz varie entre 25 et 300 ppm (volumique). La température ambiante varie entre 12 et 30 °C. Le

test a été réalisé durant six mois. Il a été validé par la mesure de l'épaisseur des échantillons de mortier avant et après l'étude, ainsi que par une étude de surface des échantillons effectuée par microscopie électronique. En parallèle un test dans lequel un débit identique d'eau distillée circule a été mis en place.

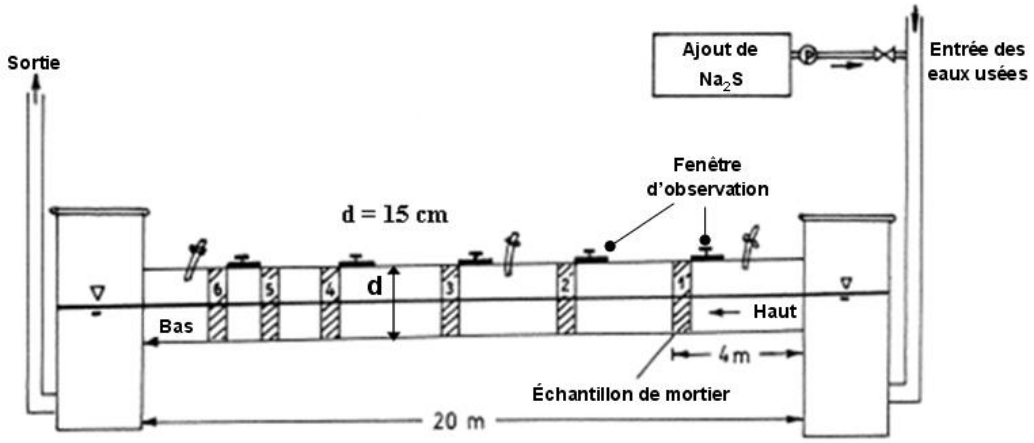

Figure 20 : schéma de principe d'un pilote d'étude développé par Mori (Mori et al., 1992)

Tests : aucune détérioration n'est observée dans le cas d'un écoulement d'eau distillée. Dans le cas d'un débit d'eaux usées, la détérioration des échantillons est vérifiée par une mesure de la perte de matière obtenue après 6 mois de test. Une analyse des produits issus de la détérioration montre la formation de gypse, produits observés dans les réseaux d'assainissement lors de la détérioration réelle des canalisations. Les détériorations sont principalement observées à l'interface liquide/air, ceci du au fait que la canalisation n'était pas thermostatée, ainsi le phénomène de condensation n'était pas focalisé au niveau du sommet de la canalisation. Ainsi, le taux de détérioration diminue progressivement en montant dans la partie atmosphérique de la canalisation. Tout comme dans les canalisations d'assainissement aucune détérioration n'est observée dans la partie immergée.

2.1.4. Chambre de simulation Heidelberger Zement (Schmidt et al., 1997)

Principe de fonctionnement : des blocs de mortier prédécoupés sont placés dans une chambre de tests étanches (figure 21). La culture du milieu bactérien (souche pure de *A.Thiooxidans*) est réalisée à part dans un compartiment dédié. Les conditions de culture sont maîtrisées. L'apport en soufre est effectué dans ce compartiment sous la forme de soufre élémentaire. La mise en contact du milieu agressif ainsi préparé et des échantillons tests se

fait par la mise en charge de la chambre test avec le milieu de culture (5 min toutes les heures). Cette étape de mise en charge peut être assimilée à une montée des eaux dans les canalisations, et à un lessivage des parois lors de la vidange du compartiment.

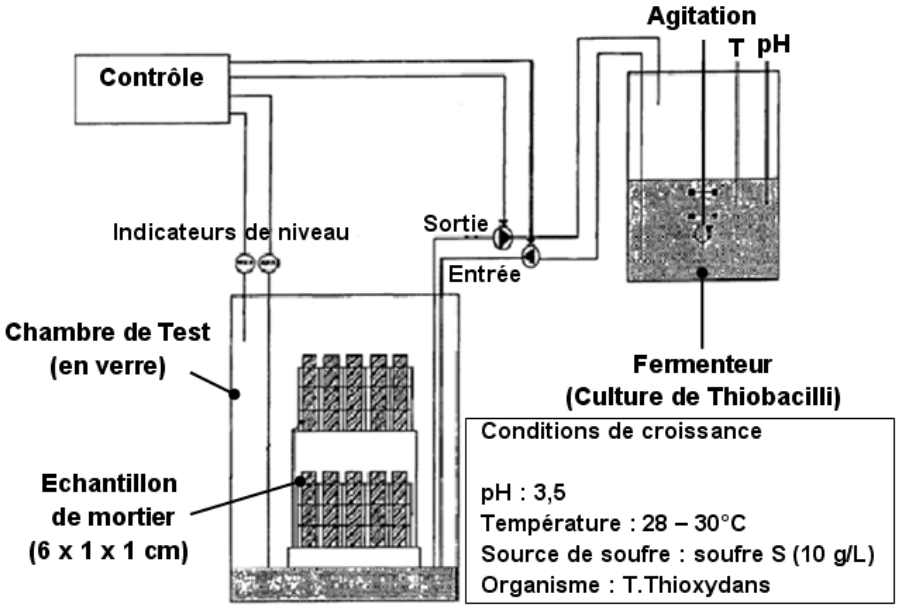

Figure 21 : schéma de principe de la chambre de simulation Heidelberger Zement développée par Schmidt et Hormann et les conditions de culture des microorganismes impliqués dans la détérioration (Schmidt et al., 1997)

Lors de l'étude menée en 1997 le test a duré 3 à 5 mois. Le suivi du test et sa validation ont été réalisés à la fin du test par la mesure sur les échantillons testés de la perte de poids et de la densité cellulaire à la surface. Cette chambre de simulation a été mise en place pour tester différents types de ciment, en particulier des ciments Portland et des ciments alumineux.

Tests : après 150 jours de test, les pertes de poids mesurées pour des ciments alumineux (3 – 4%) se sont révélées inférieures à celles mesurées pour des ciments Portland (18 – 31%). L'observation de la surface des échantillons a révélé une colonisation effective de ces mêmes surfaces.

2.1.5. Test Biologique de détérioration des bétons (Vincke et al., 1999)

Principe de fonctionnement : des blocs de bétons de différentes sortes (CEM I 42.5 et CEM III 42.5 (avec et sans polymères)) sont soumis à une attaque biogénique en présence de 4 espèces de microorganismes responsables de l'oxydation de composés soufrés en acide sulfurique (*T.intermedius, T.novellus* pour représenter des espèces mixotrophes et

modérément acidophiles, *T.neapolitanus* pour représenter une espèce autotrophe modérément acidophile, et *A.thiooxidans* pour représenter une espèce autotrophe fortement acidophile). Le test de détérioration se déroule en 4 étapes, certaines reproduisant *a priori* la croissance bactérienne et l'attaque acide, d'autres les phénomènes de lessivage des parois, ou les périodes sèches, correspondant en réseau d'assainissement aux périodes dites de temps de pluie ou de temps sec. Par ailleurs, le travail par étape peut avoir pour effet la mise en place de dynamiques de transfert liée à la création lors de chaque étape de différents gradienst de concentrations entre le milieu environnant et la surface des échantillons. Les quatre étapes du test sont les suivantes :

- Etape 1 : Incubation des échantillons sous H_2S gazeux (3 jours)
- Etape 2 : Incubation des blocs de béton en solution (10 jours) en erlenmeyer sur des tables agitantes.
- Etape 3 : Rinçage des blocs par de l'eau ultra pure (2 jours)
- Etape 4 : Séchage des blocs en atmosphère H_2S (2 jours)

La figure 22 illustre la cuve de test lors de l'étape 2, c'est-à-dire lors de la mise en solution (milieu de culture) des échantillons de ciment. Le test est réalisé par les mesures au cours du temps de l'épaisseur des échantillons et des concentrations en sulfate et en calcium dans la solution. En parallèle une étude de surface est réalisée par microscopie électronique.

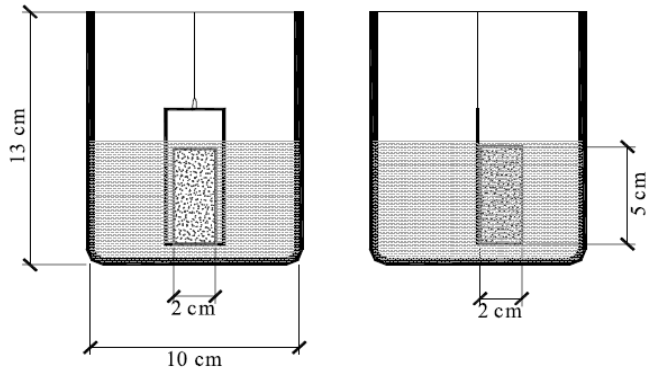

Figure 22: schéma de principe de la cuve de test lors de l'étape 2 du test de détérioration des ciments par voies biologiques. (Vincke et al., 1999)

Test : l'étape 1 par l'incubation des échantillons dans une atmosphère chargée de sulfure d'hydrogène permet une pré-acidification de la surface des échantillons et le dépôt potentiel de soufre élementaire à la surface du matériau. La mise en charge de la cuve par un milieu de culture permet, dans un milieu liquide, la colonisation de la surface des ciments par les microorganismes mis en présence (2). Il y a donc une forte diminution du pH de surface et

donc une détérioration des matériaux liée à l'activité biologique, confirmée par l'augmentation en solution des ions sulfate et des ions calcium. Après 3 cycles, c'est-à-dire 51 jours de tests, une perte de poids de 9 à 11% a été observée sur les ciments classiques, alors que cette perte de poids est estimée à 5 à 6% pour des mortiers complétés par l'ajout de polymères. D'après les auteurs (Vincke et al., 1999) cette méthode, avec un faible investissement, peut être utilisée pour tester la résistance de différents types de mortiers face à l'acide sulfurique biogénique. La procédure simule les situations les plus défavorables, en favorisant la pénétration d'H_2S, en mettant en contact le béton, les microorganismes et des nutriments, tout en lessivant régulièrement les surfaces, ce qui permet ainsi à la fin d'un cycle l'accès à une surface intacte pour les microorganismes. Cependant, de par le système par immersion dans un milieu de culture imposé, il apparait impossible de reproduire l'environnement local constitué de populations microbiennes en contact avec les matéiaux et ainsi de prendre en compte l'impact des matériaux testés sur l'activité biologique mise en jeu. De plus ce phénomène d'immersion durant 10 jours, sur des blocs de mortier de petite taille comparativement au volume de liquide, induit une neutralisation forte du pouvoir tampon du matériau, favorisant donc le travail des bacteries les plus acidophiles.

2.1.6. Biodégradation Accélérée des Ciments (Aviam et al., 2004)

Principe de fonctionnement : des échantillons de ciments ont été préparés en mélangeant 1,500 g de ciment Portland (PC 250) avec 450 mL d'une solution de soude (NaOH à 1 mol/L) à l'aide d'une bétonnière du type N-50. Chaque échantillon de ciment est alors exposé à une séquence de plusieurs cycles de détérioration, et donc à une importante quantité d'acide sulfurique dit « biogénique » produit par une culture mixte de bactéries du genre Thiobacillus (dans ce cas en particulier des espèces de type neutrophile). Cependant, un prétraitement des matrices cimentaires de 14 jours sous une atmosphère 100% CO_2 est opéré, et ce pour abaisser le pH de surface et permettre la croissance bacterienne. L'apport en soufre dans le milieu est assuré par l'ajout de thiosulfate.

Test : l'étude menée par Aviam et al en 2004 décrit une procédure mise en place pour l'accélération de la biodégradation des ciments. Après seulement 4 semaines de test il a été observé une perte de poids supérieure à 16 %. D'une manière intéressante, d'après les auteurs, l'accélération de la bio-détérioration observée dans cette étude (Aviam et al., 2004) a été obtenue en travaillant avec des cultures NSOM et *T. intermedius*, poussant durant le test à des

pH compris entre 6,2 et 6,5. Ceci alors que dans la plupart des autres procédés visant à accélérer cette bio-détérioration, des cultures ASOM (microorganisme sulfo-oxydants acidophiles) étaient généralement utilisées, conduisant en fin de cycles à des pH compris entre 0,5 et 2. En réalité, les bons résultats obtenus par Aviam et al., sont induits par une sur carbonatation initiale des échantillons. Ainsi, la dégradation rapide obtenue par ce système, certes attribuable à l'action biologique de bactéries sulfo-oxydantes, doit tout même être fortement minorée par un prétraitement drastique ayant un impact fondamental sur le pouvoir tampon du matériau et sur sa structure, phénomène accentué par le mode de test par immersion dans le milieu de culture des échantillons.

2.1.7. Oxydation du sulfure d'hydrogène en canalisation, Aalborg University (Vollertsen et al., 2008)

Principe de fonctionnement : l'injection séquencée d'un débit de sulfure d'hydrogène (H_2S) dans un pilote reproduisant une canalisation d'eaux usées, permet par la mesure en continu de la concentration en H_2S dans la phase gaz, de qualifier et de quantifier la cinétique d'oxydation de l'H_2S en condition d'assainissement. Pour cela, dans une canalisation préalablement montée (figure 23), un volume contrôlé d'eaux usées est recirculé sur une durée de deux heures avant d'être renouvelé. La préparation de la canalisation en plusieurs tronçons amovibles permet également une étude dans l'espace et dans le temps de la détérioration des matériaux. Six canalisations munies d'un revêtement en bétons de 10 tronçons chacune ont été mises en place. Le travail avec des eaux usées récupérées sur un réseau urbain permet l'ensemencement en conditions réelles des canalisations. En parallèle, l'injection maîtrisée en phase gaz d'H_2S permet, par sa mesure en continu, un suivi cinétique de son oxydation. A la fin de l'étude, des analyses de surface sur les différents tronçons permettent de visualiser et d'estimer la détérioration.

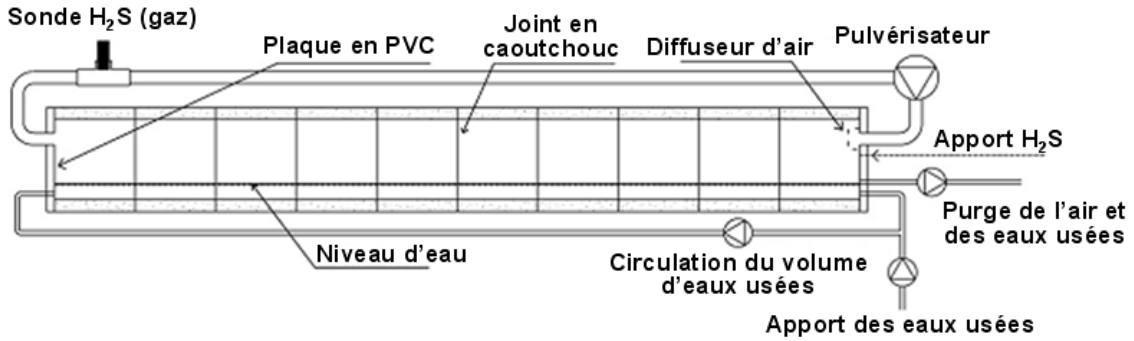

Figure 23: schéma de principe d'un pilote d'étude développé par Vollertsen (Vollertsen et al., 2008)

Test : d'après Jensen (Jensen et al., 2008) 95% de l'oxydation de l'H_2S dans les réseaux d'assainissement est due à l'activité biologique. Sans effet de saturation les taux d'oxydation augmentent avec l'augmentation de la concentration en H_2S. En ce qui concerne la détérioration des matériaux, la zone de marnage des eaux est la zone la plus fortement détériorée. Ce qui confirme certaines observations réalisées au niveau des réseaux d'assainissement.

2.1.8. Test de résistance des matériaux d'assainissement à la corrosion causée par l'acide sulfurique biogénique après la formation d'un biofilm (Wack et al., 2009) (Brevet déposé en Allemagne)

Principe de fonctionnement : dans un réacteur constitué d'une enceinte fermée contenant une phase liquide et une phase gaz, des canalisations coudées sont immergées dans une solution de culture (figure 24). L'immersion de ces canalisations tests est réalisée afin qu'une partie de la canalisation, disposée horizontalement, soit à demi-immergée, exposant l'autre partie à la phase atmosphérique du réacteur. Cette phase gazeuse est alimentée à partir de l'extérieur par l'injection d'un mélange prédéfinis d'air et d'H_2S. L'entrée du débit de gaz est réalisée au niveau de la partie immergée verticale des canalisations tests. Cette injection par le liquide doit permettre l'aspersion par pulvérisation de la partie émergée des canalisations (support de la croissance bactérienne et matrice à détériorer). L'inoculation du pilote est faîte avec des bactéries de l'espèce Thiobacilli (même si d'autres types de microorganisme peuvent être envisagés d'après les auteurs). Elle est réalisée par ajout au milieu de culture et remontée de la hauteur d'eau afin de mettre en contact le haut de la canalisation et le milieu de culture. Cette opération peut être répétée afin d'assurer la colonisation de la canalisation test (pas d'évocation de la fréquence de cette immersion). Au niveau de la phase liquide un système de recirculation permet de maîtriser la température à l'intérieur de la chambre de test. Une

régulation pH peut également être mise en place. Les mesures de contrôle sont la température, le pH, la hauteur d'eau au niveau de la phase liquide, ainsi que la concentration en H_2S dans la phase gazeuse (le brevet ne fait pas état du mode de mesure de la concentration en H_2S dans cette phase).

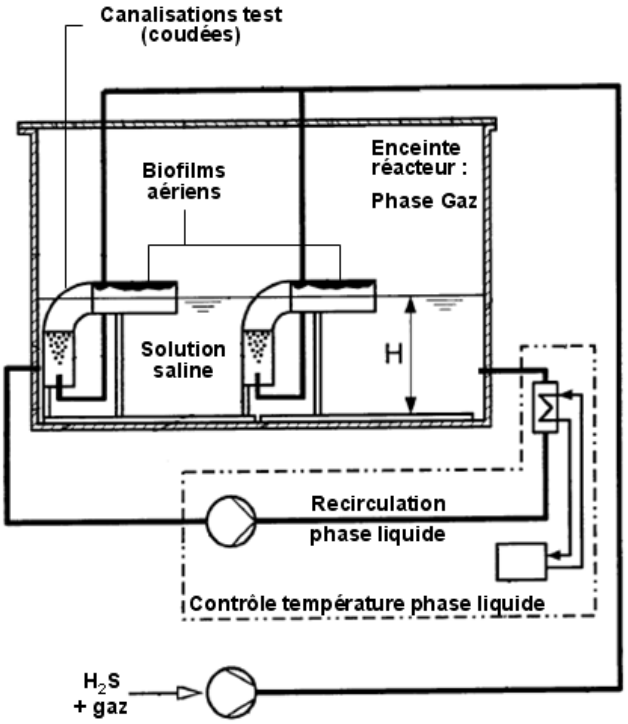

Figure 24: schéma de principe du pilote de test développé dans le cadre d'un brevet allemand par Wack (Wack et al., 2009).

Test : le brevet décrivant ce pilote de test fait état d'une croissance bactérienne assurée au bout de 4 semaines, quand une détérioration significative est observée au niveau des canalisations 6 semaines plus tard, (soit 10 semaines après le début du test). Le test décrit ne précise pas le mode d'évaluation de la détérioration (seule une mesure de la rugosité du revêtement est évoquée). Il n'est nulle part fait état de la reproductibilité des tests. En effet, de nombreux phénomènes ont été identifiés et reproduits afin de s'approcher au plus près des conditions observées en réseaux d'assainissement. Pour autant, la maîtrise des flux (mode d'aspersion en particulier) n'est pas assurée même sur les populations du genre Thiobacillus. Ce test, présenté uniquement sous la forme d'un brevet allemand, difficilement analysable a pour avantage, comme les études proposées par Mori en 1992 et par Vollersten en 2008 de travailler directement sur les produits (canalisation avec revêtement) et non sur des mortiers de laboratoire.

2.2. Récapitulatif et conclusions sur les différents systèmes expérimentaux proposés dans la littérature pour l'étude de la biodétérioration en réseau d'assainissement.

Les études présentées dans les paragraphes précédent n'avaient pas toutes vocations à proposer un test, mais leur design ainsi que les résultats obtenus ont apporté des données dans des conditions plus ou moins contrôlées et ont ainsi permis au cours des 4 dernières décennies d'améliorer et d'approfondir les connaissances sur le sujet. Le tableau 9 présente un récapitulatif des différentes études détaillées dans les paragraphes précédents. La durée de l'étude, le mode de formation du milieu de culture et la mise en contact du consortium microbien et des matériaux (par condensation, par immersion), le type d'inoculum, si l'ensemencement est unique ou répété et à quelle fréquence, la source de soufre, la quantification des flux, si une contrainte hydrodynamique est reproduite et/ou si un phénomène de lessivage de la paroi est appliquée ou crée, ainsi que les taux de détérioration mesurées (soit en perte de masse des échantillons, soit en perte d'épaisseur des échantillons), pour des mortiers différents basés sur deux types de pâte de ciment (CEM I et CAC) sont proposés.

Aujourd'hui, seul le dispositif expérimental développé à l'université de Hambourg et actuellement utilisé à l'université de Duisburg-Essen et adapté à l'IFSTTAR, par une adaptation, permet une quantification des flux de soufre réellement transformés au contact des matériaux, et donc de la quantité d'acide produit. Ainsi, il apparait que l'évolution de l'activité biologique au cours du temps, liée à l'évolution des matériaux est encore un domaine peu étudiée. Ainsi dans la plupart des systèmes expérimentaux l'influence potentielle du matériau sur l'activité biologique n'est jamais prise en compte et souvent potentiellement masquée par des volumes liquides trop importants pour être assimilables à des condensats. Dans d'autre cas, travaillant par condensation, le design expérimental ne permet tout simplement aucune évaluation des transformations intervenant dans la phase condensée.

Concernant la plupart des dispositifs expérimentaux proposés, le travail en présence d'H_2S, s'il est représentatif des conditions générales observées en réseaux d'assainissement, de par son caractère toxique, voire létal pour l'homme à certaines concentrations rencontrées sur des sites détériorés, limite la capacité de mesures et de suivi des transformations issues de l'interaction entre l'activité biologique et les matériaux. Ainsi, mise à part le banc d'essai développé à l'université d'Hambourg (aujourd'hui Duisbourg-Essen et l'IFSTTAR) où des

échantillons (limités en nombre) peuvent être disposés pour réaliser des points intermédiaires, le contrôle des conditions de transformations est réalisé *a priori*, avec une simple mesure finale de perte d'épaisseur, ou de perte de poids des échantillons. Il est également important de préciser, que mise à part le test proposé par Wack (2009), aucun travail d'essai n'est réalisé sur des produits industriels. Seuls des mortiers produits en laboratoire (dont l'avantage important concernant la reproductibilité des essais est de pouvoir être calibrés en termes de compositions, de porosité et d'homogénéité) ont été évalués.

De plus, l'un des choix majeurs effectué pour les tests proposés (hors du travail réalisé par l'université d'Aalborg en canalisation reproduite (Hvitved-Jacobsen, 2002) (Vollersten et al., 2008) (Jensen et al., 2012)) est de travailler dans le cas le plus simplifié à partir d'une souche pure (*Acidithiobacillus thiooxidans* en général), ou dans le meilleur des cas sur un consortium microbien constitué de plusieurs espèces du genre Thiobacilli (en général un mélange de 4 souches). Ce type de consortium, issu des études réalisées sur sites réels au niveau du réseau d'assainissement de la ville de Hambourg (Milde et al., 1983) (Sand and Bock, 1984), appuyé mais élargi en terme de diversité microbienne par la suite par les travaux réalisés sur le réseau de Houston (Davis et al., 1998), sur le réseau de la ville d'Ostende (Belgique) (Vincke et al., 2001) et par une étude réalisée dans un réseau du Japon (Okabe et al., 2007), ont été effectué sur des mortiers dont la base cimentaire n'est jamais spécifiée. Pour autant, de par l'ancienneté des réseaux étudiés, et les observations minéralogiques réalisées (formation de gypse pour Davis et pour Okabe, formation d'etrringite en profondeur pour Davis), il est à supposer que les matériaux utilisés étaient basés sur des ciments portland. Ainsi, si le matériau utilisé peut avoir une influence sur l'implantation, ou sur l'activité biologique, ou sur le mode de structuration des consortia microbiens mis en contact avec le matériau, les résultats obtenus à partir d'un consortium simplifié, issu d'une sélection sur des matériaux spécifiques, pourrait créer un biais. Ainsi, il apparaît intéressant dans un axe d'étude portant sur les interactions activités microbiennes / revêtement, d'inclure le revêtement en terme de facteur de sélection.

A partir de cette étude bibliographique, le chapitre suivant présente l'approche scientifique mise en œuvre afin de définir un système modèle pour l'étude de l'interaction entre les activités microbiennes (incluant la sélection) et les revêtements cimentaires utilisés, permettant la représentation et la quantification des transformations chimiques et biologiques participant à la biodétérioration des revêtements cimentaires et ainsi répondre à l'objectif industriel de la définition d'un prototype d'essai de résistance.

Tableau 9 : récapitulatif et caractéristique des différents systèmes expérimentaux développés pour l'étude de la biodétérioration des matrices cimentaires en réseau d'assainissement. Les références données en gras et en italique correspondent aux études ayant porté sur des produits commerciaux et non sur des mortiers de laboratoires.

Ref	**Durée (jours)**	**Film liquide / Immersion**	**Inoculum**	**Ensemencement régulier**	**Source de soufre**	**Quantification des flux au contact du matériau**	**1 : Simulation contraintes hydrodynamique 2 : lessivage / ruissellement**	**Taux de détérioration* / type de matériaux**			
								Perte de poids		**Perte d'épaisseur**	
								CEM I	**CAC**	**CEM I**	**CAC**
Sand (1984-1987-1994)	270	Condensation + pulvérisation	3 NSOM 1 ASOM	Durant 90 jours	H_2S ~10 ppm	-	1 : Non 2 : Oui	3.3% - 5,8%			
Sand (1987)	''	''	''	''	Thiosulfate	-	''	1.8 %			
Ehrich (1999)	150 350	Condensation + pulvérisation	3 NSOM 1 ASOM	Durant 90 jours	H_2S ~10 ppm	SO_4^{2-}	1 : Non 2 : Oui	25 % 100 %	13 % 40 %		
Mori (1992)	180	Zone de marnage	1 ASOM	Présence d'eaux usées renouvelées	H_2S ~25 à 300 ppm	-	1 : Oui 2 : Oui			***3,8 à 7,6 mm/an***	
Schmidt (1997)	150	Immersion séquencée	1 ASOM	5 min / h	S^0 (10g/l)	-	1 : Non 2 : Oui	18-31 %	3-4 %		
Vincke (1999)	51	Immersion	3 NSOM 1 ASOM	3 fois	H_2S 250 ppm	-	1 : Oui 2 : Oui	9-11 %			
Aviam (2004)	28	Immersion	2 NSOM	Non	Thiosulfate	-	1 : Non 2 : Non	16 %			
Vollersten (2008)	180	Condensation	Eaux usées	Présence d'eaux usées renouvelées	H_2S 10 – 1000 ppm	H_2S consommé	1 : Non 2 : Oui			***3,1 mm/an***	
Wack (2009)	70	Pulvérisation	Thiobacilli	Pulvérisation continue	H_2S 100 ppm	-	1 : Non 2 : Oui	Non précisés			

* : les taux de détérioration sont donnés par rapport à des pates de ciments pour identifier les différences marquées entre CEM et CAC. Chaque étude a en réalité étudiées des mortiers spécifiques. Ainsi les taux de détérioration ainsi que les pates de ciments évaluées ne sont données qu'à titre indicatif.

Chapitre II

Approche scientifique

La syntèse bibiliographique présentée au chapitre I a permis de décrire qualitativement les transformations intervenant lors de la détérioration des matrices cimentaires en réseau d'assainissement et de présenter les approches misent en oeuvre pour assurer la quantification des phénomènes (quantification assurée par des mesures de pertes de masses ou d'épaisseur des matériaux testés). Cependant, ces descriptions en réseau d'assainissement ont pour beaucoup été réalisées sur des ciments portland, ne permettant en aucune manière d'extrapoler les comportements décrits sur d'autres types de matériaux cimentaires (ciment alumineux par exemple). De la même manière, à l'échelle d'un essai de résistance, le choix des populations utilisées s'appuie généralement sur ces mêmes études, et font donc l'hypothèse d'une sélection microbienne identique en terme de populations quel que soit le revêtement testé. Il apparait donc important d'étudier les interactions entre une activité biologique « agressive » se développant sur un revêtement cimentaire et l'évolution de ce même revêtement durant cette attaque biologique sans présupposer le type de populations implantées et donc en permettant au materiau, outre un effet sur l'activité biologique, de jouer pleinement son rôle ou non de facteur de sélection.

Pour cela l'approche scientifique mise en place s'appuie sur deux points majeurs :

- Le besoin de quantification et ce afin d'assurer l'évaluation et la maitrise des processus mis en jeu, et ce aussi bien dans l'objectif (i) d'assurer la compréhension et la hiérarchisation des processus intervenant en fonction des revêtements testés, que (ii) de permettre l'évaluation de la résistance des révêtements cimentaires.

- Le besoin de travailler initialement à partir d'inoculums diversifiés et ce afin de permettre la sélection de populations via l'environnement constitué par le revêtement cimentaire et les conditions opératoires contrôlées misent en œuvres.

Ainsi, avec l'objectif d'assurer la quantification des transformations par bilans matières et d'assurer la sélection d'une activité sulfo-oxydante au contact des revêtements, le choix du susbtrat soufré utilisé apparait clé. L'utilisation d'autres composés soufrés réduits sera donc évaluée en tant que susbtrat de susbtitution à l'hydrogène sulfuré (H_2S) et ce en raison de trois facteur, (i) l'apport direct en solution, éliminant les échanges gaz-liquid problématiques pour l'assurance de bilans matières dynamiques, (ii) une plus grande stabilité du composé en conditions de culture et (ii) une facilité d'utilisation liée à l'absence de toxicité des composés utilisés.

Afin d'évaluer l'efficacité d'un tel choix, aussi bien sur la production d'acide biogénique au contact des revêtements que sur la sélection de bactéries sulfo-oxydantes à partir d'inoculum diversifié (type boue activée), la compétition entre réactions abiotique et réactions biologiques devra être étudiée. Celle-ci s'appuiera sur des études décrites dans la littérature où les stoechiométries des réactions sont proposées, parfois associées à la description des cinétiques apparentes de telle ou telle réaction. Pour autant la compétition entre réactions chimiques et réactions biologiques en fonction des conditions environmentales n'est souvent pas quantifiée. De plus, même si l'oxydation biologique de composés soufrés est largement décrite sur souche pure, la sélection d'une activité sulfo-oxydante acidophile quantifiée manque, en particulier à partir de consortium microbien issu de l'assainissement. Cette sélection, à partir d'inoculum diversifié fait appel à des compétitions entre populations microbiennes, en particulier entre microorganismes sulfo-oxydantes et nitrifiants et/ou hétérotrophes, limitant potentiellement l'implantation d'une activité sulfo-oxydantes et donc les flux d'acide biogénique produit.

Ainsi, l'objectif de ce travail de recherche est de proposer un système modèle simplifié permettant de représenter et de contrôler les transformations biologiques et chimiques participant à la biodétérioration des matrices cimentaires en réseaux d'assainissement, dans un cadre d'intensification des processus. Pour cela, une approche expérimentale par bilans matières permettra d'évaluer quantitativement les choix de simplification. Cette approche expérimentale à l'échelle système, s'appuiera sur des expériences ciblées permettant de décrire les stoechiométries et les cinétiques réactionnelles participant à la production d'acide biogénique. Un modèle dynamique couplant alors processus chimiques et processus biologiques sera proposé. Il permettra de valider et d'assurer les choix de sélection mis en œuvre. Ainsi l'attaque des revêtements cimentaires, par la sélection d'une activité sulfo-oxydante pourra étre analysée en dynamique en fonction du type de revêtement étudié. Cette analyse sera réalisée par l'étude des interactions entre revêtement cimentaire et activité microbienne permettant en terme de résistance d'évaluer aussi bien les propriétés physico-chimiques des matériaux que leur influence sur l'activité biologique.

Ce travail permettra à l'échelle du système étudié:

- L'intégration de processus chimique et biologique notamment via le développement d'un modèle dynamique.

- La validation de chemins réactionnels privilégiés ainsi que l'évaluation de certains paramètres cinétiques.
- La conception du test proposé incluant les bilans matières et l'analyse de signaux dynamiques permettant, par la compréhension des processus mis en jeu, un diagnostic de l'évolution des matériaux.
- L'analyse comparative des dégradations au sein de deux types de revêtements industriels.

Ainsi, le chapitre suivant (chapitre III), correspondant au matériel et méthode, présentera le dispositif expérimental principal développé pour assuré le système modèle retenu et présenté à la figure 17, tout en assurant une représentation fidèle des conditions rencontrées en réseau d'assainissement (en terme de température, de condensat, de charge en soufre etc...). Ce chapitre présentera également les techniques analytiques et les méthodes utilisées pour réaliser le suivi des expériences et les bilans matières nécessaires à la maitrise du système. Il y sera également présenté, les dispositifs expérimentaux supplémentaires mis en place pour approfondir la compréhension et la maitrise des processus mis en jeu.

Le chapitre IV, après le choix d'un composé soufré modèle via une synthèse bibliographique ciblée, par une comparaison de la sélection d'une activité sulfo-oxydante développée sur des revêtements CAC à partir de sulfides solubles (ion sulfur S^{2-}) et de thiosulfate ($S_2O_3^{2-}$) en tant que source de soufre, et à partir d'un consortium issue d'une boue activée en tant qu'inoculum, confrontée aux mêmes expériences réalisées en conditions abiotiques, permettra d'évaluer l'intérêt d'un tel système pour la sélection et le développement d'une activité sulfo-oxydante quantifiable au contact d'une matrice cimentaire.

Le chapitre V, hors matrices cimentaires, étudiera en fonction du pH la réactivité des thiosulfates afin d'assurer la maitrise des transformations (chimiques dans ce chapitre et ultérieurement biologiques dans le chapitre suivant) intervenant à l'échelle du dispositif expérimental. Dans ce but, associé à des expériences, un modèle dynamique sera développé et proposé assurant la qualification et la quantification des transformations ciblées.

Le chapitre VI, hors matrices cimentaires, étudiera la sélection d'une activité sulfo-oxydante acidophile à partir d'un inoculum constitué d'un consortium issu d'une boue

activée, sélection effectuée par une alimentation maitrisée en thiosulfate. L'étude se portera sur l'analyse d'une culture, à travers des analyses expérimentales et par la reprise du modèle préalablement développé au chapitre V augmenté d'un compartiment décrivant les transformations biologiques des thiosulfates.

Le chapitre VII, à partir du dispositif expérimental principal développé au chapitre IV, étudiera la sélection et le développement d'une activité sulfo-oxydante sur deux matrices cimentaires (CAC et CEM III), afin d'évaluer et l'impact de l'activité microbienne sur les matériaux et l'impact des matériaux sur l'activité microbienne. La représentativité des transformations participant à la biodétérioration des revêtements sera observée, afin d'évaluer la conception du pilote d'étude en terme de prototype pour la définition d'un essai de biodétérioration.

Par volonté d'une valorisation ultérieure des travaux présentés dans ce document, les chapitres suivants sont rédigés en anglais.

Chapter III

Materials and Methods

1. Materials and methods for the study of the interaction of the biological activity and the cementitious materials (Chapter IV and Chapter VII)

In the chapter I of this document, a simplified schema was proposed to reproduce at a lab-scale the system of an active biological consortium in contact with cementitious materials. This figure is represented again here to illustrate the system (figure 25) and explain the lab-scale pilot design based on it. The design choices to simplify the system were justified in the chapter IV. The whole system of the biodeterioration of the cementitious materials in sewer system was reproduced only by taking into account the liquid film and the cementitious material to ensure microbial activity. The gas phase and the transfer with the liquid will be avoided in order to simplify the system and to a have a better control.

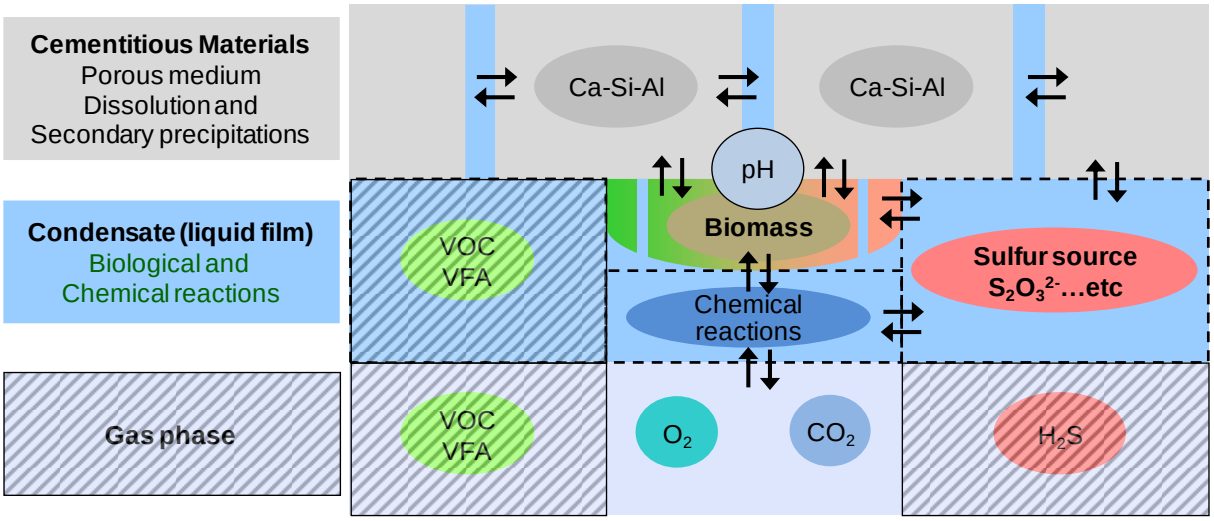

Figure 25: schema of the system proposed to study the biodeterioration of the cementitious materials in sewer systems and the interaction between biological activity and the cementitious lining.

1.1. Experimental set-up and analyses for the development of a sulfur-oxidizing activity in contact with cementitious materials

1.1.1. The sewer-pipe tested during the study

The cementitious linings are porous media composed by mortars, that were defined as a mix of bonding (cement paste in the case) of sand, water and eventually of some admixtures (Herisson, 2012) used to protect the ductile iron-cast structure of the sewer-pipe (chemical

and sacrificial protection against the agressive environments). Concerning the company Saint-Gobain PAM, the production process of the pipes and of the intern cementitious linings by centrifugation, leads inside the cementitious lining to a spatial segregation of the different compounds. The figure 26 represents a longitudinal section of a Saint-Gobain PAM sewer-pipe (inner diameter of 80 mm), and illustrates (i) the whole structure of the pipe (figure 26.A), with the ductile cast-iron structure and the inner cementitious lining (here CAC lining), and (ii) the spatial segregation inside the cementitious lining observed by SEM in the depth (figure 26.B), showing aggregates in the depth of the product, and the surface of the lining composed only by cement paste. Thus, in the case of such sewer-pipe, the biological activity selected by the environmental conditions previously described (chapter I), growth initially in contact with a porous media composed only by cement paste.

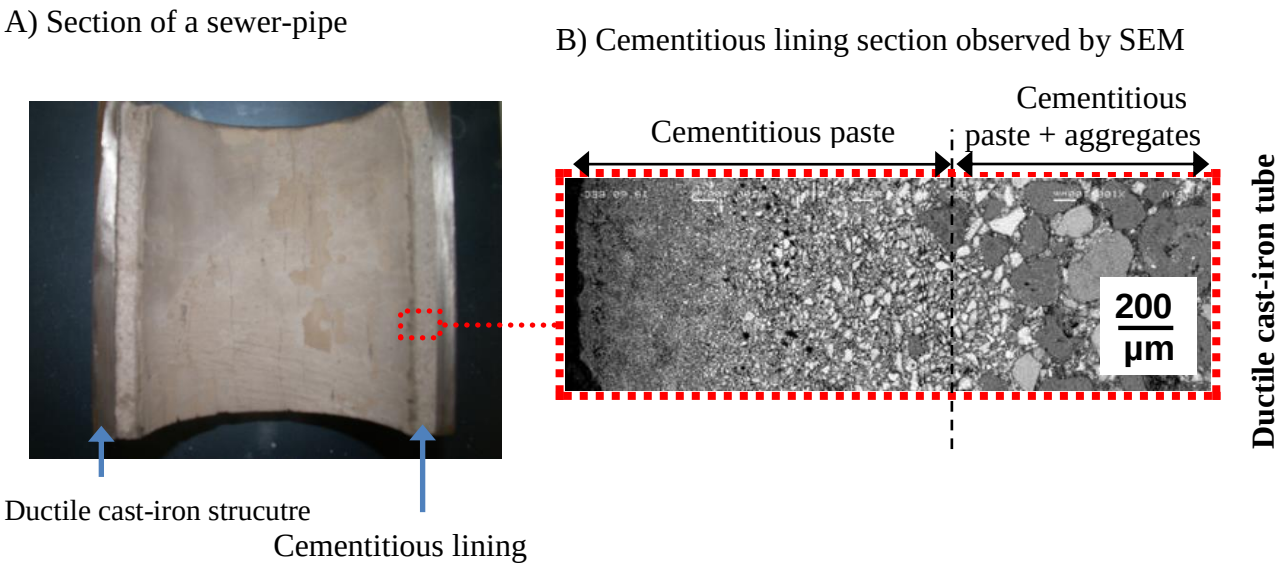

Figure 26: longitudinal section of a sewer-pipe (ductile cast-iron structure with inner lining composed by a mortar based on aluminous cement (produced by Saint-Gobain PAM) (A), and SEM observation in the depth of the cementitious lining (B).

1.1.2. Lab-scale pilot

To produce a liquid phase, assimilate to a condensate, the pilot was composed of two vertical pipe-reactors in parallel, each mainly composed of one segment cut from a real sewer pipe produced by Saint-Gobain PAM (ductile cast iron pipes with a calcium-aluminate-cement (CAC)-based internal protective lining and with BFSC-based lining (BFSC corresponding to the CEM III cement paste of the French norm) and CAC-based lining)

(figure 27). The work with two lines was choosen in order to compare different operating conditions, or system (biotic or abiotic; different linings) from the same feeding solutions.

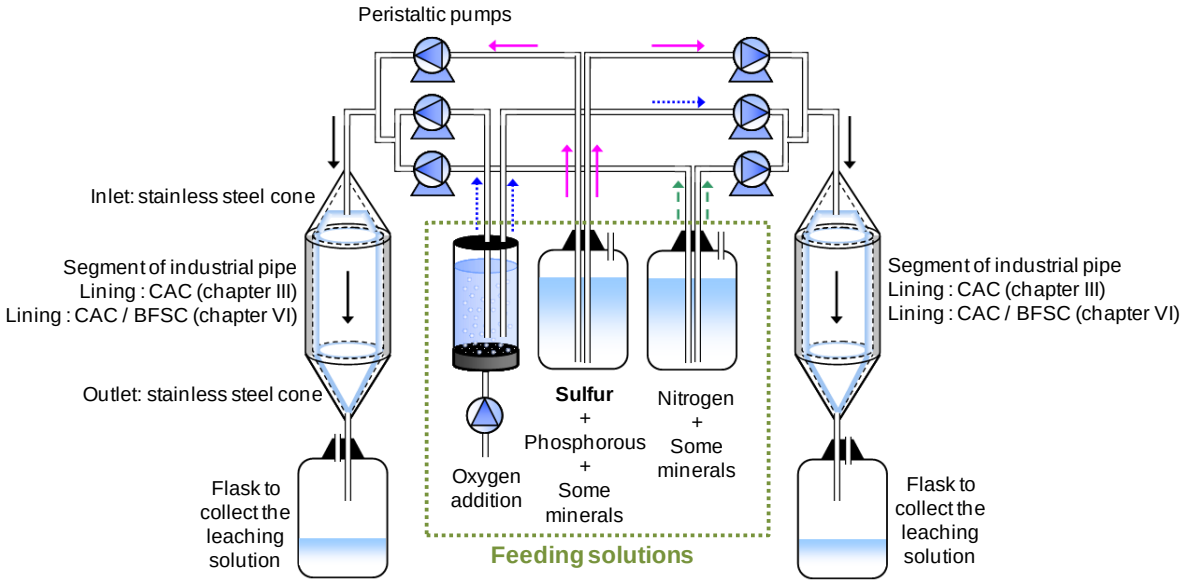

Figure 27: schema of the lab scale pilot design to reproduce the interaction between biological activity and the cementitious lining in sewers.

The segment was 200 mm long and had an internal diameter of 80 mm, equivalent to 0.05 m² of exposed concrete surface. Moreover, each pipe-reactor is composed of:

(i) An external PVC double jacket on the outside of the segment to maintain the temperature at 20 (±1)°C by circulating thermostated water, as illustrated in the figure 28.

(ii) A stainless steel cone at the inlet and another one at the outlet to collect the leaching solution in a flask. The stainless steel cones and the pipe segments were sealed by rubber rings and steel clamps.

(iii) To represent condensation and flow of water on the top part of the pipe in real sewers, a constant flow of a mineral solution was fed into the reactors by trickling. Because of the vertical position of the pipe segment, the water ran down the pipe walls by gravity. To limit the impact of preferential paths for the trickling solution, the orientation of the stainless-steel inlet cone was changed by 90 degrees every day. The water inlet-flow was fixed at 50 ml/h. This value, experimentally fixed, was estimated for a segment-pipe of 200 mm long, corresponding to intense conditions (water temperature

= 35 °C and pipe walls at 10°C). The details of this calculation were presented in the annexes of this chapter.

(iv) To ensure microbial activity, nutrients are necessary. Working in liquid conditions, the feeding solutions were provided at the inlet of the segment-pipe by three peristaltic pumps, based on three feeding compartments where mineral nutrients were separated to avoid biological growth inside the feeding solutions. The three solutions were mixed at the inlet of the segment-pipes. General composition of the mineral solution is presented in the next paragraphs.

(v) To ensure initial microbial diversity, and analyzed the selection of sulfur-oxidizing activity, depending on environmental conditions (including the composition and the structure of the cementitious lining), the inoculation was operated one time, at the beginning of the experiments. More details on the inoculation are given in the next paragraphs.

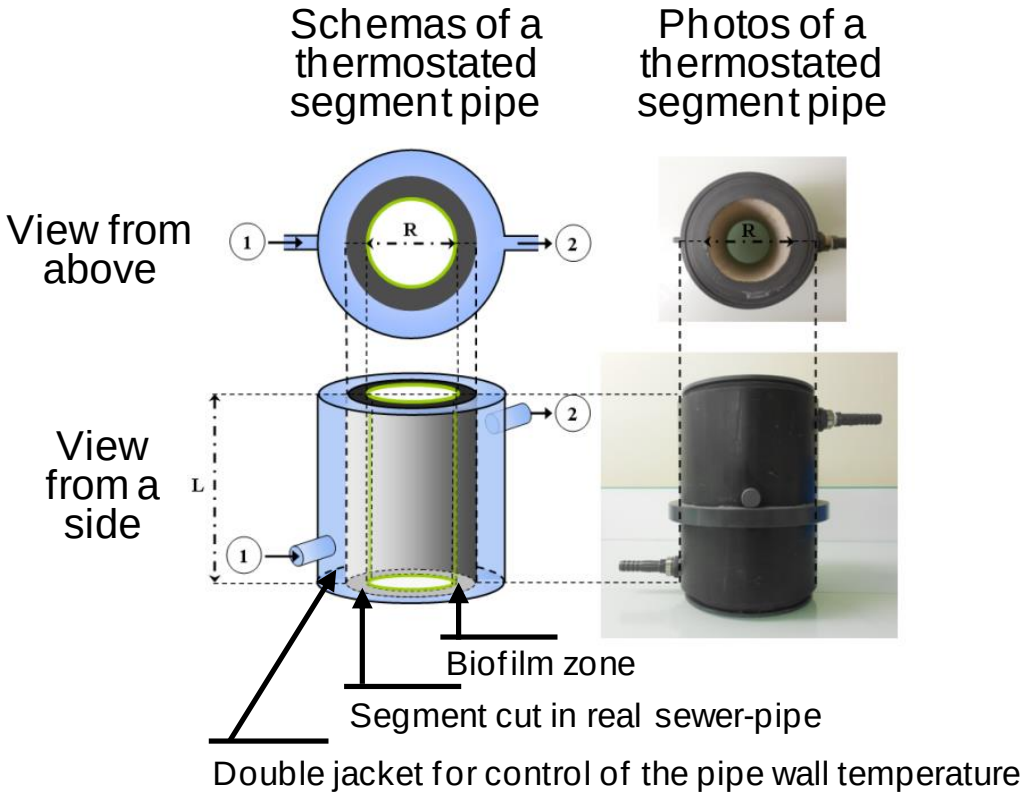

Figure 28: schema and photos of the segment-pipe (D = 80 mm and L = 200 mm) with his double jacket of PVC for the control of the temperature applied at the pipe-wall.

1.1.3. Nutrient supplies

For both pipe-reactors (figure 27), the nutrients were supplied by dripping a mix of three feeding solutions onto the inlet stainless steel cone. The initial nutrient solutions were separated in three glass tanks (5 litres each): one for the supply of sulfur, phosphorous and some others minerals (as magnesium and trace elements), one to provide nitrogen and some other mineral nutrients (as iron and manganese) and the last one, permanently aerated, to provide additional dissolved oxygen and inorganic carbon (figure 27). All the solutions were prepared with deionised water to avoid sulfate and calcium concentration. Every week, all supply tanks were emptied and washed before the preparation of new feeding solutions (twice a week for the sulfur feeding solution), and all the silicon tubing used for the connections was changed (to avoid biofilm accumulation). The different feeding solutions applied during the experiment were prepared from concentrated nutrient solutions (with no sulfate, and no calcium contribution), NH_4Cl (10 $g.l^{-1}$), $(NaPO_3)_3$ (10 $g.l^{-1}$), $MgCl_2.6H_2O$ (30 $g.l^{-1}$), $FeCl_2.4H_2O$ (1 $g.l^{-1}$), $MnCl_2.4H_2O$ (1 $g.l^{-1}$), and a solution composed of trace elements (boron oxide, cobalt, zinc, molybdenum oxide, copper and nickel).

1.1.4.1. The sulfur supply

The sulfur supply was prepared twice a week by dissolving $Na_2S.9H_2O$ crystals in four litres of deionised water. Peristaltic pumps were used to inject the feeding solutions into the inlet stainless steel cones. After 121 days of sulfide (S^{2-}) sulfur supply to both pipe-reactors (biotic and abiotic), the source of sulfur was changed to $S_2O_3^{2-}$, for an experiment lasting 143 days. The experimental pilot, the sampling method, the chemical analyses and the result treatments were kept identical. For the nutrient supplies, only the sulfur feeding solution was changed, with the dissolution of $Na_2S_2O_3$ as primary sulfur source instead of $Na_2S.9H_2O$.

The sulfur loads applied were chosen in order to obtain significant rates of concrete corrosion but to avoid any inhibition of the SOB. With respect to the transformation rate, the second step of the Pomeroy model (De Belie et al., 2004) was used to estimate a targeted sulfur load of around 0.025 $gS.m^{-2}.hr^{-1}$, even if for CAC based materials especially Pomeroy model showed limits (Alexander, Bertron and De Belie, 2013). However, this theoretical sulfur load corresponds to a calculated concrete thickness loss of about 0.85 mm/year. It refers to a recalculated material alkalinity of about 0.27 (g $CaCO_3$ / g Concrete). This load is

equivalent to 38 µmolS applied.h^{-1} in our experimental conditions. This load is divided by two at the beginning of the experiment in order to avoid inhibition and then increased when no accumulation of sulfide was found.

In the case of polythionate feeding, the sulfur was firstly provided by dissolving a thiosulfate salts ($Na_2S_2O_3$) in deionized water, and in the case of specific tests tetrathionate was used as sulfur source to evaluated the implication of this compounds in the global conversion, and its biological acidification potential. To intensify the sulfur biological reactions, the concentration of thiosulfate in the feeding solution was punctually increased.

1.1.3.2. The others nutrients

For *Thiobacillus thioparus* the maximum biomass yield measured in pure culture for a sulfur-oxidizing bacteria in autotrophic conditions (around 16 grams of $C_5H_7O_2N$ produced per mole of sulfur oxidized, equivalent to 0.14 mol$C_5H_7O_2N$/molS for example) (Alacantra et al., 2006) (Bielefeledt et al., 2010). Based on this maximal values (Y_{max}) reached on thiosulfate for SOB, nitrogen and phosphorous elements needs were calculated to be provided in excess. Nevertheless, the corresponding salt concentrations are fixed at low concentrations in order to limit a possible reaction with the cementitious materials (undesired salts precipitation of phosphorous salts for example (Herisson, 2012), and/or a negative influence of nitrogen compounds). For the same reasons no additional inorganic carbon was provided to the system, to avoid an artifact due to an over-carbonation of the material. The need of inorganic carbon for the autotrophic growth was only provided by the gas phase in contact with the trickling film of water running down on the cementitious surface.

The table 10 presents the different elements composing a bacteria cell, thus the element needs, and the method to respect the ratio and thus calculated the concentration of nutrient elements in the feeding solution, based on the oxidizable concentration of sulfur in the feeding solution. Concerning the main elements provided by soluble salts, a security factor was applied, (i) to avoid nutritional limitation of the biological growth, (ii) to enable growth of other population than sulfur-oxidizing bacteria as in real environment.

Table 10: elemental composition of bacterial cells and the elemental concentration of the feeding solution calculated, depending on the concentration of oxidizable sulfur in the feeding solution.

Main Nutrient elements	**% of element in biomass g of element / g of $C_5H_7O_2N$**	**Y_{max} x (mol of element / mol of $C_5H_7O_2N$)**	**Concentration in the feeding solution (in mol/l) calculated from the sulfur concentration (in molS/l) with excess factor**
C	53%	0.7	Brought by gas exchange
H	6%	0.98	Brought by medium
O	28%	0.28	Brought by gas exchange
$N\text{-}NH_4^+$	12.4%	0.14	4 x 0.14 x [S]
P	3%	0.11	2 x 0.11 x [S]
S	1%	0.035	Main substrate
Mg^{2+}	0.5%	0.023	2 x 0.023 x [S]
K^+	0.5%	0.014	Contained in cementitious materials
Ca^{2+}	0.5%	0.014	Contained in cementitious materials
Fe^{3+}	0.2%	0.004	2 x 0.004 x [S]
Trace elements			
Mn^{2+}	-	-	4.10^{-4} x [S]
Co^{2+}	-	-	3.10^{-4} x [S]
Zn^{2+}	-	-	1.10^{-4} x [S]
Cu^{2+}	-	-	2.10^{-5} x [S]
Mo^{2+}	-	-	4.10^{-5} x [S]
Ni^{2+}	-	-	3.10^{-5} x [S]

1.1.4. The inoculum

To evaluate the selection of sulfur-oxidizing activity on cementitious materials, inoculums with high diversity was chosen. Because biodeterioration in sewers occurred in a system with a high microbial diversity, the chosen inocula were prepared by the centrifugation of an activated-sludge from wastewater treatment plants. After centrifugation, the biological paste was applied at the surface of the cementitious lining. In the chapter IV, the activated-sludge was sampled in the wastewater treatment plant of the city of Muret (labelled AS 1 in the rest of this document). In the chapters VI and VII, the activated sludge was sampled in the wastewater treatment plant of the city of Villefranche (labelled AS 2 in the rest of this document).

To illustrate, the figure 29 proposed two photos of the experimental segment-pipes just after the application of the centrifugated activated-sludge, in the case of the experiences

realized with AS 1 (figure 29.A) (presented in the chapter IV), and of the experiences realized with AS 2 (figure 29.B) (presented in the chapter VII).

A) CAC inoculated by AS 1 day 0 (Chapter III)

B) CAC inoculated by AS 2 day 0 (Chapter VI)

Figure 29: photos of the experimental segment-pipes just after the application of the centrifugated activated-sludge for CAC lining, (A) corresponding to the experiences realized with AS 1 presented in the chapter III, (B) corresponding to the experiences realized with AS 2 presented in the chapter VI.

1.1.5. Chemical analyses of the leaching solution

1.1.5.1. Direct measurements

In the leaching solution, the total dissolved calcium concentration and the total dissolved alumina concentration were measured. pH (before 0.2 µm filtration), $S_2O_3^{2-}$, SO_4^{2-} , S^{2-}, N-NH_4^+, N-NO_2^- and N-NO_3^- -concentrations were measured (after filtration at 0.2 µm).

The pH of the leaching solution was measured by a glass electrode (SCHOTT). The concentrations of N-NO_2^-, N-NO_3^-, SO_4^{2-}, $S_2O_3^{2-}$ were measured by anionic chromatography (DIONEX: IC25, IonPacTM AS19). The sulfide concentration (S^{2-}) was quantified using a specific electrode (Radiometer analytical) in the Ion-Selective Electrode Method (APHA, 2012). The concentrations of N-NH_4^+ and the total dissolved calcium were quantified by cationic chromatography (DIONEX: ICS 2000, IonPac CS12). The N-NH_4^+ concentration measurement was punctually checked in every 10 samples by the Nessler method (APHA, 2012) and every measurement confirmed the value obtained by ionic chromatography. The

concentration of the total dissolved alumina was measured in acidified samples (HCl) by flame atomic absorption spectrophotometry (Direct Nitrous Oxide-Acetylene Flame Method) (APHA, 2012) concerning the chapter IV, and by ICP-AES (Inductively Coupled Plasma-Atomic Emission Spectrometry) concerning the chapter VII.

Concerning the chapter IV, Sulfide (S^{2-}) measurements were achieved only for the first four samples because (i) no concentration was recorded above the specific electrode limit of quantification in alkaline support solutions (specific electrode limit of quantification of 5.10^{-7} molS^{2-}.l^{-1} corresponding to 0.20% in the sulfur mass balances), and (ii) sulfur mass balances were achieved by measuring $S_2O_3^{2-}$ and SO_4^{2-} concentrations only (see results of the chapter IV).

1.1.5.2. Combined measurement

Concerning the chapters VI and VII, soluble COD measurements (NFT 90.101) were punctually realized to evaluate the lack of reduced sulfur compounds. The thiosulfate oxidation in COD is described by the equation (Eq 21):

Eq 21: $S_2O_3^{2-} + 2O_2 + H_2O \rightarrow 2SO_4^{2-} + 2H^+$

Thus, from this theoretical equation, 1g/l of thiosulfate was equivalent to 0.57 gO_2/l. For other soluble reduced sulfur compounds, as tetrathionate ($S_4O_6^{2-}$), pentathionate ($S_5O_6^{2-}$), trithionate ($S_3O_6^{2-}$) and dithionate ($S_2O_6^{2-}$) described as possible intermediates during the biological sulfur oxidation (Islander et al., 1991), the same equations were used (Eq 22, Eq 40, Eq 41 and Eq 42):

Eq 22 : $S_4O_6^{2-} + 3.5O_2 + 3H_2O \rightarrow 4SO_4^{2-} + 6H^+$ (1g$S_4O_6^{2-}$/l = 0.5 gO_2/l)

Eq 40 : $S_5O_6^{2-} + 5O_2 + 4H_2O \rightarrow 5SO_4^{2-} + 8H^+$ (1g$S_5O_6^{2-}$/l = 0.62 gO_2/l)

Eq 41 : $S_3O_6^{2-} + 2O_2 + 2H_2O \rightarrow 3SO_4^{2-} + 4H^+$ (1g$S_3O_6^{2-}$/l = 0.33 gO_2/l)

Eq 42 : $S_2O_6^{2-} + 0.5O_2 + H_2O \rightarrow 2SO_4^{2-} + 2H^+$ (1g$S_2O_6^{2-}$/l = 0.1 gO_2/l)

To validate theses theoretical equations of reduced sulfur compounds oxidation, experimental COD measurement were realized with thiosulfate and tetrathionate. The

figure 30 presents the experimental results obtained, in terms of COD values (NFT 90.101), for calibrated solutions of thiosulfate (figure 30.A) and tetrathionate (figure 30.B). The experimental values were coherent with the theoretical values (thiosulfate slope = 0.59 for 0.57 in theory; tetrathionate slope = 0.53 for 0.50 in theory). Thus, the COD measurement, combined with direct measurement of the thiosulfate and the sulfate concentration, for reduced sulfur compounds as sole source of oxidizable compounds, could be an interesting methods to achieve the sulfur mass balances (see chapter VI and VII for experimental illustrations).

A) Thiosulfate oxidation

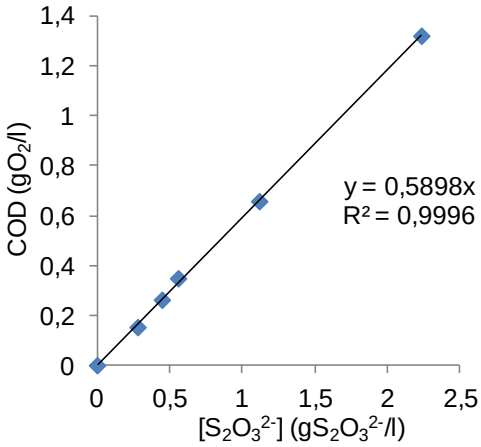

B) Tetrathionate oxidation

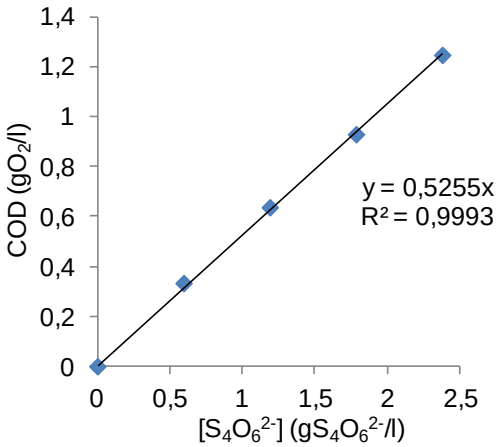

Figure 30: equivalent COD values for the oxidation of thiosulfate ($S_2O_3^{2-}$) and tetrathionate ($S_4O_6^{2-}$)

1.1.6. Sampling of the leaching solution

Regularly 20 ml was directly sampled at the outlet of the segment-pipes. After pH measurement, the solution was filtered at 0.2 µm (chapter IV: comparison between biotic and abiotic reactions; chapter VII: comparison between two cementitious materials). The filtered leaching solutions were analyzed in the day.

1.1.7. Check on stability of sulfur supply in the case of the chapter IV

To evaluate the stability of the sulfide (S^{2-}) feeding solutions, a control sample was analysed every week before the preparation of the new feeding solution. The sulfide (S^{2-}) concentration was measured in 50 ml of a solution composed of 25 ml of the supply solution sample added to 25 ml of an alkaline and antioxidant solution (1M NaOH + 0.1 M ascorbic acid). Because sulfide (S^{2-}) is reactive in presence of dissolved oxygen (Buisman et al., 1990),

SO_4^{2-} and $S_2O_3^{2-}$ concentrations were measured on the same sample to estimate the real composition of the sulfur feeding solution. The different chemical analyses were carried out in the same way as described previously.

1.2. Identification of populations[3]

At the end of the experiments different biomass samples were collected directly on the cementitious materials and used to identify the populations involved in the global transformation by 16S rRNA tag-encoded pyrosequencing. Total DNA was extracted with MoBio Ulta Clean Soil isolation kit following the manufacturer's instructions (MoBiol laboratories, Inc., USA). V1-V3 region of 16S rRNA gene was amplified using the primers 27F (5'-AGR GTT TGA TCM TGG CTC AG-3') and 519R (5'-GTN TTA CNG CGG CKG CTG-3') (Kumar et al., 2011). A single-step 30 cycle PCR using HotStarTaq Plus Master Mix Kit (Qiagen, Valencia, CA) were used under the following conditions: 94°C for 3 min, then 28 cycles of 94°C for 30 s; 53°C for 40 s and 72°C for 1 min; final extending at 72°C for 5 min. PCR products for each sample were mixed to obtain equal molar DNA for sequencing. Pyrosequencing was performed on 454 GS FLX system according to the manufacturer's instructions (Roche). Sequence analysis was performed with Mothur (Schloss et al., 2009) as follow: (1) sequences were depleted of barcodes and primers; (2) short sequences (<200bp) and ambiguous sequences were remove; (3) sequences were denoised and chimeras removed; (4) operational taxonomic units (OTUs) were defined by clustering at 3% divergence (97% similarity) (Dowd et al., 2011); OTUs were taxonomically classified using a naive Bayesian approach (Wang et al., 2009) and SILVA 111 SSU database.

[3] : the extraction, purification and amplification experiments were realized at the LISBP by Myriam MERCADE-LOUBIERE for the chapter IV and by Catherine BOTANCH for the chapter VII, the treatment of the DNA data were realized by Lucas AUER supervised by Guillermina HERNANDEZ-RAQUET.

1.3. The characterization of the behaviour of the cementitious linings[4]

For the chapter VII, at the end of the experiments, theoretical spatial zones were defined for the analyzed of the material behaviour, where the real pipe adaptation for the experiment (a) and the zones definition (b) were illustrated.

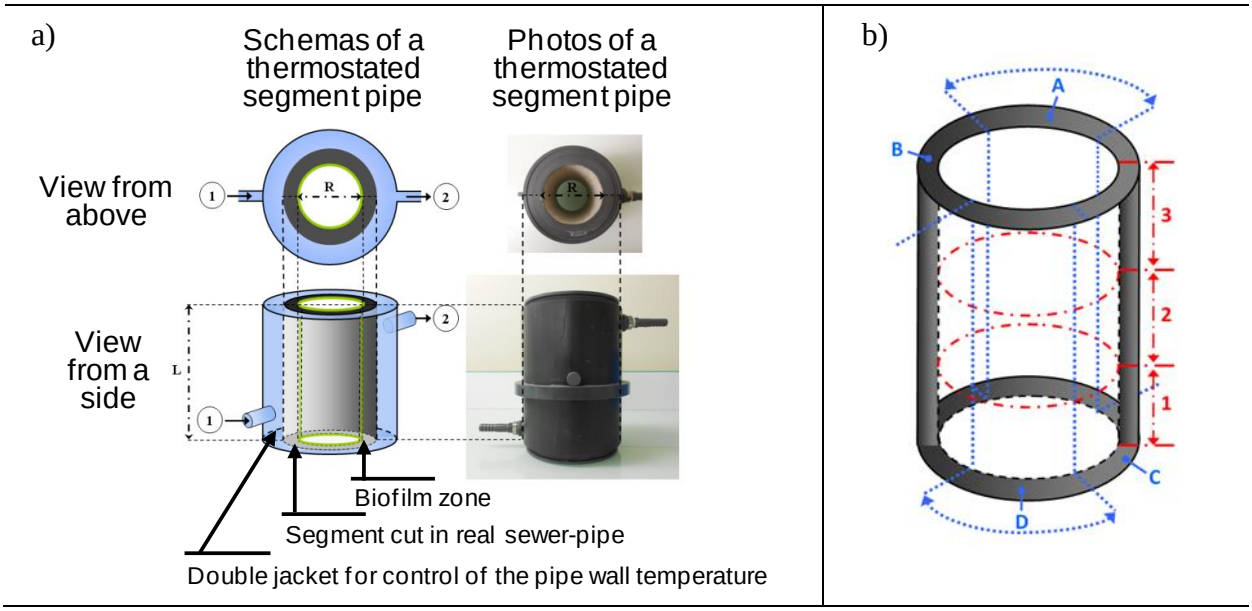

Figure 31: Illustration of the adaptation of a real pipe for the experiment of simulated microbial induced concrete corrosion (z) and the theoretical zones defined for spatial analyses of the material and the associated microbial selection (b).

1.3.1. The cementitious materials

The cementitious materials tested were, (i) Blast-Furnace-Slag Cement (BFSC) composed by Portland cement (calcium silicate $(CaO)_3.SiO_2$ and $(CaO)_2.SiO_2$) as major component and tricalcium aluminate $(CaO)_3 \cdot Al_2O_3$, tetracalcium aluminoferrite $(CaO)_4 \cdot Al_2O_3 \cdot Fe_2O_3$, and sometimes gypsum or sulfate salts as minor components) mixed with Blast-furnace waste (addition of aluminous oxides and ferric oxides and anhydrous compounds), known to have a weak resistance against biogenic sulfuric acid environment; (ii) Calcium-Aluminate Cement (CAC), composed in majority by tricalcium aluminate $(CaO)_3 \cdot Al_2O_3$, with very low percentage of sulfate salts, showing interesting behavior against acid environment (Scrivener et al., 1999) and particularly against biogenic acid (Ehrich et al.,1999) (Herisson et al.,2012).

[4] : all the analyses to characterize the cementitious materials were realized by the LMDC, via the "Division transfert de technologie" and the "Service Chimie", by Marlène FOURRE, Vanessa MAZARS, Maude SCHIETTEKATTE, Guillaume LAMBARE, Pierre NICOT and Alexandra BERTRON.

1.3.2. Characterization of the cementitious materials

At the end of the exposure period (107 days), the segment pipes were first sawn with a hand grinder to collect 5 * 5 cm specimens (ductile cast iron envelope + mortar lining). The mortar linings were then easily detached from the ductile cast iron tube. Afterwards, the mortar lining pieces were sawn more accurately with a diamond saw to prepare 1*1 cm specimens intended to microstructural testing.

1.3.2.1. Microstructural observations by scanning electron microscopy (SEM) and chemical qualification of zonal elemental composition by energy dispersive X-ray spectrometry (EDS)

Microstructural observations and chemical analyses of exposed and control specimens of mortar linings were performed using a scanning electron microscope (Jeol JSM-6380LV) fitted with an EDS detector (Rontec XFlash® 3001). Element mapping were realized by EDS. EDS uses X-ray spectrum emitted by a solid sample bombarded with a focused beam of electrons to obtain localized chemical analyses. Quantitative analyses (concentration of the elements present) measured line intensities for each elements in the sample and for the same elements in calibration Standards of known composition. X-ray intensities are measured by counting pulses generated in the detector by X-ray photons, which are emitted randomly from the sample. The ED spectra were presented with x-axis representing X-ray energy and the y-axis representing the number of counts by channel.

1.3.2.2. Chemical modifications of the linings by microanalysis (EPMA)

Chemical modifications of mortars were analysed using electron microprobe (CAMECA SX 50) (Bertron et al., 2005) (Bertron et al., 2007) (Bertron et al., 2009). The measurements were performed on flat, polished sections, according the distance to the inner surface of the lining (inoculated surface) up to the core of the specimen (about 5 mm depth). Before analyses, the polished sections were covered by metalisation of a carbon film to ensure the conduction of the electron. These analyses were performed on two specimens. A control specimen (sound lining) was also analysed. The beam was focused to obtain a analysed volume of 2*2*2 µm. The next elements were analysed: Ca, Si, Al, Fe, Mg, S, K, Na, Ti, and Mn. The analysed points were choosen with precautions to explore the hydrate paste only.

For cement paste Bertron in 2004 showed that total oxides percentages measured were always evaluated around 75%. The rest to obtain 100% include the unquantifiable elements as hydrogen, carbon as CO_2, phosphorous as P_2O_5 and some heavy-metals. The carbon and the heavy-metals count for 1 or 2% of the total oxides. The rest, around 23%, could be attribuated to the associated water of the hydrate phases of the cementitious matrices (Bertron, 2004).

1.3.2.3. Mineralogic analyses by X-ray diffraction (XRD)

Mineralogical analyses using X-ray diffraction were completed on the specimens (SIEMENS D5000) (Bertron et al., 2005) (Bertron et al., 2007) (Bertron et al., 2009). The measurements were performed on two specimens as a function of the distance to the inner surface in contact with the biofilm. These analyses were performed on the inner, slightly unbent shaped sides of the cylinders. The first analysis was done on the inner face of the specimen (in contact with the biofilm), which was then abraded and submitted to the next analysis. A control specimen (sound lining) was also analysed.

1.3.2.4. Water intrusion porosity

Water intrusion porosity tests were performed on the control specimens. The collected samples were kept in a vacuum for 4 hours to eliminate the air contained in the pores. Afterwards, the porosity of the specimens was filled with water under vacuum conditions for 12 hours. The samples were then weighed hydrostatically and then dried for 24 hours at 105°C and then weighed in air. The specific and apparent densities and the porosity were deduced from these successive weighing according to (Arliguie and Hornain, 2007).

1.3.3. Characterization of control specimens

1.3.3.1. SEM observations

The figure 32 shows SEM observations in BSE mode of cross sections of BFSC and CAC linings (control specimens). The linings, 5.6 mm thick, showed a heterogeneous, double-layer structure, causing by the production process by centrifugation: (i) the inner layer (in contact

with the biofilm), 1.6 mm thick, is a paste layer and (ii) the outer layer (in contact with the ductile cast iron tube) is a mortar layer (4.0 mm thick).

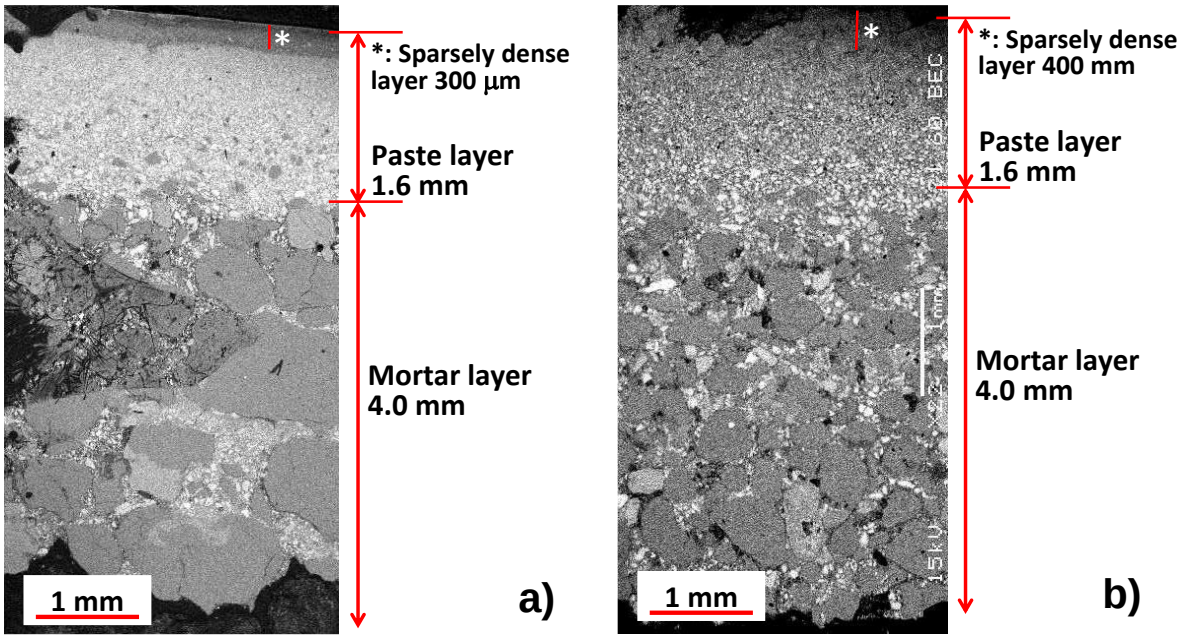

Figure 32: Observation with SEM (BSE mode) of control specimens' cross sections of mortar linings, a) BFSC and b) CAC.

CAC mortar layer showed a more compact granular packing with smaller aggregates than BFSC mortar. For both linings, the paste layer comprised a less dense layer (300 or 400 µm thick) probably linked with young age desiccation and the superficial carbonation of the lining.

No initial cracking were observed for both linings.

1.3.3.2. Water porosity of control specimen

The total porosity of control specimens of mortar linings was measured and presented in the table 11. Given the heterogeneity of the specimens, porosity was measured (i) on the paste layer (ii) on the mortar layer and (iii) on the total specimens for each type of lining. The samples in each zone were collected by sawing with a diamond saw.

Table 11: Water porosity of BFSC and CAC lining specimens.

	BFSC			CAC		
	Paste layer	Mortar layer	Tot. sample	Paste layer	Mortar layer	Tot. sample
Porosity (%)	33.8 ± 1.4	21.0 ± 1.0	24.7 ± 0.6	16.5 ± 0.6	14.6 ± 0.8	15.2 ± 0.5

CAC lining specimen shows much lower porosity than BFSC lining. In particular, the paste layer (in contact with the biofilm) of the BFSC lining is twice as more porous as the CAC lining.

1.3.3.3. Oxides composition of both paste cements for the control specimen, the theoretical neutralization capacity and the calcium content in the first 200 µm of the linings.

The table 12 presents the initial oxides composition for the cement paste of both lining.

Table 12: Oxides compositions of the cement paste for BFSC and CAC lining specimens based on mean values obtained from EPMA profiles on control specimen and porosity measurements.

BFSC paste composition in oxides									
CaO	**SiO_2**	**Al_2O_3**	**Fe_2O_3**	**MgO**	**SO_3**	**K_2O**	**TiO_2**	**Na_2O**	**Tot**
52.54 %	26.98 %	7.97 %	1.21 %	3.20 %	4.52 %	0.26 %	0.44 %	0.10 %	97.24 %
CAC paste composition in oxides									
CaO	**SiO_2**	**Al_2O_3**	**Fe_2O_3**	**MgO**	**SO_3**	**K_2O**	**TiO_2**	**Na_2O**	**Tot**
37.86 %	5.80 %	43.76 %	2.04 %	0.25 %	0.08 %	0.09 %	2 %	0.05 %	91.94 %

Due to the production of the pipe-linings by centrifugation process, the initial surfaces of the cementitious materials were only composed by the cement pastes (figure 32). Thus, after inoculation, the initial composition of the material in contact with microbial community was defined by the oxides composition presented in the table 14. Based on the oxides composition of both materials, and assuming that for 1 calcium element and 1 alumina element 2 OH^- and 3 OH^- respectively could be produced (Espinosa et al., 1996), the theoretical neutralization capacity for 1 gram of BFSC lining was 23 mmoles of H^+ neutralized, compared to 39 mmoles of H^+ neutralized for 1 gram of CAC lining (43 % more for CAC lining for the same mass of cement used).

Considering the oxides composition the volumetric mass of the cement paste was 3190 kg/m^3 for the BFSC paste and 3680 kg/m^3 for the CAC paste. Considering the oxides composition of the cement pastes and the initial porosity of the specimen, the calcium content in the first 200 µm (only composed by cement paste for both lining) for the BFSC lining was evaluated to 11180 mgCa and for the CAC lining to 11720 mgCa. Thus, in the paste layer in contact with the biological inoculum the Calcium content was quiet similar for both material (only 4.8 % more for CAC lining than for BFSC lining due to the important porosity of the initial state for BFSC lining). This data must be taken into account to analyses the calcium lixiviation during the experiments and the EPMA profiles after exposure. If decalcification occurred, the depth of the decalcified zone could be correlated to a loss of calcium.

2. Materials and methods for the study of abiotic and the biotic reactivity of thiosulfate (Chapter V and Chapter VI)

2.1. The experimental set-up for the thiosulfate abiotic conversion (Chapter V)

2.1.1. The closed batch reactor

The figure 33 represents the experimental set-up for the evaluation of the sulfur mass balance during the thiosulfate disproportionate reaction. The experimental set-up was composed by a stirred glass reactor (1.5 l of solution), isolated to the ambient air. A flow of air was continuously supply, bubbling in the bulk. The aeration served for the supply of oxygen to the solution, and as gas support for the transport of the possible gas product (as sulfur dioxide) to a trap bottle disposed at the outlet of the gas phase. The solution in the trap bottle was composed by 500 ml of soda solution (1 mol(NaOH)/l). If sulfur dioxide was produced during the thiosulfate disproportionate reaction (Johnston and McAmish, 1973), the use of soda solution will trap the acid gas.

The initial pH of the solution was controlled by the addition of HCl (37%) to the aqueous solution before the start of the reaction. The thiosulfate was added to the bulk reactor by the dissolution of pre-weighted mass of NaS_2O_3 salts (anhydrous). Then the reactor was closed. The pH and the dissolved oxygen in the bulk were measured by a glass electrode (Schott) and an optical sensor (Emmerson) respectively, and recorded on-line by the software Bios'r developed by the CRITT-GPTE (LISBP).

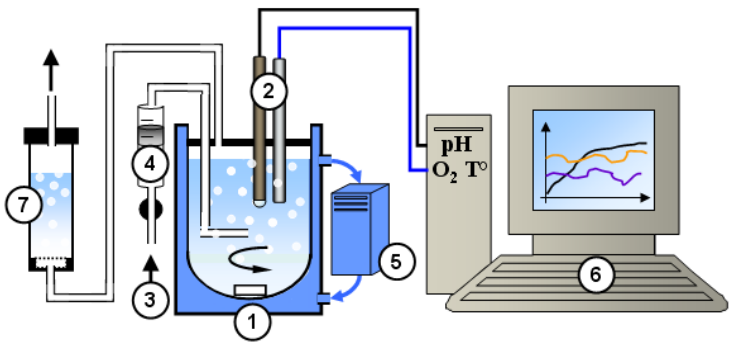

Figure 33: experimental set-up for the thiosulfate disproportionate reaction. (1) : stirred glass reactor (1.5 l), with double-jacket for the temperature control. Isolated from the ambient atmosphere. (2) : pH sensor (Schott) and dissolved oxygen sensor (Emmerson); (3) : gas inlet for the oxygen supply; (4) gas-flow meter; (5) cryostat for the temperature control; (6) on-line acquisition for the pH, the dissolved oxygen concentration and the temperature of the solution (software Bios'r); (7) trap bottle composed of a soda solution (pH = 14) for the acid-gas recovery.

With closed reactor, the analyses of the sulfur compounds were performed only at the end of the reaction. The reactor was stopped, opened, and samples were made in the different phase (bulk, trap bottle, recovery of the precipitate by filtration of the bulk solution).

2.1.2. The opened batch reactor

The figure 34 presents the experimental set-up for the dynamic experiments during the thiosulfate disproportionate reaction. The pilot was a simple adaptation of the closed batch reactor.

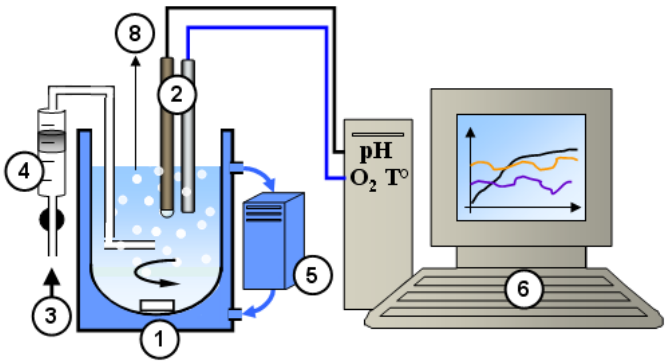

Figure 34: experimental set-up for the thiosulfate disproportionate reaction. (1) : stirred glass reactor (1 l), with double-jacket for the temperature control. (2) : pH sensor (Schott) and dissolved oxygen sensor (Emmerson); (3) : gas inlet for the oxygen supply; (4) gas-flow meter; (5) cryostat for the temperature control; (6) on-line acquisition for the pH, the dissolved oxygen concentration and the temperature of the solution (softwarel Bios'r). (8) samples of the solution.

In this configuration, during the thiosulfate disproportionate reaction several liquid samples were performed at different time (figure 34.(8)). Because the gas phase was in contact with the ambient air, in the case of sulfur dioxide stripping the achievement of the sulfur mass balance was not possible.

2.1.3. The sampling method and the chemical analyses

During the thiosulfate disproportionate reaction sulfur compounds evolutions ($S_2O_3^{2-}$ and SO_4^{2-}) were analyzed on 3 ml bulk sampling. The thiosulfate disproportionate reaction occurs in acid environment. To stop the reaction for each sample, 3 ml of soda solution (0.1 mol/l) were add to the 3 ml sample. The mixed solution was filtered at 0.2 µm. The dissolved sulfur compounds ($S_2O_3^{2-}$ and SO_4^{2-}) were analyzed by ionic chromatography (DIONEX: IC25, IonPacTM AS19).

At the end of the reaction (when the on-line measurements of pH and/or dissolved oxygen concentration stabilizing), the whole solution was filtered at 1 µm (glass-fiber filter). Then the precipitate collected was dry at 105°C during 2 hours, after the mass of the precipitate formed was quantified. In abiotic conditions, with only sulfur compounds in solution (and Na^+ and Cl^- add by the thiosulfate supply and by the hydrochloric acid supply respectively), the precipitate was assumed to be elemental sulfur.

For the closed reactor, at the end of the reaction, the ending trap solution was weighted (because during the experiment no control temperature was applied to the trap bottle, then high rate of vaporisation was observed). The mass of solution, corrected by the ambient temperature give the final volume of trap solution. The sulfur dioxide was analyzed as sulfate by ionic chromatography (DIONEX: IC25, IonPacTM AS19).

2.1.4. Measurement of the volumetric gas-liquid rate for oxygen mass transfer *(kla_{O2})*

The supply of oxygen is a key parameter for the characterisation of the secondary reactions involving the S(IV)-oxides. Before each thiosulfate disproportionate experiment, the volumetric rate for the oxygen gas-liquid mass transport (kla_{O2}) was evaluated, for the reactors configuration, by the sulfite method (Linek and Vacek, 1981) (Skobota et al., 1982). The air flow rate and the stirred velocity were fixed during the experience. Dissolved oxygen and pH were measured on-line in the same configuration of the thiosulfate disproportionate reactions. The data of the time course of the dissolved oxygen concentration ensured the kla_{O2} determination for the tested reactor configuration. The global data recorded for each kla_{O2} measurments (dissolved oxygen concentration and pH) were used after for the evaluation of the sulfite oxidation in aqueous solution (S(IV)-oxides reaction).

2.2. The experimental set-up for the thiosulfate biotic conversion (Chapter VI)

To evaluate the selection of an acidophil sulfur-oxidizing activity from an activated-sludge consortium a sequenced-batch culture were operated. A sequenced-batch was chosen to combine the advantages of a continuous culture in chemostat for the selection, and the advantages of batch system for the analyses of the dynamical phenomena.

2.2.1. The experimental setup

The figure 35 illustrates the experimental-setup operated for the selection. Feeding solutions (two flasks, one with a mix of thiosulfate add to phosphorous and some others mineral nutrient, the other with a mix of ammonium and some other mineral nutrient). The composition of the feeding solution was composed in the same way described for the experiment with cementitious linings. The table 11 presents the elemental composition of the feeding solution based on the concentration of sulfur atom in the feeding solution. The feeding solutions were provided by two peristaltic pumps, with time control. To maintain constant the reactor-volume (1 L), a waste phase was insured by a peristaltic pump with time control calibrated to obtain an outflow equivalent to the inlet-flow. The waste phase occurred always 15 min before the feeding phase.

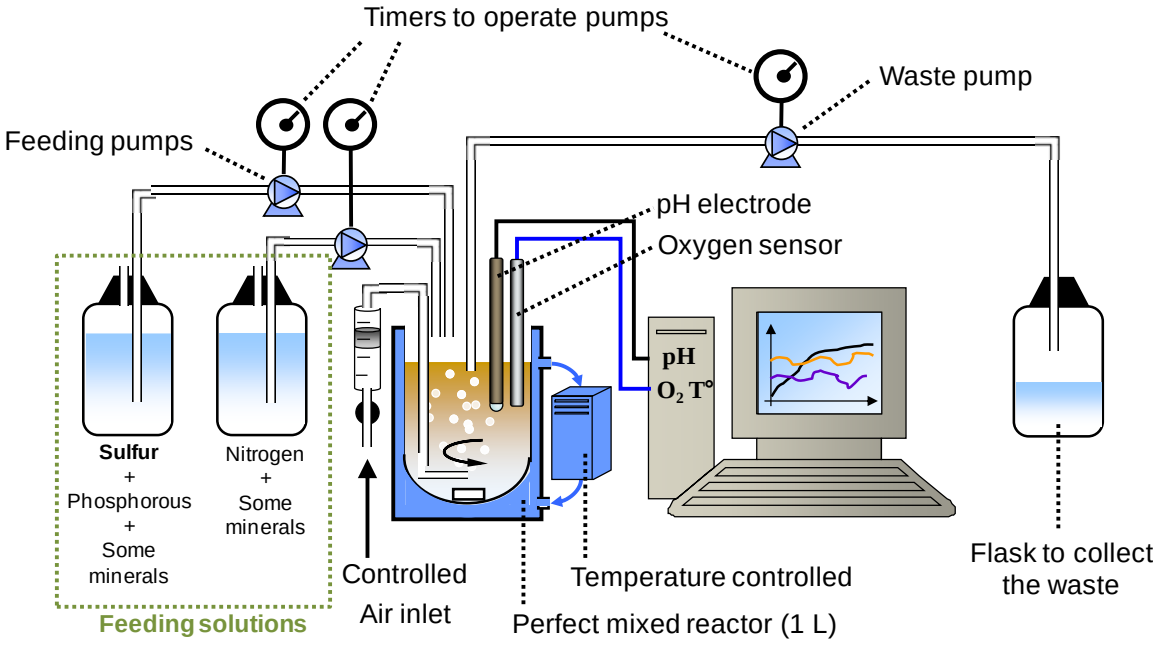

Figure 35: experimental set-up for the study of the selection of an acidophil sulfur-oxidizing activity with thiosulfate as selection factor and the study of the biological thiosulfate conversion.

In a first period of the culture, the HRT was maintained to 15.4 day (corresponding to two feeding phase and two waste phase per day). In a second period of the culture, the HRT was changed from 15.4 days to 7.3 days (corresponding to four feeding phase and four waste phase per day). Considering one thiosulfate pulse, the activity of the microbial consortium could be described by two time period, one of an intensive activity depending on the initial concentration of substrates and the microbial performances, the other when the substrates were exhausted corresponding to an endogenous respiration.

Oxygen was provided in the bulk by controlled aeration system (control of gas flow). And the solution was continuously mixed by a magnetic agitation. The temperature of the reactor was maintained at 20°C during the experiment.

2.2.2. The culture analysis

2.2.2.1. The online measurements

See page 94.

2.2.2.2. The punctual analysis

a. Particulate analysis

To evaluate the biomass selection, firstly turbidity (at 860 nm) and particulate COD were measured, (i) to observe the washout of the culture during the selection phase, (ii) to quantify the active biomass selected during the culture (in gO_2/l).

The turbidity at 860 nm was measured by the sample of 5 ml of the culture medium, stocked in a glass vial, and by the measurement in a spectrophotometer of the medium absorbance at 860 nm compared to a blank solution composed by deionised water. After the measurement, the sample was added to the culture medium. The samples were realized during the endogenous respiration period. This measurement was used as qualitative indicator of population washout occurred during the selection.

The particulate COD was measured by difference for one sample of the total COD (soluble and particulate COD) and the soluble COD obtained by the filtration at 0.2 µm of the total sample. The COD measurements were realized as described in NFT 90.101. The samples were realized during the endogenous respiration period.

b. Soluble analysis

The sampling method to analyse the soluble sulfur composes was identical to those described in the paragraph [2.1.3.] of this chapter. The concentrations SO_4^{2-}, $S_2O_3^{2-}$ were measured by anionic chromatography (DIONEX: IC25, IonPacTM AS19).

As control, to avoid undesired precipitation phenomena with sulfate, several cationic concentrations were measured in the same sample for sulfur compounds analyses. Ca^{2+}, Na^{+} were especially measured, (i) Ca^{2+} because calcium sulfate compounds are observed in real sewer environment, (ii) Na^{+} because thiosulfate was provided as sodium thiosulfate salt, and the accumulation of sodium needs to be controlled to not disturb the system.

2.2.3. The inoculum

The inoculation was realized by an activated-sludge consortium from a waste-water treatment plant near the city of Toulouse (Villefranche). The wastewater treatment plant where the sample has been realized (activated-sludge sample labeled AS 2), was different of the activated sludge sample used for the inoculation of the pipe-reactor presented in the chapter IV of this document (activated-sludge sample labeled AS 1). The sample was filtered at 400 µm, and after the filtered sample was diluted with deionized water to obtain 1 litre of inoculum at 0.8 gMES/l.

2.2. Simulation of the chemical and the biological processes by Aquasim®

The dynamic models, chemical and biological, have been developed on the modeling software Aquasim® that has been developped by Reichert (Reichert, 1994). The compartement labelled “Mixed Reactor Compartment” has been used. The description of this compartment is based on the user-manual free for access at **www.eawag.ch/forschung/siam/software/aquasim/pdf/aquasim_manual.pdf.**

This compartement describes inflow, outflow and transformations processes of substance in a completely stirred reactor with constant or variable volume (batch, fed-batch and chemostat). The equations solved by the software are:

If the volume is considered as variable (fed-bacth), the current volume of the compartement

Eq 43 : $dVr/dt = Q_{in} - Q_{out}$

where t is time, Vr is the reactor volume, Q_{in} the volumetric inflow, and Q_{out} the volumetric outflow.

The temporal change of the concentration of substances dissolved or suspended in the water is given by the following equation (Eq 44):

Eq 44 : $$dC_i/dt = I_{in,Ci}/Vr - Q_{in}/Vr + r_{Ci}$$

where C_i is the substance concentration represented by a dynamic volume state variable, $I_{in;Ci}$ is the loading of the substance described by the concentration C_i into the reactor (mass per unit of time), and r_{Ci} is the transformation rate of the substance described by the concentration C_i. This concentration rate is given as the sum of the products of the process rates times the stoichiometric coeffcients of the substance described by the concentration Ci of all processes active in the compartment.

Chapter IV

Liquid phase and sulfur substrates in contact with cementitious materials

1. Introduction

1.1. Definition of a biodeterioration essay for sewer environment

The major role of the biological activities highlighted in the deterioration of the cementitious materials occurring in sewer-networks, led to the proposition of several experimental devices during the last 40 years (see chapter I). The design of these experimental devices was always linked to the progresses of the knowledges about the several processus involved in these deteriorations.

To be efficient a test needs to reproduce and accelerate the real processes involved in the observed deteriorations. The validity of a test design, and its fiability, is based on its representativness and its reproducibility: (i) the representativness requires the knowledge about the several processes involved in the whole phenomenon. This knowledge enables the validation of the simplification ways choosen ensuring the defintion of the system, (ii) in other hand, the reproducibility of a test ensures its efficiency. This need of reproducibility requires the control of the operating conditions and the quantification in time of the transformations.

With this both objectives, the chapter I presented a literature review about the processes and the environmental conditions leading to strong deteriorations in sewer-networks. Based on it, the present paragraph will present the main choices of simplification and their arguments to obtain an experimental device (described in the M&M chapter III) to reproduce, accelerate the main phenomena involved in the deterioration of cementitious linings in sewer environements.

1.2. Proposed system for the study

1.2.1. Main choices

Microbial activity and cementitious lining deteriorations are linked. However the time scales for each compartment are different, drive in time by the microbial activity. Thus, to control the system it appears essential to quantify in time the biological transformations linked to the evolution of the linings. In that case, the adaptation of the system to ensure regular measurements for mass balances evaluation, facilitated by the use of safe compounds, and

without destruction of material, seems an interesting option for the selection and the development of a controlled microbial activity in contact with materials.

The literature review about the transformations of sulfur compounds indicated the abiotic reactivity of the dissolved sulfide (H_2S, HS^- and S^{2-}) and the production in contact with cementitious materials of more stable compounds such as thiosulfate and elemental sulfur. These compounds, unvolatile and safe for health, appear to be interesting for a test design. Moreover, the objective to realize mass balances to quanfy the acid and the sulfates fluxes produced in contact with the cementitious lining highlighted that a soluble compound such as thiosulfate ($S_2O_3^{2-}$) could be a good compromise as sulfur source.

Indeed, working with a soluble, chemically stable sulfur compound under controlled conditions, allows starting the culture on cementitious materials with an extremely diversified consortium. In that case, the control of the operating condition should ensure the selection and the development of a microbial consortium adapted to the material, and the quantification of the microbial activity by mass balances.

To evaluate these two main choices ((i) work by soluble medium with thiosulfates as a source of sulfur, (ii) starting from a diversified inoculums from wastewater environment) the following paragraphs present a synthetic literature review according to the diversity of the sulfur-oxidizing bacteria (SOB) and their adaptation to thiosulfate oxydation.

1.2.2. Diversity of the sulfur-oxidizing bacteria: example of the Thiobacillus genera or equivalent

As described in the chapter I, the biological oxidation of sulfur compounds is a complexe phenomenon, involving several abiotic reactions and several metabolic pathways (shared or specific of some microbial species) (Mason et al., 1987) (Kelly et al., 1997). To illustrate the huge diversity of sulfur-oxidizing bacteria potentially meet in sewer system, depending on the growth conditions as pH and the sulfur compounds oxidized, a literature review is proposed and presented in the table 13 and the table 14. The first objective of this literature review is to support the double choice of thiosulfate as sulfur source coupled to a diversified inoculum (sampled from wastewater) in order to select and develop a sulfur-oxidizing activity in contact with cementitious material. The second objective is to propose a data-base of microbial parameters (kinectic and stoichiomertic) of sulfur-oxidizing bacteria in order to evaluate the results obtain in the next chapters.

Table 13: literature review for microbial parameters of sulfur-oxidizing species grown under different culture systems

Species and metablism	**Culture**	**Sulfur source**	**Products of the sulfur oxidation**	**pH**	**T°**	$\mu_{SOB}(T)$ **(h^{-1})**	$Y_{X/Sub}$ **(gX /molSubstrate)**	$Y_{X/S}$ **(gX/molS)**	**maintenance (mmolsubstrate / gX.h)**	K_{Sub} **µmol/L**	**Ref**
T.neapolitanus	Chemostat	Thiosulfate	Sulfate	7.0*		0.4 (max)	13.9	6.95	21.8		Hempfling 1967
Autotrophe	"	Thiosulfate	Sulfate	6.8-7.3	28-30°C	0.43 (max)					Gottschal 1979
	Chemostat	Thiosulfate	Sulfate	6.8*	30°C	0.4	8.6 – 9.3	4.3 – 4.65	6.7 ± 1.5		Mason 1987
	"	Trithionate	Sulfate	6.8*	30°C	0.2	8.8 – 9.1	2.9 - 3	3.3 ± 0.8		"
	"	Tetrathionate	Sulfate	6.8*	30°C		15.9 – 17.2	4 – 4.3	3.6 ± 0.3		"
	Chemostat	Sulfide	Sulfate	6.8*	30°C	0.06	4.2-4.4	4.2-4.4			Stefess 1996
	"	Thiosulfate	Sulfate	6.8*	30°C	0.06	4.2-4.4	2.1-2.2			"
	"	Thiosulfate	Sulfate	6.8*	30°C	0.35 (max)					"
	Batch	Thiosulfate	Sulfate	3.7 –10		0.081 (max)	3.14 – 3.66	1.57 – 1.83			Bielefeldt 2010
Paracoccus versutus*	Chemostat	Thiosulfate	Sulfate	7.8*	30°C	0.42	7.9 – 8.3	3.95 – 4.15	1.1 ± 0.2		Mason 1987
	"	Tetrathionate	Sulfate	7.8*	30°C	no growth					"
Mixotrophe	Chemostat	Thiosulfate		7.2	28°C	0.106 (max)					Beffa 1991
	Batch	S^0		7.2	28°C	0.106 (max)					"
T.thioparus	Batch	Thiosulfate	Sulfate/S^0	7.8 – (4.4 or 6)		0.0025 – 0.0057	0.83	0.415			Starkey 1935
Autotrophe	Batch	Thiosulfate	Sulfate	6*	30°C	0.067 (max)	17.94 – 32.06	8.97 – 16.03			Alcantara 2004
	Batch	Thiosulfate	Sulfate	5.6-7.8	30°C	0.063 (max)	15.4 – 33.4	7.7 – 16.7			Bielefeldt 2010
A.Acidiphilium	Chemostat	Thiosulfate	Sulfate	3.0*	30°C	0.025	5.5 ± 0.1	2.75			Mason 1987
(T. acidophilus)		Trithionate	Sulfate	3.0*	30°C	0.025	7.0 ± 0.1	2.33			"
Mixotrophe		Tetrathionate	Sulfate	3.0*	30°C	0.025	12.5 ± 0.6	3.12			"
A.thiooxidans	Batch	S^0	Sulfate	0.9-1.0	30°C	0.0135					Sivaji Rao 1971
(T. thiooxidans)	"	"	Sulfate	2.1-2.3	30°C	0.0625					"
T.concretivorus	"	"	Sulfate	3.0-3.2	30°C	0.05					"
Autotrophe	"	"	Sulfate	4.2-4.3	30°C	0.02					"
	Chemostat	Thiosulfate	Sulfate	2.5*	30°C	0.034	6.2 (obs)	3.1			Mason 1987
	"	Tetrathionate	Sulfate	2.5*	30°C	0.034	12.1	3.02	0.4 ± 0.2		"
	Batch	S^0	Sulfate	1.5	30°C	0.11 (max)	1.97 – 3.29	1.97 – 3.29			Konishi 1995
	Semi-continuous	Thiosulfate	Sulfate	5*	28°C	growth					Masau 2001
	"	S^0		2.3*	"	no growth					"
		"	Sulfate	1.5-2.5		0.12					Chen 2002
	Batch	"	Sulfate	1.3		0.0092 (max)					Bielefeldt 2010
Starkey Novella** *Hétérotrophe*	Batch	Thiosulfate	Sulfate	7.8 – 7.2			2.08	1.04			Starkey 1935

*: culture realized with buffered solution.**: labeled as *Thiobacillus versutus* before 1995 (Katayama et al., 1995). ***: labeled as *Thiobacillus novellus* before 2000 (Kelly et al., 2000c)

Table 14: literature review for microbial parameters of sulfur-oxidizing species grown under different culture systems

Species and metablism	**Culture**	**Sulfur source**	**Products of the sulfur oxidation**	**pH**	**T°**	$\mu_{SOB}(T)$ **(h^{-1})**	$Y_{X/Sub}$ **(gX /molSubstrate)**	$Y_{X/S}$ **(gX/molS)**	**maintenance (mmolsubstrate / gX.h)**	K_{Sub} **µmol/L**	**Ref**
T.tepidarius	Chemostat	Tetrathionate	Sulfate	7*	44°C	0.44 (max)	20.5	5.125	2.6		Wood 1986
autotroph	"	Thiosulfate	Sulfate	7*	44°C	0.2	10.9	5.45	6.7		"
	"	Trithionate	Sulfate	7*	44°C	0.2	10.9	3.63	6.7		"
	"	Sulfide	Sulfate	7*	44°C	0.2	10.9	10.9	6.7		"
	Chemostat	Thiosulfate	Tetrathionate	7*	44°C	0.2				120	Lu 1988
	"	Tetrathionate	sulfate	7*	44°C	0.2				27	"
	"	Thiosulfate		4.8*	44°C	no growth					"
T. denitrificans	Chemostat	Thiosulfate	Sulfate			0.03	18.5 (/Oxygen) 11.6 (/Nitrate)	9.25 5.8			Timer-Ten Hoor 1981
autotroph	Chemostat	Thiosulfate	Sulfate	7*			20.6 (/Oxygen) 14.5 (/nitrate)	10.3 7.25			Kelly 1999
T. ferrooxidans	Chemostat	Thiosulfate	Sulfate	3*	30°C	0.016	4.9	2.45			Hazeu 1986
autotroph	"	"	"	"	"	0.021	4.9	2.45		9	"
	"	"	"	"	"	0.031	6.3	3.15		20	"
	"	"	"	"	"	0.037	5.5	2.75			"
	"	Tetrathionate	Sulfate	3*	30°C	0.006	6.3	1.575			"
	"	"	"	"	"	0.008	9.9	2.475			"
	"	"	"	"	"	0.012	9.7	2.425			"
	"	"	"	"	"	0.020	8.6	2.15		3.7	"
	"	"	"	"	"	0.023	9.0	2.25			"
	"	"	"	"	"	0.026	8.9 – 9.9	2.225-2.475			"
	"	"	"	"	"	0.030	10.3	2.575			"
	"	"	"	"	"	0.030	12.3 – 13.6	3.075-3.4		3.5	"
	"	"	"	"	"	0.14 (max)					
SOB	Semi-continuous	Thiosulfate	Sulfate	6.5-8	21°C	0.061	4.75	2.37			Schreiber 1998
Thiobacillus sp	Batch	S^0 (bio)	Sulfate	1-3.5		0.082					Tichy 1994
	"	S^0	Sulfate	1.5-3.5		0.08					"
	Chemostat	Sulfide	Sulfate	6.8*	30°C	0.06	4.2-4.4	4.2-4.4			Stefess 1996
	"	Thiosulfate	Sulfate	6.8*	30°C	0.06	8.4-8.8	4.2-4.4			"
	"	Thiosulfate	Sulfate	6.8*	30°C	0.33-0.35 (max)					"
	Batch	Sulfide	Sulfate	8-9			3.4	3.4	b = 0.13 d^{-1}		Munz 2009
	Batch	S^0	Sulfate	8-9		0.31 (max)	2.62	2.62		93.5	"
Corroded concrete	Batch	Sulfide	Sulfate	1	22°C	0.052 – 0.055					Jensen 2011

*: culture realized with buffered solution.

From the tables 13 and 14 the following remarks could be highlighted:

- Numerous studies have been realized, about numerous SOB species, cultured under several sulfur environments (as sulfide, thiosulfate, elemental sulfur or tetrathionate for example). The mode of culture were different (batch or chemostat), with controlled operating conditions as pH and temperatures.
- Microbial parameters (for kinetic and stoichiometry definition) have been fixed or evaluated. Strong variation shall be noted, depending on the SOB species, driven by the mode of culture and the sulfur source, especially for specific growth rate ($\mu_{SOB}(T)$) and net biomass yield ($Y_{X_{SOB}/S}$). These tables (tables 13 and 14) illustrate the high diversity for SOB species in terms of growth and carbon assimilation (from autotrophic bacteria, to mixotrophic bacteria)
- The high diversity in terms of specific growth rate, highly dependent of the pH conditions, illustrates the behavior and the evolution of the SOB community during the local acidification at the surface of a cementitious lining.

Moreover, the table 13 and the table 14 higlight that all SOB species are able to grow with thiosulfate as sole sulfur source, even the acidophilic species (Gosh and Bomba, 2009). Thus thiosulfate as selection factor appears jusitifed to develop SOB activity on cementitious lining based on inoculums sample from a wastewater treatment plant.

1.3. Schematic system to study the biodeterioration of cementitious lining in sewer-like environment

Some qualitative data exist on sulfur-oxidizing activity in an H_2S sewer environment (Satoh et al., 2009), and some quantitative experiments have been performed ex-situ (De Belie et al., 2004) (Bielefeldt et al., 2010) (Jensen et al., 2011). However, as described in the chapter I of this document many sulfur-oxidizing bacterial species take part in the MICC (Vincke et al., 2001) (Roberts et al., 2002) (Okabe et al., 2007). Focusing only on the sulfur requirements for growth it has been demonstrated that some sulfur-oxidizing bacteria identified in MICC cannot use hydrogen sulfide (Vollertsen et al., 2008). Actually, to our knowledge, at low pH only one study demonstrated the growth of acidophil SOB from

corroded concrete with H_2S feeding, with elemental sulfur as biological intermediate (Jensen et al., 2011). But in this study, to quantify the sulfur-oxidizing activity, the corroded concrete samples were immerged in liquid solution at pH 1. On the contrary, the main identified SOB can grow on at least one of the less reduced sulfur compounds, such as elemental sulfur, tetrathionate or thiosulfate (Kelly, 1999) (Roberts et al., 2002) (Bielefeldt et al., 2010).

The direct use of H_2S gas as sulfur substrate for the microorganisms involved in MICC limits a dynamical and quantitative analysis of the sulfur oxidizing activity by sulfur mass balances. The high reactivity of dissolved sulfide (H_2S, HS^- and S^{2-}) associated to the high toxicity of the gaseous H_2S explained this limitation. In other hand, to optimize the growth conditions and intensified the interactions between the biological activity and the evolution of the cementitious material, the control of others nutrients, as nitrogen and phosphorous as example is necessary. In a gaseous system, to represent aerosol, concentrated nutrient solutions must be sprayed regularly at the surface of the cementitious materials.

In this context, with the selection and the quantification of a SOB activity on cementious lining as main objectives, a simplified system was proposed. The figure 36, based on the figure 17 defined at the chapter I by the literature review, presented the simplification of the system to represent MICC in controlled environment.

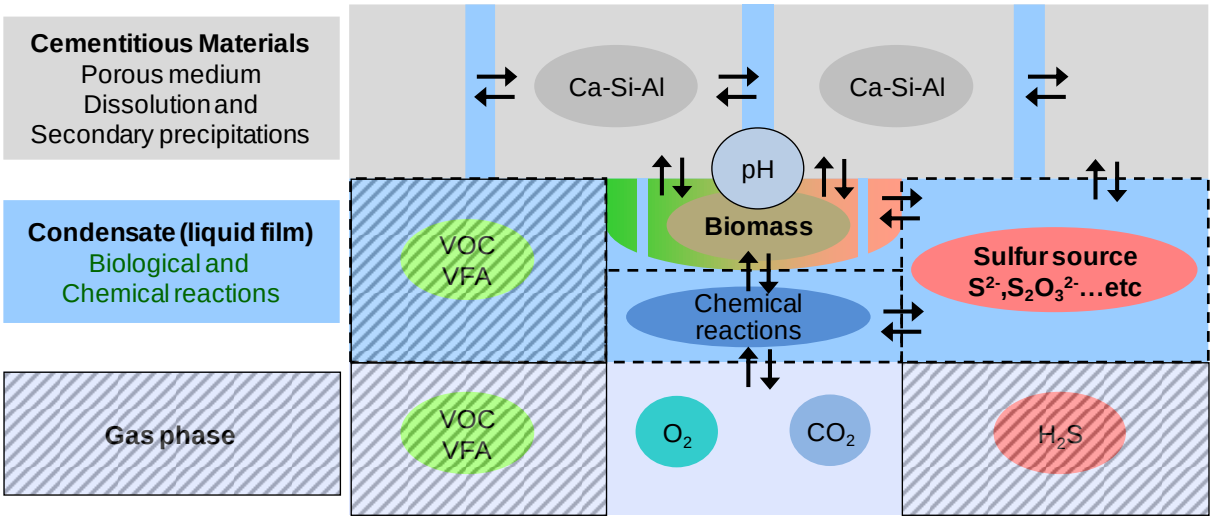

Figure 36: Simplified schema of the biotdeterioration system adapted to study the interaction between sulfur-oxidizng acivity and cementious materials (based on the schema described at figure 17 of the chapter I).

1.4. Objectives

The objective of this chapter is to improve the control of the culture conditions in order to be able to quantify biological and chemical transformations and then to elaborate a quantitative approach of a simplified MICC system defined by the interaction of SOB activity and the cementitious materials.

Sulfur mass balances will allow (i) biotic and abiotic transformations to be compared for both sulfur substrates and (ii) quantification in time the role of the sulfur-oxidizing activities developed directly in contact with the cementitious linings. The analyses of the leaching solution under different conditions (abiotic / biotic and for both sulfur substrates) will be used as a first indicator to evaluate the behaviour of the cementitious lining under different sulfur compounds environment. At the end of the experiment the biological activities selected will be confronted to the 16S rDNA identification of the selected bacterial populations.

2. Specific materials and methods

The pilot used in this chapter has been presented in the M&M section (chapter III), as the analytical techniques and methods.

2.1. Choice of the cementitious lining

For this study, a lab-scale pilot including two real pipe segments with a concrete lining composed of calcium-aluminate-cement (CAC) was designed. To differentiate between biological and chemical oxidation of the sulfur substrates, one of the pipe-segments was inoculated with a non-specified microbial population (activated-sludge consortium: AS 1) while, in the other segment, cell growth was avoided by performing no inoculation and by imposing complete nitrogen starvation in the feed. Thus, in the first reactor, both biological and chemical reactions occurred but, in the second, only chemical reactions could take place (figure 27 of the M&M).

2.2. Experimental sequences and operating conditions

The experiments were divided into four phases, illustrated in the figure 37.(i) Phase 1 from day 0 to day 70 was an acclimation phase, characterized by a regular increase in the sulfide inlet load to intensify sulfur oxidation, (figure 37.ii) Phase 2 from day 70 to day 121 was characterized by a constant sulfide inlet-load, (figure 37.iii) Phase 3 from day 121 to day 170 had a constant thiosulfate load, equivalent to the Phase 2 in terms of sulfur equivalent load, and (figure 37.iv) Phase 4 was a long-term test phase lasting from day 170 to day 264, in which the thiosulfate inlet load was increased step by step. During the acclimation phase (figure 37.i) the nitrogen inlet load was maintained constant (concentration in inlet feeding solution = 1.7 mgN-NH_4.L^{-1}). For phases 2 and 3 (figure 37. ii and iii) the nitrogen inlet load was increased and maintained constant for the biotic pipe reactor to avoid nitrogen limitation for the biological transformation. The objective of Phase 4 (figure 37.iv) was to make a long-term study at a high sulfur inlet load to expose the concrete linings to the effect of significant biological sulfur oxidation.

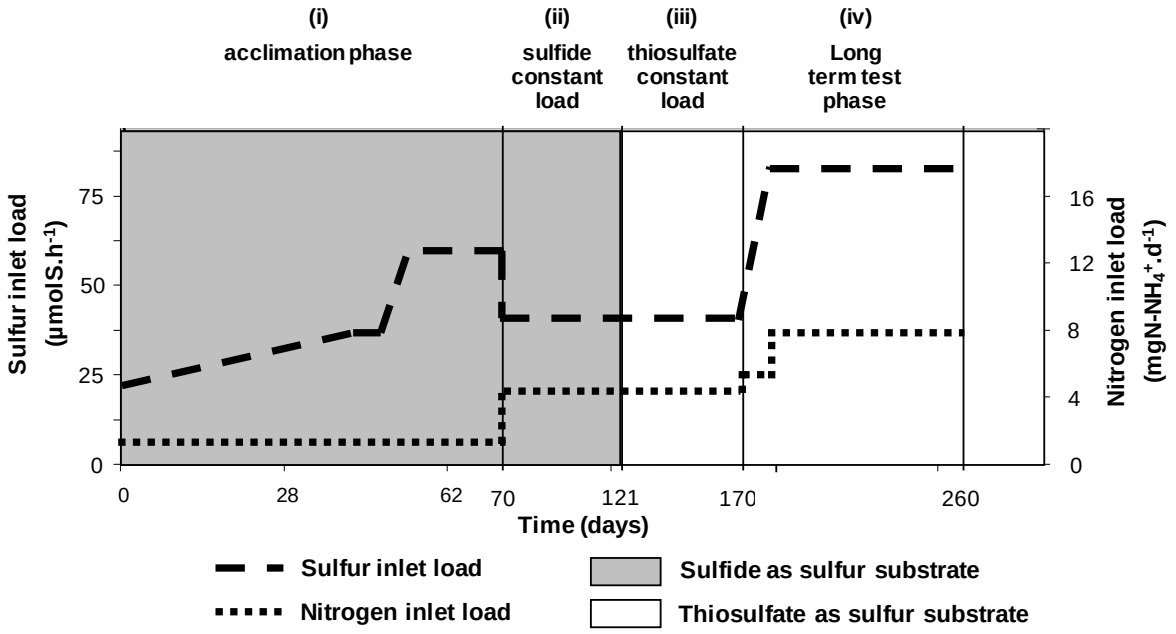

Figure 37: Experimental sequence defines as time period for abiotic and biotic segment pipe in terms of sulfur substrate used, loading of equivalent sulfur and the nitrogen loading (as ammonium) provide by the feeding solution.

3. Results and discussion

3.1. Visual observations of the abiotic and biotic pipe-reactors

The photographs presented in the figure 38 show the difference between the abiotic and the biotic pipe-reactors at day 20 (during the acclimation phase). In the abiotic pipe-reactor, the concrete surface is clearly visible (figure 38.A), while heterogeneous colonization can be observed on the concrete surface of the biotic pipe-reactor (figure 38.B), due to preferential way for the trickling feeding solution.

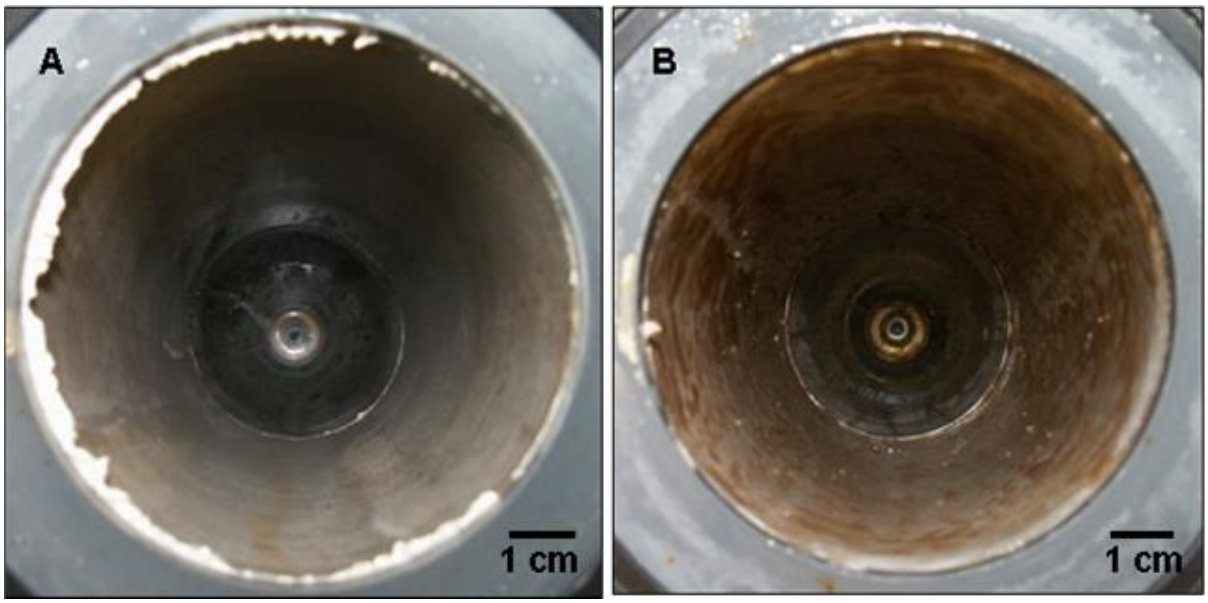

Figure 38: photos at day 20 of the abiotic pipe-reactor (A) and the biotic pipe-reactor, visual comparisons of the surface the piper-reactor, no-colonized in the case of the abiotic pipe-reactor and colonized in the case of the biotic pipe-reactor.

3.2. Comparison of sulfide (S^{2-}) and thiosulfate ($S_2O_3^{2-}$) in the feeding solution

In order to know the exact nature of the sulfur compounds fed to the pipe-reactor, the sulfur composition of the feeding solution was analysed at the beginning and at the end of each supply period. Representative initial sulfide or thiosulfate concentrations and final sulfate [SO_4^{2-}], thiosulfate [$S_2O_3^{2-}$] and sulfide [S^{2-}] concentrations found in the feeding solution are given in the figure 39 for the (S^{2-})-phase (first part of the graph) and for the ($S_2O_3^{2-}$)-phase (second part of the graph).

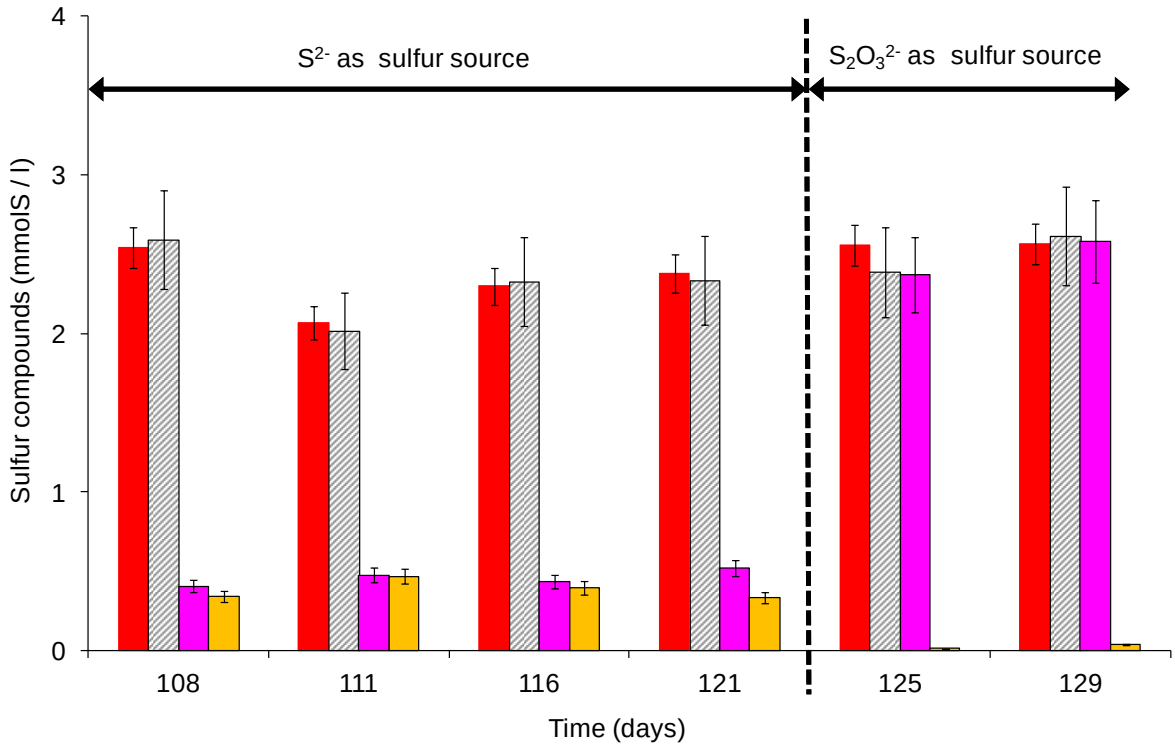

Figure 39: sulfur mass balances for the sulfur feeding solution between initial and the end of the feeding phase, for four feeding solutions of sulfide (S2-) and two feeding solutions of thiosulfate after the change of sulfur substrate. ■ : initial concentration of sulfur in the feeding solution (mmolS/l); ▨ : final total sulfur concentration in the feeding solution (S^{2-} + $S_2O_3^{2-}$ + SO_4^{2-}) (mmolS/l); ■ : final thiosulfate concentration in the feeding solution (molS/l); ■ : final sulfate concentration in the feeding solution (molS/l).

As expected from the literature, the experimental results show that soluble sulfide (S^{2-}) is not stable in the feeding solution and is partly oxidized leading to thiosulfate and sulfate. Consequently, even when S^{2-} alone is supplied and the feed is regularly renewed, a mixture of S^{2-}, $S_2O_3^{2-}$ and SO_4^{2-} is in reality fed into the reactors. In fact, from the 39 analyses performed during the (S^{2-})-phase, around 47 ± 17% of the initial S^{2-} load is oxidized before reaching the pipe-reactors and transformed into either sulfate (for 22 ± 9% of the initial S^{2-}) or thiosulfate (for 24 ± 10% of the initial S^{2-}) (figure 39). The variation in the oxidation level depends on the storage duration before renewal and on the initial S^{2-} concentration. Hence, when sulfate is formed electron donor is lost for SOB. In contrast, when thiosulfate is added into the feeding solution, it remains stable over time (see the figure 39 after the change of sulfur source after the day 121).

3.3. Competition of sulfur-oxidizing activity and nitrifying activity

Because nitrogen as ammonium is needed to ensure SOB growth with no limitation, undesired competition by nitrifying activity can occur. To evaluate this competition, sulfur and nitrogen mass balances are realized all along the experiment. Firstly the sulfur-oxidizing activity was evaluated, depending on the sulfur source, by the comparison between biotic and abiotic environment. There after, nitrifiers activity was observed and compared in the biotic pipe reactor.

3.3.1. Sulfur oxidizing activity

The figure 40 presents the pH of the leaching solution and the sulfur compounds fluxes during day 70 to day 171 for the abiotic pipe-reactor (A) and the biotic pipe-reactor (B) (during day 70 to day 121, S^{2-} was used as sulfur source, during day 121 to day 171 $S_2O_3^{2-}$ was used as sulfur source).

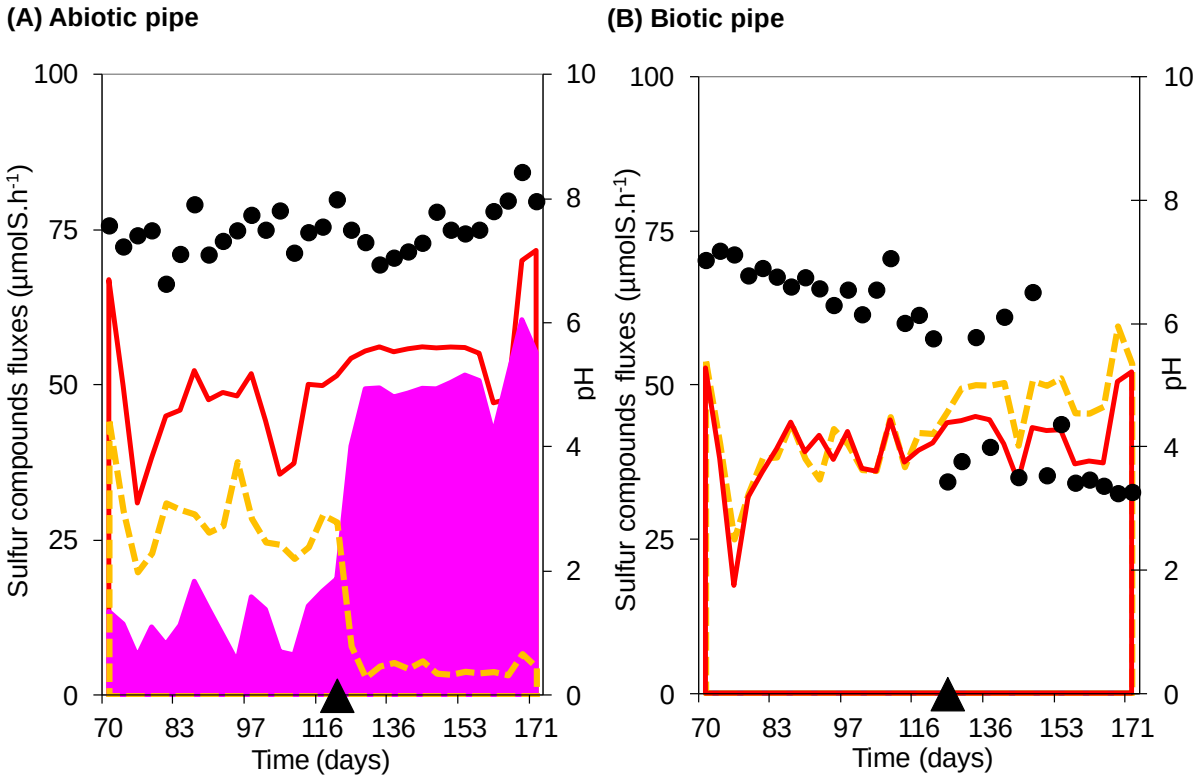

Figure 40: Analyses of the leaching solution (pH and sulfur compounds) for abiotic (A) and the biotic (B) pipe reactor. ● : pH of the leaching solution; —— : inlet sulfur fluxes (µmolS.h^{-1}); - - - : sulfate outlet fluxes in the leaching solution (µmolS.h^{-1}); ▬ : thiosulfate outlet fluxes in the leaching solution (µmolS.h^{-1}); ▲ : change of the sulfur compounds in the feeding solution (S^{2-} to $S_2O_3^{2-}$).

During the (S^{2-})-phase (from day 70 to day 121), abiotic S^{2-} oxidation on the CAC lining appears complete (sulfur mass balance recovery of 91% ± 2% for 6 sampling dates) leading to a final production of sulfate and thiosulfate (figure 40.A). A rather stable pH value around 7.5 is recorded for 51 days. During the same period in the biotic pipe reactor (figure 40.B), the sulfur mass balance also complete shows a total oxidation of initial S^{2-} to sulfate (sulfur mass balance recovery of 102% ± 5% for 15 sampling dates). This total oxidation is linked to an acidification of the medium. pH of the leaching solution decreases continuously from 7.2 to 5.8 over the same 51 days, revealing the development of a SOB activity (acidification and sulfate production) at the surface of the biotic CAC lining.

The sulfur fluxes at the pipe-reactor scale for the abiotic and biotic pipe-reactors can be described by the following mass balance equations (Eq 45) and (Eq 46) (in µmolS.h^{-1}) respectively:

Eq 45: $(50 \pm 3)\ S\text{-}S^{2-} \rightarrow (31 \pm 4)\ S\text{-}SO_4^{2-} + (14 \pm 6)\ S\text{-}S_2O_3^{2-}$ *[abiotic]*

Eq 46: $(39 \pm 3)\ S\text{-}S^{2-} \rightarrow (40 \pm 4)\ S\text{-}SO_4^{2-}$ *[biotic]*

Comparing equations 45 and 46 abiotic oxidation of S^{2-} represents a major part of the total oxidation of S^{2-} even in biotic conditions. Moreover the global differences of sulfur mass balances observed between the biotic and the abiotic pipe-reactors confirm the biological sulfur oxidation and highlights the role of thiosulfate as a major biological intermediary substrate in the experimental conditions.

At day 121sulfide (S^{2-}) is replaced by thiosulfate as the primary sulfur source. The new pH of the feeding solution is 5.8. The sulfur inlet load and the nitrogen inlet load are maintained at 41 µmolS.h^{-1} and 3.6 ± 0.1 mgN.d^{-1} respectively during the (S^{2-})-phase and at 40 µmolS.h^{-1} and 3.6 ± 0.1 mgN.d^{-1} during the ($S_2O_3^{2-}$)-phase. The only difference between this experiment and the previous one is the nature of the sulfur source.

In the abiotic pipe-reactor (figure 40.A), 95% ± 5% of the thiosulfate of the supply solution was measured as thiosulfate in the leaching solution. Therefore, only 5% ± 5% of the initial thiosulfate was oxidized to sulfate. The pH of the leaching solution was unstable (from 7 to 8.4). However no acidification of the medium was recorded. Between day 121 and day 170, 11 sulfur mass balances (mass balance recovery of 97% ± 2%) indicated that the sulfur flux could be described by the following mass balance equation (Eq 47) (µmolS.h^{-1}):

Eq 47: $(56 \pm 1)\ S\text{-}S_2O_3^{2-} \rightarrow (50 \pm 1)\ S\text{-}S_2O_3^{2-} + (4 \pm 1)\ S\text{-}SO_4^{2-}$ *[abiotic]*

In the biotic pipe-reactor, the thiosulfate was totally oxidized and transformed into sulfate (figure 40.B). Strong acidification of the leaching solution was recorded, pH decreased in three days from 5.8 to 3.44. After that, during 28 days the pH of the leaching solution was instable, oscillated between 3.5 and 6.5. At day 156, the pH of the leaching solution stabilized and then slightly decreased for the rest of the experiment. At the same time, from thirteen sulfur mass balances performed between day 121 and day 170 (mass balance recovery of 106% ± 3%), the sulfur fluxes at the pipe-reactor scale could be described by the following mass balance equation (Eq 48) ($\mu molS.h^{-1}$):

Eq 48: $43 \pm 5\ S\text{-}S_2O_3^{2-} \rightarrow 45 \pm 5\ S\text{-}SO_4^{2-}$ *[biotic]*

Considering MICC with CAC lining, closing the sulfur mass balances from soluble analyses only indicates, if secondary precipitation occurred inside the cementitious material, that only a very low part of sulfate (in the range of the uncertainty) could be trapped. This point will be illustrated and discussed in the chapter VII of this document, by several analyses of exposed cementitious linings.

For the ($S_2O_3^{2-}$)-phase the difference between abiotic sulfur mass balances (Eq 47) and biotic sulfur mass balances (Eq 48) confirms the predominant role of the biological thiosulfate oxidation. Because thiosulfate was stable in abiotic conditions comparatively to soluble sulfide (S^{2-}), the sulfur mass balance associated to the pH decrease confirms the interest of thiosulfate as sulfur substrate to select a sulfur-oxidizing activity on cementitious lining. However, the absence of any nitrifying activity must be demonstrated.

3.3.2. Nitrifying activity in competition with sulfur-oxidizing activity

After the acclimation phase (from day 0 to day 70), to avoid growth limitation by a nitrogen deficiency, the inlet nutrient load was increased from 2.2 $mgN\text{-}NH_4^+.d^{-1}$ to 3.7 $mgN\text{-}NH_4^+.d^{-1}$, giving an inlet concentration of 2.9 $mgN\text{-}NH_4^+.l^{-1}$ in the trickling solution. The figure 41 shows the ammonium inlet and outlet fluxes, the nitrate and nitrite production fluxes during the sulfide, and the subsequent thiosulfate, feeding phases. Especially between day 81 and day 121, ammonium was almost totally consumed and transformed into nitrates (nitrogen mass balance 104% ± 10% for 12 analyses).

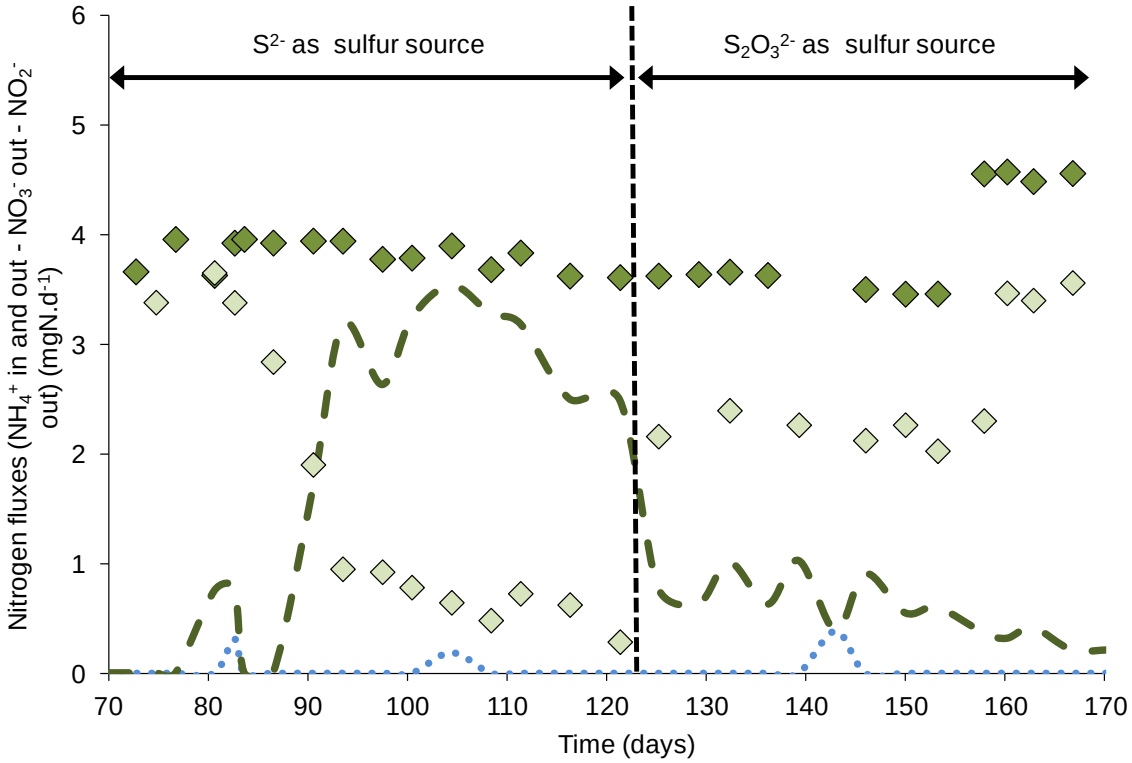

Figure 41: Analyses of nitrogen compounds in the leaching solution for the biotic-pipe reactor. ◆ : ammonium inlet fluxes (mgN.d^{-1}); ◇ : ammonium outlet fluxes in the leaching solution (mgN.d^{-1}); – – –: nitrate fluxes produced in the leaching solution (mgN.d^{-1}); ••••• : nitrite fluxes produced in the leaching solution (mgN.d^{-1}).

Hence, under S^{2-} feeding a nitrifying activity was recorded, consuming a huge part of the ammonium flux. This nitrifying activity could be in competition with the sulfur oxidizing activity for the ammonium and for the oxygen needs.

The total oxidation of sulfide (S^{2-}), thiosulfate ($S_2O_3^{2-}$) and ammonium (NH_4^+) and their influence on the acidity of the medium are described by the following equations respectively (Eq 49, Eq 21 and Eq 50).

Eq 49: $S^{2-} + 2\,O_2 \rightarrow 2\,SO_4^{2-}$

Eq 21: $S_2O_3^{2-} + 2\,O_2 + H_2O \rightarrow 2\,SO_4^{2-} + 2\,H^+$

Eq 50: $NH_4^+ + 2\,O_2 + H_2O \rightarrow NO_3^- + 2H_3O^+$

The mean production of 3 mgN-NO_3^-.d^{-1} during the highest ammonia conversion corresponded to an oxygen consumption of 3.1 mgO_2/d^{-1}. The total oxidation of S^{2-} in the biotic pipe reactor, during the period from day 70 to day 121 corresponded to an oxygen demand of 77 mgO_2.d^{-1}. Thus the necessary oxygen demand to produce nitrate corresponded

to 4% of the total necessary oxygen demand to oxide the sulfur compounds and only ammonium limitation must be taken into account.

With thiosulfate as sulfur source the ammonium consumption decreased from 3 $mgN.d^{-1}$ to 1.5 $mgN.d^{-1}$. This decrease was confirmed by the drastic decrease in nitrate production (figure 41), suggesting that, in these pH conditions (strongly acid), nitrifying bacteria were no longer efficient. During this period, the nitrate produced slightly decreased, illustrating the regularly wash-out of the nitrifying activity. Thus, using stable sulfur source, as thiosulfate, intensifies the biological acidification for a same flux of equivalent of sulfur at the inlet of the pipe-reactor, leading to a more selective environment, hence limiting the development of nitrifying activity.

When the maximum nitrate production was measured at 1 $mgN\text{-}NO_3^-.d^{-1}$ (figure 41), the acid fluxes due to the nitrification and to the thiosulfate oxidation could be evaluated (from Eq 50 and Eq 21) at 32 $\mu molH^+.d^{-1}$ and to 1200 $\mu molH^+.d^{-1}$ respectively. Thus in the experimental conditions with thiosulfate as sulfur source, the nitrification contributed to less than 3% of the total acidity biologically produced.

Therfore, the used of thiosulfate as sulfur source, compared to soluble sulfide (S^{2-}), ensure a more drastic selection of acidophilic SOB, limiting the development of non-desired nitrifying bacteria, ensuring the establishment of sulfur biogenic acid production in contact with cementitious material.

3.3.1. Biomass samples and population identification

To confirm the origin of microbial activity, at the end of the experiment, the biotic pipe-reactor was open and four biofilm samples from different zones of the pipe-reactor were collected for DNA extraction, purification and sequencing experiments in order to identify the established bacteria.

The table 15 shows the results obtained after the pyro-sequencing of the DNA. For the four samples, *Thiobacillus denitrificans* was one of the major species identified, accounting for 59.8%, 28.5%, 12.1% and 52.6% of the total clones for sample 1 to 4 respectively. These results confirmed the selection of sulfur-oxidizing-bacteria by the operating conditions and the nature of the sulfur substrate. *Thiomonas thermosulfata (or thermosulfatus)* accounted for

10.5% of the total clones in sample 4. Originally, *Thiomonas thermosulfata* was isolated from sewage sludge samples enriched with elemental sulfur (Shooner et al., 1996). This bacterial specie is a facultative autotrophic strictly aerobic bacterium able to grow on thiosulfate at pH varying between neutral and around 2.5.

Table 15: Ratio of the different species obtained by sequencing analysis from the four biomass samples, and comparison to a thiosulfate batch culture with the same activated sludge inoculums (only the populations with the most important contribution are showed)

Name	% Sample 1	% Sample 2	% Sample 3	% Sample 4
Thiobacillus denitrificans	59,8	28,5	12,1	52,6
Thiomonas thermosulfata	0,2	1,1	3,8	10,5
Rhodanobacter thiooxidans	0	0	0,8	1,2
Pandoraea pnomenusa	0	0	0	0
Dokdonella koreensis	4	16,3	0,13	3,6
Methylotenera spp,	2,5	2,6	24,5	10,9
Edaphobacter modestum	0,03	0	17,6	0,06
Methyloversatilis spp,	1,6	1,6	0	0,5
Roseomonas ludipueritiae	2,8	16	2.1	2,9
Nitrospira cf, moscoviensis	2,4	1,9	0,4	0,9
Nitrospira sp,	2,1	0,9	0,3	0,9
Nitrosomonas oligotropha	1	0,2	0,1	0,5
others	~ 23.6	~ 30.9	~ 38.2	~ 15.4

In the four samples (table 15), bacteria that were not known for their sulfur-oxidizing capacity were also identified. The major ones were: (i) *Edaphobacter modestum,* for 17.6% of the total clones in sample 3, (ii) *Methylotenera* spp, for 24.5% of the total clones in sample 3 and 10.9% of the total clones in sample 4, (iii) *Dokdonella koreensis* for 16.3%, 4% and 3.6% of the total clones in samples 2, 1 and 4 respectively.

Edaphobacter modestum is a member of the Acidobacteriaceae family. Its identification confirmed the global acidification of the medium in the biotic pipe-reactor (Koch et al., 2008).

Nitrifying bacteria (*Nitrospira sp*, *Nitrosomonas*) are identified in the four samples. Nevertheless, the amount of clones was equivalent to 5.5% for sample 1, and never exceeded 3% for the other samples (table 15). At the same time, sulfur-oxidizing bacteria represented 16.7% of the total clones identified in sample 3 and 60.1%, 29.6% and 64.3% in samples 1, 2 and 4 respectively. These results demonstrated the predominance of the sulfur-oxidizing-

bacteria over the other species of microorganisms and confirmed thiosulfate as a good substrate for promoting sulfur-oxidizing activity in contact with cementitious materials.

The sequencing of the four samples highlighted the selection of sulfur-oxidizing bacteria from a non-specified initial consortium (activated-sludge: AS 1) by the operating conditions and the choice of sulfur substrate.

The aims of this study are, firstly to produce a soluble phase in contact with cementitious products enabling the selection and the growth of SOB, secondly to validate the impact of these biological transformations on the cementitious linings. The selection of sulfur-oxidizing activity was demonstrated. However, the reactivity of the cementitious linings must be now evaluated.

3.4. Lixiviation of the cementitious material under soluble sulfide (S^{2-}) biological environment and thiosulfate ($S_2O_3^{2-}$) biological environment.

Oxidation of sulfur compounds should cause concrete deterioration, especially in the biotic conditions where it led to acidification of the bulk liquid and sulfate production in contact with cementitious materials (Eq 21). The figure 42 presents the sum of calcium in the leaching solution for the biotic and the abiotic pipe reactors (figure 42.A) and the associated pH of the leaching solutions (figure 42.B), during the (S^{2-})-phase and the ($S_2O_3^{2-}$)-phase.

For the abiotic pipe-reactor, the sum of dissolved calcium in the leaching solution shows a linear trend, whatever the sulfur compounds used and the equivalent sulfur inlet fluxes. The rate of calcium lixiviation (rCa) for the abiotic pipe reactor is 3.4 $mgCa.d^{-1}$. In contrast, for the biotic pipe-reactor, the calcium lixiviation rate is much higher than in the abiotic pipe reactor reaching 12.6 $mgCa.d^{-1}$ with sulfide (S^{2-}) as sulfur source (x4 compared to abiotic system) and 24.5 $mgCa.d^{-1}$ with thiosulfate ($S_2O_3^{2-}$) as sulfur source for a same substrate flux. At day 145 (20 days after the change from S^{2-} to $S_2O_3^{2-}$ as sulfur source), the calcium lixiviation rate was reduced, but was still superior to the abiotic lixiviation rate (figure 42.A).

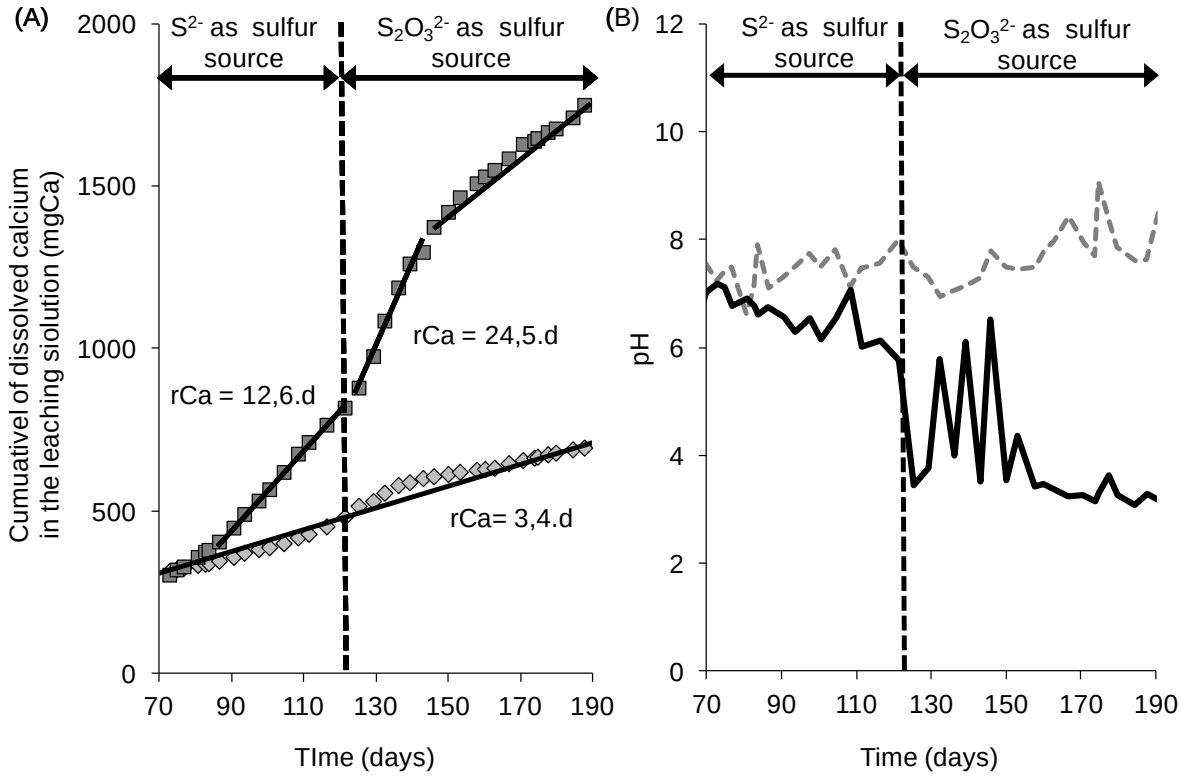

Figure 42: total calium in the leaching solution for the abiotic pipe reactor and the biotic pipe reactor, with the pH evolution of the leaching solutions. ■ : total calcium in the leaching solution of the biotic pipe reactor (mgCa); ◇ : total calcium in the leaching solution of the abiotic pipe reactor (mgCa); ▬ : pH of the leaching solution of the biotic pipe reactor; ▬ ▬ : pH of the leaching solution of the abiotic pipe reactor,

With thiosulfate as sulfur source, in the abiotic pipe reactor, the pH of the leaching solution was relatively stable (range from 7.5 to 9) and quiet similar to the pH values recorded in the same conditions with sulfide (S^{2-}) as sulfur source (figure 42.B). In the biotic pipe reactor, the change of the sulfur source, led to a drastic biological acidification of the leaching solution, leading to a stronger calcium lixiviation (from day 125). During this time period, pH instability in the leaching solution was recorded. The stronger lixiviation of calcium during the same period (from day 125) indicated for some pH values in the same range than with S^{2-} different behavior of the cementitious material in terms of calcium lixiviation. Thus, pH appears to not be a direct indicator of the attack of the material, but must be coupled to the sulfate production (sulfur-oxidizing activity) and the calcium dissolution (indicator of the evolution of the cementitious material) to reveal the interaction between the microbial communities and the cementitious materials.

No dissolved alumina was detected for the two pipe-reactors, confirming the different behaviour of the alumina compared to the calcium during acid attacks, and the interesting performances of the CAC linings in a biotic, slightly acidic environment.

3.5. Thiosulfate versus dissolved sulfide for investigating MICC

For efficient control of MICC environmental conditions and for the quantitative evaluation of biotic transformations and then evaluate the behaviour of cementitious linings under controlled environment, the use of a sulfur substrate, stable in abiotic conditions, is a crucial issue. The criteria for chosing a soluble sulfur compounds lean on the capacity to induce a quick acidification of the local medium and a local production of sulfate in order to, (i) limit nitrifiers colonization and mainly select SOB communities, (ii) accelerate the biodeterioration by the combination of acid and sulfate biological production.

The use of H_2S in the gaseous state greatly increases the difficulties of performing mass balances due to (i) the abiotic precipitation of elemental sulfur at the surface of the cementitious materials (ii) the necessary safety precautions, making the collection of the leaching solution difficult. Working with soluble sulfur compounds should therefore be preferred in the case where analyses against time of the biological activity and quantification of the biogenic acid fluxes produced in contact with the cementitious linings are wanted. As excepted from the literature results and shown in these experiments, two main disadvantages of using dissolved sulfide (S^{2-}) as a substrate for a test of cement resistance to corrosion can be pointed out: firstly a significant loss of sulfur resource for biological transformation occurs due to spontaneous sulfide abiotic oxidation (around 64% ± 13% of the initial sulfide load in our condition). This leads to a decrease in the biological acidification potential. Secondly, as acidification is slow at the beginning of a test, bacterial competition can occur, leading to the establishment of autotrophic nitrifying bacteria and thus to a preferential transformation of ammonia to nitrate. This can lead to a SOB nitrogen growth limitation, and a competition for oxygen.

As a consequence, thiosulfate appears to be an interesting substrate to developed acidophil sulfur-oxidizing activity in contact with cementitious linings. It is stable over time under abiotic conditions at neutral or alkaline pH. This potential of thiosulfate to favour sulfur-oxidizing bacteria, even acidophilic, has been reported in the literature (Parker and Prisk, 1953) (Kelly, 1999) (Roberts et al., 2002), especially in opened system (Pronk et al., 1990b). However, based on the comparison of the abiotic and biotic sulfur mass balances (Eq 47 and Eq 48), the quantitative evaluation of the biotic thiosulfate oxidation may be incorrect. Indeed, at pH around 3 in the leaching solution of the biotic pipe-reactor abiotic thiosulfate disproportionate reaction may occurred (Pronk et al., 1990c). However, this reaction

consumes acid (Johnston and McAmish, 1973), the low pH values recorded in the leaching solution confirmed the predominant contribution of biotic thiosulfate oxidation in the global sulfur transformation.

4. Conclusions

The objectives of this chapter were firstly to evaluate the possibility to establish sulfur-oxidizing activity at the surface of cementitious linings by the production of a controlled liquid phase, secondly to assess thiosulfate versus dissolved sulfide as substrate for the controlled development of microbial populations involved in Microbial induced concrete corrosion (MICC) and, thirdly, to compare the biotic and abiotic transformations both qualitatively and quantitatively, according to the substrate supplied to the system. Using a lab-scale pilot enable representing the liquid phase in contact with cementitious materials, mass balances on sulfur compounds and other minerals, such as nitrogenous compounds, calcium and alumina, were performed for an abiotic and a biotic pipe-reactor composed by the same cementitious lining (Calcium Aluminates Cement). The following conclusions are noteworthy:

The reproduction of liquid phase enables the control of the sulfur fluxes applied at the surface of cementitious linings, thus, by sulfur mass balance achievement in abiotic and biotic conditions, to underline the correlation of the abiotic stability of the sulfur source and the enhancement of a sulfur-oxidizing activity.

Under dissolved sulfide (S^{2-}) feeding, a low biological selection pressure is imposed and consequently nitrifying bacteria establishment occurs. Abiotic sulfide oxidations limit the implantation of sulfur-oxidizing bacteria and thus the biological acidification of the pipe walls.

The experimental results showed fast, strong biological acidification in the thiosulfate environment (pH values of the leaching solutions around 3.5) and the limitation of nitrifying bacteria. The comparison between the abiotic and biotic pipe-reactors demonstrated the **efficiency of the biological thiosulfate oxidation in intensifying the dissolution of the CAC lining**. Calcium lixiviation rate was 7 folds higher in the biotic than in the abiotic conditions for the highest lixiviation rates, and during 69 days of thiosulfate feeding 5 folds

higher. The sequencing analyses, on **four final biofilm samples, confirmed the physico-chemical analyses at the pipe-reactor scale, in terms of sulfur-oxidizing bacteria selection**, and the competition with other autotrophic bacteria.

Even if thiosulfate disproportionate reaction under acid environment needs further experimentation (see the chapter V), it has been demonstrated that thiosulfate, chemically stable in alkaline and neutral pH conditions, is an appropriate substrate for bacteria involved in acidification and thus in MICC. By using this component instead of dissolved sulfide (S^{2-}) a much more convenient experimental device and experimental protocol can be set up for further laboratory MICC studies.

The experimental results at a pilot scale identified interesting design and operating conditions to produce sulfur-oxidizing environment at the surface of cementitious materials from a diversified activated-sludge consortium. Thus in the chapter VII of this document, the interaction between sulfur-oxidizing activity and two cementitious linings will be evaluate, in terms of the cementitious lining behaviours and sulfur-oxidizing activities. Before that, to ensure the control of the system, and validate the experimental approach, the stability of thiosulfate in acid environment must be evaluated and quantified (objective of the chapter V), and the selection from an activated sludge consortium of acidophil sulfur-oxidizing activity by a thiosulfate pressure needs specific investigations to be evaluated too (objective of the chapter VI).

Chapter V

Chemical reactivity of thiosulfate

1. Introduction

Thiosulfate ($S_2O_3^{2-}$) is an intermediate in the sulfur cycle in real environment, as water sediments (Jorgensen, 1990), or hydrothermal waters (Xu et al., 1998), or in sewer systems (Okabe 2007), especially where microbial activity was detected. In some sulfur environments its low concentration detection is linked to a high affinity with the microorganisms involved in the sulfur cycle (Jorgensen, 1990) and its chemical reactivity in specific conditions (Druschel et al., 2003) (Okabe et al., 2007).

In sewers system, under hydrogen sulfur atmosphere, sulfur-oxidizing-bacteria (SOB) are involved in the deterioration of the concrete infrastructures, by the acidification of the surface medium linked to a sulfate production. Thiosulfate is a reduced sulfur compound with a high affinity as energy source for numerous SOB (Parker and Prisk, 1953) (Kelly, 1999), including acidophilic bacteria as *Thiobacillus acidophilus* (Okabe et al., 2007) or *Acidithiobacillus thiooxidans* (Mason et al., 1987).

The chapter IV demonstrated the interest of thiosulfate as a reduced sulfur substrate to reproduced acidophilic sulfur-oxidizing conditions in contact with cementitious linings. The major interest of this compound for a laboratory test based on microbial induced concrete corrosion is its stability, allowing the total amount of reduced sulfur to be entirely available for biological oxidation. However, in acidic environment thiosulfate is chemically reactive and can decompose by a disproportionate reaction in colloidal sulfur (S^0) that may latter precipitate as crystal of elemental sulfur (S_8), and in S(IV)-oxides such as sulfite (SO_3^{2-}) and bisulfite (HSO_3^-) (Johnston and McAmish, 1973) generally described by the (Eq 51) (Zaiser et al., 1948):

Eq 51: $S_2O_3^{2-} + H^+ \rightarrow S_{colloïdal} + HSO_3^-$

The figure 43, based on the figure 7 adapted from Islander (Islander et al., 1991), focused on the thiosulfate oxidation, by microbial activity and by chemical reaction (disproportionate reaction in that case), depending on the pH conditions. Thus, this figure illustrates the competitions that can occur in a biotic aerobic and acidic environment. As described in the chapter I (literature review), the production of elemental sulfur stabilized sulfur for biological oxidation. However, the production of S(IV)-oxides (as sulfite (SO_3^{2-}), bisulfite (HSO_3^-) and sulfurous acid (H_2SO_3)), cause of the high reactivity of these compounds with oxygen, lead to an abiotic production of sulfate (Linek and Vacek, 1981) (Wilkinson et al., 1993). In the case

of the sulfite oxidation, no acid is produced during this reaction, and moreover the thiosulfate disproportionate reaction leads to an increase of the medium pH (as described by the equation (Eq 51), and illustrated in the figure 43).

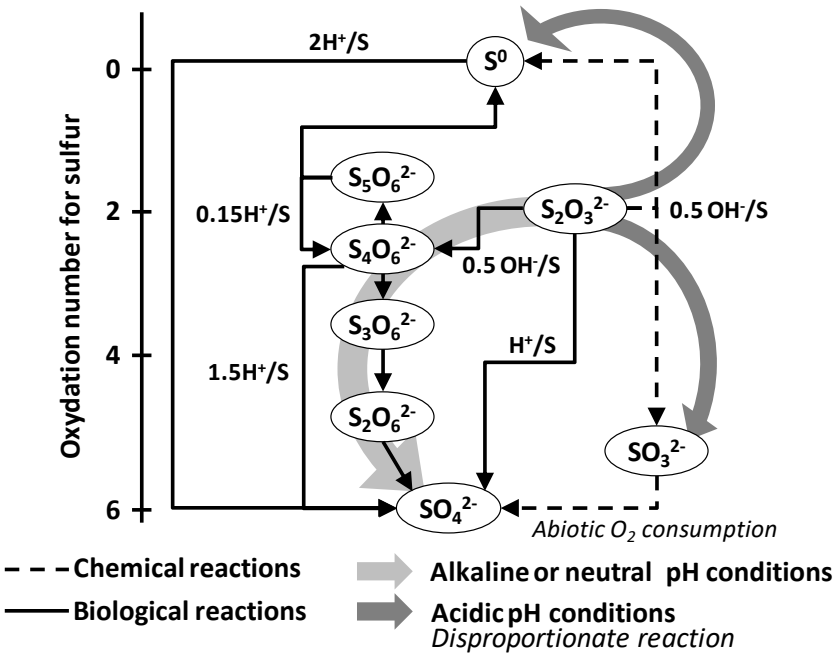

Figure 43: Illustration of the thiosulfate conversions by sulfur-oxidizing bacteria and by the disproportionate reaction depending on the local pH conditions, with the proton production/consumption for each reaction, and the intermediary compounds.

With an objective to control the sulfur substrate stability for the achievement of accurate sulfur mass balances, and to maximize biogenic acid production in contact with a cementitious material, the chemical reactivity of thiosulfate must be qualified and quantified in terms of stoichiometry and kinetic. The influence of thiosulfate transformation on the pH definition of the medium must also be analyzed and predicted.

To summarize, without any control of the kinetic of thiosulfate chemical transformations, it is not possible to ensure that thiosulfate remains available for biological reactions. For that, an experimental approach was proposed, coupled to the development of a dynamical model. In a fisrt step a literature review on the thiosulfate disproportionate reaction is firstly presented.

1.1. Bibliography on the thiosulfate disproportionate reaction

1.1.1. The thiosulfate disproportionate reaction

The global disproportionate reaction of thiosulfate ($S_2O_3^{2-}$) was described generally by the equation (Eq 51). Others studies showed the importance of the formation of bithiosulfate ($HS_2O_3^-$) during the disproportionate reaction (Dinegar et al., 1951) (Davis, 1958) (Johnston and McAmish, 1973). Bithiosulfate is the acid form of the thiosulfate and the base form of the thiosulfuric acid ($H_2S_2O_3$). The equations (Eq 52) and (Eq 53) presented the acid-base equilibrium describing the concentrations in solution of these three compounds:

Eq 52: $H_2S_2O_3 + H_2O \overset{Ka_{T1}}{=} HS_2O_3^- + H_3O^+$

Eq 53: $HS_2O_3^- + H_2O \overset{Ka_{T2}}{=} S_2O_3^{2-} + H_3O^+$

with Ka_{T1} = 0.45 (Dinegar 1951) or 0.25 (Page 1953) and Ka_{T2} = 0.01 for dilute solution and 0.062 for moderate thiosulfate concentration (Dinegar 1951) or 0.019 for zero ionic strength (Page 1953) or 0.05 to 0.06 for 0.035 ionic strength value (Johnston and McAmish, 1973).

In acidic environment the formation of bithiosulfate leads to the reactivity of the "thiosulfate" compounds and then to the disproportionate reaction. Different sequences of reactions have been proposed and described by the equations (Eq 54, Eq 55) according to Dinegar in 1951:

Eq 54: $HS_2O_3^- + S_2O_3^{2-} \rightarrow (HS_2O_3.S_2O_3^{2-})$

Eq 55: $(HS_2O_3.S_2O_3^{2-}) \rightarrow S_2 + HSO_3^- + SO_3^{2-}$

where S_2 was the precursor prior to the formation of S_8 molecule leading thus to colloidal sulfur.

Another description of this transformation is given by the equations (Eq 56, Eq 57, Eq 58) according to Davis in 1958:

Eq 56: $HS_2O_3^- + S_2O_3^{2-} \rightarrow HS_3O_3^- + SO_3^{2-}$

Eq 57: $HS_3O_3^- + S_2O_3^{2-} \rightarrow HS_4O_3^- + SO_3^{2-}$

The reaction sequence continues until $HS_9O_3^-$ is formed leading to S_8 production by the following reaction:

Eq 58 : $HS_9O_3^- \rightarrow S_8 + HSO_3^-$

Johnston and McAmish in 1973 confirmed that the bimolecular process (Eq 56) was the limiting reaction and proposed a kinetic reaction for the formation of elemental sulfur described by the equation (Eq 59):

Eq 59: $d[S]/dt = k_{dis}.[H^+].[S_2O_3^{2-}]^2$

where the compound inside square brackets "*[compounds]"* corresponds to the concentration of the concerned species in solution (see the paragraph [4.2.] in the annexes of this chapter for the definition of the species activity in solution), *R* is the perfect gas constant, $k_{dis} = (1.64 \pm 0.13) \times 10^{11} \times exp^{(-15930 \pm 160)/R.T}$ (in $l^2.mol^{-2}.s^{-1}$), and *T* is the temperature in Kelvin.

Moreover, the thiosulfate disproportionate reaction could not be observed for pH values over 4.6 (Pascal, 1961), that is in good agreement with the proposition of a previous formation of bithiosulfate ($HS_2O_3^-$) before observing the decomposition of the "thiosulfate" compounds.

In a first approach, through the development of a dynamical model, specific experiments will be confronted to these stoichiometric and kinetic definitions proposed in the literature.

1.1.2. The influence of the thiosulfate disproportionate reaction on a sulfur-oxidizing activity

In a more global vision of thiosulfate transformations under aerobic environment, the S(IV)-oxides (SO_3^{2-}, HSO_3^- and H_2SO_3) will react at different rates with dissolved oxygen to directly produced sulfur(VI)-oxides as sulfate (SO_4^{2-}) and/or bisulfate (HSO_4^-) depending on the pH of the solution (Wilkinson et al., 1993) (Lancia et al., 1999). More details on these chemical reactions are presented at the annexes of this chapter. Moreover, in strong acidic environment, the possible formation of H_2SO_3 by acid-base equilibrium, in aerated conditions could lead to the volatilization of sulfur dioxide described by the equation (Eq 60):

Eq 60: $SO_2\,(gas) \overset{H_{SO_2/water}}{=} H_2SO_3\,(liq)$

where $H_{SO_2/water}$ is the Henry constant of the sulfur dioxide in water, considering the hydration reaction as an instantaneous reaction.

To grow sulfur-oxidizing-bacteria under autotrophic metabolism, bacteria need reduced sulfur compounds as energy source, oxygen as final electron acceptor, except for some species such as *Thiobacillus denetrificans* or *Thiomocrospira denetrificans* (Kelly, 1999) which could grow under anoxic conditions (nitrate as final electron acceptor). In addition a specific pH range is also required that depends on the growth optimal condition (Kelly, 1989). In these conditions, associated with the description proposed in the introduction of this chapter, if the conversion rate of the thiosulfate disproportionate reaction is faster than the biological conversion in acidic conditions, the system will be drive in the opposite way of local acid production.

In this context, to qualify and quantify the thiosulfate disproportionate reaction and ensure the control of the system, an experimental system and the equations needed to describe the whole system are presented in the following paragraphs.

1.2. The description of the thiosulfate disproportionate reaction system

The kinetic description will allow the dynamic determination of pH and oxygen concentration that are key parameters involved in the reactions. The figure 44 illustrates the simplification of the whole system studied in this chapter.

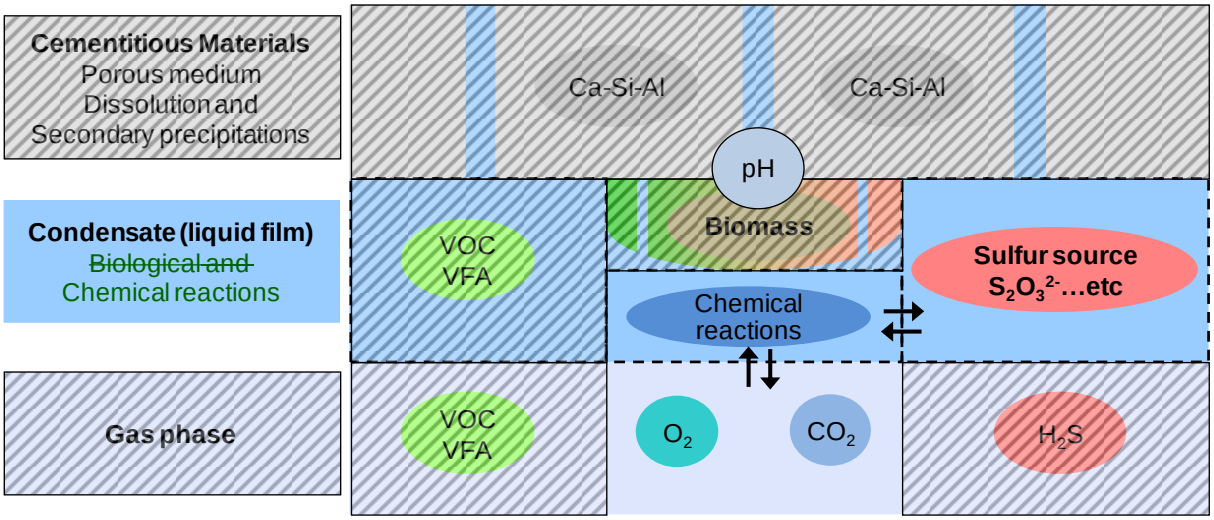

Figure 44: simplification of whole system studied in the chapter IV in order to focalize on the liquid/solid interactions only.

To describe kinetically this disproportionate reaction and evaluate for different conditions the behavior of the sulfur species, the pH evolution and the oxygen consumption, the kinetic description of secondary reactions involving S(IV)-oxides are necessary. This description is presented in the annexes of this document, as other secondary reactions (carbon dioxide absorption and inorganic carbon acid-base equilibrium) involved in the pH definition of the system and because in biological system, with autotrophic bacteria (as several SOB), carbon dioxide is the main carbon source to support growth.

The figure 45 summarizes the reactions involved in the thiosulfate disproportionate reaction system (see the annexes of this chapter for more details on the secondary reactions). Symbol “(ok)” “(?)” and “(??)” respectively indicate if the reactions are kinetically well known in the literature, described but with no clear data, or not defined.

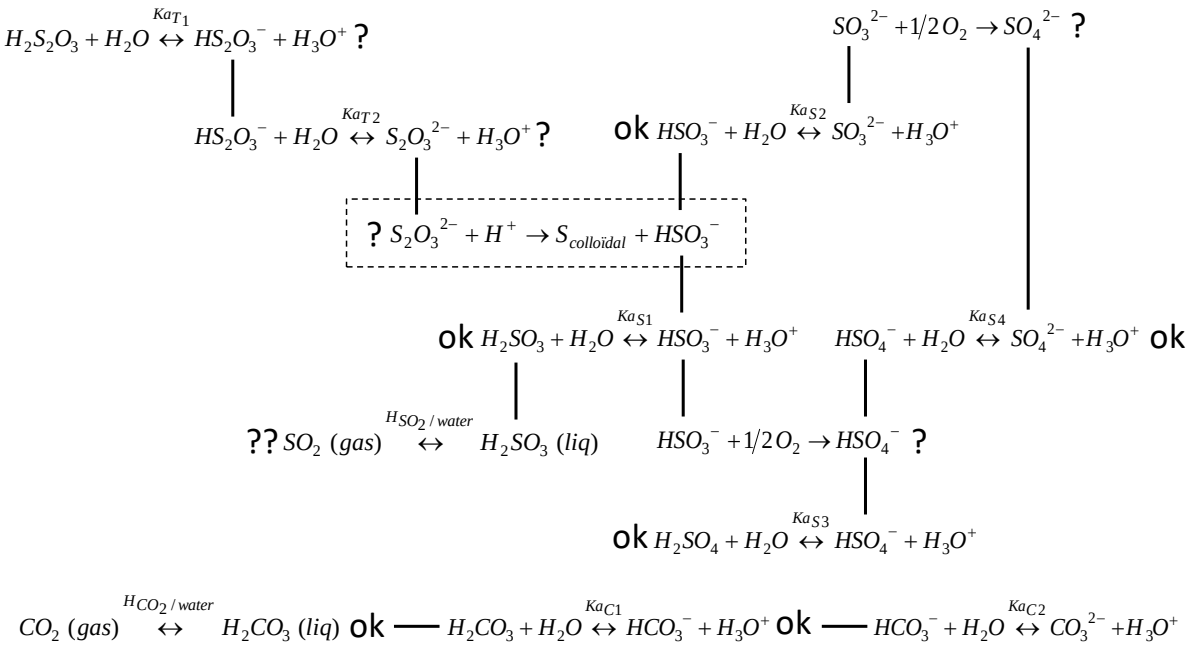

Figure 45: the description of the thiosulfate disproportionate reaction by global stoechiometric reactions (↔ equilibrium phenomena, → irreversible reactions). The symbol (ok) indicates a kinetic process known in the literature; the symbol (?) indicates a kinetic process described in the literature but with no clear datas; the symbol (??) indicates kinetics processes with no kinetic description. (Johnston and McAmish, 1973) (Ulrich et al., 1986) (Lide, 1990) (Wilkinson et al., 1993) (Sperandio and Paul, 1997) (Lancia et al., 1999) (Musvoto et al., 2000).

The whole system to describe thiosulfate transformation is complex, linked to irreversible reactions, equilibrium reactions and gas-liquid exchanges. The relative contribution of various reactions involved in the thiosulfate disproportionate reaction system is not well known, especially in complex system including the pH evolution and the gas-liquid exchanges. Hence, using a combined experimental and modelling approach, the contribution of this work will be a better quantitative description of this system. Dynamic measurements of pH, dissolved oxygen concentration and sulfur compounds will be thus used in order to discriminate between the possible reaction pathways.

The work sequences in this chapter are as follow:

In a first part, this chapter develops an experimental approach[5], to evaluate, validate or adapt by contrasted conditions and mass balances analyses the previous description of the global reaction (figure 45), and to accumulate data results with contrasted conditions of pH,

[5] : Some of the experiments and the first tests of the kinetic models were realized in collaboration with Mohamed Arezki CHEKROUN during his master internship (Master Recherche GPE UPS-INP-INSA Toulouse University) (First semester, year 2012).

initial thiosulfate concentration and oxygen mass transfer for a further development of a dynamic model.

In a second part, a global description of the thiosulfate disproportionate reaction is proposed (sulfur compounds concentration, pH of the solution, dissolved oxygen concentration). This description was segmented in three blocks of reactions and physical process, according to the literature and the experimental results. Based on this description by mass balance and kinetic equations a dynamic model was developed on Aquasim® (Reichert, 1994). The acid-base equilibrium reactions were described as kinetic processes by the method proposed by Musvoto in 1997 and developed and applied to different experimental context (Musvoto et al., 1998) (Musvoto et al., 2000) (Rensenburg et al., 2003).

At the end of this work, a calibrated chemical model will be obtained. It will be used in the next chapter of this work in combination with the biological model in order to predict the global transformation of thiosulfate in a complex environment.

2. Specific materials and methods

2.1. The material

Two experimental batch reactors were used to describe and quantify the thiosulfate disproportionate reaction: (i) a closed system with gas trap bottle to notably investigate the possible loss of volatile sulfur intermediate, and (ii) an opened reactor to realize dynamic samples and analyze versus time the fate of the sulfur compounds. These reactors (batch) and the analytical techniques and methods used in this chapter V are described in the M&M (chapter III).

2.2. Description of the experimental procedure

Five experiments described in the table 16 were run under different operating conditions, i.e. different initial concentrations of thiosulfate ($S_2O_3^{2-}$), different initial pH values and different kla_{O2}). The experiments Exp_$S_2O_3^{2-}$_a, the Exp_$S_2O_3^{2-}$_b, Exp_$S_2O_3^{2-}$_c were operated in the open-reactor configuration. The Exp_$S_2O_3^{2-}$_d, Exp_$S_2O_3^{2-}$_e were operated in the closed configuration.

Table 16: Operating initial conditions for the thiosulfate disproportionate reactions tested.

Name of the experiments	Temperature (°C)	Initial pH	Initial [$S_2O_3^{2-}$] (mol/l)	Initial [O_2] (mgO_2/l)	kl.a_{O2} (h^{-1})
Exp_$S_2O_3^{2-}$_a	20.5 ± 1	1.22	5 x10^{-2}	8.8	0.7* ± 0.25
Exp_$S_2O_3^{2-}$_b	20.4 ± 1	1.32	2.5 x10^{-2}	8.78	0.7* ± 0.25
Exp_$S_2O_3^{2-}$_c	20.5 ± 1	5.7	2.6 x10^{-2}	8.78	0.7* ± 0.25
Exp_$S_2O_3^{2-}$_d	19 ± 1	2.03	2.5 x 10^{-2}	NM	2.5 ± 0.25
Exp_$S_2O_3^{2-}$_e	20 ± 1	2.53	1 x 10^{-2}	9.07	2.2 ± 0.25

NM : no measures caused by a failure of the dissolved oxygen sensor.
*: surface aeration

2.3. Development and evaluation of the mathematical model

The mathematical model of figure 45 is developed on the Aquasim® software. It is based on compartments or blocks that results from the experimental approach (described in the first part of the results paragraphs) with an ascendant method, from the simplest one to the

complete description of the system. Each block describes a part of the thiosulfate disproportionate reaction system and all blocks are interconnected.

To define the partial orders of the kinetic laws, different sets of partial orders were tested for each kinetic. For each set, the parameters estimation tool of the Aquasim® software was used to evaluate the best values of the associated rate constants. The numerical results were compared to the experimental data, and the rate constant was estimate by the "simplex" method, tool of the modelling software Aquasim® described in the user manual (at www.eawag.ch/forschung/siam/software/aquasim/pdf/aquasim_manual.pdf, page 151).

To evaluate the best model definitions the mean square deviations between numerical results and experimental results for the thiosulfate concentration *(Dev_S_2O_3)*, the sulfate concentration *(Dev_SO_4)*, the dissolved oxygen concentration *(Dev_O_2)* and the pH *(Dev_pH)* were calculated. For each experience tested and each parameter, the mean square deviation was divided by the mean value of these parameters for all the experiments (*(mean(Dev_S_2O_3)* as example for thiosulfate concentration). Thus all the deviations were expressed in the same range, and a moderate summation could be applied to define a parameter called "Model evaluation" enables underlining the model definition with the minimum deviation to all the experimental data. The equation (Eq 61) presents an example of the definition of the parameter "Model evaluation" for x experiences, where only y measurements of the dissolved oxygen concentration were usable.

Eq 61: Model evaluation

$$= \frac{\left(x.\frac{Dev\_S_2O_3}{mean(Dev\_S_2O_3)} + y.\frac{Dev\_O_2}{mean(Dev\_O_2)} + x.\frac{Dev\_SO_4}{mean(Dev\_SO_4)} + x.\frac{Dev\_pH}{mean(Dev\_pH)} \right)}{x + y + x + x}$$

3. Results and discussion

3.1. Experimental results and description of the thiosulfate disproportionate reaction as a physico-chemical system

The photographs in the figure 46 present for the Exp_$S_2O_3^{2-}$_a the formation of a pale-yellow precipitate during the thiosulfate disproportionate reaction in acid environment. The precipitation of a pale-yellow solid was observed for all the experiments, except for the Exp_$S_2O_3^{2-}$_c for an initial pH at 5.7. These first observations suggest the formation of S^0 that is in good agreement with the pH dependency of the thiosulfate disproportionate reaction and its pH limit (Pascal, 1961) (Johnston and McAmish, 1973).

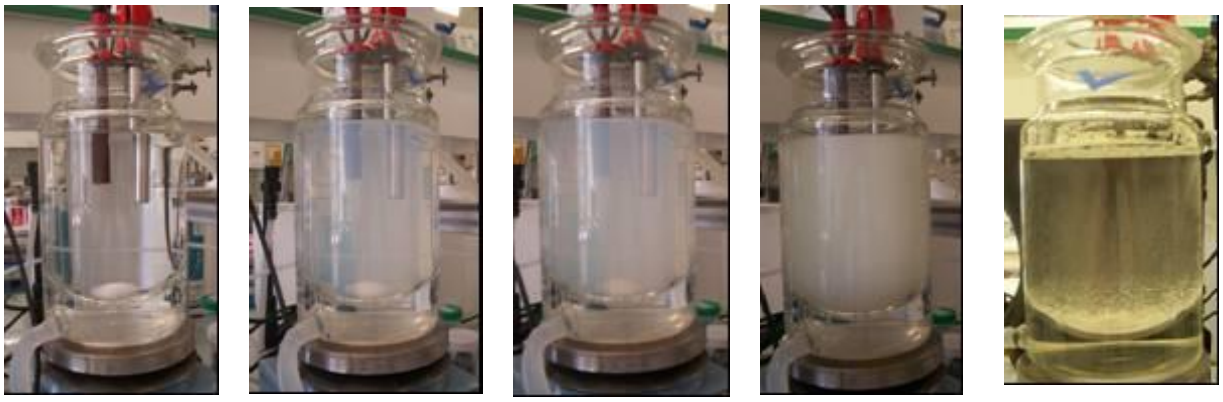

t = 0h before the thiosulfate injection	----------During a few minutes to an hour ----------	End of the experience (46 h) Mixing stopped

Figure 46: photos of the open reactor during the experience Exp_$S_2O_3^{2-}$_a for the thiosulfate disproportionate reaction.

3.1.1. Evaluation of the thiosulfate and pH dependencies, and influence of the thiosulfate disproportionate reaction on the definition of the aqueous solution

3.1.1.1. The pH dependency

The experience Exp_$S_2O_3^{2-}$_c was realized at an initial pH of 5.7 (a pH value above the critical pH value to observe the decomposition of the thiosulfate (Pascal 1961)). The figure 47 shows the time course of the different parameters measured during the experience Exp_$S_2O_3^{2-}$_c. During 95 hours neither changes of the thiosulfate concentration in the reactor

nor modification of pH and dissolved oxygen concentration are observed at an initial pH of 5.7. Obviously, neither sulfate nor precipitate is formed during this experience.

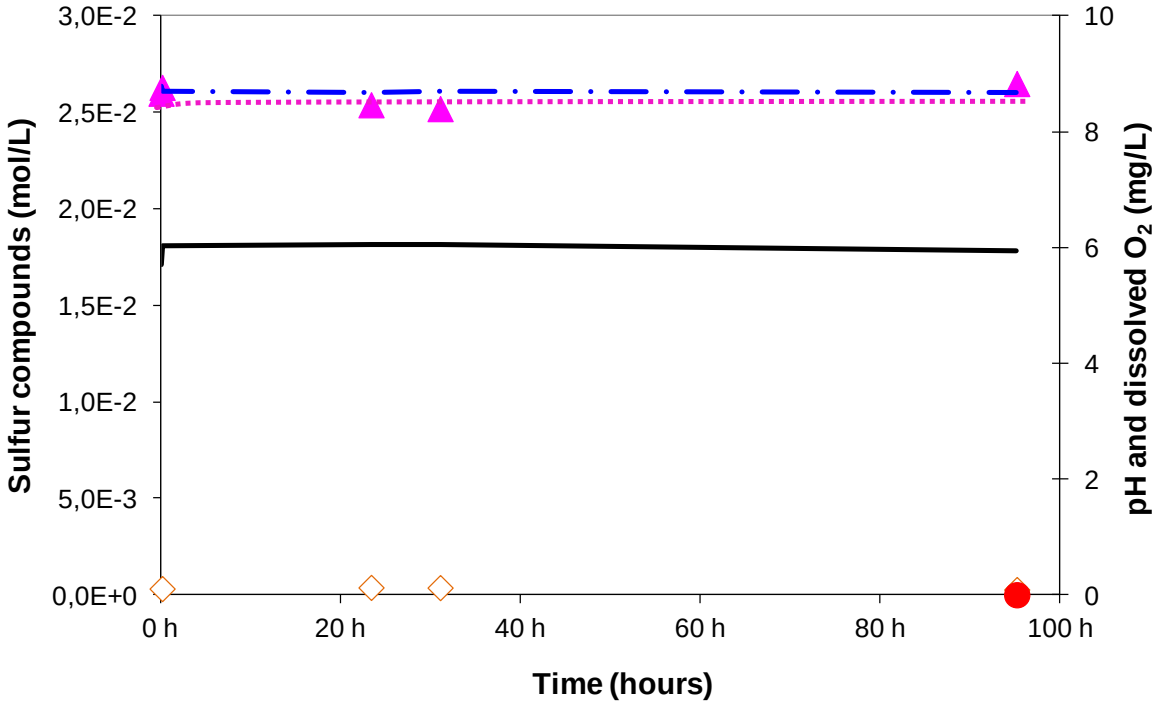

Figure 47: Exp_$S_2O_3^{2-}$_c – time course of the different parameters measured. : the thiosulfate concentration ($S_2O_3^{2-}$) (mol/l); : the sulfate concentration (SO_4^{2-}) (mol/l); : the mass of precipitate expressed as equivalent of loss sulfur (molS/l); : dissolved oxygen concentration (mgO_2/l); : pH measurement.

The experiments Exp_$S_2O_3^{2-}$_c , Exp_$S_2O_3^{2-}$_b and Exp_$S_2O_3^{2-}$_d (figure 47, figure 48 and figure 49) operated for the same initial thiosulfate concentration at different initial pH conditions illustrate the pH dependency of the thiosulfate disproportionate reaction. After 23 hours, for both reactions with thiosulfate consumption (figure 48 and figure 49), the thiosulfate consumption rates were:

- $d[S_2O_3^{2-}]/dt$ = - 0.96 $mmol.l^{-1}.h^{-1}$ for an initial pH = 1.32 (after 22.6 hours), corresponding to a thiosulfate consumption of 87% of the initial quantity.
- $d[S_2O_3^{2-}]/dt$ = - 0.27 $mmol.l^{-1}.h^{-1}$ for an initial pH = 2.03 (after 22.9 hours), corresponding to a thiosulfate consumption of 26% of the initial quantity.

The kinetic law of the thiosulfate disproportionate reaction is acid dependent. Lower is the initial pH, higher is the consumption rate.

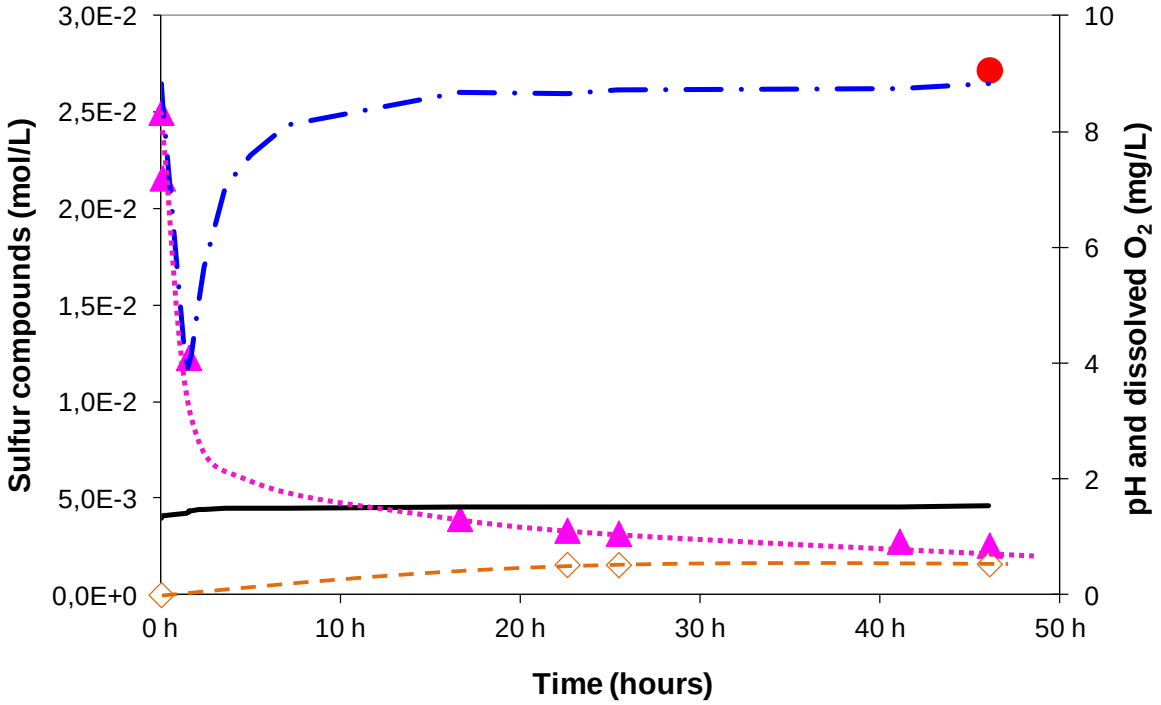

Figure 48: Exp_$S_2O_3^{2-}$_b – time course of the different parameters measured. : the thiosulfate concentration ($S_2O_3^{2-}$) (mol/l); : the sulfate concentration (SO_4^{2-}) (mol/l); : the mass of precipitate expressed as equivalent of loss sulfur (molS/l); : dissolved oxygen concentration (mgO_2/l); : pH measurement.

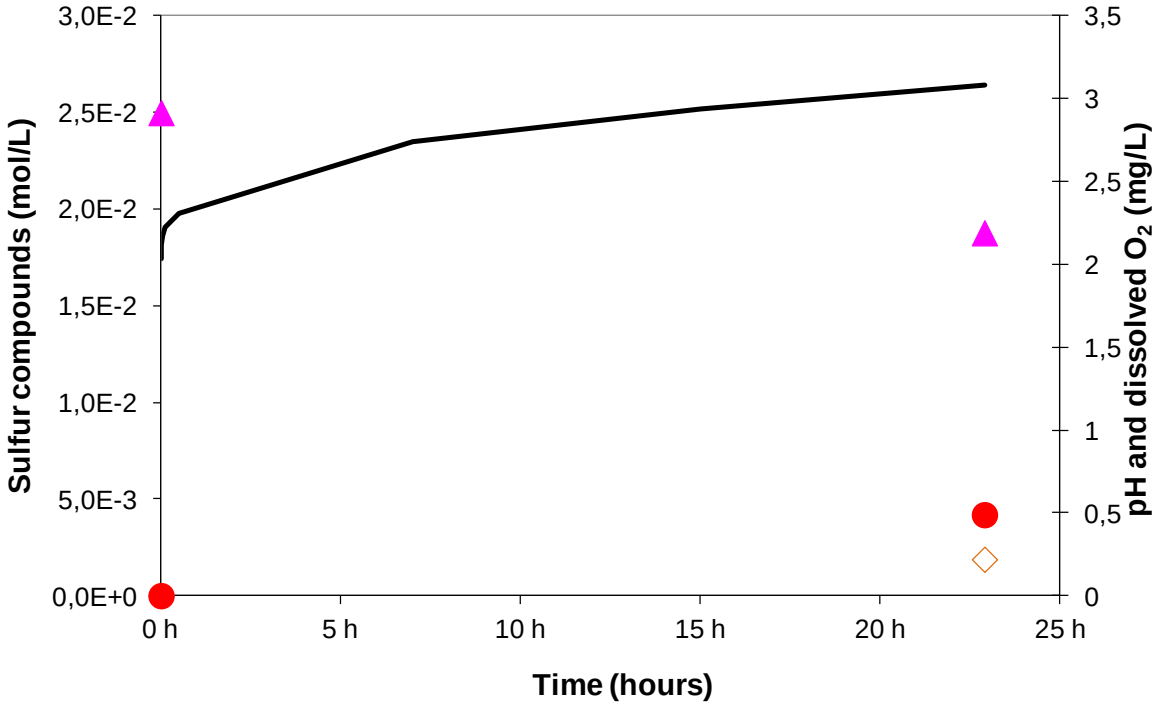

Figure 49: Exp_$S_2O_3^{2-}$_d – time course of the different parameters measured. : the thiosulfate concentration ($S_2O_3^{2-}$) (mol/l); : the sulfate concentration (SO_4^{2-}) (mol/l); : the mass of precipitate expressed as equivalent of loss sulfur (molS/l); : pH measurement..

As a conclusion, the dependency of thiosulfate disproportionate reaction with pH is confirmed and kinetic data are now available.

3.1.1.2. The thiosulfate concentration dependency

The figure 48 and the figure 50 show the time course of the parameters measured during Exp_$S_2O_3^{2-}$_b and Exp_$S_2O_3^{2-}$_a respectively. At low initial pH the formation of a pale-yellow precipitate (figure 46) was confirmed by the consumption of thiosulfate ($S_2O_3^{2-}$) in the aqueous solution (figure 48 and figure 50). For both Exp_$S_2O_3^{2-}$_b and Exp_$S_2O_3^{2-}$_a an increase in the pH of the solution was recorded confirming acid consumption during the thiosulfate disproportionate reaction. The production of SO_4^{2-} and the consumption of dissolved oxygen in the first moment of the reaction could indicate the intermediary formation of S(IV)-oxides during the thiosulfate disproportionate reaction.

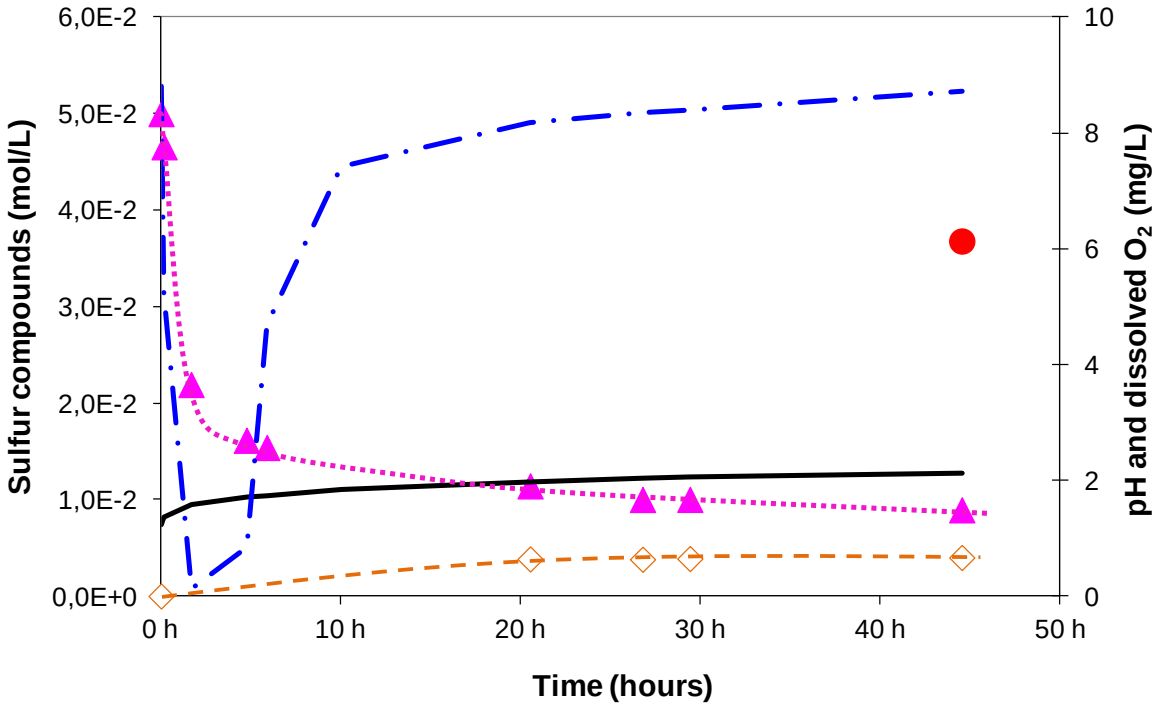

Figure 50: Exp_$S_2O_3^{2-}$_a – time course of the different parameters measured. : the thiosulfate concentration ($S_2O_3^{2-}$) (mol/l); : the sulfate concentration (SO_4^{2-}) (mol/l); : the mass of precipitate expressed as equivalent of loss sulfur (molS/l); : dissolved oxygen concentration (mgO_2/l); : pH measurement.

The experiments Exp_$S_2O_3^{2-}$_a and Exp_$S_2O_3^{2-}$_b indicate a thiosulfate concentration dependency for the thiosulfate disproportionate reaction. For similar initial pH conditions (1.22 and 1.32 respectively) an initial thiosulfate concentration of:

- $[S_2O_3^{2-}]_0$ = 5 x 10^{-2} mol/l leads to an initial consumption rate $d[S_2O_3^{2-}]/dt$ = -16.8 mmol.l^{-1}.h^{-1} when an initial thiosulfate concentration,
- $[S_2O_3^{2-}]_0$ = 2.5 x 10^{-2} mol/l leads to an initial consumption rate $d[S_2O_3^{-2}]/dt$ = -8.3 mmol.l^{-1}.h^{-1}.

Thus the higher the initial thiosulfate concentration is faster the initial consumption rate is.

3.1.1.3. Influence of the thiosulfate disproportionate reaction on pH

The table 17 presents the experimental conditions for the different experiments tested, and the experimental mass balance obtained at the end of the experiments. An important variation in the H_3O^+ consumption per mole of consumed thiosulfate (1.34 for Exp_$S_2O_3^{2-}$_a, and 0.75 for Exp_$S_2O_3^{2-}$_b) was recorded. These results indicated that the apparent stoichiometry for acid consumption is not constant.

Table 17 : Experimental stoichiometric equations for the thiosulfate disproportionate reactions tested.

Experiments	**Initial pH**	**Initial $[S_2O_3^{2-}]$ (mol/l)**	**kl.a_{O2} (h^{-1})**	**Stoichiometric equations of the global reaction based on the consumed thiosulfate**
Exp_$S_2O_3^{2-}$_a	1.22	5 x10^{-2}	0.7*	$S_2O_3^{2-}$ + 1.34 H_3O^+ → 0.83 S^0 + 0.09 SO_4^{2-} + NM
Exp_$S_2O_3^{2-}$_b	1.32	2.5 x10^{-2}	0.7*	$S_2O_3^{2-}$ + 0.75 H_3O^+ → 1.20 S^0 + 0.09 SO_4^{2-} + NM
Exp_$S_2O_3^{2-}$_c	5.7	2.6 x10^{-2}	0.7*	No reaction
Exp_$S_2O_3^{2-}$_d	2.03	2.5 x 10^{-2}	2.5	$S_2O_3^{2-}$ + 1.40 H_3O^+ → 0.67 S^0 + 0.30 SO_4^{2-} + 0.30 SO_2(stripped)
Exp_$S_2O_3^{2-}$_e	2.53	1 x 10^{-2}	2.2	$S_2O_3^{2-}$ + 1.20 H_3O^+ → 0.27 S^0 + 0.30 SO_4^{2-} + 0.31 SO_2(stripped)

NM : sulfur compound not measured because of volatilization due to the use of the open configuration of the reactor.

*: surface aeration

The equation generally used to present the thiosulfate disproportionate is not confirmed by the experimental results obtained in the open system because of a possible gas stripping. Indeed, volatilization of a sulfur compound is kla_{O2}-dependent.

3.1.2. SO_2 volatilization of at low pH conditions

The figure 49 shows the time course of the different parameters measured during the experience Exp_$S_2O_3^{2-}$_d. The experience Exp_$S_2O_3^{2-}$_d was operated with the reactor in the closed configuration. Thus, the gas phase passed through a soda trap bottle. The figure 51 shows the total sulfur mass balance and the different fractions for the sulfur species at the start and at the end of the experience.

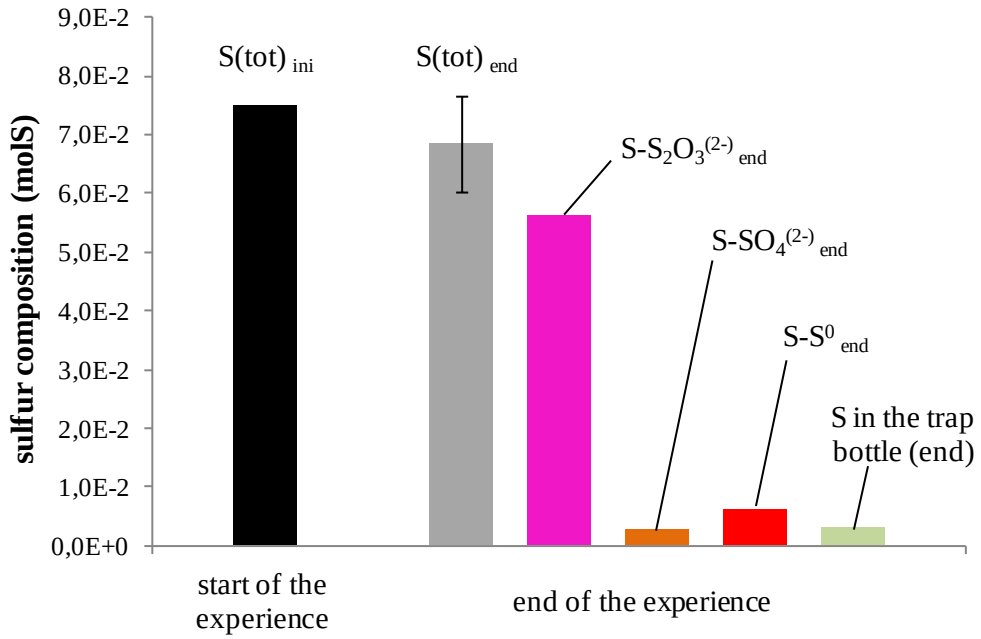

Figure 51: Exp_$S_2O_3^{2-}$_d – sulfur mass balance and fraction of the different sulfur species. ■ : the total quantity of sulfur at the initial time (t = 0 h); ■ : the total quantity of sulfur recovery at the end of the experience (t = 23h); ■ : the sulfur quantity recovery under thiosulfate form at the end of the experience; ■ : the sulfur quantity recovery under sulfate form at the end of the experience; ■ : the sulfur quantity recovery by precipitation at the end of the experience; ■: the sulfur quantity recovery by the trap-bottle at the end of the experience (sulfur striped during the reaction).

During the experience Exp_$S_2O_3^{2-}$_d only 26% of the initial sulfur (as thiosulfate) was transformed (figure 49 and figure 51). However, at the end of the experience, 92 ± 10% of the initial sulfur was recovery (thiosulfate + sulfate + sulfur precipitated + sulfur striped in the gas phase). In the soda trap-bottle 4% of the initial sulfur was analyzed as sulfate. This results, linked to the oxygen consumption recorded during the experiments Exp_$S_2O_3^{2-}$_a, Exp_$S_2O_3^{2-}$_b, Exp_$S_2O_3^{2-}$_e, confirmed the formation of S(IV)-oxides and the possible volatilization of a part of the sulfur as sulfur dioxide (SO_2) during the thiosulfate disproportionate reaction.

3.1.3. Towards a model for the description of the thiosulfate disproportionate reaction in aqueous solution

The figure 52 based on the literature review and the experimental results presented previously, illustrates the chemical species and the processes (chemical and physical) involved in the description of the system. The thiosulfate disproportionate reaction is described as a bimolecular process between the thiosulfate form ($S_2O_3^{2-}$) and its associated acid form ($HS_2O_3^-$), in accordance with literature results (Dinegar et al., 1951) (Johnston and McAmish, 1973).

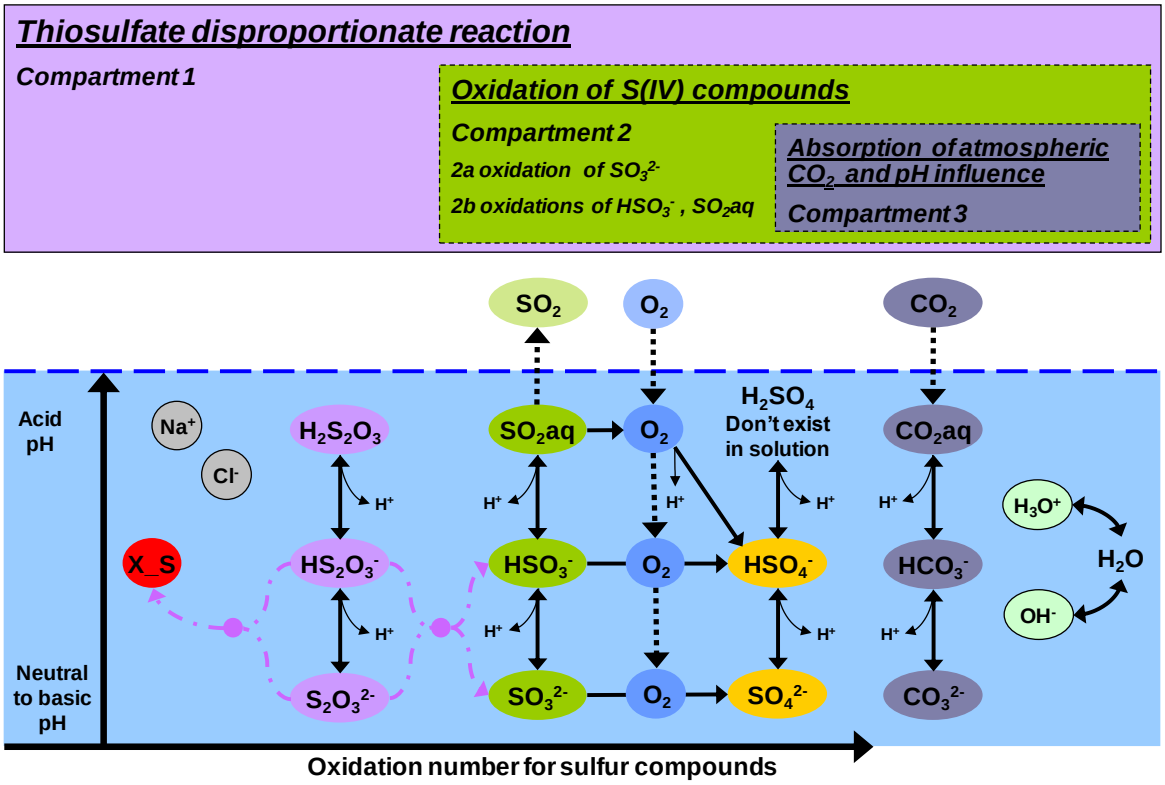

Figure 52: Schematic representation of the thiosulfate disproportionate system, composed by three compartment including specific chemical and physical processes. Compartment 1: the thiosulfate disproportionate system including the all processes. Compartment 2: reactivity of the sulfur(IV) oxides including oxidations reactions, acid-base equilibriums and gas-liquid mass transfer of the sulfur dioxide. Compartment 3: the absorption of the carbon dioxide in aqueous solution, including the mass transfer process and the acid-base equilibriums.
: $S_2O_3^{2-}$ disproportionate reaction; : equilibriums; : irreversible reactions; : gas-liquid mass transfer.

The system of the thiosulfate disproportionate reaction was decomposed in three reactive compartments:

- The Compartment 1 describes the whole thiosulfate disproportionate system, with all the processes involved.

- The Compartment 2 describes the S(IV)-oxides reactions, as acid-base equilibriums, oxidation reactions and the gas-liquid exchanges of the oxygen and the sulfur dioxide. The compartment 2 could be separated in two sub-compartments, corresponding to the sulfite (SO_3^{2-}) oxidation (2a), and to the bisulfite (HSO_3^-) and the sulphurous acid (H_2SO_3 noted SO_2aq) oxidations (2b), depending on the pH.
- The Compartment 3 describes the absorption of the atmospheric carbon dioxide (CO_2) and the influence of this physical process on the pH definition by the description of the carbon dioxide acid-base equilibrium in aqueous solution. To describe the pH of the liquid, the water ionisation equilibrium process was joined to the Compartment 3.

The ionic species Na^+ and Cl^- (added during the experiments as NaS_2O_3, and HCl) were joined to the global description as non-reactive compounds because they are included in the ionic strength definition, thus on the activity definition for each species in solution (for further explanations see paragraph *[1.5.2.]* of the annexes of this chapter).

The Compartment 1 depends on the Compartments 2 and 3, but the Compartment 2 can be studied independently of the thiosulfate disproportionate reaction. However, the Compartment 2 is always dependent of the Compartment 3 for the definition of the global parameters (as pH). The Compartment 3 can be studied independently of the Compartment 2.

3.2. The model development for the dynamic simulation of the thiosulfate disproportionate system.

First the Compartment 3 was developed and validated, then the Compartment 2 was tested, and finally the Compartment 1 was added and the whole tested.

The development of the model, concerning the compartment 3 and 2a are presented in annexes of this chapter. Only the model representing the whole system of the thiosulfate disproportionate reaction is presented in this chapter.

3.2.1. Kinetic definitions previously described in the literature (Compartment 1 and Compartment 2b)

As presented in the introduction of this chapter, the thiosulfate disproportionate reaction was described by Johnston in 1973 by the equation (Eq 55) and (Eq 59).

Eq 55: $(HS_2O_3.S_2O_3^{2-}) \rightarrow S_2 + HSO_3^- + SO_3^{2-}$

where S_2 was the precursor to the condensation of S_8 molecule thus for the formation of colloidal sulfur.

Eq 59: $d[S]/dt = k_{dis}.[H^+].[(S_2O_3^{2-}]^2$ for 2.1 < pH < 2.7, 15°C < T < 45°C and μ = 0.035 mol/l.

The bisulfite oxidation was described by Connick and Zhang in 1996 by the equation (Eq 62) and (Eq 63) and by the equation (Eq 62) and (Eq 64) for Lancia in 1999, and presented in the annexes of this chapter.

Eq 62: $HSO_3^- + 1/2\,O_2 \rightarrow HSO_4^-$

Eq 63: $-d[O_2]/dt = k_{obs}.[HSO_3^-]^2.[H_3O^+]^{-2}$ with k_{obs} = 3.6 x 10^6 mol.l^{-1}.s^{-1}.

defined at pH = 4.5 for a ionic strength μ = 0.05 mol/l

Eq 64: $-d[HSO_3^-]/dt = k_u.[HSO_3^-]^{3/2}$ with k_U = 428.4 $l^{1.5}$.$mol^{-0.5}$.h^{-1}.

3.2.2. The model definition for the thiosulfate disproportionate system (Compartment 1)

The table 18 presents the stoichiometric matrix for the mathematical description of the thiosulfate disproportionate system in aerated aqueous solution (Compartment 1).

The table 19 presents the kinetic rates for all the processes involved in the mathematical description of the thiosulfate disproportionate system in aerated aqueous solution (Compartment 1).

The table 20 and the table 21 present the different parameters used in Aquasim® for the resolution of the mathematical model presented in the table 18 and the table 19.

Table 18: Parameters State variables, kinetic processes and stoechiometric ratio for the mathematical description of the thiosulfate disproportionate reaction in aerated aqueous solution (Compartment 1).

State Variables		Description	$[H_3O^+]$	$[OH^-]$	$[Na^+]$	$[Cl^-]$	$[O_2]$	$[H_2S_2O_3]$	$[HS_2O_3^-]$	$[S_2O_3^{2-}]$	$[H_2CO_3]$	$[HCO_3^-]$	$[CO_3^{2-}]$	$[H_2SO_3]$	$[HSO_3^-]$	$[SO_3^{2-}]$	$[H_2SO_4]$	$[HSO_4^-]$	$[SO_4^{2-}]$	S^0
		Unit	mol/L	mol/L	mol/L	mol/L	mol/L	mol/L	mol/L	mol/L	mol/L	mol/L	mol/L	mol/L	mol/L	mol/L	mol/L	mol/L	mol/L	mol/L
		Expression	H	OH	Na	Cl	O2	H2S2O3	HS2O3	S2O3	CO2aq	HCO3	CO3	SO2aq	HSO3	SO3	H2SO4	HSO4	SO4	X_S
Processes	**Acid –base equilibriums**	Water_deionization_f	1	1																
		Water_deionization_r	-1	-1																
		$CO_2aq \rightarrow HCO_3^- + H^+$	1								-1	1								
		$HCO_3^- + H^+ \rightarrow CO_2aq$	-1								1	-1								
		$HCO_3^- \rightarrow CO_3^{2-} + H^+$	1									-1	1							
		$CO_3^{2-} + H^+ \rightarrow HCO_3^-$	-1									1	-1							
		$SO_2aq \rightarrow HSO_3^- + H^+$	1											-1	1					
		$HSO_3^- + H^+ \rightarrow SO_2aq$	-1											1	-1					
		$HSO_3^- \rightarrow SO_3^{2-} + H^+$	1												-1	1				
		$SO_3^{2-} + H^+ \rightarrow HSO_3^-$	-1												1	-1				
		$H_2S_2O_3 \rightarrow HS_2O_3^- + H^+$	1					-1	1											
		$HS_2O_3^- + H^+ \rightarrow H_2S_2O_3$	-1					1	-1											
		$HS_2O_3^- \rightarrow S_2O_3^{2-} + H^+$	1						-1	1										
		$S_2O_3^{2-} + H^+ \rightarrow HS_2O_3^-$	-1						1	-1										
		$H_2SO_4 \rightarrow HSO_4^- + H^+$	1														-1	1		
		$HSO_4^- + H^+ \rightarrow H_2SO_4$	-1														1	-1		
		$HSO_4^- \rightarrow SO_4^{2-} + H^+$	1															-1	1	
		$SO_4^{2-} + H^+ \rightarrow HSO_4^-$	-1															1	-1	
	Irreversible reactions	$HSO_3^- + O_2 \rightarrow HSO_4^-$					-1								-2			2		
		$SO_3^- + O_2 \rightarrow SO_4^-$					-0.5									-1			1	
		$S_2O_3^{2-} + HS_2O_3^- \rightarrow S(IV) + S_8$							-1	-1					1	1				2
	Transfers	$O_2gas \rightarrow O_2aq$					1													
		$CO_2gas \rightarrow CO_2aq$									1									

Table 19: Kinetic rates per processes for the mathematical description of the the thiosulfate disproportionate reaction in aerated aqueous solution (Compartment 1).

		Reaction definitions	Rates	Descriptions
Processes	**Acid –base equilibriums**	Water_deionization_f	kw*Kw	Irreversible reaction: $2H_2O \rightarrow H_3O^+ + OH^-$
		Water_deionization_r	kw*fm*OH*fm*H	Irreversible reaction: $2H_2O \leftarrow H_3O^+ + OH^-$
		$CO_2aq \rightarrow HCO_3^- + H^+$	kC1*KaC1*CO2aq	Irreversible reaction: $H_2CO_3 + H_2O \rightarrow HCO_3^- + H_3O^+$
		$HCO_3^- + H^+ \rightarrow CO_2aq$	kC1*fm*HCO3*fm*H	Irreversible reaction: $H_2CO_3 + H_2O \leftarrow HCO_3^- + H_3O^+$
		$HCO_3^- \rightarrow CO_3^{2-} + H^+$	kC2*KaC2*fm*HCO3	Irreversible reaction: $HCO_3^- + H_2O \rightarrow CO_3^{2-} + H_3O^+$
		$CO_3^{2-} + H^+ \rightarrow HCO_3^-$	kC2*fd*CO3*fm*H	Irreversible reaction: $HCO_3^- + H_2O \leftarrow CO_3^{2-} + H_3O^+$
		$SO_2aq \rightarrow HSO_3^- + H^+$	kS(IV)1*KaS(IV)1*SO2aq	Irreversible reaction: $H_2SO_3 + H_2O \rightarrow HSO_3^- + H_3O^+$
		$HSO_3^- + H^+ \rightarrow SO_2aq$	kS(IV)1*fm*HSO3*fm*H	Irreversible reaction: $H_2SO_3 + H_2O \leftarrow HSO_3^- + H_3O^+$
		$HSO_3^- \rightarrow SO_3^{2-} + H^+$	kS(IV)2*KaS(IV)2*fm*HSO3	Irreversible reaction: $HSO_3^- + H_2O \rightarrow SO_3^{2-} + H_3O^+$
		$SO_3^{2-} + H^+ \rightarrow HSO_3^-$	kS(IV)2*fd*SO3*fm*H	Irreversible reaction: $HSO_3^- + H_2O \leftarrow SO_3^{2-} + H_3O^+$
		$H_2S_2O_3 \rightarrow HS_2O_3^- + H^+$	kT1*KaT1*H2S2O3	Irreversible reaction: $H_2S_2O_3 + H_2O \rightarrow HS_2O_3^- + H_3O^+$
		$HS_2O_3^- + H^+ \rightarrow H_2S_2O_3$	kT1*fm*HS2O3*fm*H	Irreversible reaction: $H_2S_2O_3 + H_2O \leftarrow HS_2O_3^- + H_3O^+$
		$HS_2O_3^- \rightarrow S_2O_3^{2-} + H^+$	kT2*KaT2*fm*HS2O3	Irreversible reaction: $HS_2O_3^- + H_2O \rightarrow S_2O_3^{2-} + H_3O^+$
		$S_2O_3^{2-} + H^+ \rightarrow HS_2O_3^-$	kT2*fd*S2O3*fm*H	Irreversible reaction: $HS_2O_3^- + H_2O \leftarrow S_2O_3^{2-} + H_3O^+$
		$H_2SO_4 \rightarrow HSO_4^- + H^+$	kS(VI)1*KaS(VI)1*H2SO4	Irreversible reaction: $H_2SO_4 + H_2O \rightarrow HSO_4^- + H_3O^+$
		$HSO_4^- + H^+ \rightarrow H_2SO_4$	kS(VI)1*fm*HSO4*fm*H	Irreversible reaction: $H_2SO_4 + H_2O \leftarrow HSO_4^- + H_3O^+$
		$HSO_4^- \rightarrow SO_4^{2-} + H^+$	kS(VI)2*KaS(VI)2*fm*HSO4	Irreversible reaction: $HSO_4^- + H_2O \rightarrow SO_4^{2-} + H_3O^+$
		$SO_4^{2-} + H^+ \rightarrow HSO_4^-$	kS(VI)2*fd*SO4*fm*H	Irreversible reaction: $HSO_4^- + H_2O \leftarrow SO_4^{2-} + H_3O^+$
	Irreversible reactions	$HSO_3^- + O_2 \rightarrow HSO_4^-$	Connick 1995 or Lancia 1999	Bisulfite oxidation: $2HSO_3^- + O_2 \rightarrow 2HSO_4^-$
		$SO_3^- + O_2 \rightarrow SO_4^-$	kSO3*((fd*SO3)^2) *(O2)	Sulfite oxidation: $SO_3^{2-} + 0.5\ O_2 \rightarrow SO_4^{2-}$
		$S_2O_3^{2-} + HS_2O_3^- \rightarrow S(IV) + S_2$	Johnston 1973	Thiosulfate disproportionate reaction: $S_2O_3^{2-} + HS_2O_3^- \rightarrow S_2 + HSO_3^- + SO_3^{2-}$
	Transfers	$O_2gas \rightarrow O_2aq$	KlaO2*EO2*(sat_O2-O2)	Oxygen absorption: $O_2gas \rightarrow O_2aq$
		$CO_2gas \rightarrow CO_2aq$	KlaCO2*ECO2*(sat_CO2-CO2aq)	Carbon dioxode absorption: $CO_2gas \rightarrow CO_2aq$

Table 20: Equilibrium parameters values and/or expressions used for the mathematical description of the thiosulfate disproportionate system in aerated aqueous solution (Compartment 1).

Parameters	Description	Values or Expressions	Unities	Ref
T	Experimental temperature	Experimental data	K	Experimental data
Zi	Valence of the specie i	Depends on the valence of the i specie	-	-
μ	Ionic strength (Ci = concentration of the specie i)	$0.5 \times \Sigma(Ci \times Zi^2)$	-	(Loewenthal et al., 1989)
A	Dependent temperature constant	$1.825 \times 10^6 \times (78.3 \times T)^{-1,5}$		(Loewenthal et al., 1989)
fm	Monovalent activity coefficient	$10^{(A \times Zi \times ((\mu \times 0.5/(1 + \mu^{0.5})) - 0.3 \times \mu)}$	-	(Loewenthal et al., 1989)
fd	Divalent activity coefficient	$10^{(A \times \mu^2 \times ((\mu \times 0,5/(1 + \mu^{0.5})) - 0.3 \times \mu)}$	-	-
Kw	Water ionisation constant	$3.46 \times 10^{-24} \times \exp(0.0729 \times T)$	-	(Lide, 1990)
Ka_{C1}	First acid-base equilibrium constant (CO_2aq)	$10^{(- (3404.7/T - 14.8435 + 0.03279 \times T))}$	-	(Loewenthal et al., 1989)
Ka_{C2}	Second acid-base equilibrium constant (CO_2aq)	$10^{(- (2902.47/T - 6.498 + 0.02379 \times T))}$	-	(Loewenthal et al., 1989)
$Ka_{S(IV)1}$	First acid-base equilibrium constant (SO_2aq)	$10^{(- 4.74 + (853/T))}$		(Maahs, 1982)
$Ka_{S(IV)2}$	Second acid-base equilibrium constant (SO_2aq)	$10^{(- 9.278 + (621.9/T))}$		(Maahs, 1982)
$Ka_{S(VI)1}$	First acid-base equilibrium constant (H_2SO_4)	100 (totalement dissocié en solution)		(Lide, 1990)
$Ka_{S(VI)2}$	Second acid-base equilibrium constant (H_2SO_4)	$9.895 \times 10^{-8} \times T^3 - 8.949 \times 10^{-5} \times T^2 + 0.02671 \times T^{-2} + 2.62$		(lide, 1990)
Ka_{T1}	First acid-base equilibrium constant ($H_2S_2O_3$)	0.25		(Page, 1953)
Ka_{T2}	Second acid-base equilibrium constant ($H_2S_2O_3$)	$10^{-1.70}$		(Page, 1953)
$H_{CO2/water}$ (T)	Carbon dioxide Henry constant (temperature)	$83400 \times \exp^{0,0254 \times T}$	Pa	relation (USPEA)
Sat_O2aq (T)	Dissolved oxygen saturation concentration	$7.2044x10^{-7}xT^4 - 0.00090733xT^3 + 0.42974xT^2 - 90.817xT + 7238.6$		Adapted from solublity data
pH	pH of the aqueous solution	-log(fm x H)		-

Table 21: Kinetic parameters values and/or expressions used for the mathematical description of the thiosulfate disproportionate system in aerated aqueous solution (Compartment 1).

Parameters	Description	Values or Expressions	Unities	Ref
kw	Rate constant water dionization reaction	3.6×10^{13}	$l.mol^{-1}.h^{-1}$	(Musvoto et al, 2000)
kC1	Rate constant 1° acid-base eq (CO_2aq)	3.6×10^{10}	$l.mol^{-1}.h^{-1}$	(Musvoto et al, 2000)
kC2	Rate constant 2° acid-base eq (CO_2aq)	3.6×10^{13}	$l.mol^{-1}.h^{-1}$	(Musvoto et al, 2000)
kS(IV)1	Rate constant 1° acid-base eq (SO_2aq)	10^{10}	$l.mol^{-1}.h^{-1}$	defined
kS(IV)2	Rate constant 2° acid-base eq (SO_2aq)	10^{10}	$l.mol^{-1}.h^{-1}$	defined
kS(VI)1	Rate constant 1° acid-base eq (H_2SO_4)	10^{10}	$l.mol^{-1}.h^{-1}$	defined
kS(VI)2	Rate constant 2° acid-base eq (H_2SO_4)	10^{10}	$l.mol^{-1}.h^{-1}$	defined
kT1	Rate constant 1° acid-base eq ($H_2S_2O_3$)	10^{10}	$l.mol^{-1}.h^{-1}$	defined
kT2	Rate constant 2° acid-base eq ($H_2S_2O_3$)	10^{10}	$l.mol^{-1}.h^{-1}$	defined
$\mathbf{k_{SO3}}$	Rate constant for the sulfite oxidation	1.63×10^{10}	$L^2.mol^{-2}.h^{-2}$	From this study
$\mathbf{k_{HSO3}}$	Rate constant for the bisulfite oxidation	1.296×10^{10} $l^2.mol^{-2}.h^{-1}$ or 2×428.4 $l^{1.5}.mol^{-1.5}.h^{-1}$	/	Connick 1995 or Lancia 1999
$\mathbf{k_{dis}}$	Rate constant for the thiosulfate disproportionate reaction	$(1.64 \pm 0.13) \times 10^{11} \times exp^{(-15930 \pm 160)/R.T)}$	$L^2.mol^{-2}.h^{-2}$	Johnston 1973
a	Volumetric interfacial area	Surface libre du réacteur (aération de surface) = 7,85 $m^2.m^{-3}$	$m^2.m^{-3}$	Experimental data
KlaO2	Volumetric rate oxygen transfer	Donnée expérimentale (aération de surface = 0,7 h^{-1})	h^{-1}	-
klO2	Rate oxygen transfer	KlaO2 / a	$m.h^{-1}$	-
KlaCO2	Volumetric rate carbon dioxide transfer	$KlaO2 \times (D_{CO2aq}(T)/D_{O2}(T))^{0.5}$	h^{-1}	(Spérandio, 1997)
Hatta	Hatta number for the oxygen transfer	$kSO3x(2/(1+1))x(D_{O2}(T)x3600)x([O_2]^{(1-1)})x([SO_3^{2-}]^2)^{0.5})/klO2$		(Danckwerts, 1970)
EO2	Enhancement factor for the oxygen transfer	$(1+Hatta^2)^{0.5}$		(Danckwerts, 1970)
ECO2	Enhancement factor for the carbon dioxide transfer	$1+((D_{CO3(2-)}(T) \times [CO_3^{2-}])/(D_{CO2aq}(T) \times [CO_2aq^{sat}]))$	-	(Bosch et al., 1989)

3.2.3. Simulations obtained with literature data (Compartment 1 and Compartment 2b)

The figure 53 shows the simulation results obtained with the kinetic definitions proposed by the equation (Eq 63) and the equation (Eq 64) from the literature, for the experiments Exp_$S_2O_3^{2-}$_a and Exp_$S_2O_3^{2-}$_c. The definition of the thiosulfate disproportionate reaction does not fit the experimental data for the thiosulfate consumption. For the experiment Exp_$S_2O_3^{2-}$_c (with no thiosulfate reaction recorded experimentally), the kinetic definition tested simulated an important thiosulfate consumption. Concerning the dissolved oxygen consumption, the kinetic expression for the oxidation of S(IV)-oxides with zero order for oxygen concentration induced the simulation of negative oxygen concentration. Thus the definition of the kinetic law can lead to numerical problems.

To represent the thiosulfate disproportionate system, the definition of new kinetic laws was necessary.

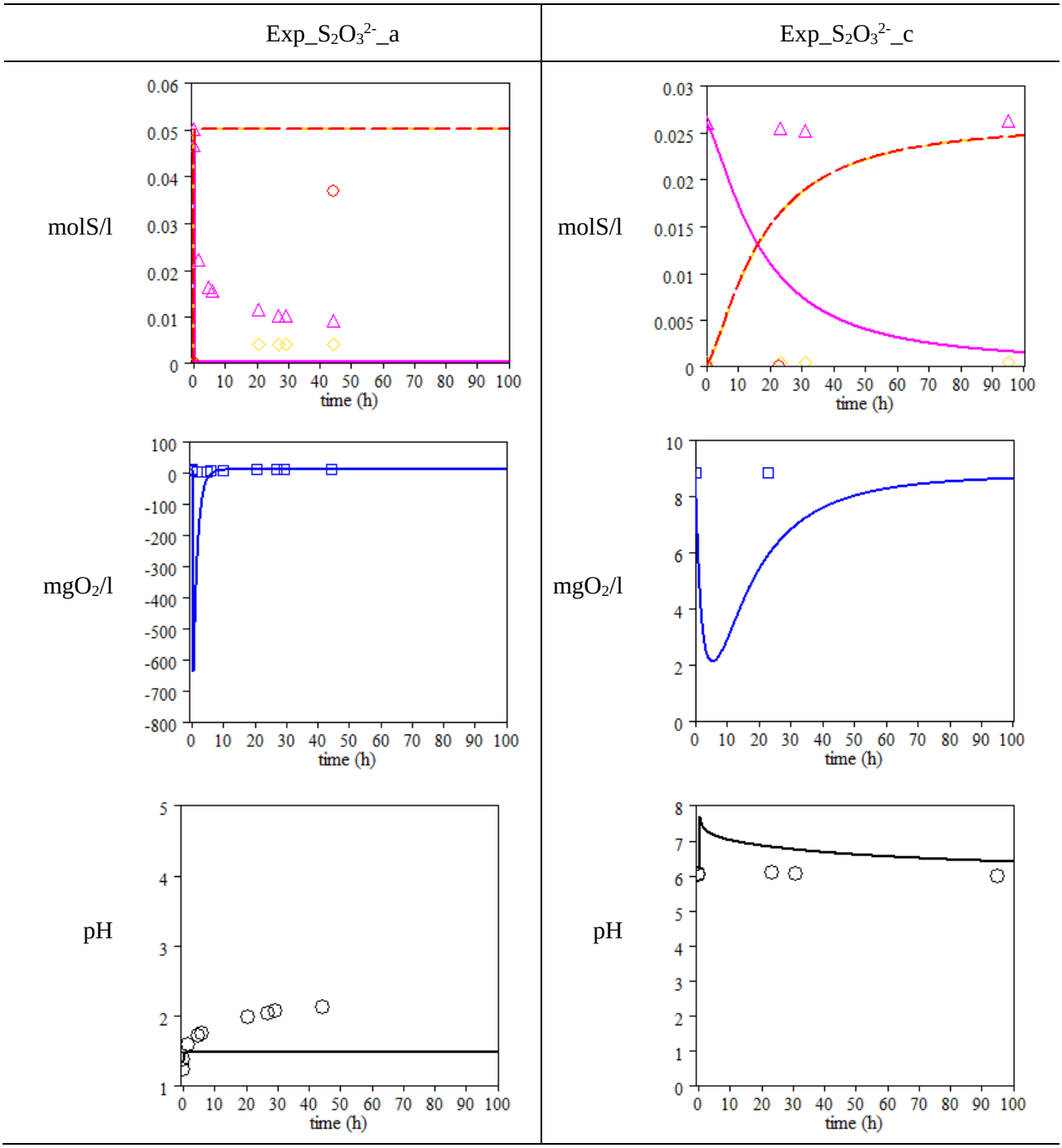

Figure 53: Simulation results with Johnston and Connick kinetic definition (Exp_$S_2O_3^{2-}$_a and – Exp_$S_2O_3^{2-}$_c). Experimental data: △: the thiosulfate concentration ($S_2O_3^{2-}$) (mol/l); ◇: the sulfate concentration (SO_4^{2-}) (mol/l); ○ : the mass of precipitate expressed as equivalent of loss sulfur (molS/l); □ : the dissolved oxygen concentration; ○ : the pH.
Numerical data: ——— : the thiosulfate concentration ($S_2O_3^{2-}$) (mol/l); ——— : the sulfate concentration (SO_4^{2-}) (mol/l); – – : the colloidal sulfur (eqmolS/l); ——— : dissolved oxygen concentration (mgO_2/l); ——— : pH measurement.

3.2.4. New proposal for the thiosulfate disproportionate reaction description

Because bimolecular reaction between $S_2O_3^{2-}$ and HS_2O^{3-} is the limiting reaction (Dinegar et al., 1951) (Johnston and McAmish, 1973), the thiosulfate disproportionate reaction could be described by the equation (Eq 65) for the stoichiometry and by the equation (Eq 66) for the kinetic.

Eq 65: $S_2O_3^{2-} + HS_2O_3^- \rightarrow S_2 + HSO_3^- + SO_3^{2-}$

Eq 66: $-\frac{d(S_2O_3^{2-})}{dt} = k_{dis}.(f_d.[S_2O_3^{2-}])^s.(f_m.[HS_2O_3^-])^t$

where, (s) is the order of the reaction in thiosulfate, (t) the order of the reaction in bithiosulfate, (f_d) is the activity coefficient for the divalent species, (f_m) is the activity coefficient for the monovalent species, and (k_{dis}) is the rate constant (in $l^{s+t-1}.mol^{1-s-t}.h^{-1}$).

For the description of the oxygen consumption, the S(IV)-oxides oxidation must be described by the equation (Eq 62) for the stoichiometry and by the equation (Eq 67) for the kinetic.

Eq 62: $HSO_3^- + 1/2\,O_2 \rightarrow HSO_4^-$

Eq 67: $-\frac{d[HSO_3^-]}{dt} = k_{HSO3}.(f_m.[HSO_3^-])^o.[O_2]^p$

where, (o) is the order of the reaction in bisulfite (HSO_3^-), (p) the order of the reaction in dissolved oxygen, (f_m) is the activity coefficient for the monovalent species and k_{HSO3} is the rate constant (in $l^{o+p-1}.mol^{1-o-p}.h^{-1}$).

The next paragraph presents numerical experiences to evaluate the different parameters and to confirm the kinetic laws proposed in the above section. In a first step, to evaluate the kinetic laws of the thiosulfate disproportionate reaction (only thiosulfate and bithiosulfate concentrations dependent) and the S(IV)-oxides oxidation (HSO_3^- and H_2SO_3), the pH evolution during the numerical experiments was fixed by the experimental pH dynamic. Then the acid-base equilibrium is used to recalculate the speciation of all the species in solution. Then, in a final step, the quality of the simulations based on the proposed kinetic laws in the real conditions, including pH determination, will be evaluated.

3.2.4.1. Determination of partial orders and constant rate associated for the thiosulfate disproportionate reaction

The table 22 presents the kinetic laws tested and the associated *Dev_S_2O_3* obtained. Seven reaction definitions were tested with different partial orders (s and t) and associated rate constant (k_{dis}).

Table 22: Model definition and evaluation for the thiosulfate disproportionate kinetic (partial orders and rate constant)

Thiosulfate disproportionate reaction			**Mean square deviation**
s	***t***	***k_{dis}*** [a]	**Dev_S_2O_3**
1	1	158	2.15E-05
1	1.5	2993	**2.76E-06**
1	2	5.46E+04	**2.40E-06**
1.5	1.5	47208	3.52E-06
1.5	2	9.67E+05	**2.03E-06**
1.5	2.5	1.84E+07	5.17E-06
2	2	1.68E+07	2.78E-06

a: in $l^{s+t-1}.mol^{1-s-t}.h^{-1}$

The parameter (*Dev_S_2O_3*) enables evaluating the quality of the model definition for the description of the thiosulfate consumption during the thiosulfate disproportionate reaction depending on pH and under different experimental conditions. In the next paragraphs, the three more accurate model definitions are used to identify kinetic parameters of secondary reactions.

3.2.4.2. Determination of partial orders and constant rates associated for the oxidation of bisulfite (HSO_3^-) involved in the definition of the whole system

During the thiosulfate disproportionate reaction, stripping of sulfur dioxide (SO_2gas) due to the formation of S(IV)-oxides was recorded, together with the gas-liquid mass transfer conditions.

To take into account this stripping phenomenon the equation (Eq 68) was added to the model definition. It introduced the relation between the volumetric rate of oxygen mass

transfer definition ($kl.a_{O2}$) and the volumetric rate of the sulfur dioxide mass transfer definition ($kl.a_{SO2}$).

Eq 68: $$-\frac{d[H_2SO_3]}{dt} = kl.a_{O_2} \cdot \left(\frac{kl.a_{SO_2}}{kl.a_{O_2}}\right).[H_2SO_3]$$

where $[H_2SO_3]$ is the concentration of the sulphurous acid (in mol/l), ($kl.a_{O_2}$) is the volumetric rate for the gas-liquid mass transfer of oxygen (measured in h^{-1}) and $\left(\frac{kl.a_{SO_2}}{kl.a_{O_2}}\right)$ is the parameters linked the measures of $kl.a_{O2}$ to the volumetric rate for the gas-liquid mass of sulfur dioxide $kl.a_{SO2}$.

For each set of parameters, the mean square deviations between experimental data and numerical data, for dissolved oxygen concentration (Dev_O_2) and sulfate concentration (Dev_SO_4), were calculated. The best model definition was evaluated by the calculation of the parameter "Model evaluation" determined by the equation (Eq 69).

Eq 69: $$Model\ evaluation = \frac{\left(4.\frac{Dev\_S_2O_3}{mean(Dev\_S_2O_3)} + 3.\frac{Dev\_O_2}{mean(Dev\_O_2)} + 4.\frac{Dev\_SO_4}{mean(Dev\_SO_4)}\right)}{4+3+4}$$

The table 23 presents the model definitions tested and the results obtained for the mean square deviations and the "Model evaluation". For all the numerical experiments, the parameter $\left(\frac{kl.a_{SO_2}}{kl.a_{O_2}}\right)$ was determined in the same range order ($\left(\frac{kl.a_{SO_2}}{kl.a_{O_2}}\right)$ = 0.996 ± 0.004)[6]. Thus the variations in the "Model evaluation" for each kinetic law tested were due to the chemical reaction definitions only. For the three thiosulfate disproportionate kinetics identified in the previous paragraph (low $Dev\_S_2O_3$), the "Model evaluation" eliminated the definition with s = 1 and t = 1.5. For the two last thiosulfate disproportionate kinetics (s = 1, t = 2, and s = 1.5, t = 2) the bisulfite oxidation with (o = 1, p = 1) and (o = 1.5, p = 1) were clearly identified as the best definitions for the kinetic model.

[6] : at 20°C the ratio $\sqrt{\frac{DSO_2}{DO_2}}$ is equal to 0.84, but can be not used as relation to determine $kl.a_{SO_2}$ due to the Henry constant limitation.

Table 23: Model definition and evaluation for the thiosulfate disproportionate kinetic (partial orders and rate constant) and the bisulfite oxidation at low pH (partial orders and rate constant)

Thiosulfate disproportionate reaction			**Mean square deviation**	**Bisulfite oxidation**				**Mean square deviation between the numerical data and the experimental data for the model evaluation**		
s	***t***	k_{dis} [a]	**Dev_S_2O_3**	***o***	***p***	k_{HSO3} [b]	**kla$_{SO2}$ /kla$_{O2}$**	**Dev_O_2**	**Dev_SO_4**	**Model evaluation [c]**
1	1	158	2.15E-05							
1	1.5	2993	**2.76E-06**	1	1	599	0.996	1.34	5.77E-07	1.35
				1.5	1	12907	0.998	1.03	1.94E-07	0.91
				2	1	2.72E+05	0.999	0.93	1.78E-07	0.87
				4	1	8.02E+10	0.999	1.32	5.85E-07	1.35
1	2	5.46E+04	**2.40E-06**	1	1	534	0.987	0.905	1.08E-07	**0.74**
				1.5	1	12594	0.992	0.7	2.95E-07	0.84
				2	1	2.65E+05	0.996	0.602	5.38E-07	1.03
				4	1	6.20E+10	0.997	0.787	1.06E-07	1.54
1.5	1.5	47208	3.52E-06							
1.5	2	9.67E+05	**2.03E-06**	1	1	599	0.998	0.865	8.61E-08	**0.66**
				1.5	1	13232	0.999	0.609	1.47E-07	**0.63**
				2	1	2.90E05	0.999	0.552	3.26E-07	0.77
				4	1	6.96E+10	0.996	0.723	8.72E-07	1,30
1.5	2.5	1.84E+07	5.17E-06							
2	2	1.68E+07	2.78E-06							

a: in $l^{s+t-1}.mol^{1-s-t}.h^{-1}$

b: in $l^{o+p-1}.mol^{1-o-p}.h^{-1}$

c = [4.Dev_S_2O_3/mean(Dev_S_2O_3) + 3.Dev_O_2/mean(Dev_O_2) + 4. Dev_SO_4/mean(Dev_SO_4)] /11

3.2.4.3. Evaluation of partial orders and constant rates associated for the oxidation of sulfurous acid involved in the definition of the whole system

To evaluate the possible influence of the oxidation of H_2SO_3 for a better definition of the model, the same method was applied with different kinetic laws (bisulfite oxidation (Eq 67) and sulphurous acid oxidation (Eq 70)).

Eq 70: $$-\frac{d[H_2SO_3]}{dt} = k_{SO_2} \cdot [H_2SO_3]^q \cdot [O_2]^r$$

where, (q) is the order of the reaction in bisulfite (H_2SO_3), (r) the order of the reaction in dissolved oxygen, k_{SO2} is the rate constant (in $l^{q+r-1}.mol^{1-q-r}.h^{-1}$).

The influence of this additional reaction was evaluated by the comparison between the numerical results obtained with sulphurous acid oxidation and without.

The table 24 presents the results obtained for the different kinetic definitions. As for the definition without sulphurous acid oxidation, the parameter $\left(\frac{kla_{SO_2}}{kla_{O_2}}\right)$ was consistent for all the numerical experiments. The "Model evaluation" indicated five interesting model definitions, three with the description of the sulphurous acid oxidation and two without.

Table 24: Model definition and evaluation for the thiosulfate disproportionate kinetic (partial orders and rate constant) and the bisulfite oxidation at low pH (partial orders and rate constant) with and without sulfurous acid oxidation.

Thiosulfate disproportionate reaction			**Bisulfite oxidation**			**Sulphurous acid oxidation**			**Mean square deviation between the numerical data and the experimental data for the model evaluation**				
s	**t**	k_{dis} [a]	**o**	**p**	k_{HSO3} [b]	**q**	**r**	k_{SO2} [c]	**klaSO2 /klaO2**	**Dev_O2**	**Dev_S2O3**	**Dev_SO4**	**Model [d] evaluation**
1	2	5.46E+04	1	1	534				0.987	0.905	2.40E-06	1.08E-07	0.89
			1.5	1	12594				0.992	0.7	2.40E-06	2.95E-07	0.97
			2	1	2.65E+05				0.996	0.602	2.40E-06	5.38E-07	1.15
			4	1	6.20E+10				0.997	0.787	2.40E-06	1.06E+06	1.72
1.5	2	9.67E+05	1	1	599				0.998	0.865	2.03E-06	8.61E+06	**0.79**
			1.5	1	13232				0.999	0.609	2.03E-06	1.47E-07	**0.74**
			2	1	2.90E+05				0.999	0.552	2.03E-06	3.26E-07	0.88
			4	1	6.96E+10				0.996	0.723	2.03E-06	8.72E-07	1.46
1	2	5.46E+04	1	1	233	1	1	257	0.999	0.771	2.40E-06	3.52E-07	1.06
			1.5	1	2627	1.5	1	5290	0.999	0.42	2.40E-06	2.42E-07	**0.80**
			2	1	1.83E+05	2	1	3.18E+04	0.997	0.474	2.40E-06	6.29E-07	1.18
1.5	2	9.67E+05	1	1	157	1	1	333	0.999	0.64	2.03E-06	1.64E-07	**0.77**
			1.5	1	2849	1.5	1	5533	0.999	0.379	2.03E-06	2.48E-07	**0.73**
			2	1	2.16E+04	2	1	1.05E+05	0.999	0.277	2.03E-06	4.46E-07	0.87

a: in $l^{s+t-1}.mol^{1-s-t}.h^{-1}$

b: in $l^{o+p-1}.mol^{1-o-p}.h^{-1}$

c: in $l^{q+r-1}.mol^{1-q-r}.h^{-1}$

d = [4.Dev_S_2O_3/mean(Dev_S_2O_3) + 3.Dev_O_2/mean(Dev_O_2) + 4.Dev_SO_4/mean(Dev_SO_4)] /11

3.2.4.4. Determination of the numerical parameters to define the system of the thiosulfate disproportionate reaction

The last step for the determination of the best model definition was the simulation of the experiments with the complete model structure (pH as a variable). For these numerical experiments the parameter $\left(\frac{kl.a_{SO_2}}{kl.a_{O_2}}\right)$ was fixed (= 0.996).

The table 25 presents the definition of the five kinetic models tested (issue from the best model definitions evaluated in the table 24) and the results obtained. The mean square deviation for the pH was calculated, and added to the definition of the parameter "Model evaluation". The results obtained, indicated that the more consistent model definition was s = 1.5, t = 2, o = 1, p = 1, q = 1 and r = 1 with k_{dis} = 9.67 x 10^5 $l^{2.5}$.$mol^{-2.5}$.h^{-1}, k_{HSO3}= 157 l.mol^{-1}.h^{-1} and k_{SO2}= 333 l.mol^{-1}.h^{-1}.

Table 25: Model definition and evaluation for the thiosulfate disproportionate kinetic (partial orders and rate constant) and the bisulfite oxidation at low pH (partial orders and rate constant) with and without sulfurous acid oxidation for the complete model (pH calculation).

Thiosulfate disproportionate reaction			**Bisulfite oxidation**			**Sulphurous acid oxidation**			**Mean square deviation between the numerical data and the experimental data for the model evaluation**				
s	**t**	k_{dis} [a]	**o**	**p**	k_{HSO3} [b]	**q**	**r**	k_{SO2} [c]	**Dev_O_2**	**Dev_pH**	**Dev_S_2O_3**	**Dev_SO_4**	**Model [d] Evaluation**
1.5	2	9.67E+05	1	1	599				1.02	0.0675	2.50E-06	2.91E-07	1.13
1.5	2	9.67E+05	1.5	1	13232				0.78	0.060	2.29E-06	1.83E-07	0.92
1	2	5.46E+04	1.5	1	2627	1.5	1	5290	0.38	0.074	1.30E-06	6.35E-07	1.02
1.5	2	9.67E+05	1	1	157	1	1	333	0.36	0.083	1.83E-06	2.61E-07	**0.88**
1.5	2	9.67E+05	1.5	1	2849	1.5	1	5533	0.36	0.083	1.83E-06	5.17E-07	1.05

a: in l^{s+t-1}.mol^{1-s-t}.h^{-1}

b: in l^{o+p-1}.mol^{1-o-p}.h^{-1}

c: in l^{q+r-1}.mol^{1-q-r}.h^{-1}

d = [4.Dev_S_2O_3/mean(Dev_S_2O_3) + 3.Dev_O_2/mean(Dev_O_2) + 4.Dev_SO_4/mean(Dev_SO_4) + 5.Dev_pH/(mean(Dev_pH] /16

The figure 54 shows the simulation results with the model definition proposed compared to the experimental data for all the experiments (sulfur compounds, pH and dissolved oxygen). For all experimental conditions tested, the different parameters are quiet well described quantitatively and dynamically. The numerical model enables the description of the pH evolution depending only on the initial composition of the system.

To be improved and extended to the definition of more complex systems (for example the case of transformation in contact with cementitious materials), the evaluation of the possible homogenous catalysis by dissolved compounds as cationic species (calcium, magnesium, iron) should be assessed and could be an interesting development of the model proposed in this chapter.

The table 26 presents the stoichiometric matrix for the final mathematical description of the thiosulfate disproportionate system in aerated aqueous solution. Compared to the first matrix presented at the table 17 of this chapter, the stoichiometric definition of the thiosulfate disproportionate reaction was modified, one irreversible oxidation (for SO_2aq oxidation by O_2) and a liquid-gas exchange process (sulfur dioxide volatilization) have been added.

The table 27 presents the final kinetic rates for all the processes involved in the mathematical description of the thiosulfate disproportionate system in aerated aqueous solution, with the processes additions described for the stoichiometric matrix (table 18).

The table 28 and the table 29 present the different parameters used for the resolution of the final mathematical model presented in the table 26 and the table 27.

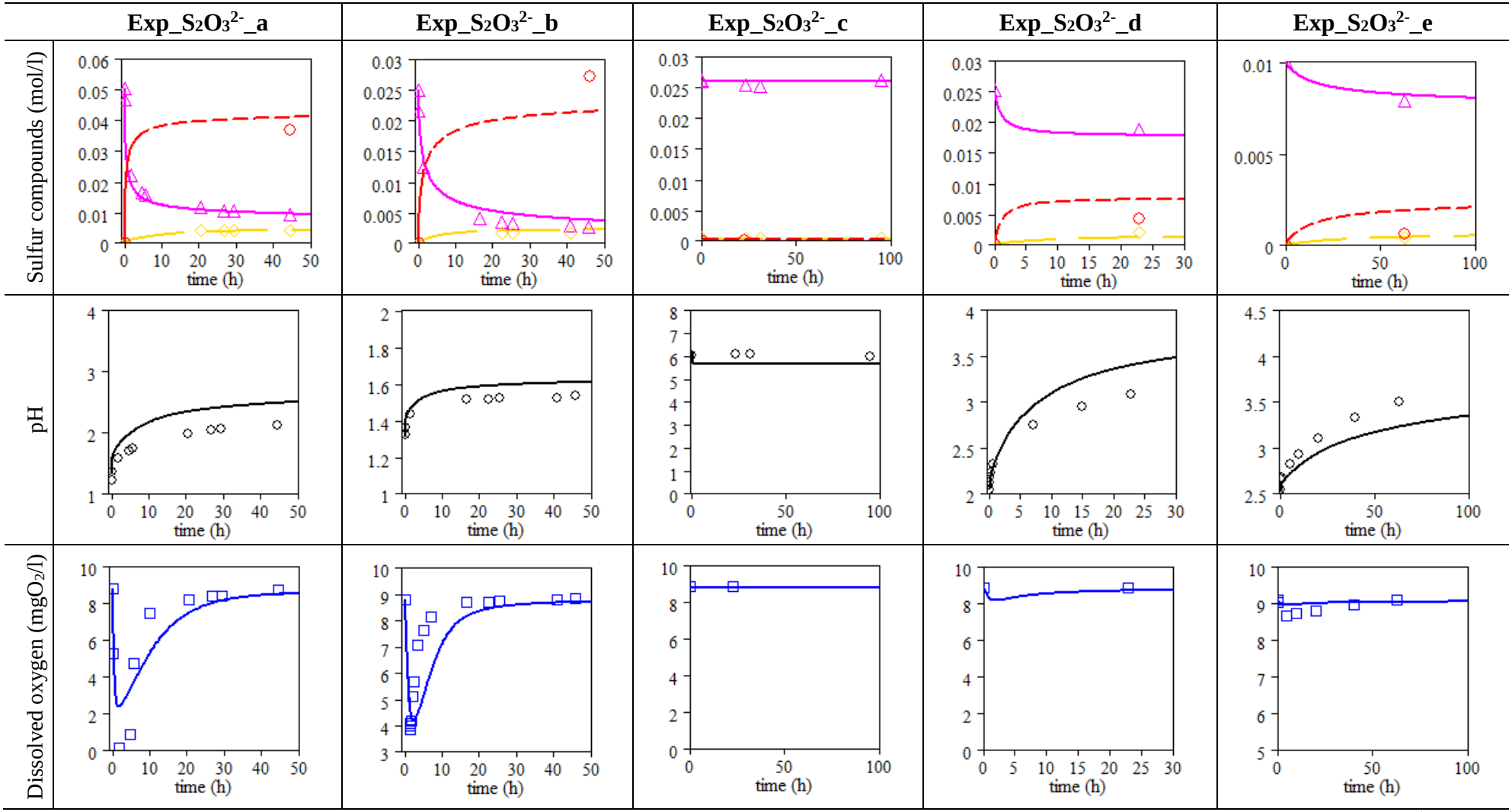

Figure 54: Simulation results for the kinetic model definition (Exp_$S_2O_3^{2-}$_a to Exp_$S_2O_3^{2-}$_e). Experimental data: △: the thiosulfate concentration ($S_2O_3^{2-}$) (mol/l); ◇: the sulfate concentration (SO_4^{2-}) (mol/l); ○ : the mass of precipitate expressed as equivalent of loss sulfur (molS/l); □ : the dissolved oxygen concentration; ○ : the pH. Numerical data: ▬ : the thiosulfate concentration ($S_2O_3^{2-}$) (mol/l); ▬ : the sulfate concentration (SO_4^{2-}) (mol/l); ▬ ▬ : the colloidal sulfur (eqmolS/l); ▬ : dissolved oxygen concentration (mgO_2/l); ▬ : pH measurement.

Table 26: Final parameters state variables, kinetic processes and stoechiometric ratio for the mathematical description of the thiosulfate disproportionate reaction in aerated aqueous solution.

State Variables		Description	$[H_3O^+]$	$[OH^-]$	$[Na^+]$	$[Cl^-]$	$[O_2]$	$[H_2S_2O_3]$	$[HS_2O_3^-]$	$[S_2O_3^{2-}]$	$[H_2CO_3]$	$[HCO_3^-]$	$[CO_3^{2-}]$	$[H_2SO_3]$	$[HSO_3^-]$	$[SO_3^{2-}]$	$[H_2SO_4]$	$[HSO_4^-]$	$[SO_4^{2-}]$	S^0
		Unit	mol/L	mol/L	mol/L	mol/L	mol/L	mol/L	mol/L	mol/L	mol/L	mol/L	mol/L	mol/L	mol/L	mol/L	mol/L	mol/L	mol/L	mol/L
		Expression	H	OH	Na	Cl	O2	H2S2O3	HS2O3	S2O3	CO2aq	HCO3	CO3	SO2aq	HSO3	SO3	H2SO4	HSO4	SO4	X_S
Processes	**Acid –base equilibriums**	Water_deionization_f	1	1																
		Water_deionization_r	-1	-1																
		$CO_2aq \rightarrow HCO_3^- + H^+$	1								-1	1								
		$HCO_3^- + H^+ \rightarrow CO_2aq$	-1								1	-1								
		$HCO_3^- \rightarrow CO_3^{2-} + H^+$	1									-1	1							
		$CO_3^{2-} + H^+ \rightarrow HCO_3^-$	-1									1	-1							
		$SO_2aq \rightarrow HSO_3^- + H^+$	1											-1	1					
		$HSO_3^- + H^+ \rightarrow SO_2aq$	-1											1	-1					
		$HSO_3^- \rightarrow SO_3^{2-} + H^+$	1												-1	1				
		$SO_3^{2-} + H^+ \rightarrow HSO_3^-$	-1												1	-1				
		$H_2S_2O_3 \rightarrow HS_2O_3^- + H^+$	1					-1	1											
		$HS_2O_3^- + H^+ \rightarrow H_2S_2O_3$	-1					1	-1											
		$HS_2O_3^- \rightarrow S_2O_3^{2-} + H^+$	1						-1	1										
		$S_2O_3^{2-} + H^+ \rightarrow HS_2O_3^-$	-1						1	-1										
		$H_2SO_4 \rightarrow HSO_4^- + H^+$	1														-1	1		
		$HSO_4^- + H^+ \rightarrow H_2SO_4$	-1														1	-1		
		$HSO_4^- \rightarrow SO_4^{2-} + H^+$	1															-1	1	
		$SO_4^{2-} + H^+ \rightarrow HSO_4^-$	-1															1	-1	
	Irreversible reactions	$SO_2aq + O_2 \rightarrow HSO_4^- + H^+$	1				-0.5							-1				1		
		$HSO_3^- + O_2 \rightarrow HSO_4^-$					-0.5								-1			1		
		$SO_3^- + O_2 \rightarrow SO_4^-$					-0.5									-1			1	
		$S_2O_3^{2-} + HS_2O_3^- \rightarrow S(IV) + S_8$							-1	-1					1	1				2
	Transfers	$O_2gas \rightarrow O_2aq$					1													
		$CO_2gas \rightarrow CO_2aq$									1									
		$SO_2aq \rightarrow SO_2gas$												-1						

Table 27: Final kinetic rates per processes for the mathematical description of the thiosulfate disproportionate reaction in aerated aqueous solution.

		Reaction definitions	Rates	Descriptions
Processes	**Acid –base equilibriums**	Water_deionization_f	kw*Kw	Irreversible reaction: $2H_2O \rightarrow H_3O^+ + OH^-$
		Water_deionization_r	kw*fm*OH*fm*H	Irreversible reaction: $2H_2O \leftarrow H_3O^+ + OH^-$
		$CO_2aq \rightarrow HCO_3^- + H^+$	kC1*KaC1*CO2aq	Irreversible reaction: $H_2CO_3 + H_2O \rightarrow HCO_3^- + H_3O^+$
		$HCO_3^- + H^+ \rightarrow CO_2aq$	kC1*fm*HCO3*fm*H	Irreversible reaction: $H_2CO_3 + H_2O \leftarrow HCO_3^- + H_3O^+$
		$HCO_3^- \rightarrow CO_3^{2-} + H^+$	kC2*KaC2*fm*HCO3	Irreversible reaction: $HCO_3^- + H_2O \rightarrow CO_3^{2-} + H_3O^+$
		$CO_3^{2-} + H^+ \rightarrow HCO_3^-$	kC2*fd*CO3*fm*H	Irreversible reaction: $HCO_3^- + H_2O \leftarrow CO_3^{2-} + H_3O^+$
		$SO_2aq \rightarrow HSO_3^- + H^+$	kS(IV)1*KaS(IV)1*SO2aq	Irreversible reaction: $H_2SO_3 + H_2O \rightarrow HSO_3^- + H_3O^+$
		$HSO_3^- + H^+ \rightarrow SO_2aq$	kS(IV)1*fm*HSO3*fm*H	Irreversible reaction: $H_2SO_3 + H_2O \leftarrow HSO_3^- + H_3O^+$
		$HSO_3^- \rightarrow SO_3^{2-} + H^+$	kS(IV)2*KaS(IV)2*fm*HSO3	Irreversible reaction: $HSO_3^- + H_2O \rightarrow SO_3^{2-} + H_3O^+$
		$SO_3^{2-} + H^+ \rightarrow HSO_3^-$	kS(IV)2*fd*SO3*fm*H	Irreversible reaction: $HSO_3^- + H_2O \leftarrow SO_3^{2-} + H_3O^+$
		$H_2S_2O_3 \rightarrow HS_2O_3^- + H^+$	kT1*KaT1*H2S2O3	Irreversible reaction: $H_2S_2O_3 + H_2O \rightarrow HS_2O_3^- + H_3O^+$
		$HS_2O_3^- + H^+ \rightarrow H_2S_2O_3$	kT1*fm*HS2O3*fm*H	Irreversible reaction: $H_2S_2O_3 + H_2O \leftarrow HS_2O_3^- + H_3O^+$
		$HS_2O_3^- \rightarrow S_2O_3^{2-} + H^+$	kT2*KaT2*fm*HS2O3	Irreversible reaction: $HS_2O_3^- + H_2O \rightarrow S_2O_3^{2-} + H_3O^+$
		$S_2O_3^{2-} + H^+ \rightarrow HS_2O_3^-$	kT2*fd*S2O3*fm*H	Irreversible reaction: $HS_2O_3^- + H_2O \leftarrow S_2O_3^{2-} + H_3O^+$
		$H_2SO_4 \rightarrow HSO_4^- + H^+$	kS(VI)1*KaS(VI)1*H2SO4	Irreversible reaction: $H_2SO_4 + H_2O \rightarrow HSO_4^- + H_3O^+$
		$HSO_4^- + H^+ \rightarrow H_2SO_4$	kS(VI)1*fm*HSO4*fm*H	Irreversible reaction: $H_2SO_4 + H_2O \leftarrow HSO_4^- + H_3O^+$
		$HSO_4^- \rightarrow SO_4^{2-} + H^+$	kS(VI)2*KaS(VI)2*fm*HSO4	Irreversible reaction: $HSO_4^- + H_2O \rightarrow SO_4^{2-} + H_3O^+$
		$SO_4^{2-} + H^+ \rightarrow HSO_4^-$	kS(VI)2*fd*SO4*fm*H	Irreversible reaction: $HSO_4^- + H_2O \leftarrow SO_4^{2-} + H_3O^+$
	Irreversible reactions	$SO_2aq + O_2 \rightarrow HSO_4^- + H^+$	kSO2*(SO2aq)*(O2)	Sulphurous acid oxidation: $H_2SO_3 + 0.5\ O_2 \rightarrow HSO_4^- + H_3O^+$
		$HSO_3^- + O_2 \rightarrow HSO_4^-$	kHSO3*(fm*HSO3)*(O2)	Bisulfite oxidation: $HSO_3^- + 0.5\ O_2 \rightarrow HSO_4^-$
		$SO_3^- + O_2 \rightarrow SO_4^-$	kSO3*((fd*SO3)^2)*(O2)	Sulfite oxidation: $SO_3^{2-} + 0.5\ O_2 \rightarrow SO_4^{2-}$
		$S_2O_3^{2-} + HS_2O_3^- \rightarrow S(IV) + S_2$	kdis*(fd*S2O3)^1.5)*(fm*HS2O3)^2	Thiosulfate disproportionate reaction: $S_2O_3^{2-} + HS_2O_3^- \rightarrow S_2 + HSO_3^- + SO_3^{2-}$
	Transfers	$O_2gas \rightarrow O_2aq$	KlaO2*EO2*(sat_O2-O2)	Oxygen absorption: $O_2gas \rightarrow O_2aq$
		$CO_2gas \rightarrow CO_2aq$	KlaCO2*ECO2*(sat_CO2-CO2aq)	Carbon dioxide absorption: $CO_2gas \rightarrow CO_2aq$
		$SO_2aq \rightarrow SO_2gas$	KlaO2*(KlaSO2/KlaO2)*SO2aq	Sulfur dioxide stripping: $SO_2aq \rightarrow SO_2gas$

Table 28: Equilibrium parameters values and/or expressions used for the final mathematical description of the thiosulfate disproportionate system in aerated aqueous solution.

Parameters	Description	Values or Expressions	Unities	Ref
T	Experimental temperature	Experimental data	K	Experimental data
Zi	Valence of the specie i	Depends on the valence of the i specie	-	-
μ	Ionic strength (Ci = concentration of the specie i)	$0.5 \times \Sigma(Ci \times Zi^2)$	-	(Loewenthal et al., 1989)
A	Dependent temperature constant	$1.825 \times 10^6 \times (78.3 \times T)^{-1,5}$		(Loewenthal et al., 1989)
fm	Monovalent acitivity coefficient	$10^{\wedge}(A \times Zi \times ((\mu \times 0.5/(1 + \mu^{0.5})) - 0.3 \times \mu)$	-	(Loewenthal et al., 1989)
fd	Divalent acitivity coefficient	$10^{\wedge}(A \times \mu^2 \times ((\mu \times 0,5/(1 + \mu^{0.5})) - 0.3 \times \mu)$	-	(Loewenthal et al., 1989)
Kw	Water ionization constant	$3.46 \times 10^{-24} \times \exp(0.0729 \times T)$	-	(Lide, 1990)
Ka_{C1}	First acid-base equilibrium constant (CO_2aq)	$10^{\wedge}(- (3404.7/T - 14.8435 + 0.03279 \times T))$	-	(Loewenthal et al., 1989)
Ka_{C2}	Second acid-base equilibrium constant (CO_2aq)	$10^{\wedge}(- (2902.47/T - 6.498 + 0.02379 \times T))$	-	(Loewenthal et al., 1989)
$Ka_{S(IV)1}$	First acid-base equilibrium constant (SO_2aq)	$10^{\wedge}(- 4.74 + (853/T))$		(Maahs, 1982)
$Ka_{S(IV)2}$	Second acid-base equilibrium constant (SO_2aq)	$10^{\wedge}(- 9.278 + (621.9/T))$		(Maahs, 1982)
$Ka_{S(VI)1}$	First acid-base equilibrium constant (H_2SO_4)	100 (totalement dissocié en solution)		(Lide, 1990)
$Ka_{S(VI)2}$	Second acid-base equilibrium constant (H_2SO_4)	$9.895 \times 10^{-8} \times T^3 - 8.949 \times 10^{-5} \times T^2 + 0.02671 \times T^{-2} + 2.62$		(Lide, 1990)
Ka_{T1}	First acid-base equilibrium constant ($H_2S_2O_3$)	0.25		(Page, 1953)
Ka_{T2}	Second acid-base equilibrium constant ($H_2S_2O_3$)	$10^{-1.70}$		(Page, 1953)
$H_{CO2/water}$ (T)	Carbon dioxide Henry constant (temperature)	$83400 \times \exp^{0,0254 \times T}$	Pa	relation (USPEA)
Sat_O2aq (T)	Dissolved oxygen saturation concentration	$7.2044x10^{-7}xT^4 - 0.00090733xT^3 + 0.42974xT^2 - 90.817xT + 7238.6$		Adapted from solublity data
pH	pH of the aqueous solution	-log(fm x H)		-

Table 29: Kinetic parameters values and/or expressions used for the final mathematical description of the thiosulfate disproportionate system in aerated aqueous solution

Parameters	Description	Values or Expressions	Unities	Ref
kw	Rate constant water dionization reaction	3.6×10^{13}	$l.mol^{-1}.h^{-1}$	(Musvoto et al, 2000)
kC1	Rate constant 1° acid-base eq (CO_2aq)	3.6×10^{10}	$l.mol^{-1}.h^{-1}$	(Musvoto et al, 2000)
kC2	Rate constant 2° acid-base eq (CO_2aq)	3.6×10^{13}	$l.mol^{-1}.h^{-1}$	(Musvoto et al, 2000)
kS(IV)1	Rate constant 1° acid-base eq (SO_2aq)	10^{10}	$l.mol^{-1}.h^{-1}$	defined
kS(IV)2	Rate constant 2° acid-base eq (SO_2aq)	10^{10}	$l.mol^{-1}.h^{-1}$	defined
kS(VI)1	Rate constant 1° acid-base eq (H_2SO_4)	10^{10}	$l.mol^{-1}.h^{-1}$	defined
kS(VI)2	Rate constant 2° acid-base eq (H_2SO_4)	10^{10}	$l.mol^{-1}.h^{-1}$	defined
kT1	Rate constant 1° acid-base eq ($H_2S_2O_3$)	10^{10}	$l.mol^{-1}.h^{-1}$	defined
kT2	Rate constant 2° acid-base eq ($H_2S_2O_3$)	10^{10}	$l.mol^{-1}.h^{-1}$	defined
$\mathbf{k_{SO3}}$	Rate constant for the sulfite oxidation	1.63×10^{10}	$l^2.mol^{-2}.h^{-1}$	From this study
$\mathbf{k_{HSO3}}$	Rate constant for the bisulfite oxidation	157	$l.mol^{-1}.h^{-1}$	From this study
$\mathbf{k_{SO2}}$	Rate constant for the sulphurous acid oxidation	333	$l.mol^{-1}.h^{-1}$	From this study
$\mathbf{k_{dis}}$	Rate constant for the thiosulfate disproportionate reaction	9.67×10^{5}	$l^{2.5}.mol^{-2.5}.h^{-1}$	From this study
a	Volumetric interfacial area	Surface libre du réacteur (aération de surface) = 7,85 $m^2.m^{-3}$	$m^2.m^{-3}$	Experimental data
KlaO2	Volumetric rate oxygen transfer	Donnée expérimentale (aération de surface = 0,7 h^{-1})	h^{-1}	Experimental data
klO2	Rate oxygen transfer	KlaO2 / a	$m.h^{-1}$	Experimental data
KlaCO2	Volumetric rate carbon dioxide transfer	$KlaO2 \times (D_{CO2aq}(T)/D_{O2}(T))^{0.5}$	h^{-1}	(Spérandio et al., 1997)
KlaSO2/KlaO2	Volumetric rate sulfure dioxide paramater / KlaO2	0.996		From this study
Hatta	Hatta number for the oxygen transfer	$kSO3.\ (2/(1+1)).(D_{O2}(T)x3600).([O_2]^{(1-1)}).([SO_3^{2-}]^2)^{0.5})/klO2$		(Danckwerts, 1970)
EO2	Enhancement factor for the oxygen transfer	$(1+Hatta^2)^{0.5}$		(Danckwerts, 1970)
ECO2	Enhancement factor for the carbon dioxide transfer	$1+((D_{CO3(2-)}(T).[CO_3^{2-}])/(D_{CO2aq}(T).[CO_2aq^{sat}]))$	-	(Bosch et al., 1989)

3.2.5. Conclusion and discussion on the proposed model

Based on deviations observed between experimental measurements and simulations by a model based on previously described kinetic laws, a new model is proposed. Its definition has been built step by step in order to fit with experimental dynamics of the components involved in the thiosulfate chemical transformation system. The thiosulfate disproportionate reaction is describes as a system, including irreversible cascade reactions, acid-base equilibriums and liquid-gas exchanges.

This new model allows quantitative and dynamic prediction of the thiosulfate chemical transformation in acidic and aerobic conditions, including the definition of the concentration of the sulfur intermediaries, the precipitation of elemental sulfur, the pH and the dissolved oxygen concentration in time. Taking into account the order of magnitude of the chemical reaction rates, competition with biological transformations by SOB would be possible but is strongly pH and thiosulfate concentration dependent.

In the context of thiosulfate use as selection factor for the establishment of acidophil sulfur-oxidizing activity in contact with cementitious linings, the thiosulfate concentrations tested in this chapter and necessary to observed thiosulfate consumption were at the maximum 125 folds higher and at the minimum 25 folds higher than the concentration used in the chapter IV of this document, where acidification and sulfur-oxidizing activity selection were observed.

4. Conclusions

The objective of this chapter was to assess if a competition between chemical and biological transformations of thiosulfate can occur during a real biological test. Therefore the work performed was directed to study and to predict the chemical transformation of thiosulfate in dynamic and at different pH and operation conditions. Experiments and modeling have been used in order to reach this goal.

Chemical transformations and model development

The experiments confirmed the reactivity of thiosulfate in acid environment, showing the precipitation of elemental sulfur and the production of S(IV)-oxides. The experimental set-up validated the oxygen consumption due to secondary reactions involving the oxidation of the S(IV)-oxides. At low pH (pH > 3), the loss of sulfur was attributed to the stripping of sulfur dioxide.

Based on experimental results a dynamic model was developed with the definition of the kinetic laws of the reactions involved in the chemical system. Combined with equilibriums described by dynamic processes, **the model is able to simulate, in function of the pH, thiosulfate chemical transformation**, sulfate production, elemental sulfur production, sulfur loss by the stripping of sulfur dioxide, oxygen consumption, pH evolution and carbon dioxide absorption and speciation in solution.

The kinetic of the thiosulfate disproportionate reaction is pH and thiosulfate concentration dependent, (strong dependency on thiosulfate concentration) described by the next equation, where the reaction rate (k_{dis}) was determined as 9.67 x 10^5 $l^{2.5}.mol^{-2.5}.h^{-1}$.

Eq 66: $$-\frac{d(S_2O_3^{2-})}{dt} = k_{dis}.(f_d.[S_2O_3^{2-}])^s.(f_m.[HS_2O_3^{-}])^t$$

Consequence for the set up of a biological test

The usefulness of a biological test depends on its capacity to accelerate the interesting processes involved in the biodeterioration of the cementitious linings. The quantification of the thiosulfate transformation highlights that **the thiosulfate concentration (instead of S^{2-})**

applied at the inlet of the pipe-reactor (in chapter IV) could be improved without disturbing the biological system (see chapter VII).

In the case of selections and cultures of sulfur-oxidizing bacteria with thiosulfate as substrate (objective of the next chapter (VI)), the experimental measurement of pH, thiosulfate consumption and dissolved oxygen, compared to the model proposed here will enable (i) evaluating the part of abiotic thiosulfate transformation in a more complex system, and (ii) by combining with a biological model determining biological parameters such as the specific maximal growth rate and the observed biomass yield of the selected sulfur-oxidizing bacteria under the specific experimental conditions.

Chapter VI

Biological oxidation of thiosulfate

1. Introduction

To simplify the system and to work without hydrogen sulfur, thiosulfate use as sulfur substrate enabled the selection of sulfur-oxidizing bacteria (SOB) and the production of sulfate and acid in contact with cementitious materials. To a better control of the thiosulfate reactivity and to aim the biological conversions during a thiosulfate feeding the chapter V studied the abiotic reactivity of thiosulfate under neutral and acid environment. To get more insights on the use of thiosulfate as an appropriate substrate of sulfur-oxidizing bacteria from activated-sludge, the acid production potential on this component has been assessed. Therefore, the biological conversion of thiosulfate during the bacterial selection, on an open free long term continuous culture was operated (in a stirred reactor, with temperature regulation, without cementitious material and without pH regulation). The figure 55 presents the schema of the whole system considered in this document and the part that is specifically studied in this chapter.

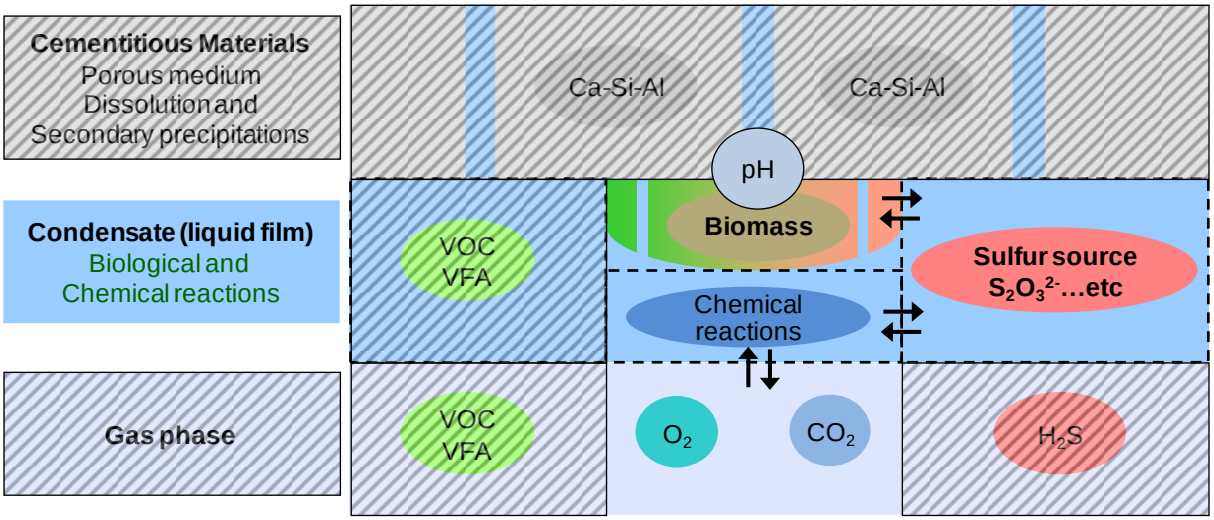

Figure 55: the part of the whole system studied in the chapter VI

The aim of this chapter is firstly to evaluate the selection of sulfur-oxidizing bacteria from an activated sludge consortium, and secondly to estimate the microbial performances of the selected bacteria by analytical methods in a first time and by the definition of a dynamical model. This model enables describing the sulfur-oxidizing culture in a second time.

In order to help the interpretation of results from the microbial culture performed, a literature overview, previously presented (table 13 and table 14 at the chapter IV), was realized to identify the diversity of chemolithotrophic SOB possibly selected from an activated sludge, considering the culture conditions (type of reactor, pH and temperature), the

sulfur source used, the specific growth rate and the biomass yield observed. This overview will allow to compare the microbial performances observed during the selection to pure cultures, and to evaluate the interest of activated sludge as inoculum. To complete this literature review, to improve the interpretation of the selection mode and the use of thiosulfate as selection factor, the fate of the thiosulfate consumption by chemolithotrophic SOB described in the literature will be presented. Then a microbial selection in continuous culture will be described and analyzed, by using mass balances combined to the chemical model presented in the chapter V. Finally, based on the experimental results, a dynamical model will be proposed to describe the culture behavior, coupling biological and physico-chemical processes.

1.1. The oxidation of thiosulfate by chemolithotrophic sulfur-oxidizing bacteria

The aim of this paragraph, in the context of the selection of chemolithotrophic SOB activity by thiosulfate feeding, is to present the main modes of biological conversion of thiosulfate by the chemolithotrophic SOB. Firstly two sulfur oxidation pathways involving thiosulfate described in the literature are presented; secondly several experimental results with SOB illustrated these both different pathways, depending on the species and on the culture conditions.

1.1.1. Description of two thiosulfate oxidation pathways

The oxidation pathway of thiosulfate ($S_2O_3^{2-}$) by chemolithotrophic sulfur-oxidizing bacteria seems to be species and environment dependent (Kelly et al., 1997) (Masau et al., 2001) (Gosh et al., 2009). Indeed, different metabolic pathways could be involved in the thiosulfate oxidation, with the participation of several intermediates (Gosh et al., 2009). Considering the thiosulfate oxidation, two main pathways have been identified (Gosh et al., 2009): (i) the Kelly-Friedrich pathway called also PSO pathway for Sulfur Oxidation by *Paracoccus*. In that case, thiosulfate is converted directly into sulfate without the formation of any detectable intermediate (Sauvé et al., 2007) (this pathway is conventional with the phototrophic sulfur bacteria). (ii) The S_4I pathway (for tetrathionate ($S_4O_6^{2-}$) intermediate)

where tetrathionate is first formed during the thiosulfate oxidation and then oxidized into sulfate (Kelly et al., 1997).

The figure 56 presents the PSO pathway (Kelly, 1989) (Kelly et al., 1997) (Friedrich et al., 2001) (Sauvé et al., 2007). Through this pathway thiosulfate, but also other reduced sulfur compounds as sulfide (HS^-) and elemental sulfur (S_8), are oxidized into sulfate as end product by a multi-enzyme complex constituted by thiosulfate induced periplasmic protein SoxXA, SoxYZ, SoxB and SoxCD. This common pathway (only observed in facultatively sulfur-oxidizing organisms growing at neutral or near-neutral pH) shows the adaptability for some bacteria (*Starkey novella*; *Paracoccus versutus*) to grow on different sulfur substrates.

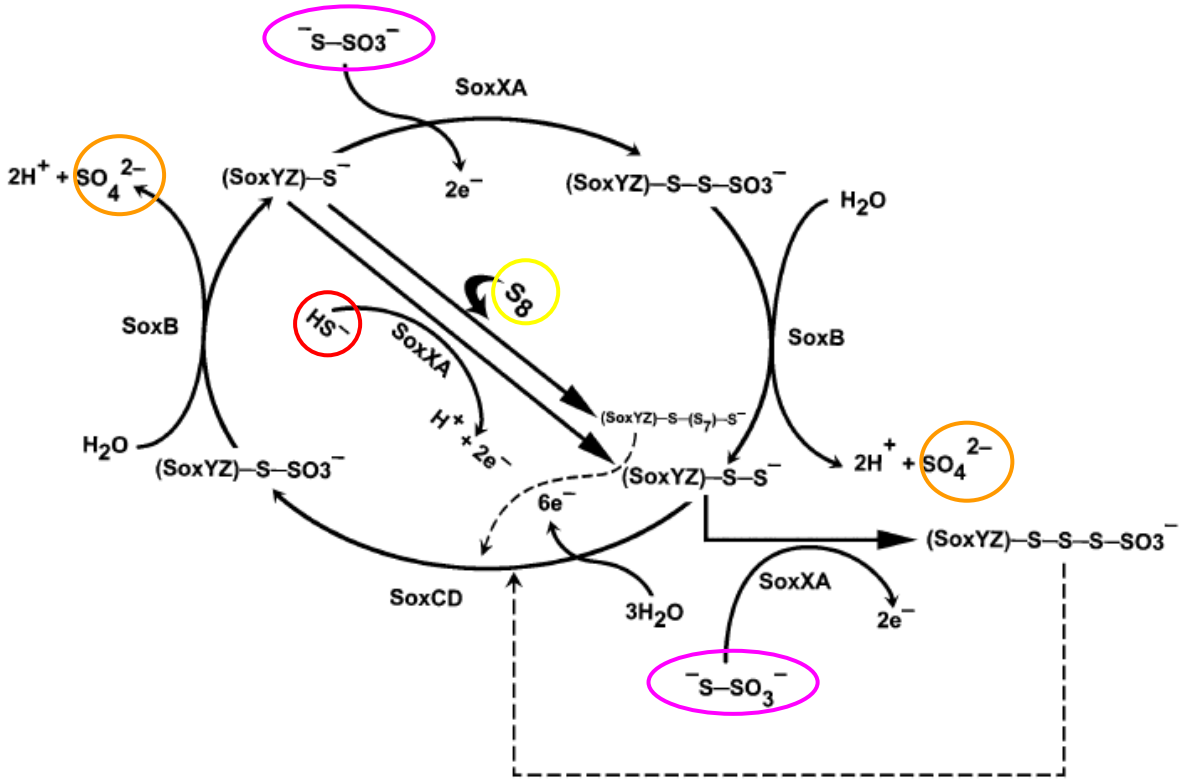

Figure 56: Reduced sulfur compounds oxidation by the PSO pathway as established in Paracoccus sp. (Friedrich et al., 2001), involving the enzymatic complex SOX (from Gosh et al., 2009). O: thiosulfate; O: sulfide (HS^-); O elemental sulfur; O: produced sulfate.

From the PSO pathway, the biological oxidation of thiosulfate to sulfate can be defined by the equation (Eq 21).

Eq 21: $S_2O_3^{2-} + 2\,O_2 + H_2O \rightarrow 2\,SO_4^{2-} + 2\,H^+$

The figure 57 presents the schematic representation of the S_4I pathway adapted by Gosh (Gosh et al., 2009) and as it was proposed by Kelly in 1989 and supported by Kelly et al., in 1997 for *Thermithiobacillus tepidarius*, and later by studies in *Acidithiobacillus caldus* (Hallberg et al., 1996) and in *Tetrathiobacter kashmirensis* (Dam et al., 2007). To illustrate the acid production linked to the sulfur compounds oxidation, the OH^- and the H^+ produced for each intermediary reactions have been added to the scheme.

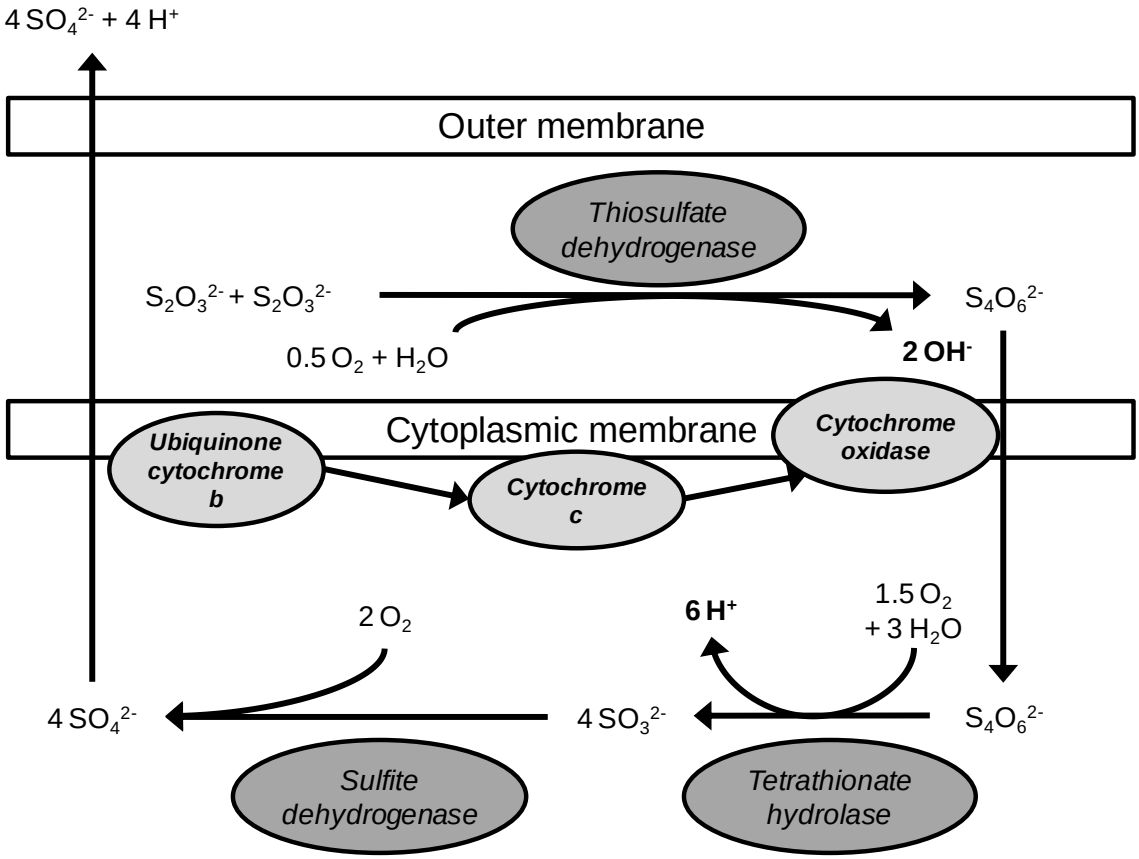

Figure 57: Thiosulfate oxidation in chemolithotrophic bacteria by the S_4I pathway as proposed in *Thermithiobacillus tepidarius* (Kelly, 1989) (Kelly et al., 1997), adapted from Gosh et al., 2009.

Thiosulfate oxidation via S_4I was observed in several obligately chemolithotrophic species as *Acidithiobacillus*, *Thermithiobacillus* and *Halothiobacillus* (Gosh et al., 2009). By this pathway, thiosulfate ($S_2O_3^{2-}$) was firstly oxidized into tetrathionate ($S_4O_6^{2-}$), and then tetrathionate was oxidized into sulfate (SO_4^{2-}) with sulfite (SO_3^{2-}) as intermediate. This pathway could be resumed by the successive equations (Eq 71 , Eq 72 and Eq 73), which are equivalent, in term of mass balance to the equation (Eq 21) describing the direct PSO pathway.

Eq 71: $2\,S_2O_3^{2-} + 0.5\,O_2 + H_2O \rightarrow S_4O_6^{2-} + 2\,OH^-$

Eq 72: $S_4O_6^{2-} + 1.5\,O_2 + 3\,H_2O \rightarrow 4\,SO_3^{2-} + 6\,H^+$

Eq 73: $4\,SO_3^{2-} + 2\,O_2 \rightarrow 4\,SO_4^{2-}$

By the S_4I pathway, the total oxidation of thiosulfate into sulfate leads to the same total stoichiometric, compared to PSO pathway. However, the stoichiometric equations shows that the thiosulfate oxidation in two steps, with tetrathionate as intermediate, leads to a first oxidation with a hydroxide production, that was compensed in the second step by the acid production linked to the tetrathionate oxidation.

1.1.2. Experimental confirmation of two thiosulfate oxidation pathways

Masau in 2001 has shown, for *Acidithiobacillus thiooxidans*, the coextience of two oxidative pathways and indicated a pH dependency for the use of one over the other. At pH 5, the oxidation stoichiometry shows that tetrathionate does not participate to the global oxidation of thiosulfate (elemental sulfur and sulfurous acid are presented as main intermediates). On contrary, at pH 2.3 tetrathionate appeared to be produced (with elemental sulfur and sulfurous acid as intermediate also and/or by disproportionate reaction forming thiosulfate and sulfate).

A reason given by several studies to explain the switch in the oxidative pathway is the unstability of thiosulfate at low pH. Thus, bacteria converted thiosulfate into tetrathionate which is more stable in acidic environment (Druschel et al., 2003c). Nevertheless, this theory does not explain why the S_4I pathway is also observed in alkalophilic and neutrophilic SOB (Gosh et al., 2009).

Even if some global biological conversion of sulfur compounds are described, a lot of particular pathways are still observed for SOB species, with the formation of sulfur globule (out or in the cells) (Steudel, 1989), and/or formation of long chain of polythionates as for *A.ferrooxidans* (Steudel et al., 1987). Gosh, in their article review in 2009, indicated mono-sulfonic acid ($HS_2SO_3^-$) as a possible key intermediate in some tetrathionate oxidation, explaining the possible formation of long chain sulfur compounds by this way.

At a reactor scale, the figure 58 presents the adaptation of some results proposed in the literature for the thiosulfate conversion by some sulfur-oxidizing species in batch culture (Starkey, 1935) (Parker and Prisk, 1953). (a) and (b) present results for neutrophil species (Starkey, 1935), and (c) and (d) for acidophil species (Parker and Prisk, 1953).

(a) Thiobacillus specie
(adapted from Starkey 1935)
Starkey Novella (since 1995)

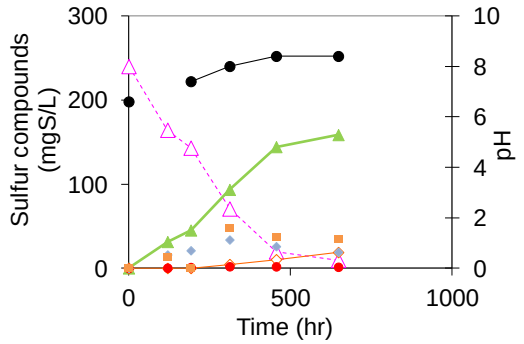

(b) Thiobacillus Thioparus
(adapted from Starkey 1935)

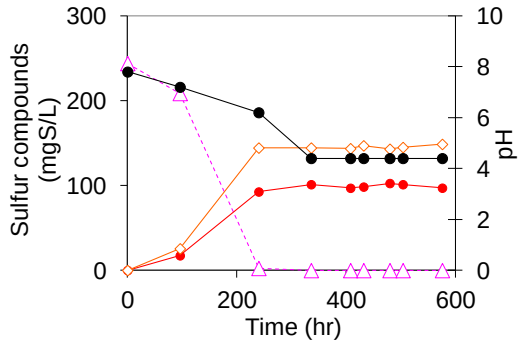

(c) Thiobacillus thiooxidans
(adapted from Parker 1953)
Acidithiobacillus thiooxidans

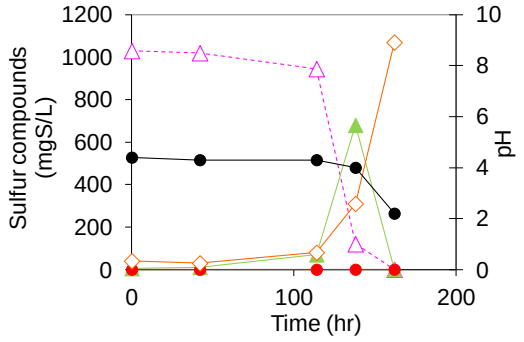

(d) Thiobacillus thiooxidans
(adapted from Parker 1953)
Acidithiobacillus thiooxidans

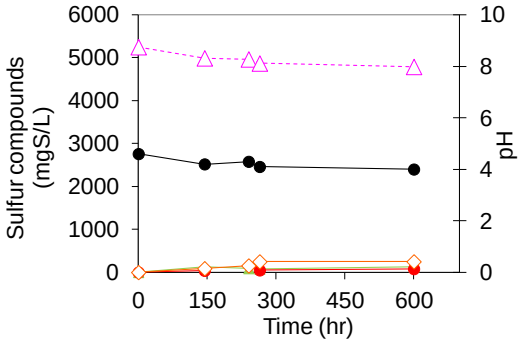

Figure 58: adaptation of results obtained by Starkey in 1935 and Parker 1953 during batch culture of thiobacilli species (neutrophil and acidophil) with thiosulfate as sulfur substrate. : thiosulfate concentration [$S_2O_3^{2-}$] (mgS/l); : S(VI) oxides concentration (mgS/l); : tetrathionate concentration [$S_4O_6^{2-}$] (mgS/l); : trithionate concentration (mgS/l); : pentathionate concentration (mgS/l); : pH measurements.

Considering the neutrophil species (*Starkey novella* and *Thiobacillus thioparus*), the thiosulfate conversion was completely different, with production of polythionates (with tetrathionate as major intermediate) for *Starkey novella* (figure 58.a) and a basification of the medium. For *Thiobacillus thioparus* (figure 58.b) the acidification of the medium linked to a sulfate and elemental sulfur production was observed. Concerning the acidophil specy, *Acidithiobacillus thiooxidans*, two initial thiosulfate concentrations are presented (figure 58.c

$[S_2O_3^{2-}]_0$ = 1000 mgS/l and figure 58.d $[S_2O_3^{2-}]_0$ = 5000 mgS/l). Thiosulfate at high concentration could lead to inhibition phenomena (no thiosulfate consumption during 600 hours with an initial thiosulfate concentration of 5000 mgS/l). When thiosulfate oxidation occurred (figure 58.c), during a first phase, low thiosulfate consumption rate was recorded with sulfate production.Then after 100 hours an acceleration in the thiosulfate consumption was linked to tetrathionate production with weak acidification, and then tetrathionate consumption led to strong acidification and strong sulfate production.

In 1994 Wentzien studied with thiosulfate and tetrathionate the growth of *Thiobacillus intermedius* (today *Thiomonas intermedia*) and *Thiobacillus versutus* (today *Paracoccus versutus*) (Wentzien et al., 1994). The two behaviours are also identified. *Thiobacillus intermedius* oxidized thiosulfate via tetrathionate to sulfate, with the detection of intermediates as trithionate ($S_3O_3^{2-}$) and penthathionate ($S_5O_6^{2-}$) due to the formation of highly reactive compounds as mono-sulfonic acid ($HS_2SO_3^-$). With tetrathionate as sulfur source, some thiosulfate could be detected, explained by the reaction of trithionate with tetrathionate, and/or the hydrolysis of trithionate (Wentzien et al., 1994). For *Thiobacillus versutus* (*Paracoccus versutus*) no intermediate could be detected.

Thus, metabolic studies and experimental datas at reactor scale, confirmed the possible description of the thiosulfate oxidation through two different pathways, depending on the SOB specy cultivated. Based on these results the selection preformed in this chapter could be analysed in terms of thiosulfate oxidation. In a further step, the description of the stoichiometric thiosulfate conversion will enable proposing and evaluating a dynamical model.

1.2. Culture system chosen and objectives

A preliminary experiment, by a fed-batch culture, presented in annexes of this chapter, by the comparison of the chemical model developed in the Chapter V, confirmed the possible perturbation of the system by precipitation phenomena due to the instability of the thiosulfate at low pH, but also highlighted, in complex environment as mineral solution, the possible precipitation of sulfate salts due to the strong accumulation of S(VI)-oxides in solution.

A culture operated by a sequenced-batch system was chosen to combine advantages of a chemostat culture for the limitation of disturbance linked to secondary reactions and the

establishment at a global scale of stationary system, and of a batch culture which enable the analyse of dynamical phenomena.

Three objectives were carried out in parallel: (i) to observe the selection of sulfur oxidizing activity from activated-sludge consortium by thiosulfate feeding; (ii) to evaluate the sulfur-oxidizing activity in terms of kinetics and stoichiometry in the experimental conditions; (iii) to describe in dynamic the thiosulfate conversion and proposed a dynamical model enable to evaluate the optimal biological performances of the selected activity to compare to literature data for pure cultures identified during microbially induced concrete corrosion.

2. Specific materials and methods

2.1. Culture system and analytical method

The reactor used for the sequenced-batch culture was presented in the M&M (chapter III), as the analytical methods used.

2.2. Temperature dependency of the specific growth rate

Because conversion rates are pH and temperature dependent, to compare the rate of the sulfur-oxidizing activity selected by the sequenced-batch culture to the literature data, the operating conditions must be equivalent.

Acidithiobacillus thiooxidans is often considered as the last specie involved in the microbially induced concrete corrosion and was used as representative specie to simulate the last step of the acidification phenomenon. In 1942, Vogler studied *Acidithiobacillus thiooxidans* and quantified the rate of oxygen consumption in function of the temperature culture (Vogler et al., 1942). Based on theses experimental results, an Arrhenius function has been calculated (see annexes of this chapter for details of this calculation) and applied for the evaluation of the specific growth rate at different temperature for *Acidithiobacillus thiooxidans*. For example, Mason in 1987 at 30°C and pH = 2.5 fixed for *Acidithiobacillus thiooxidans* a specific growth rate in chemostat culture to 0.025 h^{-1}. If this specific growth rate

was the maximum available for this strain at these operating conditions, at 20°C, corrected by the Arrhenius function determined here, the specific growth rate will be equal to 0.0086 h^{-1}.

2.3. Evaluation of potential precipitation of sulfate salts by the calculation of the Saturation Index (SI)

The accumulation of sulfate in the medium, due to the sulfur-oxidizing activity could lead, in mineral medium to the precipitation of some sulfate salts. To evaluate this eventuality, for all the samples, as defined for one example by the equation (Eq 74), the saturation index (SI) was calculated for four compounds (*$CaSO_4$*; *$CaSO_4.2H_2O$*; *$NaSO_4.H_2O$*; *$NaSO_4.10H_2O$*).

Eq 74: $$SI_{(CaSO_4)} = log\left(\frac{(Ca^{2+}).(SO_4^{2-})}{Ks_{CaSO_4}}\right)$$

where $SI_{(CaSO_4)}$ is the saturation index for the sulfate calcium salts; (Ca^{2+}) and (SO_4^{2-}) are the activity in solution of Ca^{2+} and SO_4^{2-} (mol/l), and Ks_{CaSO_4} is the solubility constant of the sulfate calcium salt considered.

The sulfate calcium salts were chosen due to: (i) the high affinity of Ca^{2+} ion with SO_4^{2-} ion, (ii) the secondary precipitation of calcium salts observed during real microbial induced concrete corrosion and (iii) the preliminary observation of calcium precipitation in a fed-batch culture realized and presented in annexes of this chapter. The sulfate sodium salts because thiosulfate was provided by NaS_2O_3 salt, and thus sodium accumulated to high concentration during the culture. The equilibrium constant used were from the Minteq-database. Negative SI values indicated concentrations under the concentration defined by the equilibrium constant, thus no precipitation phenomenon could occur. Null values indicated concentrations at the concentrations excepted for the equilibrium state, then precipitation phenomenon occurs.

2.4. Analyze of the sulfur-oxidizing activity by measurement of dynamical oxygen consumption

The culture by a continuous sequenced-batch culture with sequential pulses of thiosulfate, enable measuring the oxygen consumption due to the sulfur-oxidizing activity. The dissolved

oxygen concentration, during a thiosulfate pulse, results of the sulfur-oxidizing activity (chemical and biological) and the physical absorption of the oxygen in the solution. The equation (Eq 75) describes the evolution of the dissolved oxygen concentration during a thiosulfate pulse, considering the system, for each pulse, as a batch system (the O_2 provided by the liquid addition considering as negligible, because the liquid volume added for each pulse was equivalent at 3% of the culture volume).

Eq 75: $\frac{d[O_2]}{dt} = kl.a_{O_2}.([O_2^{Sat}](T) - [O_2]) - OUR(t)$

Where $\frac{d[O_2]}{dt}$ is the variation of the dissolved oxygen concentration (in mol.l^{-1}.h^{-1}); $kl.a_{O2}$ is the volumetric gas-liquid rate for oxygen mass transfer (in h^{-1}); $[O_2^{Sat}](T)$ is the dissolved oxygen saturation concentration (in mol/l), $[O_2]$ is the dissolved oxygen concentration in the aqueous solution (in mol/l); and *OUR(t)* is the oxygen uptake rate at t time (in mol.l^{-1}.h^{-1}).

Thus, by the definition of the volumetric gas-liquid rate for the oxygen mass transfer ($kl.a_{O2}$) during the experiment (sulfite method, Linek and Vacek, 1981), and the measurement of the dissolved oxygen concentration during the experiment, the dynamic *OUR(t)* could be calculated from the equation (Eq 75).

3. Results and discussion

The sequenced-batch culture was divided in two culture-periods. The first period was operated from day 0 to day 30 with a hydraulic retention time of 14.6 days (HRT), to limit the washout of the culture, and to impose the microbial selection from the biological acidification of the culture medium. During this period, the thiosulfate loading was regularly increased. The main objective of this part was to select and intensify the sulfur-oxidizing activity and to evaluate the growth parameters of the selection. The second period was operated from day 30 to day 70 with a HRT = 7.3 days, to stabilized and purified the culture, with the objective to estimate the observable biomass yield of the selected bacteria.

3.1. Selection phase

3.1.1. Macroscopic analysis parameters

The figure 59 presents the global parameters describing the culture (as pH, S(VI)-oxides produced, OUR_{max} , particulate COD...) during the culture (day 0 to day 30 and day 30 to day 70).

During the first period (day 0 to day 30), two pulses of thiosulfate per day were applied, each followed by a waste phase (corresponding to a HRT = SRT = 14.6 days). During this period, to intensify the thiosulfate conversion, the inlet thiosulfate flux was increased regularly (from 23 to 429 $mgS_2O_3^{2-}.l^{-1}.d^{-1}$). A pH value of 2.3 was reached in 3 days and slowly decreased to reach the value 1.6 after 30 days. The maximum OUR (OUR_{max}) values, recorded for each thiosulfate pulse, increased during the 30 days of this period and can be correlated to S(VI)-oxides production. Thus, the operating conditions applied in this reactor ensured the selection and the development of a sulfur-oxidizing activity. The turbidity of the reactor (Optical density at 860 nm) decreased continually, even if the sulfur-oxidizing activity increased. This is the result of the decay and the washout of the initial non-adapted microorganisms.

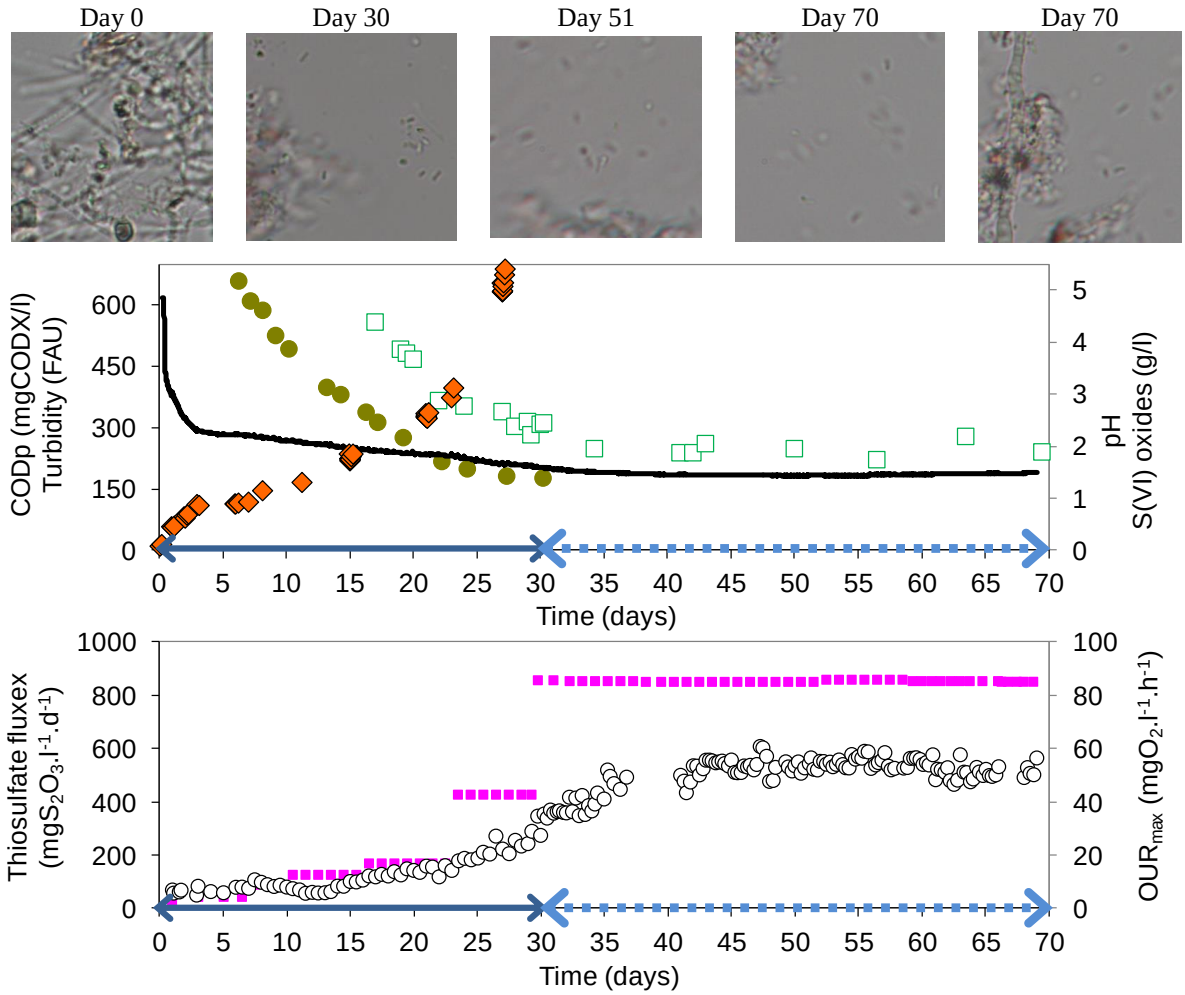

Figure 59: Sequenced-batch culture (inoculated by activated sludge consortium) feeding by thiosulfate as only sulfur substrate. ■ : inlet thiosulfate fluxes ($mgS_2O_3.l^{-1}.d^{-1}$); ○: OUR max for each pulse ($mgO_2.l^{-1}.h^{-1}$); ▬ : pH measurements; ◆ : S(VI)-oxides (g/l); □ : particulate COD (mgCOD-X/l); ● : Turbidity (FAU = OD at 860 nm); ⟷ : period with HRT = 14.6 d ; ⟷ : period with HRT = 7.3 d.

During the second time period of the culture (day 30 to day 70), the number of thiosulfate pulses per day was increased (from 2 to 4/day). The frequency of the waste phase was increased also (so, for a day, the inlet-flow was equal to the outlet-flow). The thiosulfate concentration in the supply was identical to the concentration applied during the first period. Thus the thiosulfate load was stabilized and two folds higher than the inlet load applied during the first period of the sequenced-batch culture (figure 59). From the day 37 and to the day 40 the OUR_{max} calculations were eliminated because biofilm grows on the Oxygen sensor disturbed the dissolved oxygen concentration analyses. However, after the sensor rinsing, from the day 40 to the end of the culture (day 70), the OUR_{max} calculation showed stabilization of the sulfur-oxidizing activity. At the same time the particulate COD measurement and pH (ranged between 1.45 and 1.5) stabilized also.

The photos, taken along the culture time, presented in the figure 59 illustrated the selection. Other microscopic observations are given in the figure 60 and highlighted the simplification of the suspended solids contents with the following trends: (i) development of free bacteria (rod shape); (ii) elimination of the filamentous bacteria; (iii) diminution of the aggregate structure. The decrease of the particulate COD in the liquid also confirmed this behaviour. Moreover no precipitation was visually observed (visual culture control and microscopic observations).

Day 0 (HRT = 14.6 d) 10 µm	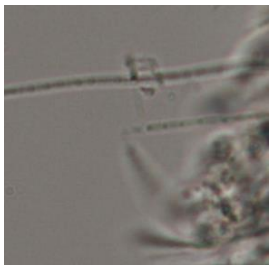	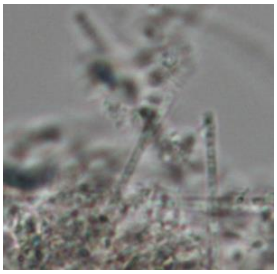	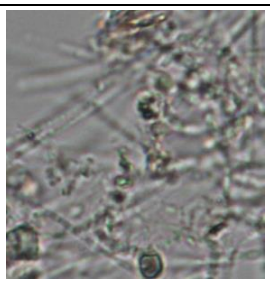
Day 7 (HRT = 14.6 d) 10 µm	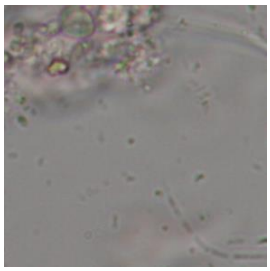	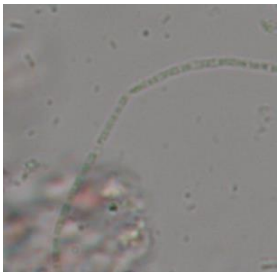	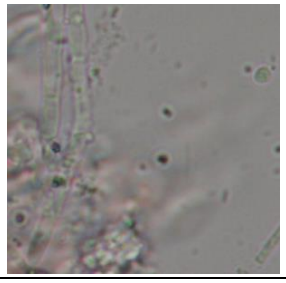
Day 17 (HRT = 14.6 d) 10 µm	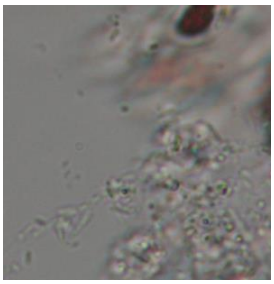	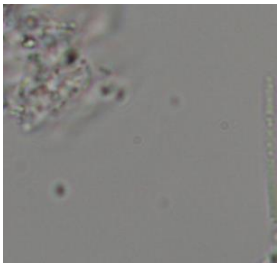	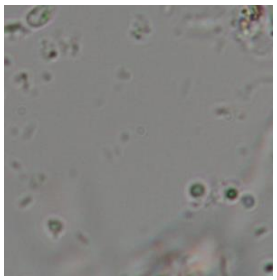
Day 30 (HRT = 14.6 d) 10 µm	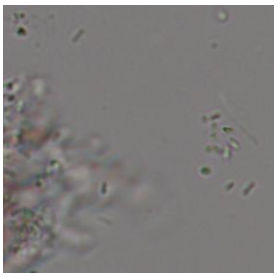	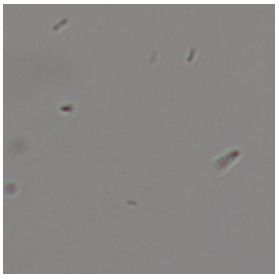	
Day 30	HRT changing (14.6 days to 7.3 days)		
Day 51 (HRT = 14.6 d) 10 µm	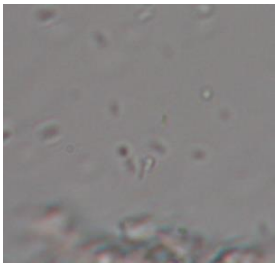	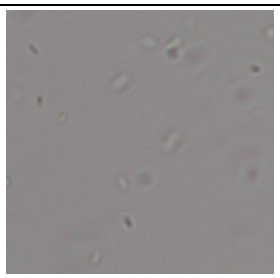	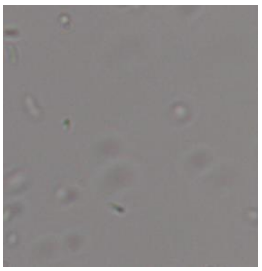
Day 70 (HRT = 14.6 d) 10 µm	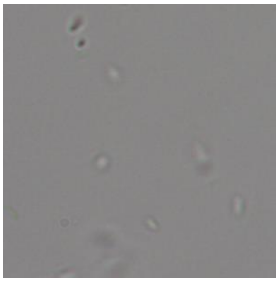	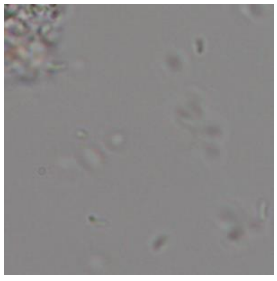	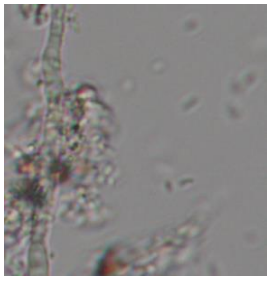
Day 70	End of the culture		

Figure 60: Visual observations of the sequenced-batch culture (microscopy x1000).

3.1.2. Analyses of the precipitation potential during the culture

3.1.2.1. Evaluation of the precipitation of sulfate salts

To evaluate the precipitation potential of sulfate salts during the sequenced-batch culture and ensure sulfur conversion analyses, the method of the saturation index (SI) was applied (see material and methods [2.3.] of this chapter). The figure 61 presents the saturation index (SI) calculated for four compounds ($CaSO_4$; $CaSO_4.2H_2O$; $NaSO_4.H_2O$; $NaSO_4.10H_2O$).

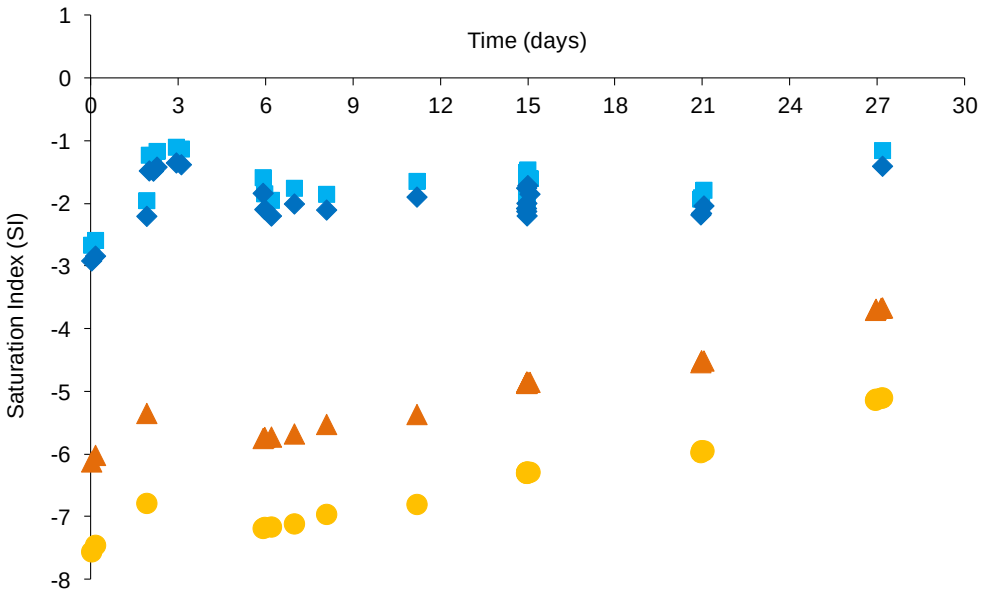

Figure 61: Saturation Index (SI) calculated for four compounds during the sequenced-batch culture (time period day 0 to day 30 - HRT = 14.6 days). ■: $CaSO_4,2H_2O$; ◆: $CaSO_4$; ▲: $NaSO_4,10H_2O$; ● : $NaSO_4,H_2O$.

The saturation index, for the four compounds, never reached a null value, indicating that none of the compounds have precipitated during the first period of the sequenced batch reactor.

3.1.2.2. Evaluation of the precipitation of elemental sulfur by the thiosulfate disproportionate reaction

To evaluate the possible loss of sulfur substrate by the thiosulfate disproportionate reaction (production of elemental sulfur slowly biodegradable by the selected microorganisms and the stripping of sulfur dioxide as described in the chapter V), the dynamical model developed previously was used (with pH as data for the model resolution) (see chapter V for more

details). The figure 62 presents the simulated results taking into account only the abiotic reaction (lines) compared to the experimental measurements (symbols).

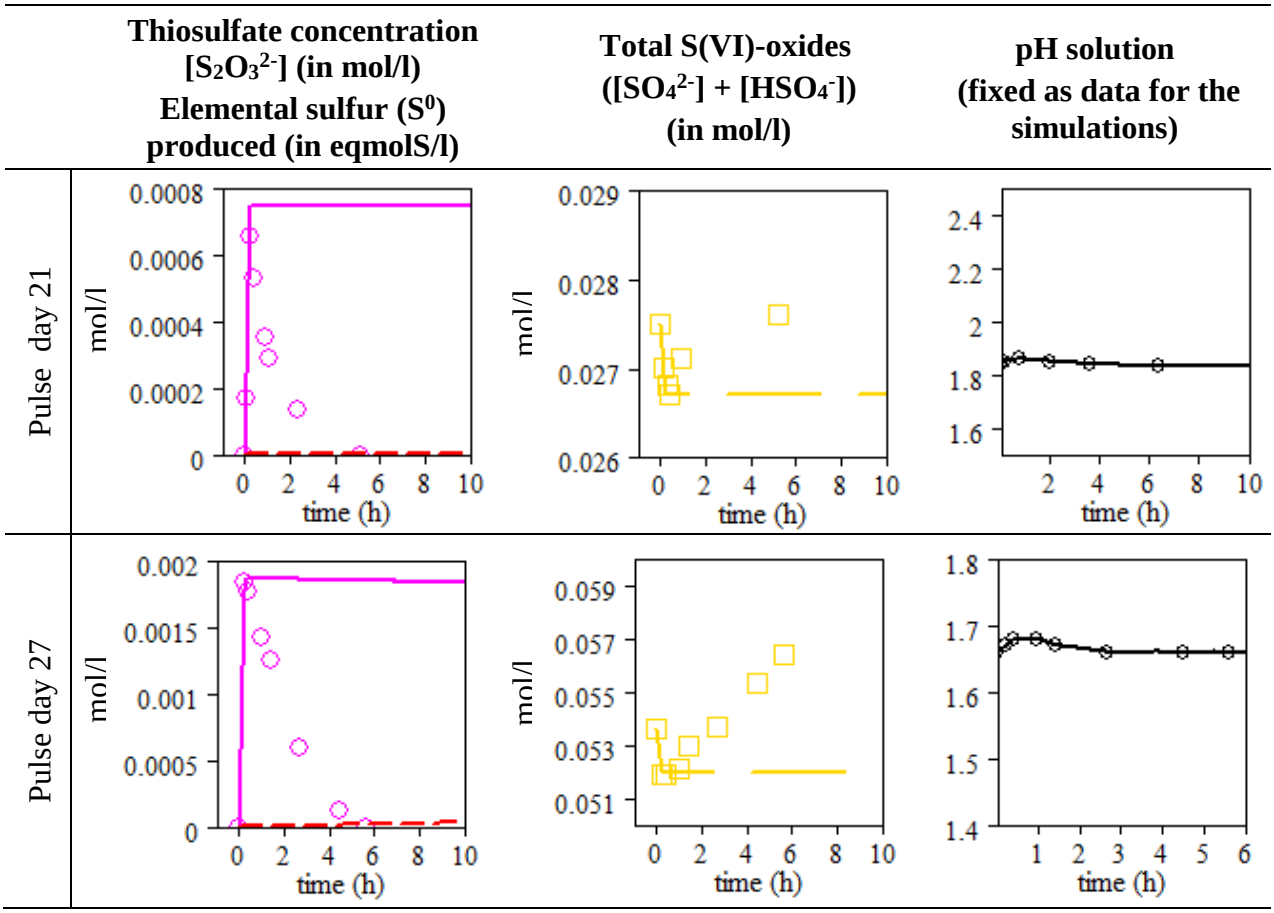

Figure 62: Simulations of thiosulfate pulses for the sequenced-batch culture (day 21) (day 27) with pH as data for the evaluation of the abiotic thiosulfate disproportionate reaction in the definition of the global conversion phenomena. Experimental data: △ : thiosulfate concentration [$S_2O_3^{2-}$] (mol/l); ◇ : S(VI)-oxides (mol/l); ○: pH measurements. Numerical data: ▬: thiosulfate concentration [$S_2O_3^{2-}$] (mol/l); ▬ ▪: elemental sulfur produced [S^0] (eqmolS/l); ▬ ▪: S(VI)-oxides (mol/l); ▬: solution pH.

The simulated results for the two pulse events shows that elemental sulfur production linked to abiotic thiosulfate consumption is very low compared to the experimental thiosulfate consumption. Using the results of the simulation obtained 6 hours after the pulse (experimental ending of the thiosulfate consumption), without biological processes, the simulation estimates that only 1% of the initial sulfur is converted to elemental sulfur (days 27), and 1% is lost by sulfur dioxide stripping. Thus, in the controlled feeding conditions, even in acid conditions, the thiosulfate consumption is only due to the biological conversion. No significant loss of sulfur substrate for the biological oxidation due to the

thiosulfate disproportionate reaction and the conversion of thiosulfate into elemental sulfur and sulfur dioxide is noted.

3.1.3. Dynamic response of microbial activity to thiosulfate pulses

In figure 63 and figure 64, for one pulse, the thiosulfate concentration, the produced S(VI)-oxides concentration, the dissolved oxygen concentration profile and the oxygen uptake rate calculated (*OUR(t)*), are presented. The initial pulse of thiosulfate was of 86 mg$S_2O_3^{2-}$/l (figure 63), and 214 mg$S_2O_3^{2-}$/l (figure 64).

For each thiosulfate pulse, immediate oxygen consumption was recorded, linked to thiosulfate consumption. However, for each pulse, the oxygen profile clearly showed a specific feature. Indeed, just after the thiosulfate pulse, the oxygen uptake rate (*OUR(t)*) reached a high value. After, during a first step of the thiosulfate consumption the *OUR(t)* decreased. However, in a second step, the *OUR(t)* increased suddenly and slightly decreased until the substrate (thiosulfate) was exhausted. Then the *OUR(t)* stabilized at a low value corresponding to a residual endogenous respiration and/or residual respiration on intermediates compounds taking into account the complex reactivity of the sulfur compounds.

Therefore an unconventional *OUR(t)* profile is observed, that revealed a complex reactivity with transient processes though, at the end leading to the biological oxidation of thiosulfate to sulfate.

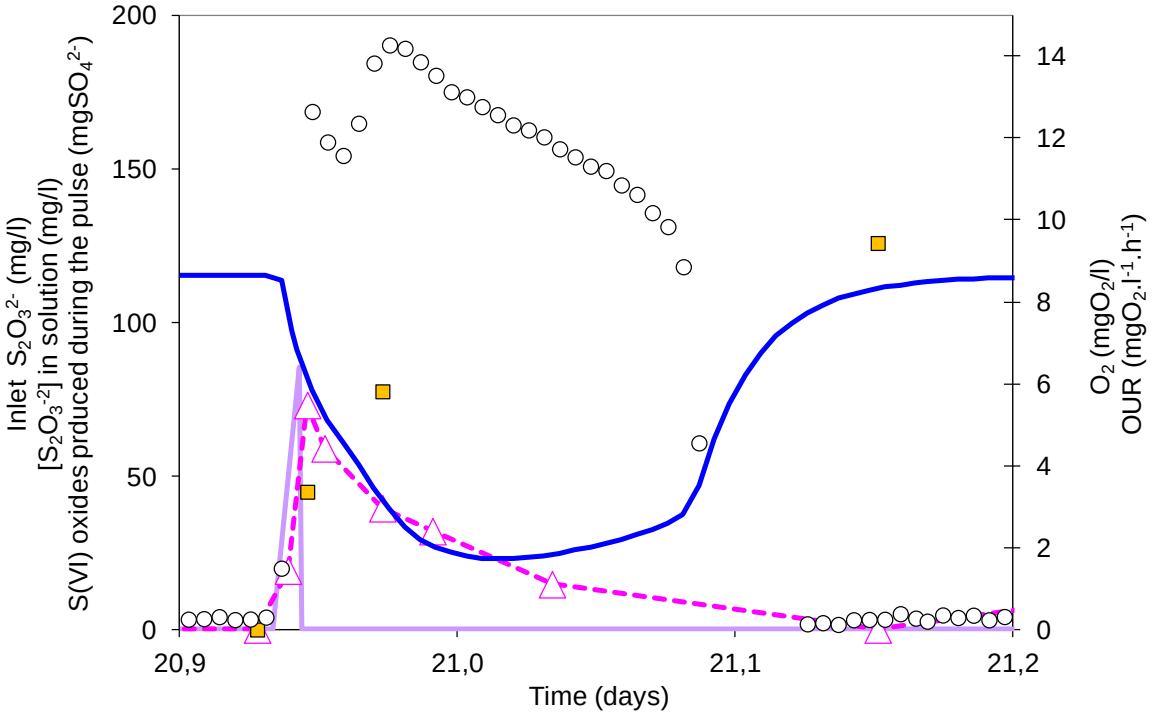

Figure 63: Sequenced-batch culture – HRT = 14.6 days – thiosulfate pulse (86 $mgS_2O_3^{2-}$/l per pulse). : thiosulfate pulse; : thiosulfate concentration (mgS_2O_3/l);; S(VI)-oxides produced during the pulse ($mgSO_4^{2-}$); : dissolved oxygen concentration (mgO_2/l); : OUR ($mgO_2.l^{-1}.h^{-1}$).

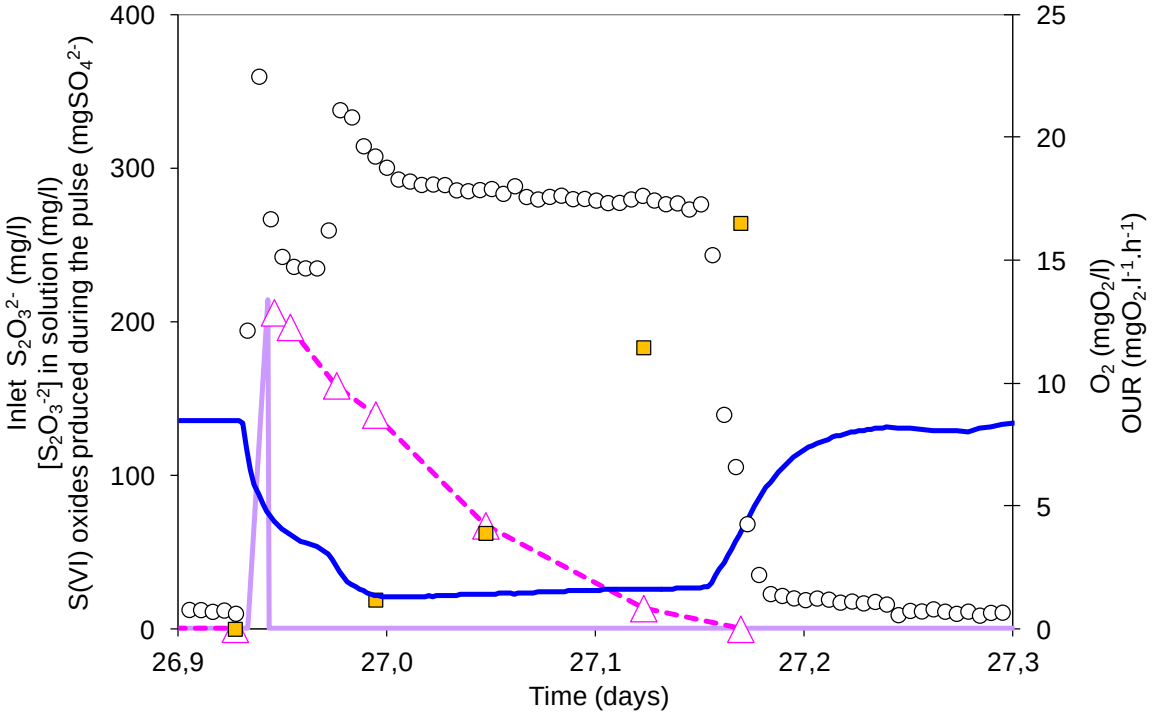

Figure 64: Sequenced-batch culture – HRT = 14.6 days – thiosulfate pulse (214 $mgS_2O_3^{2-}$/l per pulse). : thiosulfate pulse; : thiosulfate concentration (mgS_2O_3/l); S(VI)-oxides produced during the pulse ($mgSO_4^{2-}$); : dissolved oxygen concentration (mgO_2/l); : OUR ($mgO_2.l^{-1}.h^{-1}$).

To illustrate this phenomenon, and its permanent behavior, the figure 65 presents for five consecutive and identical thiosulfate pulses (214 mg$S_2O_3^{2-}$/l per pulse), the time course of the dissolved oxygen concentration and the associated calculation of the *OUR(t)*.

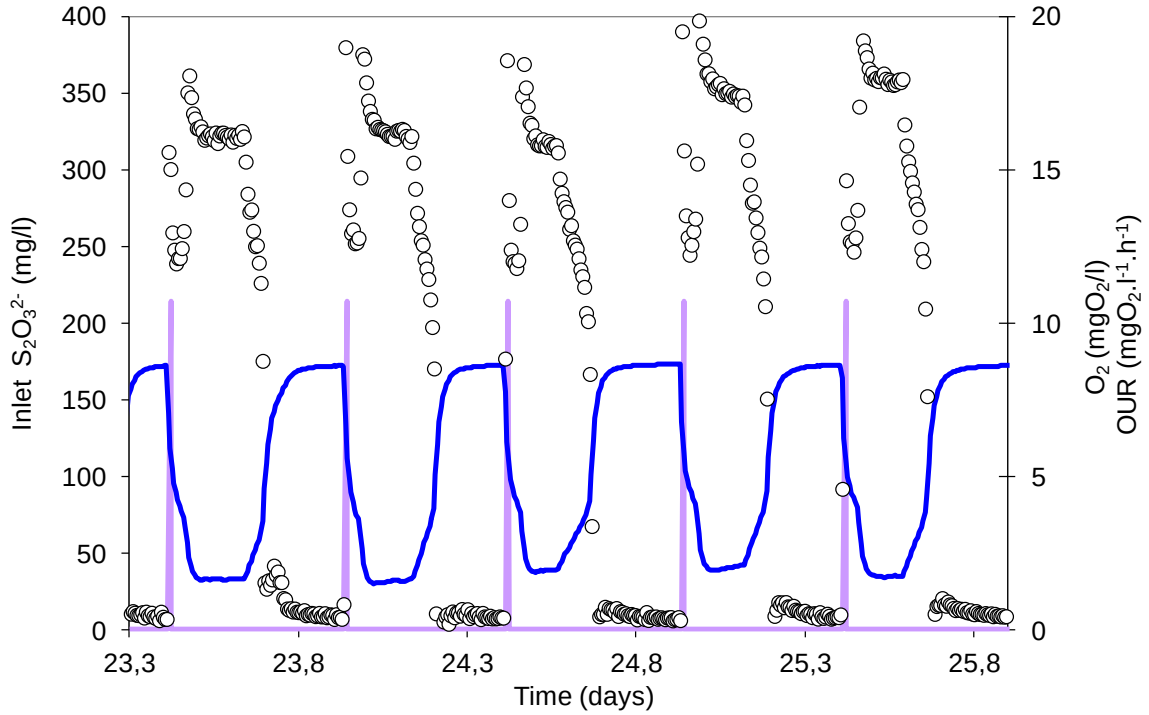

Figure 65: Sequenced-batch culture – HRT = 14.6 days – five thiosulfate pulses (214 mg$S_2O_3^{2-}$/l per pulse). : thiosulfate pulses; : dissolved oxygen concentration (mgO_2/l); ○: OUR (mgO_2.l^{-1}.h^{-1}).

The evolution of the thiosulfate concentration after the thiosulfate pulses (figure 63 and figure 64) indicated that the OUR(t) deceleration was not due to a fast conversion of the thiosulfate, because thiosulfate are still available when the deceleration-acceleration occurred. To investigate deeper these phenomenon, sulfur mass balances and oxygen mass balances were realized and presented further.

At the culture scale (figure 59), the analyses of the OUR_{max}, of the produced S(VI)-oxides, of the pH and of the particulate COD indicate the selection and the stabilization of a sulfur-oxidizing activity with a specific thiosulfate conversion highlighted. A growth period is observed (from day 0 to day 40) illustrated by the OUR_{max} and the S(VI)-oxides measurements in the figure 59 and a stabilization phase of the culture is observed from day 40 to day 70.

3.1.4. Selected populations by the operating conditions

To evaluate the interest of thiosulfate as selection factor combined to activated-sludge consortium to obtain acidophil SOB, two biomass samples were realized during the culture for rDNA-16s analyzes. One at the end of the first period (day 30) when turbidity and particulate COD measurement indicated the importance of residual biomass of the inoculum, one at the end of the culture (day 70), when oxygen consumption, thiosulfate consumption and particulate COD was stable since 30 days (4 folds the HRT).

The first sample (day 30) revealed that 64% of the rDNA-16s identified corresponds to the genera *Acidithiobacillus* corresponding to the species *T.acidophilus* and *T.thiooxidans* described in the table 13 in the chapter IV. The second sample (day 70) indicated that the genera *Acidithiobacillus* represents 98% of the indentified rDNA-16s established in the reactor. These results confirms firstly the selection of an acidophil SOB, secondly the possibility by the control of the environmental conditions to strongly selected and enriched a culture from an initial activated-sludge consortium.

3.1.5. Performance of sulfur-oxidizing bacteria selected under thiosulfate environment

For the model development, the analyses of the biological performances is the purpose of this paragraphs, with firstly the estimation of the observable specific growth (μ_{SOB}^{obs}), and secondly the estimation of the observable biomass yield ($Y^{obs}_{X_{SOB}/S_2O_3^{2-}}$).

3.1.5.1. Estimation of the net specific growth rate of the selected SOB

During the first period of the sequenced-batch culture several parameters (S(VI) oxides concentration and OUR_{max}) indicated growth of the sulfur-oxidizing activity. Because the reactor was operated under stable condition (HRT = 14.6 days), with a liquid volume injected for each pulse negligible (3% of the total volume), the sequenced-batch culture could be approximated in time to a continuous reactor. Thus the mass balance for the sulfur-oxidizing bacteria must be expressed by the equation (Eq 76).

Eq 76: $V.\frac{dX_{SOB}}{dt} = Q.X_{SOB}^{in} - Q.X_{SOB}^{out} + \mu_{SOB}^{obs}.X_{SOB}.V$

where X_{SOB} is the concentration of the sulfur-oxidizing bacteria (in gCOD-X/l); X_{SOB}^{in} is the concentration of sulfur-oxidizing bacteria at the inlet of the reactor (= 0 for the culture) (in gCOD-X/l), X_{SOB}^{out} is the concentration of the sulfur-oxidizing bacteria at the outlet of the reactor (here $X_{SOB}^{out} = X_{SOB}$); V is the reactor volume (in litre); Q is the inlet and the outlet water-flow (in l/d); μ_{SOB}^{obs} is the observable specific growth for the sulfur-oxidizing bacteria involved in the global sulfur oxidation (in d^{-1}) (this kinetic parameter include growth and decay).

To determine the time-course of the active microorganism during the growth period, the equation (Eq 76) could be converted to the equation (Eq 77).

Eq 77: $X_{SOB} = X_{SOB}^{(0)}.exp^{[(\mu_{SOB}^{obs} - \frac{Q}{V}).t]}$

where $X_{SOB}^{(0)}$ is the concentration of sulfur-oxidizing bacteria at t = 0 of the concerning period (in gCOD-X/l) and t is the time of the culture (in days).

Because OUR_{max} measurement is proportional to the active biomass, the equation (Eq 77) could be adapted to express the evolution of the OUR_{max} during time by the equation (Eq 78).

Eq 78: $OUR_{max} = OUR_{max}^{(0)}.exp^{[(\mu_{SOB}^{obs} - \frac{Q}{V}).t]}$

where $OUR_{max}^{(0)}$ is the maximum oxygen uptake rate for the thiosulfate pulse at t = 0 of the concerning period (in $mgO_2.l^{-1}.h^{-1}$).

In a first approximation, if S(VI)-oxides production was mainly considered, the same approach could be used with the S(VI)-oxides values described by the equation (Eq 79) (confirmed by the evaluation of the chemical disproportionate reaction in the paragraph [*3.1.2.2.*] and by the absence of sulfate salts precipitation [3.1.2.1.]).

Eq 79: $[S(VI) - oxides] = [S(VI) - oxides]^{(0)}.exp^{[(\mu_{SOB}^{obs} - \frac{Q}{V}).t]}$

where $[S(VI)-oxides]^{(0)}$ is the S(VI)-oxides concentration at t = 0 of the concerning period (in mol/l).

For a chosen period, μ_{SOB}^{obs} is the only unknown parameter in the equations (Eq 78) and (Eq 79). To estimate μ_{SOB}^{obs} the excel solver was used, for the period beginning at day 11 and finishing at day 30. The results obtained with the OUR_{max} data and the S(VI)-oxides data were μ_{SOB}^{obs} = 0.16 d^{-1} and μ_{SOB}^{obs} = 0.15 d^{-1} respectively at 20°C.

The figure 66 illustrates the numerical values obtained for the exponential growth models with corresponding μ_{SOB}^{obs} values compared to analytical measurements (time period day 11 to day 30).

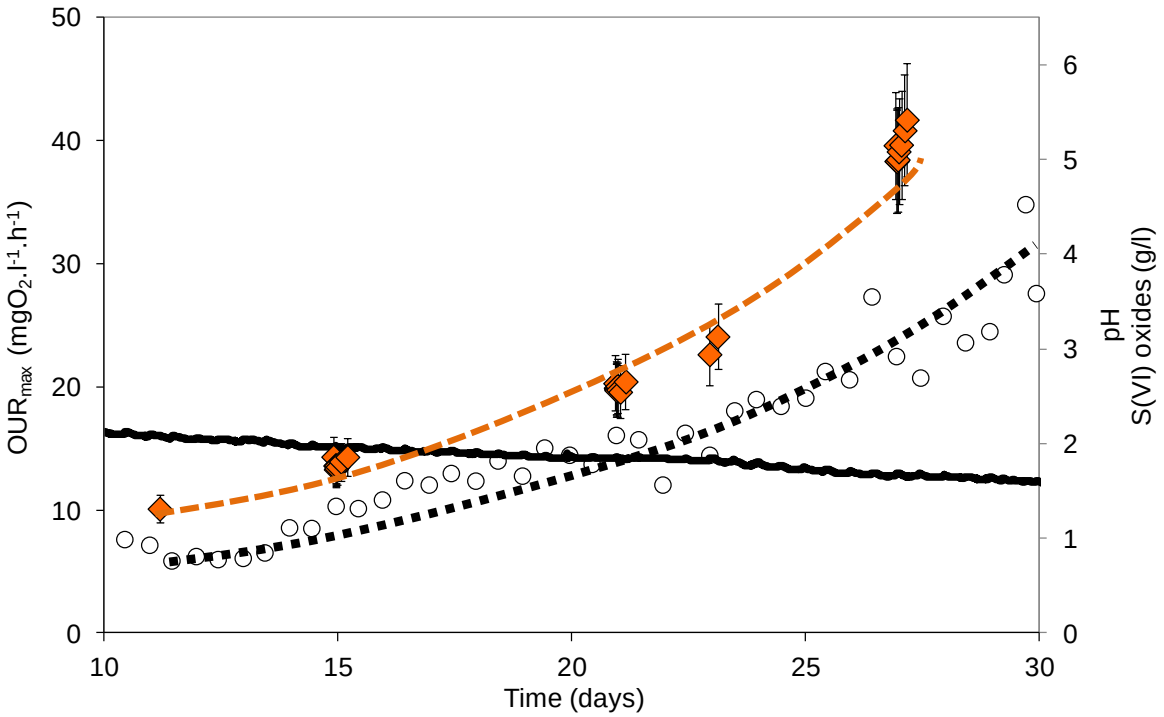

Figure 66: S(VI)-oxides and OURmax measurements compared calculated values based on exponential growth mode for the time period day 11 to day 30 – HRT = 14.6 days) and the pH measurement.
Experimental data. ◆: S(VI) oxides (g/l); ○: OUR_{max} ($mgO_2.l^{-1}.h^{-1}$); ——: pH measurement.
Numerical values (exponential growth model). – – : S(VI) oxides (g/l); ·····: OUR_{max} ($mgO_2.l^{-1}.h^{-1}$).

The numerical values, calculated with exponential growth model in a continuous reactor, showed good agreements with the analytical measurements. Based on the results obtained for the two model descriptions, the μ_{SOB}^{obs} values could be estimated to 0.155 d^{-1} (for a pH ranged between 2.09 and 1.59, and a temperature culture at 20°C). Thus, during the first time period

of the sequenced-batch culture the SOB growth rate was two folds faster than the imposed HRT (14.6 days equivalent to a dilution rate of 0.0685 d^{-1}).

3.1.5.2. Estimation of the net biomass yield ($Y^{obs}_{X_{tot}/S_2O_3^{2-}}$) of the selected SOB

Because the system was in steady state during the last 30 days of the sequenced-batch culture, the net biomass yield could be calculated (particulate COD produced per mole of sulfur substrate eliminated). During the last 30 days the particulate COD analyses gave a mean value of 248 ± 30 mgCOD/l with a standard deviation of 18 mgCOD/l (figure 59). Because abiotic elemental sulfur production was negligible (see paragraph [*3.1.4.2.*] of this chapter), the stable value of total particulate COD measurement (X_{tot}) defined the total particulate compounds produced during the culture. The stable X_{tot} measurement was composed by the catalytic biomass (X_{SOB}) produced during the growth phase (substrate consumption) and endogenous products (X_e) linked to the decay of the microorganisms. With the particulate compounds produced assimilated to the general formula $C_5H_7O_2N$ (considering the sulfur assimilation negligible, less than 1% of the biomass), the stable value (X_{tot}) during the second period was equivalent to 0.175 gX/l. The thiosulfate balance in a continuous system was described by the equation (Eq 80).

Eq 80: $$V.\frac{d[S_2O_3^{2-}]}{dt} = Q.[S_2O_3^{2-}]^{in} - Q.[S_2O_3^{2-}] - \mu_{SOB}^{obs} \cdot \frac{X_{tot}}{Y^{obs}_{X_{SOB}/S_2O_3^{2-}}}.V$$

where $[S_2O_3^{2-}]$ is the thiosulfate concentration at t time (in mol/l); $[S_2O_3^{2-}]^{in}$ is the thiosulfate concentration at the inlet of the reactor (in mol/l) equal to 0.054 mol$S_2O_3^{2-}$/l and $Y^{obs}_{X_{SOB}/S_2O_3^{2-}}$ is the observable conversion yield for particulate compounds production (in gX/mole of $S_2O_3^{2-}$ eliminated).

Under stationary conditions, because $\frac{d[S_2O_3^{2-}]}{dt} = 0$ and the thiosulfate was totally eliminated and μ_{SOB}^{obs} is equal to Q/V (0.14 d^{-1} in the experimental conditions), thus the equation (Eq 80) gave $Y^{obs}_{X_{SOB}/S_2O_3^{2-}}$ defined by the equation (Eq 81).

Eq 81: $Y^{obs}_{X_{SOB}/S_2O_3^{2-}} = \frac{X_{tot}}{[S_2O_3^{2-}]^{in}}$

In these conditions, the $Y_{X_{SOB}/S_2O_3^{2-}}$ is equal to 3.24 ± 0.39 gX/mol$S_2O_3^{2-}$, thus $Y^{obs}_{X_{SOB}/S_2O_3^{2-}}$ = 0.029 ± 0.004 mol$C_5H_7O_2N$ / mol$S_2O_3^{2-}$. This biomass yield value was in accordance with some values measured for pure culture of sulfur-oxidizing species and presented in the table 13 and table 14 of the chapter IV.

3.1.6. Preliminary conclusions

The experiments on semi-continuous culture allowed to observe the establishment and the growth of sulfur-oxidizing activity and to evaluate the kinetic and stoichiometric parameters of the selected population. The results showed the efficiency of the culture conditions to select, enrich and maintain acidophilic SOB. Moreover, the chemical model developed in the chapter V applied to the experimental data indicated the negligible contribution of the thiosulfate disproportionate reaction in the global transformation of the thiosulfate. It is thus concluded that thiosulfate is a convenient sulfur substrate to be used to produce biogenic acid.

To compare with other acidophil SOB, the table 31 (adapted from the table 13 and the table 14) presents in acid conditions the specific growth rate of some sulfur-oxidizing culture described in the literature and their associated biomass yield for different sulfur substrate. For *Thiobacillus thiooxidans* the Arrhenius temperature correction adapted from Vogler (1942) was applied (see paragraph [2.2]). This temperature correction was also applied to the experimental data proposed by Jensen 2011 for undetermined acidophil sulfur-oxidizing bacteria grown on corroded concrete. A comparison for the same sulfur substrate was proposed (thiosulfate), and then comparisons with elemental sulfur or sulfide as sulfur substrate were presented.

Concerning the net biomass yield conversion, the value determined experimentally (for thiosulfate as substrate) is lower than those given in the literature (around 50% lower, table 30). The feeding by pulses enhances the part of the maintenance in the energetic balance that can explain the difference observed with real chemostat culture.

Table 30: microbial parameters obtained during the selection of the sulfur-oxidizing activity in the experimental conditions with thiosulfate and tetrathionate as energy source compared to microbial parameters.

Species	**Culture Reactor**	**Sulfur Substrate**	**Oxidation product**	**pH**	**T°**	**Specific growth rate of the culture (h^{-1})**	**Yculture (gX/molS)**	**Ref**
T.Acidophilus	Chemostat	$S_2O_3^{2-}$	Sulfate	3.0	30°C	0.025	2.75	Mason 1987
= A.acidophilus	-	$S_4O_6^{2-}$	Sulfate	3.0	30°C	0.025	3.12	-
T.Thiooxidans	Chemostat	$S_2O_3^{2-}$	Sulfate	2.5	30°C	0.034 *(0.012)**	3.1	Mason 1987
= A.thiooxidans	-	$S_4O_6^{2-}$	Sulfate	2.5	30°C	0.034 *(0.012)**	3.02	-
T.Ferroxidans	Chemostat	$S_2O_3^{2-}$	Sulfate	3.0	30°C	0.037	2.75	Hazeu 1986
	-	$S_4O_6^{2-}$	Sulfate	3.0	30°C	0.030	3.4	-
Sulfur-oxidizing microorganisms	**Semi-continuous**	**$S_2O_3^{2-}$**	**Sulfate**	**1.45-1.5**	**20°C**	**0.006**	**1.62 ± 0.20**	**This study**
T.Thiooxidans	Batch	S^0	Sulfate	2.1-2.3	30¨C	0.0625 *(0.021)**		Sivaji Rao 1971
= A.thiooxidans	Batch	S^0	Sulfate	1.5	30°C	0.11 *(0.038)**		Konishi 1995
	Batch	S^0	Sulfate	1.3	22°C	0.0092 *(0.0074)**		Bielefeldt 2010
Thiobacilli sp.	Batch	(S^0 bio)	Sulfate	1.5-3.5		0.082		Tichy 1994
From correded concrete	Batch	Sulfide	Sulfate	1	22°C	0.055 *(0.044)**		Jensen 2011

** : the specific growth rate in italic indicated the recalculated specific growth at 20°C by the temperature correction adapted from Vogler 1942*

The specific growth rate is temperature and pH dependent, and could be substrate dependent. In chemostat the specific growth was fixed by the HRT of the culture. The specific growth rates presented in the table 30 are the highest values tested by the authors. In that case, *Acidithiobacillus acidophilus* and *Acidithiobacillus thiooxidans* (genera selected here) present equivalent performances in the experimental conditions. Considering *A.thiooxidans* as a representativ culture, optimal pH was determined by Bielefeldt (Bielfeldt et al., 2010) to 1.9, and ranged according to Sivaji Rao (Sivaji Rao and Berger, 1971) between 2.1 and 2.3. Thus the specific growth rate of the bacteria selected from the activated sludge determined experimentally (20°C) must be compared with the values corrected by the Arrhenius constant (indicated with a star). The higher specific growth rate (with thiosulfate or tetrathionate as sulfur substrate) recorded by Mason (1987) was quiet similar to this determined during the sequenced-batch culture (0.012 h^{-1} compared to 0.006 h^{-1}).

Compared to the heterogeneous values determined with elemental sulfur in batch culture, the values (0.021 h^{-1}, 0.038 h^{-1} and 0.0074 h^{-1}) determined in the sequenced-batch culture are in the same order than Bielefeldt values (0.0074 h^{-1}), but lower than theses determined by Sivaji Rao (1971) (0.021 h^{-1}) and Konishi (1995) (0.038 h^{-1}) . The energy recovery from the oxidation of elemental sulfur, compared to thiosulfate is a possible explanation of these differences for the specific growth rate.

The biological model, developed further, will determine the maximum specific growth rate for the SOB selected and will highlight the similitude with maximum specific growth rate recorded with pure culture of *A.thioxidans* and *A.acidophilus*, even on elemental sulfur as substrate. For that, the fate of the thiosulfate must be firstly described to improve the definition of the system and then enable the development of the dynamical model.

3.2. Conversion of thiosulfate in the experimental conditions

To propose a dynamic model describing the culture and the estimation of the biological parameters, the dynamic description of the thiosulfate and the associated stoichiometry are necessary. The first paragraphs focus on the stoichiometric description of the thiosulfate conversion. In the next section, based on the phenomenological description of the thiosulfate conversion, a dynamic model adapted from the chemical model presented in the chapter V, will be developed.

3.2.1. Analyze of the thiosulfate conversion during the culture by oxygen and sulfur mass balances

The total chemical oxidation of thiosulfate into sulfate could be expressed by the equation (Eq 21).

Eq 21: $S_2O_3^{2-} + 2O_2 + H_2O \rightarrow 2SO_4^{2-} + 2H^+$

For total chemical oxidation of thiosulfate, the ratio $O_2/S_2O_3^{2-}$ is equal to 2.

Autotrophic growth of SOB was involved in the oxidation of the reduced sulfur compounds, and $Y_{X_{SOB}/S_2O_3^{2-}}$ = 0.029 mol$C_5H_7O_2N$ / mol$S_2O_3^{2-}$ was evaluated for the total

elimination of thiosulfate. Thus the biological oxidation of thiosulfate during the culture can be described by the equation (Eq 82).

Eq 82: $$S_2O_3^{2-} + 1.855\,O_2 + 0.116\,CO_2 + 0.029\,HCO_3^- + 0.029\,NH_4^+ + 1.029\,H_2O \rightarrow 2\,SO_4^{2-} + 2\,H^+ + 0.029\,C_5H_7O_2N$$

Hence the theoretically ratio $O_2/S_2O_3^{2-}$ is equal to 1.855.

The figure 67 indicates the stability of the system in terms of oxygen consumption during the last 25 days. The ratio $O_2/S_2O_3^{(2-)}$ was equal to 1.67 ± 0.28 (quiet similar to the theoretically ratio (1.855) excepted for the equation (Eq 82)). The deviation of oxygen consumption could be attributed to the experimental measurements coupled to the weak loss of sulfur compounds (1% due to the thiosulfate disproportionate reaction and 0.5% to 1% of the biomass produced composed by assimilated sulfur). Therefore, comparing the experimental and the theoretical ratio $O_2/S_2O_3^{(2-)}$ it can be stated that the biological oxidation was the major process involved in the thiosulfate conversion. However, the specific oxygen profile indicates a specific conversion of the thiosulfate that is the purpose of the next sections.

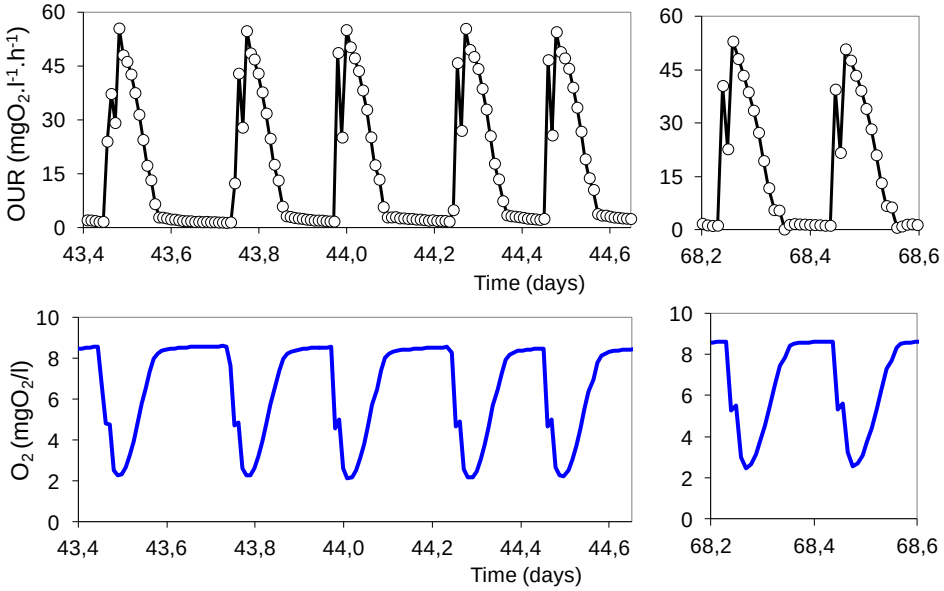

Figure 67: five consecutive thiosulfate pulses in the middle of the period and two thiosulfate pulses at the end of the second period of the sequenced-batch culture – HRT = 7.3 days – thiosulfate pulses (214 $mgS_2O_3^{2-}$/l per pulse). ——: dissolved oxygen concentration (mgO_2/l); —○—: OUR ($mgO_2.l^{-1}.h^{-1}$).

3.2.2. Kinetic analysis of tetrathionate oxidation as biological intermediate

As presented in the paragraph [1.2.1.], tetrathionate is a potential candidate for biological intermediate during the oxidation of thiosulfate, as it was also suggested on the *OUR(t)* profile (figure 67). To study the possible role of tetrathionate during the culture, four tetrathionate pulses were tested during the stable phase of the second period of the sequenced-batch culture (tetrathionate quantity per pulse equivalent in mole of sulfur of the thiosulfate pulses, so 9.81 x 10^{-4} mol$S_4O_6^{2-}$ compared to 1.97 x 10^{-3} mol$S_2O_3^{2-}$). The first objective was to evaluate the potentiality of the formation of this compound during the thiosulfate biological conversion. The second objective, in the case of a biological response, was to analyse the stoichiometry of the tetrathionate biological oxidation by oxygen and sulfur mass balance.

3.2.2.1. Oxygen profiles with tetrathionate as sulfur source

The figure 68 presents the experimental results obtained for three identical tetrathionate pulses with the experimental results obtained for the thiosulfate pulses just after or just before the tetrathionate pulses. The presented experimental data were the oxygen profile during the pulses and the calculated *OUR(t)*. The tetrathionate pulses were designed by the numbers (1), (2) and (3) in the chronologic order.

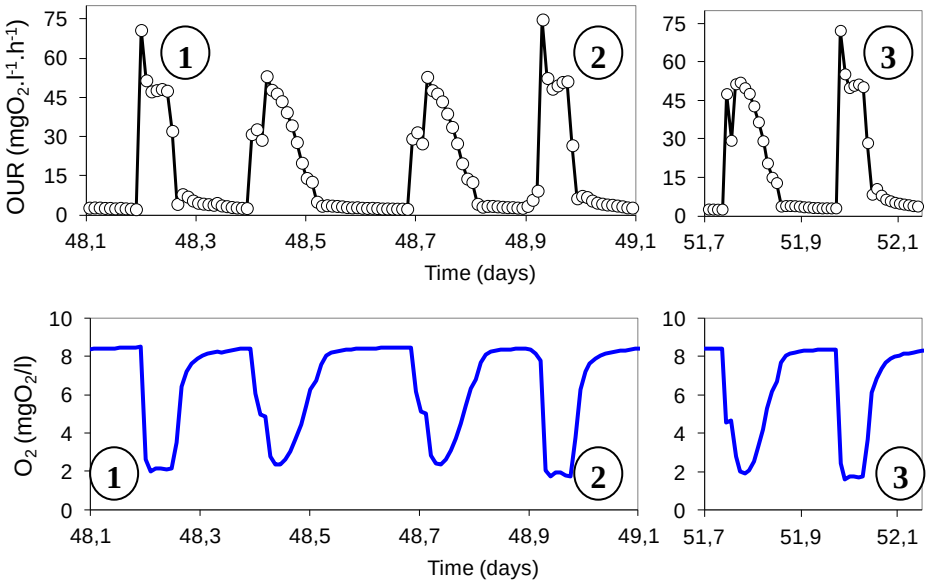

Figure 68: three tetrathionate pulses tested and thiosulfate pulses associated during the second period of the sequenced-batch culture – HRT = 7.3 days – tetrathionate pulses (221 mg$S_4O_6^{2-}$/l per pulse), thiosulfate pulses (214 mg$S_2O_3^{2-}$/l per pulse). ——: dissolved oxygen concentration (mgO_2/l); —○—: OUR (mgO_2.l^{-1}.h^{-1}). The tetrathionate pulses are designed by the number (1), (2) and (3).

The use of tetrathionate led to immediate oxygen consumption, but the dissolved oxygen profiles for the tetrathionate differs clearly from the profiles recorded during the thiosulfate pulses (no deceleration-acceleration phenomena recorded for the oxygen consumption). The sharp *OUR(t)* decrease at the end of the tetrathionate consumption demonstrates the high affinity of the active sulfur-oxidizing biomass for the tetrathionate as sulfur substrate (confirming the literature data for acidophilic Thiobacilli species cultivated under tetrathionate environment (Hazeu et al., 1986) (Pronk et al., 1990c)). If tetrathionate was biologically produced as intermediate, it can be an explanation of the acceleration of OUR observed during thiosulfate consumption.

After the increase of the *OUR(t)*, the quick decrease and the stabilization to lower values may be caused by a constant substrate limitation. Indeed stabilization of the *OUR(t)* at a constant value argues for a limitation where the limiting compounds is continustly fed to the system. Thus only oxygen and/or carbon dioxide must be considered. As $[O_2]$ is always higher than 2 mg/l, only carbon dioxide limitation can explain the *OUR(t)* profiles. Thus, for the development of the dynamical model the consumption of the carbon dioxide will must be taken into account to describe correctly the system.

3.2.2.2. Biological oxidation of tetrathionate during the culture

The dynamic consumption of the tetrathionate was evaluated during one tetrathionate pulse. For that, because 1g of $S_4O_6^{2-}$ is equivalent to 0.5 gCOD, the soluble COD was measured during the last tetrathionate pulse tested (day 63) (221 mg$S_4O_6^{2-}$/l), before, during and after the tetrathionate pulse. The figure 69 presents the dissolved oxygen concentration and the *OUR(t)* calculation associated, the soluble COD concentration during the tetrathionate pulse and the thiosulfate concentration before the tetrathionate pulse (because thiosulfate is quantifiable by COD measurement).

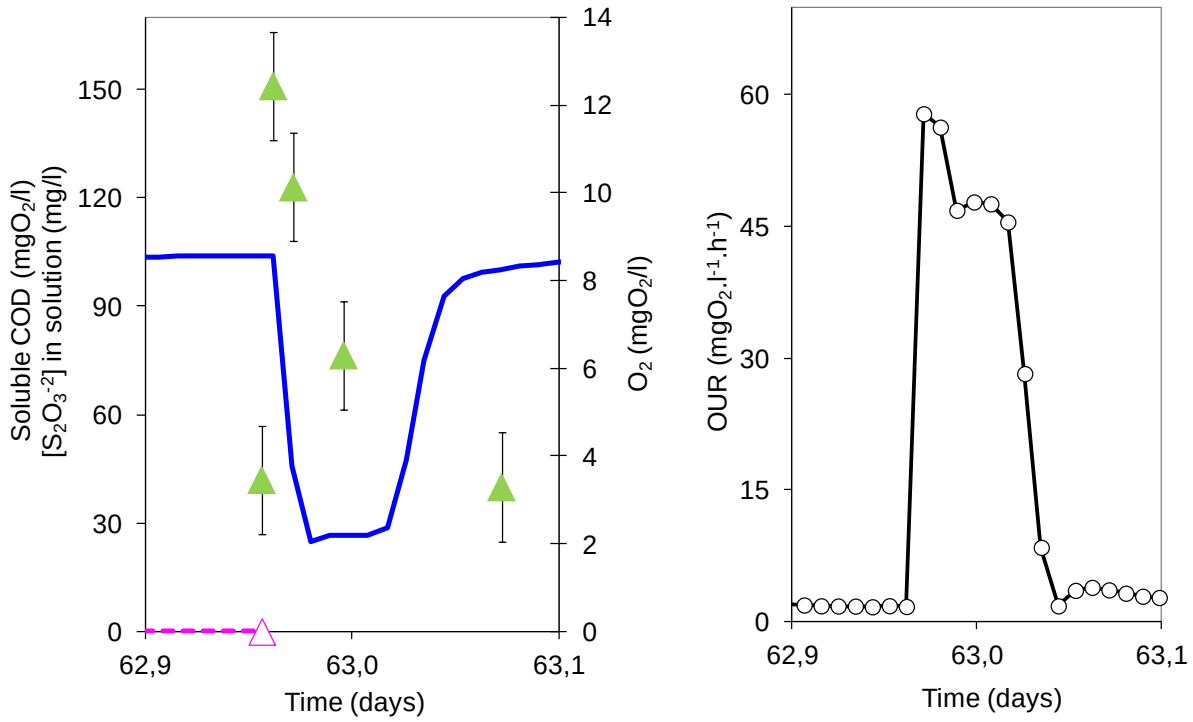

Figure 69: last tetrathionate pulse tested (day 63) with soluble COD measurements (221 $mgS_4O_6^{2-}$/l per pulse). ▬: dissolved oxygen concentration (mgO_2/l); ▬○▬: OUR(t) ($mgO_2.l^{-1}.h^{-1}$); ▬△▬: thiosulfate concentration (mgS_2O_3/l); ▲: soluble COD (mgO_2/l).

Before the tetrathionate pulse the soluble COD concentration was equal to 42 mgCOD/l, with thiosulfate concentration null, thus no thiosulfate interferences had to be taken into account for the COD measurement. Just after the tetrathionate pulse the soluble COD concentration increased directly to 151 ± 15 mgCOD/l, thus 109 ± mgCOD/l were added to the medium corresponding to the 218 ± 24 $mgS_4O_6^{2-}$/l added by the tetrathionate pulse (theoretical ratio) compared to the 220 $mgS_4O_6^{2-}$/l really added. During the oxygen consumption phase, the soluble COD concentration decreased to reach the initial value (40 mgCOD/l) at the end of the oxygen consumption and then stabilized. Thus all the soluble COD added by the tetrathionate pulse was consumed, confirming the total consumption of tetrathionate during the pulse.

To evaluate the stability of the tetrathionate biological oxidation, the table 31 presents the experimental ratio $O_2/S_4O_6^{2-}$ obtained for the four tetrathionate pulses tested during the sequenced-batch culture (first pulse realized day 48, last pulse realized day 63).

Table 31: Determination of the experimental ratio $O_2/S_4O_6^{2-}$ for the four pulses of tetrathionate used during the sequenced-batch culture.

Tetrathionate pulse [day of the culture]	**Tetrathionate /pulse (mol $S_4O_6^{2-}$)**	**Oxygen consumed /pulse (mol O_2)**	**Ratio $O_2/S_4O_6^{2-}$**	**Mean values for the ratio $O_2/S_4O_6^{2-}$**	**Standard deviation for the ratio $O_2/S_4O_6^{2-}$**
(1) [day 48]	9.81×10^{-4}	2.60×10^{-3}	2.65 ± 0.45	2.75 ± 0.47	± 0.18
(2) [day 49]	9.81×10^{-4}	2.70×10^{-3}	2.75 ± 0.47		
(3) [day 52]	9.81×10^{-4}	2.94×10^{-3}	3 ± 0.51		
(4) [day 63]	9.81×10^{-4}	2.54×10^{-3}	2.59 ± 0.44		

The mean value for the ratio $O_2/S_4O_6^{2-}$ is 2.75 (± 0.47) with a standard deviation of 0.18 for four evaluation of the ratio. The stability of the ratio values indicates the stability of the tetrathionate conversion during the second time period of the sequenced-batch culture.

Based on the experimental results and their analysis, a dynamical model will be developed in the next sections of this chapter, to describe the kinetic and stoichiometry of the thiosulfate conversion by selected acidophil SOB, and to estimate for this population the maximum specific growth rates and the specific biomass yields on thiosulfate and on tetrathionate.

3.3. Development of dynamic model to describe the thiosulfate conversion by selected SOB

To develop a dynamic model able to describe the consumption of thiosulfate at low pH in presence of acidophil SOB activity, a bottom-up method was proposed, from a simple system as a first step to more and more complex system. Different controls and experimental validations were performed during the development. The figure 70 presents a schematic description of the model proposed for the conversion of thiosulfate in biological acidic environment, and the sequence proposed for the development and the validation (step by step) of the model structure and the parameters values.

The chemical model indicated the weak contribution of the thiosulfate disproportionate reaction in the global thiosulfate consumption. Moreover the pH was relatively stable during the last 55 days of the sequenced-batch culture (from 1.95 to 1.45). Therefore the thiosulfate disproportionate reaction was considered negligible for the definition of the microbial activity in the culture conditions obtained during this study.

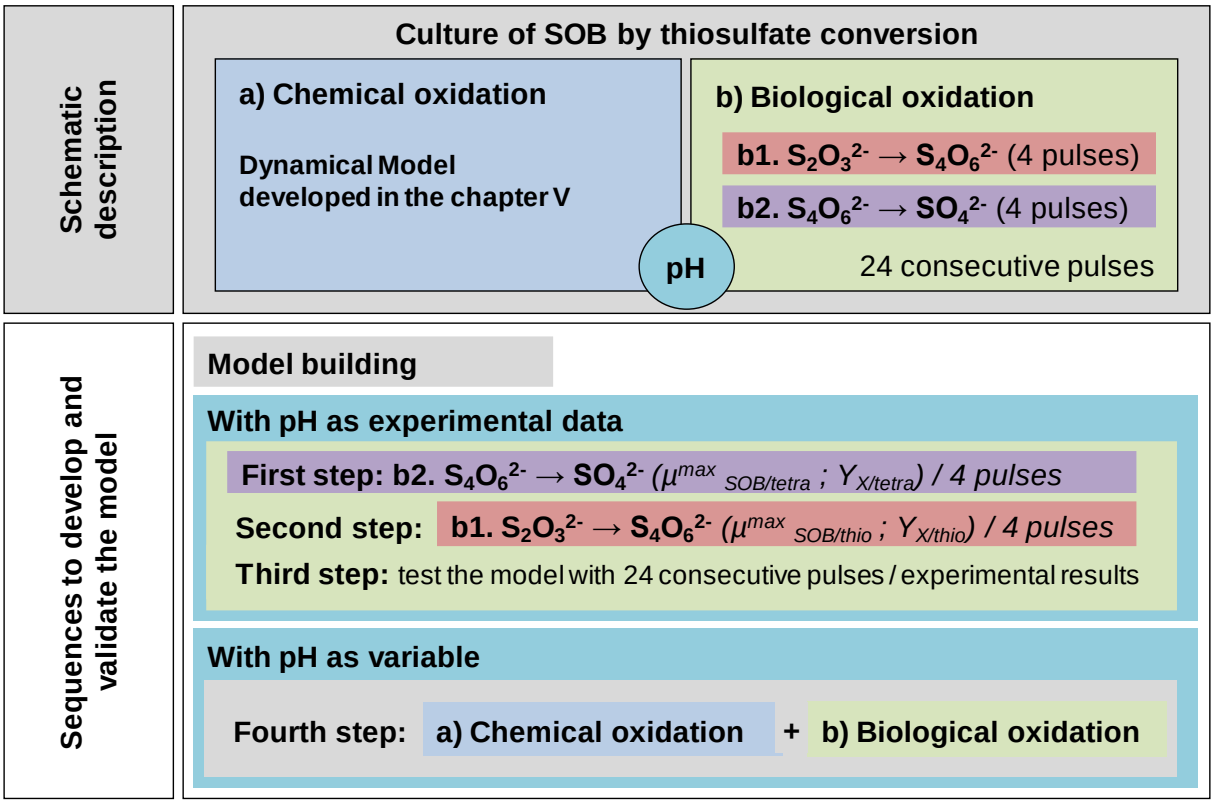

Figure 70: description of the experimental construction for the study of the thiosulfate reactivity, and the sequence to build the dynamical model with chemical and biological oxidation of thiosulfate with tetrathionate as biological intermediate.

Model development followed through steps (as illustrated at the figure 70):

In a first step, through comparison to experimental data, the biological conversion of tetrathionate was studied. Evaluation of the specific growth rate and of the specific biomass yield conversion (one kinetic was used to calibrate the parameters, the four tetrathionate pulse showing stable conversion of tetrathionate). In a second step, the thiosulfate conversion was added in the model together, with tetrathionate biological production. It allowed evaluating the specific parameters of the tetrathionate production (four different thiosulfate pulse were tested). In a third step, the dynamic multisubstrate model was tested during several consecutive pulses (from day 15 to day 27 of the culture). In a fourth step, the pH definition and the thiosulfate disproportionate reaction was inluded to allow the complete description of the system, i.e. the time course of thiosulfate and tetrathionate transformations, oxygen consumption and pH.

The mathematical model presented in this part only objective to understand experimental results. None optimization procedure for the calibration of the parameters was developed. The parameters values obtained, only determine the range of maximum specific growth rates and of the sequential biomass yield for the two steps of the biological conversion of thiosulfate.

3.3.1. Dynamic biological oxidation of tetrathionate

Tetrathionate was produced during the thiosulfate biological oxidation, and oxidized as sulfur substrate into S(VI)-oxidises. Tetrathionate was stable in acidic environment (Druschel et al., 2003c), thus its biological oxidation could be considered as a unique reaction at the end of the process. Thus for a tetrathionate pulse only the tetrathionate oxidation could be considered independent of the others biological reactions.

At pH relatively stable, a simple model can be used to evaluate the microbial parameters (μ_{SOB}^{max} the maximum specific growth rate and $Y_{X_{SOB}/S_4O_6^{2-}}$ biomass yield).

The mass balance equation for the production of 1 mole of X_{SOB} (1 mole of $C_5H_7O_2N$) is described by the equation (Eq 83).

Eq 83: $$Y_1.S_4O_6^{2-} + (3.5\,Y_1 - 5)\,O_2 + 4\ CO_2 + HCO_3^- + NH_4^+ + (3 + 1/Y_1)\,H_2O \rightarrow (4\,Y_1)\,SO_4^{2-} + (6\,Y_1)\,H^+ + C_5H_7O_2N$$

where:

$Y_1 = \frac{1}{Y_{X_{SOB} / S_4O_6^{2-}}}$ is the inverse value of the biomass Yield conversion (in mol$S_4O_6^{2-}$/molX).

The dynamical biomass production is described by the equation (Eq 84) based on the Monod model if decay was neglected (valid approximation during substrate pulses).

Eq 84: $$V.\frac{dX_{SOB}}{dt} = \mu_{SOB}^{max} . \frac{[S_4O_6^{2-}]}{K_{S_4O_6^{2-}} + [S_4O_6^{2-}]} . \frac{[O_2]}{K_{O_2} + [O_2]} . \frac{[CO_2aq]}{K_{CO_2} + [CO_2aq]} . X_{SOB} . V$$

where μ_{SOB}^{max} is the maximum specific growth rate (in h^{-1}); $K_{S_4O_6^{2-}}$ is the half saturation constant for tetrathionate (in mol/l); K_{O_2} is the half saturation constant for dissolved oxygen (mol/l); K_{CO_2} is the half saturation constant for dissolved carbon dioxide (mol/l).

The table 32 presents the different values used as microbial parameters to define the biological oxidation of tetrathionate during the sequenced-batch culture.

Table 32: microbial parameters used to define the biological oxidation of tetrathionate during the sequenced-batch culture.

Parameters	Unity	values	Ref.
μ_{SOB}^{max}	h^{-1}	0.020	Manual estimation (Aquasim®)
$Y_{X_{SOB} / S_4O_6^{2-}}$	molX/mol$S_4O_6^{2-}$	0.043	Manual estimation (Aquasim®)
$K_{S_4O_6^{2-}}$	mol/l	3.5×10^{-6}	(Hazeu, 1986) value for T.Ferrooxidans [a]
K_{O_2}	mol/l	1.56×10^{-5}	Equivalent to 0.5 mgO_2/l [b]
K_{CO_2}	mol/l	1×10^{-7}	Low value to test [c]

[a]: value determined for specific strain, but value corresponding to pH conditions, specific growth rate and substrate.

[b]: value fixed in accordance with experimental data (lower dissolved oxygen concentration never lower than 1 mgO_2/l)

[c]: low value to simulated lowest dissolved oxygen concentrations with carbon dioxide limitation

The oxygen and the carbon dioxide supply were simulated as described in the chapter V, paragraph [3.2.2.2] and paragraph [3.2.2.] (with measured kla_{O2} equal to 7.3 h^{-1}).

The figure 71 presents the experimental data compared to the numerical data obtained from the model (resolved by Aquasim®). Looking at the curves in figure 71 allows comparing experimental and simulated values of tetrathionate and O_2 concentrations and the simulated *OUR(t)*.

Simulated data and experimental data (tetrathionate pulse, day 63) (Aquasim®)

Tetrathionate concentration	Dissolved oxygen concentration	Oxygen uptake rate (*OUR(t)*)
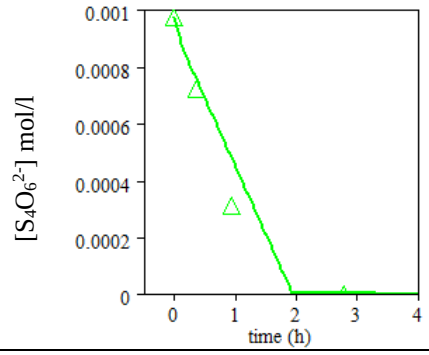	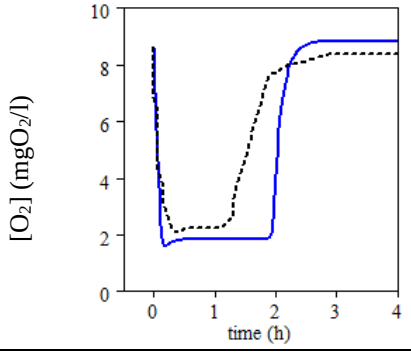	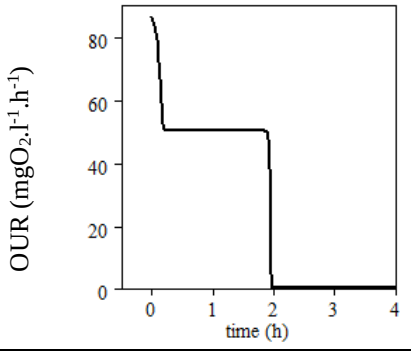

Figure 71: experimental and numerical data for tetrathionate pulse. △: experimental data for tetrathionate concentration (mol/l); ——: numerical data for tetrathionate concentration (mol/l); ▪▪▪▪▪▪: experimental data for oxygen concentration (mgO_2/l); ——: numerical data for oxygen concentration (mgO_2/l); ——: numerical data for OUR ($mgO_2.l^{-1}.h^{-1}$).

The simulated data for the *OUR(t)* fits rather well with the experimental *OUR(t)* (see figure 69). The model represents dynamically the tetrathionate and the oxygen consumption. The figure 72 shows the simulated data for dissolved carbon dioxide concentration during the tetrathionate pulse, that could explain by a CO_2 limitation the shape in two phase of the *OUR(t)*. Indeed, just after the tetrathionate pulse, due to fast biological reaction, the carbon dioxide (for autotrophic growth) decreased quickly to reach limitation value. Thus the carbon dioxide limitation explains the shape of the OUR profiles. The OUR plateau obtained during the end of the tetrathionate oxidation was due to the rate of the physical absorption of the atmospheric carbon dioxide. The values, quiet similar for the experimental data and the numerical data (around 45 – 50 $mgO_2.l^{-1}.h^{-1}$) indicate the good representation of this physical process during the biological oxidation of sulfur compounds.

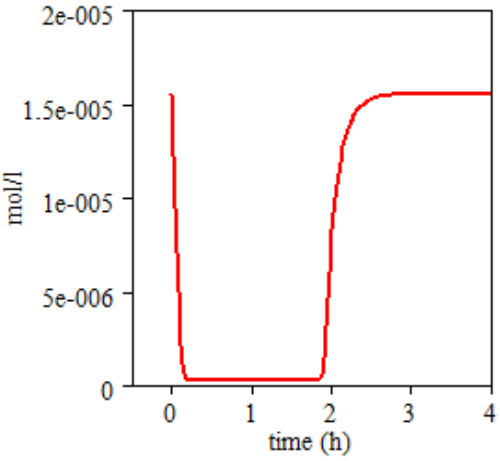

Figure 72: simulated data for the dissolved carbon dioxide concentration during the tetrathionate pulse represented in the figure 71(mol/l).

To represent tetrathionate consumption, the maximum specific growth rate was estimated to 0.020 h^{-1} (at 20°C), value in the range order of the maximum specific growth rate proposed in the literature for several pure cultures of Thiobacilli species (0.025 h^{-1} for *Acidithiobacillus acidophilus* at 30°C and 0.012 h^{-1} for *Acidithiobacillus thiooxidans* at 20°C (table 30)).

The biomass yield for tetrathionate conversion ($Y_{Xtot / S_4O_6^{2-}}$) determined for the mathematical description of tetrathionate pulse was fixed to 0.043 molX/mol$S_4O_6^{2-}$ (or 4.86 gVSS/mol$S_4O_6^{2-}$), corresponding in the global conversion of thiosulfate to the second step of the biological reaction. Thus for the thiosulfate oxidation, considering the entire conversion of thiosulfate into tetrathionate, the biomass yield for the second step of the reaction could be estimated theoretically to 0.0215 mole of biomass for one mole of thiosulfate converted to tetrathionate. Because the global biomass yield ($Y_{X_{tot} / S_2O_3^{2-}}$) evaluated experimentally was 0.029 molX/mol$S_2O_3^{2-}$, the specific biomass yield during the first step of the biological reaction (oxidation of thiosulfate to tetrathionate) is evaluated to 0.0075 molX/mol$S_2O_3^{2-}$.

These values indicate, for thiosulfate pulse, that the biomass production occurred mainly during the second step of the biological reaction, during the tetrathionate oxidation. 74% of the biomass was produced during the oxidation of tetrathionate to sulfate, and only 26% was produced during the first step corresponding to the oxidation of thiosulfate into tetrathionate. Considering the theoretical biomass production calculated for the total oxidation of thiosulfate and for the two oxidative steps (based on the free Gibbs energies and presented in annexes of this chapter) (Kelly, 1999), the theoretical ratios, 83% of the biomass produced by the

tetrathionate oxidation for 17% produced by thiosulfate oxidation, were in accordance with the values determined from the combination of the experimental data and the estimation of the simulated parameters.

3.3.2. Dynamic biological oxidation of thiosulfate

One microbial specie was involved in the two steps of the thiosulfate oxidation. Therefore, one specific growth rate is sufficient to describe the full thiosulfate oxidation. The switch between both sulfur substrates can be included by in a specific growth rate equation, (Eq 85) for the thiosulfate oxidation, and equation (Eq 86) for the tetrathionate oxidation (based on the equation (Eq 84)).

Eq 85:

$$\frac{dX_{SOB}}{dt} = \mu_{SOB}^{max}(1).\frac{[S_2O_3^{2-}]}{K_{S_2O_3^{2-}} + [S_2O_3^{2-}]}.\frac{[O_2]}{K_{O_2} + [O_2]}.\frac{[CO_2]}{K_{CO_2} + [CO_2]}.\frac{Ki_{S_4O_6^{2-}}}{Ki_{S_4O_6^{2-}} + [S_4O_6^{2-}]}.X_{SOB}$$

where $\mu_{SOB}^{max}(1)$ is the maximum specific growth rate (in h^{-1}); $K_{S_2O_3^{2-}}$ is the half saturation constant for thiosulfate (in mol/l); $Ki_{S_4O_6^{2-}}$ is the biological inhibition constant to the tetrathionate.

Eq 86:

$$\frac{dX_{SOB}}{dt} = \mu_{SOB}^{max}(2).\frac{[S_4O_6^{2-}]}{K_{S_4O_6^{2-}} + [S_4O_6^{2-}]}.\frac{[O_2]}{K_{O_2} + [O_2]}.\frac{[CO_2]}{K_{CO_2} + [CO_2]}.\frac{Ki_{S_2O_3^{2-}}}{Ki_{S_2O_3^{2-}} + [S_2O_3^{2-}]}.X_{SOB}.$$

where $\mu_{SOB}^{max}(2)$ is the maximum specific growth rate (in h^{-1}); $K_{S_4O_6^{2-}}$ is the half saturation constant for tetrathionate (in mol/l); $Ki_{S_2O_3^{2-}}$ is the biological inhibition constant to thiosulfate.

To avoid a simultaneous growth on both substrates and simulate the switch in the substrates consumption, a simple comparison of the observable specific growth rate ($\mu_{SOB}^{obs}(S_2O_3^{2-})$ and $\mu_{SOB}^{obs}(S_4O_6^{2-})$ corresponding to the maximum specific growth rate for thiosulfate and tetrathionate respectively corrected by the Monod terms and the inhibitions

terms) determined which substrate is used by a switch function described by the equation (Eq 87).

Eq 87: if $\mu_{SOB}^{obs}(S_2O_3^{2-}) > \mu_{SOB}^{obs}(S_4O_6^{2-})$ then $\mu_{SOB}^{max}(1) = \mu_{SOB}^{obs}(S_2O_3^{2-})$ else $\mu_{SOB}^{max}(1) = 0$, and if $\mu_{SOB}^{obs}(S_2O_3^{2-}) < \mu_{SOB}^{obs}(S_4O_6^{2-})$ then $\mu_{SOB}^{max}(2) = \mu_{SOB}^{obs}(S_4O_6^{2-})$ else $\mu_{SOB}^{max}(2) = 0$ end if.

The mass balance equations for the production of 1 mole of X_{SOB} (in mole of $C_5H_7O_2N$) are described by the equation (Eq 88) for the thiosulfate oxidation (first reaction) and by the equation (Eq 89) for the tetrathionate oxidation (second reaction).

Eq 88: $$(133.33).S_2O_3^{2-} + (28.33)O_2 + 4\ CO_2 + HCO_3^- + NH_4^+ + (1.0075)H_2O \rightarrow (66.665)S_4O_6^{2-} + (133.33)OH^- + C_5H_7O_2N$$

Eq 89: $$(23.26).S_4O_6^{2-} + (76.4)O_2 + 4\ CO_2 + HCO_3^- + NH_4^+ + (3.043)H_2O \rightarrow (93)SO_4^{2-} + (139.5)H^+ + C_5H_7O_2N$$

The parameters used for the numerical simulation of the biological oxidation of thiosulfate are presented in the table 33. The inhibition constant were adjusted to obtained valid representation of the thiosulfate consumption, of the oxygen consumption and of the *OUR(t)* calculation.

Table 33: microbial parameters used to define the biological oxidation of thiosulfate described by two biological steps during the sequenced-batch culture.

Parameters	unity	values	Ref.
$\mu_{SOB}^{max}(1)\ and\ (2)$	h^{-1}	0.020	From paragraph [3.3.1.]
$Y_{Xtot/S_2O_3^{2-}}$	molX/mol$S_2O_3^{2-}$	0.0075	From paragraph [3.3.1.]
$Y_{Xtot/S_4O_6^{2-}}$	molX/mol$S_4O_6^{2-}$	0.043	From paragraph [3.3.1.]
$Ki_{S_2O_3^{2-}}$	mol/l	0.0025	Manual estimation (Aquasim®)
$Ki_{S_4O_6^{2-}}$	mol/l	0.001	Manual estimation (Aquasim®)
$K_{S_2O_3^{2-}}$	mol/l	2×10^{-5}	(Hazeu 1986) value for T.Ferrooxidans [a]
$K_{S_4O_6^{2-}}$	mol/l	3.5×10^{-6}	(Hazeu 1986) value for T.Ferrooxidans [a]
K_{O_2}	mol/l	1.56×10^{-5}	Equivalent to 0.5 mgO_2/l [b]
K_{CO_2}	mol/l	1×10^{-7}	Low value to test [c]

[a]: value determined for specific strain, but value corresponding to pH conditions, specific growth rate and substrate.
[b]: value fixed in accordance with experimental data (lower dissolved oxygen concentration never lower than 1 mgO_2/l)
[c]: low value to simulated lowest dissolved oxygen concentrations with carbon dioxide limitation

The figure 73 shows the numerical data obtained for the four thiosulfate pulses tested compared to the experimental data. The consumption of thiosulfate and the production-consumption of tetrathionate are presented, the dissolved oxygen concentration and the calculated *OUR(t)* also.

Experimental data and numerical data for four thiosulfate pulses

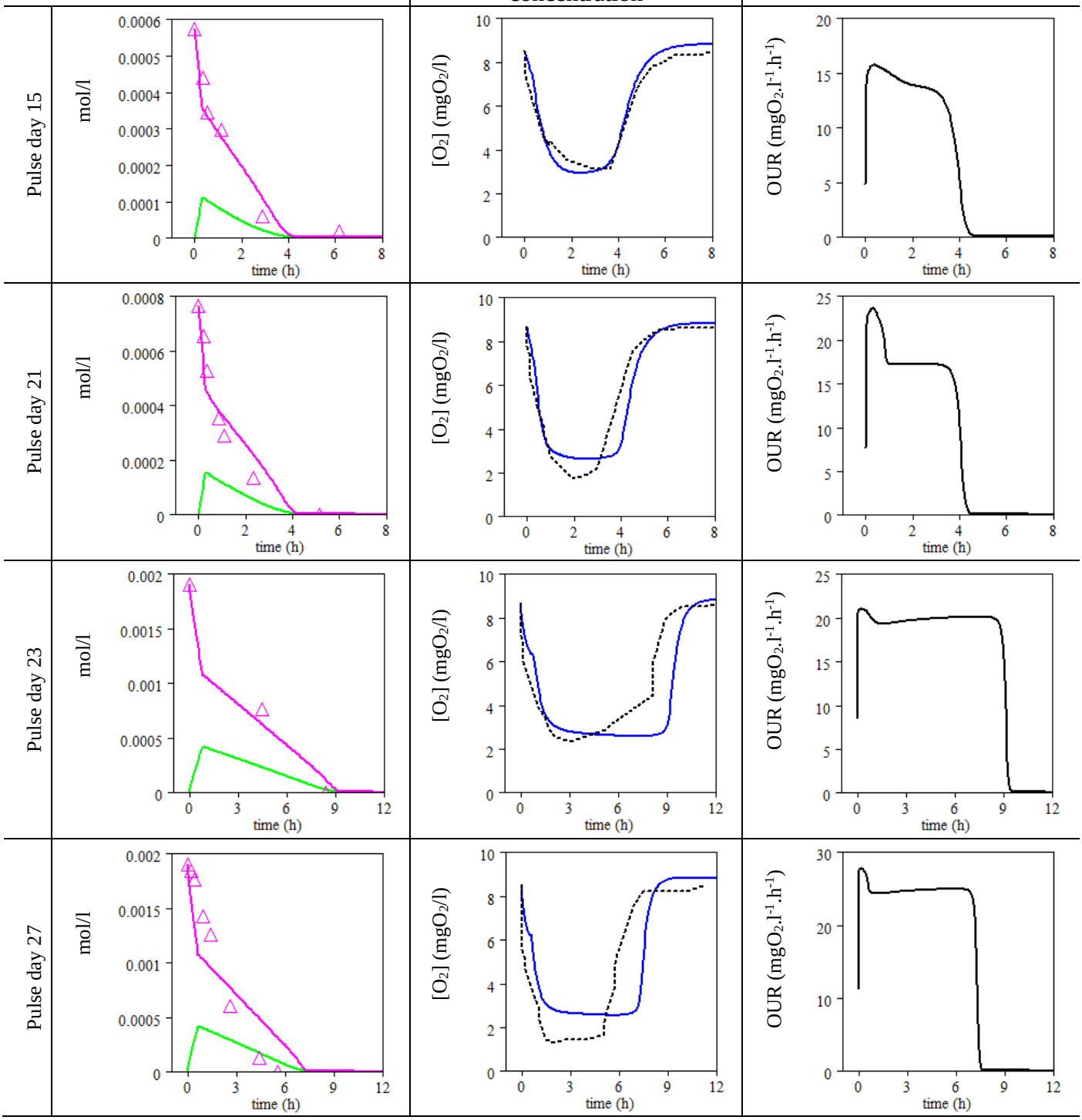

Figure 73: experimental and numerical data for four thiosulfate pulses.
Numerical data: △: experimental data for thiosulfate concentration (mol/l); ——: numerical data for thiosulfate concentration; ——: numerical data for tetrathionate concentration (mol/l); ·····: experimental data for oxygen concentration (mgO_2/l); ——: numerical data for oxygen concentration (mgO_2/l); ——: numerical data for *OUR(t)* ($mgO_2.l^{-1}.h^{-1}$).

The different parameters are rather well simulated. The work with preferential substrate and one global population with one way for growth defined in two biological steps, enables the qualitative description of the deceleration-acceleration phenomenon observed for the oxygen profiles (thus the *OUR(t)* calculations) during the thiosulfate pulses.

For the four pulses, the numerical model simulates a phenomenon of deceleration-acceleration of the oxygen consumption faster than this recorded experimentally. Moreover, for the pulses day 23 and day 27, especially for the day 27, the rate of the oxygen consumption, defined by the carbon dioxide limitation is underestimated. Vogler in 1942, showed for *Acidithiobacillus thiooxidans*, that the fixation of carbon dioxide could be decoupled of the reduced sulfur compounds oxidation by the storage of energy in the cell during the sulfur oxidation and the energy release for CO_2 fixation in the absence of sulfur oxidation.

3.3.3. Control of the model definition during growth period (24 consecutive pulses)

To evaluate the interest of the model to describe the sequenced-batch culture, the model was tested during 12 days of the culture (from the day 15 to the day 27), thus during 24 consecutives pulses. The microbial parameters determined in the previous paragraphs of this chapter were applied without modification.

The figure 74 presents the simulated results obtained compared to the experimental data during this period (0 hour is equivalent to day 15 and 288 hours correspond to the day 27). The thiosulfate consumption and the tetrathionate production-consumption are presented, the evolution of the biomass and the sulfate production are presented as control of the growth simulation.

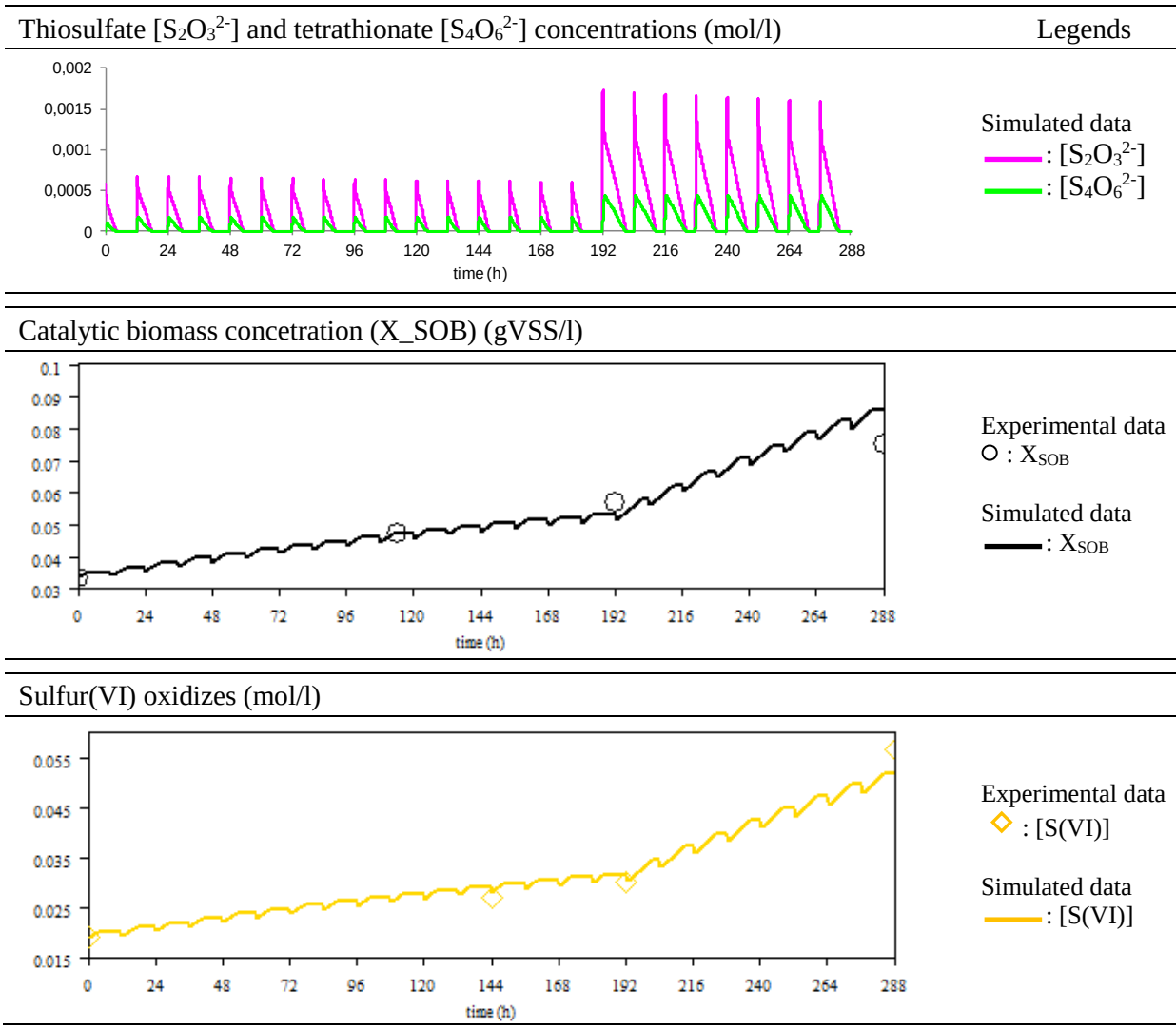

Figure 74: experimental and numerical data for growth period (24 thiosulfate pulses).

The simulated data obtained, from dynamical model applied for several consecutive pulses, describe the global behaviour of the selected sulfur-oxidizing bacteria during the culture. The sulfate production (expressed in S(VI)-oxides) and the evolution of the biomass are in accordance with the simulated data. To complete these results, the figure 75 focus on two consecutive thiosulfate pulses and presents the oxygen profiles and the associated *OUR(t)* calculations (from numerical and experimental data). Even during several consecutive thiosulfate pulses, the model describes the specific oxygen profiles (with deceleration-acceleration phenomenon for the oxygen consumption), and thus describes the associated specific *OUR(t)* profiles compared to the experimental *OUR(t)* profiles obtained and presented in the figure 67 of the paragraph [3.2.1.] of this chapter.

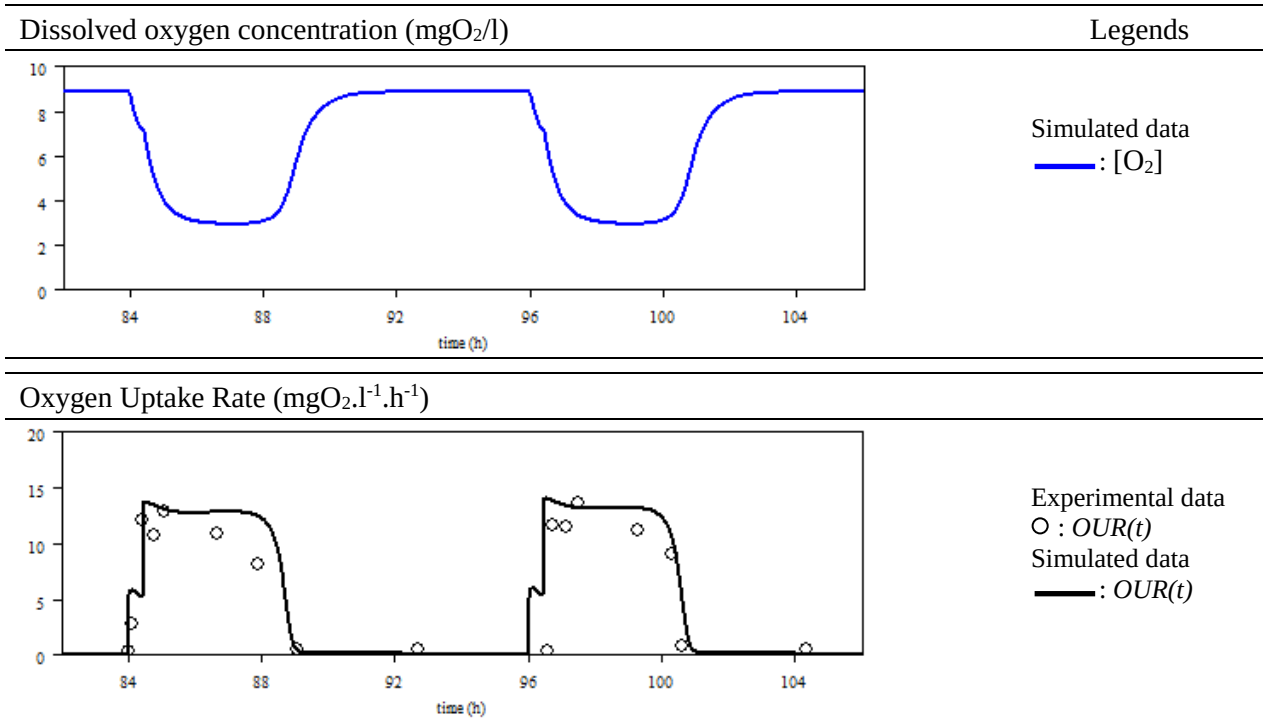

Figure 75: experimental and numerical data for growth period (example of 2 consecutive thiosulfate pulses).

For further exploration, because the deterioration of cementitious materials was linked to the local pH definition and the local sulfate production, the biological model defined in this paragraph for the microbial parameters estimation was implemented to the chemical model defined in the chapter V of this document, and the four thiosulfate pulses recording were tested to evaluate the good definition of the model for the dynamic definition of the system.

3.3.4. Biological and chemical model for thiosulfate conversion and pH definition

Without modification of the parameters used for the model definition, the figure 76 presents the results obtained for two pulses with connection of the biological and the chemical model, with pH considerate as variable (for these simulations only the initial values were fixed).

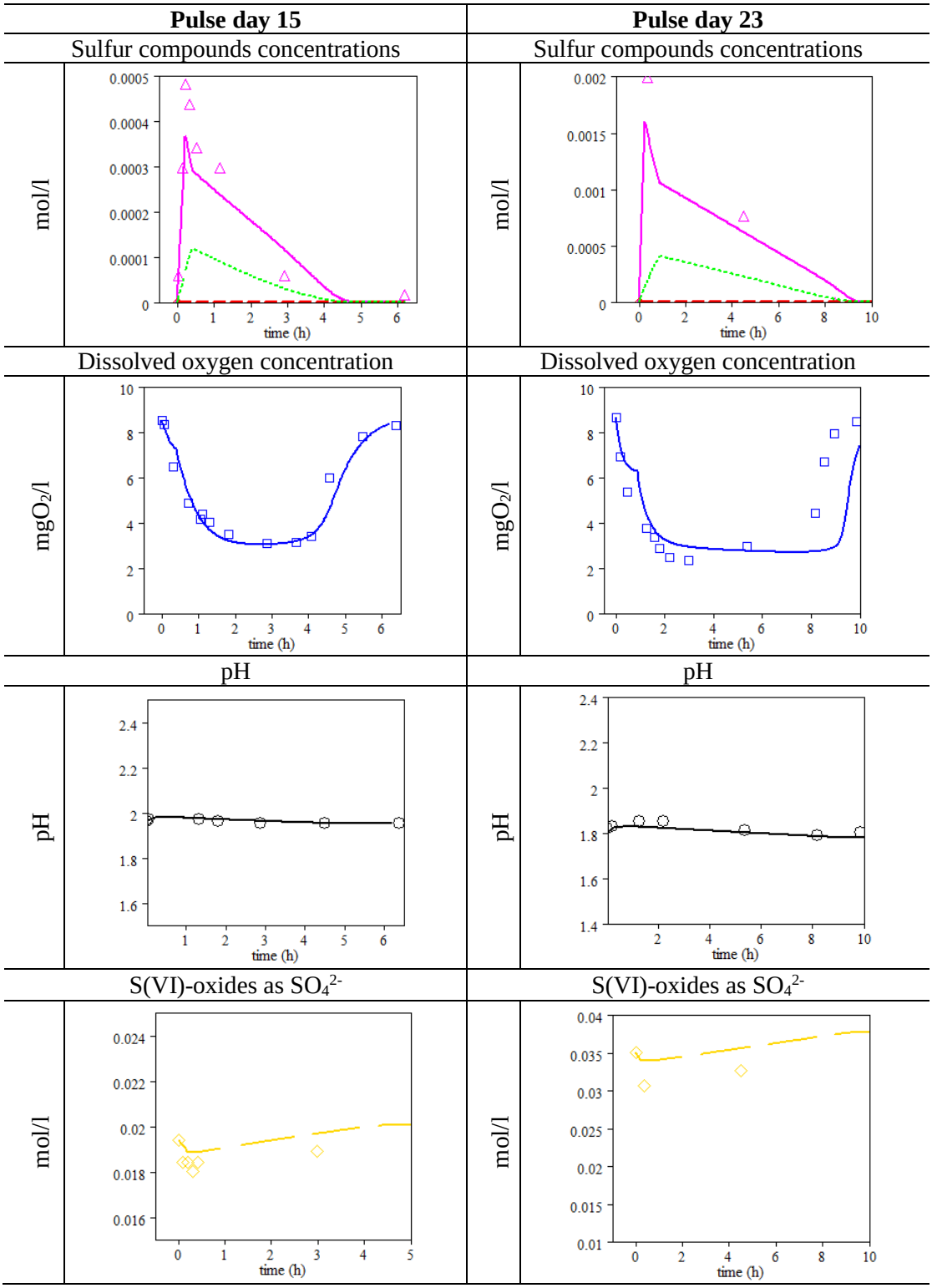

Figure 76: coupled chemical and biological processes experimental and numerical data for two thiosulfate pulses (pulse day 15 and pulse days 23).
Experimental data: △ : thiosulfate concentration (mol/l); □: dissolved oxygen concentration (mgO_2/l); ○: pH; ◇ : concentration of S(VI)-oxides produced.
Simulated data: —: thiosulfate concentration (mol/l); ····: tetrathionate concentration (mol/l); – –: loss of sulfur compounds by elemental sulfur precipitation (eqmolS/l); —: oxygen concentration (mgO_2/l); —: pH; – –: concentration of S(VI)-oxides produced.

The simulated results showed that the model describes dynamically the pH without other data for the system definition than the initial conditions. The simulated data compared to experimental for thiosulfate concentration, shows a deviation, especially during the thiosulfate supply (15 minutes for supply duration). This phenomenon could be explained by the biological metabolism which needs some lag time to reach its maximum enzymatic potential and thus its maximum rate to oxidize the sulfur compounds in the experimental conditions. This biological phenomenon, not represented in the numerical model, can explain also, the lag time between the simulation results and the experimental results concerning the specific phenomenon of deceleration-acceleration observed for the oxygen profiles (figure 76). In other hand, the use of microbial parameters determined without chemical competition, could also explain these difference between simulated data and experimental data.

However, the coupling of biological reactions with chemical reactions confirms the weak participation of the thiosulfate disproportionate reaction in the thiosulfate conversion, in some controlled supply conditions, even with a medium at acid pH (range from pH = 2 to pH = 1.45).

The model enables the description of the biomass, thiosulfate and tetrathionate conversion, the biotic and the abiotic production of S(VI)-oxidizes, the abiotic elemental sulfur and S(IV)-oxidizes production, the oxygen consumption, the carbon dioxide absorption and biological consumption, and the pH.

4. Conclusions

The results presented here from a **sequenced-batch culture confirmed the interest of thiosulfate as a substrate for biogenic acid production and selection of acidophil sulfur-oxidizing activity from an activated sludge consortium because**, (i) numerous SOB are able to grow under thiosulfate environment, (ii) thiosulfate is a stable substrate in controlled concentration conditions, even in acid environment, and does not limit the intensification of the biological activity, (iii) **the biological sulfur-oxidizing activity is in the same order than pure cultures in terms of specific growth rate** (max = 0.020 h^{-1}; observed = 0.006 h^{-1}) and biomass yields $Y_{X_{SOB}/S_2O_3^{2-}}$ = 0.029 mol$C_5H_7O_2N$/mol$S_2O_3^{2-}$.

By the confrontation of experimental data with the development of a dynamical model, the thiosulfate conversion was described by the combination of chemical and mainly biological reactions. **The formation of tetrathionate as an important biological intermediate was identified** and confirmed the literature data for some special way for the biological oxidation of thiosulfate. In this culture conditions, the biological oxidation of thiosulfate could be described in two steps, the biological oxidation of thiosulfate into tetrathionate and the biological oxidation of tetrathionate into sulfate, which is the acidification step. The model definition enabled the estimation of the proper microbial parameters to define the two biological steps.

The development of a complex biological and chemical dynamical model ensures, the definition of a part of a control pilot for biodeterioration of cementitious materials. With thiosulfate as sulfur source, it ensures the control of the global transformations involved in the acidification and in the sulfate production.

The selection of acidophil SOB from activated-sludge, using thiosulfate as selection factor, was demonstrated, even if for validation numerous experiences with activated-sludge consortium from different origin need to be realized. The possible formation of tetrathionate was highlighted and quantified. In this context, in the next chapter two cementitious materials will be inoculated by the same activated-sludge consortium used in this chapter (AS 2). A thiosulfate selection will be applied to evaluate: (i) the system biological activity/cementitious lining as representativ system for MICC simulation (ii) the selection of sulfur-oxidizing activities and the thiosulfate conversion and (iii) the design of the pilot to discriminate between two cementitious linings in terms of resistance to biogenic acid attacks (and their influence versus time on the selected biological activity).

Chapter VII

Mortar linings degradation by biogenic acid produced in contact with the materials

1. Introduction

1.1. Context of the study

In the sewer network, strong deteriorations of the cementitious materials are primarily related to the production in stagnant zones, volatilization and condensation on the top of pipe-walls of hydrogen sulfur (H_2S). Thereafter, in contact with cementitious materials, H_2S under moisture environment leads by chemical oxidations to different reduced sulfur compounds (elemental S^0, thiosulfate $S_2O_3^{2-}$ etc…) (Islander et al., 1991) (Okabe et al., 2007) (Herisson et al., 2012). Sulfur-oxidizing bacteria (SOB) are able to grow on oxidation of these reduced sulfur compounds, leading to acidification of the local liquid in contact with the cementitious material and to local production of sulfate (SO_4^{2-}) as an end product (Islander et al., 1991) (Okabe et al., 2007) (Herisson et al., 2012) (Alexander and Fourie 2011).

The biodeterioration of the cementitious materials in the sewer networks is considered as a surface processes, where decalcification occurred due to the high solubility of calcium oxides in acid environment ($K_{s\ Ca(OH)2} = 10^{-5.2}$ (Minteq database)). The decalcification phenomenon could be described by the equations (Eq 28 and Eq 84), where the equation (Eq 84) presents the biological thiosulfate conversion and the associated acid and sulfate production. The equation (Eq 28) defines the solubility equilibrium of the Portlandite ($Ca(OH)_2$). The decalcification phenomenon in surface of the materials was linked in the depths to the migration of the sulfates produced by the microorganisms (Roberts et al., 2002) (Herisson et al., 2012). During this migration secondary expansive precipitation occurred, in a first step caused by the formation of gypsum ($CaSO_4.2H_2O$) coming from the reaction of the biogenic sulfuric acid (Eq 83) with the Portlandite and/or the Silicate-Calcium oxides of the cement paste (Eq 27, Eq 30 and Eq 31). In a second step, if alumina compounds are presents in the material, by the reaction of the gypsum and the alumina compounds forming ettringite ($CaO.Al_2O_3.3CaSO_4,32H_2O$) (Eq 32) (Monteny et al., 2000).

Inside the porous media the precipitation of expansive compounds as gypsum (always discussed (Tian and Cohen, 2000)) and in a more important way ettringite leads to local swelling of the cementitious material causing cracks, then increasing the local porosity, and then after accelerating the penetration of the aggressive agents (Ehrich et al., 1999) (Monteny et al., 2000) (Roberts et al., 2002).

In the case of an ettringite formation, the increase of the porosity intensifies the acid penetration and then the deteriorated front displaced in the depth of the cementitious matrix changing the local conditions (as pH), leading to the decomposition of the secondary ettringite crystal, forming gypsum ($CaSO_4.2H_2O$) and alumina gel ($Al_2O_3.3H_2O$) as described by the equation (Eq 90) (Lamberet, 2005).

Eq 90: $3\ CaO.Al_2O_3.3\ CaSO_4.32\ H_2O \rightarrow 3Ca^{2+} + Al_2O_3.3H_2O + 3\ (CaSO_4.2H_2O) + 26\ H_2O$

1.2. Objective

In this chapter two different cementitious materials centrifugated on the inner surface of ductile cast-iron pipes (produced by the industrial centrifugation process of Saint-Gobain PAM) had been exposed to biogenic acid (produced by microbial community selected under thiosulfate environment). The objectives were to (i) evaluate the activities of SOB attached to the lining surface, (ii) look at the degradation of the cementitious matrix in the experimental conditions, (iii) highlight or/not the impact of the material on the biological colonization and the biological activity, (iv) discuss the representativity of the reactions and transformations observed in the experimental conditions with respect to the transformations occurring in real sewers.

1.3. Materials and methods: short description

The pilot defined in the M&M for the chapter IV was used with an increase of the thiosulfate inlet-fluxes. The table 34 presents in sulfur atom equivalent the evolution of the sulfur compounds concentration in the feeding solutions, for the different time period of the experiment. For each increase of the sulfur concentration in the feeding solution, the other nutrients were increased in proportion as describes in M&M. It was inoculated by activated-sludge consortium (AS 2) from a waste-water treatment plant (Muret near the city of Toulouse).

Table 34: equivalent sulfur concentration in the feeding solution (thiosulfate and tetrathionate) per period for the cementitious materials tested in the chapter VII.

Day 0 to day 22	**Day 22 to day 37**	**Day 37 to day 51**	**Day 51 to day 58**	**Day 58 to day 80**	**Day 80 to day 104***	**Day 104 to day 107**
$S_2O_3^{2-}$	$S_2O_3^{2-}$	$S_2O_3^{2-}$	$S_2O_3^{2-}$	$S_2O_3^{2-}$	$S_2O_3^{2-}$	$S_4O_6^{2-}$
1.08×10^{-3} molS/l in	1.62×10^{-3} molS/l in	2.67×10^{-3} molS/l in	3.21×10^{-3} molS/l in	4.22×10^{-3} molS/l in	6.32×10^{-3} molS/l in	6.12×10^{-3} molS/l in

*: end of the thiosulfate feeding, sample in different zone for the microbial population analyzes

The figure 77 illustrates, from the schema of the whole system of the microbial induced concrete corrosion, the part of the system treated in this chapter. The reduced sulfur source was thiosulfate fed by trickling the solution at the surface of a segment of real sewer-pipes.

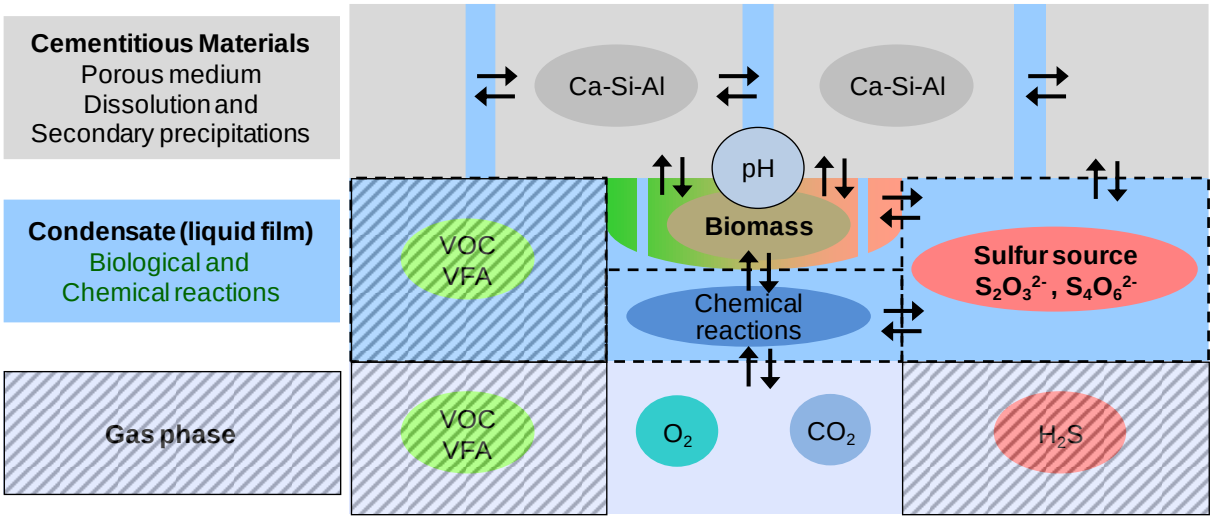

Figure 77: Part of the whole system studied in the chapter VII, based on the figure 17 defined at the chapter I.

The behaviors of the two materials were analyzed against time by evaluating in the leaching solution the products of thiosulfate transformation, the lixiviated calcium and the alumina. At the end of the experiment, the characterization of spatial chemical and the microstructure of both materials were performed, compared with their corresponding initial specimen (by SEM observations, EPAM profiles and DRX analyses).

2. Results

2.1. Visual observations of the biofilms

The figure 78 shows some photos of both inoculated pipes (BFSC and CAC lining) during the experiments, and the theoretical spatial zonation. The photos for the day 0 showed the result of inoculation of the activated-sludge before the starting of the feeding. During the experiments, for both cementitious materials, the non-adapted biomass was washed out from the system (visually loss of biomass covering from day 0 to day 44 for both cementitious materials). From day 44 to day 104, for BFSC lining, the biofilm was heterogeneous, but visually spread on the whole surface, compared with the CAC lining, where the biofilm was regularly washed out (around 1/3 of the surface was highly colonized at the day 104, whereas the surface showed a very thin biofilm).

Exposed to the same thiosulfate fluxes, with an identical feeding and the same inoculum, the feature of the developed biofilm appears qualitatively very different.

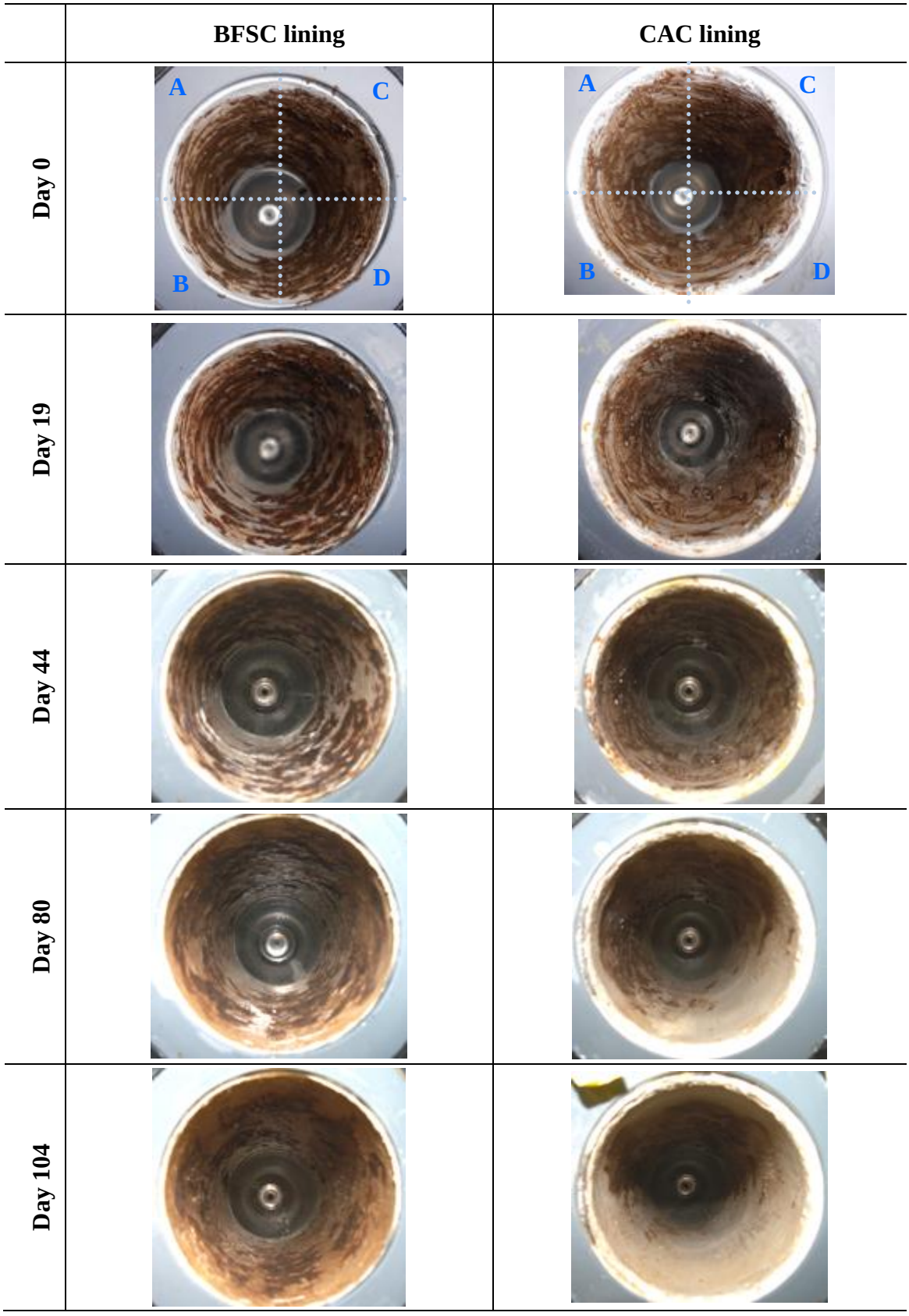

Figure 78: Photos of the biofilms evolutions in contact with BFSC and CAC linings during thiosulfate feeding and the definition of the zones used for the further local analyses.

To complete the visual observations presented in the figure 78, the figure 79 shows global photos for both pipes at the last day (day 107), and some zoom on particular zones. The differences between both materials in terms of biofilm development was highlighted (figure 79.a and figure 79.b). The heterogeneous structures of the biofilms were observed on both materials. On the BFSC lining, the biofilm colonized the whole surface, but with structure of different density (figure 79.a). On the CAC lining, the biofilm seemed to be concentrated, mainly in one zone (figure 79.b).

Mineral precipitates were observed, especially for the BFSC lining. It looked like white filaments perpendicular to the surface (see the figure 79.c). White deposits on the surface of the dense zone of the biofilm (see the figure 79.d) were also observed. As the zoomed zones showed for the CAC lining (figure 79.e) is characteristic of the structure of the developped biofilm. It can be concluded that no particular mineral precipitates were visualized on the CAC lining.

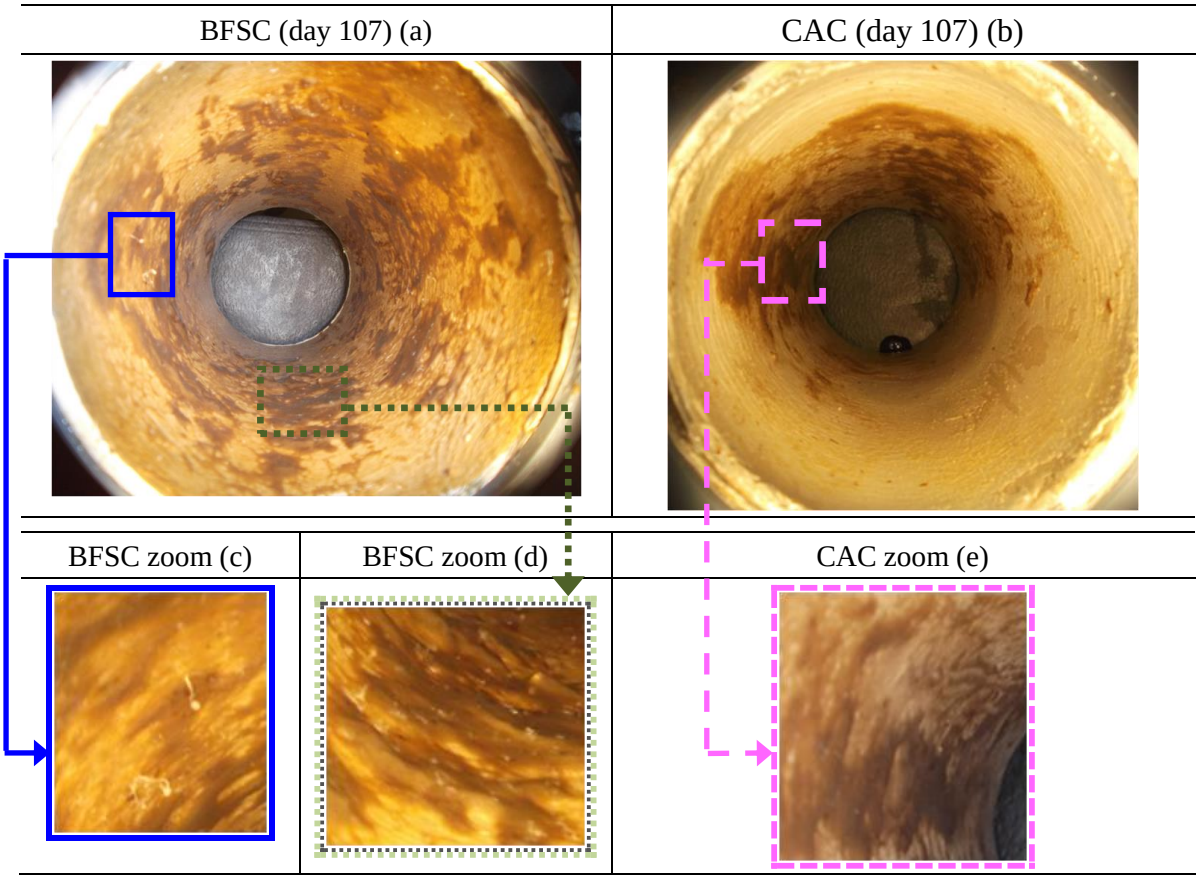

Figure 79: Photos of the biofilms in contact with BFSC and CAC linings at day 107, and particular observations.

At the end of the experiment, the surfaces of both cementitious materials were washed with deionised water from wash bottle to avoid abrasive constraints, and conserve the surface material in contact with the biofilm. On the CAC linings, the biofilm appeared to be drier than on the BFSC lining, with a stronger attachment to the material. This fact could indicate particular behaviour of the microbial communities on CAC lining compared to BFSC lining.

The visual observation presented in this paragraph highlighted a different biological fate in terms of colonization and structure of the biofilm. To go deeper in the understanding of the processes involved in the whole transformation for both cementitious materials the fate of thiosulfate is presented in the next paragraph.

2.2. Thiosulfate transformation and sulfur-oxidizing activity

2.2.1. CAC lining: thiosulfate conversion

The figure 80 presents, for CAC lining, the pH and sulfur compounds (thiosulfate and S(VI)-oxides versus time) in the leaching solution. The continuous line showed the gradual increase of the thiosulfate concentration in the feeding solution, in percentage of the initial concentration applied (that was 1.08 x 10^{-3} molS-$S_2O_3^{2-}$/l). Thiosulfate (full area corresponding to thiosulfate at the outlet of the system) were consumed and led to a corresponding S(VI)-oxides production (dotted line) and to the acidification of the leaching solution. At day 17 the pH of the leaching solution reached a value around 4.35 (black points).It then continuously decreased to reach the value of 3.15 day 104. Mass balance on S compounds (dashed line) showed that after 10 days of operation a loss of S is occurring. As described in the previous section, two hypotheses can be proposed to explain this lack of S, (i) the total conversion of the consumed thiosulfate to sulfate with a penetration and secondary precipitation of a part of sulfate into the cementitious matrix, (ii) the formation of biological sulfur intermediate, that are not quantified yet, as observed for the biological selection studied in the chapter VI. These hypotheses will be discussed latter. However, in the case where the sulfur conversion would not be complete, S(VI)-oxides production and decrease of pH of the leaching solution are significant and indicated the selection of a SOB activity on CAC lining.

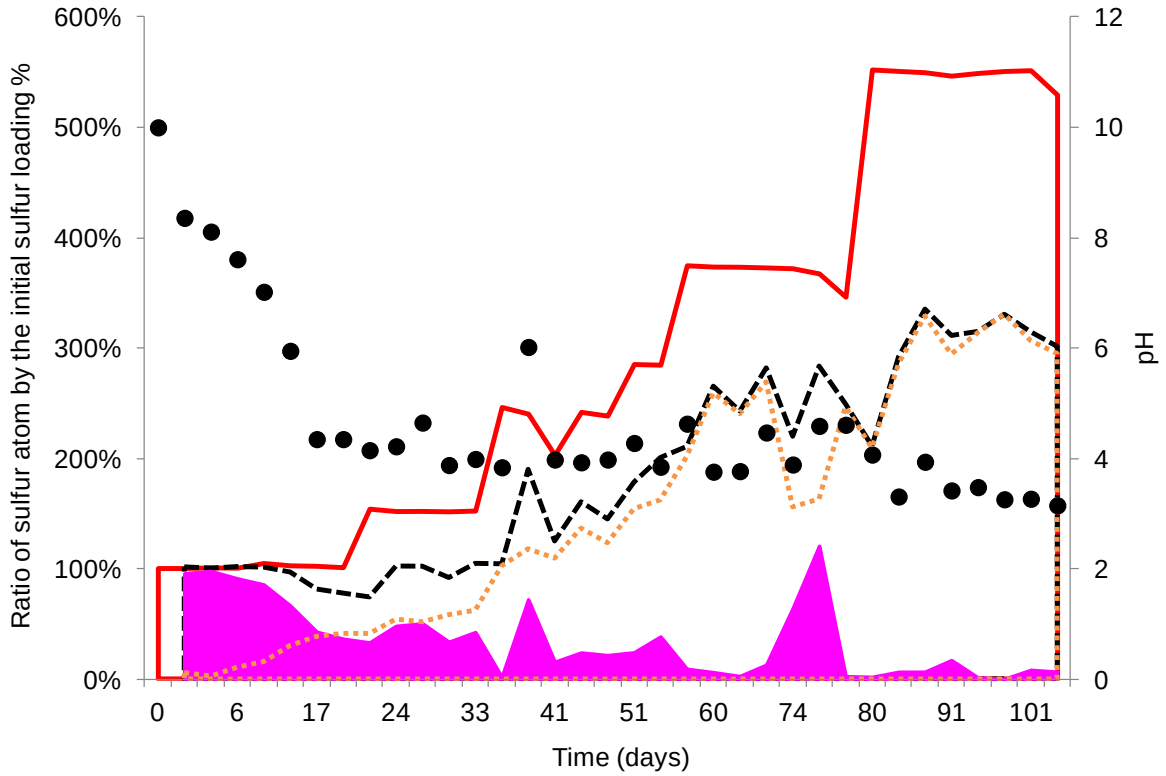

Figure 80: Analyses of the leaching solution for the CAC lining, pH and thiosulfate conversion. ●: pH of the leaching solution; ——: % sulfur atom as thiosulfate in the feeding solution compared to the composition of the initial feeding solution; .....: % sulfur atom as S(VI)-oxides in the leaching solution; ▬: % sulfur atom as thiosulfate in the leaching solution; – – –: sum of % sulfur atom measured in the leaching solution.

2.2.2. BFSC lining: thiosulfate conversion

The figure 81 presents, for inoculated BFSC lining, the pH and sulfur compounds (thiosulfate and S(VI)-oxides versus time) in the leaching solution. As for the CAC lining, a thiosulfate consumption was recorded with a production of S(VI)-oxides linked to an acidification of the medium during the first 60 days. In 17 days the leaching solution reached a pH value of 4.37. Following pH slowly decreased to reach 3.84 at day 37. Then pH was quiet instable, with alternance of basification phase and acidification phase indicating a different behavior of the system cementitious material and microbial community for BFSC lining compared to CAC lining.

As for CAC lining the sulfur mass balance did not close from day 22. However after day 60, an important quantity of thiosulfate was not consumed. This observation may be linked to the instability of the pH. The SOB activity was disturbed by environmental conditions. At the same time, after day 60, for high loading of thiosulfate, the concentration of S(VI)-oxides stabilized in the leaching solution, with a higher deviation of the sulfur mass

balance. Thus, the same two hypotheses proposed to explain the observations for the CAC lining can be renewed.

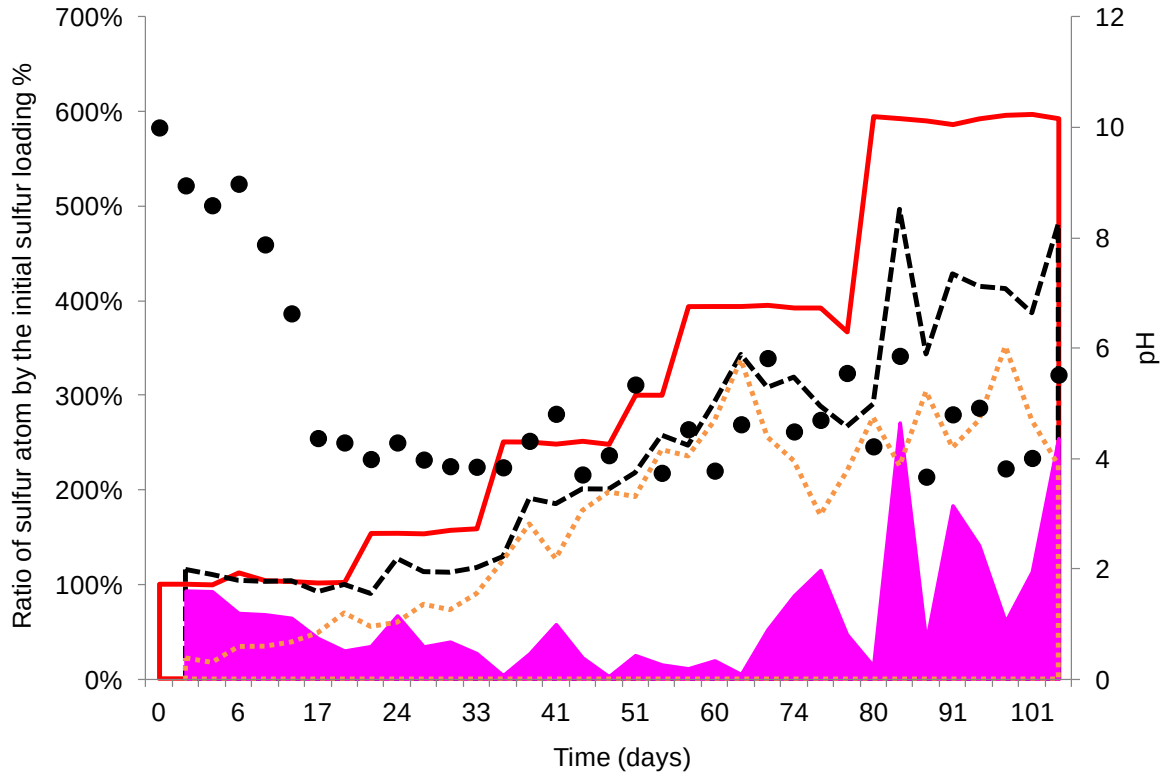

Figure 81: Analyses of the leaching solution for the BFSC lining, pH and thiosulfate conversion. ●: pH of the leaching solution; ——: % sulfur atom as thiosulfate in the feeding solution compared to the composition of the initial feeding solution; .....: % sulfur atom as S(VI)-oxides in the leaching solution; ▬ : % sulfur atom as thiosulfate in the leaching solution; – – : sum of % sulfur atom measured in the leaching solution.

2.2.3. Analyses of the fate of sulfur

2.2.3.1 Soluble COD analyses

To evaluate the fate of the sulfur compounds during the transformations, soluble COD measurements were realized (as in M&M and in chapter VI). For 12 samples, soluble COD mass balances were performed as described in the figure 82. These soluble COD mass balances enbled evaluating if soluble oxidizable S compounds are still present in the leaching solution at the outlet of the segment pipes, or if the loss of sulfur compounds must be attribuated to an immobilization of sulfur compounds at the surface or inside the cementitious matrix.

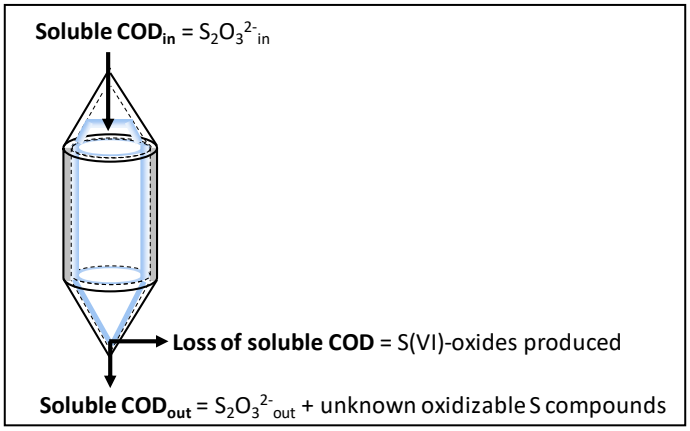

Figure 82: schema for the COD mass balances calculation during the SOB selection on cementitious linings.

The figure 83 presents the results obtained for 12 soluble COD mass balances operated during the experiment on the inoculated CAC lining. The full line shows the conversion in COD of the inlet thiosulfate concentration; the dark area shows the equivalent COD of thiosulfate at the outlet of the segment-pipe; the clear area shows the soluble COD measurement in the leaching solution at the outlet of the segment-pipe; and the dashed line shows soluble COD mass balances including the loss of oxidizable sulfur compounds by the biological production of S(VI)-oxides.

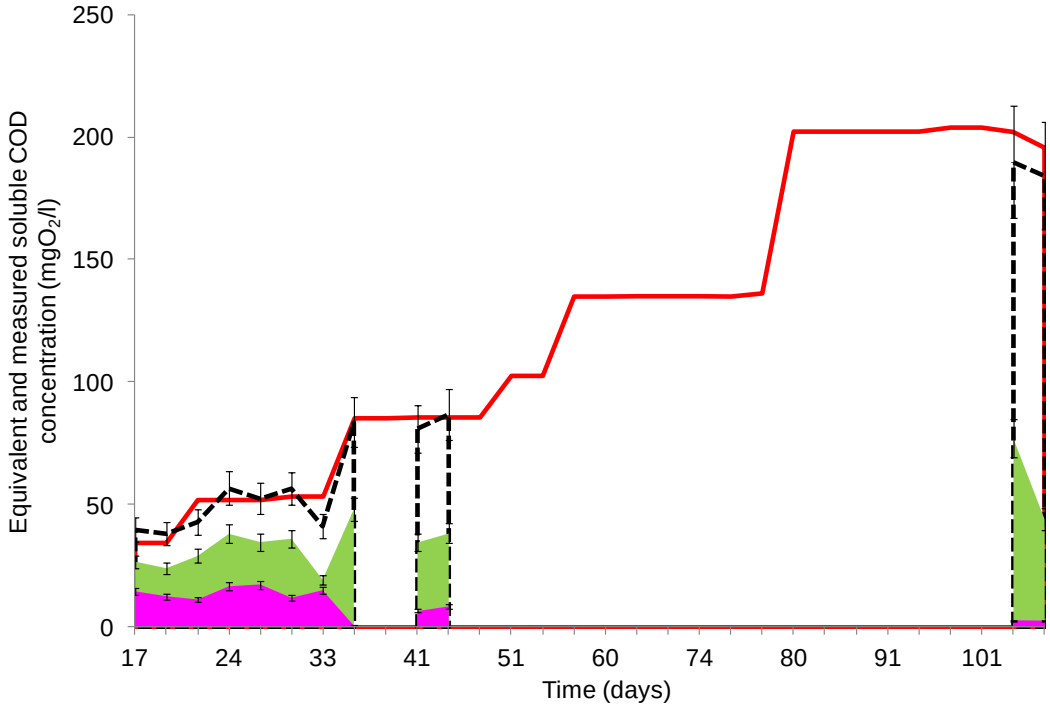

Figure 83: soluble COD mass balance (mgO_2/l) for the inoculated CAC lining. ——: COD equivalent for thiosulfate concentration in the feeding solution; ▬ : soluble COD measurement in the leaching solution (mgO_2/l); ▬ : COD equivalent for thiosulfate concentration in the leaching solution. – – : COD equivalent (sum of measured COD concentration and equivalent sulfur(VI) oxides in the leaching solution).

The figure 84 presents the results obtained for BFSC lining. The figure 83 and the figure 84 show, for all the samples tested, that COD mass balances, considering the loss of soluble COD by biological production of S(VI)-oxides, closed very well for both cementitious materials. Thus, if secondary precipitation occurred inside the materials, compared to the quantity of sulfur provide as thiosulfate, the majority of converted sulfur remained in soluble form. The lack of sulfur that was not quantified previously, i.e. due in majority to the production of soluble sulfur intermediates which remains in the leaching solution. The figure 83 and figure 84 confirmed this proposition by the comparison of the direct soluble COD measurement (clear area) and the COD equivalent of the thiosulfate measured in the leaching solution (dark area). The direct soluble COD concentrations were always superior of the thiosulfate equivalent (for both cementitious materials) indicating production of intermediate oxidizable compounds.

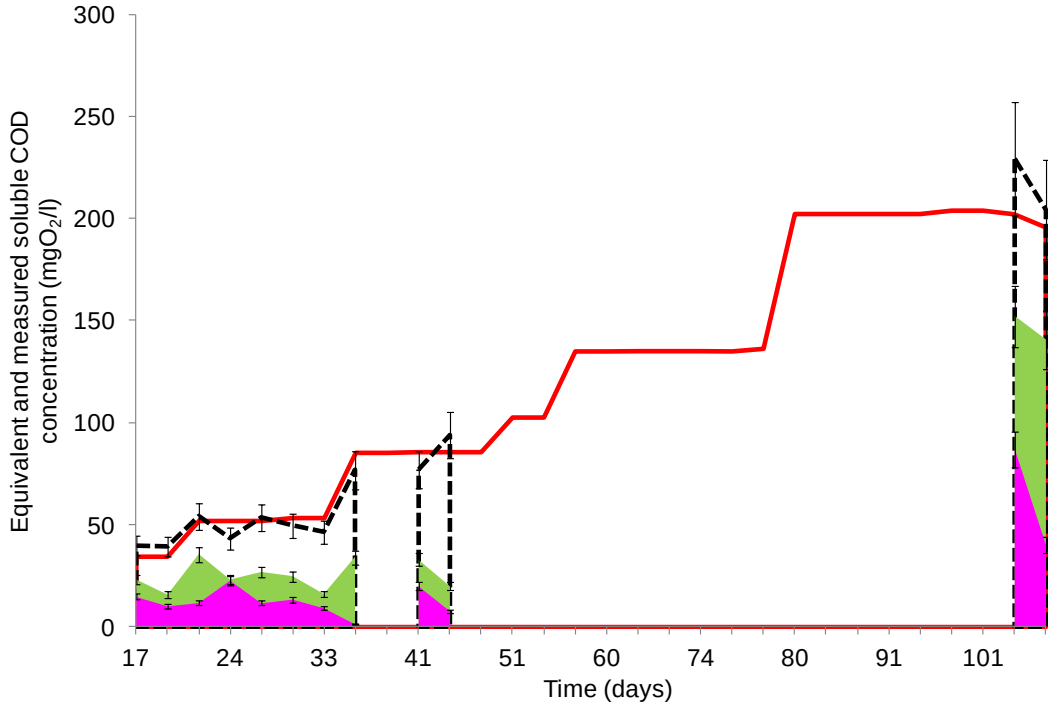

Figure 84: soluble COD mass balance (mgO_2/l) for the inoculated BFSC lining. ——: COD equivalent for thiosulfate concentration in the feeding solution; ▬ : soluble COD measurement in the leaching solution (mgO_2/l); ▬ : COD equivalent for thiosulfate concentration in the leaching solution. – – : COD equivalent (sum of measured COD concentration and equivalent S(VI)-oxides in the leaching solution).

2.2.3.2. Evaluation of biological sulfur intermediate

As demonstrated in the previous paragraph, for both linings, soluble sulfur intermediate production can explain the lack of sulfur to close the sulfur mass balances (figure 80 and

figure 81). In that case, using theoretical sulfur compounds, the soluble COD measurement enables the estimation of the equivalent sulfur compounds. To evaluate the best sulfur compound, considering only one sulfur compound as the major intermediate, four compounds were theoretically tested: tetrathionate ($S_4O_6^{2-}$), trithionate ($S_3O_6^{2-}$), dithionate ($S_2O_6^{2-}$) and pentathionate ($S_5O_6^{2-}$) (Islander et al., 1991).

The table 35 presents for both linings, the theoretical sulfur mass balances considering all the sulfur intermediate, based on the soluble COD measurements and the COD equivalent of the sulfur compounds presented in the M&M.

Table 35: sulfur mass balances with different theoretical intermediate sulfur compounds by the conversion of soluble COD measurement and the thiosulfate concentration in the leaching solution.

Day	**Sulfur substrates**	**CAC lining**				**BFSC lining**			
		$S_4O_6^{2-}$	**$S_3O_6^{2-}$**	**$S_2O_6^{2-}$**	**$S_5O_6^{2-}$**	**$S_4O_6^{2-}$**	**$S_3O_6^{2-}$**	**$S_2O_6^{2-}$**	**$S_5O_6^{2-}$**
17		120 %	133 %	226 %	115 %	118 %	127 %	188 %	115 %
20		115 %	128 %	211 %	110 %	116 %	122 %	163 %	114 %
22		88 %	100 %	186 %	83 %	111 %	127 %	241 %	104 %
24		115 %	130 %	233 %	109 %	83 %	84 %	85 %	83 %
30		106 %	118 %	201 %	101%	107 %	117 %	190 %	103 %
33	$S_2O_3^{2-}$	112 %	129 %	241 %	106 %	96 %	103 %	156 %	93 %
37		78 %	81 %	102 %	77 %	89 %	93 %	125 %	87 %
40		106 %	126 %	264 %	98 %	95 %	109 %	205 %	90 %
42		99 %	111 %	193 %	95 %	92 %	97 %	136 %	90 %
44		106 %	119 %	206 %	101%	114 %	124 %	198 %	109 %
104		99 %	112 %	204 %	94 %	118 %	130 %	210 %	113 %
107	$S_4O_6^{2-}$	97 %				112 %			
Mean values		**103 %**	116 %	204 %	**98 %**	**100 %**	106 %	167 %	**97 %**
Ecart type		± 12 %	± 15 %	± 42 %	± 11 %	± 12 %	± 16 %	± 49 %	± 11 %

For both cementitious materials, two sulfur compounds (tetrathionate and pentathionate) enabled obtaining a good agreement with soluble COD measurements and theoretical closure of the sulfur mass balances. Thus, one or the other compound could be used as theorectical compound to describe the global fate of the thiosulfate biological conversion.

Because, in the chapter VI of this document tetrathionate was identified as major intermediate in the biological thiosulfate oxidation, to evaluate the possibility of identical

global conversion of thiosulfate even in contact with cementitious material, the last feeding solution was prepared with tetrathionate as unique sulfur source as presented in the table 35. In the figure 83 for CAC lining and in the figure 84 for BFSC lining, the last point corresponds of results obtained with tetrathionate. For both materials, with tetrathionate as sole sulfur source, tetrathionate were consumed as soluble COD, linked to the pH decreases and the increase of produced S(VI)-oxides in the leaching solution.

2.2.4. Sulfur-oxidizing activity comparison for both cementitious materials

As just seen sulfur mass balances could be achieved only considering soluble sulfur compounds (thus sulfate quantity possibly trapped in the materials could be considered as negligible in term of fate of sulfur, but not necessarily negligible to analyse the behaviour of the materials, see further for the materials analyses). The global SOB activity can be evaluated from the consumption of the thiosulfate, and the acidification capacity from the S(VI)-oxides produced.

The figure 85 presents the thiosulfate conversion for both linings and for an abiotic CAC lining as a reference (see results from chapter IV) (figure 85.a). The total S(VI)-oxides measured in the leaching solution during the experiments are also given (figure 85.b). Firstly the comparison between biotic and abiotic results confirmed the predominance of biological transformations in the thiosulfate conversion (figure 85.a). Secondly, during the first 60 days of the experiments, the thiosulfate conversion appeared similar for both materials, with a quasi complete conversion. However, at the same time the total S(VI)-oxides measured in the leaching solution was 10-30% higher on the BFSC lining than on CAC lining (figure 85.b), indicating an higher acidification potential for the microbial community on BFSC lining during the first times of the transformations. After 80 days, for the last increase of the thiosulfate loading, the thiosulfate conversion was complete on the CAC lining, whereas environmental conditions (pH instability) on BFSC limited the thiosulfate conversion, as presented in the figure 81. At the same time the total S(VI)-oxides measured in the leaching solution reached the same order of magnitude for both material indicating an equivalent acidification after 104 days of experiments, but with a different behaviour during time for both material.

Discussion on the representativity of the amount of reduced sulfur transformed and of the acid produced will be discussed at the end of this chapter.

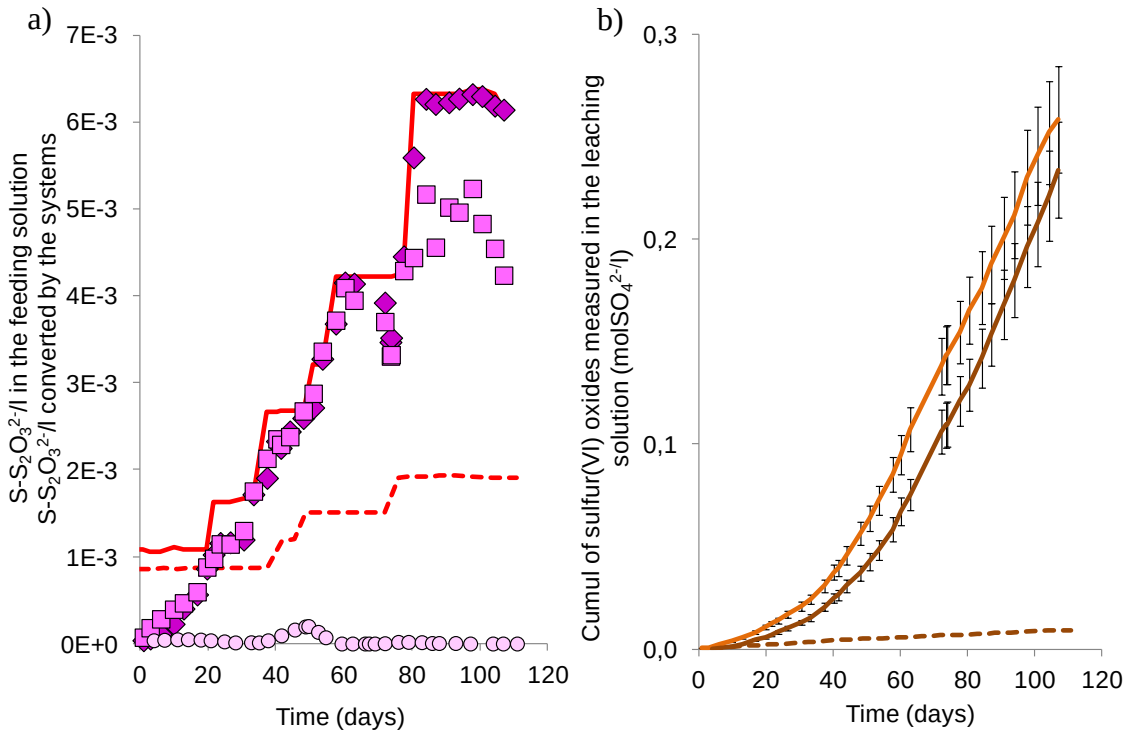

Figure 85: (a) concentration of converted thiosulfate compared to thiosulfate in the feeding solution for inoculated CAC lining, inoculated BFSC lining and abiotic CAC lining (results from the chapter IV of this document). ——: concentration thiosulfate in the feeding solution for the biotic experiments (molS-$S_2O_3^{2-}$/l); – – : concentration of sulfur atom as thiosulfate in the feeding solution for the abiotic experiment on CAC (molS-$S_2O_3^{2-}$/l); □ : thiosulfate concentration converted by biotic BFSC lining (molS-$S_2O_3^{2-}$/l); ◆: thiosulfate concentration converted by biotic CAC lining (molS-$S_2O_3^{2-}$/l); ○: thiosulfate concentration converted by abiotic CAC lining (molS-$S_2O_3^{2-}$/l) (results from the chapter IV of this document). (b) total S(VI)-oxides in the leaching solution for inoculated CAC lining, inoculated BFSC lining and abiotic CAC lining (results from the chapter IV of this document). —— : total S(VI)-oxides in the leaching solution on biotic BFSC lining (molSO_4^{2-}); —— : total S(VI)-oxides in the leaching solution on biotic CAC lining (molSO_4^{2-}); – – : total S(VI)-oxides in the leaching solution on abiotic CAC lining (molSO_4^{2-}).

2.3. Calcium and alumina lixiviation

The figure 86 presents the pH of the leaching solution, the calcium and the alumina concentration in the leaching solution for both cementitious materials.

Firstly, as expected from the pH measurement, the calcium concentrations in the leaching solutions confirmed the lixiviation from both cementitious materials.

Secondly, considering only the CAC lining (figure 86.a), even if the calcium and the alumina in the initial matrix are in the same proportion, *i.e.* 37.86 % in calcium oxides and 43.76 % in alumina oxides (see table 12 in the M&M), the behaviours of this both elements,

during the lixiviation were completely different. The lixiviation of the calcium was immediate (in a low proportion), and could be correlated to the thiosulfate inlet fluxes and the S(VI)-oxides produced in the leaching solution (which correspond to the biological potential of acidification). On contrary, the alumina concentration in the leaching solution was around zero during 90 days of the experiment, and from day 98 to day 104 the concentration in the leaching solution was around 1.3×10^{-4} molAl/l compared to 1.1×10^{-3} molCa/l for the calcium.

From day 98 to day 104 the alumina concentration in the leaching solution corresponds to a mean value of 3.5 mgAl/l. Herisonn evaluated a biological impact of the dissolved alumina for some concentrations 100 folds higher (Herisson, 2012). Thus, in the experimental conditions, the difference for both materials in terms of biofilm structure and covering can not be attribuated to the dissolution of the aluminous compounds, even if local conditions and concentration can not be reached by the experimental device.

Inoculated CAC lining (a)

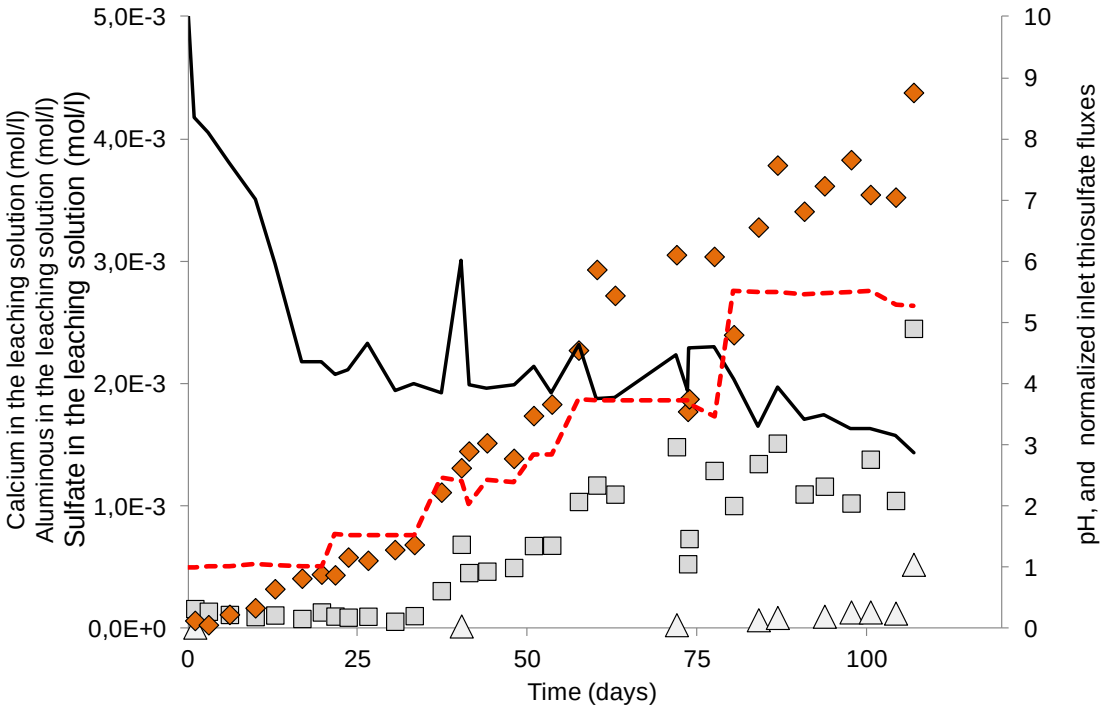

Inoculated BFSC lining (b)

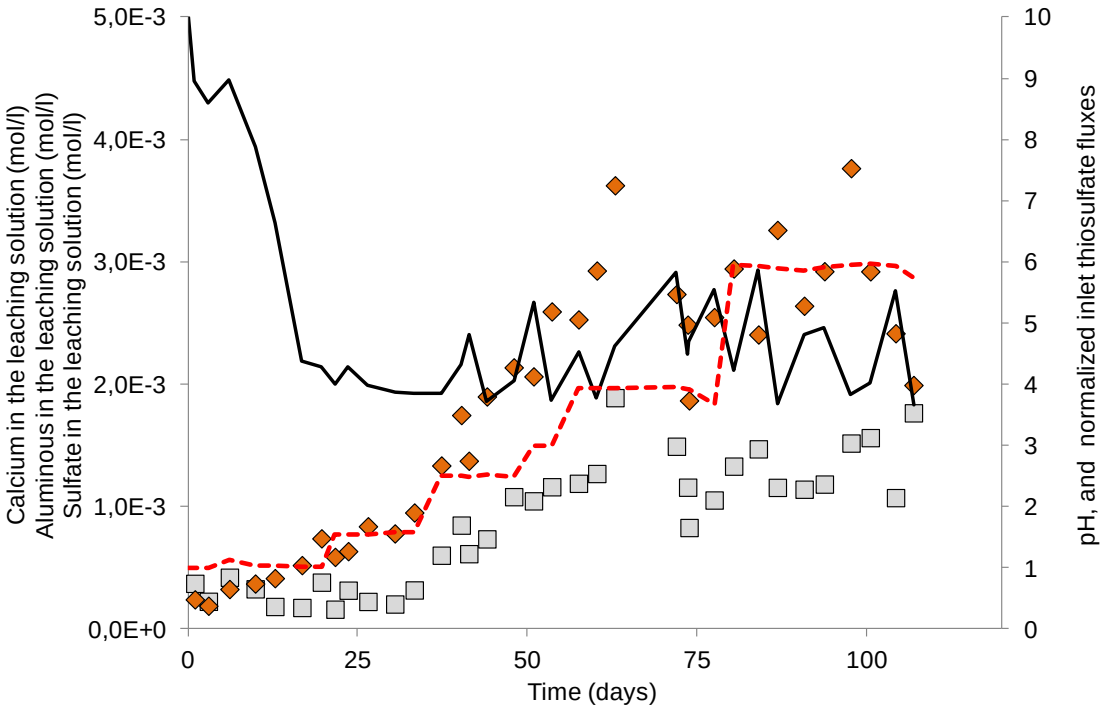

Figure 86: (a) for CAC lining, (b) for BFSC. ——— : pH of the leaching solution; ◆: sulfate concentration in the leaching solution (mol/l); ▢ : calcium concentration in the leaching solution (mol/l); △ : alumina concentration in the leaching solution (mol/l); – – : normalized thiosulfate inlet fluxes.

These first results confirmed the previously behaviour of the CAC paste in acid environment (above pH = 3) (Scrivener et al., 1999) (Herisson, 2012), with release of calcium but entrapment of alumina inside the cementitious matrix. From day 107, as described in the previous paragraph, tetrathionate was used as the sole sulfur source, the pH slightly decreased from 3.15 to 2.87, with a direct and significant increase of the calcium and the alumina concentrations in the leaching solution, confirming the pH dependency of the calcium and alumina lixiviation (Scrivener et al, 1999) (Alexander and Fourie, 2011).

For BFSC lining, the low alumina content in the initial matrix gives no quantifiable measurements of alumina in the leaching solution.

Concerning the calcium lixiviation, the lixiviaition rate followed the thiosulfate transformation for both materials (figure 86 (a and b)). To illustrate this similar behaviour of the calcium lixiviation for both lining, but highlighted quantitative and kinetic differences, the figure 87 presents the total calcium versus time in the leaching solution for both inoculated linings (BFSC and CAC) and for abiotic CAC as reference, with rate of lixiviation in mole of calcium per days for different time periods.

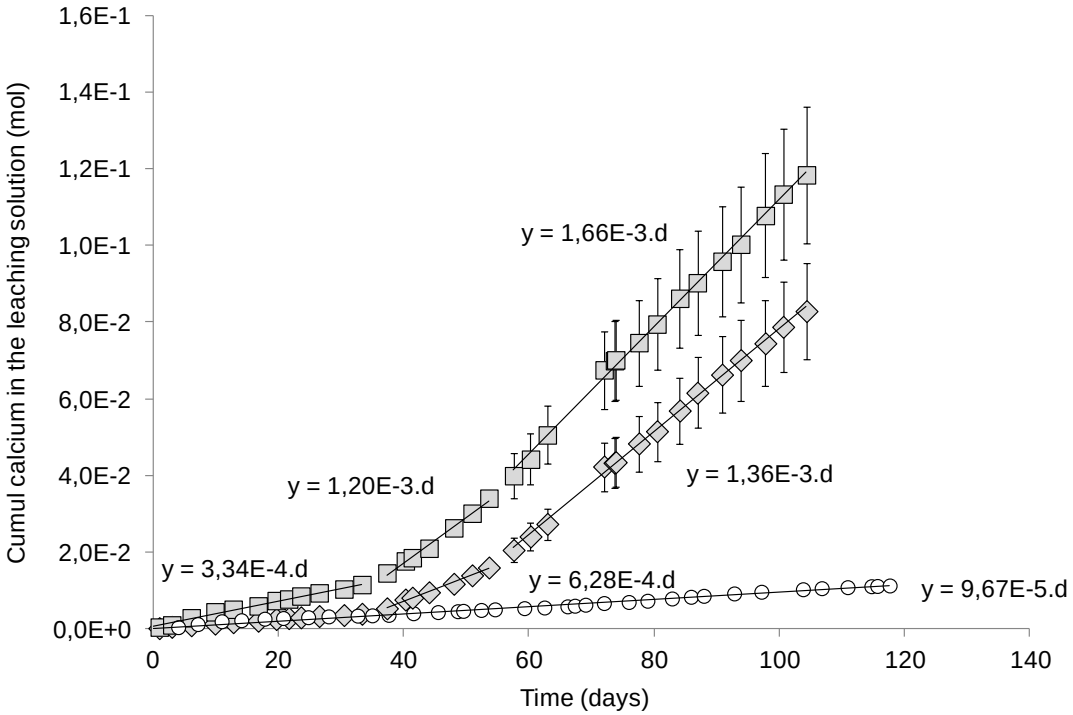

Figure 87: total calcium in the leaching solution during the experiments with inoculated CAC and BFSC lining, and with abiotic CAC lining. ◇: total calcium in the leaching solution for inoculated CAC lining (mol); □ : cumul of calcium in the leaching solution for inoculated BFSC lining (mol); ○ : total calcium in the leaching solution for abiotic CAC lining (mol).

During the first 33 days the calcium lixiviation rate for the inoculated BFSC lining was 3.5 folds higher than for the inoculated CAC lining (which is similar to the abiotic rate during the same time period) (figure 87), when the amount of calcium in the first 200 µm of cementitious matrix under the inoculated surface was quiet similar (M&M).

An important difference between BFSC lining and CAC lining was the fate of the pH of the leaching solution during the last period (from day 60 to day 104) with the linear calcium lixiviation. For BFSC lining the global pH was instable, with some values around 4 and the next measurement above 5.5. The thiosulfate conversion was impacted by this pH instability (as described in the figure 81 and in the figure 85.a), indicating as described in the literature a sensibility to the pH conditions of the sulfur-oxidizing bacteria, highlighting at minima the selection of slightly acidophilic bacteria for BFSC lining. However, the calcium lixiviation seemed to be not impacted by this pH instability revealing a clear difference of both materials against the same inoculum, feeding under the same environmental conditions. This particular evolution of the pH of the leaching solution was discussed further, after the analyses of microstructural and chemical fates of the exposed cementitious matrix.

2.4. Characterization of the cementitious materials exposed

To evaluate the behaviour of both materials under simulated microbial induced concrete corrosion, and understand interactions between microbial activity and material transformations, the two exposed materials were analyzed at the end of the experiments (107 days).

2.4.1. Global Cementitious lining inspections using SEM observations coupled with EDS zonal analyses

Because biomass development was heterogeneous, especially for CAC lining, different spatial zones were defined for the material analyzes. The figure 88 presents the schema defined in the figure 31 in the M&M for the spatial zones definition. Illustrations of this segmentation on photos of BFSC and CAC lining at the end of the experiments are also provided.

For BFSC lining the SEM analyzes were realized on the zone D (D1, D2, D3) and for the CAC lining on the zone C under evident dense biofilm (C1 and C2) and on the zone B where slightly colonisation was observed (B1).

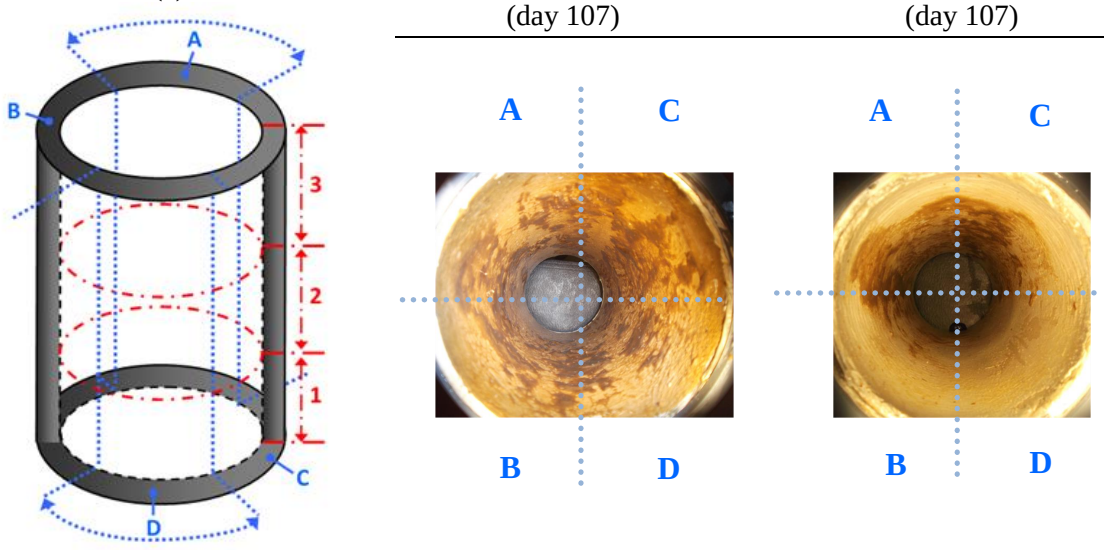

Figure 88: (a) spatial zones definition for segment pipes used during the experiments, and illustration on photos at the end of the experiments for BFSC lining (b) and CAC lining (c).

2.4.1.1. BFSC lining exposed: SEM characterizations (BSE mode)

The figure 89 presents for the vertical D1, D2 and D3 zone the SEM observations, with associated local EDS spectrum.

In the figure 89, the paste layer (a – dotted circles) match the inoculated surface. The SEM observations revealed the presence of micro-cracks in the whole exposed BFSC specimens, both in the paste and in the mortar layers. Some zonal EDS spectrum indicated sulfur accumulation at different depth of the material (D3 red zone and D1 blue zone). To illustrate the general cracking phenomenon, the figure 89 presents for the zone D2 a SEM observation of the zone (figure 90.a), some zoom on several cracking zones (figure 90.c.d.e) and after abrasion of the first 400 µm a wide observation of the cracking network create inside the matrix (figure 90.b). At 300 µm depth from the surface, a thicker crack, almost parallel to the surface is notably visible (figure 90.a.d.e).

BFSC lining exposed

	SEM photos (polish section, LV, BSE, x50)			Zonal EDS spectrum (dotted circle)	Zonal EDS spectrum (dashed and full line circles)
	Iron-cast	Mortar layer (c)	Paste + anhydrous (b)	Paste layer (a)		
BFSC D3	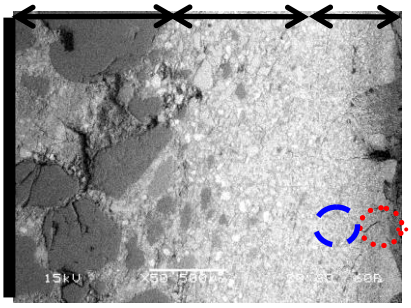 500 µm			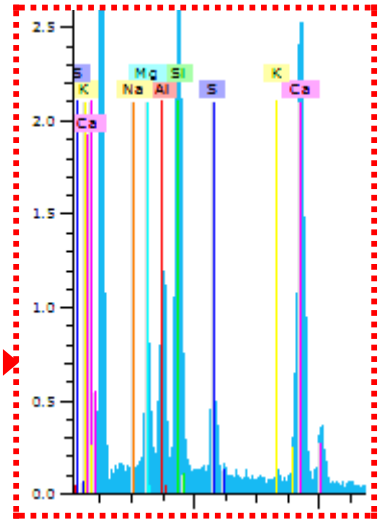	For dashed circle See figure 91
BFSC D2	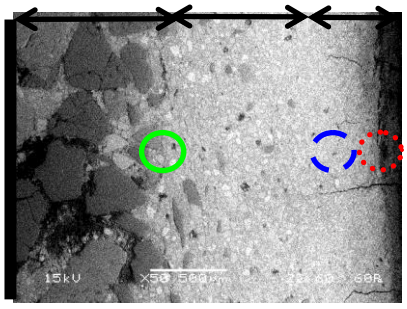 500 µm			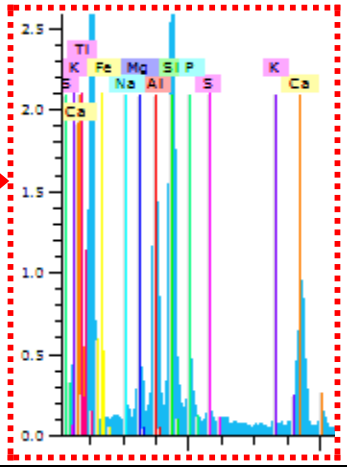	For dashed and full line circles See figure 91
BFSC D1	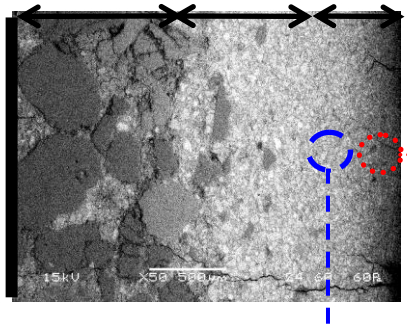 500 µm			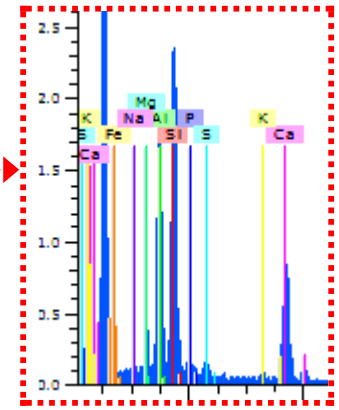	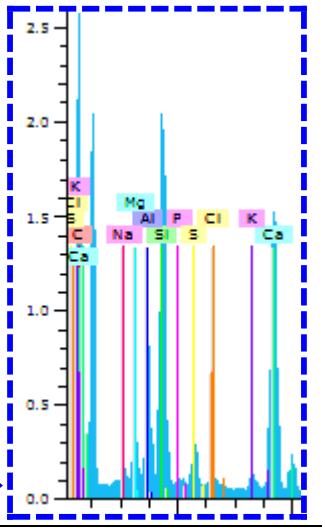

Figure 89: SEM global observations of zone D of BFSC lining, and local EDS analyses.

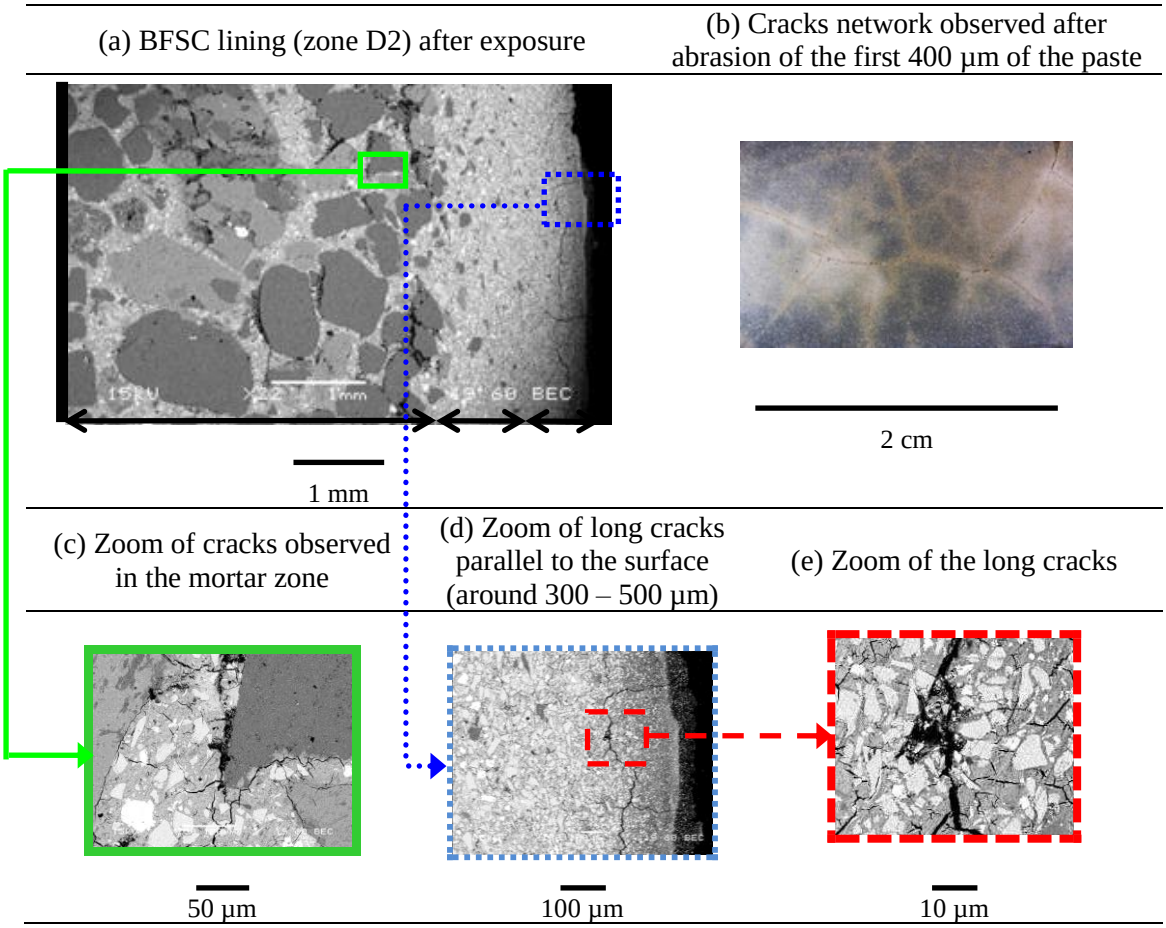

Figure 90: Micro-cracking zones observed by SEM observations on zone D2 of exposed BFSC lining.

In the figure 89, the EDS analyses showed that the location of the crack matches the transition between (i) Zone (a), a partly decalcified layer and (ii) Zone (b) (the rest of the specimen) enriched in sulfur. The decalcification was stronger in the D1 zone (end of the pipe reactor), than in D3 zone (inlet of the pipe reactor). Fact that can be in agreement with the biological thiosulfate conversion in two steps, with tetrathionate as intermediate, thus the biological acidification occurring during the tetrathionate oxidation (Eq 22).

The local EDS analyses in the matrix depth for the D2 and D3 zone are presented in the figure 91. Elemental composition similar to ettringite is observed almost everywhere in the paste layer and notably in the porosity of the matrix and in the cracks. Elemental gypsum composition was also detected at the beginning of the mortar layer, in the depth of the matrix, corresponding to the cracking zones described in the figure 90. Thus, it is observed that, for BFSC lining, the lixiviation of the calcium recorded during the experiment was associated with penetration of sulfate into the matrix and locally precipitation of ettringite and/or

gypsum depending on the local pH and concentration conditions. However, the formation of secondary ettringite needs the formation of gypsum as precursor, thus after 107 days of exposure the important ettringite formation revealed an advanced step of microbial induced concrete corrosion.

Local SEM observations BFSC lining exposed (D2)

(SEM, polish section, LV, BSE, x700) (zonal EDS spectrum) secondary precipitation

D3 (b)

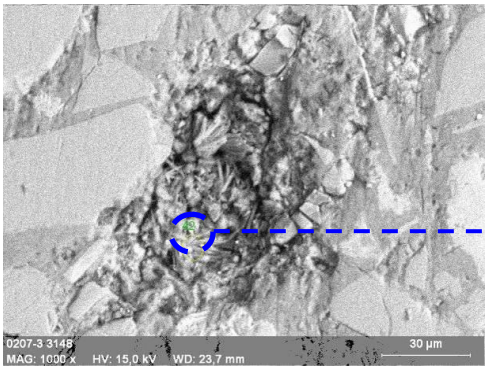

30 µm

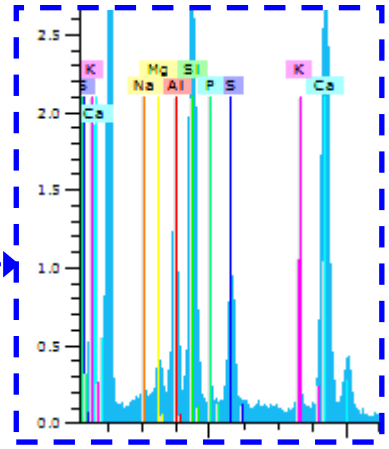

D2 (b)

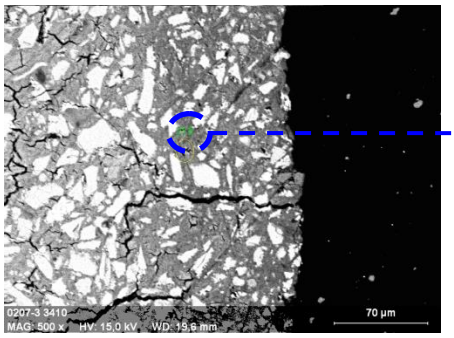

70 µm

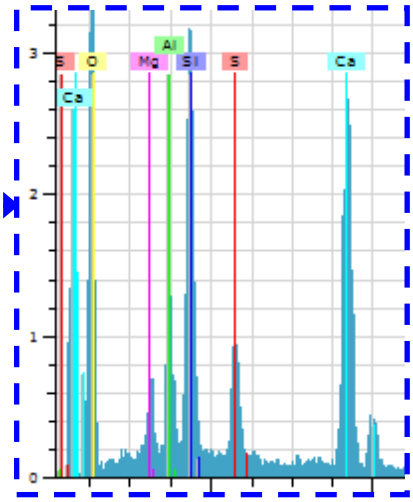

CaO = 37.40 %
Al_2O_3 = 9.06 %
SO_3 = 16.28 %
(~ Ettringite)

Initial specimen
CaO = 45.2 %
Al_2O_3 = 6.9 %
SO_3 = 3.9 %

D2 (c)

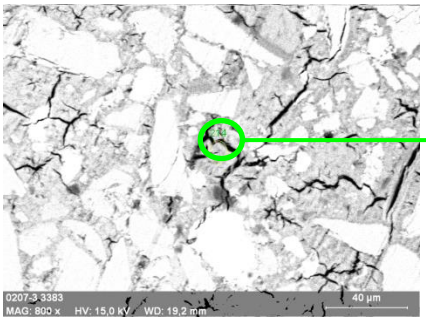

40 µm

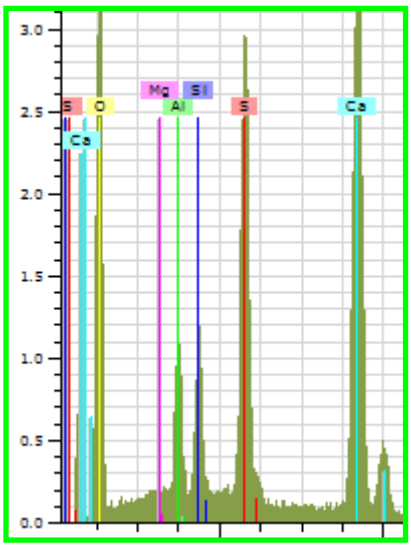

CaO = 46.23 %
Al_2O_3 = 7.56 %
SO_3 = 36.99 %
(~ Gypsum)

Initial specimen
CaO = 45.2 %
Al_2O_3 = 6.9 %
SO_3 = 3.9 %

Figure 91: Local SEM observations on zone D2 of BFSC lining and EDS analyses.

2.4.1.2. CAC lining: SEM characterizations (BSE mode)

The figure 92 presents SEM observations and EDS analyses for C1 and C2 zones (zones under biofilm visualisation at the end of the experiment) and for the B1 zone (zone without biofilm visualisation at the end of the experiments). The paste layer (figure 92 dotted circle) matched the inoculated surface. No crack due to the exposition was visible anywhere in the specimen[7]. The paste showed high density and compactness except in a 100 µm-thick layer (in contact with the biofilm), very porous, decalcified and slightly enriched in sulfur (figure 92.C2).

In zone B1 where dense biofilm were not observable at the end of the experiment no decalcification was recorded. It is important to notice that deterioration is thus a local phenomenon, caused by the local SOB activity. Moreover, the time course of the surface biomass covering (photos of the biofilms in the figure 78) showed that biofilm was implanted on zone B1 during the first 44 days. Thus, the decalcification phenomenon occurred more intensively during the last 63 days, observations that was quantitatively confirmed by the calcium lixiviation measurements presented as sum in the figure 87. In the case of the zones with dense biofilm structure still remained at the end of the experiment (C1 and C2), some sulfur was accumulated inside the decalcified layer (100 – 200 µm), but sulfate produced by the biofilm was not able to further penetrate into the matrix. Thus no secondary precipitation was observed and consequently that no cracks appeared on CAC lining.

[7] : the cracks observed (figure 92) are due to the manipulation of the sample with extremely fragile surface layer (cut section).

CAC lining exposed					
	SEM photos (polish section, LV, BSE, x50)			Zonal EDS spectrum (dotted circle zone)	Zonal EDS spectrum (dashed circle zone)
Iron-Cast	Mortar layer (c)	Paste + anhydrous (b)	Paste layer (a)	Paste layer (a)	Mixte zone (b)
CAC C2	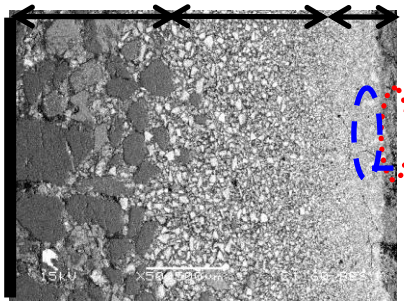 500 µm			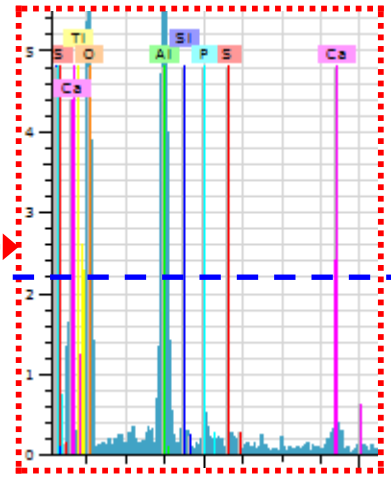 CaO = 7.54 % Al_2O_3 = 77.31 % **(Decalcification)**	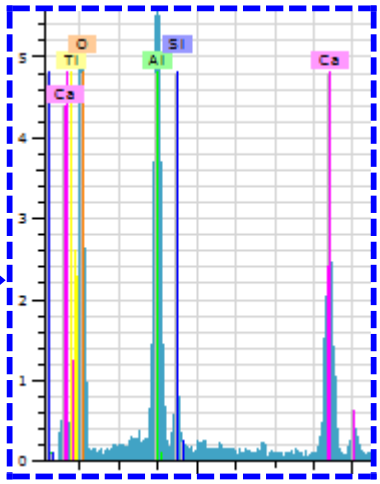 CaO = 43.41 % Al_2O_3 = 46.40 % **(Sound paste)**
CAC C1	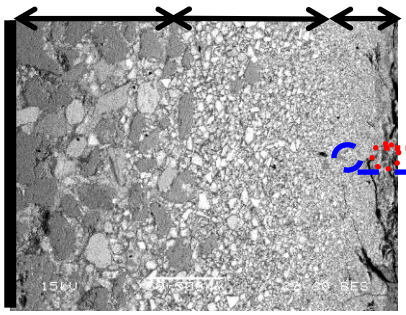 500 µm			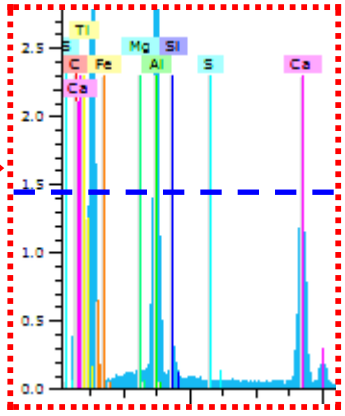	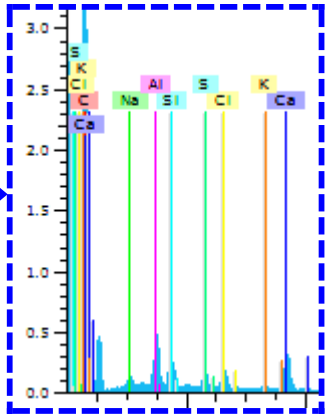
CAC B1	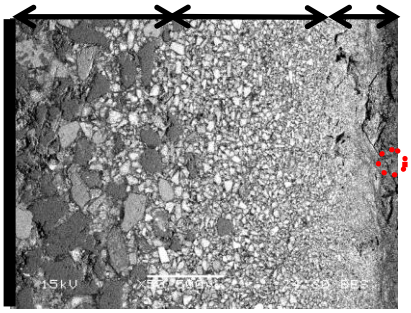 500 µm			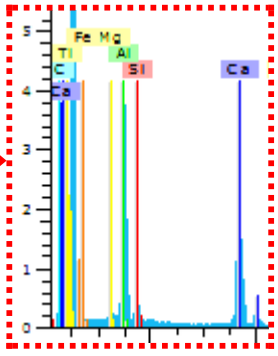	

Figure 92: SEM global observations on zone C (under biofilm zones) and B (without biofilm) of CAC lining, and local EDS analyses.

2.4.2. Chemical composition profiles and microstrucutral analyses

To investigate deeper chemical state of the cement paste for both exposed materials, and evaluate their different behaviour, EPMA profiles were realized on the cement paste of the zone D2 for BFSC lining and of zone B1 (with disperse colonization) and C1 and C2 (under dense biofilm structure) for CAC lining. XRD analyses were performed from the surface to depth of the cementitious matrix to define the mineralogic structure of the exposed linings.

To assist the analyses of the EPMA profiles, the oxides compositions of the control specimen were presented in the table 36 (mean values of EPMA profiles on control specimens).

Table 36 : Oxides compositions of the control specimen for BFSC lining and CAC lining

BFSC lining composition in oxides								
CaO	**SiO_2**	**Al_2O_3**	**Fe_2O_3**	**MgO**	**SO_3**	**K_2O**	**TiO_2**	**Na_2O**
45.23 %	23.20 %	6.89 %	1.06 %	2.77 %	3.87 %	0.23 %	0.38 %	0.04 %
CAC lining composition in oxides								
CaO	**SiO_2**	**Al_2O_3**	**Fe_2O_3**	**MgO**	**SO_3**	**K_2O**	**TiO_2**	**Na_2O**
29.53 %	4.53 %	34.12 %	1.25 %	0.19 %	0.06 %	0.07 %	2.48 %	0.04 %

2.4.2.1. BFSC lining exposed

The figure 93 presents the EPMA profiles obtained on the zone D2 of the exposed BFSC lining. Zones (a), (b) and (c) represents the decalcified surface layer, the paste + anhydrous mixed middle zone and the mortars layer respectively. The measurement of the total oxides confirmed the matter loss in zone (a), confirmed the loss of calcium oxides in good agreement with the amount of Ca^{2+} recorded from the profiles and correlated to the lixiviated calcium. Contents of Al_2O_3 and SiO_2 are maintained in this zone.

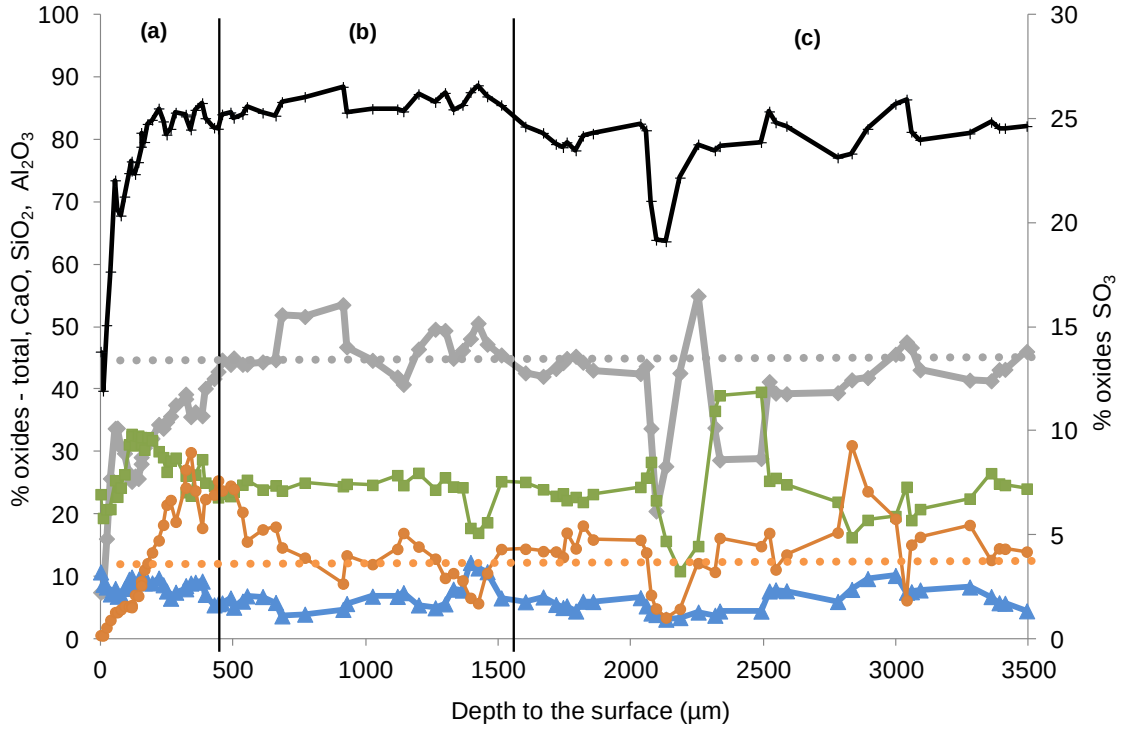

Figure 93: EPMA profiles of cement paste on zone D2 of BFSC lining after exposure. + : total oxides (in %); ◆ : CaO (in %); ■ : SiO_2 (in %); ▲ : Al_2O_3 (in %); ● : SO_3 (in %). ••• : mean value of CaO for initial cement paste (in %); ••• : mean value of SO_3 for initial cement paste (in %). (a) decalcified zone; (b) zone of paste cement + anhydrous; (c) mortar zone.

At the end of the decalcified Zone (from 300 µm to 500 µm), sulfur oxide accumulation was recorded compared to the mean value of sulfur oxide in the initial cement paste (table 14.III). The depth of this sulfur oxide accumulation corresponded to the cracking zone presented in the figure 90, where ED spectra indicate the possible formation of secondary ettringite. Another sulfur oxides accumulation was recorded deeper in the matrix (between 2800 and 3000 µm to the surface, in the mortar zone (c)) corresponding to deep cracking zones presented in the figure 95 where ED spectra identified elemental composition closed to the gypsum composition (figure 96.D2). The initial sulfur oxides content was 3.87% (table 37), based on the EPMA profiles of 3500 µm depth, the final content of sulfur oxides is increased to 4.24% (figure 93).

The figure 94 shows the mineralogical characterization by XRD of the BFSC lining specimen exposed for Zones (a) and (b) described previously in the figure 93 and for the surface of the specimen (in contact with the biofilm). The surface of the BFSC specimen was mainly amorphous (figure 94). The XRD analyses on the Zone (a) showed the precipitation of calcite and the peaks of anhydrous residual grains of C_3S and merwinite (component of slag)

can be seen. In the paste layer of Zone (b), the XRD analysis confirmed that ettringite had precipitated. In the mortar layer, the presence of intense peaks of aggregates did not allow the crystallised phases of the cement paste to be adequately observed and identified. In particular, gypsum could not be detected whereas chemical analyses by EDS showed typical spectrum of this phase at the beginning of the mortar layer (figure 89).

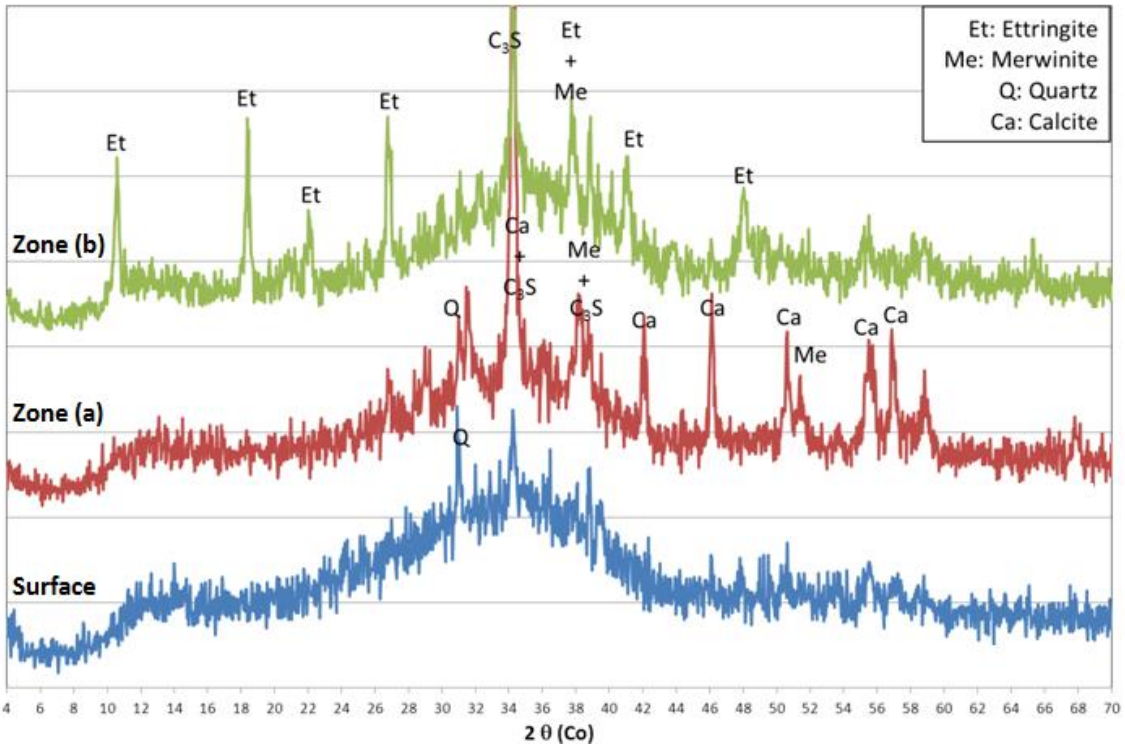

Figure 94: Mineralogical analysis by XRD of zone D2 for the BFSC lining exposed to the test. X-ray patterns of the various zones of surface and of the core of the paste layer.

2.4.2.2. CAC lining exposed

The figure 95 presents the EPMA profiles obtained on the zone B1 (with disperse colonization at the end of the experiment) for the exposed CAC lining. No decalcification was observed in this zone. After 107 days of exposure, the CaO and the Al_2O_3 profiles were equivalent to the mean values obtained for initial specimens.

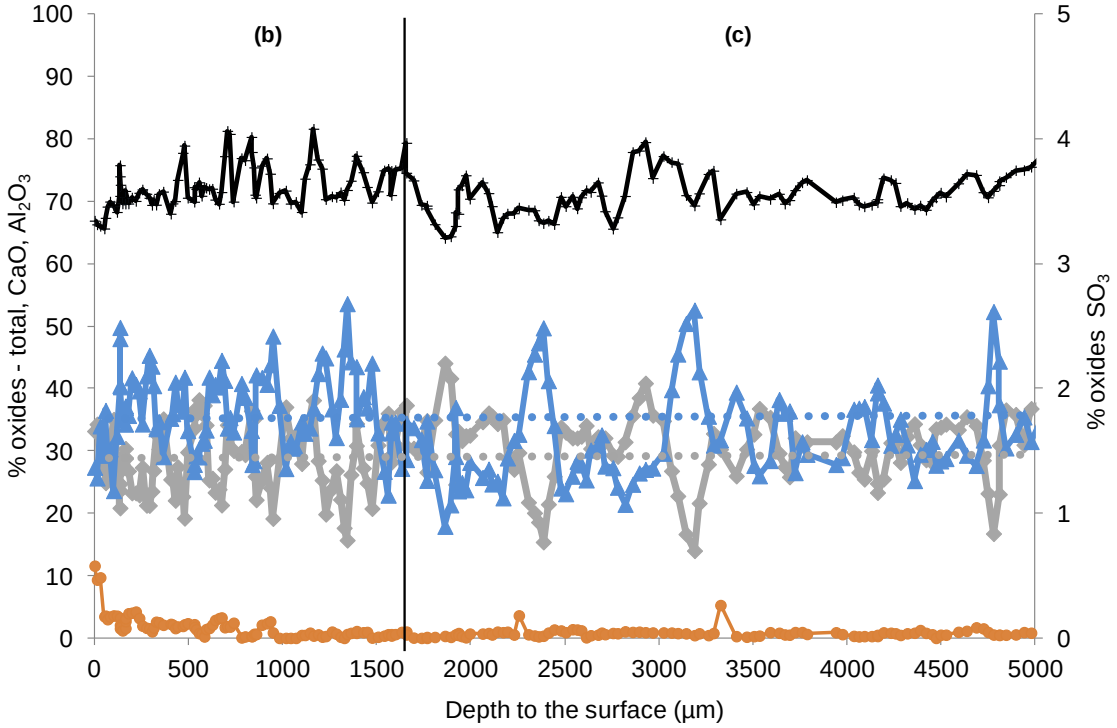

Figure 95: EPMA profiles of cement paste on zone B1 of CAC lining after exposure. + : total oxides (in %); ◆ : CaO (in %); ▲ : Al_2O_3 (in %); ● : SO_3 (in %). • • • : mean value of CaO for initial cement paste (in %); • • • : mean value of Al_2O_3 for initial cement paste (in %). (b) zone of sane paste cement + anhydrous; (c) mortar zone.

The figure 96 presents the results of EPMA analyses under colonized zone C1 and C2 along the distance from the inoculated surface. For both profiles of colonized zones, the surface zone, a layer of 100-150 µm thick (a), is decalcified, enriched in sulfur (up to 1.7% of SO_3 vs. an average of 0.06 % in the rest of the paste) and contains almost only alumina oxides, confirming the weak lixiviation of alumina oxides during the experiment. Layer (b) the composition in oxides is almost constant and matches the composition of the control specimen.

(1) Zone C1 CAC lining after 107 days of exposure

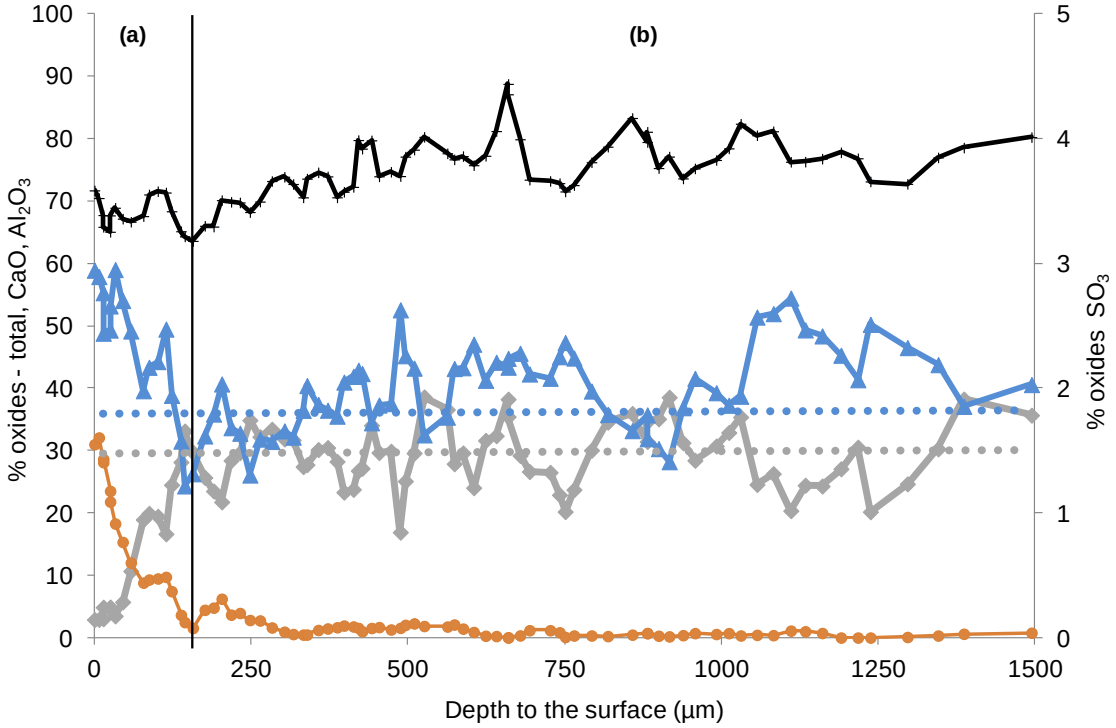

(2) Zone C2 CAC lining after 107 days of exposure

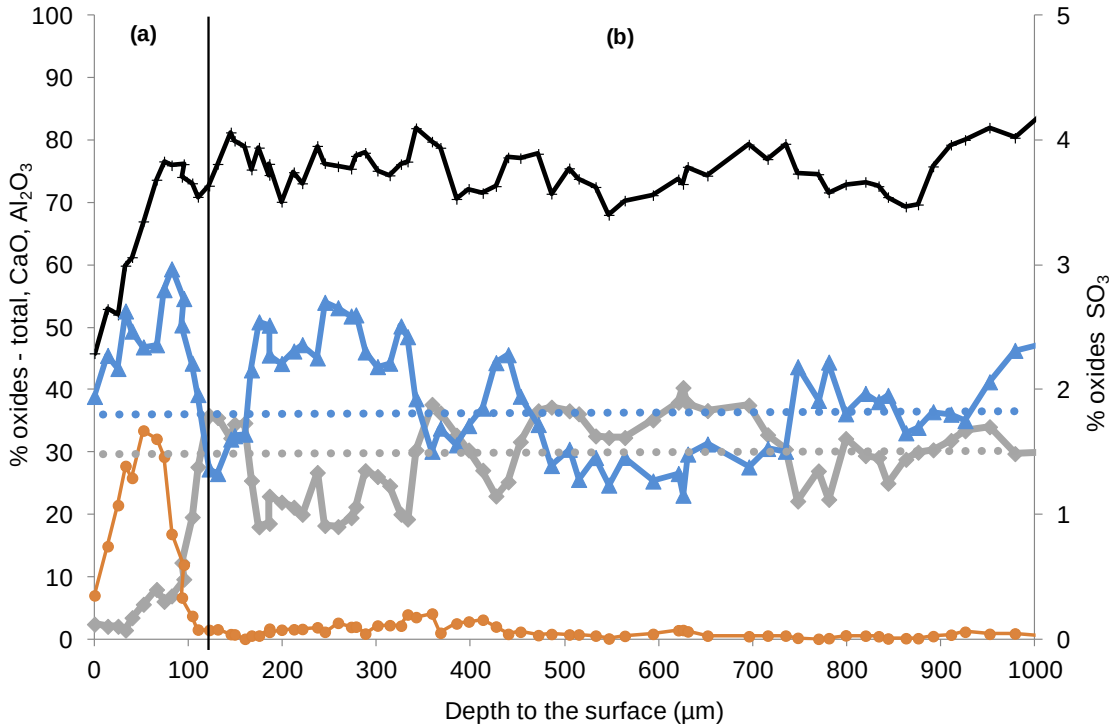

Figure 96: EPMA profiles of cement paste on zone C1(1) and C2(2) of CAC lining after exposure. + : total oxides (in %); ◆ : CaO (in %); ▲ : Al_2O_3 (in %); ● : SO_3 (in %); • • • : mean value of CaO for initial cement paste (in %); • • • : mean value of Al_2O_3 for initial cement paste (in %). (a): decalcified zone; (b) zone of sane paste cement + anhydrous; (c) mortar zone.

The figure 97 shows the mineralogical characterization by XRD of the CAC lining specimen after exposure to biogenic acid for the Zone (a) described previously (zone in contact with the biofilm) and for the Zone (b) corresponding to the core of the paste layer (about 1400 µm depth on the figure 96).

The core of the paste layer shows typical anhydrous (*CA*, $C_{12}A_7$ and hydrated (C_3AH_6, *AH*) crystallized phases of CAC matrix. In the layer in contact with the biofilm, the structure is mainly amorphous with formation of AH_3 and dissolution of C_4AH_6 and of the other crystallised phases, confirming the loss of calcium during the microbial induced concrete corrosion, and indicating as describes in the literature (Scrivener et al., 1999) (Lamberet, 2005) (Alexander and Fourie, 2011) the formation of alumina gel (AH_3) reducing the local porosity due to the material lixiviation and then limiting the transport of sulfate in the depth of the CAC matrix.

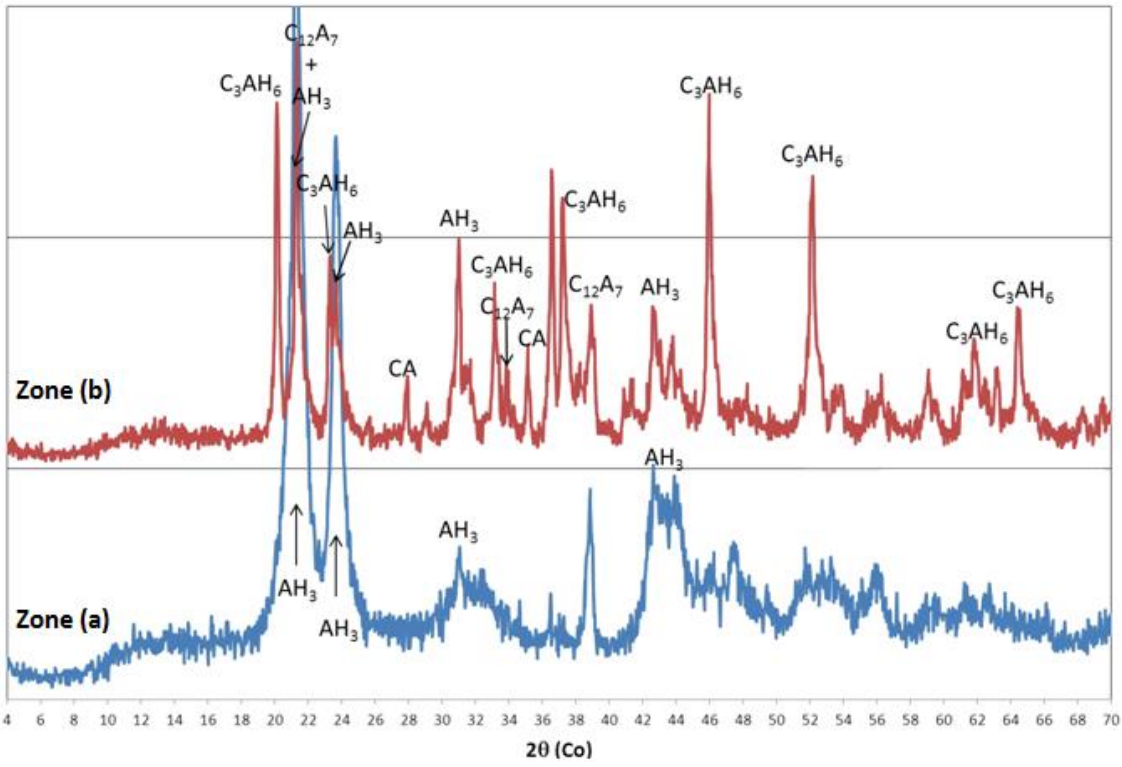

Figure 97: Mineralogical analysis by XRD of zone C2 for the CAC lining exposed. X-ray patterns of the gel zone and of the core of the paste layer

Thus the sulfur oxides accumulation observed by EDS analyses and EPMA profiles in the decalcified zone under the biofilm not appeared as crystallized forms (no gypsum, no ettringite observation). In that case, for CAC lining, two hypotheses could be proposed to explain this specific accumulation of sulfur oxides, (i) the adsorption of soluble sulfur oxides

(as thiosulfate, sulfate and/or other polythionate) on the amorphous zone, (ii) the important role of the alumina gel for the reduction of the local porosity and the resulting sulfur oxides profiles as a consequence of sulfate diffusion through the surface layers.

2.4.3. Two different behaviors for CAC lining and BFSC lining

Decalcification occurred for both materials under biogenic acid environment. However, a thinner decalcification zone was observed for CAC lining compared to the BFSC lining (due to the acid resistance of the material and also of the difference in the initial porosity). No huge penetration of sulfur was observed for CAC lining, indicating the specific role of the alumina fate after calcium lixiviation at the surface of the material. The CAC lining stopped the sulfate penetration and then no secondary precipitation occurred, and then no cracking zones could be observed at this state of the microbial induced concrete corrosion. For BFSC, the important penetration of sulfate inside the cementitious matrix led to the precipitation of expansive secondary ettringite, with the formation of a microcracks network under decalcified zone.

3. Discussions

To complete the analyses and evaluate the experimental device as an efficient qualitative and quantitative tool to optimize the process, three aspects will be treated in the next paragraphs, (i) the quantitative evaluation, for acidification and Ca^{2+} lixiviation, (ii) the pH time courses as phenomenologic signal of the deterioration progress, and (iii) the maximization of the biocorrosion process, in particular concerning the sulfur source.

3.1. Quantitative aspects

3.1.1. Mean decalcified depth calculation by calcium mass balances

The total calcium in the leaching solution during the experiements was compared to the loss of calcium estimated by the EPMA profiles. For both materials, taking into account the initial composition (table 36) and the initial porosity of the paste layers (table 11) (only zone where decalcification occurred) the amount of calcium dissolved was calculated in function of the depth of the decalcified zone.

For both cementitious lining the total calcium in the leaching solution used for the theoretical estimation of the decalcified depth was measured and presented in the figure 87. After 107 days of exposure the amounts of calcium in the leaching solutions were 4980 ± 750 mgCa for the BFSC lining and 3600 ± 540 mgCa for the CAC lining. Based on these values, for each EPMA profiles, two depths of decalcified zone were calculated, (i) a theoretical depth corresponding of a zone with a total decalcification, (ii) a theoretical depth corresponding of a semi-decalcified zone. The results, compared to EPMA profiles, are presented in the next figures (figure 98 and figure 99) in terms of the theoretical depth calculations for decalcified zones; in the figure 98 for the CAC lining (EPMA profile on zone C1 and C2) and in the figure 99 for the BFSC lining (EPMA profile on zone D2). The total decalcification zones are presented by full line, the semi-decalcification zone by dashed line, and experimental depth of decalcification observed by EPMA analyses by dotted lines.

(1) Zone C1 CAC lining – CaO profiles after 107 of exposure

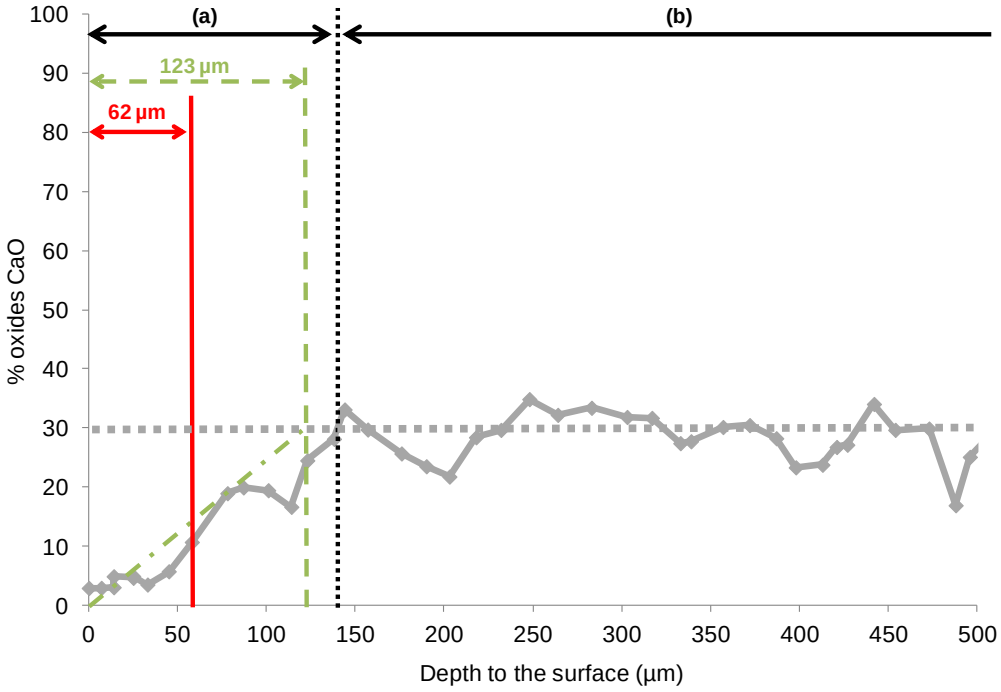

(2) Zone C2 CAC lining – CaO profile after 107 days of exposure

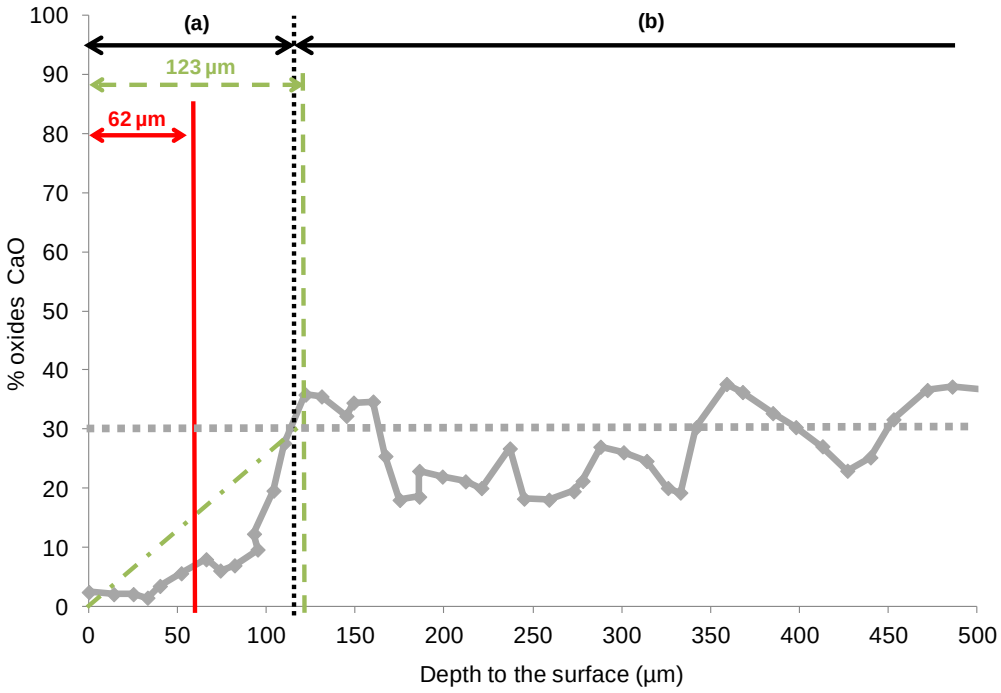

Figure 98: CaO EPMA profiles on zone C1(1) and C2(2) of CAC lining after exposure and calculation of theoretical decalcified depths by the cumul of the calcium in the leaching solution. ◆: CaO (in %); ● ● ●: mean value of CaO for initial cement paste (in %); •••••: depth of the decalcified zone by comparison of the CaO content of the control specimen and EPMA profiles; ▬ : calculated depth of decalcified zone for homogenous total decalcification; ▬ ▬ : calculated depth of decalcified zone for homogenous semi-decalcification; ▬ · ▬ : theoretical CaO profile for zone with semi-decalcification; (a): decalcified zone; (b) zone of sane paste cement + anhydrous; (c) mortar zone.

The figure 98, concerning the CaO profile by EPMA analyses for the exposed CAC lining (zone C1 and C2), shows that the theoretical calculation of a theoretical decalcified depth matched quiet well the experimental determinations, if a semi-decalcification (dashed lines) was taken into account to describe the experimental decalcified zone (dotted line). Thus, the EPMA profiles on the zone C1 and C2 for the CAC lining seemed to represent the mean phenomenon.

The figure 99, concerning the CaO profile by EPMA analyses for the exposed BFSC lining (zone D2) shows that the theoretical calculation of a theoretical decalcified depths mismatched the experimental determination. On BFSC lining, the decalcification zone was deeper but the decalcification profile was less sharp than for the CAC lining (figure 98 and figure 99).

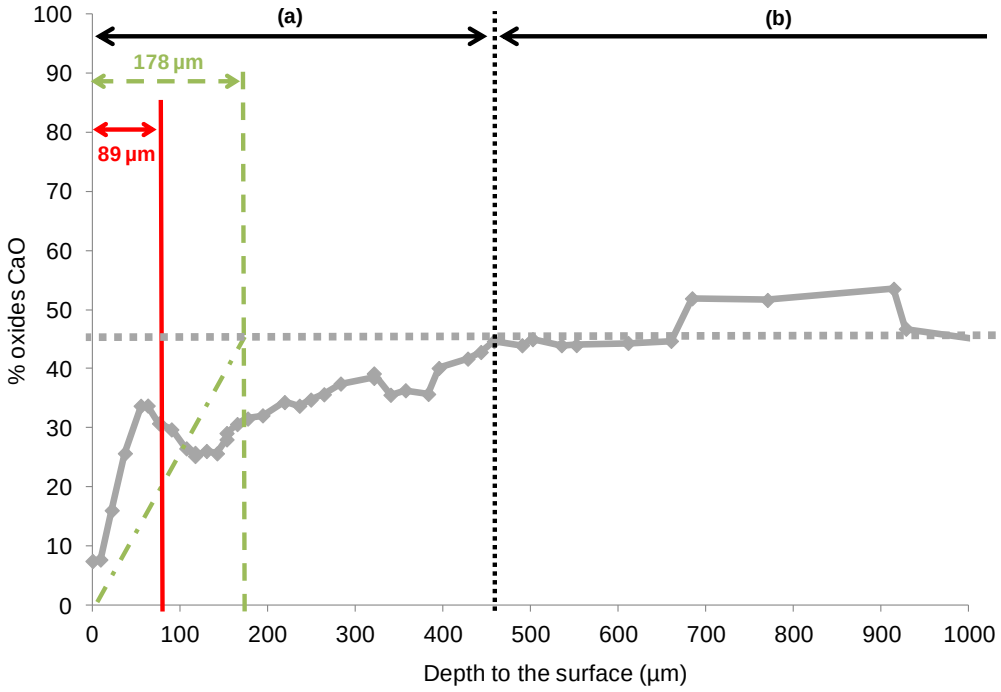

Figure 99: CaO EPMA profiles on zone D2 of BFSC lining after exposure and calculation of theoretical decalcified depths by the cumul of the calcium in the leaching solution. ◆: CaO (in %); ● ● ●: mean value of CaO for initial cement paste (in %); •••••: depth of the decalcified zone by comparison of the CaO content of the control specimen and EPMA profile; ▬ : calculated depth of decalcified zone for homogenous total decalcification; ▬ ▬ : calculated depth of decalcified zone for homogenous semi-decalcification; ▬ · ▬ : theoretical CaO profile for zone with semi-decalcification; (a): decalcified zone; (b) zone of sane paste cement + anhydrous; (c) mortar zone.

This phenomenon could be due to the high initial porosity and its increase during the deterioration phenomenon, leading to (i) a competition between the transport and the reaction for the acidity biologically produced, (ii) the migration of the microorganisms inside the

porous media and a local production of acid and sulfate. Thus, the surface layer was not totally decalcified even if the deteriorated front continuously penetrated inside the porous media. Moreover, the identification for BFSC lining of secondary precipitate of sulfate calcium salts in the zone between 300 µm and 500 µm could also explain the particular CaO profile in the partially decalcified zone, revealing an accumulation of calcium by secondary precipitated structures, linked to the acid attack and the migration of sulfate.

Thus, in the case of no secondary precipitation (CAC), the sole quantification of the lixiviated Ca^{2+}, coupled with an analysis of the initial linings (CaO content and porosity), should enable the evaluation of the deterioration progress in terms of depth of decalcification. The identification of secondary precipitation will be described in a further paragraph [3.2].

3.1.2. Acid produced in contact with the cementitious linings

Most of the studies using thiosulfate to simulated MICC worked in immerged system with free bacteria (no attached biomass in contact with cementitious material) producing acid and sulfate (Aviam et la., 2004) (Bielefeldt et al., 2010). As said by Ehrich in 1999 and Herisson in 2012, these biological tests works in some ways like chemical tests.

The pilot design proposed in this study focused the microbial colonization and production of biogenic acid only in contact with the cementitious material. But, in the case of a short hydraulic retention time (unkown in the experimental conditions), compared to the characteristic time for diffusive transport and reaction, a part of the acid produced at the surface of the biofilm could be not react with the material, and thus not be efficient for the study of the biodeterioration. In that case, if acid potential was calculated only based on the biological products as sulfate and tetrathionate, the biocorrosion could be overestimated.

To evaluate the efficiency of the acidity production in term of deterioration, the total acidity produced by the microorganisms was calculated and compared to the lixiviation products, taking into account the global sulfur mass balances and associated respectively the acidity or alkalinity production in accordance with the mass balance reactions (Eq 21, Eq 71, Eq 72 and Eq 73). Thus, as described in the figure 100, with the biological oxidation of thiosulfate defined in two steps, with tetrathionate as intermediate, the acid production (H^+ prod) could be calculated by sulfur mass balances. On the other hand, because no or low concentration of alumina was recorded during the experiments with CAC, the neutralization

capacity for both materials could be associated to the dissolution of $Ca(OH)_2$ only. Thus for 1 mole of calcium released from the cementitious matrix 2 moles of OH^- were released to. Thus in a stoichiometric model the ratio of the cumulated calcium in the leaching solution and the cumulated acid produced by the biological reactions must be $Ca^{2+}{}_{out} / H^{+}{}_{prod}$ if all the acid produced has reacted with the cementitious materials, considering the continuous dissolution of $Ca(OH)_2$ due to favorable pH conditions (valid during the last 90 days).

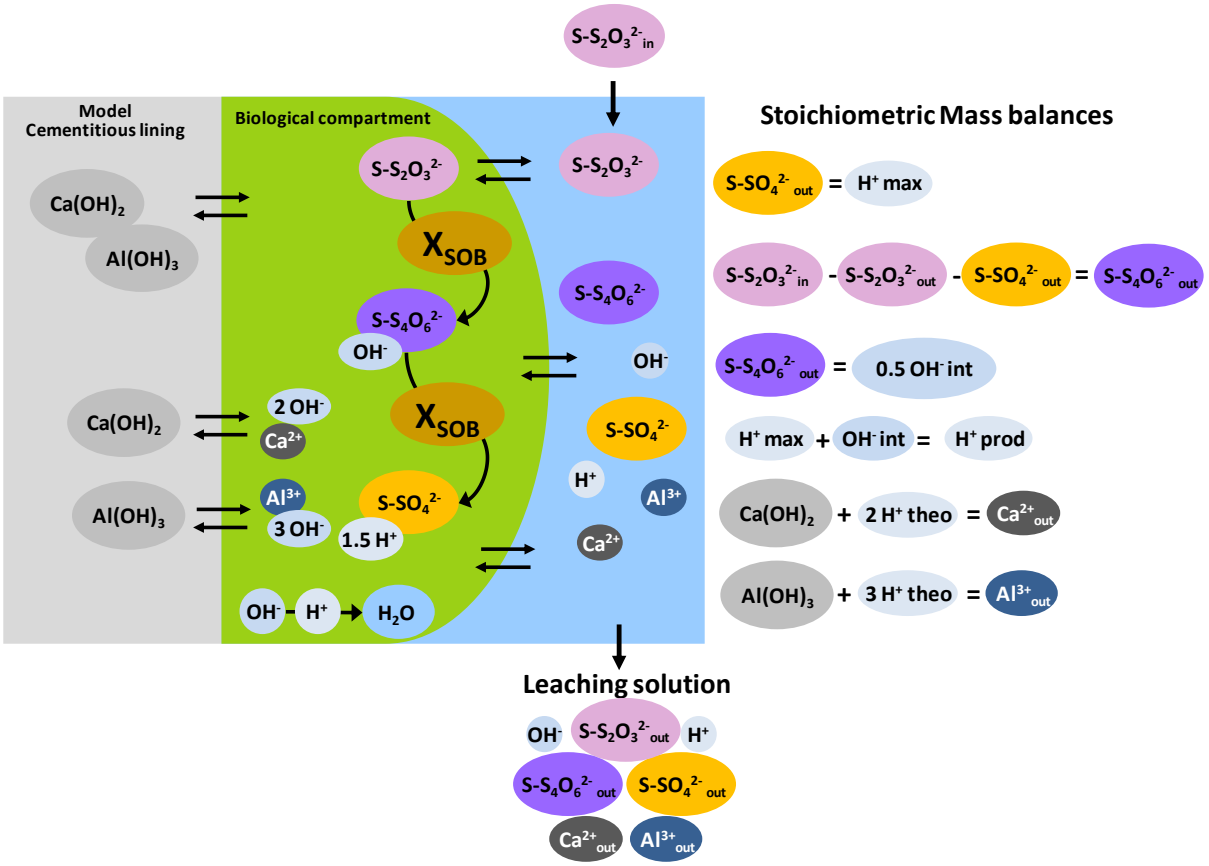

Figure 100: simplified schema and reactive model to describe the main processes involved in the lixiviation of the cementitious linings, and the illustration of the mass balances system to evaluate the acidproduction and the associated reactivity of the cementitious lining, based on the stoichiometric equations (Eq 20, Eq 71, Eq 72,and Eq 73); H^+max: the total theoretical H^+ produced linked to the sulfate production; OH^- int: the total OH^- produced during the production of the sulfur intermediate (tetrathionate); H^+prod: the H^+ produced by biological processes; H^+theo: the theoretical H^+ corresponding to the dissolution of theoretical compounds describing the cementitious matrix..

As discussed in the paragraph [2.2.3.1] of this chapter, the quantity of sulfate produced by the microbial community and trapped in the cementitious matrix, could be neglected for both materials tested. Thus the acidity associated to the production of sulfate could be evaluated by the total sulfate measured in the leaching solution.

The table 37 presents the results obtained for both materials in terms of total production of biogenic acid and the associated experimental ratio ($Ca^{2+}_{out} / H^{+}_{prod}$).

Table 37: Total biogenic acid production and calcium lixiviation associated

	SO_4^{2-} produced (molS)	H^+ max produced (= SO_4^{2-}) ($molH^+$)	$S_4O_6^{2-}$ not converted (molS)	OH^- int produced (= 0.5 x $S_4O_6^{2-}$) ($molOH^-$)	H^+ prod (= $H^+_{max} - OH^-_{int}$) ($molH^+$)	Ca^{2+} out in the leaching solution ($molCa^{2+}$)	$Ca^{2+}_{out} / H^{+}_{prod}$
BFSC	0.259	0.259	0.133	0.0665	0.1925	0.124	*0.64*
CAC	0.234	0.234	0.158	0.079	0.155	0.090	*0.58*

For both materials, the ratio calculated was in the range of the theoretical ratio excepted (0.5). Thus all the acidity produced by the microbial community was produced in contact with the material and had a direct impact on its dissolution. No comparison is possible between the two values obtained, due to the high uncertainty resulting from the calculation method through several experimental mass balances.

Even if this ratio could not be used to quantify precisely the process, this results indicate the direct relation between total SOB activity and the behavior of the cementitious matrix, thus as presented in the next paragraph the pH measurement in the leaching solution become an good indicator in time of the behavior of the whole system (biological activity and material).

3.2. pH time course in the leaching solution as signal of the evolution of the dynamic system SOB activity and cementitious lining

Two materials were tested under similar biological potential transformation, and as expected in the literature strong differences in terms of behaviour were recorded (Erhrich et al., 1999) (Alexander and Fourie, 2011). Considering the pH of the leaching solution, for CAC lining regular acidification were measured (figure 80), whereas for BFSC lining during the acid phase, the pH of the leaching solution appeared to be instable (figure 81). The major difference between CAC and BFSC lining was the precipitation of secondary compounds

observed inside the cementitious matrix. This secondary precipitation could explain the pH by the combination of the equation (Eq 21) and the equation (Eq 31). The formation of Gypsum was explain by the reaction of the biogenic sulfuric acid (H_2SO_4) and the Portlandite ($Ca(OH)_2$) (Eq 31). In the case of the biological oxidation of thiosulfate (Eq 83), the ratio H^+/SO_4^{2-} was equal to 1 (instead of 2 for H_2S total conversion). The equation (Eq 31) could be converted to the equation (Eq 91) for the biological acid produced by the system, and then could explain the punctual alkalinity increase in the leaching solution due to the local precipitation.

Eq 91: $Ca(OH)_2 + HSO_4^- + H_2O \rightarrow CaSO_4.2H_2O + OH^-$

Moreover SOB activity is pH dependent. At the reactor scale, the first step of the biological conversion of thiosulfate, the tetrathionate production is associated to alkalinity production (Eq 71), contrary to the sulfate production (Eq 22). This altenance, linked in a first step by the pH disturbance caused by the secondary precipitation, may explain the variation observed only on the BFSC lining.

These local processes highlight specific interactions of the microbial community and chemical and mineralogical local transformations of the cementitious matrix. In the case of the CAC lining no secondary precipitation of sulfate calcium salts was observed when no pH disturbance was recorded. For the CAC lining the associated pH of the leaching solution decreased slightly during the experiments (figure 80).

In the case of a test development, with thiosulfate as sulfur source, this pH instability could indicate the time when secondary precipitation occurred and an advanced deterioration like for the tested BFSC lining. To evaluate this observation, others experiences should be performed in similar conditions on same linings exposed during different time periods.

3.3. The choice of the sulfur source to intensify the acid production in contact with the cementitious lining.

Compared to the use of H_2S (Eq 17), with a ratio of biogenic acid production ($H^+/ SO_4^{2-} = 2$), the use of thiosulfate as sulfur source (Eq 21) leads to a ratio of biogenic acid production ($H^+/ SO_4^{2-} = 1$). With the objective to intensify the deterioration of the cementitious matrix by biological reactions, the direct use of tetrathionate (as sole source) could limit the pH

disturbances linked to the SOB activity (Eq 22), due to a higher ratio of biogenic acid production ($H^+/ SO_4^{2-} = 1.5$).

The use of tetrathionate with no intermediate reaction will avoid the first biological basification occurring during the thiosulfate oxidation (highlighted in the chapter VI and this chapter). As demonstrated in the chapter VI, confirming the literature review presented in the tables 13 and 14 of the chapter IV, the kinetics are equivalent for the thiosulfate and the tetrathionate, depending on the microbial species involved in the transformations. Moreover, as for the thiosulfate, numerous SOB are able to grow on tetrathionate, even the acidophilic species (see table 13 and 14 in the chapter IV), indicating that tetrathionate should be a more interesting selection factor for SOB activity. In other hand with a biomass yield slightly lower than for thiosulfate (chapter VI), the biomass production could limit a little the quantity of SOB involved in the transformation and thus the robustness of the process. However, the use of tetrathionate, due to the kinetic performances and the immediate acidification should limit the heterogeneous reactivity of the microbial consortium, and optimized the deterioration along of the segment-pipe. Moreover, in regard to the literature results and those obtained in this study, the acid potential of this compounds should lead to an acceleration of the selection, thus to a faster establishment of SOB activity and a better resistance of the SOB activity to the pH disturbances caused by the reactivity of the cementitious linings.

4. Conclusions

The use with an adapted laboratory pilot of thiosulfate as sulfur substrate to reproduced MICC shows interesting results. As for the culture in perfect mixed reactor, the use of thiosulfate in a control environment, led to a fast selection of viable acidophilic SOB from an initial activated-sludge consortium, independently of the support material. The pathway of conversion of thiosulfate appeared to be the same than for free cultures, with tetrathionate as the main biological sulfur intermediate. The experiences with two different cementitious materials, known to have different behaviour against biogenic acid attacks, showed coherent global transformations of the materials, with a **better resistance of CAC lining compared to BFSC lining**. In accordance with the literature, **the biogenic acid** produced at the surface of the materials **led to a decalcification of the surface layers** of the materials (depth of the decalcified zone linked to the intensity of the acid attack). It is observed **for the BFSC lining** a penetration of the associated produced sulfate into the matrix, **precipitating as** secondary compounds like **gypsum and ettringite** in a most part, causing swelling and thus cracking inside the porous medium, intensifying then the biodeterioration process.

In other hand, **for CAC lining**, the materials analyses confirmed the important role of the **formation of alumina gel** during the decalcification for the protection of the material. In contrast to BFSC lining, the formation of alumina gel in the decalcified zone **limited the porosity, thus the penetration of sulfate** inside the matrix, and thus precipitation and damage deeper in the cementitious material.

The regular analyses in time of the leaching solution, with pH, calcium and alumina released from the cementitious materials, and the **mass balances of soluble sulfur compounds**, associated to the chemical and micro-structural analyses of the materials, indicated the capacity of the experimental device to record the evolution of the cementitious material. The soluble sulfur mass balances revealed a **SOB activity starting faster on BFSC lining than on CAC lining** during the first 60 days of the experiences. Thus CAC lining, moreover to present better resistance to acid attack, reduced in the first time the acid-production (10 to 30 % less during the 60 first days).

The visual observations of the colonized surfaces, during the 107 days of the cultures, showed clear difference in covering surface for both materials. On BFSC lining, the whole

surface appeared to be covered with heterogeneity in the thickness of the biofilm implanted. On CAC lining, a dense biofilm was observable only on 1/3 of the surface materials, biofilm that appeared to be dryer under the same environmental condition. Thus, **the CAC lining have also an impact on the microbial community colonization** and its development at the surface of the material. The reasons of this observable phenomenon were not known actually. A bacteriostatic impact of the released alumina contained in the material could be an explanation, but this subject was always discussed in the literature today and the concentrations of alumina in the leaching solution were so low that this argument seems not to be coherent with the experimental results obtained in this study (global SOB activity equivalent at the end of the experiment on both material, even with notable differences in the covering surface). In other way, the surface properties of the different materials could have specific interactions with biofilm.

The experiences realized in this study, link and quantify the reciprocal influence of a cementitious material and biological activity. The dynamical measurements in the leaching solution, assured by sulfur mass balances in particularly, coupled at the end of the experiences of chemical and micro-structural analyses, enable the phenomenological description of the biogenic acid attack for each material, confirming the literature observations for the resistance of BFSC lining and CAC lining against biogenic acid produced by microbial community. Thus, **an experimental set-up for the study and the evaluation of the MICC on industrial products is developed, controlled and validated in terms of representativness**.

Conclusions Générales et Perspectives

1. Conclusions Générales

L'enjeu industriel de ce travail de recherche, réalisé au sein du LISBP et supporté par le centre de recherche et de développement de l'entreprise Saint-Gobain PAM, était de **développer un dispositif expérimental permettant d'évaluer la résistance de revêtements cimentaires** dans des conditions de biodétérioration assimilables à celles rencontrées **en réseaux d'assainissement**, résistance pouvant être la résultante d'une résistance physico-chimique propre aux revêtements et d'une influence des revêtements eux-mêmes ou de leur évolution sur la colonisation ou l'activité biologique. Cet objectif se positionnait dans le cadre normatif « NF EN 598 » imposant l'unique évaluation de la résistance des matériaux cimentaires face aux environnements « agressifs » rencontrés en réseaux d'assainissement par des essais chimiques long terme (6 mois) peu représentatifs de la réalité biologique présente dans les réseaux.

1.1. Apports de l'étude pour la définition d'un essai de biodétérioration

Pour assurer la maitrise et l'intensification des phénomènes une étude bilbiographique a permis de proposer un **dispositif expérimental visant à réduire le temps de colonisation d'un consortium « agressif »**, sans passer par une pré-acidification chimique peu représentative du système étudié. **Deux choix majeurs en termes de fonctionnement de l'essai ont été proposés**, (a) **le travail sans H_2S** comme substrat soufré, par l'**utilisation de thiosulfate**, et (b) l'**inoculation unique du système** au temps initial **via un consortium mixte issu de boues-activées** prélevées sur stations d'épuration.

- Le choix des thiosulfates a été motivé en terme de facteur de sélection d'une activité sulfo-oxydante par, (i) son identification en tant qu'intermédiaire réactionnel lors des transformations abiotiques de l'H_2S, (ii) sa large utilisation par toutes les espèces sulfo-oxydantes identifiées en réseaux d'assainissement, (iii) la stabilité abiotique de celui-ci en condition de pH alcalin ou neutre, permettant de contrôler les flux de soufre apporté, et de maximiser les transformations biologiques recherchées.

- Le choix d'une inoculation initiale unique à partir d'un consortium diversifié issue de la filière de l'assainissement a été motivé par, (i) la volonté d'assurer une diversité microbienne initiale, permettant par rapport aux matériaux évalués l'implantation du

consortium le plus adapté aux transformations étudiées, sans présupposition des populations microbiennes impliquées, (ii) par le contrôle des conditions opératoires permettant la définition d'un milieu de croissance sélectif et donc de l'implantation, telle qu'elle existe en réseau d'assainissement, d'une activité microbienne complexe mais spécifiquement adaptée.

Les différents points concernant ces deux choix ont ainsi été évaluées à travers différentes expériences, et ce afin de confirmer les hypothèses émises et d'assurer ultérieurement la maitrise de la sélection microbienne et des transformations biologiques en terme d'activité sulfo-oxydante :

- Une première étude expérimentale réalisée à partir d'un inoculum diversifié a permis de révéler **l'intérêt des thiosulfates en tant que facteur de sélection d'une activité sulfo-oxydante** sur des revêtements de type CAC.

- Par la suite, dans l'objectif de comprendre et de maitriser les transformations abiotiques des thisosulfates, une approche de simulation numérique appuyée sur des expériences de laboratoire a été mise en place. **Le modèle développé permet la description dynamique** de l'évolution des concentrations des thiosulfates et des produits de réactions, tels que les sulfates, le soufre élémentaire, ainsi que la description de la consomation en oxygène **en fonction des conditions opératoires** (pH, concentration en thiosulfate).

- Basé sur l'analyse expérimentale de la culture microbienne et le modèle dynamique préalablement développé, **la sélection et le maintien d'une activité acidophile sulfo-oxydante à partir d'un consortium issu d'une boue-activée a été validé expérimentalement.**

- En suivant, un compartiment décrivant les transformations biologiques a été implémenté au modèle chimique, ainsi **l'oxydation biologique des thiosulfates a été décrite en deux étapes d'oxydations, avec un intermédiaire tetrathionate**. Le modèle dynamique rend ainsi compte de la faible inlfuence des réactions chimiques en conditions d'alimnentation contrôlées. Ainsi, **la production d'acide sulfurique biogénique (production de sulfates et de protons) est décrite stoechiométriquement et cinétiquement** dans les conditions d'expériences.

- Par la suite, basée sur la description des transformations chimiques et biologiques des thiosulfates, **la sélection d'une activité sulfo-oxydante sur deux types de revêtements cimentaires en 15 semaines** ont permis, par des bilans matières (i) l'**évaluation du devenir de deux types de revêtements** (CEM III et CAC) face à une attaque biogénique, (ii) l'**évaluation temporelle de l'impact du type de revêtement sur la sélection et l'intensité de l'activité sulfo-oxydante sélectionnée au contact du matériau**, (iii) et donc la **discrimination entre deux types de revêtements**.

Ainsi, d'un point de vu industriel le dispositif expérimental a permis de confirmer que les **mortiers à base de pâte de ciment du type CAC**, en comparaison à un revêtement dit CEM III, propose une **résistance accrue face à la biodétérioration** intervenant en réseau d'assainissement et ce par des propriétés physico-chimiques limitant l'impact de l'acide biogénique sur la matrice, et sur une première phase de la colonisation (60 jours dans le cas de l'étude accélérée) par un impact négatif sur l'implantation d'une activité sulfo-oxydante entre 10% et 30% de celle enregistrée sur un revêtement du type CEM III.

Pour autant, **la définition d'un essai de biodétérioration impose** avant tout **que celui-ci soit représentatif, reproductible et accéléré.**

1.2. Evaluation de le réprésentativité de l'essai proposé

Afin d'assurer la reproduction en conditions contrôlées des transformations clés impliquées dans l'attaque biologique (production d'acide et de sulfate par des microorganismes sulfo-oxydants se développant au contact des matériaux), l'étude s'est attachée à reproduire en conditions maitrisées le condensat formé au sommet des canalisations, tout en accentuant les phénomènes entrainant une intensification de la dissolution des matériaux. **Ce double objectif technique a été atteint en travaillant par le ruissellement d'une solution nutritive minérale après un ensemencement de la surface des canalisations**. Dans un second temps, les expériences réalisées en laboratoire, par la quantification de la production d'acide biogénique au contact de deux types de revêtements (basés sur des pâtes de ciment de type CEM III ou CAC) et **l'analyse du devenir de ces matériaux ont permis de qualifier les choix en terme de représentativité du système pilote**:

- Production d'acide et de sulfate au contact des matériaux en très grande majorité liée à l'activité biologique (95% des sulfates produits).

- Lixiviation du calcium des matrices cimentaires en réponse à cette attaque biologique localisée à la surface des revêtements.
- Cinétique de lixiviation du calcium plus importante pour le revêtement basé sur une pâte de ciment de type CEM III par rapport à une pâte de type CAC.
- Dans le cas du revêtement basé sur une pâte de ciment de type CEM III l'observation généralisée d'un phénomène de fissuration de la matrice, induite par la formation au sein de la pâte de ciment de précipités secondaires, majoritairement de l'ettringite, avec en profondeur des échantillons la détection de gypse au contact des granulats.
- Dans le cas du revêtement basé sur une pâte de ciment de type CAC, la formation en surface du matériau d'un gel d'alumine assurant la protection physico-chimique du matériau, limitant ainsi la pénétration de l'acide et des sulfates et donc la précipitation de composés secondaires sources de fissurations importantes.

1.3. Evaluation de la reproductivité de l'essai proposé

La reproductibilité de l'essai reste encore à confirmer expérimentalement. Cependant, le contrôle des conditions opératoires telles que la température, les flux de matières appliquées à la paroi, couplé à une approche par bilans matières a montré la maitrise des conditions de croissances et donc de l'activité biologique sulfo-oxydante, moteur principal de la biodétérioration.

1.4. Evaluation de l'accélération de l'essai proposé

L'observation et la quantification de détériorations importantes de revêtements après 15 semaines d'expositions indiquent l'accélération des processus étudiés. Pour autant, afin d'évaluer un facteur d'accélération du procédé proposé, dans les conditions opératoires présentées, des analyses équivalentes sur sites réels, sont à mettre en œuvre.

2. Perspectives

Les perspectives proposées abordent dans un premier temps le développement et la validation expérimentale de l'essai de biodétérioration. Les paragraphes suivant proposent dans un second temps, le couplage d'une approche expérimentale et d'une approche modélisation, qui associée aux expériences proposées, faisant écho aux questions soulevées durant ce projet de recherche, devrait permettre d'approfondir les connaissances et ainsi d'améliorer la description, la quantification et donc la maitrise des phénomènes participant à la biodétérioration des matrices cimentaires en réseau d'assainissement.

2.1. Validation de l'essai de biodétérioration

Le dispositif expérimental proposé a montré à travers différentes approches, sa pertinence et son efficacité, en particulier sur l'étude des intéractions entre activité microbienne et devenir des revêtements cimentaire**.** Afin de valider le dispositif expérimental en tant qu'essai de biodétérioration il est nécessaire d'évaluer sa reproductibilité et de quantifier l'accélération des processus mis en jeu. Pour cela, après une adaptation des modes d'apport de la solution de culture, afin d'optimiser et de sécuriser le ratio flux d'acide produit et surface exposée, il apparait nécessaire de multiplier les expériences :

- Sur des matériaux identiques, dans des conditions identiques pour évaluer la reproductibilité du dispositif, et donc la sensibilité du dispositif.
- Sur des revêtements différents, dans des conditions identiques pour évaluer la discrimination entre différents produits.
- Dans des conditions opératoires différentes, en particulier la température, pour évaluer l'intensification des processus.
- De confronter ces expériences à des résultats obtenus sur des sites réels instrumentés afin d'évaluer le facteur d'accélération. Ce facteur d'accélération permettrait d'évaluer l'impact des matériaux en terme d'implantation d'une activité sulfo-oxydante et donc d'évaluer un gain en durée de vie des revêtements testés.

De plus, le développement d'un test nécessite une mesure quantifiable et comparable afin d'évaluer les performances des revêtements les uns par rapport aux autres, et ce également par

rapport à des vitesses de détériorations observées sur site réel. Actuellement, au niveau du dispositif proposé, même si une quantification des cations lixiviés est assurée, ainsi que les sulfates et l'acide produit biologiquement, la complexité du phénomène de biodétérioration couplant dissolution en surface du produit et précipitation de composés secondaires à l'interieur du revêtement, nécessite encore une évaluation des mesures pertinentes permettant la définition d'indicateurs quantitatifs d'évaluation de la résistance des revêtements.

En termes d'accélération des processus mis en jeu, la charge en composés soufrés à l'entrée sera augmentée, de plus, l'utilisation de tetrathionate en tant que source de soufre devrait permettre une accentuation, pour la même quantité de soufre oxydé, de la production d'acide.

2.2. Activité microbienne durant la détérioration des matrices cimentaires

Les expériences proposées pour confirmer les performances de l'essai, associée à une étude quantitative et qualitative des activtés et des populations microbiennes, permettront l'étude conjointe des interactions entre les communautés microbiennes et les différerents types de revêtements testés et ce par :

- Une analyse physico-chimiques des interactions eau / matériaux et leur possible impact sur la composition et la structure des consortia microbiens selectionés.
- Une analyse quantitive de la biomasse cultivée, de sa composition (C/N/P), et des populations sélectionnées, et ce en fonction des conditions de croissances et des revêtements supports.
- Une analyse des molécules structurelles des aggrégats microbiens (exopolymères), afin d'évaluer leurs rôles dans la biodétérioration (actions directes sur les matériaux, structuration et maintien des microorganismes au contact des matériaux) et leurs specificités en fonction des conditions de croissances et des revêtements supports.
- La structure du système d'étude permet également d'envisager le contrôle de l'implantation d'une activité hétérotrophe conjointe à l'implantation d'une activité sulfo-oxydante, et ainsi d'assurer par une approche relative, le rôle peu étudié des acitivtés microbiennes associées (bacétériennes et/ou fongiques), et ce toujours en fonction des conditions de croissances couplées aux revêtements supports.

2.3. Modélisation des transformations

A partir de la même approche que celle proposée durant ce projet de recherche, couplant expériences ciblées et développement d'un modèle dynamique, les conditions d'utilisations du modèle pourront être augmentées, en particulier en ce qui concerne l'influence de certains composés participant à la définition de la phase soluble lors de la dissolution des matériaux, tels que les ions calcium, les ions aluminium, les ions ferreux… etc.

Associées aux analyses dynamiques réalisées au niveau des lixiviats et sur les matériaux, un modèle de transports/réactions pourra être proposé afin de représenter dans le temps l'évolution à l'échelle pilote des interactions consortia microbiens et revêtements cimentaires. Une telle approche numérique devrait permettre :

- Dans un premier temps, de quantifier l'importance des précipitations secondaires en termes d'accélération des processus (gypse et ettringite) ou de ralentissement (gel d'hydroxyde d'aluminium).
- Dans un second temps d'évaluer et de proposer des modes de représentation de la détérioration des revêtements cimentaires.

Liste des références

A, B

Abtp,2006, Renforcement d'ouvrages d'assainissement visitables au moyen de matériaux composites. Annales du Bâtiment et des Travaux Publics, 3, 51-60.

Alcantara, S.,2004, Sulfur formation by steady-state continuous cultures of a sulfoxidazing consortium and Thiobacillus thioparus ATCC 23645. Environ. Technol., 25, 1151-1157.

Alexander, M. G.et Fourie, C. W.,2001, Acid resistance of calcium aluminate cement in concrete sewer pipe mixtures. Calcium Aluminate Cements 2001, 633-645.

Alexander, M.G., Goyns, A. and Fourie, C.W., 2008, Experiences with a full-scale experimental sewer made with CAC and other cementitious binders in Virginia, South Africa. Proceedings, Calcium Aluminate Cements, The Centenary Conference, Bracknell: IHS BRE Press, 279-292.

Alexander, M. G.et Fourie, C.,2011, Performance of sewer pipe concrete mixtures with portland and calcium aluminate cements subject to mineral and biogenic acid attack. Materials and Structures, 44, 313-330.

Alexander, M., Bertron, A., and De Belie, N., 2013. Performance of Cement-Based Materials in Aggressive Aqueous Environments: state of the art. RILEM, Book, Springer.

Allahverdi, A.et Skvara, F.,2000a, Acidic corrosion of hydrated cement based materials - Part 2. Kinetics of the phenomenon and mathematical models. Ceramics-Silikaty, 44, 152-160.

Allahverdi, A.et Skvara, F.,2000b, Acidic corrosion of hydrated cement based materials Part 1. - Mechanism of the phenomenon. Ceramics-Silikaty, 44, 114-120.

Allahverdi, A.et Skvara, F.,2005, Sulfuric acid attack on hardened paste of geopolymer cements Part 1. Mechanism of corrosion at relatively high concentrations. Ceramics-Silikaty, 49, 225-229.

Allahverdi, A.et Skvara, F.,2006, Sulfuric acid attack on hardened paste of geopolymer cements Part 2. corrosion mechanism at mild and relatively low concentrations. Ceramics-Silikaty, 50, 1-4.

Aouad, G. (2006) Influence de Pseudomonas Aeruginosa sur la dégradation des silicates. Strasbourg, Université Louis Pasteur.

Apha (2012) Standard Methods for the Examination of Water and Wastewater, 22nd Edition, Portland, American Public Health Association (APHA), American Water Works Association (AWWA) & Water Environment Federation (WEF).

Arliguie, G.et Hornain, H. (2007) GranDuBé: Grandeurs associées à la Durabilité des Bétons, Presses des Ponts.

Atkins, M., Glasser, F. P.et Kindness, A.,1992, Cement hydrate phase: Solubility at 25°C. Cement and Concrete Research, 22, 241.

Aviam, O., Bar-Nes, G., Zeiri, Y.et Sivan, A.,2004, Accelerated biodegradation of cement by sulfur-oxidizing bacteria as a bioassay for evaluating immobilization of low-level radioactive waste. Applied and Environmental Microbiology, 70, 6031-6036.

Baldensperger, Guarraiaet Humphreys,1974, Scanning electron microscopy of Thiobacilli grown on colloidal sulfur. Archive of Microbiology, 99, 323-329.

Beddoe, R. E.et Dorner, H. W.,2005, Modelling acid attack on concrete: Part I. The essential mechanisms. Cement and Concrete Research, 35, 2333-2339.

Beffa, T., Berczy, M.et Aragnok, M.,1991, Chemolithoautotrophic growth on elemental sulfur (S°) and respiratory oxidation of S° by Thiobacillus versutus and another sulfur-oxidizing bacterium. FEMS Microbiology Letters, 84, 285-290.

Beller, H. R., Chain, P. S. G., Letain, T. E., Chakicherla, A., Larimer, F. W., Richardson, P. M., Coleman, M. A., Wood, A. P.et Kelly, D. P.,2006, The genome sequence of the obligately chemolithoautotrophic, facultatively anaerobic bacterium Thiobacillus denitfificans. Journal of Bacteriology, 188, 1473-1488.

Berland, J. M.et Juery, C. (2003) Colloque national du Cercle Français de l'Eau "Quel financement pour la politique de l'eau de demain".

Berndt, M. L.,2011, Evaluation of coatings, mortars and mix design for protection of concrete against sulphur oxidising bacteria. Construction and Building Materials, 25, 3893-3902.

Bertron, A. (2004) Durabilité des matériaux cimentaires soumis aux acides organiques: cas particulier des effluents d'élevage. Laboratoire Matériaux et Durabilité des Constructions, INSA-UPS. Toulouse, Institut National des Sciences Appliquées.

Bertron, A., Duchesne, J.et Escadeillas, G.,2005a, Accelerated tests of hardened cement pastes alteration by organic acids: analysis of the pH effect. Cement and Concrete Research, 35, 155-166.

Bertron, A., Duchesne, J.et Escadeillas, G.,2005b, Attack of cement pastes exposed to organic acids in manure. Cement & Concrete Composites, 27, 898-909.

Bertron, A., Duchesne, J.et Escadeillas, G.,2007, Degradation of cement pastes by organic acids. Materials and Structures, 40, 341-354.

Bertron, A., Escadeillas, G., De Parseval, P.et Duchesne, J.,2009, Processing of electron microprobe data from the analysis of altered cementitious materials. Cement and Concrete Research, 39, 929-935.

Bertron, A., Escadeillas, G.et Duchesne, J.,2004, Cement pastes alteration by liquid manure organic acids: Chemical and mineralogical characterization. Cement and Concrete Research, 34, 1823-1835.

Bielefeldt, A., Guadalupe, M., Gutierrez-Padilla, M. G. D., Ovtchinnikov, S., Silverstein, J.et Hernandez, M.,2010, Bacterial Kinetics of Sulfur Oxidizing Bacteria and Their Biodeterioration Rates of Concrete Sewer Pipe Samples. Journal of Environmental Engineering-Asce, 136, 731-738.

Blight, K. R.et Ralph, D. E.,2008, Aluminium sulphate and potassium nitrate effects on batch culture of iron oxidising bacteria. Hydrometallurgy, 92, 130-134.

Borichewski,1967, Keto acids as growth-limiting factors in autrophic growth of thiobacillus thiooxidans. Journal Bacteriology, 93, 597 - 599.

Bosch, H., Versteeg, G. F.et Vanswaaij, W. P. M.,1989, Gas-Liquid Mass-Transfer with Parallel Reversible-Reactions.1. Absorption of CO_2 into Solutions of Sterically Hindered Amines. Chemical Engineering Science, 44, 2723-2734.

Buisman, C., Ijspeert, P., Janssen, A.et Lettinga, G.,1990, Kinetics of Chemical and Biological Sulfide Oxidation in Aqueous-Solutions. Water Research, 24, 667-671.

Butler, J. N.,1964, Ionic Equilibrium: A Mathematical Approach. Adison Westley, Reading, Mass, USA.

C, D

Carpentier, S.,2000, Renforcement d'un réseau d'assainissement unitaire. Chantiers de France, 332, 46-47.

Chabrelie, A., 2010. Mechanisms of degradation of concrete by external sulfate ions under laboratory and field conditions. Phd dissertation. EPFL, Lausanne.

Chang, J. H., Hocheng, H., Chang, H. Y.et Shih, A.,2008, Metal removal rate of Thiobacillus thiooxidans without pre-secreted metabolite. Journal of Materials Processing Technology, 201, 560-564.

Chen, K. Y.et Morris, J. C.,1972, Kinetics of Oxidation of Aqueous Sulfide by O2. Environmental Science & Technology, 6.

Chen, M. C., Zhang, Y. K., Zhong, B. H., Qiu, L. Y.et Liang, B.,2002, Growth kinetics of thiobacilli strain HSS and its application in bioleaching phosphate ore. Ind.Eng. Chem. Res., 41, 1329-1334.

Chistoserdova, L.,2011, Methylotrophy in a Lake: from Metagenomics to Single-Organism Physiology. Applied and Environmental Microbiology, 77, 4705-4711.

Cho, K. S.et Mori, T.,1995, A Newly Isolated Fungus Participates in the Corrosion of Concrete Sewer Pipes. Water Science and Technology, 31, 263-271.

Cohen, M. D.et Mather, B.,1991, Sulfate Attack on Concrete - Research Needs. Aci Materials Journal, 88, 62-69.

Col (2008) Colloque sur le développement durable des réseaux hydraulique. Colloque sur le développement durable des réseaux hydraulique. Bordeaux.

Connick, R.E., and Zhang Y.X., 1996. Kinetics and mechanism of the oxidation of HSO_3^- by O_2. 2. The manganese(II)-catalyzed reaction. Inorg. Chem., 35(16), 4613-4621.

CSTB-AGHTM (1989) Réhabilitation des réseaux d'assainissement. Synthèse des résultats de l'enquête menée en 1989, commission "Assainissement" de l'AGTHM, Groupe de travail "Réhabilitation".

Dam, B., Mandal, S., Ghosh, W., Das Gupta, S.K., and Roy, P., 2007. The S4-intermediate pathway for the oxidation of thiosulfate by the chemo-lithoautotroph *Tetrathiobacter kashmirensis* and inhibition of tetrathionate oxidation by sulfite. Res. Microbiol., 158,330-338

Danckwerts, P. V. (1970) Gas-liquid reactions, New York, McGraw-Hill Book Co.

Davis, R.E., 1958, Displacement Reactions at the Sulfur Atom. I. An Interpretation of the Decomposition of Acidified *Thiosulfate*. J. Am. Chem. Soc., 80(14),3565-3569.

Davis, J. L., Nica, D., Shields, K.et Roberts, D. J.,1998, Analysis of concrete from corroded sewer pipe. International Biodeterioration & Biodegradation, 42, 75-84.

De Belie, N., Monteny, J., Beeldens, A., Vincke, E., Van Gemert, D.et Verstraete, W.,2004, Experimental research and prediction of the effect of chemical and biogenic sulfuric acid on different types of commercially produced concrete sewer pipes. Cement and Concrete Research, 34, 2223-2236.

De Belie, N., Monteny, J.et Taerwe, L.,2002, Apparatus for accelerated degradation testing of concrete specimens. Materials and Structures, 35, 427-433.

De Muynck, W., De Belie, N.et Verstraete, W.,2009, Effectiveness of admixtures, surface treatments and antimicrobial compounds against biogenic sulfuric acid corrosion of concrete. Cement and Concrete Composites, 31, 163.

De Windt, L.et Devillers, P.,2010, Modeling the degradation of Portland cement pastes by biogenic organic acids. Cement and Concrete Research, 40, 1165-1174.

Diercks, M., Sand, W.et Bock, E.,1991, Microbial Corrosion of Concrete. Experientia, 47, 514-516.

Dinegar, R.H., Smellie, R.H., La Mer V.K., 1951, Kinetics of the Acid Decomposition of Sodium Thiosulfate in Dilute Solutions. J. Am. Chem. Soc., 73(5),2050-2054.

Dopson, M., Baker-Austin, C., Koppineedi, P. R.et Bond, P. L.,2003, Growth in sulfidic mineral environments: metal resistance mechanisms in acidophilic micro-organisms. Microbiology-Sgm, 149, 1959-1970.

Dowd, S. E., Hanson, J. D., Rees, E., Wolcott, R. D., Zischau, A. M., Sun, Y., White, J., Smith, D. M., Kennedy, J.et Jones, C. E.,2011, Survey of fungi and yeast in polymicrobial infections in chronic wounds. Journal of Wound Care, 20, 40-47.

Druschel, G. K., Hamers, R. J.et Banfield, J. F.,2003a, Kinetics and mechanism of polythionate oxidation to sulfate at low pH by O_2 and Fe^{3+}. Geochimica Et Cosmochimica Acta, 67, 4457-4469.

Druschel, G. K., Hamers, R. J., Luther, G. W.et Banfield, J. F.,2003b, Kinetics and mechanism of trithionate and tetrathionate oxidation at low pH by hydroxyl radicals. Aquatic Geochemistry, 9, 145-164.

Druschel, G. K., Luther, G. W.et Banfield, J. F.,2003c, Intermediate sulfur species in pyrite oxidation pathways. Abstracts of Papers of the American Chemical Society, 225, U916-U916.

E, F, G

Ehrich, S. (1998) Untersuchungen zur biogenen Schwefelsäurekorrosion von zementgebundenen Baustoffen. Hamburg, Hamburg University.

Ehrich, S., Helard, L., Letourneux, R., Willocq, J.et Bock, E.,1999, Biogenic and chemical sulfuric acid corrosion of mortars. Journal of Materials in Civil Engineering, 11, 340-344.

Ehrlich, H. L.et Newman, D. K. (2009) Geomicrobiology, Taylor & Francis Group.

Fattuhi, N. I.et Hughes, B. P.,1988, The performance of cement paste and concrete subjected to sulphuric acid attack. Cement and Concrete Research, 18, 545.

Fattuhi, N. I.et Hughes, B. P.,1989a, Ductility of Reinforced-Concrete Corbels Containing Either Steel Fibers or Stirrups. Aci Structural Journal, 86, 644-651.

Fattuhi, N. I.et Hughes, B. P.,1989b, Reinforced Steel Fiber Concrete Corbels with Various Shear Span-to-Depth Ratios. Aci Materials Journal, 86, 590-596.

Fischer, J., Quentmeier, A., Gansel, S., Sabados, V.et Friedrich, C. G.,2002, Inducible aluminum resistance of Acidiphilium cryptum and aluminum tolerance of other acidophilic bacteria. Archives of Microbiology, 178, 554-558.

Ghosh, W.et Bomba, D.,2009, Biochemistryandmolecular biologyof lithotrophic sulfuroxidation by taxonomicallyand ecologicallydiverse bacteria and archaea. FEMS Microbiol Rev, 33, 999-1043.

Girardi, F., Vaona, W.et Di Maggio, R.,2010, Resistance of different types of concretes to cyclic sulfuric acid and sodium sulfate attack. Cement & Concrete Composites, 32, 595-602.

Goldberg, R. N.et Parker, V. B.,1985, Thermodynamics of Solution of So2(G) in Water and of Aqueous Sulfur-Dioxide Solutions. Journal of Research of the National Bureau of Standards, 90, 341-358.

Gottschal, J. C., De Vries, S.et Kuenen, J. G.,1979, Competition between the facultatively chemolithotrophic Thiobacillus A2, an obligately chemolithotrophic Thiobacillus and a heterotrophie Spirillum for inorganic and organic substrates. Arch. Microbiol., 121, 241-249.

Graw, K. U.et Gruschwitz, C.,2000, Approaches for sewer network maintenance and rehabilitation planning. Lacer, 5, 541-550.

Grube, H.et Rechenberg, W.,1989, Durability of Concrete Structures in Acidic Water. Cement and Concrete Research, 19, 783-792.

Gu, J.-D., Ford, T. E., Berke, N. S.et Mitchell, R.,1998, Biodeterioration of concrete by the fungus Fusarium. International Biodeterioration & Biodegradation, 41, 101.

Guadalupe, M., Gutierrez-Padilla, M. G. D., Bielefeldt, A., Ovtchinnikov, S., Hernandez, M.et Silverstein, J.,2010, Biogenic sulfuric acid attack on different types of commercially produced concrete sewer pipes. Cement and Concrete Research, 40, 293-301.

Gubner (1998) Biofilms and accelerated low-water corrosion of carbon steel piling in tidal water. University of Portsmouth.

Guida, L., Saidi, Z., Hughes, M. N.et Poole, R. K.,1991, Aluminum Toxicity and Binding to Escherichia-Coli. Archives of Microbiology, 156, 507-512.

Gutiérrez-Padilla, M. G. D., Bielefeldt, A., Ovtchinnikov, S., Hernandez, M.et Silverstein, J.,2010, Biogenic sulfuric acid attack on different types of commercially produced concrete sewer pipes. Cement and Concrete Research, 40, 293.

H, I

Haile, T., Nakhla, G.et Allouche, E.,2008, Evaluation of the resistance of mortars coated with silver bearing zeolite to bacterial-induced corrosion. Corrosion Science, 50, 713.

Haile, T., Nakhla, G., Allouche, E.et Vaidya, S.,2010, Evaluation of the bactericidal characteristics of nano-copper oxide or functionalized zeolite coating for bio-corrosion control in concrete sewer pipes. Corrosion Science, 52, 45.

Hallberg, K.B., Dopson, M., Bo, E., Rje Lindstro, M., 1996. Journal of Bacteriology, 6-11.

Harrison,1984, The acidophilic Thiobacilli and other acidophilic bacteria that share their habitat. Annual Review of Microbiology, 38, 265-292.

Hazeu, W., Biileveld, W., Grotenhuis, J.T.C., Kakes, E., Kuenen,J.G., 1986, Kinetics and energetics of reduced sulfur oxidation by chemostat cultures of *Thiobacillus ferrooxidans*. Antonie van Leeuwenhoek, 52(6), 507-518.

Hazeu, Battenburg, Bos, Pas, V. D.et Kuenen, 1988, The production and utilization of intermediary elemental sulphur during the oxidation of reduced sulphur compounds by Thiobacillus ferrooxidans. Archive of Microbiology, 150, 574-579.

Hempfling, W. P.et Vishniac, W.,1967, Yield coefficients of Thiobacillus neapolitanus in continuous culture. J Bacteriol., 93, 874-878.

Herisson, J. (2012) Biodétérioration des matériaux cimentaires dans les ouvrages d'assainissement – Etude comparative du ciment d'aluminate de calcium et du ciment Portland. Structures et Matériaux. Paris, Université Paris-Est.

Herisson, J., Van Hullebusch, E. D., Moletta-Denat, M., Taquet, P.et Chaussadent, T.,2012, Toward an accelerated biodeterioration test to understand the behavior of Portland and calcium aluminate cementitious materials in sewers networks. International Biodeterioration & Biodegradation.

Hernandez, M., Marchand, E. A., Roberts, D.et Peccia, J.,2002, In situ assessment of active Thiobacillus species in corroding concrete sewers using fluorescent RNA probes. International Biodeterioration & Biodegradation, 49, 271-276.

Hormann, Hofmannet Schmidt (1997) Stability of concrete against biogenic sulphuric acid corrosion, a new method for determination. Proceedings of the 10th International Congress on the Chemistry of Cement. Gothenburg.

Hvitved-Jacobsen, T. (2002) Sewer Processes: Microbial and Chemical Process Engineering of Sewer, CRC Press LLC.

Hvitved-Jacobsen, T., Jütte, P., Nielsen, N.et Jensen, N. A. (1988) Hydrogen sulphide control in municipal sewers. Pretreatment in Chemical Water and Wastewater Treatment, proceedings of the 3rd International Gothenburg Symposium. Gothenburg, Sweden.

Hvitved-Jacobsen, T., Raunkjr, K.et Nielsen, P. H.,1995, Volatile fatty acids and sulfide in pressure mains. Water Science and Technology, 31, 169.

Hvitved-Jacobsen, T., Vollertsen, J.et Tanaka, N.,1999, Wastewater quality changes during transport in sewers - An integrated aerobic and anaerobic model concept for carbon and sulfur microbial transformations (vol 38, pg 257, 1998). Water Science and Technology, 39, 233-+.

Ifen,2006, L'assainissement en France en 1998 et 2001, Enquête "les collectivités locales et l'environnement", Volet assainissement. Les dossiers de l'Ifen, 3, 29.

Islander, R. L., Devinny, J. S., Mansfeld, F., Postyn, A.et Hong, S.,1991, Microbial Ecology of Crown Corrosion in Sewers. Journal of Environmental Engineering-Asce, 117, 751-770.

Ismail,1993, Effect of carbonation on microbial corrosion of concrete. journal of Construction Management and Engineering, 20, 133-138.

Israel, D., Macphee, D.et Lachowski, E.,1997, Acid attack on pore-reduced cements. Journal of Materials Science, 32, 4109.

J, K

Jauberthie, R., Robu, I., Lanos, C., Mortreuil, F.et Camps, J. P.,1998, X-ray diffraction characterization of the superficial attack of cement pastes in sulfate solutions. Journal De Physique Iv, 8, 519-523.

Jaworska, M.et Urbanek, A.,1997, The influence of carbon dioxide concentration in liquid medium on elemental sulphur oxidation by Thiobacillus thiooxidans. Bioprocess Engineering, 16, 361-365.

Jensen, H. S. (2009) Hydrogen sulfide induced concrete corrosion of sewer networks. Section of Environmental Engineering. Aalborg, Aalborg University.

Jensen, H. S., Lens, P. N. L., Nielsen, J. L., Bester, K., Nielsen, A. H., Hvitved-Jacobsen, T.et Vollertsen, J.,2011, Growth kinetics of hydrogen sulfide oxidizing bacteria in corroded concrete from sewers. Journal of Hazardous Materials, 189, 685-691.

Jensen, H. S., Nielsen, A. H., Hvitved-Jacobsen, T.et Vollertsen, J.,2008, Survival of hydrogen sulfide oxidizing bacteria on corroded concrete surfaces of sewer systems. Water Science And Technology, 57, 1721-1726.

Jensen, H. S., Nielsen, A. H., Hvitved-Jacobsen, T.et Vollertsen, J.,2009a, Modeling of Hydrogen Sulfide Oxidation in Concrete Corrosion Products from Sewer Pipes. Water Environment Research, 81, 365-373.

Jensen, H. S., Nielsen, A. H., Lens, P. N. L., Hvitved-Jacobsen, T.et Vollertsen, J.,2009b, Hydrogen sulphide removal from corroding concrete: Comparison between surface removal rates and biomass activity. Environmental Technology, 30, 1291-1296.

Jensen, N. A.,1995, Empirical modeling of air-to-water oxygen transfer in gravity sewers. Water Environment Research, 67, 979-991.

Jiang, F., Leung, D. H.-W., Li, S., Chen, G.-H., Okabe, S.et Van Loosdrecht, M. C. M.,2009, A biofilm model for prediction of pollutant transformation in sewers. Water Research, 43, 3187.

Johnston, F.et Mcamish, L.,1973, A Study of the Rates of Sulfur Production in Acid Thiosulfate Solutions Using S-35. Journal of Colloid and Interface Science, 42, 112 - 119.

Jorgensen, B.B., 1990, The sulfure cycle of freshwater sediments: Role of thiosulfate. Lirnnol. Oceanogr., 35(6), 1329-1342.

Joseph, A. P., Keller, J., Bustamante, H.et Bond, P. L.,2012, Surface neutralization and H_2S oxidation at early stages of sewer corrosion: Influence of temperature, relative humidity and H2S concentration. Water Research, 46, 4235 - 4245.

Kaempfer, W.et Berndt, M.,1999, Estimation of service life of concrete pipes in sewer networks. Durability of Building Materials and Components, 8, 36-45.

Kawai, F., Zhang, D. M.et Sugimoto, M.,2000, Isolation and characterization of acid- and Al-tolerant microorganisms. Fems Microbiology Letters, 189, 143-147.

Kelly, D. P.,1982, Biochemistry of the Chemolithotrophic Oxidation of Inorganic Sulfur. Philosophical Transactions of the Royal Society of London Series B-Biological Sciences, 298, 499-528.

Kelly D.P., 1989. Physiology and biochemistry of unicellular sulfur bacteria, In: Autotrophic Bacteria. HG. *Schlegel* and B. Bowien (Ed), 193-213.

Kelly, D. P.,1999, Thermodynamic aspects of energy conservation by chemolithotrophic sulfur bacteria in relation to the sulfur oxidation pathways. Archive Microbiology, 171, 219-229.

Kelly, D. P., Mcdonald, I. R.et Wood, A. P.,2000c, Proposal for the reclassification of Thiobacillus novellus as Starkeya novella gen. nov., comb. nov., in the alpha-subclass of the Proteobacteria. International Journal of Systematic and Evolutionary Microbiology, 50, 1797-1802.

Kelly, D. P., Shergill, J. K., W.P., L.et Wood, A. P.,1997, Oxidative metabolism of inorganic sulfur compounds by bacteria. Antonie van Leeuwenhoek, 71, 95-107.

Kelly, D. P.et Wood, A. P.,2000a, Confirmation of Thiobacillus denitrificans as a species of the genus Thiobacillus, in the beta-subclass of the Proteobacteria, with strain NCIMB 9548 as the type strain. International Journal of Systematic and Evolutionary Microbiology, 50, 547-550.

Kelly, D. P.et Wood, A. P.,2000b, Reclassification of some species of Thiobacillus to the newly designated genera Acidithiobacillus gen. nov., Halothiobacillus gen. nov. and Thermithiobacillus gen. nov. Int. J. Syst. Evol. Microbiol., 50, 511-516.

King, A. D., Ponting, J. D., Sanshuck, D. W., Jackson, R.et Mihara, K.,1981, Factors Affecting Death of Yeast by Sulfur-Dioxide. Journal of Food Protection, 44, 92-97.

Koch, I. H., Gich, F., Dunfield, P. F.et Overmann, J.,2008, Edaphobacter modestus gen. nov., sp nov., and Edaphobacter aggregans sp nov., acidobacteria isolated from alpine and forest soils. International Journal of Systematic and Evolutionary Microbiology, 58, 1114-1122.

Konishi, Y., Asai, S.et Yoshida, N.,1995, Growth-Kinetics of Thiobacillus Thiooxidans on the Surface of Elemental Sulfur. Applied and Environmental Microbiology, 61, 3617-3622.

Krotonarou, A.et Hoffman, M. R.,1991, Catalytic auto-oxidation of hydrogen-sulfide in wastewater. Environmental Science & Technology, 25, 1153-1160.

Kumar, P. S., Brooker, M. R., Dowd, S. E.et Camerlengo, T.,2011, Target Region Selection Is a Critical Determinant of Community Fingerprints Generated by 16S Pyrosequencing. Plos One, 6.

L, M

Lamberet, S. (2005) Durabilty of ternary binders based on portland cement, calcium aluminate cement and calcium sulfate. Section des matériaux. Lausanne, Ecole polytechnique et fédérale de Lausanne.

Lancia, A., Musmarra, D., Prisciandari, M., Tammaro, M., 1999, Catalytic oxidation of calcium bisulfite in the wet limestone-gypsum flue gas desulfurization process. Chemical Engineering Science, 54, 3019-3026.

Larreur-Cayol, S., Bertron, A.et Escadeillas, G.,2011, Degradation of cement-based materials by various organic acids in agro-industrial waste-waters. Cement and Concrete Research, 41, 882-892.

Le Gauffre, P., Joannis, C., Breysse, D., Gibello, C.et Desmulliez, J. J. (2004) Gestion patrimoniale des réseaux d'assainissements urbains, Guide méthodologique, Lavoisier.

Lea (1970) The chemistry of Cement and Concrete, London, Edward Arnold Ltd.

Lemaître, C., Pébère, N.et Festy, D. (1998) Biodétérioration des matériaux.

Lerm (2007) Pathologies des réseaux d'assainissement, Dossier technique. IN WWW.LERM.FR (Ed.).

Letourneux, R.et Scrivener, K. L.,1999, The resistance of calcium aluminate cements to acid corrosion in sea water applications. Modern concrete materials: binders, additions and admixtures.

Lide, D. R. (1990) CRC Handbook of Chemistry and Physics, Boca Raton (FL), CRC Press.

Linek, V.et Vacek, V.,1981, Chemical-Engineering Use of Catalyzed Sulfite Oxidation-Kinetics for the Determination of Mass-Transfer Characteristics of Gas-Liquid Contactors. Chemical Engineering Science, 36, 1747-1768.

Loewenthal, R. E., Ekama, G. A.et Marais, G.,1989, Mixed Weak Acid-Base Systems.1. Mixture Characterization. Water Sa, 15, 3-24.

Loewenthal, R. E., Wentzel, M. C., Ekama, G. A.et Marais, G. R.,1991, Mixed Weak Acid-Base Systems.2. Dosing Estimation, Aqueous Phase. Water Sa, 17, 107-122.

Lu, W.P., Kelly, D.P., 1988, Kinetic and Energetic Aspects of Inorganic Sulphur Compound Oxidation by *Thiobacillus tepidarius.* Microbiology, 134(4),865-876.

Maahs, H.G., 1982, Sulfur-dioxide/water equilibria between 0 and 50 C. An examination of data at low concentrations in Heterogeneous Atmospheric Chemistry, Geophysical Monograph 26. Am. Geophys. Union, Washington, D.C., 187-195.

Macdonald, T. L.et Martin, R. B.,1988, Aluminum Ion In Biological-Systems. Trends In Biochemical Sciences, 13, 15-19.

Madsen, H. I., Hvitved-Jacobsen, T.et Vollertsen, J.,2006, Gas phase transport in gravity sewers - A methodology for determination of horizontal gas transport and ventilation. Water Environment Research, 78, 2203-2209.

Maeda, T., Negishi, A., Komoto, H., Oshima, Y., Kamimura, K.et Sugio, T.,1999, Isolation of Iron-Oxidizing Bacteria from Corroded Concretes of Sewage Treatment Plants. Journal of Bioscience and Bioengineering, 88, 300-305.

Malik, A., Dastidar, M. G.et Roychoudhury, P. K.,2004, Factors limiting bacterial iron oxidation in biodesulphurization system. International Journal of Mineral Processing, 73, 13-21.

Masau, R. J. Y., Oh, J. K.et Suzuki, I.,2001, Mechanism of oxidation of inorganic sulfur compounds by thiosulfate-grown Thiobacillus thiooxidans. Canadian Journal of Microbiology, 47, 348-358.

Mason, J., Kelly, D. P.et Wood, A. P.,1987, Chemolithotrophic and Autotrophic Growth of Thermothrix thiopura and Some Thiobacilli on Thiosulphate and Polythionates, and a Reassessment of the Growth Yields of Thx. thiopuru in Chemostat Culture. Journal of General Microbiology, 133, 1249-1256.

Metcalfet Eddy (2003) Wastewater engineering: treatment and reuse, New York, McGraw-Hill.

Meyer, W. J.,1980, Case-Study of Prediction of Sulfide Generation and Corrosion in Sewers. Journal Water Pollution Control Federation, 52, 2666-2674.

Milde, K., Sand, W.et Bock, E.,1983, Thiobacilli of the corroded concrete walls of Hamburg sewer system. Journal of General Microbiology, 129, 1327-1333.

Monteny, J., De Belie, N., Vincke, E., Verstraete, W.et Taerwe, L.,2001, Chemical and microbiological tests to simulate sulfuric acid corrosion of polymer-modified concrete. Cement and Concrete Research, 31, 1359-1365.

Monteny, J., Vincke, E., Beeldens, A., De Belie, N., Taerwe, L., Van Gemert, D.et Verstraete, W.,2000, Chemical, microbiological, and in situ test methods for biogenic sulfuric acid corrosion of concrete. Cement and Concrete Research, 30, 623-634.

Mori, T., Nonaka, T., Tazaki, K., Koga, M., Hikosaka, Y.et Noda, S.,1992, Interactions of Nutrients, Moisture and Ph on Microbial Corrosion of Concrete Sewer Pipes. Water Research, 26, 29-37.

Mortezania, S.et Othman, F.,2012, Cost analysis of pipes for application in sewage systems. Materials & Design, 33, 356-361.

Munz, G., Gori, R., Mori, G., Lubello, C., 2009, Monitoring biological sulphide oxidation processes using combined respirometeric and titrimetric techniques. Chemosphere, 76, 644-650.

Musvoto, E. V., Wentzel, M. C., Loewenthal, R. E.et Ekama, G. A.,1997, Kinetic-based model for mixed weak acid/base systems. Water Sa, 23, 311-322.

Musvoto, E.V., Wentzel, M.C., Loewenthal, R.E. et Ekama, G.A., 1998. Mathematical modelling of integrated chemical, physical and biological treatment of wastewaters. *Research Report W97*, Dept. Civil Eng., Univ. Cape Town, Rondebosch 7701, Cape Town, South Africa.

Musvoto, E. V., Wentzel, M. C., Loewenthal, R. E.et Ekama, G. A.,2000, Integrated chemical-physical processes modelling - I. Development of a kinetic-based model for mixed weak acid/base systems. Water Research, 34, 1857-1867.

N, O

Nica, D., Davis, J. L., Kirby, L., Zuo, G.et Roberts, D. J.,2000, Isolation and characterization of microorganisms involved in the biodeterioration of concrete in sewers. International Biodeterioration & Biodegradation, 46, 61-68.

Nielsen, A. H., Hvitved-Jacobsen, T.et Vollertsen, J.,2005a, Kinetics and stoichiometry of sulfide oxidation by sewer biofilms. Water Research, 39, 4119-4125.

Nielsen, A. H., Hvitved-Jacobsen, T.et Vollertsen, J.,2006a, Recent findings on sinks for sulfide in gravity sewer networks. Water Science and Technology, 54, 127-134.

Nielsen, A. H., Hvitved-Jacobsen, T.et Vollertsen, J.,2008b, Effects of pH and iron concentrations on sulfide precipitation in wastewater collection systems. Water Environment Research, 80, 380-384.

Nielsen, A. H., Lens, P., Vollertsen, J.et Hvitved-Jacobsen, T.,2005b, Sulfide-iron interactions in domestic wastewater from a gravity sewer. Water Research, 39, 2747-2755.

Nielsen, A. H., Vollertsen, J.et Hvitved-Jacobsen, T.,2003, Determination of kinetics and stoichiometry of chemical sulfide oxidation in wastewater of sewer networks. Environmental Science & Technology, 37, 3853-3858.

Nielsen, A. H., Vollertsen, J.et Hvitved-Jacobsen, T.,2006b, Kinetics and stoichiometry of aerobic sulfide oxidation in wastewater from sewers - Effects of pH and temperature. Water Environment Research, 78, 275-283.

Nielsen, A. H., Vollertsen, J.et Jacobsen, T. H.,2004, Chemical sulfide oxidation of wastewater - effects of pH and temperature. Water Science and Technology, 50, 185-192.

Nielsen, A. H., Vollertsen, J., Jensen, H. S., Wium-Andersen, T.et Hvitved-Jacobsen, T.,2008a, Influence of pipe material and surfaces on sulfide related odor and corrosion in sewers. Water Research, 42, 4206.

Nielsen, A. H., Yongsiri, C., Hvitved-Jacobsen, T.et Vollertsen, J.,2005c, Simulation of sulfide buildup in wastewater and atmosphere of sewer networks. Water Science and Technology, 52, 201-208.

Norsker, N. H., Nielsen, P. H.et Hvitved-Jacobsen, T.,1995, Influence of Oxygen on Biofilm Growth and Potential Sulfate Reduction in Gravity Sewer Biofilm. Water Science and Technology, 31, 159-167.

Ochoa Chavez, J. C. (2009) Analyse de l'influence de l'hydodynamique locale sur le détachement des biofilms. Toulouse, INSA Toulouse.

Okabe, S., Odagiri, M., Ito, T.et Satoh, H.,2007, Succession of sulfur-oxidizing bacteria in the microbial community on corroding concrete in sewer systems. Applied and Environmental Microbiology, 73, 971-980.

P, Q

Page, F. M.,1953, The dissociation constants of thiosulphuric acid. J. Chem. Soc., 1719-1724.

Parker, C. D.,1945, The corrosion of concrete. I. The isolation of a species of bacterium associated with corrosion of concrete exposed to atmospheres containing hydrogen sulphide. Experimental Biology and Medecine Journal, 23, 81-90.

Parker, C. D.,1951, Mechanics of Corrosion of Concrete Sewers by Hydrogen Sulfide. Sewage and Industrial Wastes, 23, pp. 1477-1485.

Parker, C. D.et Jackson, D. (1965) The microbial flora of concrete surfaces. Hydrogen Sulfide Corrosion of Concrete Sewers, Technical Paper. Melbourne, Australia, Melbourne and Metropolitan Board of Works.

Parker, C. D.et Prisk, J.,1953, The oxidation of inorganic compounds of sulphur by various sulphur bacteria. J. gen. Microbial., 8, 344-364.

Pascal, P. (1961) Nouveau traité de chimie minérale, Paris, Masson et Cie, Editeurs.

Pavlik, V.,1994a, Corrosion of Hardened Cement Paste by Acetic and Nitric-Acids.1. Calculation of Corrosion Depth. Cement and Concrete Research, 24, 551-562.

Pavlik, V.,1994b, Corrosion Of Hardened Cement Paste By Acetic And Nitric-Acids.2. Formation And Chemical-Composition Of The Corrosion Products Layer. Cement And Concrete Research, 24, 1495-1508.

Pavlik, V.,1996, Corrosion of hardened cement paste by acetic and nitric acids.3. Influence of water cement ratio. Cement and Concrete Research, 26, 475-490.

Pomeroy, R. D.et Boon, A. G. (1990) The problem of hydrogen sulphide in sewers, Westminter, Acer John Taylor.

Pomeroy, R. D.et Parkhurst, J. D.,1977, Forecasting of Sulfide Buildup Rates in Sewers. Progress in Water Technology, 9, 621-&.

Pronk, J. T., Debruijn, P., Vandijken, J. P., Bos, P.et Kuenen, J. G.,1990a, Energetics of Mixotrophic and Autotrophic-C1-Metabolism by Thiobacillus-Acidophilus. Archives of Microbiology, 154, 576-583.

Pronk, J. T., Meesters, P. J. W., Vandijken, J. P., Bos, P.et Kuenen, J. G.,1990b, Heterotrophic Growth of Thiobacillus-Acidophilus in Batch and Chemostat Cultures. Archives of Microbiology, 153, 392-398.

Pronk, J. T., Meulenberg, R., Hazeu, W., Bos, P.et Kuenen, J. G.,1990c, Oxidation of Reduced Inorganic Sulfur-Compounds by Acidophilic Thiobacilli. Fems Microbiology Reviews, 75, 293-306.

Pronk, J. T., Meulenberg, R., Vandenberg, D. J. C., Batenburgvandervegte, W., Bos, P.et Kuenen, J. G.,1990d, Mixotrophic and Autotrophic Growth of Thiobacillus-Acidophilus on Glucose and Thiosulfate. Applied and Environmental Microbiology, 56, 3395-3401.

R

Raven, J. A.et Scrimgeour, C. M.,1997, The influence of anoxia on plants of saline habitats with special reference to the sulphur cycle. Annals of Botany, 79, 79-86.

Reichert, P.,1994, Aquasim - a Tool for Simulation and Data-Analysis of Aquatic Systems. Water Science and Technology, 30, 21-30.

Rendell, F.et Jauberthie, R.,1999, The deterioration of mortar in sulphate environments. Construction and Building Materials, 13, 321-327.

Rendell, F.et Jauberthie, R. (2002) Ammonium sulfate attack on cement mortar. IN MPG BOOKS (Ed.) Concrete for extreme conditions: Proceedings of international conference. Bodmin, Cornwall.

Rerau (2002-2004) Restructuration des collecteurs visitables, Guide technique, Lavoisier.

Revertegat, E., Richet, C.et Gégout, P.,1992, Effect of pH on the durability of cement pastes. Cement and Concrete Research, 22, 259.

Rigdon, J. H.et Beardsley, C. W.,1956, Corrosion of concrete by autotrophes. Corrosion, 14, 60-62.

Roberts, D. J., Nica, D., Zuo, G.et Davis, J. L.,2002, Quantifying microbially induced deterioration of concrete: initial studies. International Biodeterioration & Biodegradation, 49, 227-234.

Romben, L.,1978, Aspects on testing methods for acid attack on concrete. CBI Forsk 78, 1, 1-61.

Roux, S. (2008) Evaluation des risques de biodégradation des bétons en contact avec une eau douce naturelle. Strasbourg, École Doctorale Mathématiques, Sciences de l'Information et de l'Ingénieur.

Roux, S., Feugeas, F., Géraud, Y.et Cornet, A. (2008) Caractérisation de la porosité de différents matériaux cimentaires pour l'étude de leur résistance à la biodégradation, influence des milieux. XXVIe Rencontres Universitaire Génie Civil. Nancy.

S

Sadowski, A. G. (2005) Synthèse sur l'hydrogène sulfuré et son traitement, Rapport du Laboratoire de Recherche SHU-ENGEES.

Sand, W.,1987, Importance of Hydrogen-Sulfide, Thiosulfate, and Methylmercaptan for Growth of Thiobacilli during Simulation of Concrete Corrosion. Applied and Environmental Microbiology, 53, 1645-1648.

Sand, W.,1997, Microbial mechanisms of deterioration of inorganic substrates--A general mechanistic overview. International Biodeterioration & Biodegradation, 40, 183.

Sand, W.et Bock, E.,1984, Concrete corrosion in the Hamburg sewer system. Environmental Technology Letters, 5, 517-528.

Sand, W.et Bock, E.,1991, Biodeterioration of Mineral Materials by Microorganisms - Biogenic Sulfuric and Nitric-Acid Corrosion of Concrete and Natural Stone. Geomicrobiology Journal, 9, 129-138.

Sand, W., Bock, E.et White, D. C.,1987, Biotest System for Rapid Evaluation of Concrete Resistance to Sulfur-Oxidizing Bacteria. Materials Performance, 26, 14-17.

Sand, W., Milde, K.et Bock, E.,1983, Simulation of concrete corrosion in a strictly controlled H2S-breeding chamber. G. Rossi and A.E. Torma (ed), 667-677.

Sato, H., Hirose, T., Kimura, T., Moriyama, Y.et Nakashima, Y.,2001, Analysis of malodorous volatile substances of human waste: Feces and urine. Journal of Health Science, 47, 483-490.

Satoh, H., Odagiri, M., Ito, T.et Okabe, S.,2009, Microbial community structures and in situ sulfate-reducing and sulfur-oxidizing activities in biofilms developed on mortar specimens in a corroded sewer system. Water Research, 43, 4729-4739.

Saucier, F.et Lamberet, S. (2009) Calcium aluminate concrete for sewers: going from qualitative to quantitative evidence of performance. Concrete in aggressive aqueous environments, performance, testing and modeling. Toulouse.

Sauve, V., Bruno, S., Berks, B.C. et Hemmings, A.M., 2007, The SoxYZ complex carries sulfur cycle intermediates on a peptide swinging arm. J Biol Chem, 282, 23194-23204.

Schloss, P. D.,2009, A High-Throughput DNA Sequence Aligner for Microbial Ecology Studies. Plos One, 4.

Schloss, P. D., Westcott, S. L., Ryabin, T., Hall, J. R., Hartmann, M., Hollister, E. B., Lesniewski, R. A., Oakley, B. B., Parks, D. H., Robinson, C. J., Sahl, J. W., Stres, B., Thallinger, G. G., Van Horn, D. J.et Weber, C. F.,2009, Introducing mothur: Open-Source, Platform-Independent, Community-Supported Software for Describing and Comparing Microbial Communities. Applied and Environmental Microbiology, 75, 7537-7541.

Schmidt, M., Hormann, K., Hofmann, F. J.et Wagner, E.,1997, Beton mit erhöhtem Widerstand gegen Säure und Biogene Schwefelsäurekorrosion. Concrete Precasting Plant Technology, 4, 64-70.

Schneider, U.et Chen, S. W.,2005, Deterioration of high-performance concrete subjected to attack by the combination of ammonium nitrate solution and flexure stress. Cement and Concrete Research, 35, 1705-1713.

Schreiber, D.C., Pavlostathis, S.G., 1998, Biological oxidation of thiosulfate in mixed heterotrophic/autotrophic cultures. Water Reasearch, 32(5), 1363-1372.

Schroeter, L. (1996) Sulfur dioxide: Applications in Foods, Beverages and pharmaceuticals, Long Island City, Scientific Commitee for Food.

Scrivener, K. L.,2009, Importance of microstructural understanding for durable and sustainable concrete. Concrete Repair, Rehabilitation and Retrofitting Ii, 11-17.

Scrivener, K. L., Cabiron, J.-L.et Letourneux, R.,1999, High-performance concretes from calcium aluminate cements. Cement and Concrete Research, 29, 1215.

Shakhashiri, B. Z. (1992) Chemical Demonstrations, Volume 3: A Handbook for Teachers of Chemistry.

Sharma, K. R.et Yuan, Z. (2010) Kinetic of chemical sulfide oxidation under high dissolved oxygen levels. 6th International Conference on Sewer Processes and Networks. Surfers Paradise, Gold Coast, Australia.

Sharma, K. R., Yuan, Z., De Haas, D., Hamilton, G., Corrie, S.et Keller, J.,2008, Dynamics and dynamic modelling of H2S production in sewer systems. Water Research, 42, 2527.

Shooner, F., Bousquet, J.et Tyagi, R. D.,1996, Isolation, phenotypic characterization, and phylogenetic position of a novel, facultatively autotrophic, moderately thermophilic bacterium, Thiobacillus thermosulfatus sp nov. International Journal of Systematic Bacteriology, 46, 409-415.

Sivaji Rao, S.G. et Berger, L.R.,1971, The Requirement of Low pH for Growth of Thiobacillus thiooxidans. Arch. Mikrobiol., 79, 338-334.

Sotemann, S.W., Musvoto, E.V., Wentzel, M.C. et Ekama, G.A., 2005, Integrated biological, chemical and physical processes kinetic modelling Part 1 - Anoxic-aerobic C and N removal in the activated sludge system. Water Sa, 31, 529-544.

Sperandio, M., et Paul, E., 1997. Determination of carbon dioxide evolution rate using on-line gas analysis during dynamic biodegradation experiments. Biotechnology and Bioengineering, 53(3), 243-252.

Stanier, R. Y., Ingraham, J. L., Wheels, M. L.et Paainter, P. R. (1986) The Microbial World, Englewood Cliffs.

Starkey, R. L.,1935, Productsof the oxidation of thiosulfate by bacteria in mineral media. J Gen Physiol., 18, 325-349.

Stefess, G. C., Torremans, R. A. M., De Schrijver, R., Robertson, L. A.et Kuenen, J. G.,1996, Quantitative measurement of sulphur formation bysteady-state and transient-state continuous cultures of autotrophicThiobacillus species. Appl. Microbiol. Biotechnol., 45, 169-175.

Steudel, R., 1987. Recent Developments in the Chemistry of Elemental Sulfur and Sulfur-Rich Compounds. Int. Symposium *Elemental Sulfur in Agriculture*, Proceedings, Acropolis, Nice, France, 1, 7-16.

Steudel, R., 1989. On the Nature of the "Elemental sulfur" (S^0) produced by sulfur-oxidizing-bacteria, a model for S^0 globules. In: Autotrophic Bacteria. HG. *Schlegel* and B. Bowien (Ed), 289-303.

Steudel, R.,1996, Mechanism for the formation of elemental sulfur from aqueous sulfide in chemical and microbiological desulfurization processes. Industrial & Engineering Chemistry Research, 35, 1417-1423.

Suez (2008) Outils de modélisation d'émission d'H2S. Suez Environnement.

Suzuki, I., Lee, D., Mackay, B., Harahuc, L.et Oh, J. K.,1999, Effect of various ions, pH, and osmotic pressure on oxidation of elemental sulfur by Thiobacillus thiooxidans. Applied and Environmental Microbiology, 65, 5163-5168.

Sydney, R., Esfandi, E.et Surapaneni, S.,1996, Control concrete sewer corrosion via the crown spray process. Water Environment Research, 68, 338-347.

T, U

Taeil, P.et Hyoungkwan, K.,2013, A data warehouse-based decision support system for sewer infrastructure management. Automation in Construction, Volume 30, Pages 37–49.

Tanaka, N.et Hvitved-Jacobsen, T.,1998, Transformations of wastewater organic matter in sewers under changing aerobic/anaerobic conditions. Water Science and Technology, 37, 105-113.

Tazaki, K., Mori, T.et Nonaka, T.,1992, Microbial Jarosite and Gypsum from Corrosion of Portland-Cement Concrete. Canadian Mineralogist, 30, 431-444.

Tazawa, E. I., Morinaga, T.et Kawai, K. (1994) Deterioration of concrete derived from metabolites of microorganisms. Proceedings of 3rd CANMET/ACI International Conference on Durability of Concrete.

Thistlethwayte (1972) Control of Sulfide in Sewerage Systems, Michigan, Butterworth Pty. Ltd.

Thistlethwayte, D. K.et Goleb, E. E. (1972) Sewers and storm water. The composition of sewer air. Proc. of 16th Internationnal Congress. Jerusalem, Advances in Wat. Poll. Res.

Tian, B.et Cohen, M. D.,2000, Does gypsum formation during sulfate attack on concrete lead to expansion? Cement and Concrete Research, 30, 117.

Tichy, R., Janssen, A., Grotenhuis, J.T.C., Lettings, G., Rulkens, W.H., 1994, Possibilities for using biologically-produced sulphur for cultivation of *Thiobacilli* with respect to bioleaching processes. Bioresource Technology, 48(3), 221-227.

Timer-ten Hoor, A., 1981, Cell yield and bioenergetics of Thiomicrospira denitrificans compared with Thiobacillus denitrificans. Antonie Van Leeuwenhoek, 47(3), 231-43.

Torii, K.et Kawamura, M.,1994, Effects Of Fly-Ash And Silica Fume On The Resistance Of Mortar To Sulfuric-Acid And Sulfate Attack. Cement And Concrete Research, 24, 361-370.

Trüper, H. G.,1984, Microorganisms and sulphur cycle. Studies in Inorganic Chemistry, 351-365.

Tulliani, J. M., Montanaro, L., Negro, A.et Collepardi, M.,2002, Sulfate attack of concrete building foundations induced by sewage waters. Cement and Concrete Research, 32, 843-849.

Tuovinen, O., Niemelã¤, S.et Gyllenberg, H.,1971, Tolerance of<i>Thiobacillus ferrooxidans</i> to some metals. Antonie van Leeuwenhoek, 37, 489.

Ulrich, R.K., Rochelle, G.T., and Pradas, R.E., 1986. Enhanced oxygen absorption into bisulphite solutions containing transition metal ion catalysts. Chemical Engineering Science, 41(8), 2183-2191.

Usepa (1974) Process design manual for sulfide control in sanitary sewerage systems, EPAEPA 625/1-74-005.

V, W

Van Rensburg, P., Musvoto, E. V., Wentzel, M. C.et Ekama, G. A.,2003, Modelling multiple mineral precipitation in anaerobic digester liquor. Water Research, 37, 3087-3097.

Vincke, E., Boon, N.et Verstraete, W.,2001, Analysis of the microbial communities on corroded concrete sewer pipes - a case study. Applied Microbiology and Biotechnology, 57, 776-785.

Vincke, E., Van Wanseele, E., Monteny, J., Beeldens, A., De Belie, N., Taerwe, L., Van Gemert, D.et Verstraete, W.,2002, Influence of polymer addition on biogenic sulfuric acid attack of concrete. International Biodeterioration & Biodegradation, 49, 283-292.

Vincke, E., Verstichel, S., Monteny, J.et Verstraete, W.,1999, A new test procedure for biogenic sulfuric acid corrosion of concrete. Biodegradation, 10, 421-428.

Vollertsen, J., Hvitved-Jacobsen, T.et Nielsen, A. H.,2005, Stochastic Modeling of chemical oxygen demand transformations in gravity sewers. Water Environment Research, 77, 331-339.

Vollertsen, J., Nielsen, A. H., Jensen, H. S.et Hvitved-Jacobsen, T.,2008a, Modeling the formation and fate of odorous substances in collection systems. Water Environment Research, 80, 118-126.

Vollertsen, J., Nielsen, A. H., Jensen, H. S., Wium-Andersen, T.et Huitued-Jacobsen, T.,2008b, Corrosion of concrete sewers - The kinetics of hydrogen sulfide oxidation. Science of the Total Environment, 394, 162-170.

Wack, H., Pape, F.et Merretig-Bruns (2009) PATENT: Verfahreb und Bioreaktor zur Erzeugung eines Biofilm. Bundesrepublik Deutschland Deutsches Patent und Markenamt. Deustschland.

Wang, Z., Gerstein, M.et Snyder, M.,2009, RNA-Seq: a revolutionary tool for transcriptomics. Nature Reviews Genetics, 10, 57-63.

Wentzien, S., Sand, W., Albertsen, A., Steudel, R., 1994. Thiosulfate and tetrathionate degradation as well as biofilm generation by *Thiobacillus intermedius* and *Thiobacillus versutus* studied by microcalorimetry, HPLC, and ion-pair chromatography. Archives of Microbiology, 161(2), 116-125.

Wentzien, S. W.et Sand, W.,2004, Tetrathionate disproportionation by Thiomonas intermedia K12. Engineering in Life Sciences, 4, 25-30.

Werey, C., Rozan, A., Wittner, C., Le Gat, Y., Le Gauffre, P., Nirsimloo, K.et Leclercq, C.,2012, Gestion patrimoniale des réseaux d'assainissement: de l'état des réseaux à la planification de leur réhabilitation − Outils, méthodes et perspectives. Sciences Eaux et Territoires, 9, p.44-p.53.

Wilkinson, P.M., Doldbrsum, B., Crames, P.H.M.E., Van Dierendonck, L.L., 1993, The kinetics of uncatalyzed sodium sulfite oxidation. Chemical Engineeing Science, 48(5), 933-941.

Wilmot, P. D., Cadee, K., Katinic, J. J.et Kavanagh, B. V.,1988, Kinetics of Sulfide Oxidation by Dissolved-Oxygen. Journal Water Pollution Control Federation, 60, 1264-1270.

Wood, A.P.& Kelly, D.P., 1986, Chemolithotrophic metabolism of newly-isolated moderately thermophilic, obligately autotrophic Thiobacillus *tepidarus*. Arch. Microbiol., vol. 144(16),71-77.

X, Y, Z

Xu, Y., Choonen, M.A.A.S., Ordstrom, D.K.N., Unningham, K.M.C., All, J.W.B., 1998, Sulfure geochemistry of hydrothermal waters in Yellowstone National Park: I. The origin of thiosulfate in hot spring waters. Geochimica et Cosmochimica Acta, 62(23),3729-3743.

Yamanaka, T., Aso, I., Togashi, S., Tanigawa, M., Shoji, K., Watanabe, T., Watanabe, N., Maki, K.et Suzuki, H.,2002, Corrosion by bactera of concrete in sewerage systems and inhibitory effects of formats on their growth. Water Research, 36, 2636-2642.

Yongsiri, C., Hvitved-Jacobsen, T., Vollertsen, J.et Tanaka, N.,2003, Introducing the emission process of hydrogen sulfide to a sewer process model (WATS). Water Science and Technology, 47, 319-320.

Yongsiri, C., Vollertsen, J.et Hvitved-Jacobsen, T.,2004a, Effect of temperature on air-water transfer of hydrogen sulfide. Journal of Environmental Engineering-Asce, 130, 104-109.

Yongsiri, C., Vollertsen, J.et Hvitved-Jacobsen, T.,2004c, Hydrogen sulfide emission in sewer networks: a two-phase modeling approach to the sulfur cycle. Water Science and Technology, 50, 161-168.

Yongsiri, C., Vollertsen, J.et Hvitved-Jacobsen, T.,2005, Influence of wastewater constituents on hydrogen sulfide emission in sewer networks. Journal of Environmental Engineering-Asce, 131, 1676-1683.

Yongsiri, C., Vollertsen, J., Rasmussen, M.et Hvitved-Jacobsen, T.,2004b, Air-water transfer of hydrogen sulfide: An approach for application in sewer networks. Water Environment Research, 76, 81-88.

Yoon, J. H., Kang, S. J.et Oh, T. K.,2006, Dokdonella koreensis gen. nov., sp nov., isolated from soil. International Journal of Systematic and Evolutionary Microbiology, 56, 145-150.

Yoshida, N., Murooka, Y.et Ogawa, K.,1998, Heavy metal particle resistance in Thiobacillus intermedius 13-1 isolated from corroded concrete. Journal of Fermentation and Bioengineering, 85, 630-633.

Zaiser, E.M. and La Mer, V.K., 1948, J.Colloid Sci, 3, 571.

Zajic, J. E. (1969) Microbial Biogeochemistry, New York and London, Academic Press.

Zeebe, R. E.,2011, On the molecular diffusion coefficients of dissolved CO2, HCO3-, and CO32- and their dependence on isotopic mass. Geochimica Et Cosmochimica Acta, 75, 2483-2498.

Zemaitis, J. F. (1986) Handbook of aqueous electrolyte thermodynamics: Theory & application, New York, Design Institute for Physical Property Data sponsored by the American Institute of Chemical Engineers.

Zhang, L., De Schryver, P., De Gusseme, B., De Muynck, W., Boon, N.et Verstraete, W.,2008, Chemical and biological technologies for hydrogen sulfide emission control in sewer systems: A review. Water Research, 42, 1.

Zivica, V.et Bajza, A.,2001, Acidic attack of cement based materials - a review. Part 1. Principle of acidic attack. Construction and Building Materials, 15, 331-340.

Zivica, V.et Bajza, A.,2002, Acidic attack of cement-based materials - a review Part 2. Factors of rate of acidic attack and protective measures. Construction and Building Materials, 16, 215-222.

Annexes - Chapter III

I.
Théorie des équilibres gaz-liquide

II.
Bases théoriques du transfert de chaleur dans une canalisation

III.
Bases théoriques du transfert de chaleur dans une canalisation

I. Théorie des équilibres gaz-liquide

Concernant le paragraphe [1.1.2.] du chapitre III, au sein des deux zones de travail (vaporisation et condensation), le procédé est régi par un équilibre Gaz/Liquide. Le paragraphe suivant, afin de développer un modèle se propose de présenter la théorie de ces équilibres.

En termes de nomenclature, les exposants L et V correspondent respectivement à la phase liquide et à la phase vapeur, quand les indices i font références aux différents composés susceptibles de constituer les différentes phases. T correspond à la température de travail (vaporisation ou condensation), P à la pression au sein du pilote, alors que x et y correspondent respectivement à la fraction molaire du composé dans la phase liquide et dans la phase gaz considérée. $H_{i\text{-}S(T)}$ représente la constante de Henry du composé i dans le solvant S à la température T, et γ_i représente le coefficient d'activité du composé i.

L'équation de base de l'équilibre gaz-liquide est l'égalité des fugacités (f) de chaque composé dans les deux phases (Eq 92) :

Eq 92 : $f_i^{L}{}_{(T,P,x)} = f_i^{V}{}_{(T,P,y)}$

Au niveau de la phase gaz la fugacité peut s'écrire pour chaque composé i :

Eq 93 : $f_i^{V}{}_{(T,P,y)} = y_i.\phi_i^{V}{}_{(T,P,y)} \cdot P$

La pression au sein de l'ensemble du pilote étant faible (P = 1 bar), la phase gaz, quelle que soit la zone de travail, peut être assimilée à un mélange de gaz parfaits, donc :

Eq 94 : $\phi_i^{V}{}_{(T,P,y)} = 1 \rightarrow f_i^{V}{}_{(T,P,y)} = y_i \cdot P$

Au niveau de la phase liquide,

l'eau est considérée comme étant le solvant, sa fugacité peut donc s'écrire :

Eq 95 : $f_i^{L}{}_{(T,P,x)} = x_i.\gamma_i.P_{i(T)}^{sat}.exp\left[\int_{P_i^{sat}}^{P} \frac{v_i^*}{RT} dP\right]$

Avec l'expression $exp\left[\int_{P_i^{sat}}^{P} \frac{v_i^*}{RT} dP\right]$ correspondant au facteur correctif de Poynting

L'état de référence choisi pour la phase liquide est pure ce qui implique que pour l'eau :

$x_{eau} = 1$ et $\gamma_{eau} = 1$, et $P - P_{eau}^{sat}$ est faible alors le facteur correctif de Poynting = 1, donc :

Eq 96 : $f_{eau(T,P,x)}^{L} = x_{eau}.P_{eau(T)}^{sat}$

Dans le cas des solutés i la fugacité en phase liquide s'écrit :

Eq 97 : $f_i^{L}{}_{(T,P,x)} = x_i.\gamma'_i.H_{i-S(T)}.exp\left[\int_{P_{eaui}^{sat}}^{P} \frac{\bar{v}_i^{\infty}}{RT} dP\right]$

Les solutés sont très dilués donc $\gamma_i^L = 1$ et $P - P_{eau}^{sat}$ est faible, alors le facteur correctif de Poynting = 1

Donc, pour les différents solutés i l'expression de la fugacité est :

Eq 98 : $f_i^{L}{}_{(T,P,x)} = x_i.H_{i-S(T)}$

Nous avons donc à l'équilibre :

Dans le cas du solvant avec P = 1 bar:

Eq 99 : $y_{eau}.P = x_{eau}.P_{eau(T)}^{sat}$

Dans le cas des solutés avec P = 1 bar

Eq 100 : $x_i.H_{i-S(T)} = y_i.P$

A partir de ces équations, il est possible pour une température et une pression connue de calculer, pour un ou plusieurs composés, la répartition à l'équilibre de chacun de ces composés entre une phase liquide et une phase gaz. Pour cela il est nécessaire de déterminer pour un solvant tel que l'eau, et pour différentes températures, les constantes de Henry de chaque composé intervenant dans le procédé à modéliser.

II. Bases théoriques du transfert de Chaleur dans une canalisation[8]

1. Défintion théorique du problème

Soit un tube de longueur L et de diamètre D (figure 101), dans lequel circule un fluide à la vitesse moyenne u_m (ou vitesse de débit). Ce fluide pénètre dans le tube à la température T_1 et ressort à la température T_2. Soit T_0, la température de la paroi fixée et constante (isotherme). Dans notre cas $T_0 < T_1$.

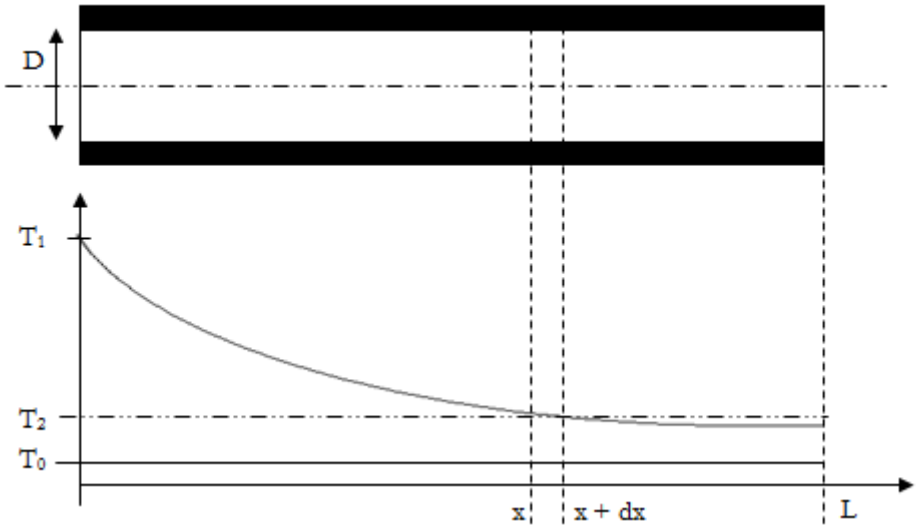

Figure 101: schéma théorique d'une canalisation pour la résolution de l'évolution de la température au sein du fluide traversant la canalisation

Soit T la température du fluide à l'abscisse x. Soit un élément de tube de largeur dx et L la longueur totale de la canalisation. Le flux de chaleur reçu par le fluide à partir de cet élément est :

Eq 101 : $\partial\Phi = h\,.(T_0 - T).dS = h..(T_0 - T).\pi.D.dx$

avec h : coefficient d'échange de chaleur par convection ($W.m^{-2}.K^{-1}$)

ce flux sert à refroidir de dT le fluide traversant cet élément, c'est-à-dire :

Eq 102 : $\partial\Phi = \dot{m}\,.Cp.dT$

[8] : (Manuel Thermique 2° édition Bernard Eyglunent ; Transfert de chaleur : Applications industrielles 1990 J.Cabrol)

avec $\dot{m}$ m le débit de masse du fluide de chaleur massique. Or :

Eq 103 : $\dot{m} = s.\rho.u_m = \frac{\pi.D^2}{4}.\rho.u_m$

avec s : section (m^2)

ρ : masse volumique du fluide (kg/m^3)

u_m : vitesse moyenne (m/s)

D : diamètre de la canalisation (m)

Cp : chaleur spécifique (kJ/kg)

Ainsi :

Eq 104 : $\partial\Phi = \frac{\pi.D^2}{4}.\rho.u_m.Cp.dT$

En égalant les relations (1) et (4) on obtient :

Eq 105 : $h..(T_0 - T).\pi.D.dx = \frac{\pi.D^2}{4}.\rho.u_m.Cp.dT$

c'est-à-dire :

Eq 106 : $\frac{dT}{T - T_0} = \frac{4.h}{D.\rho.u_m.Cp}.dx = \frac{4.M}{D}.dx$

Avec M : nombre adimensionnel de Margoulis.

En supposant que le nombre de Margoulis (transfert total/transfert convection) soit constant le long de la canalisation, on a :

Eq 107 : $Ln(T_0 - T) = \frac{4.M}{D}.x + Cte$

Soit :

Eq 108 : $T_0 - T = K.exp^{(-\frac{4.M}{D}.x)}$

Quand x = 0, $T_0 - T_1 = K$

Soit :

Eq 109 : $T = T_0 - (T_0 - T_1).exp^{(-\frac{4.M}{D}.x)}$

Donc à partir de l'équation (9), pour une longueur de canalisation donnée, il est possible de calculer la température moyenne du gaz en sortie de canalisation. Pour cela il faut déterminer le nombre de Margoulis pour le fluide considérés.

Eq 110 : $M = \frac{h}{\rho.u_m.Cp}$

Pour déterminer le nombre de Margoulis il est donc nécessaire au préalable de déterminer le coefficient d'échange de chaleur par convection h dans le cas considéré.

Calcul du coefficient d'échange de chaleur par convection (h)

Dans le cas d'un échange de chaleur par convection forcée h est fonction d'un nombre adimensionnel **Nu** (Nusselt) *(caractérise échange thermique entre le fluide et la paroi)* qui est lui-même fonction de deux nombre adimensionnel **Re** (Reynolds) *(caractérise l'écoulement)* et Pr (Prandlt) *(caractérise les propriétés thermiques du fluide).*

Eq 111 : $Nu = h.D/\lambda$ avec λ : conductivité thermique du fluide ($W.m^{-1}.K^{-1}$)

Eq 112 : $Re = \rho.u_m.D/\mu$ avec μ : viscosité dynamique du fluide ($kg.m^{-1}.s^{-1}$)

Eq 113 : $Pr = \mu.Cp/\lambda$

Ainsi le coefficient d'échange spécifique h du fluide est donnée par l'équation suivante :

Eq 114 : $h = Nu.\lambda /D$

Pour un écoulement laminaire différentes corrélations permettent de déterminer le nombre de Nusselt (Nu). Une, proposée par Loison, fait intervenir le nombre A = (x/D).(1/Re.Pr), et définit une valeur moyenne empirique du nombre de Nusselt ($\overline{Nu}$) le long d'une canalisation par l'équation suivante (Eq 115):

Eq 115 : $\overline{Nu} = 2{,}34 . A^{-0{,}33}$

Ainsi dans le cas d'un air sec, le coefficient d'échange de chaleur h peut être calculé, considérant un air humide (y = fraction molaire en eau dans la phase gaz, calculée à partir des équilibres gaz-liquide décrit en partie I de ces annexes), la corrélation suivante est alors utilisée :

Eq 116 : $h_{air\ humide} = h.10^{(2{,}46 . y)}$

Ainsi, le nombre de Margoulis (M) en fonction de la longueur de la canalisation peut être calculé, et ainsi en utilisant l'équation (Eq 109), la température de la phase gaz, à une certaine distance de l'entrée, par rapport à une température d'entrée, une température constante à la paroi, et une vitesse de circulation de la phase gaz au sein de la canalisation peut être estimée[9].

2. Estimation du profil de température

Le tableau 38 présente les données utilisées pour réaliser la résolution du système

Tableau 38: valeurs types utilisées pour le calcul de l'évolution de la température de la phase gaz le long d'une canalisation.

Diamètre canalisation	80 mm	D
Surface d'échange de la canalisation	dépend de la longueur de la canalisation	S_{ech}
Masse volumique de l'air	1,20 kg/m^3	ρ
Vitesse moyenne de circulation de l'air	0,135 m/s	v
Chaleur spécifique de l'air	1 J.g^{-1}.K^{-1}	Cp
Viscosité dynamique de l'air	1,88E-5 kg.m^{-1}.s^{-1}	μ
Conductivité thermique de l'air	0,026 W.K^{-1}.m^{-1}	λ
Température d'entrée	35°C	T_1
Température à la paroi	10°C	T_0
Fraction molaire d'eau dans le gaz à la température d'entrée	0.06	$y_{eau/air}$

[9] : de nombreuses corrélations permettant de définir le nombre de Nusselt existent et ce en fonction des conditions. Certaines ont été testées (Hausen) et (Sieder et Tate). Il a été présenté dans ce paragraphe celle qui permettait de représenter au mieux les données expérimentales présentées dans le chapitre III.

Dans ce cas le nombre de Reynolds confirme bien l'écoulement laminaire du fluide (Re = 688), le nombre Prandlt est égale à 0,72. Dans ces conditions le long d'une canalisation de 0.8 m, le tableau suivant (tableau 39) présente les températures calculées.

Tableau 39: résultats des séquences de calculs pour l'évaluation de l'évolution de la température de la phase gaz le long d'une canalisation thermostatée, dans les conditions d'expériences présentées au tableau 38.

Longueur	**A**	**Nusselt**	**h $_{air\ sec}$**	**h $_{air\ humide}$**	**Margoulis**	**Température théorique**
0 cm	0,00E+00					35,0 °C
1 cm	2,51E-04	36,1	11,73	16,48	0,102	33,8 °C
2 cm	5,02E-04	28,7	9,33	13,11	0,081	33,1 °C
3 cm	7,52E-04	25,1	8,16	11,47	0,071	32,5 °C
4 cm	1,00E-03	22,8	7,42	10,43	0,064	32,0 °C
5 cm	1,25E-03	21,2	6,90	9,69	0,060	31,5 °C
6 cm	1,50E-03	20,0	6,49	9,12	0,056	31,1 °C
7 cm	1,76E-03	19,0	6,17	8,67	0,054	30,7 °C
8 cm	2,01E-03	18,2	5,91	8,30	0,051	30,4 °C
9 cm	2,26E-03	17,5	5,68	7,98	0,049	30,0 °C
10 cm	2,51E-03	16,9	5,49	7,71	0,048	29,7 °C
20 cm	**5,02E-03**	**13,4**	**4,36**	**6,13**	**0,038**	**27,1 °C**
42 cm	1,05E-02	10,5	3,42	4,80	0,030	23,4 °C
62 cm	1,56E-02	9,2	3,00	4,22	0,026	21,1 °C
80 cm	2,01E-02	8,5	2,76	3,88	0,024	19,6 °C

Pour une longueur de 20 cm, correspondant à la longueur d'un tronçon utilisé dans le dispositif expérimental par ruissellement, la température théorique en sortie de ce tronçon dans ces conditions d'expériences est de 27,1°C. Cette température, réutilisée dans les équations présentées dans le chapitre III, paragraphe [1.1.2.], permet de calculer le débit théorique condensée correspondant.

III. Ruissellement d'un film liquide pour reproduire le phenomene de condensation

La vitesse de circulation de l'air au niveau des phases aérienne des réseau d'assainissement a été évaluée dans une gamme allant de 0,05 à 0,22 m/s (Madsen et al., 2006). Dans ce type d'environnement le taux d'humidité relactive de la phase gaz est généralement très élevée, comprise entre 90 et 100 % (Joseph et al., 2012). De plus, comme l'a montré Joseph (2012), et Jean Herisson (Herisson, 2012), une température élevée et un important taux d'humidité au niveau de la phase aérienne des réseaux d'assainissement favorisent les réactions chimiques et biologiques impliquées dans les transformations étudiées, conduisant ainsi à une intensification de l'acidification du milieu.

Afin d'évaluer le flux d'eau apporté à la surface d'une canalisation par un phenomene de condensation, des expériences préliminaire, basées sur les études théoriques présentées aux précédentes sections de ces annexes, ont été réalisées sur une canalisation teste. La figure 102 présente le schéma du pilote conçu pour étudier le phénomène de condensation dans un système intensifié.

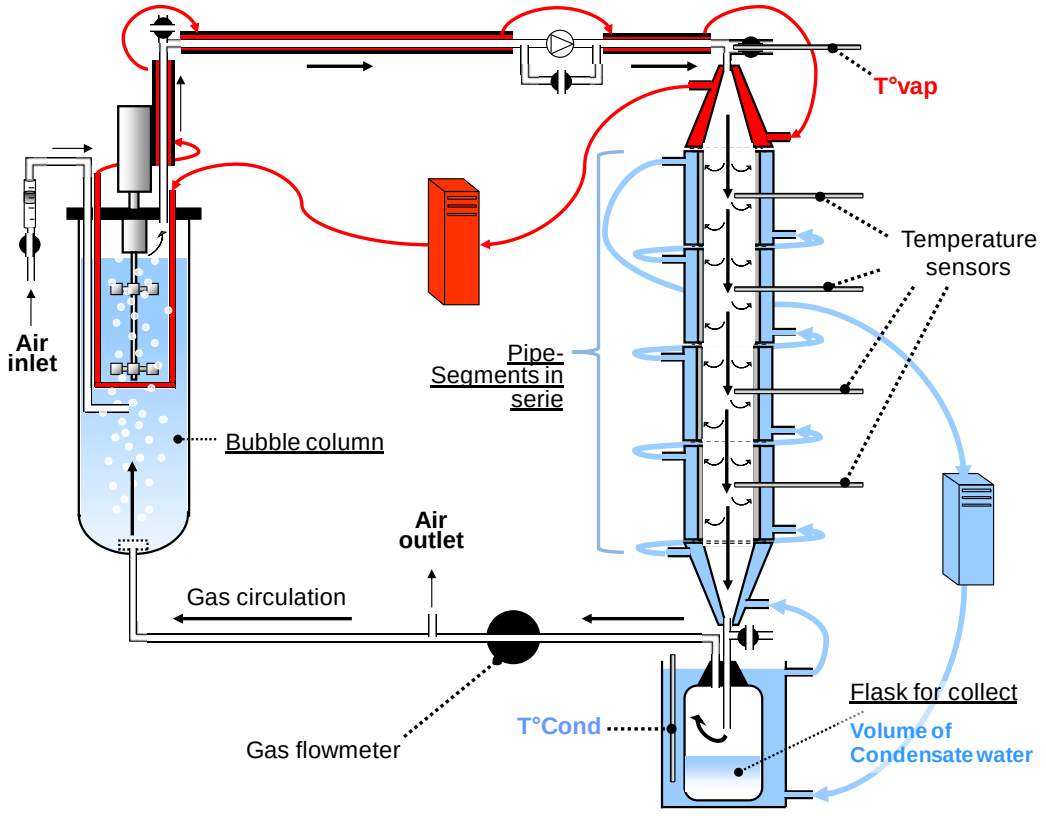

Figure 102: schéma du pilote expérimentale conçu pour évaluer les flux de condensat produit à la paroi d'une canalisation modèle en fonction des conditions opératoires.

Un débit d'air (mesurer par un débitmètre massique) traverse une colonne d'eau thermostatée (température de vaporisation : T°vap) pour une obtenir une phase gaz à 100 % en humidité relative. La phase gaz ainsi constituée est transportée à température constante vers une canalisation test (composée de quatre tronçons en série, tronçons présentés dans le matériel et méthodes, soit une canalisation de 4 x 0,2 m de long). La canalisation test est thermostatée au paroi à une température appelée « température de condensation : T°cond ». Ainsi, à travers la canalisation un phénomène de condensation se produit à la paroi de la canalisation. Expérimentalement, plusieurs sondes température ont été installées afin de mesurer l'évolution de la température de la phase gaz le long de la canalisation. A la sortie de la canalisation, la phase liquide condensée, après ruissellement, est collectée dans bouteille en verre thermostatée à la température de condensation. Punctuellement, le volume de condensat est mesuré par pesée, ainsi le débit condensé en fonction des conditions opératoires est calculées.

Plusieurs conditions opératoires ont été testées (debit d'air, temperature de vaporisation et température de condensation). Le tableau 40 présente les conditions opératoires utilisées pour l'évaluation du débit d'eau condensé.

Tableau 40: conditions opératoires de vaporization / condensation pour l'évaluation du debit d'eau condense dans la confinguration du pilote de laboratoire (figure 103)

Manip	**Température de vaporisation T°vap (°C)**	**Température de condensation T°cond (°C)**	**Débit d'air (m^3/h)**
1	36.5	16.7	0.035
2	36.5	16.6	0.555
3	42.4	25.4	0.498
4	43.0	19.1	0.498

Dans une première approche, les valeurs théoriques obtenues à partir de la resolution des équilibres thermodynamiques ont été calculées. Pour ça, basé sur la théorie des équilibres gaz-liquide décrit précédement, et appliqué au conditions opératoires décrites au tableau 40, le debit molaire d'air passant à travers le sytème a été calculé l'équation suivante (Eq 117) issue de l'équation des gaz parfaits :

Eq 117 : $N_{air} = \frac{P_{atm} \cdot Q_{air}}{R \cdot T°_{cond}}$

avec N_{air} est le debit molaire de gaz sec (mol/h); P_{atm} est la pression atmosphérique (Pa); Q_{air} est le debit volumétrique d'air (m^3/h); R est la constante des gaz parfaits (equal to 8.3144 $J.K^{-1}.mol^{-1}$) est $T°_{cond}$ est la température de condensation (K).

Ainsi, les fractions molaires d'eau à l'équilibre en phase gaz à l'entrée de la canalisation (y_{vap}) (à T°vap) et celle en sortie de canalisation (y_{cond}) (à T°cond) sont calculées par les équations suivantes (Eq 118 and Eq 119):

Eq 118 : $$y_{vap} = \frac{P^{Sat}_{(T°vap)}}{P_{atm}}$$

Eq 119 : $$y_{cond} = \frac{P^{Sat}_{(T°cond)}}{P_{atm}}$$

avec $P^{Sat}_{(T°vap)}$ est la pression de vapeur saturante à la température de vaporisation (Pa), et $P^{Sat}_{(T°cond)}$ est la pression de vapeur saturante à la temperature de condensation (Pa) (valeurs utlisées issues de Roustan, 2003).

Le debit de condensate peut alors être calculé par la perte théorique d'eau dans la phase gaz entre l'entrée et la sortie de la canalization test. Ainsi, le débit d'eau condensé (Q_{cond} en ml/h) est décrit par l'équation suivante (Eq 120):

Eq 120 : $$Q_{cond} = 1000.(y_{vap} - y_{cond}).N_{air} / 55.55$$

avec y_{vap}, y_{cond} et N_{air} défénis précédement, et 55.55 est une valeur approximative de la quantité de moles d'eau contenues dans un litre d'eau à 20°C.

La figure 103 presente les debits condensat experimentaux (symbols) et theorique (lignes) obenue pour différentes conditions opératoires testées présentées au tableau 40. Les debits théoriques de condensate ont été calculé par la methode proposée précédement (Eq 117, Eq 118, Eq 119 and Eq 120).

Les résultats théoriques des débits d'eau condensée en fonction des conditions opératoires permettent de représenter les résultats expérimentaux obtenus pour différentes conditions expérimentales. Ainsi, pour une canalisation longue de 0,8 m le travail à l'équilibre est validé, et ce si on prend en compte une mise en régime du système d'environ 5h.

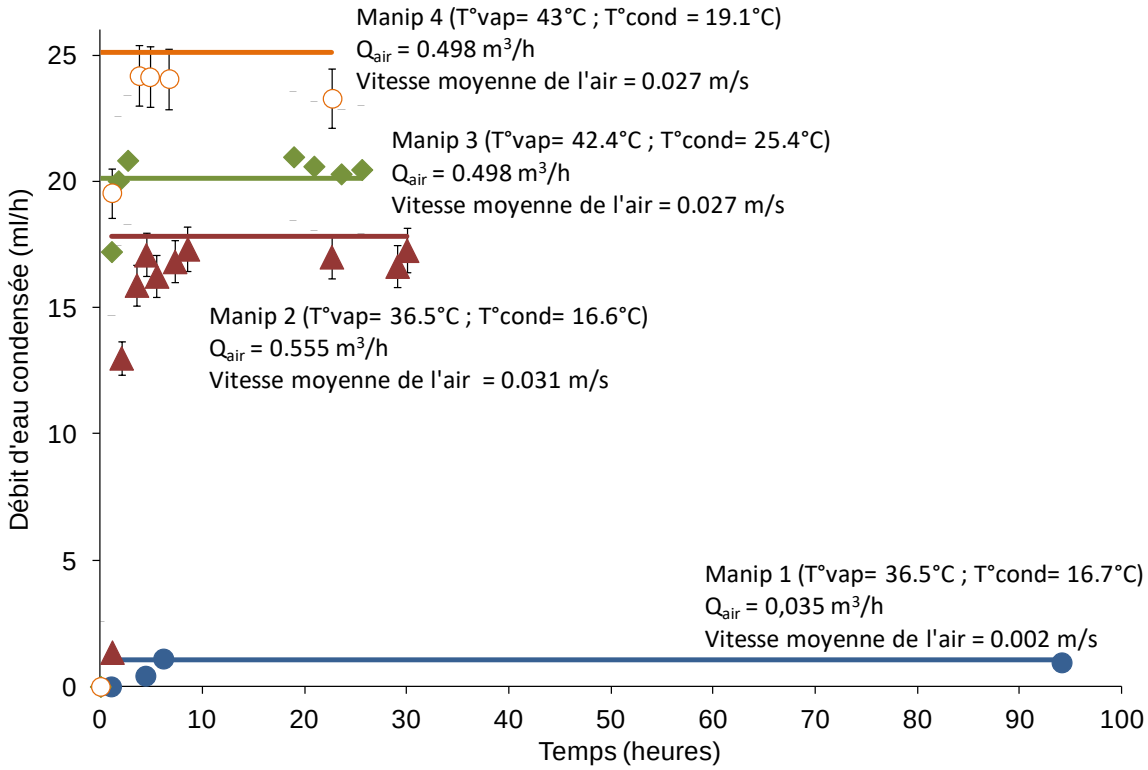

Figure 103: flows of condensate water at the pipe walls for different operating conditions exposes in the Tableau 40, for a pipe length of 1 m. Symbols represents the experimental measurements. Lines the calculated values by the hypothesis of gas-liquid equilibrium. Experimental data. ● : manip 1 ; ▲ : manip 2 ; ◆ : manip 3 ; ○ : manip 4.

Durant ces experiences, la temperature au sein de la phase gaz a été mesurée à different emplacement le long de la canalization test. La figure 104 présente les profiles de temperature pour trois des conditions expérimentales testées (Manip 2, Manip 3 et la Manip 4), et les profiles de temperatures théoriques qui ont été calculées pour chaque condition à partir des bases théoriques du transfert de chaleur présentées précédement.

Prémièrement, les profils expérimentaux, pour les trois conditions présentées, montrent l'obtention d'une température de la phase gas en sortie de canalisation (80 cm de long) équivalente aux températures appliquées à la paroi. Ainsi, le phénomène de condensation est bien maximal, et la possibilité de travailler à l'équilibre est bien confirmer. Ensuite, la bonne représentation, par la théorie, des profils expérimentaux, permet d'extrapoler pour différentes conditions de travail, pour différentes dimension de canalisation (20 cm) la température de sortie et donc le potentiel d'eau condensée en fonction des conditions opératoires et de la dimension de la canalisation, dans le cas d'une circulation de l'air laminaire.

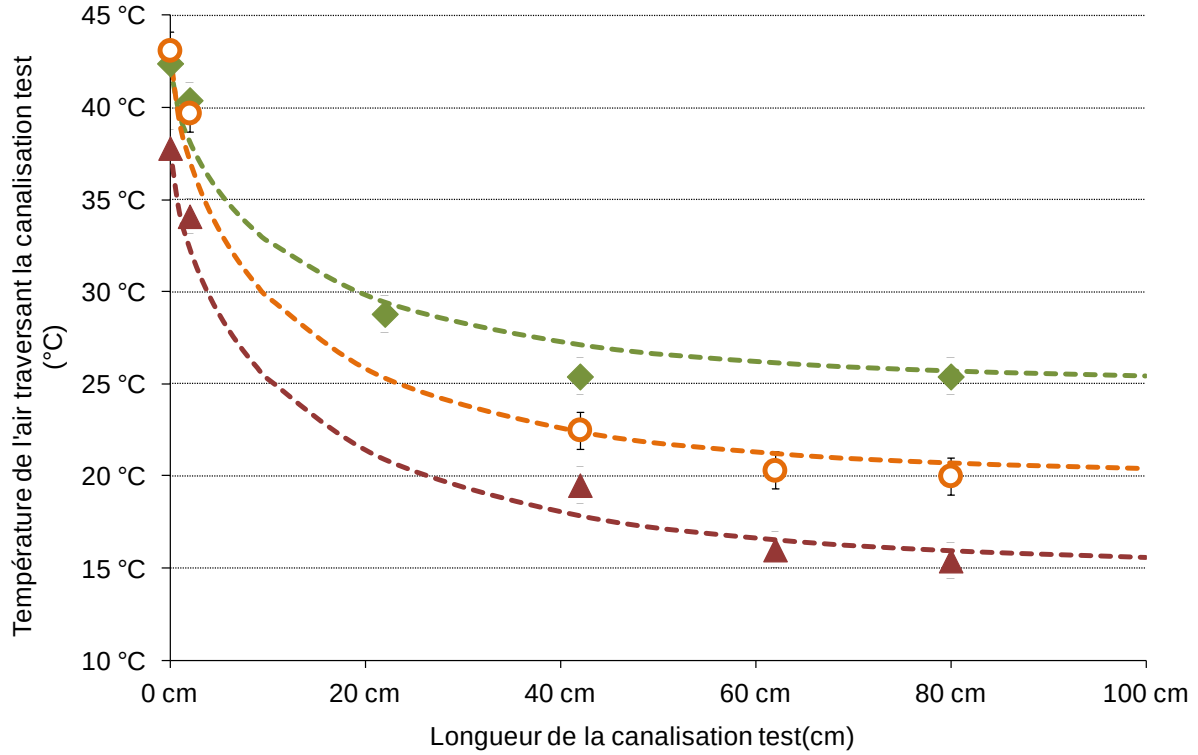

Figure 104: experimental measurement of the temperature at different positions all along the pipe reactor for different experimental condition of vaporization / condensation, compared to theoretical temperature profiles in a simple pipe (see the annexes of this chapter for the details of the calculation). ▲ : manip 2 ; ◆ : manip 3 ; ○ : manip 4.

Ainsi, pour une vitesse de circulation de l'air dans la canalisation fixée à 0,135 m/s (moitié de la vitesse maximale de circulation de l'air enregistrée en réseau d'assainissement par Madsen), correspondant à un débit d'air de 2,44 m^3/h (Re = 688, confirmant l'écoulement lamainaire), différentes températures de travail ont été testées théoriquement pour déterminer un débit d'eau condensée correspondant à des conditions intense de condensation. Par exemple, pour une canalisation de 20 cm de long, et des températures opératoires $T°_{vap}$ = 35°C et $T°_{wall}$ = 10°C, le modèle de transfert de chaleur donne une température en sortie de canalisation de 27°C. En utilisant cette température en tant que $T°_{cond}$ dans le modèle d'équilibre, un débit d'eau condensée théorique Q_{cond} = to 37.1 ml/h est déterminé.

Avec l'objectif de reproduire par ruissellement un phenomène intensifié de condensation, tout en assurant la séparation des solutions d'alimentations pour éviter toute profilération en amont de l'interaction avec la matrice cimentaire, le débit d'entrée a été fixé à 50 ml/h (valeur minimale stable obtenue en travaillant avec une pompe peristaltique munie de trois têtes de pompe.)

Annexes - Chapter V

I.

Specific bibliography on the secondary reactions involved in the definition of the thiosulfate disproportionate reaction and their mathematical formulation

II.

Experiences and numerical simulations of the secondary reactions involved in the description of the thiosulfate disproportionate reaction

I. Specific bibliography on the secondary reactions involved in the definition of the thiosulfate disproportionate reaction and their mathematical formulation

To describe kinetically the thiosulfate disproportionate reaction and evaluate for different conditions the behavior of the sulfur species, the pH evolution and the oxygen consumption, the secondary reactions involved S(IV)-oxides, need to be kinetically described also. This part of the document focus on the compartments 2 and 3 presented in the Figure 9 of the chapter V of this document.

1. The oxidation of the S(IV)-oxides under oxic conditions

The S(IV)-oxides gathers three sulfur compounds, the sulfite (SO_3^{2-}), the bisulfite (HSO_3^-) and the sulfur dioxide (SO_2 or H_2SO_3 in the hydrate form named sulfurous acid). In solution the concentrations of these compounds are defined by the acid-base equilibrium reactions described by the equations (Eq 121) and (Eq 122). As mentioned, H_2SO_3 is also a volatile compound in equilibrium in the gas phase with SO_{2gas}, and the concentrations of these compounds were defined by the equation (Eq 11 in the chapter V).

Eq 121: $H_2SO_3 + H_2O \overset{Ka_{S(IV)1}}{=} HSO_3^- + H_3O^+$

with $Ka_{S(IV)1} = (HSO_3^-).(H_3O^+)/(H_2SO_3)$, where $Ka_{S(IV)1}$ is the acid-base equilibrium constant (different values of $Ka_{S(IV)1}$ are reported from the literature in the table 40).

Eq 122: $HSO_3^- + H_2O \overset{Ka_{S(IV)2}}{=} SO_3^{2-} + H_3O^+$

with $Ka_{S(IV)2} = (SO_3^{2-}).(H_3O^+)/(HSO_3^-)$, where $Ka_{S(IV)2}$ is the acid-base equilibrium constant (different values of $Ka_{S(IV)2}$ are reported from the literature in the table 41).

Table 41 : Different values of the acid-base equilibrium constants of the S(IV)-oxides system ($Ka_{S(IV)1}$ and $Ka_{S(IV)2}$) and the associated references.

Ref	$Ka_{S(IV)1}$ (25°C)	Ref	$Ka_{S(IV)2}$ (25°C)
Scott 1967	0.0127	Scott 1967	6.4×10^{-8}
Schroeter 1966	0.0166	Schroeter 1966	6.31×10^{-8}
Huss 1977	0.0138	Eigen 1961	6.31×10^{-8}
Maahs 1982	$10^{(-4.74 + 853/T)}$	Maahs 1982	$10^{(-9.278 + 621.9/T)}$
Goldberg 1985	0.0139	Goldberg 1985	6.7×10^{-8}
Zemaitis 1986	0.0195	Zemaitis 1986	5.488×10^{-8}

T = temperature (K)

Sulfite (SO_3^{2-}) and bisulfite (HSO_3^-) are well known to be reactive with dissolved oxygen (Linek and Vacek, 1981) (Wilkinson et al., 1993) (Lancia et al., 1999). The stoichiometric reactions were described by the equations (Eq 123) for the sulfite, and (Eq 124) for the bisulfite:

Eq 123: $SO_3^{2-} + 1/2\,O_2 \rightarrow SO_4^{2-}$

Eq 124: $HSO_3^- + 1/2\,O_2 \rightarrow HSO_4^-$

In 1995 Brandt et Eldik reviewed the oxidation of the S(IV)-oxides, uncatalyzed and catalyzed reactions (Brandt et al., 1995). The table 42 adapted from a table of this study, reported the values of the rate constant for uncatalyzed reaction at different pH conditions. The values of the rate constants for the S(IV)-oxides uncatalyzed oxidation were given for a constant dissolved oxygen concentration. Thus, the kinetic law could be described by the equation (Eq 125).

Eq 125: $d[S(IV)]/dt = -k_{S(IV)}.[S(IV)]$

where d[S(IV)]/dt is the evolution during time of total concentration of S(IV)-oxidizes in solution ($mol.l^{-1}.s^{-1}$), $k_{S(IV)}$ is the apparent rate constant of the reaction (s^{-1}), and [S(IV)] is the total concentration of the S(IV)-oxides in solution (mol/l).

The table 42 shows the increase of the rate reaction with the increase of the pH, that could indicated a higher reactivity of the sulfite (SO_3^{2-}) than the bisulfite (HSO_3^-) under oxic conditions. These data are not in agreement with others results presented by Wilkinson in 1993. At the same time, for the same conditions of experiment (pH < 8.2 correspond to the predominance zone of sulfite), with dionized water as support the rate constant was 7.3 times

higher than with milli-R/Q water, indicating the important role of ionic species in the catalyzed reaction of sulfite (Linek and Vacek, 1981) (Ulrich et al., 1984) (Wilkinson et al., 1993) (Brandt et al., 1995).

Table 42: Rate constants for some uncatalyzed oxidation reactions of S(IV)-oxides for different pH conditions (adapted from Brandt 1995), and the S(IV)-oxides speciation for two different combinations of acid-base equilibrium constant (Ka_{S1} and Ka_{S2}).

pH	T°C	$k_{S(IV)}$ (s^{-1})	(AD) H_2SO_3	(AD) HSO_3^-	(AD) SO_3^{2-}	(BC) H_2SO_3	(BC) HSO_3^-	(BC) SO_3^{2-}
3	25	1,18E-07	7,30%	92,69%	0,01%	4,87%	95,12%	0,01%
4	25	1,72E-07	0,78%	99,15%	0,07%	0,51%	99,44%	0,05%
5	25	9,19E-07	0,08%	99,26%	0,67%	0,05%	99,40%	0,55%
6	25	1,63E-06	0,01%	93,71%	6,28%	0,00%	94,79%	5,20%
8,2	25	1,30E-05[a]	0,00%	8,61%	91,39%	0,00%	10,31%	89,69%
8,9	25	1,30E-05[a]	0,00%	1,84%	98,16%	0,00%	2,24%	97,76%
8,2	25	9,50E-05[b]	0,00%	8,61%	91,39%	0,00%	10,31%	89,69%
8,9	25	9,50E-05[b]	0,00%	1,84%	98,16%	0,00%	2,24%	97,76%

a : with milli-R/Q water ; b: with deionized water

AD : Ka_{S1} (A) = 0.0127 (Scott 1967); $Ka_{S2} = 6.7 \times 10^{-8}$ (Goldberg 1985)

BC : Ka_{S1} (B) = 0.01952 (Zemaitis 1986); $Ka_{S2} = 5.488 \times 10^{-8}$ (Zemaitis 1986)

The table 42 shows for two combinations of acid-base equilibrium constants the ratio of the different S(IV)-oxides in accordance with the pH conditions. The choice of the constants was determined by the maximum variation and the minimum variation between the set of constants reported in the table 41. The comparison between the different calculated ratios indicates a weak difference between the both set of constants (less than 2% at pH 8.2 for the HSO_3^- ion). In some pH conditions, the calculation of the predominant species enable highlighting a rate constant for specific oxidation reactions. For example, between pH 4 and 5, HSO_3^- represents more than 99% of the total S(IV)-oxides in solution, thus the rate constant determined in these conditions could be attributed directly to the uncatalyzed oxidation of HSO_3^- by the oxygen (1.72×10^{-7} s^{-1} < $k_{HSO3(-)}$ < 9.19×10^{-7} s^{-1}). For a pH value ranged from 8.2 to 8.9, SO_3^{2-} is the predominant compounds (90% at pH = 8.2, and 98% at pH = 8.9). Although the pH conditions were different, thus the SO_3^{2-} concentration, the rate constant were the same, at pH 8.2 and 8.9, for the set of two experiments with milli-R/Q water, and the set of two experiments with dionized water (1.30×10^{-5} s^{-1} and 9.5×10^{-5} s^{-1} respectively, corresponding to the values of the rate constant $k_{SO3(2-)}$).

Concerning the kinetic of the uncatalyzed oxidation of bisulfite (HSO_3^-) by dissolved oxygen, Connick in 1995, for reaction at pH 4.5, 25°C with ionic strength of 0.05 mol/l, proposed a kinetic law described by the equation (Eq 126).

Eq 126: $d(O_2)/dt = -k_{obs} . [HSO_3^-]^2 . [H_3O^+]^{-2} . [O_2]^0$

with $k_{obs} = 3.6 \times 10^6$ mol.l^{-1}.s^{-1}

Lancia in 1996 proposed a kinetic law independent of the oxygen concentration and with a 3/2 order in HSO_3^- concentration (Lancia 1999), described by the equation (Eq 127), where k_U is the kinetic constant for the uncatalyzed reaction, $k_U = 1.19 \times 10^{-4}$ m$^{1.5}$.mol$^{-0.5}$.s^{-1}, corresponding to $k_U = 428.4$ l$^{1.5}$.mol$^{-0.5}$.h^{-1}.

Eq 127: $d(HSO_3^-)/dt = -k_u . [HSO_3^-]^{3/2}$

The oxidation of sulfite (SO_3^{2-}) by dissolved oxygen is strongly environment dependent. In fact the pH, the water quality as presence of trace metal as manganese, iron, copper, cobalt or nickel could accelerate the oxidation of sulfite by dissolved oxygen (Linek and Vacek, 1981). The reaction pathways differ considerably from a condition to another (Wilkinson et al., 1993). The table 43 shows some examples of the impact of catalyst use on the oxidation reaction rate at a pH solution of 5 (here kinetic law corresponding to the equation (Eq 125)), and the impact of this reaction on the gas-liquid mass transfer of oxygen, by the calculation of the enhancement factor EO2 (Ulrich et al., 1984) (for the definition of the enhancement factor see annexes of this document (Danckwerts, 1970)). In their review article, Linek and Vacek in 1981 concluded that the law kinetic of the oxidation of sulfite by oxygen with and without catalyst had a 0 order in oxygen and a 3/2 order in SO_3^{2-} ion (Linek and Vacek, 1981). Some other studies presented different reaction orders, as 0 in O_2 and 1 in SO_3^{2-} (Ulrich et al., 1984), or as 1 order in O_2 for uncatalyzed reaction (Wilkinson et al., 1993).

The presence of thiosulfate in solution inhibits the catalysis of the oxidation of sulfite by manganese by a scavenging effect of the thiosulfate on manganese (Ulrich et al., 1984).

In 1993, Wilkinson et al., have demonstrated a good description of the evolution of the pH solution during the S(IV)-oxides by taking into account the acid-base equilibrium and activities of the different species in solution. For that, the acid-base equilibrium of the

products (S(VI)-oxides as sulfate (SO_4^{2-}) and bisulfate (HSO_4^-)) must to be involved in the whole description.

Table 43: Comparison of catalytic activities with air oxidation of 10 mmol/l of sulfur(IV) oxides in 300 mmol/l of sulfur(VI) oxides at pH 5, 50°C and 400 rpm agitation. Reaction rate for $[O_2] = 6 \times 10^{-5}$ mol/l (from Ulrich 1984))

Catalyst (mmol/l)	Interface		Enhancement factor EO2	Homogenous oxidation rate ($mmol.l^{-1}.s^{-1}$)
	pH	S(IV)-oxides (mmol/l)		
[Mn] = 5	4.2	9.2	2.5	1.2
[Mn] = 10	3.9	8.5	5.0	5.5
[Fe] = 0.1	4.1	9.1	3.1	1.9
[Fe] = 10	4.2	9.3	2.4	1.1
[Co] = 10	4.3	9.4	1.9	0.6
[Ni] = 10	4.6	9.7	1.1	0.1
[Cr] = 10	4.2	9.2	2.7	1.4
[Cu] = 10	3.7	7.8	7.3	11.5

2. The acid-base equilibrium for the S(VI)-oxides

The S(VI)-oxides gathers three sulfur compounds, the sulfate (SO_4^{2-}), the bisulfate (HSO_4^-) and the sulfuric acid (H_2SO_4) which is totally dissociated in solution. The acid-base equilibriums are described by the equations (Eq 128) and (Eq 129):

Eq 128: $$H_2SO_4 + H_2O \overset{Ka_{S(VI)1}}{=} HSO_4^- + H_3O^+$$

with $Ka_{S(VI)1} = (HSO_4^-).(H_3O^+)/(H_2SO_4)$, where $Ka_{S(VI)1}$ is the acid-base equilibrium constant of a strong acid, thus, this compounds does not exist in solution, $Ka_{S(VI)1} >> 1$.

Eq 129: $$HSO_4^- + H_2O \overset{Ka_{S(VI)2}}{=} SO_4^{2-} + H_3O^+$$

with $Ka_{S(VI)2} = (SO_4^{2-}).(H_3O^+)/(HSO_4^-)$, where $Ka_{S(VI)2}$ is the acid-base equilibrium constant (different values of $Ka_{S(VI)2}$ are reported from the literature in the table 44).

Table 44: Different values of the acid-base equilibrium constant $Ka_{S(VI)2}$ of the S(VI)-oxides system and the associated references.

Ref	$Ka_{S(VI)2}$ (25°C)
Robinson 1970	0.012
Wilkinson 1993	0.012
Adapted from Stergarsek 1996 (from Brewer 1982)	$9.895 \times 10^{-8} \times T^3 - 8.948 \times 10^{-5} \times T^2 + 0.0267 \times T - 2.62$

T = temperature (K)

Moreover, if the description of the pH is a key parameter in the global reaction, Wilkinson highlighted that at neutral and basic pH the absorption of atmospheric carbon oxide (CO_2) could disturb the pH definition and then the kinetics processes (Wilkinson et al., 1993).

3. The description of the atmospheric carbon dioxide (CO_2) absorption in solution and the definition of pH solution

The carbon dioxide (CO_2) composed the air (concentration ~ 0.035% of the natural air composition). In solution, after hydration reaction, the carbon dioxide is a diacid. Thus, absorption of carbon dioxide in solution impacts the pH of the solution. The reactions involved in this phenomena are described by the equilibrium equations, (Eq 130) corresponding to the gas-liquid equilibrium, (Eq 131) corresponding to the first acid-base equilibrium, and (Eq 132) corresponding to the second acid-base equilibrium.

Eq 130: $CO_2(gas) \overset{H_{CO_2/water}(T)}{=} H_2CO_3(liq)$

where $H_{CO_2/water}(T)$ is the Henry constant of the sulfur dioxide in water, considering the hydration reaction as an immediate reaction and the temperature dependency.

Eq 131: $H_2CO_3 + H_2O \overset{Ka_{C1}}{=} HCO_3^- + H_3O^+$

with $Ka_{C1} = (HCO_3^-).(H_3O^+)/(H_2CO_3)$, where $Ka_{C1} = 10^{-(3404.7 / (T - 14.8435 + 0.03279 \times T)}$ (Loewenthal et al 1989).

Eq 132: $HCO_3^- + H_2O \overset{Ka_{C2}}{=} CO_3^{2-} + H_3O^+$

with $Ka_{C2} = (CO_3^{2-}).(H_3O^+)/(HCO_3^-)$, where $Ka_{C2} = 10^{-(2902.4 / (T - 6.498 + 0.02379 \times T)}$ (Loewenthal et al., 1989).

The pH variation of a solution, due to an abiotic or a biotic reaction, modifies the carbon dioxide equilibria in aqueous solution, thus the quantity of carbon dioxide stripped (if acidification occurs) or absorbed (if basification occurs). The definition of the carbon dioxide equilibriums in aqueous solution is crucial for further applications, with autotrophic bacteria especially. In fact the autotrophic bacteria grow with the consumption of an energy source (as reduced sulfur compounds for sulfur-oxidizing-bacteria) to fixe carbon for cellular production from the dissolved carbon dioxide. Then the definition of the absorption and the speciation of the carbon dioxide in aqueous solution ensure the definition of an essential substrate for autotrophic growth.

4. The dynamic description of acid-base equilibrium reactions

The description of the thiosulfate disproportionate system (figure 52 of the chapter V of this document) included gas-liquid mass transfer process, irreversible reactions (as the thiosulfate disproportionate reaction, the oxidations of the S(IV)-oxides) and acid-base equilibriums. The need to describe the system in dynamic (for the evaluation of the kinetic laws and further comparisons with the biological oxidation of thiosulfate) required dynamical description of the equilibrium processes.

4.1. Acid-base equilibrium as two contrary kinetic reactions **(Musvoto et al., 2000)**

Musvoto et al, in 1997, proposed a dynamic description of equilibriums for weak acid/base system (the kinetic model was developed on Aquasim®). The principle was to describe the equilibrium process as two kinetic reactions, with contrary kinetic laws: a forward reaction (r_f) and a reverse reaction (r_r), defined by different rate constants linked each other by the equilibrium constant (Musvoto et al., 1997) (Musvoto et al., 2000) (Sötemann et al., 2004) (Manas et al., 2012). For example the equation (Eq 133) described an equilibrium process.

Eq 133: $a.A+b.B \overset{Ka}{=} c.C+d.D$

where *Ka* is the equilibrium constant, and a, b, c, d are the stoichiometric definitions of A, B, C and D compounds respectively. The equilibrium constant *Ka* is defined by the following equation (Eq 134).

Eq 134: $Ka = {(C)^c.(D)^d}\Big/{(A)^a.(B)^b}$

where (A), (B), (C) and (D) are the activity in solution of the species A, B, C and D respectively (see paragraph [3.2.1.2.] for the definition of the activity of one specie in aqueous solution).

The forward reaction (r_f) is defined by the following equation (Eq 135).

Eq 135: $a.A+b.B \rightarrow c.C+d.D$

with the kinetic law (r_f) defined by the following equation (Eq 136).

Eq 136: $r_f = k_f.(A)^a.(B)^b$

where k_f is the homogenous rate constant of the forward reaction (r_f).

The reverse reaction (r_r) for the equilibrium defined by the equation (Eq 133) is described by the following equation (Eq 137).

Eq 137: $c.C+d.D \rightarrow a.A+b.B$

with the kinetic law (r_r) defined by the following equation (Eq 138).

Eq 138 : $r_r = k_r.(C)^c.(D)^d$

where k_r is the homogenous rate constant of the forward reaction (r_r), (C) and (D) are the activity in solution of the C and D species respectively.

These kinetic reactions ((r_f) and (r_r)) represent the equilibrium process if the homogenous rate constants (k_f and k_r) respect the following equation (Eq 139).

Eq 139: $Ka = k_f / k_r$

Thus the equilibrium process is described by the equation (Eq 140) which is in agreement with the equilibrium definition presented by the equation (Eq 134).

Eq 140: $k_r . Ka .(A)^a .(B)^b = k_r .(C)^c .(D)^d$

This method has been developed for all the acid-base equilibriums presented in this chapter.

4.2. The activity of one specie in undiluted solution (Loewenthal et al., 1989)

In an undiluted solution, the equilibrium processes are defined, not by the direct concentrations of the different species involved in the reaction, but by the activity of these. In an undiluted solution the influence of others species must be taking into account on the definition of the equilibrium processes. The activity of the compound A is described by the equation (Eq 141).

Eq 141: $(A) = f_A .[A]$

where *(A)* is the activity of the specie A (in mol/l), *[A]* the concentration of the specie A (in mol/l), and f_A the activity coefficient associated to the specie A.

The activity coefficient f_A represents the influence of the solution composition on the different species in solution. The activity coefficient definition f_A is dependent of the ionic strength μ of the solution, which is defined by the following equation including all the ionic species in solution (Eq 142).

Eq 142: $\mu = \frac{1}{2}\sum C_i . Z_i^2$

where C_i is the concentration of the ionic specie (i) in solution (mol/l), and Z_i is the charge of the ionic specie (i) in solution.

4.3. The final expression by dynamic processes of an equilibrium reaction in undiluted solution

Based on the equations developed in the paragraphs (4.1 and 4.2) the equilibrium process defined by the equation (Eq 133) could be represented in a dynamic model by the final equation (Eq 143).

Eq 143: $k_r \,.\, Ka \,.(\, f_A.[A])^a \,.(\, f_B.[B])^b = k_r \,.\,(\, f_C.[C])^c \,.\,(\, f_D.[D])^d$

where [A], [B], [C] and [D] are the concentration in solution of the species A, B, C and D respectively (in mol/l); f_A, f_B, f_C and f_D are the activity coefficients of the species A, B, C and D respectively (expressions depending on the charge of the associated specie).

By this method proposed and developed by Musvoto (Musvoto et al., 1997) (Musvoto et al., 2000), and adapted in this document, the acid-base equilibrium reactions could be easily integrated to a dynamic model if the ionic strength of the solution is defined at each step of the calculation procedure.

II. Experiences and numerical simulations of the secondary reactions involved in the description of the thiosulfate disproportionate reaction

1. The absorption of the atmospheric carbon dioxide in aqueous solution and the pH definition (Compartment 3).

1.1. The system definition of the carbon dioxide absorption in aqueous solution

1.1.1. The equilibrium system CO_2gas-H_2CO_3-HCO_3^--CO_3^{2-}

The pH of an aqueous solution was defined by several acid-base equilibrium reactions. In contact with atmospheric air, some compounds are able to transfer from the gas phase to the liquid phase, and/or transfer from the liquid phase to the gas phase. Concerning the absorption of the carbon dioxide and the influence of this physical process on the solution pH definition, the system was described in the introduction of this chapter. To resume, in solution the carbon dioxide speciation was defined by the acid-base equilibrium equations (Eq 144) and (Eq 145).

Eq 144: $H_2CO_3 + H_2O \overset{Ka_{C1}}{=} HCO_3^- + H_3O^+$

with $Ka_{C1} = (HCO_3^-).(H_3O^+)/(H_2CO_3)$, where $Ka_{C1} = 10^{-(3404.7 / (T - 14.8435 + 0.03279 \times T)}$ (Loewenthal et al 1989).

Eq 145: $HCO_3^- + H_2O \overset{Ka_{C2}}{=} CO_3^{2-} + H_3O^+$

with $Ka_{C2} = (CO_3^{2-}).(H_3O^+)/(HCO_3^-)$, where $Ka_{C2} = 10^{-(2902.4 / (T - 6.498 + 0.02379 \times T)}$ (Loewenthal et al., 1989).

To be solved the system must be completed by the description of the water ionization defined by the equation (Eq 146).

Eq 146: $H_2O \overset{Kw}{=} H_3O^+ + OH^-$

with $Kw = (H_3O^+).(OH^-)$, where Kw = 3.46 x 10^{-24} x $\exp^{(0.0729 \text{ x } T)}$ with T in Kelvin (adapted from Lide 1990).

The gas-liquid mass transfer is described by the equilibrium defined by the equation (Eq 147).

Eq 147: $CO_2\,(gas) \overset{H_{CO_2/water}(T)}{=} H_2CO_3\,(liq)$

where $H_{CO_2/water}(T)$ is the Henry constant of the sulfur dioxide in water, considering the hydration reaction as an immediate reaction and the temperature dependency.

1.1.2. The physical definition of the gas-liquid mass transfer of the carbon dioxide

The equation (Eq 147) defined the different concentrations at an equilibrium state. The absorption of the carbon dioxide in solution is a dynamic process, linked to a perturbation of an equilibrium system. In fact, the equilibrium defined the limit of the absorption process. To be described dynamically, a kinetic process must be proposed to represent in time the absorption of the carbon dioxide. Based on the double-film model, with a transfer resistance defined only in liquid phase, the gas-liquid mass transfer of the carbon dioxide could be described by the equation (Eq 148).

Eq 148: $\frac{d[CO_2aq]}{dt} = kl.a_{CO_2}.([CO_{2_{aq}}^{Sat}] - [CO_2aq])$

where Kla_{CO2} is the volumetric rate of gas-liquid mass transfer of the carbon dioxide (h^{-1}), and $[CO_2aq]$ is the concentration of the dissolved carbon dioxide (assimilated to the concentration of the H_2CO_3 specie) (in mol/l), and $[CO_{2_{aq}}^{Sat}]$ is the saturation concentration of the dissolved carbon dioxide (in mol/l).

The value of the saturation concentration of the dissolved carbon dioxide $[CO_{2_{aq}}^{Sat}]$ must be evaluated by the resolution of the gas-liquid equilibrium equation (Eq 147) which defines the equilibrium concentration of dissolved carbon dioxide from the air composition by the equation (Eq 149).

Eq 149: $y_{CO_2} . P = x_{CO_2} . H_{CO_2 / eau}(T)$

where P is the system pressure (atmospheric pressure here), y_{CO_2} is the molar fraction of carbon dioxide in the gas phase (ambient air here), and x_{CO_2} is the molar fraction of the carbon dioxide in the liquid phase.

Thus, considering a $y_{CO_2} \approx 0.000388$, the depending temperature value of the saturation concentration of the dissolved carbon dioxide $[CO_{2aq}^{Sat}](T)$ could be expressed by the equation (Eq 150).

Eq 150: $[CO_{2aq}^{Sat}](T) = \frac{y_{CO_2} . P}{H_{CO_2 / eau}(T)} . \frac{\rho_{H_2O}(T)}{M_{H_2O}}$

Where $\rho_{H_2O}(T)$ is the volumetric mass of water (g/l) (depending of the temperature), and M_{H_2O} is the molar mass of water (= 18.017 g/mol).

The CO_2 gas-liquid transfer in aqueous solution was well studied (Sperandio et al., 1996) (Musvoto et al., 1998), (Manas et al., 2012). The rate constant for the mass transport of the carbon dioxide (kla_{CO2}: volumetric gas-liquid mass transport rate for the carbon dioxide) could be described in function of the volumetric gas-liquid mass transport rate of the dioxygen (kla_{O2}), by the following equation (Eq 151):

Eq 151: $kla_{CO_2} = kla_{O_2} . \left(\frac{D_{CO_2aq}(T)}{D_{O_2aq}(T)} \right)^{0.5}$

where $D_{CO_2aq}(T)$ is the diffusion coefficient of carbon dioxide in the water, and $D_{O_2aq}(T)$ is the diffusion coefficient of oxygen in the water.

The expressions of the diffusion coefficients used in this document (with temperature dependency relations) are presented in the table 45.

Table 45: diffusion coefficient expressions and temperature dependency relations.

Diffusion coefficient in water ($m^2.s^{-1}$)	Dependent temperature relation (T in Kelvin)	Range of temperature	Ref
$D_{CO_2aq}(T)$	$1.46836\ x\ 10^{-8}\ x\ (\frac{T}{217.206}-1)^{1.997}$	0 – 100°C	(Zeebe et al., 2011)
$D_{CO_3^{2-}}(T)$	$5.4468\ x\ 10^{-9}\ x\ (\frac{T}{210.265}-1)^{2.1929}$	0 – 100°C	(Zeebe et al., 2011)
$D_{O_2aq}(T)$	$5.44\ x\ 10^{-13}\ x\ exp^{(0.0281\ x\ T)}$	10 – 30°C	Adapted from Roustan 2003
$D_{SO_2aq}(T)$	$3.87\ x\ 10^{-13}\ x\ exp^{(0.0281\ x\ T)}$	10 – 30°C	Adapted from Roustan 2003

1.1.3. Influence of equilibrium reactions in solution on the definition of the gas-liquid mass transfer of the carbon dioxide (enhancement factor ECO_2)

Due to the equilibrium equations, in high pH conditions, the carbon dioxide predominant form is carbonate form (CO_3^{2-}). In these conditions, the physical absorption of the atmospheric carbon dioxide in a basic aqueous solution is following by two equilibrium reactions (acid-base reaction), thus an enhancement factor could accelerated the physical mass transport (Bosch et al., 1989) (Versteeg et al., 1990) (Anderko et al., 1998).

Bosch in 1989, for approximation, assimilated the global reaction of the carbon dioxide absorption in basic solution to a reaction between the dissolved carbon dioxide ($CO_2aq = H_2CO_3$) and the carbonate (CO_3^{2-}) producing bicarbonate (HCO_3^-) described by the equation (Eq 152).

Eq 152: $CO_2aq + CO_3^{2-} + H_2O \rightarrow 2HCO_3^-$

Based on the double-film model, this expression leads to an approximation of the enhancement factor for the absorption of atmospheric carbon dioxide in aqueous solution (E_{CO_2}) defined by the equation (Eq 153).

Eq 153: $E_{CO_2} \approx 1 + \frac{D_{CO_3^{2-}}(T).[CO_3^{2-}]_b}{D_{CO_2aq}(T).[CO_2]_i}$

where $D_{CO_2aq}(T)$ is the diffusion coefficient of carbon dioxide in the water, $D_{CO_3^{2-}}(T)$ is the diffusion coefficient of carbonate in the water (expressions in the table 45), $[CO_3^{2-}]_b$ the carbonate concentration in the bulk, and $[CO_2]_i$ the concentration of dissolved carbon dioxide at the air-liquid interface (in approximation the carbon dioxide saturation concentration $[CO_{2aq}^{Sat}]$).

The volumetric mass transport rate for the carbon dioxide defined by the equation (Eq 151), could then be expressed by the equation (Eq 154).

Eq 154: $$kla_{CO_2} = E_{CO_2} \cdot kl.a_{O_2} \cdot \left(\frac{D_{CO_2aq}(T)}{D_{O_2aq}(T)} \right)^{0.5}$$

1.1.4. The definition of the Compartment 3: mathematic model

To describe the absorption of gaseous carbon dioxide in a aqueous solution and the influence of this physical process on the pH solution, the system includes, the water ionization equilibrium, 2 acid-base equilibriums, one gas-liquid mass transport process, thus 7 kinetic processes, defining the evolution of 5 variables ($[H_3O^+]$, $[OH^-]$, $[H_2CO_3]$, $[HCO_3^-]$, $[CO_3^{2-}]$, if gaseous carbon dioxide concentration was considering constant).

1.2. The experimental and simulation results for the carbon dioxide absorption

1.2.1. Experiments and experimental results

To evaluate the model definition, several experiments were operated in open batch reactor. The table 46 reports the experiments and the operating conditions. The experiments were realized by the addition of concentrated soda solution (0.1 mol/l) to a 1 l volume of dionized water and the recording of the pH time course. The end of the experience were defined when the pH signal was stabilized.

Table 46: Operating initial conditions for the study of the carbon dioxide absorption in aqueous solution (Compartment 3).

Name of the experiments	Temperature (°C)	Volume of NaOH added	Initial pH	Initial [Na^+] (mol/l)*	kla_{O2} (h^{-1})
Exp_CO_2_a	29.7 ± 1	100 µl	9.02	10.10^{-6}	0.70 ± 0.25
Exp_CO_2_b	30.1 ± 1	300 µl	9.47	30.10^{-6}	0.70 ± 0.25
Exp_CO_2_c	30.5 ± 1	400 µl	9.60	40.10^{-6}	0.70 ± 0.25
Exp_CO_2_d	20.0 ± 1	4.5 mL	10.65	450.10^{-6}	0.70 ± 0.25
Exp_CO_2_e	25.0 ± 1	2.5 mL	10.34	250.10^{-6}	0.70 ± 0.25
Exp_CO_2_f	20.5 ± 1	1.5 mL	10.15	150.10^{-6}	0.70 ± 0.25

* : Na^+ in solution by the addition of concentrate soda solution at the start of the experiments

The figure 105 illustrated the pH and the dissolved oxygen time course during the experience Exp_CO2_a, before and after the addition of 100 µl of NaOH (0.1 mol/l). The dissolved oxygen was not impacted by the NaOH injection, stabilized quickly to the saturation value.

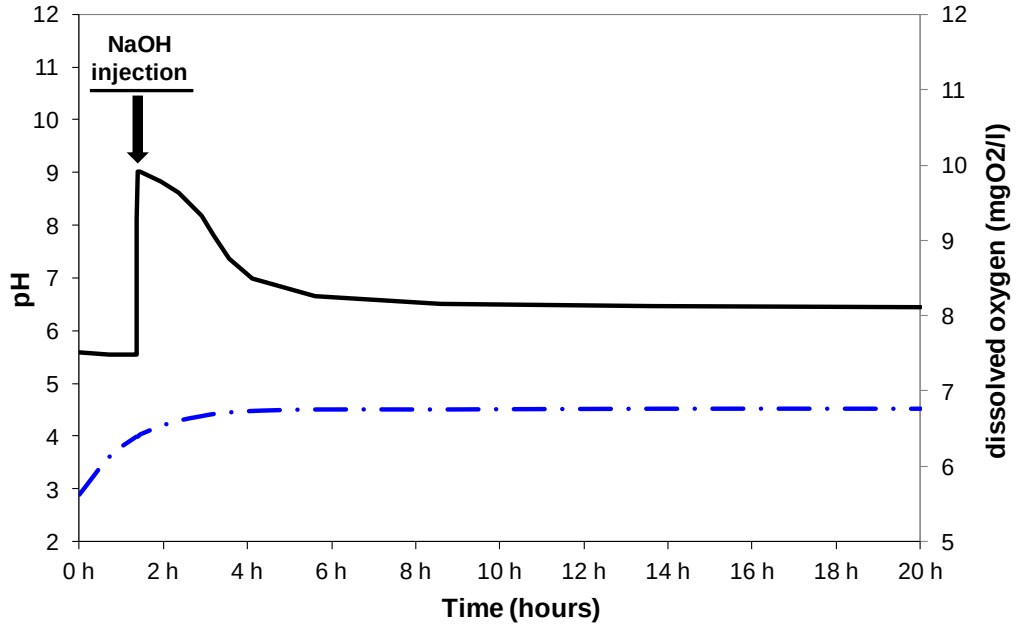

Figure 105: Exp_CO_2_a – time course of the different parameters measured. - · - : dissolved oxygen concentration (mgO_2/l); ——— : pH measurement.

Before the NaOH injection (figure 105), the pH was stable around 5.6. Directly after the injection, the pH increase to 9.02 and then decrease. In a first part of the reaction (during 4 hours) the pH decrease from 9.02 to 6.65 with a curve profile. After 4 hours, the pH was quiet stable (slowly decrease from 6.65 to 6.44 in 14 hours).

The injection of NaOH increased the pH, thus change the concentration of the different species in solution. At pH 5.6, the predominant form of the carbon dioxide in solution was H_2CO_3 ($\%H_2CO_3$ = 94% of the total dissolved inorganic carbon). At pH 9.02 the speciation of the dissolved carbon dioxide was $\%H_2CO_3$ = 0.25%, $\%HCO_3^-$ = 94.75%, $\%CO_3^{2-}$ = 5%, thus in contact with ambient air (relative constant concentration of CO_2), the gas-liquid equilibrium was perturbed leading to an absorption process. The absorption of gaseous carbon dioxide dissolved a diacide in solution, then the pH of solution decrease, and the dynamic pH definition was composed by the absorption process and the acid-base equilibriums.

1.2.2. The model definition for the carbon dioxide absorption

The table 47 presents the stoechiometric matrix for the mathematical description of the carbon dioxide absorption. Two variables ($[Na^+]$ and $[O_2]$) were add to the 5 variables defined in the paragraph [1.2.4.].

Table 47: State variables, kinetic processes and stoechiometric ratio for the mathematical description of the carbon dioxide absorption in aqueous solution (Compartment 3).

State Variables		Description	$[H_3O^+]$	$[OH^-]$	$[Na^+]$	$[O_2]$	$[H_2CO_3]$	$[HCO_3^-]$	$[CO_3^{2-}]$
		Unit	mol/L	mol/L	mol/L	mol/L	mol/L	mol/L	mol/L
		Expression	H	OH	Na	O2	CO2aq	HCO3	CO3
Processes	**Acid –base equilibriums**	Water_deionization_f	1	1					
		Water_deionization_r	-1	-1					
		$CO_2aq \rightarrow HCO_3^- + H^+$	1				-1	1	
		$HCO_3^- + H^+ \rightarrow CO_2aq$	-1				1	-1	
		$HCO_3^- \rightarrow CO_3^{2-} + H^+$	1					-1	1
		$CO_3^{2-} + H^+ \rightarrow HCO_3^-$	-1					1	-1
	Gas-liquid Transfer	$O_2gas \rightarrow O_2aq$				1			
		$CO_2gas \rightarrow CO_2aq$					1		

The sodium ($[Na^+]$) was added, because the initial basification of the solution was realized by NaOH addition. Even if sodium is a non-reactive compounds in the context of the experiment, its concentration defined the ionic strength, thus the activity coefficient for the reactive compounds. The oxygen was also added, because to define the volumetric rate for carbon dioxide transfer *(kla_{CO2})*, volumetric rate for oxygen mass transfer *(kla_{O2})* was needed.

The table 48 presents the kinetic rates for all the processes involved in the mathematical description of the carbon dioxide absorption in aqueous solution.

Table 48: Kinetic rates per processes for the mathematical description of the carbon dioxide absorption in aqueous solution (Compartment 3).

		Reaction definitions	Rates	Descriptions
Processes	**Acid –base equilibriums**	Water_deionization_f	kw*Kw	Irreversible reaction: $2H_2O \rightarrow H_3O^+ + OH^-$
		Water_deionization_r	kw*fm*OH*fm*H	Irreversible reaction: $2H_2O \leftarrow H_3O^+ + OH^-$
		$CO_2aq \rightarrow HCO_3^- + H^+$	kC1*KaC1*CO2aq	Irreversible reaction: $H_2CO_3 + H_2O \rightarrow HCO_3^- + H_3O^+$
		$HCO_3^- + H^+ \rightarrow CO_2aq$	kC1*fm*HCO3*fm*H	Irreversible reaction: $H_2CO_3 + H_2O \leftarrow HCO_3^- + H_3O^+$
		$HCO_3^- \rightarrow CO_3^{2-} + H^+$	kC2*KaC2*fm*HCO3	Irreversible reaction: $HCO_3^- + H_2O \rightarrow CO_3^{2-} + H_3O^+$
		$CO_3^{2-} + H^+ \rightarrow HCO_3^-$	kC2*fd*CO3*fm*H	Irreversible reaction: $HCO_3^- + H_2O \leftarrow CO_3^{2-} + H_3O^+$
	Gas-liquid Transfer	$O_2gas \rightarrow O_2aq$	KlaO2*(O2sat-O2)	Oxygen absorption: $O_2gas \rightarrow O_2aq$
		$CO_2gas \rightarrow CO_2aq$	KlaCO2*ECO2*(CO2sat-CO2aq)	Carbon dioxide absorption: $CO_2gas \rightarrow CO_2aq$

O_2 is the concentration of dissolved oxygen *[O2aq]* ; O2sat is the saturation concentration of dissolved oxygen in the experimental conditions (temperature) $[O_{2aq}^{Sat}](T)$; CO2aq is the concentration of carbon dioxide *[CO2aq]*; CO2sat is the saturation concentration of carbon dioxide depending of the experimental conditions $[CO_{2aq}^{Sat}](T)$ as defined at the equation (Eq 150).

The table 49 presents the different parameters used for the resolution of the mathematical model presented in table 47 and table 48. To describe the carbon dioxide absorption in aqueous solution all the parameters values or expression used were from the literature.

The gas-liquid oxygen mass transfer was described by the double-film model, with the mass resistance transfer localized in the liquid film only. The equation (Eq 155) defined the oxygen absorption in aqueous solution.

Eq 155: $$\frac{d[O_2aq]}{dt} = kl.a_{O_2}.([O_{2aq}^{Sat}](T) - [O_2aq])$$

where kla_{O2} is the volumetric gas-liquid rate for oxygen mass transfer (h^{-1}), $[O_{2aq}^{Sat}](T)$ is the dissolved oxygen saturation concentration (mol/l), $[O_2aq]$ is the dissolved oxygen concentration in the aqueous solution.

Experimentally the (kla_{O2}) is determined by the sulfite method (Linek and Vacek, 1981) (Skobota et al., 1982).

Table 49: Parameters values and/or expressions used for the mathematical description of the carbon dioxide absorption.

Parameters	Description	Values or Expressions	Unities	Ref
T	Experimental temperature	Experimental data	K	Experimental data
Zi	Valence of the specie i	Depends on the valence of the i specie	-	-
μ	Ionic strength (Ci = concentration of the specie i)	$0.5 \times \Sigma(Ci \times Zi^2)$	-	(Loewenthal et al., 1989)
A	Dependent temperature constant	$1.825 \times 10^6 \times (78.3 \times T)^{-1,5}$		(Loewenthal et al., 1989)
fm	Monovalent acitivity coefficient	$10\text{^}(A \times Zi \times ((\mu \times 0.5/(1 + \mu^{0.5})) - 0.3 \times \mu)$	-	(Loewenthal et al., 1989)
fd	Divalent acitivity coefficient	$10\text{^}(A \times \mu^2 \times ((\mu \times 0,5/(1 + \mu^{0.5})) - 0.3 \times \mu)$	-	-
Kw	Water ionization constant	$3.46 \times 10^{-24} \times \exp(0.0729 \times T)$	-	(Lide, 1990)
Ka_{C1}	First acid-base equilibrium constant (CO_2aq)	$10\text{^}(- (3404.7/T - 14.8435 + 0.03279 \times T))$	-	(Loewenthal et al., 1989)
Ka_{C2}	Second acid-base equilibrium constant (CO_2aq)	$10\text{^}(- (2902.47/T - 6.498 + 0.02379 \times T))$	-	(Loewenthal et al., 1989)
$H_{CO2/water}$ (T)	Carbon dioxide Henry constant (temperature)	$83400 \times \exp^{0,0254 \times T}$	Pa	relation (USPEA)
kw	Rate constant water dionization reaction	3.6×10^{13}	h^{-1}	(Musvoto et al, 2000)
kC1	Rate constant 1° acid-base eq (CO_2aq)	3.6×10^{10}	h^{-1}	(Musvoto et al, 2000)
kC2	Rate constant 2° acid-base eq (CO_2aq)	3.6×10^{13}	h^{-1}	(Musvoto et al, 2000)
KlaO2	Volumetric rate oxygen transfer	Experimental data	h^{-1}	-
KlaCO2	Volumetric rate carbon dioxide transfer	$KlaO2 \times (D_{CO2aq}(T)/D_{O2}(T))^{0.5}$	h^{-1}	(Spérandio and Paul, 1997)
ECO2	Enhancement factor for the carbon dioxide transfer	$1+((D_{CO3(2-)}(T) \times [CO_3^{2-}])/(D_{CO2aq}(T) \times [CO_2aq^{sat}]))$	-	(Bosch et al., 1989)
pH	pH of the aqueous solution	$-\log(f_m \times H)$		-

1.2.3. The simulation results (Aquasim®)

The figure 106 presents the pH simulations results obtained for the 6 experiments reported in the table 46. The numerical experiments were simulated with the same volumetric gas-liquid rate for oxygen mass transfer (0.7 h^{-1}), which is the mean value obtained by the sulfite method for the experimental configuration (mechanical stirring and surface aeration).

The simulation results showed good agreements between the experimental data and the numerical data (figure 106). The model enables the simulation of the pH time course of an aqueous solution during carbon dioxide absorption (without modification of the literature parameters). The model describes the tendencies of the dynamical process in different conditions and the equilibrium state obtained at the end. The miss match between some experimental data and numerical data (Exp_CO_2_b, Exp_CO_2_d), could be due to the uncertainty measurement of the kla_{O2}. Surface aeration was chosen for these experiments because low volumetric gas-liquid rate impose a slow absorption phenomena, thus a good pH definition in time. But work with surface aeration made experiments extremely sensitive to slight modifications in the reactor configuration, and explain the uncertainty add in the table 46 to the kla_{O2} definition. In fact, parameters estimations (Aquasim®) for the *klaO2* determination (Exp_CO_2_b, Exp_CO_2_d) gave good agreements in the pH definition for kla_{O2}_b = 0.95 h^{-1}, and kla_{O2}_d = 0.55 h^{-1}. Thus the uncertainty of the kla_{O2} measurement was defined at ± 0.25 h^{-1}.

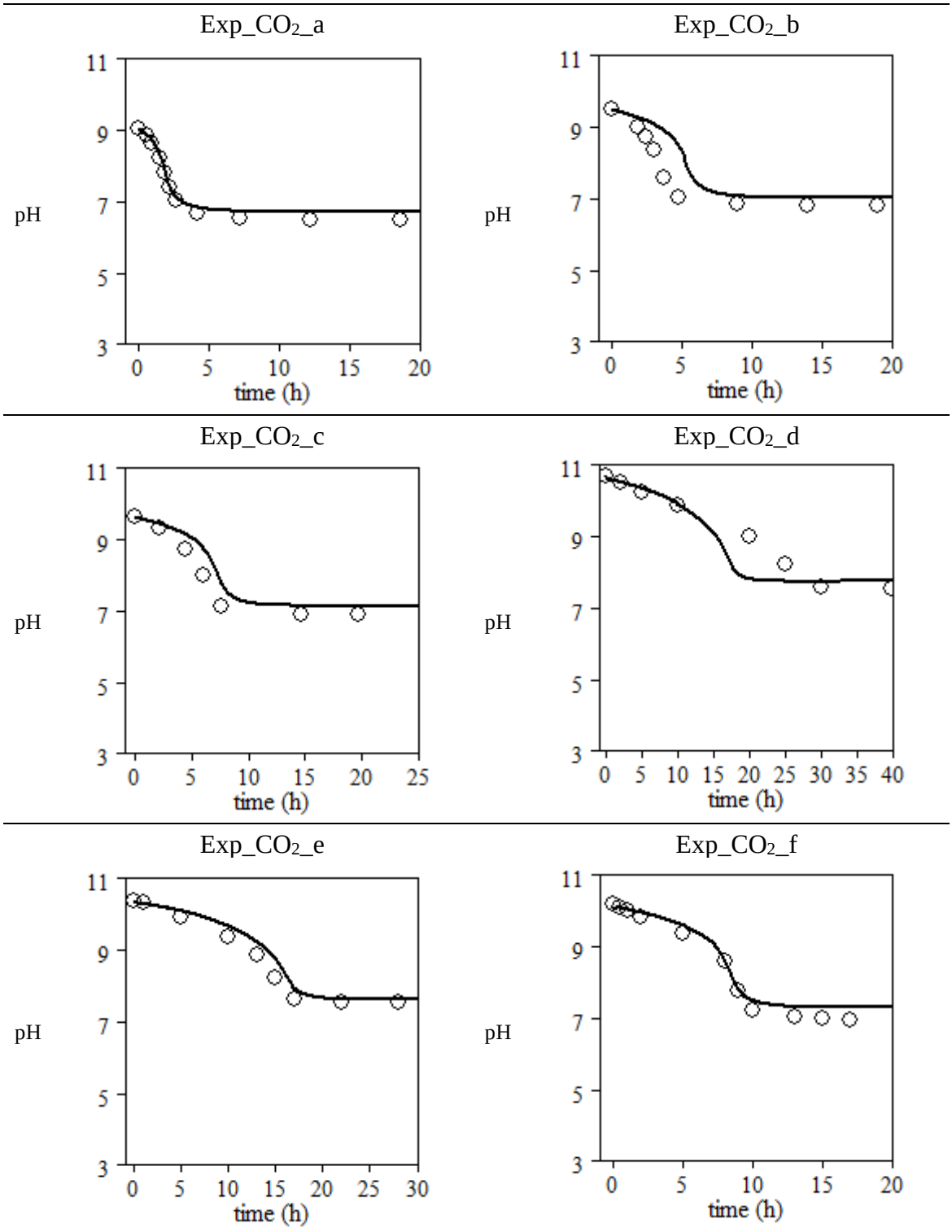

Figure 106: Simulation results for the pH calculation during the carbon dioxide absorption in aqueous solution. The kla_{O2} was fixed for all the experience (0.7 h^{-1}). ○ : the pH values from experimental data; ▬▬ : the pH simulation results.

The figure 107 shows the pH simulation results obtained for the experiments Exp_CO_2_e and Exp_CO_2_f, with and without the calculation of the enhancement factor for the carbon dioxide absorption. These simulation results indicate the interesting approximation proposed by Bosch in 1989 to define the carbon dioxide absorption in aqueous solution, and the necessary, at high pH, to take into account the impact of the equilibrium reactions on the gas-liquid mass transfers.

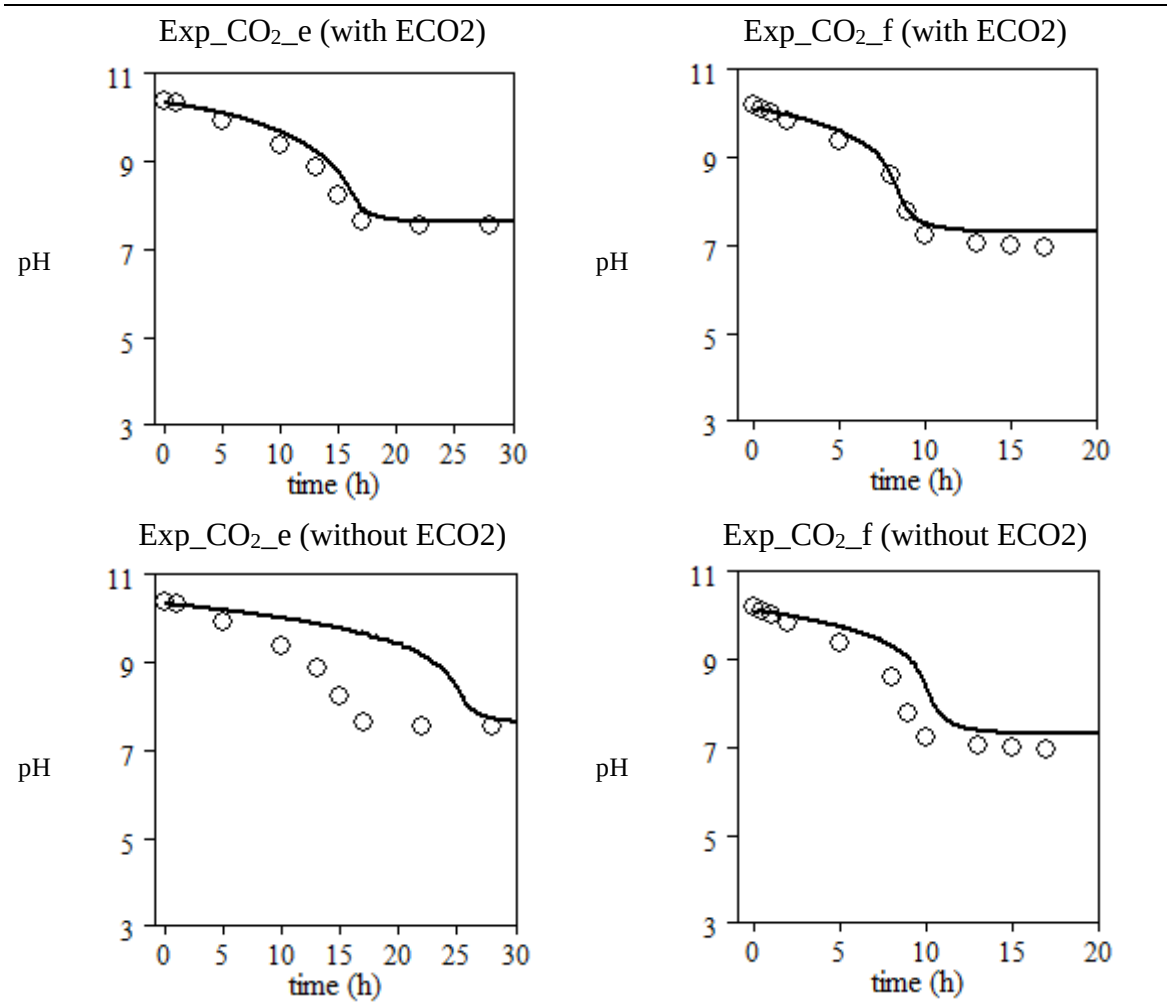

Figure 107: Simulation results for the pH calculation during the carbon dioxide absorption in aqueous solution with and without enhancement factor; Exp_CO2_e and Exp_CO2_f ; (kla_{O2}= 0.7 h^{-1}). ○ : the pH values from experimental data; ▬▬ : the pH simulation results.

The Compartment 3, describing the absorption of carbon dioxide in aqueous solution, was defined. The next paragraph developed the same approach for the reaction of sulfite (SO_3^{2-}) in aerated aqueous solution.

2. The reactions of sulfite (SO_3^{2-}) in aerated aqueous solution and the pH definition (Compartment 2a).

The mathematical model developed for the Compartment 3 was completed to describe the behavior of sulfite (SO_3^{2-}) in aerated aqueous solution, the impact on the concentration of the different compounds in solution (S(IV)-oxides, oxygen, S(VI)-oxides), and on the pH definition.

2.1. The system definition of the S(IV)-oxides in aerated aqueous solution

2.1.1. The equilibrium system SO_2gas-H_2SO_3-HSO_3^--SO_3^{2-} and the pH conditions for sulfite (SO_3^{2-}) predominance

The S(IV)-oxides speciation in solution and the pH definition in presence of these compounds, was defined by a gas-liquid equilibriums (Eq 156) and 2 acid-base equilibriums, the equation (Eq 157) describing the first acid-base equilibrium, and the equation (Eq 158) describing the second acid-base equilibrium.

Eq 156: $SO_2\,(gas) \overset{H_{SO_2/water}}{=} H_2SO_3\,(liq)$

where $H_{SO_2/water}$ is the Henry constant of the sulfur dioxide in water, considering the hydration reaction as an immediate reaction.

Eq 157: $H_2SO_3 + H_2O \overset{Ka_{S(iV)1}}{=} HSO_3^- + H_3O^+$

with $Ka_{S(IV)1} = (HSO_3^-).(H_3O^+)/(H_2SO_3)$, where $Ka_{S(IV)1}$ is the acid-base equilibrium constant (different values of $Ka_{S(IV)1}$ are reported from the literature in the table 40 of the chapter V of this document).

Eq 158: $HSO_3^- + H_2O \overset{Ka_{S(IV)2}}{=} SO_3^{2-} + H_3O^+$

with $Ka_{S(IV)2} = (SO_3^{2-}).(H_3O^+)/(HSO_3^-)$, where $Ka_{S(IV)2}$ is the acid-base equilibrium constant (different values of $Ka_{S(IV)2}$ are reported from the literature in the table 41).

To study the reactivity of sulfite (SO_3^{2-}) only, pH conditions must be evaluated, firstly to eliminate the loss of compounds by sulfur dioxide stripping (SO_2gas), secondly to obtained sulfite as the predominant S(IV)-oxides in solution. The table 42 presented in these annexes showed for different pH the speciation of the S(IV)-oxides. At pH 8.9 sulfite represents around 98% of the total S(IV)-oxides in solution, thus at above this pH value only sulfite oxidation could be considered.

2.1.2. The sulfite (SO_3^{2-}) oxidation in distilled water (Compartment 2a)

The sulfite oxidation in solution is generally described by the equation (Eq 123).

Different kinetic laws were proposed in the literature with important differences, for the kinetic law definition as well as for the homogenous rate value (see paragraph [1.] of theses annexes).

In a first approach, some controlled experiments were operated and then kinetic laws were directly tested with the model developed further to evaluate the existing description for the sulfite oxidation in aqueous solution.

The kinetic laws tested were based on the laws proposed, (i) by Brandt in 1995 with a 0 order in oxygen and a 1 order in sulfite, with a homogenous rate constant evaluated at 9.5×10^{-5} s^{-1} in dionized water, (ii) by Wilkinson in 1993 with a 1 order in O_2 for the uncatalyzed reaction. The global kinetic laws for the sulfite oxidation could be defined by the equation (Eq 159).

Eq 159: $$\frac{d[SO_3^{2-}]}{dt} = k_{SO3}.(f_d.[SO_3^{2-}])^n.[O_2]^m$$

where $[SO_3^{2-}]$ is the sulfite concentration (in mol/l); $[O_2]$ is the dissolved oxygen concentration (in mol/l); f_d is the activity coefficient for divalent ionic species; n is the reaction order in sulfite; m is the reaction order in dissolved oxygen; k_{SO3} is the homogenous rate constant (in $mol^{(1-n-m)}.l^{(-1+n+m)}.h^{-1}$).

To be completed, because sulfate was product during the sulfite oxidation, the acid-base equilibriums defining the concentration of the S(VI)-oxides in solution (Eq 128 and Eq 129), and influencing the pH definition must be taken into account.

2.1.3. The physical definition of the gas-liquid mass transfer of the oxygen

The sulfite oxidation occurred in presence of dissolved oxygen. In the reactor configuration, the oxygen was supplied by the bulk aeration (surface or bubbling system). In these conditions, the physical gas-liquid oxygen mass transfer was described at the paragraph *[1.2.2.]* of these annexes, by the equation (Eq 155).

2.1.4. Influence of an irreversible reaction on the definition of the gas-liquid mass transfer of the oxygen (enhancement factor E_{O2})

As presented at the paragraph *[1.]*, the sulfite oxidation in aerated aqueous solution influences the physical gas-liquid oxygen mass transfer (Ulrich et al., 1984).

When a gas-liquid mass transfer is followed in the liquid phase by a chemical reaction, the expression of the absorbed flux must be changed to take into account the influence of the chemical reaction on the physical transfer process. Thus, for the film model, the physical gas-liquid mass transfer described by the equation (Eq 155), must be modified and represented by the equation (Eq 160).

Eq 160: $$\frac{d[O_2aq]}{dt} = E_{O2}.kl.a_{O_2}.([O_{2_{aq}}^{Sat}](T) - [O_2aq])$$

where Kla_{O2} is the volumetric gas-liquid rate for oxygen mass transfer (h^{-1}), $[O_{2_{aq}}^{Sat}](T)$ is the dissolved oxygen saturation concentration (mol/l), $[O_2aq]$ is the dissolved oxygen concentration in the aqueous solution, and E_{O2} is the enhancement factor.

The enhancement factor E_{O2} is essentially dependent of a dimensionless number, the Hatta number, which represents the ratio between the maximum conversion in the diffusion liquid film and the maximum quantity of oxygen pass through the liquid-film by diffusion only. In

the case of chemical reaction described by the equation (Eq 159), the Hatta number was defined by the equation (Eq 161) (Danckwerts, 1970).

Eq 161: $$Ha = \frac{1}{k_L(O_2)}\sqrt{\frac{2}{m+1}.\, D_{O_2aq}(T).k_{SO_3}[O_2aq]^{(m-1)}.(f_d.[SO_3^{2-}])^n}$$

where $[SO_3^{2-}]$ is the sulfite concentration (in mol/l); $[O_2]$ is the dissolved oxygen concentration (in mol/l); f_d is the activity coefficient for divalent ionic species; n is the reaction order in sulfite; m is the reaction order in dissolved oxygen; k_{SO3} is the homogenous rate constant (in $mol^{(1-n-m)}.l^{(-1+n+m)}.h^{-1}$); $D_{O_2aq}(T)$ is the diffusion coefficient of oxygen in water (in $m^2.s^{-1}$); $k_L(O_2)$ is the oxygen rate mass transfer trough the liquid film ($m.s^{-1}$) (calculated in surface aerated condition from the kla_{O2} experimentally measured and (a) the volumetric interfacial surface give by the geometry of the experimental reactor ($a = 7.85\ m^2.m^{-3}$)).

The value of the Hatta number (Ha) indicates if the irreversible reaction has or not an impact on the gas-liquid mass transfer. In the case of different gas-liquid mass transport theories the table 50 (from Haroun 2008) presents the main number Hatta ranges (for the film model (Whitman, 1923)) and the expression of the enhancement factor (E_{O2}).

Numerous definitions of the enhancement factor were proposed in the literature (Danckwerts, 1970). The purpose of this paragraph is not a review of this aspect, but a presentation of some mathematical solutions for the definition of a dynamical model. In these conditions, the expression of the enhancement factor (E_{O2}) proposed by Danckwerts was tested (Eq 162), because in a first approximation, even under or above the Ha ranges the expression gives good agreements with excepted enhancement factor. For example, for a Hatta number at 0.1, the equation (Eq 162) gives an enhancement factor at 1.005 (≈ 1 excepted), for a Hatta number at 5 the equation (Eq 162) gives an enhancement factor at 5.1 (≈ 5 excepted).

Eq 162 : $$E_{O2} = \sqrt{1 + Ha^2}$$

The calculation of the Hatta number during each simulation enables the final evaluation of this choice for the expression of the enhancement factor of the oxygen mass transfer (E_{O2}), by the confrontation of the Hatta number values to the ranges presented in the table 50.

Table 50: Hatta number ranges and enhancement factor expressions for different theories of gas-liquid mass transport (Haroun 2008).

Ha ranges	Two-film theory (1924)	Higbie penetration theory (1935)	Danckwerts theory (1951)
Ha < 0.3 Slow reaction	$E_{O2} = 1$	$E_{O2} = 1$	$E_{O2} = 1$
0.3 < Ha < 3 Moderately fact reaction	$E_{O2} = \frac{Ha}{tanh(Ha)}$	$E_{O2} = X$ **	$E_{O2} = \sqrt{1 + Ha^2}$
Ha > 3 Fast reaction	$E_{O2} = Ha$	$E_{O2} = Ha$	$E_{O2} = Ha$
3 < Ha < 10Ei* Instantaneous reaction	$E_{O2} = Ei$	$E_{O2} = (1 + Ei).\sqrt{\frac{D_{SO_3^{2-}}(T)}{D_{O_2aq}(T)}}$	

*: Ei is the instantaneous enhancement factor ; $Ei = 1 + \frac{D_{SO_3^{2-}}(T).[SO_3^{2-}]}{\frac{1}{2}.D_{O_2aq}(T).[O_2aq]}$

**: $X = Ha.\left[1 + \frac{\pi}{8Ha^2}.erf\left(\frac{2Ha}{\sqrt{\pi}}\right) + \frac{1}{2}e^{\left(-\frac{4Ha^2}{\pi}\right)}\right]$

2.1.5. The definition of the Compartment 2a: mathematic model

To describe the sulfite oxidation and its influence on the pH definition of an aqueous solution, the system includes the variables and parameters describe for the Compartment 3 added by specific parameters described in the upper paragraphs. 4 acid-base equilibriums was added, thus 16 kinetic processes must be taken into account to define the evolution of 11 variables ($[H_3O^+]$, $[OH^-]$, $[H_2CO_3]$, $[HCO_3^-]$, $[CO_3^{2-}]$, $[O_2aq]$, $[SO_3^{2-}]$, $[HSO_3^-]$, $[H_2SO_3]$, $[SO_4^{2-}]$, $[HSO_4^-]$).

2.2. The experimental and simulation results for the sulfite (SO_3^{2-}) reactions in aerated aqueous solution (Compartment 2a)

2.2.1. Experiments and experimental results (Compartment 2a)

To evaluate the model definition, several experiments were operated in open batch reactor. The table 51 reports the experiments and the operating conditions. The experiments were realized by the addition of sodium sulfite (Na_2SO_3) at different concentrations. The pH and the dissolved oxygen were measured on-line. The four experiments Exp_SO_3^{2-}_a, Exp_SO_3^{2-}_b, Exp_SO_3^{2-}_c, Exp_SO_3^{2-}_d, were operated with distilled water, without initial pH modification, with the same configuration for the aeration process (surface aeration), with the same operating temperature (around 30°C). The experience Exp_SO_3^{2-}_e was operated after the addition of NaOH solution to determine a high initial pH. The experiments Exp_SO_3^{2-}_f and Exp_SO_3^{2-}_g were operated with distilled water, without initial pH modification, but with aeration process by bubbling.

For all the experiments the initial pH defined the pH of the aqueous solution just before the sulfite addition.

Table 51: Operating initial conditions for the study of the sulfite oxidation in aerated aqueous solution (Compartment 2a).

Name of the experiments	T (°C)	Initial pH*	Initial [SO_3^{2-}] (mol/l)	Initial [Na^+] (mol/l)	Initial [O_2aq] (mgO_2/l)	$kl.a_{O2}$ (h^{-1})
Exp_SO_3^{2-}_a	30.8 ± 1	5.41	3.21×10^{-3}	6.42×10^{-3}	7.19	0.70 ± 0.25
Exp_SO_3^{2-}_b	30.7 ± 1	5.77	1.73×10^{-3}	3.46×10^{-3}	6.92	0.70 ± 0.25
Exp_SO_3^{2-}_c	29.8 ± 1	5.41	8.32×10^{-4}	1.66×10^{-3}	7.12	0.70 ± 0.25
Exp_SO_3^{2-}_d	29.3 ± 1	5.33	1.31×10^{-3}	2.62×10^{-3}	7.07	0.70 ± 0.25
Exp_SO_3^{2-}_e	20.25 ± 1	10.81	1.19×10^{-3}	3.03×10^{-3}	8.71	0.70 ± 0.25
Exp_SO_3^{2-}_f	20.5 ± 1	6.30	6.135×10^{-3}	1.23×10^{-2}	8.82	7.13 ± 0.25
Exp_SO_3^{2-}_g	20.5 ± 1	4.17	5.778×10^{-3}	1.15×10^{-2}	8.43	7.28 ± 0.25

*: the initial pH defines the pH of the aqueous solution just before the sulfites injection.

The figure 108 and figure 109 show the pH and the dissolved oxygen concentration time courses recorded for the experiments Exp_SO_3^{2-}_a and Exp_SO_3^{2-}_e. For the experiment

Exp_SO_3^{2-}_a, with distilled water initially, the addition of sulfite led to an immediate increase of the pH, mainly due to the S(IV)-oxides acid-base equilibriums (Eq 157) and (Eq 158). At the same time the concentration of dissolved oxygen decreased immediately to zero, due to the oxidation of the sulfite by the dissolved oxygen (Eq 159). Then, due to the conversion of sulfite in solution (loss of a base) the pH of the solution decreased in time. During the same period the dissolved oxygen concentration maintained null. When all the sulfites in solution were oxidized, the pH began to stabilize, and the dissolved oxygen concentration increased, due to the oxygen absorption by the physical gas-liquid mass transfer only. At the end of the experiment the dissolved oxygen concentration stabilized at the saturation concentration.

The volumetric gas-liquid rate ($kl.a_{O2}$) was directly measured, for each experiment, by the sulfite method, from the experimental data of the rise of dissolved oxygen concentration.

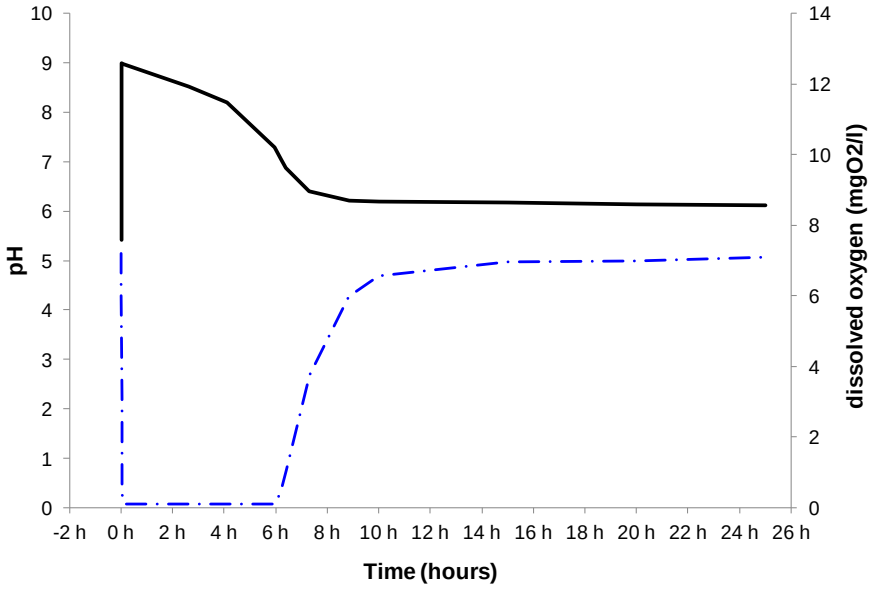

Figure 108: Exp_SO_3^{2-}_a – time course of the different parameters measured. ▬ · ▬ : dissolved oxygen concentration (mgO_2/l); ▬▬ : pH measurement.

For the experiment Exp_SO_3^{2-}_e (figure 109), the initial pH was fixed at high pH (around 10.80) by addition of NaOH to the solution. In that case, during all the experiment, the sulfite (SO_3^{2-}) was clearly the predominant form for the S(IV)-oxides. As for the experiment Exp_SO_3^{2-}_a (figure 108), the concentration of the dissolved oxygen decreased immediately after the sulfite addition. The slightly decrease of the pH during the experiment must be attributed to absorption of carbon dioxide described previously (Compartment 3).

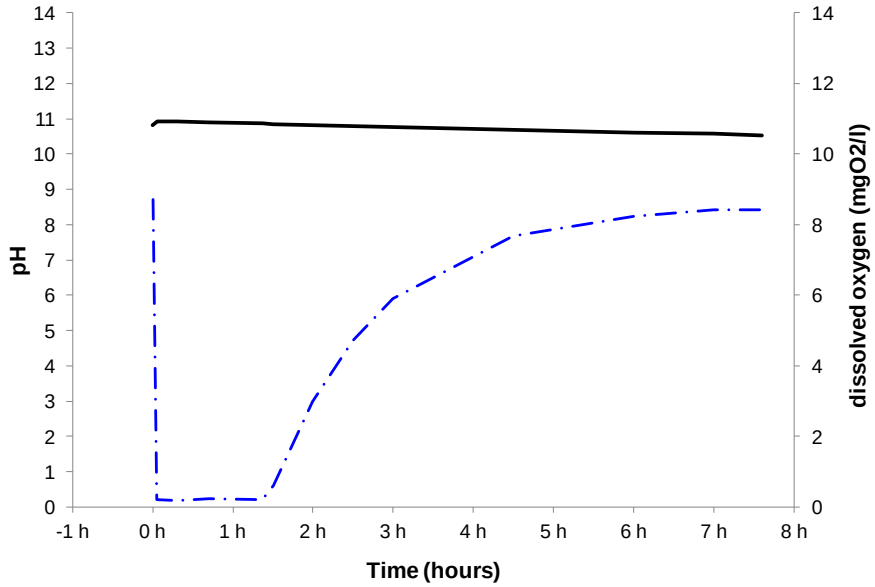

Figure 109: Exp_SO_3^{2-}_e – time course of the different parameters measured. ▬ ▪ ▬ : dissolved oxygen concentration (mgO_2/l); ▬▬ : pH measurement.

2.2.2. The model definition for the sulfite (SO_3^{2-}) reactions in aerated aqueous solution (Compartment 2a)

The table 52 presents the stoichiometric matrix for the mathematical description of the sulfite oxidation in aerated aqueous solution (Compartment 2a).

In that case the sodium ($[Na^+]$) was maintained for the system description, because the sulfite addition was ensure by dissolution of sodium sulfite salt (Na_2SO_3). Even if sodium is a non-reactive compounds in the context of the experiment, its concentration defined the ionic strength, thus the activity coefficient for the reactive compounds.

The table 53 presents the kinetic rates for all the processes involved in the mathematical description of the sulfite oxidation in aerated aqueous solution.

The table 54 and the table 55 present the different parameters used for the resolution of the mathematical model presented in table 52 and table 53. To describe the sulfite oxidation system (Compartment 2a) carbon dioxide absorption in aqueous solution all the parameters values or expression used here were from the literature.

Table 52: Parameters State variables, kinetic processes and stoichiometric ratio for the mathematical description of the sulfite oxidation in aerated aqueous solution (Compartment 2a).

State Variables		Description	$[H_3O^+]$	$[OH^-]$	$[Na^+]$	$[Cl^-]$	$[O_2]$	$[H_2CO_3]$	$[HCO_3^-]$	$[CO_3^{2-}]$	$[H_2SO_3]$	$[HSO_3^-]$	$[SO_3^{2-}]$	$[H_2SO_4]$	$[HSO_4^-]$	$[SO_4^{2-}]$
		Unit	mol/L	mol/L	mol/L	mol/L	mol/L	mol/L	mol/L	mol/L	mol/L	mol/L	mol/L	mol/L	mol/L	mol/L
		Expression	H	OH	Na	Cl	O2	CO2aq	HCO3	CO3	SO2aq	HSO3	SO3	H2SO4	HSO4	SO4
Processes	**Acid –base equilibriums**	Water_deionization_f	1	1												
		Water_deionization_r	-1	-1												
		$CO_2aq \rightarrow HCO_3^- + H^+$	1					-1	1							
		$HCO_3^- + H^+ \rightarrow CO_2aq$	-1					1	-1							
		$HCO_3^- \rightarrow CO_3^{2-} + H^+$	1						-1	1						
		$CO_3^{2-} + H^+ \rightarrow HCO_3^-$	-1						1	-1						
		$SO_2aq \rightarrow HSO_3^- + H^+$	1								-1	1				
		$HSO_3^- + H^+ \rightarrow SO_2aq$	-1								1	-1				
		$HSO_3^- \rightarrow SO_3^{2-} + H^+$	1									-1	1			
		$SO_3^{2-} + H^+ \rightarrow HSO_3^-$	-1									1	-1			
		$H_2SO_4 \rightarrow HSO_4^- + H^+$	1											-1	1	
		$HSO_4^- + H^+ \rightarrow H_2SO_4$	-1											1	-1	
		$HSO_4^- \rightarrow SO_4^{2-} + H^+$	1												-1	1
		$SO_4^{2-} + H^+ \rightarrow HSO_4^-$	-1												1	-1
	Oxidation	$SO_3^- + O_2 \rightarrow SO_4^-$					-0.5						-1			1
	Gas-liquid transfer	$O_2gas \rightarrow O_2aq$					1									
		$CO_2gas \rightarrow CO_2aq$						1								

Table 53: Kinetic rates per processes for the mathematical description of the sulfite oxidation (Compartment 2a).

		Reaction definitions	Rates	Descriptions
Processes	**Acid –base equilibriums**	Water_deionization_f	kw*Kw	Irreversible reaction: $2H_2O \rightarrow H_3O^+ + OH^-$
		Water_deionization_r	kw*fm*OH*fm*H	Irreversible reaction: $2H_2O \leftarrow H_3O^+ + OH^-$
		$CO_2aq \rightarrow HCO_3^- + H^+$	kC1*KaC1*CO2aq	Irreversible reaction: $CO_2aq + H_2O \rightarrow HCO_3^- + H_3O^+$
		$HCO_3^- + H^+ \rightarrow CO_2aq$	kC1*fm*HCO3*fm*H	Irreversible reaction: $CO_2aq + H_2O \leftarrow HCO_3^- + H_3O^+$
		$HCO_3^- \rightarrow CO_3^{2-} + H^+$	kC2*KaC2*fm*HCO3	Irreversible reaction: $HCO_3^- + H_2O \rightarrow CO_3^{2-} + H_3O^+$
		$CO_3^{2-} + H^+ \rightarrow HCO_3^-$	kC2*fd*CO3*fm*H	Irreversible reaction: $HCO_3^- + H_2O \leftarrow CO_3^{2-} + H_3O^+$
		$SO_2aq \rightarrow HSO_3^- + H^+$	kS(IV)1*KaS(IV)1*SO2aq	Irreversible reaction: $SO_2aq + H_2O \rightarrow HSO_3^- + H_3O^+$
		$HSO_3^- + H^+ \rightarrow SO_2aq$	kS(IV)1*fm*HSO3*fm*H	Irreversible reaction: $SO_2aq + H_2O \leftarrow HSO_3^- + H_3O^+$
		$HSO_3^- \rightarrow SO_3^{2-} + H^+$	kS(IV)2*KaS(IV)2*fm*HSO3	Irreversible reaction: $HSO_3^- + H_2O \rightarrow SO_3^{2-} + H_3O^+$
		$SO_3^{2-} + H^+ \rightarrow HSO_3^-$	kS(IV)2*fd*SO3*fm*H	Irreversible reaction: $HSO_3^- + H_2O \leftarrow SO_3^{2-} + H_3O^+$
		$H_2SO_4 \rightarrow HSO_4^- + H^+$	kS(VI)1*KaS(VI)1*H2SO4	Irreversible reaction: $H_2SO_4 + H_2O \rightarrow HSO_4^- + H_3O^+$
		$HSO_4^- + H^+ \rightarrow H_2SO_4$	kS(VI)1*fm*HSO4*fm*H	Irreversible reaction: $H_2SO_4 + H_2O \leftarrow HSO_4^- + H_3O^+$
		$HSO_4^- \rightarrow SO_4^{2-} + H^+$	kS(VI)2*KaS(VI)2*fm*HSO4	Irreversible reaction: $HSO_4^- + H_2O \rightarrow SO_4^{2-} + H_3O^+$
		$SO_4^{2-} + H^+ \rightarrow HSO_4^-$	kS(VI)2*fd*SO4*fm*H	Irreversible reaction: $HSO_4^- + H_2O \leftarrow SO_4^{2-} + H_3O^+$
	Oxidation	$SO_3^- + O_2 \rightarrow SO_4^-$	kSO3*((fd*SO3)^n) *(O2^m)	Sulfite oxidation: $SO_3^{2-} + 0.5\ O_2 \rightarrow SO_4^{2-}$
	Gas-liquid transfer	$O_2gas \rightarrow O_2aq$	KlaO2*EO2*(sat_O2-O2)	Oxygen absorption: $O_2gas \rightarrow O_2aq$
		$CO_2gas \rightarrow CO_2aq$	KlaCO2*ECO2*(sat_CO2-CO2aq)	Carbon dioxide absorption: $CO_2gas \rightarrow CO_2aq$

Table 54: Equilibrium parameters values and/or expressions used for the mathematical description of the sulfite oxidation (Compartment 2a).

Parameters	Description	Values or Expressions	Unities	Ref
T	Experimental temperature	Experimental data	K	Experimental data
Zi	Valence of the specie i	Depends on the valence of the i specie	-	-
μ	Ionic strength (Ci = concentration of the specie i)	$0.5 \times \Sigma(Ci \times Zi^2)$	-	(Loewenthal et al., 1989)
A	Dependent temperature constant	$1.825 \times 10^6 \times (78.3 \times T)^{-1,5}$		(Loewenthal et al., 1989)
Fm	Monovalent acitivity coefficient	$10\text{^}(A \times Zi \times ((\mu \times 0.5/(1 + \mu^{0.5})) - 0.3 \times \mu)$	-	(Loewenthal et al., 1989)
Fd	Divalent acitivity coefficient	$10\text{^}(A \times \mu^2 \times ((\mu \times 0,5/(1 + \mu^{0.5})) - 0.3 \times \mu)$	-	-
Kw	Water ionization constant	$3.46 \times 10^{-24} \times \exp(0.0729 \times T)$	-	(Lide, 1990)
Ka_{C1}	First acid-base equilibrium constant (CO_2aq)	$10\text{^}(- (3404.7/T - 14.8435 + 0.03279 \times T))$	-	(Loewenthal et al., 1989)
Ka_{C2}	Second acid-base equilibrium constant (CO_2aq)	$10\text{^}(- (2902.47/T - 6.498 + 0.02379 \times T))$	-	(Loewenthal et al., 1989)
$Ka_{S(IV)1}$	First acid-base equilibrium constant (SO_2aq)	$10\text{^}(- 4.74 + (853/T))$ (a) ou $10^{-1,76}$ (b)		(a) (Maahs, 1982)
$Ka_{S(IV)2}$	Second acid-base equilibrium constant (SO_2aq)	$10\text{^}(- 9.278 + (621.9/T))$ (a) ou $10^{-7,20}$ (b)		(a) (Maahs, 1982)
$Ka_{S(VI)1}$	First acid-base equilibrium constant (H_2SO_4)	100 (totalement dissocié en solution)		
$Ka_{S(VI)2}$	Second acid-base equilibrium constant (H_2SO_4)	$9.895 \times 10^{-8} \times T^3 - 8.949 \times 10^{-5} \times T^2 + 0.02671 \times T^{-2} + 2.62$		
$H_{CO2/water}$ (T)	Carbon dioxide Henry constant (temperature)	$83400 \times \exp^{0,0254 \times T}$	Pa	relation (USPEA)
Sat_O2aq (T)	Dissolved oxygen saturation concentration	$7.2044x10^{-}7xT^4-0.00090733xT^3+0.42974xT^2-90.817xT+7238.6$		Adapted from solublity data
pH	pH of the aqueous solution	-log(fm x H)		-

Table 55: Kinetic parameters values and/or expressions used for the mathematical description of the sulfite oxidation (Compartment 2a).

Parameters	Description	Values or Expressions	Unities	Ref
kw	Rate constant water dionization reaction	3.6×10^{13}	$l.mol^{-1}.h^{-1}$	(Musvoto et al, 2000)
kC1	Rate constant 1° acid-base eq (CO_2aq)	3.6×10^{10}	$l.mol^{-1}.h^{-1}$	(Musvoto et al, 2000)
kC2	Rate constant 2° acid-base eq (CO_2aq)	3.6×10^{13}	$l.mol^{-1}.h^{-1}$	(Musvoto et al, 2000)
kS(IV)1	Rate constant 1° acid-base eq (SO_2aq)	10^{10}	$l.mol^{-1}.h^{-1}$	Defined
kS(IV)2	Rate constant 2° acid-base eq (SO_2aq)	10^{10}	$l.mol^{-1}.h^{-1}$	Defined
kS(VI)1	Rate constant 1° acid-base eq (H_2SO_4)	10^{10}	$l.mol^{-1}.h^{-1}$	Defined
kS(VI)2	Rate constant 2° acid-base eq (H_2SO_4)	10^{10}	$l.mol^{-1}.h^{-1}$	Defined
kSO3	Rate constant for the sulfite oxidation	Tested	/	Evaluated in this study
n	Sulfite order of the sulfite oxidation	To determine	-	Evaluated in this study
m	Oxygen order of the sulfite oxidation	To determine	-	Evaluated in this study
a	Volumetric interfacial surface	(surface aeration = 7,85 $m^2.m^{-3}$)	$m^2.m^{-3}$	Experimental data
KlaO2	Volumetric rate oxygen transfer	Experimental data (surface aeration = 0,7 h^{-1})	h^{-1}	-
klO2	Rate oxygen transfer	KlaO2 / a	$m.h^{-1}$	-
KlaCO2	Volumetric rate carbon dioxide transfer	$KlaO2 \times (D_{CO2aq}(T)/D_{O2}(T))^{0.5}$	h^{-1}	(Spérandio, 1996)
Hatta	Hatta number for the oxygen transfer	$kSO3x(2/(1+1))x(D_{O2}(T)x3600)x([O_2]^{(1-1)})x([SO_3^{2-}]^2)^{0.5})/klO2$	-	(Danckwerts, 1970)
EO2	Enhancement factor for the oxygen transfer	$(1+Hatta^2)^{0.5}$	-	(Danckwerts, 1970)
ECO2	Enhancement factor for the carbon dioxide transfer	$1+((D_{CO3(2-)}(T) \times [CO_3^{2-}])/(D_{CO2aq}(T) \times [CO_2aq^{sat}]))$	-	(Bosch et al., 1989)

2.2.3. The simulation results obtained for the kinetic describes in the literature for the sulfite oxidation in aerated aqueous solution (Compartment 2a) (Aquasim®)

The general kinetic law for the sulfite oxidation was previously described the (Eq 159).

Two equations from the literature were firstly tested, (i) n = 1 and m = 0 with $k_{SO3} = 9.5 \times 10^{-5}$ s^{-1} (Brandt 1995) ($k_{SO3} = 0.324$ h^{-1}), (ii) n = 1 and m = 1 with two values of the rate constant (k_{SO3}).

The figure 110 presents the simulation results compared to the experimental dissolved oxygen concentration and pH values for the experiments Exp_SO_3^{2-}_a, Exp_SO_3^{2-}_c and Exp_SO_3^{2-}_g, using the Brandt kinetic law. The model describes the oxygen consumption and the decrease of the pH. But the experimental data are not correlated to the simulation results. For all the experiments the mean square deviation between the numerical results and the experimental data was calculated, for the pH values as well as for the dissolved oxygen concentration (noted Dev_pH for the mean square deviation between the numerical pH values and the experimental pH data, and Dev_O_2 for the mean square deviation between the numerical dissolved oxygen concentration and the experimental data). The table 56 resumes the mean square deviation obtained for all the model definition (Compartment 2a) used in this study (for the experiments Exp_SO_3^{2-}_a, Exp_SO_3^{2-}_b, Exp_SO_3^{2-}_c, Exp_SO_3^{2-}_d, Exp_SO_3^{2-}_f, Exp_SO_3^{2-}_g).

With the rate constant $k_{SO3} = 0.324$ h^{-1} (figure 110), the oxidation kinetics seemed to be too slow, especially for the experiments Exp_SO_3^{2-}_c and Exp_SO_3^{2-}_g, where the oxygen consumption simulated is clearly inferior of the oxygen consumption recorded during the experiments.

n = 1 ; m = 0 ; k_{SO3} = 9.5 x 10^{-5} s^{-1} = 0.324 h^{-1} (Brandt 1995)

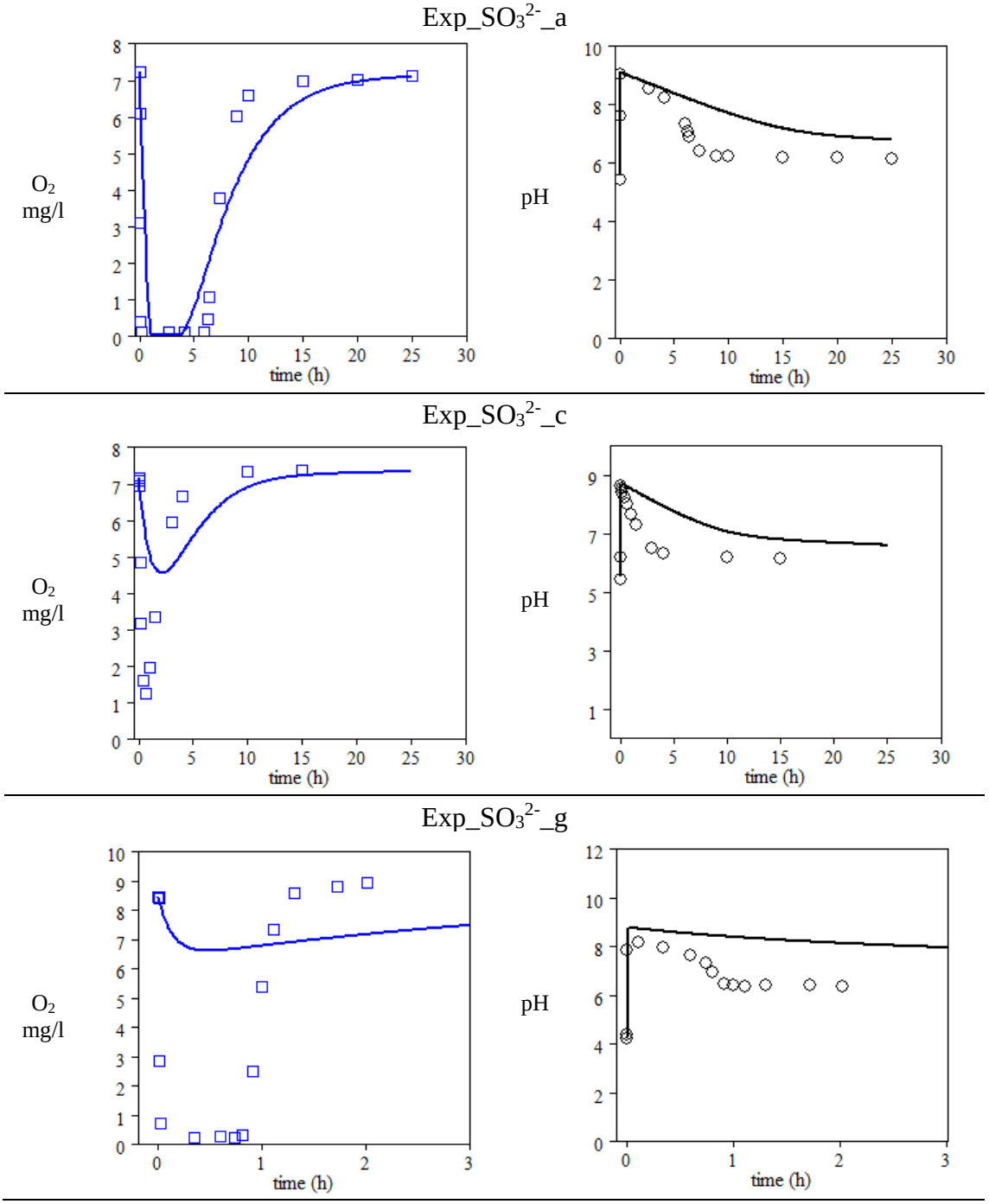

Figure 110: Simulation results compared to the experimental data for the pH and the dissolved oxygen concentration during the experiments Exp_SO_3^{2-}_a - Exp_SO_3^{2-}_c - Exp_SO_3^{2-}_g . n = 1 ; m = 0 ; k_{SO3} = 9.5 x 10^{-5} s^{-1} = 0.324 h^{-1} (Brandt 1995). □ : experimental values for the dissolved oxygen concentration (mgO_2/l) ; ——: simulation of the dissolved oxygen concentration (mgO_2/l); ○ : the experimental values for pH ; ——: simulation of the pH.

To evaluate the kinetics definition, the value of the rate constant k_{SO3} was increased (three values were tested $k_{SO3} = 0.95\ h^{-1}$, $1.3\ h^{-1}$, $3\ h^{-1}$). The simulated results compared to the experimental data, for $k_{SO3} = 3\ h^{-1}$, are presented in the figure 111. The increase of the rate constant seems to improve the model definition for the experiments Exp_SO_3^{2-}_c and Exp_SO_3^{2-}_g (figure 111/figure 110) but at the same time the simulated oxygen consumption for the experiment Exp_SO_3^{2-}_a were more important. However, the comparison for Dev_O_2 and Dev_pH (table 56) indicated an improvement of the model accuracy by the increase of the rate constant k_{SO3}.

Table 56: kinetic law definitions tested for the numerical experiments, and the corresponding mean square deviation between numerical results and experimental results, for the pH and the dissolved oxygen concentration (for the experiments Exp_SO_3^{2-}_a, Exp_SO_3^{2-}_b, Exp_SO_3^{2-}_c, Exp_SO_3^{2-}_d, Exp_SO_3^{2-}_f, Exp_SO_3^{2-}_g).

Definition of the kinetic law for the sulfite oxidation	Dev_O_2[a]	Dev_pH[b]
n = 1, m = 0, $k_{SO3} = 0.324\ h^{-1}$ *(Brandt 1995)*	9.76	1.76
n = 1, m = 0, $k_{SO3} = 0.95\ h^{-1}$ *(adapted from Brandt 1995)*	4.45	0.79
n = 1, m = 0, $k_{SO3} = 1.3\ h^{-1}$ *(adapted from Brandt 1995)*	3.59	0.59
n = 1, m = 0, $k_{SO3} = 3\ h^{-1}$ *(adapted from Brandt 1995)*	3.07	0.42
n = 1, m = 1, $k_{SO3} = 9 \times 10^4\ l.mol^{-1}.h^{-1}$ *(adapted from Wilkinson 1993)*	4.96	0.84
n = 1, m = 1, $k_{SO3} = 5 \times 10^5\ l.mol^{-1}.h^{-1}$ *(adapted from Wilkinson 1993)*	5.56	0.53
n = 3/2, m = 1, $k_{SO3} = 3.5 \times 10^7\ l^{3/2}.mol^{-3/2}.h^{-1}$ *(from this study)*	4.49	0.27
n = 2, m = 1, $k_{SO3} = 1.63 \times 10^{10}\ l^2.mol^{-2}.h^{-1}$ *(from this study)*	0.73	0.1

a: mean square deviation between numerical and experimental results for the dissolved oxygen concentration
b: mean square deviation between numerical and experimental results for pH

The simulated results presented in the figure 110 and in the figure 111 indicated the discordance of the model definition with the experimental data, because the improvement of some numerical experiment leads to a loss of accuracy for other numerical experiments, even if the global mean square deviation decreases with the increase of the rate constant k_{SO3}.

n = 1 ; m = 0 ; k_{SO3} = 3 h^{-1} (adapted from Brandt 1995)

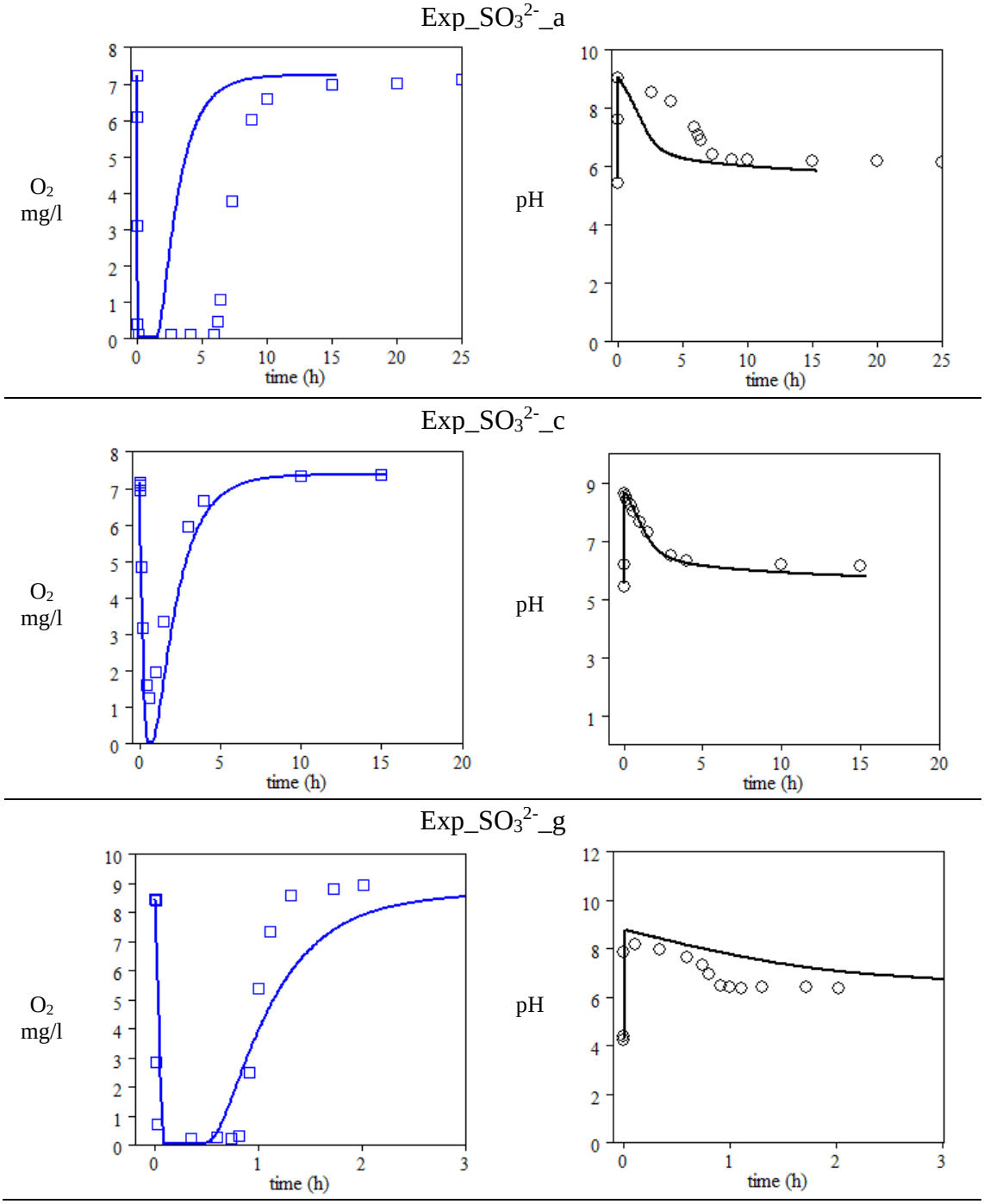

Figure 111: Simulation results compared to the experimental data for the pH and the dissolved oxygen concentration during the experiments Exp_SO_3^{2-}_a - Exp_SO_3^{2-}_c - Exp_SO_3^{2-}_g . n = 1 ; m = 0 ; k_{SO3} = 3 h^{-1} (adapted from Brandt 1995). ▢ : experimental values for the dissolved oxygen concentration (mgO_2/l) ; ——: simulation of the dissolved oxygen concentration (mgO_2/l); ○ : the experimental values for pH ; ——: simulation of the pH.

The figure 112 presents the simulation results compared to the experimental dissolved oxygen concentration and pH values for the experiments Exp_SO_3^{2-}_a, Exp_SO_3^{2-}_c and Exp_SO_3^{2-}_g, using the kinetic law adapted from Wilkinson. In this kinetic proposition, a general value of the rate constant (k_{SO3}) was not defined. To evaluate the model definition, two values of the rate constant (k_{SO3}) were previously tested (k_{SO3} = 9 x 10^4 l.mol^{-1}.h^{-1} and 5 x 10^5 l.mol^{-1}.h^{-1}).

Compared to the simulated results presented in the figure 110 and in thefigure 111, this kinetic law seems to represent the system with a better accuracy for all the experiments, for the dissolved oxygen concentration as well as for the pH definition. Nevertheless, the mean square deviation calculated for these numerical experiments showed accuracy in the same range than the kinetic law previously tested (table 56).

However, regarding to the oxygen consumption the kinetic seems to be too slow again with k_{SO3} = 9 x 10^4 l.mol^{-1}.h^{-1} (figure 114). Thus, a higher value for the rate constant was tested (k_{SO3} = 5 x 10^5 l.mol^{-1}.h^{-1}). The figure 113 presents the results obtained for this rate constant definition. A significant increase in the rate constant (x 5.5) modified the results but not the accuracy of the numerical simulation (gain accuracy for Dev_pH with a loss of accuracy for Dev_O_2).

Two kinetic laws, from the literature, were tested, with different rate constants. None of them could describe, with an interesting accuracy, the dynamic system of the sulfite oxidation in different conditions. However, the kinetic law with an order 1 in oxygen seems to improve the shape definition of the system, even if no rate constants could unified the different experiments. Thus the equation (Eq 159) could be adapted and the following equation (Eq 163) could be proposed to describe the sulfite oxidation kinetic.

Eq 163: $$\frac{d[SO_3^{2-}]}{dt} = k_{SO3} . (f_d . [SO_3^{2-}])^n . [O_2]$$

n = 1 (tested) ; m = 1 ; k_{SO3} = 9 x 10^4 $l.mol^{-1}.h^{-1}$ (adapted from Wilkinson 1993)

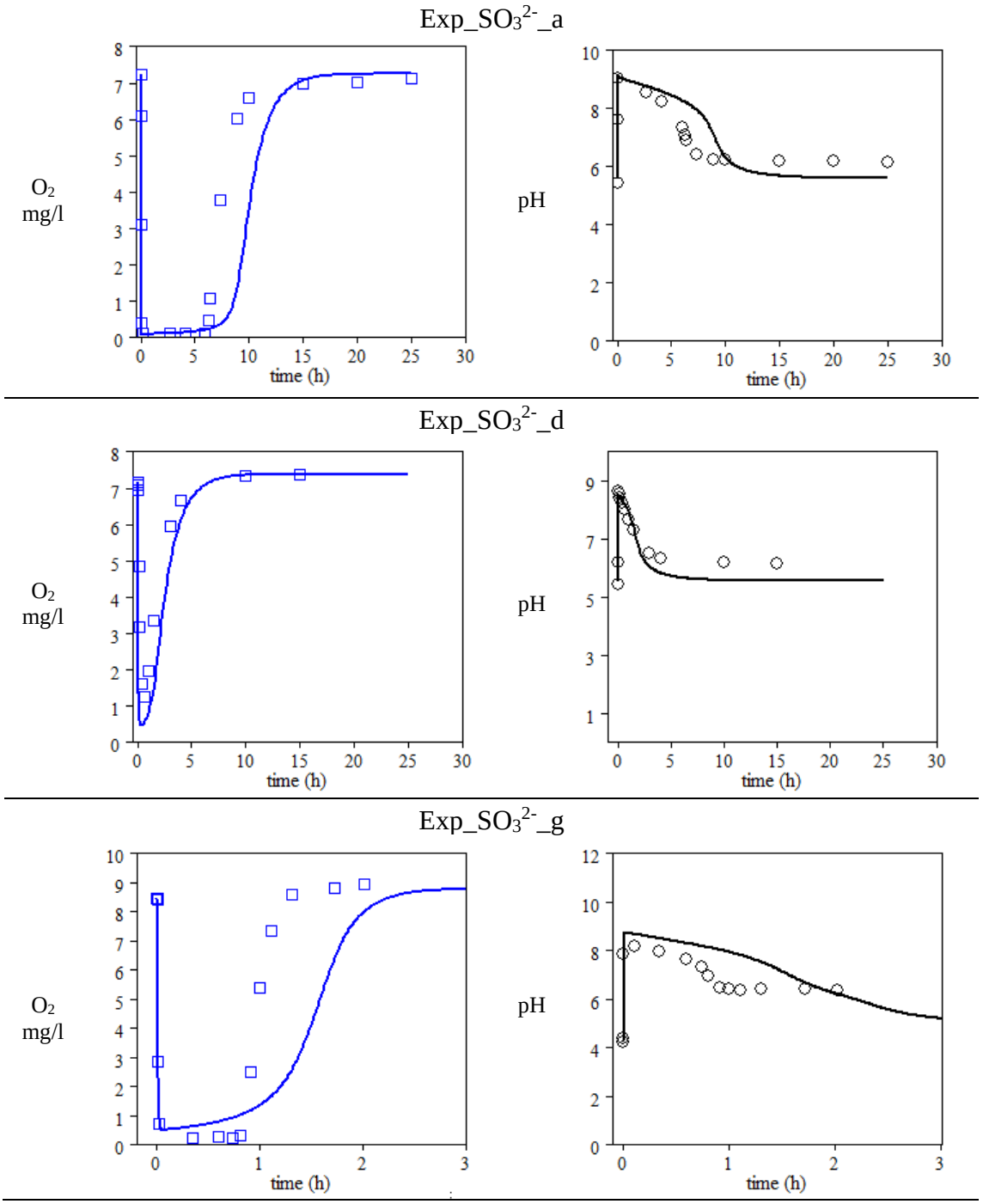

Figure 112: Simulation results compared to the experimental data for the pH and the dissolved oxygen concentration during the experiments Exp_SO_3^{2-}_a - Exp_SO_3^{2-}_c - Exp_SO_3^{2-}_g . n = 1 ; m = 1 ; k_{SO3} = 9 x 10^4 $l.mol^{-1}.h^{-1}$ (adapted from Wilkinson 1993). □ : Experimental values for the dissolved oxygen concentration (mgO_2/l) ; ——: simulation of the dissolved oxygen concentration (mgO_2/l); ○ : the experimental values for pH ; ——: simulation of the pH.

n = 1 (tested) ; m = 1 ; k_{SO3} 5 x 10^5 $l.mol^{-1}.h^{-1}$ (adapted from Wilkinson 1993)

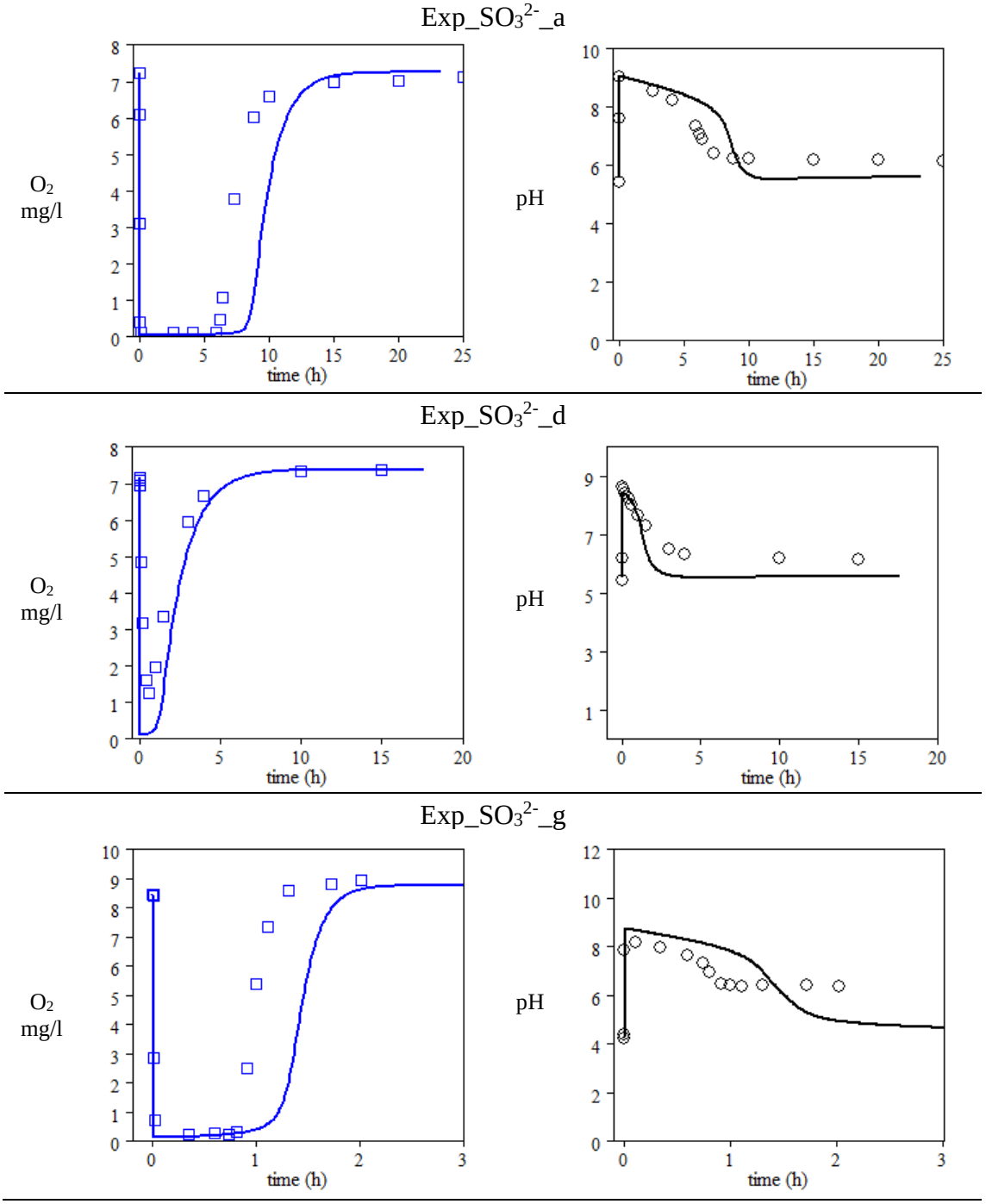

Figure 113: Simulation results compared to the experimental data for the pH and the dissolved oxygen concentration during the experiments Exp_SO_3^{2-}_a - Exp_SO_3^{2-}_c - Exp_SO_3^{2-}_g . n = 1 ; m = 1 ; k_{SO3} = 5 x 10^5 $l.mol^{-1}.h^{-1}$ (adapted from Wilkinson 1993). □ : Experimental values for the dissolved oxygen concentration (mgO_2/l) ; ——: simulation of the dissolved oxygen concentration (mgO_2/l); ○ : the experimental values for pH ; ——: simulation of the pH.

2.2.4. The adaptation of the sulfite oxidation kinetic definition and the simulation results obtained (Compartment 2a) (Aquasim®)

The stoichiometric equation defining the sulfite oxidation was described by the equation (Eq 123) with the kinetic law defined by the equation (Eq 163).

For the evaluation of the kinetic law, two n values were tested (n = 1.5, and n = 2). For each value of n the best rate constant (k_{SO3}) was evaluated by testing different values. The best results obtained for each n value, with the rate constant associated, are presented in the table 56. For n = 1.5, although none improvement of the model was observed for the dissolved oxygen concentration definition, the Dev_O_2 was in the same order of magnitude than for the other kinetic laws previously tested, an improvement of the pH definition was recorded. For n = 2, a clear improvement of the accuracy was obtained, for Dev_O_2 as well as for Dev_pH.

The figure 114 and figure 115 present the simulation results compared to the experimental data for the experiments Exp_SO_3^{2-}_a, Exp_SO_3^{2-}_b, Exp_SO_3^{2-}_c, and for the experiments Exp_SO_3^{2-}_d, Exp_SO_3^{2-}_e, Exp_SO_3^{2-}_g respectively. For all the experiments, the dissolved oxygen concentration and the pH were simulated with an interesting accuracy compared to the experimental data. The kinetic law for the sulfite oxidation in aerated aqueous solution (distilled water) could be described by the equation (Eq 164).

Eq 164: $-\frac{d[SO_3^{2-}]}{dt} = k_{SO3}.(f_d.[SO_3^{2-}])^2.[O_2]$ with k_{SO3} = 1.63 x 10^{10} $l^2.mol^{-2}.h^{-1}$

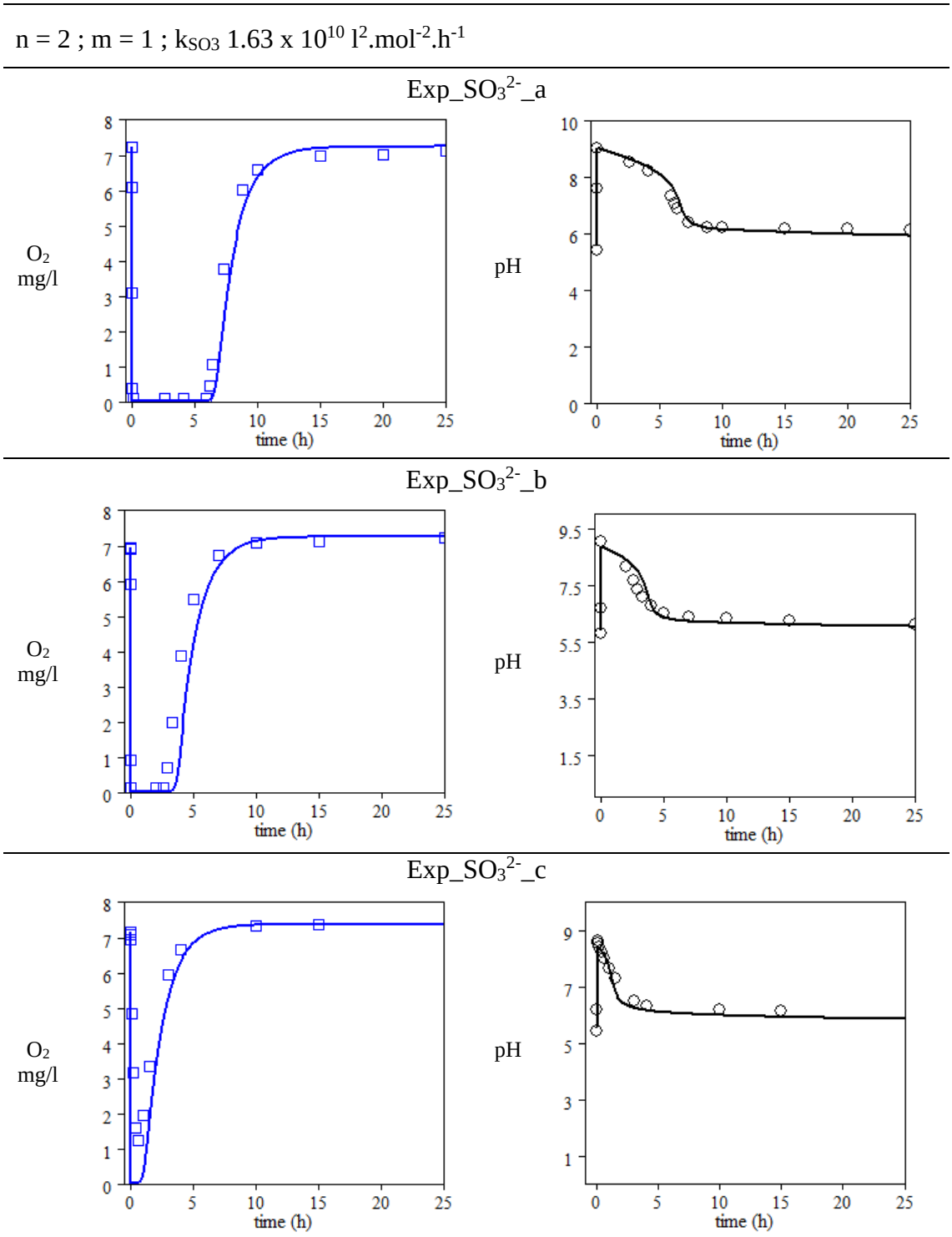

Figure 114: Simulations results compared to the experimental data for the pH and the dissolved oxygen concentration during the experiments Exp_SO_3^{2-}_a - Exp_SO_3^{2-}_b - Exp_SO_3^{2-}_c ; n = 2 ; m = 1 ; k_{SO3} = 1.63 x 10^{10} $l^2.mol^{-2}.h^{-1}$ (adapted from Wilkinson 1993). □ : Experimental values for the dissolved oxygen concentration (mgO_2/l) ; ——: simulation of the dissolved oxygen concentration (mgO_2/l); ○ : the experimental values for pH ; ——: simulation of the pH.

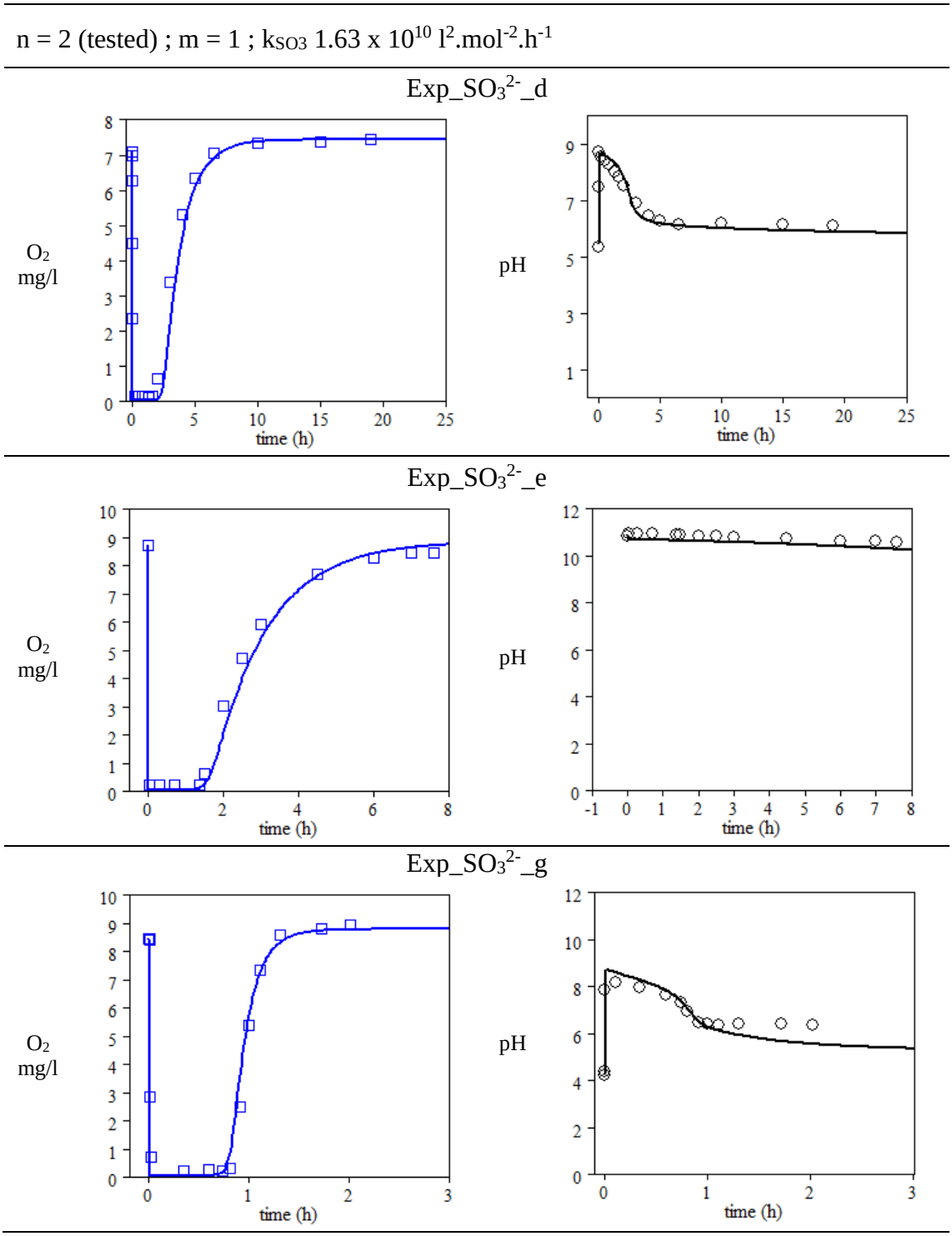

Figure 115: Simulations results compared to the experimental data for the pH and the dissolved oxygen concentration during the experiments Exp_SO_3^{2-}_d - Exp_SO_3^{2-}_e - Exp_SO_3^{2-}_g ; n = 2 ; m = 1 ; k_{SO3} = 1.63 x 10^{10} $l^2.mol^{-2}.h^{-1}$ (adapted from Wilkinson 1993). ☐ : Experimental values for the dissolved oxygen concentration (mgO_2/l) ; ——: simulation of the dissolved oxygen concentration (mgO_2/l); ○ : the experimental values for pH ; ——: simulation of the pH.

To define the numerical model, especially the oxygen absorption, hypotheses have been made. The enhancement factor (E_{O2}) was defined by the equation proposed by Danckwerts, corresponding to Hatta numbers ranging between 0.3 and 3. Thus, for each experiment, the Hatta number corresponding of the simulation must be include in this range to have an enhancement correctly defined. The figure 116 presents for each experiment the Hatta numbers calculation during the first hour. For each experiment (expected for the experiment Exp_SO_3^{2-}_c), the initial Hatta number was in the range fixed. For the experiment Exp_SO_3^{2-}_c, an initial Hatta number of 0.22 was determined. At this Hatta number value, the enhancement factor (E_{O2}) must be equal to 1 (table 50). Using the equation (Eq 162) defining the enhancement factor from the Hatta number calculation E_{O2} = 1.024 was obtained. This deviation corresponds to an increase of 2.4% of the physical gas-liquid rate. With the decrease of the Hatta number during the experiment (due to the decrease in the sulfite oxidation kinetic), this deviation decrease also, minimizing the deviation (maximum of 4.4% for Ha = 0.299).

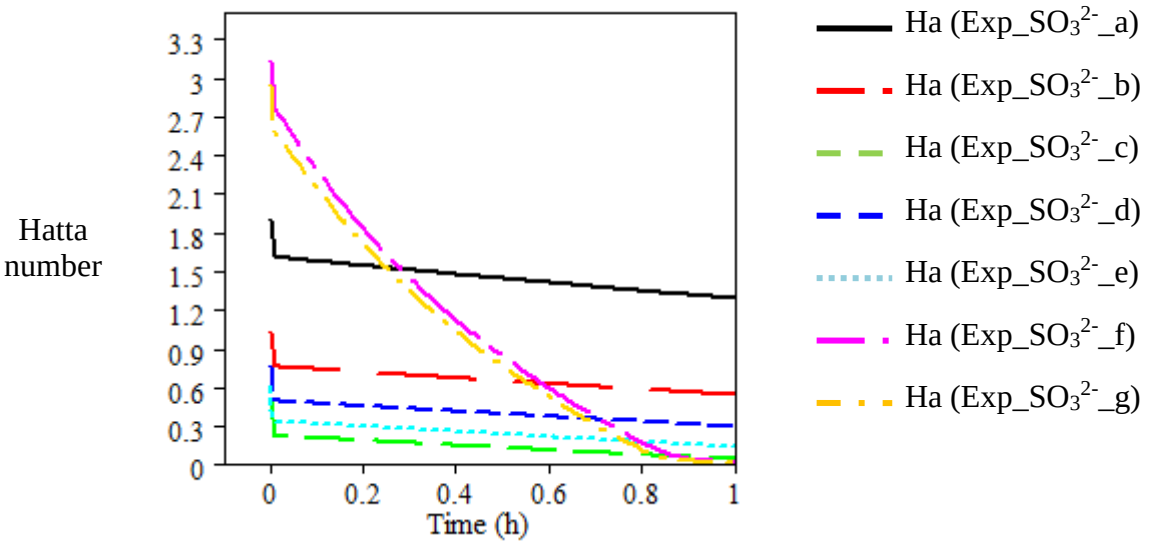

Figure 116: The Hatta number values calculated during the numerical simulation of the sulfite oxidation, concerning the oxygen absorption in the liquid phase for the experiments Exp_SO_3^{2-}_a, Exp_SO_3^{2-}_b, Exp_SO_3^{2-}_c, Exp_SO_3^{2-}_d, Exp_SO_3^{2-}_e, Exp_SO_3^{2-}_f, Exp_SO_3^{2-}_g.

The expression of the enhancement factor for the experiment is in a good agreement with the theory of the absorption in presence of an irreversible reaction (Danckwerts, 1970). The mathematical model proposed enables simulated sulfite oxidation in aerated aqueous solution for different operating conditions (sulfite concentration, pH and kla_{O2}). The the figure 117

illustrates the interest of including the carbon dioxide absorption for the model definition. With the same rate constant (k_{SO3} = 1.63 x 10^{10} $l^2.mol^{-2}.h^{-1}$), the dissolved oxygen concentration simulation is the same, with and without carbon dioxide absorption. However, the pH simulation differed. A significant decrease in the accuracy of the pH definition is recorded (with carbon dioxide absorption simulation Dev_pH_a = 0.03 and Dev_pH_b = 0.07, when without Dev_pH_a = 0.39 and Dev_pH_b = 0.48).

n = 2 (tested) ; m = 1 ; k_{SO3} 1.63 x 10^{10} $l^2.mol^{-2}.h^{-1}$

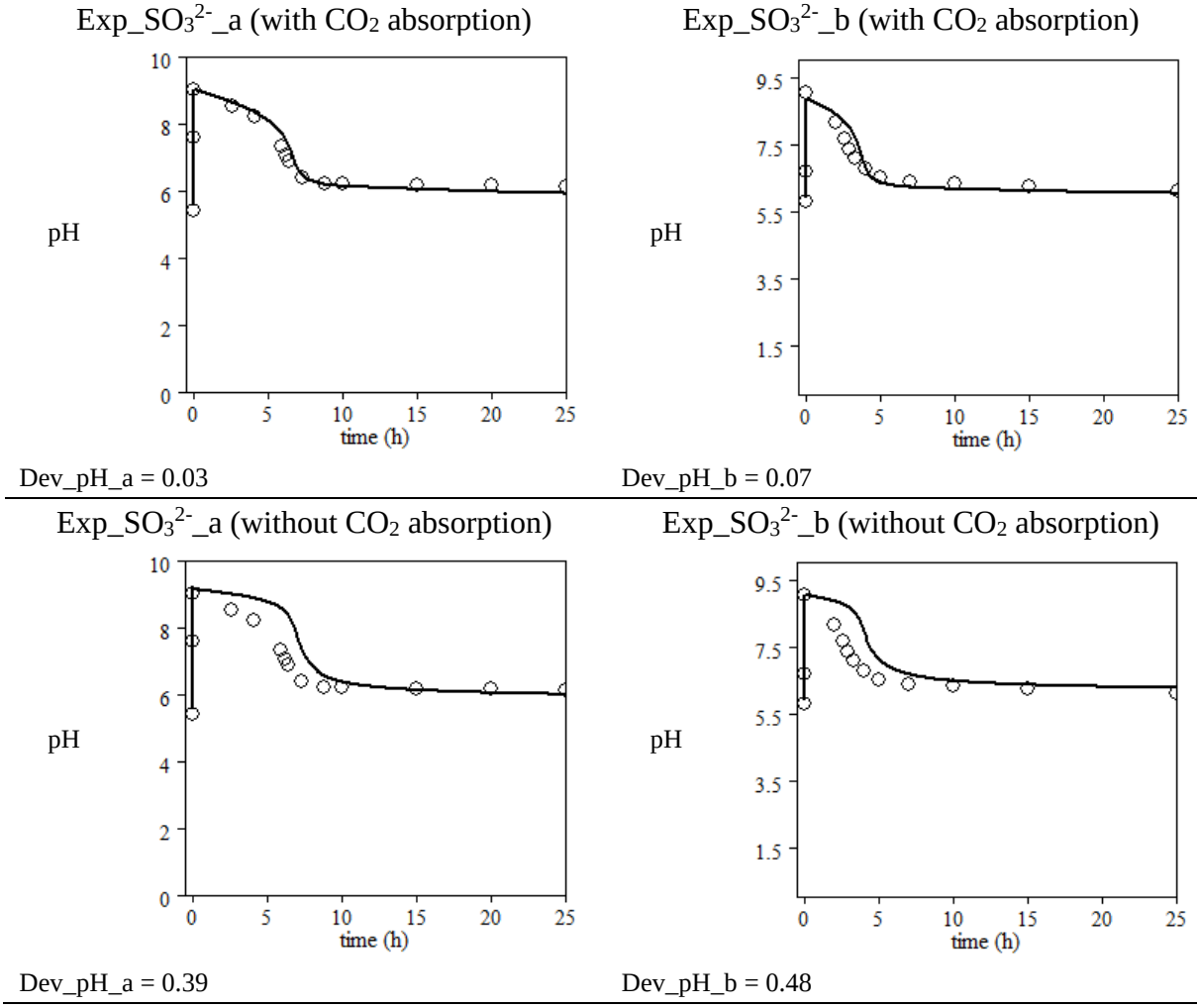

Figure 117: the implication of the carbon dioxide absorption in the definition (Compartement 3) of the sulfite oxidation (Compartment 2a). Comparison in the pH simulation for the experiments Exp_SO_3^{2-}_a, and Exp_SO_3^{2-}_b, with and without the simulation of the carbon dioxide absorption. The dissolved oxygen concentration was not modified.

2.2.5. Conclusions for the mathematical definition of the Compartment 2a

A mathematical model was proposed that could describe for different operating conditions the sulfite oxidation, in terms of (i) S(IV)-oxides speciation and consumption, (ii) oxygen consumption, (iii) S(VI)-oxides production and speciation, (iv) pH definition, (v) carbon dioxide absorption and speciation in relation with the pH definition. A kinetic law was adapted from the literature and proposed (Eq 164).

Annexes: Chapter VI

I.
Preliminary experiments in fed-batch culture to the selection of sulfur-oxidizing activity

II.
Arrhenius constant evaluation for Acidithiobacillus thioxidans

III.
Evaluation of the maximum biomass yield by free Gibbs energy calculations

I. Preliminary experiments in fed-batch culture to the selection of sulfur-oxidizing activity

1. Evaluation of the abiotic contribution in the biological thiosulfate conversion (fed-batch culture)

1.1. Description in time of the fed-batch culture

The figure 118 presents the time-course of the thiosulfate concentration [$S_2O_3^{2-}$], the S(VI)-oxides concentration, the pH measured during the fed-batch culture and some microscopic observation of the culture. The fed-batch culture was inoculated with an activated-sludge consortium from a wastewater treatment plant near the city of Toulouse (France),completed with nutrient solution to obtained initial culture at 0.8 gTSS/l.

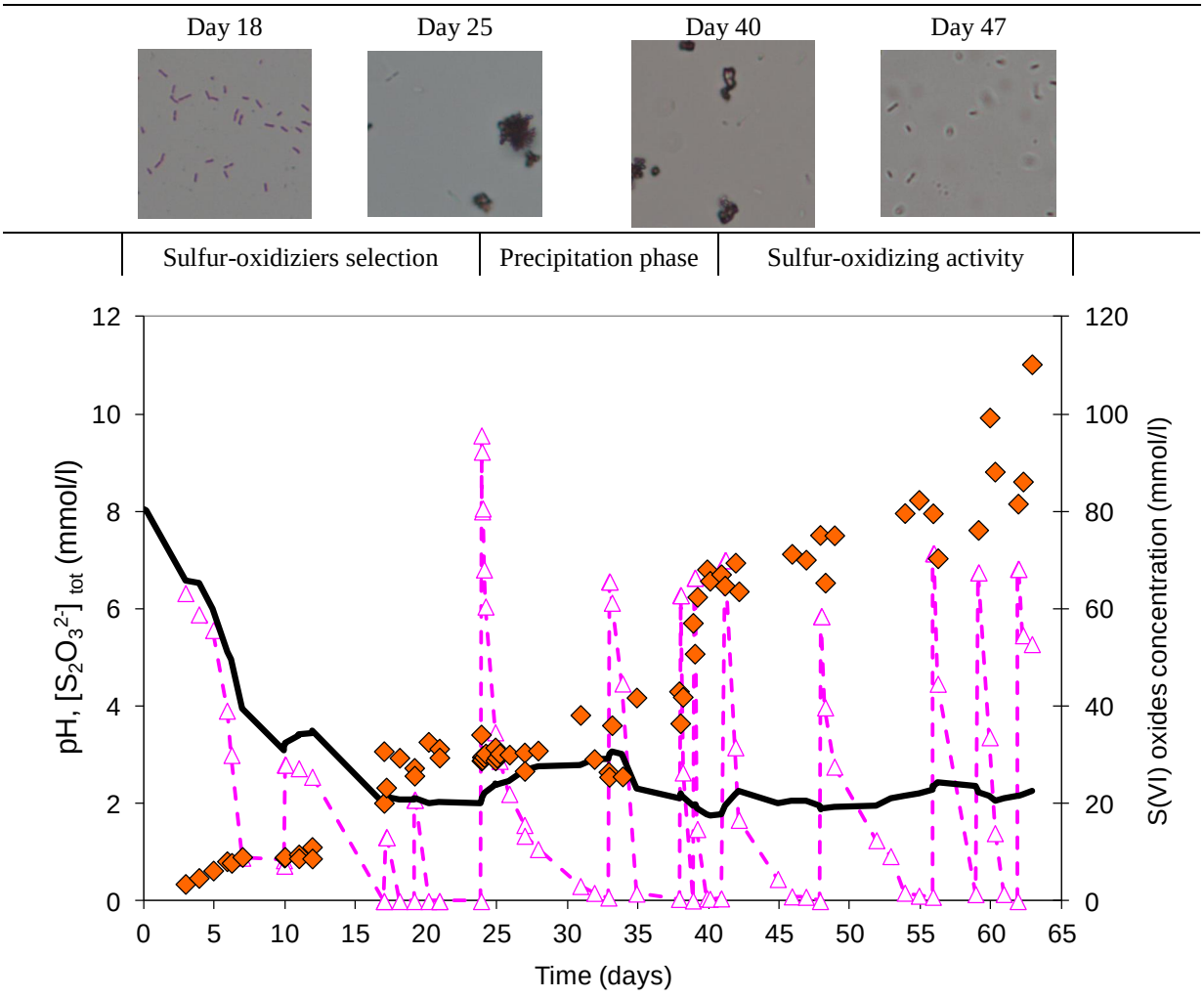

Figure 118: Fed-Batch culture of activated sludge inoculum on thiosulfate as only sulfur substrate (surface aeration). – △ – : thiosulfate concentration measured [$S_2O_3^{2-}$] (mmol/l); ◆ : S(VI) oxides (mol/l) (mmol/l); ▬ : pH measurements.

After the pulses (1) and (2) pH decrease directly (figure 118), and after the pulse (3) (day 3), the pH reached the value 3 at the day 10. After the pulse (4) (day 10) a first phase with a pH increase was recorded, following by a pH decrease reaching the value 2 at the day 17. During this global acidification phenomenon S(VI)-oxides production was observed, linked to thiosulfate consumption (figure 118).

Microscopic observations (x1000) at day 18 (figure 118 completed by thefigure 119), after safranine coloration, indicated that free microbial organisms with rod shape still existed in the reactor in spite of the very low pH establishment (value around 2 from the day 17 to the day 24). Sulfur-oxidizing activity only could explain the global evolution of the different parameters. Thus, from an initial consortium not adapted to the sulfur oxidation, thiosulfate seemed to be an interesting substrate to operate sulfur-oxidizers selection.

At day 24 (figure 118), because thiosulfate disproportionate reaction was pH and thiosulfate dependent (see chapter V to this document), to evaluate the part of the abiotic reaction in the thiosulfate conversion, an important thiosulfate pulse (pulse (7)) (important in quantity compared to the previous thiosulfate pulses providing to the culture) was used to ensure dynamic measurements of thiosulfate consumption and pH variation analyses. At low pH (around 2) an important thiosulfate conversion led to an important precipitation phenomenon combined to a basification of the culture medium (figure 118).

The precipitation phenomenon was illustrated by the microscopic observations (figure 119 – Day 24 just after the pulse (7)), where black and yellow-pale point could be observed just after the thiosulfate pulse, and by global observations of the reactor at the beginning of the culture (brown classical colour for an activated-sludge consortium) and at day 25 where a white and dense particulate structure could be observed in the culture.

Because the observations (after the day 18) were realized on fresh samples, with very intense motile bacteria, the free rod shape microorganisms were often represented on the photography by halo circle. The black points and the yellow-pale points were immobile thus considered as inorganic material. Five hours after the pulse (7) (day 24), the microscopic observations indicated an increase in the precipitation phenomenon (figure 119 – Day 24 – 5h after the pulse (7)), and the formation of larger aggregates. This tendency was confirmed by the microscopic observations realized the day 25, where larger aggregates were identified (figure 119 – Day 25). During this precipitation event a loss of free bacteria seems to be observed.

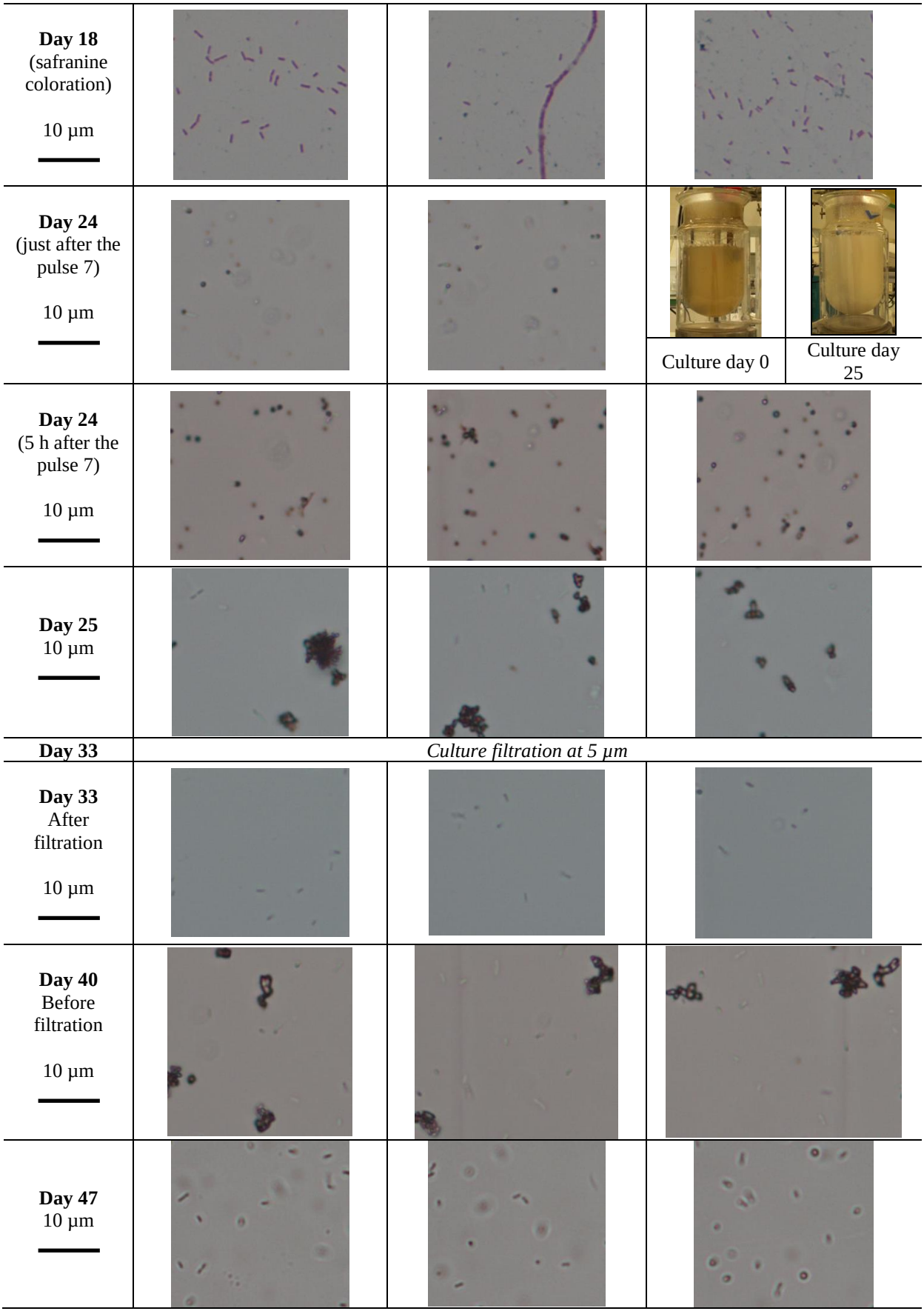

Figure 119: Visual observations of the fed-batch culture (microscopy x1000 and external reactor photography).

At the end of the pulse (7) (day 33), the whole culture was filtered (at 5 µm) to eliminate the larger aggregates, and thiosulfate pulse intensity was decreased to limit precipitation phenomenon. The figure 119 (Day 33) shows the microscopic observation of the culture after filtration and just before the thiosulfate pulse (8) (day 33).

Because, the initial pH was near 3 and the pulse (8) (day 33) was less intense than the pulse (7) (day 24), small basification was recorded (figure 118), quickly following by an acidification period (linked to thiosulfate consumption and S(VI)-oxides production, indicating biological sulfur-oxidizing activity). Thus the precipitation events and the filtration did not eliminate the totality of the sulfur-oxidizing bacteria.

During the period from the day 35 to the day 40, the pH decreased constantly from 3.1 to 1.8 (with little increases at each thiosulfate pulse which could be attributed to the thiosulfate disproportionate reaction in a first analyze). However precipitation phenomenon was newly observed (figure 119 - day 40). Another filtration was realized before the pulse (11) (day 41). After that, the microscopic observations showed no intense precipitation phenomenon, although weak basifications were recorded at the beginning of some thiosulfate pulses (figure 118).

During the last period (from day 41 to day 65), concerning five thiosulfate pulses, the pH oscillated around 1.89 and 2.45. S(VI)-oxides production was recorded linked to thiosulfate consumption. At the same time, free rod shape bacteria colonized the medium (see the difference in the figure 119 for the bacteria density recorded by microscopic observations at day 33 and day 47). At the end of the culture (day 65) a biomass sample was realized for further populations identification.

To conclude on this descriptive paragraph, the use of thiosulfate as major energy source selected sulfur oxidizing activity with strong acidity potential (pH 2 reached in 17 days), but in some conditions precipitation phenomenon seems to limit the biological activity, by an increase of the pH solution, by a possible loss of sulfur substrate and by a possible interaction in solution of minerals aggregates and free bacteria.

The next two paragraphs analyze the possible sulfur loss by sulfur mass balances and the precipitation phenomenon by the confrontation of the experimental results to the abiotic model developed in the chapter V of this document.

1.2. Loss of sulfur by sulfur mass balances analyses

The table 57 presents the sulfur mass balances realized for different time periods of the fed-batch culture by the measurement of the thiosulfate consumption and the S(VI)-oxides production. From day 0 to day 24, where no intense precipitation phenomenon was observed, the sulfur mass balance was achieved at 95%, confirming the absence of loss of sulfur substrate during this time period (by sulfur dioxide volatilisation due to the thiosulfate disproportionate reaction for example). Elemental sulfur could be a substrate for sulfur-oxidizing bacteria, thus finally converted to S(VI)-oxides (but no microscopic observation revealed important mineral precipitation during this time period). From day 24 to day 41, where strong precipitation phenomenon was observed (figure 119), with two filtration events operated, the sulfur mass balances could not be achieved (only 63% of the sulfur provided was analyzed as S(VI)-oxides). In that case, if elemental sulfur was produced, filtration eliminated it, thus limiting the sulfur mass achievement.

Table 57: Sulfur mass balances for different time periods of the fed-batch culture, and for the whole experiment, by cumulating thiosulfate consumed and the sulfate produced.

Time periods	**Pulses**	**Sulfur supply (mol S-$S_2O_3^{2-}$)**	**Sulfate produced (mol S-SO_4^{2-})**	**Sulfur mass balances recovery**
Day 0 to 24	(1) (2) (3) (4) (5) (6)	36×10^{-3}	34×10^{-3}	95%
Day 24 to 41	(7) (8) (9) (10)	60×10^{-3}	38×10^{-3}	63%
Day 41 to 48	(11)	14×10^{-3}	10×10^{-3}	80%
Day 48 to end	(12) (13) (14) (15)	52×10^{-3}	45×10^{-3}	88%
Total	“	160×10^{-3}	110×10^{-3}	69%

From day 41 to day 48, and from day 48 to the end of the culture the sulfur mass balances indicated a decrease in the precipitation phenomenon. During these two time periods no filtration events were operated. Thus, the loss of sulfur in the sulfur mass balances could be attributed to, (i) the formation of an intermediary sulfur compounds, (ii) the production of elemental sulfur precipitated and not oxidized (iii) the stripping of sulfur dioxide during the thiosulfate disproportionate reaction.

1.3. The precipitation phenomena investigated by the confrontation of the experimental data and the dynamical model developed in the chapter V of this document

To evaluate the possible role of the thiosulfate disproportionate reaction during the fed-batch culture, the dynamical model developed in the chapter V of this document was used for different thiosulfate pulses (4), (7) and (11) (figure 118). For the pulse (4) (day 10), corresponding to the first time period described in the table 57, the numerical results presented in the figure 120 showed that conditions are not favourable to the abiotic thiosulfate disproportionate reaction. Thus no elemental sulfur was produced confirming the microscopic observations and the sulfur mass balances recorded during the time period form day 0 to day 24 (table 57). During this period, the thiosulfate consumption could be attributed to the biological activity only. Thus, the increase of the pH just after the pulse (4) (day 10) (figure 118), linked to a thiosulfate consumption but not directly followed by a sulfate production should be attributed to a biological conversion. The production of intermediaries as tetrathionate for example described in the chapter I of this document could explain this special behaviour in the first step of thiosulfate oxidation. The following acidification was associated to S(VI)-oxides production indicating an production and an accumulation of the intermediary sulfur substrate and then it's consumption.

For the pulse (7) (day 24), corresponding to the second period in the table 57, the numerical results (figure 120) showed that abiotic thiosulfate disproportionate reaction occurred at these experimental conditions, thus elemental sulfur was produced, confirming the visual and microscopic observations realised during the experiment (figure 119). However, the abiotic thiosulfate disproportionate reaction could not explain the whole thiosulfate consumption, and the huge increase of the pH solution. Thus, because a weak S(VI)-oxides production was recorded during this time period, the biological production of an intermediary sulfur compound with a base production as described above seems to be an interesting explanation. The simulated results (figure 120) obtained for the pulse (11) (day 41) corresponding to the third period in the table 57, show the same global tendencies, (i) with an initial pH increase superior to the increase expected by the abiotic thiosulfate disproportionate reaction only, (ii) with a thiosulfate consumption higher than the rate expected by the abiotic reaction only. But in that case, after an initial increase of the pH an acidification phenomenon was recorded, indicating as for the pulse (4) a delay for the acid production probably due to

the biological production of an intermediary sulfur compounds consumed in a second biological step.

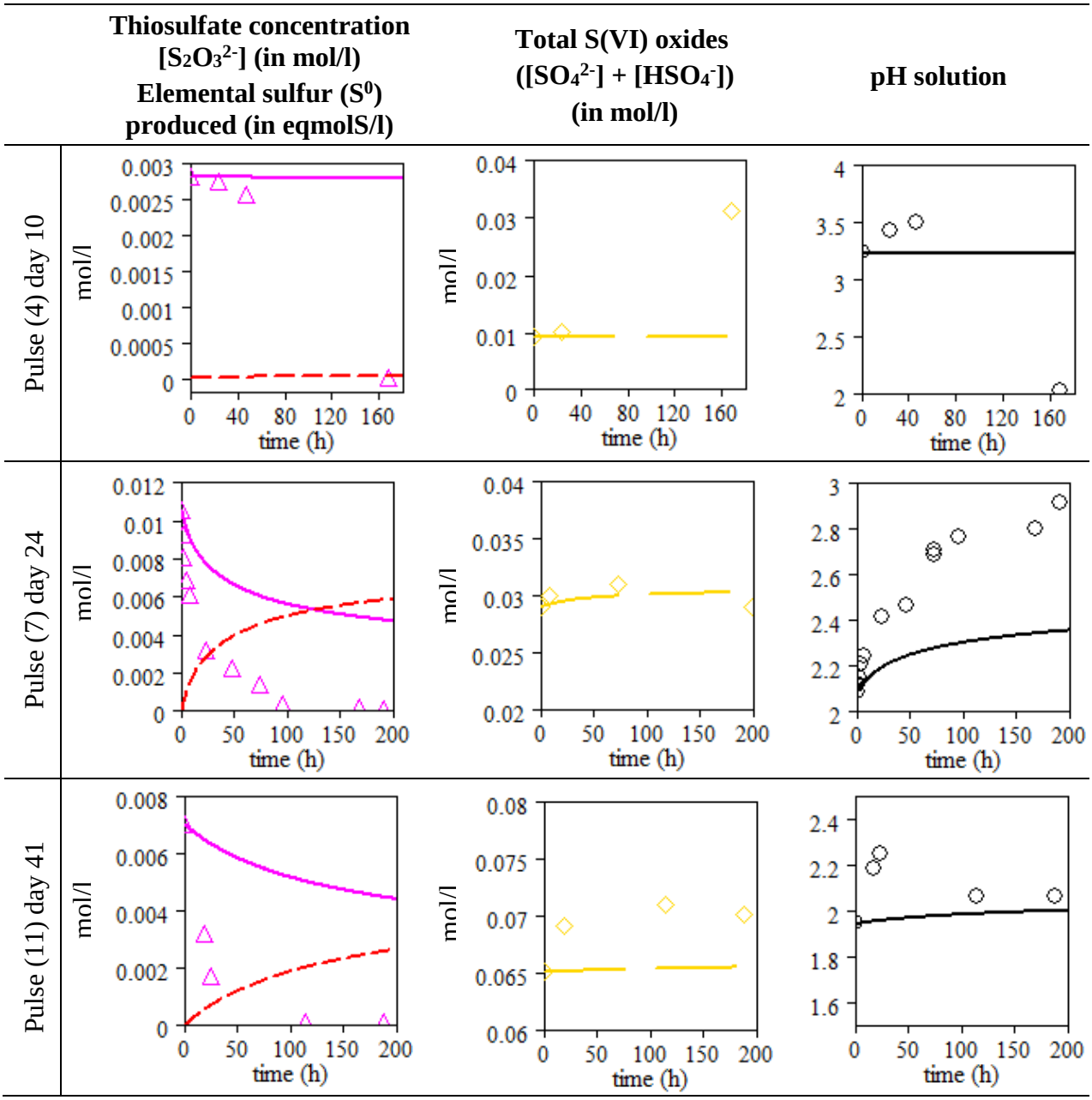

Figure 120: Simulations of thiosulfate pulses (4) (7) (11) by the abiotic model developed in the chapter V of this document. Experimental data: △ : thiosulfate concentration [$S_2O_3^{2-}$] (mol/l); ◇ : S(VI)-oxides (mol/l); ○: pH measurements. Numerical data: ▬: thiosulfate concentration [$S_2O_3^{2-}$] (mol/l); ▬ ▪ : elemental sulfur produced [S^0] (eqmolS/l); ▬ ▪ : S(VI)-oxides concentration (mol/l); ▬ : solution pH.

The figure 120 revealed the importance of the biological activity even in the basification phenomenon. To clearly evaluate the part of the abiotic thiosulfate disproportionate reaction

in the global conversion, the model was adapted considering pH and thiosulfate concentration as known data and not as variables. In that case the simulation for the thiosulfate pulses (7) and (11) presented in the figure 121 confirmed the importance of the biological activity in the global conversion of thiosulfate. The biological activity clearly limited the effect of the abiotic thiosulfate disproportionate reaction, by a fast consumption of the thiosulfate and by an initial over basification of the medium.

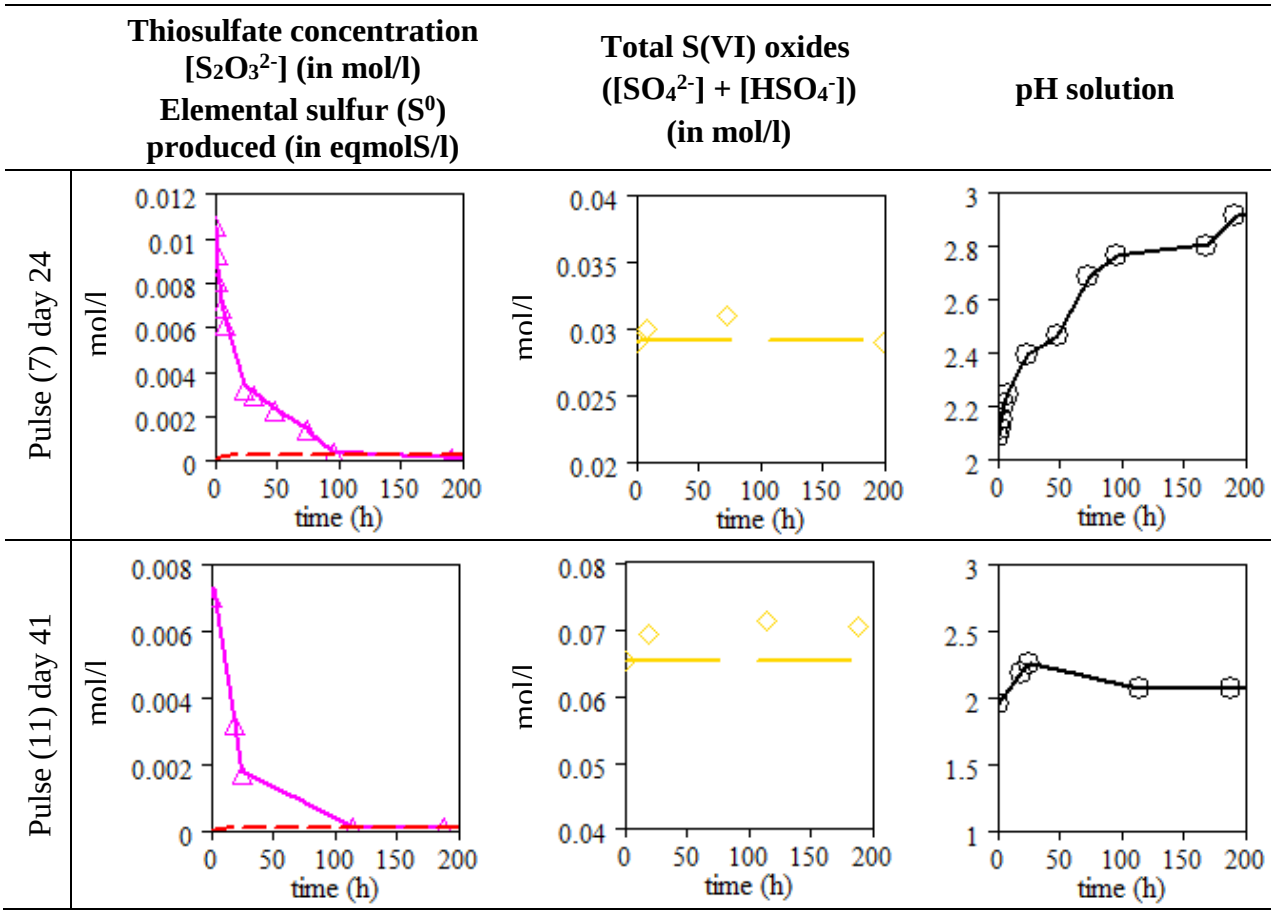

Figure 121: Simulations of thiosulfate pulses (7) (11) with pH and thiosulfate experimental data as inlet data for the evaluation of the abiotic thiosulfate disproportionate reaction in the definition of the global conversion phenomena. Experimental data: △ : thiosulfate concentration [$S_2O_3^{2-}$] (mol/l); ◇ : S(VI)-oxides (mol/l); ○: pH measurements. Numerical data: ▬: thiosulfate concentration [$S_2O_3^{2-}$] (mol/l); ▬ ▪: elemental sulfur produced [S^0] (eqmolS/l); ▬ ▪: S(VI)-oxides (mol/l); ▬: solution pH.

In these conditions, even if elemental sulfur was produced (around less than 2% of the total S-$S_2O_3^{2-}$ consumed) the precipitation phenomena could not be attributed to the abiotic thiosulfate disproportionate reaction only.

1.4. The precipitation phenomena investigated by supplementary analyses

Because the culture was realized with activated-sludge as initial medium, complete with feed solution (composed by mineral nutrients) an important quantity of calcium was initially dissolved in the culture. The figure 122 presents the time course of the sulfate concentration and the dissolved calcium concentration during the fed-batch culture. During the first 38 days, the analyzed of the dissolved calcium concentration recorded a slightly decrease; even during the period after the pulse (7) (day 24). But after the pulse (8) (day 33) and during the pulses (9) and (10) (day 38 and 39), an important loss of dissolved calcium was observed linked to a significant production of S(VI)-oxides, but with a sulfur mass balance achievement only of 63% (table 57) (filtration event operated during this period). These results could indicate aside the abiotic thiosulfate disproportionate reaction the precipitation of sulfate calcium salts.

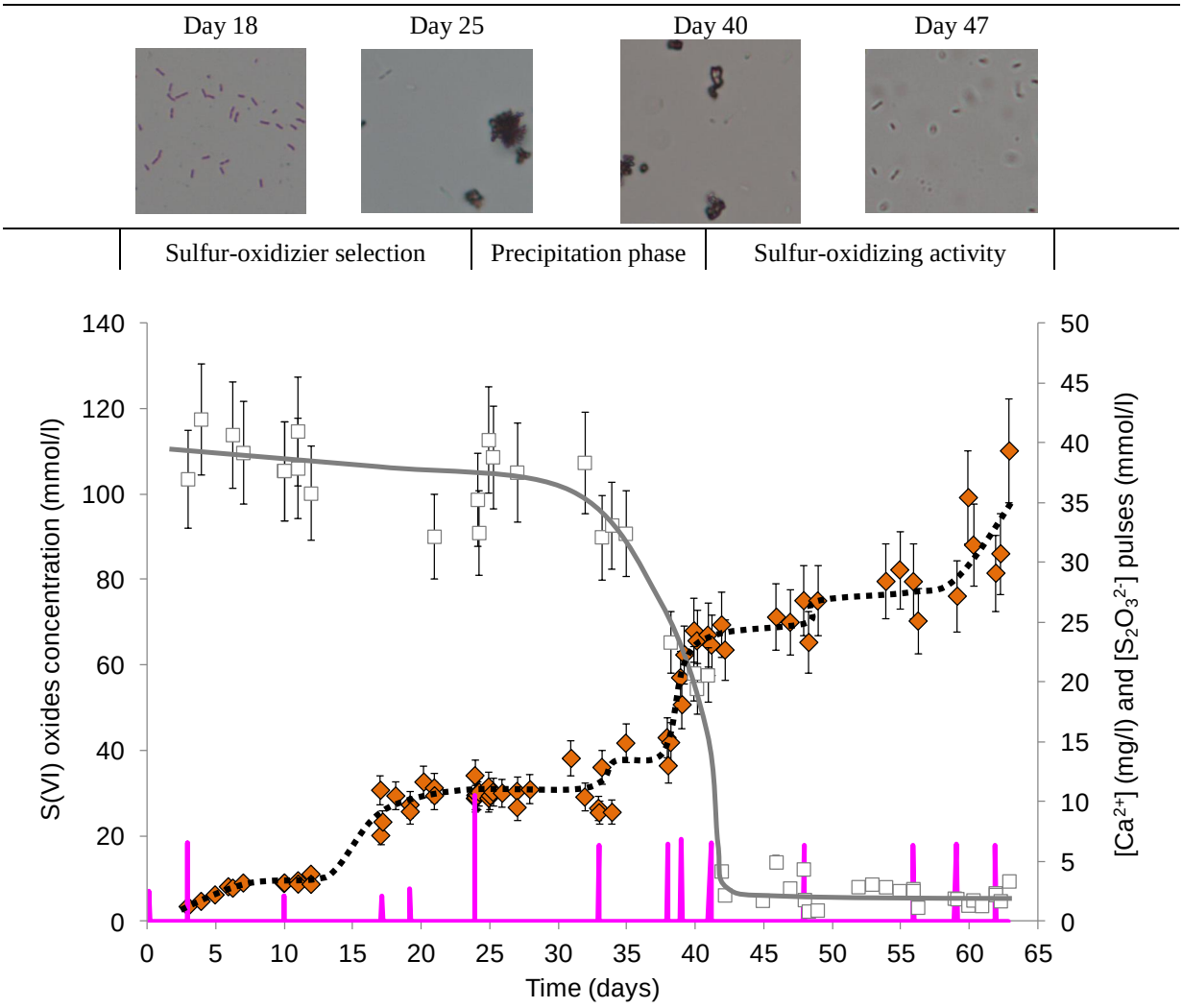

Figure 122: Evolution of the sulfate concentration and the dissolved calcium concentration during the fed-batch culture. ▬: the thiosulfate pulses (mmol/l); ◆: the S(VI) oxides concentration (mmol/l); ▪▪▪: the global evolution of the sulfate concentration; □: the dissolved calcium concentratio [Ca^{2+}] (mg/l); ▬: the global evolution of the dissolved calcium concentration.

To evaluate this eventuality, for all the samples, the saturation index (SI) was calculated for four compounds ($CaSO_4$; $CaSO_4.2H_2O$; $NaSO_4.H_2O$; $NaSO_4.10H_2O$) (figure 121). The sulfate calcium salts were chosen due to the analytical results (figure 124). The sulfate sodium salts because thiosulfate was provided by NaS_2O_3 salt, and thus sodium accumulated to high concentration during the fed-batch culture.

The figure 123 presents the Saturation Index (SI) calculated during the fed-batch culture for the four compounds chosen (taking into account the sulfate concentration at each time by the pH values and S(VI)-oxides concentration measurements). The equilibrium constant used were from the Minteq-database. Negative SI values indicated concentrations under the concentration defined by the equilibrium constant, thus no precipitation phenomenon could occur. Positive SI values indicated concentrations over the concentrations excepted for the equilibrium state, thus obligatory precipitation phenomenon occurs.

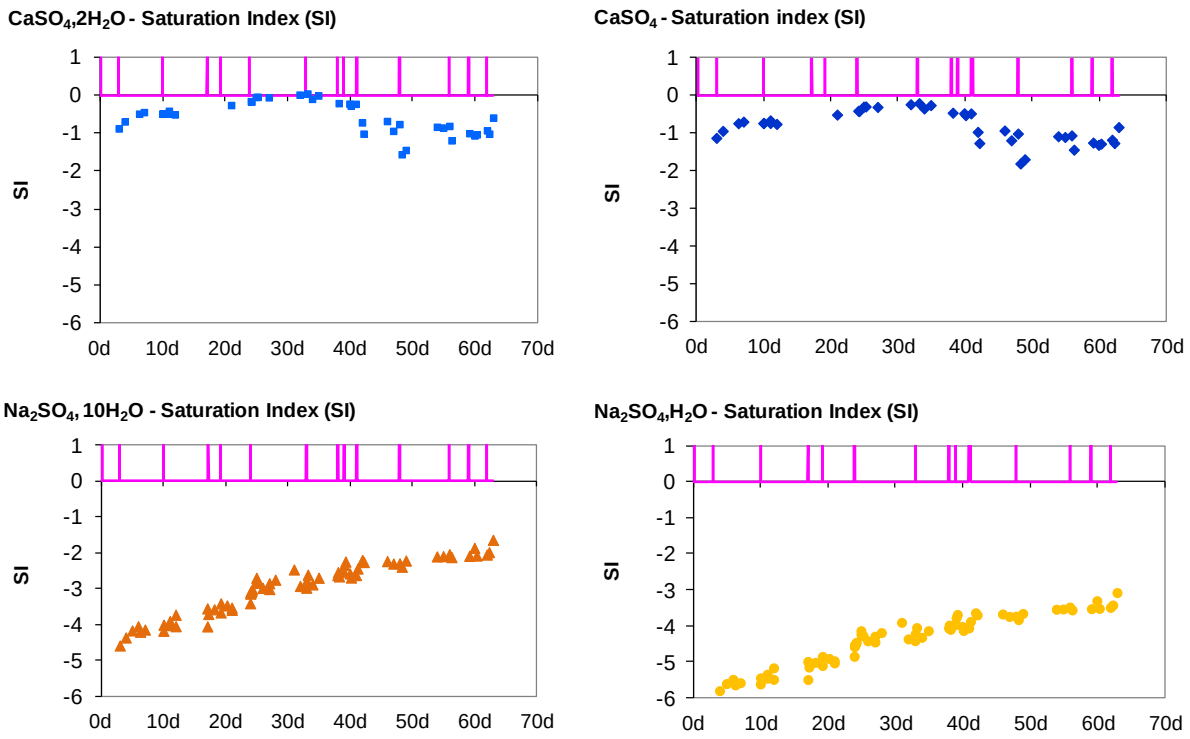

Figure 123: Saturation Index (SI) calculated during the fed-batch culture for four compounds (■: $CaSO_4,2H_2O$; ◆: $CaSO_4$; ▲: $NaSO_4,10H_2O$; ● : $NaSO_4,H_2O$).

The SI calculated for the sodium salts (figure 123), were negative all the time, indicating that no precipitation of these compounds could occur during the fed-batch culture. For the calcium salts, the SI values for the *$CaSO_4$* and *$CaSO_4.2H_2O$* were negative at the beginning of the fed-batch culture (figure 123). The SI values are more negative for *$CaSO_4$* than for

$CaSO_4.2H_2O$ due to the equilibrium constants used showing a favorable precipitation of $CaSO_4.2H_2O$ in water saturated conditions. During the fed-batch culture, the SI values approach null values for $CaSO_4.2H_2O$ at day 24 (pulse (7)) and stay near null values until day 41, indicating the concentrations of dissolved calcium and sulfate at the equilibrium values, thus a fast precipitation phenomenon during all this period (confirming the visual and microscopic observations (paragraphs [3.1.1.]) and the sulfur mass balances realized (paragraph [3.1.2.]).

After day 41, no intense precipitation phenomenon was observed (figure 119), confirmed by the SI values calculated for this period.

1.5. The selected populations during the fed-batch culture

At the end of the fed-batch culture, a biomass sample was realized by centrifugation, freezing by immersion in liquid nitrogen and conserved at -80°C. The results of 16S rRNA tag-encoded pyrosequencing are presented at the figure 124.

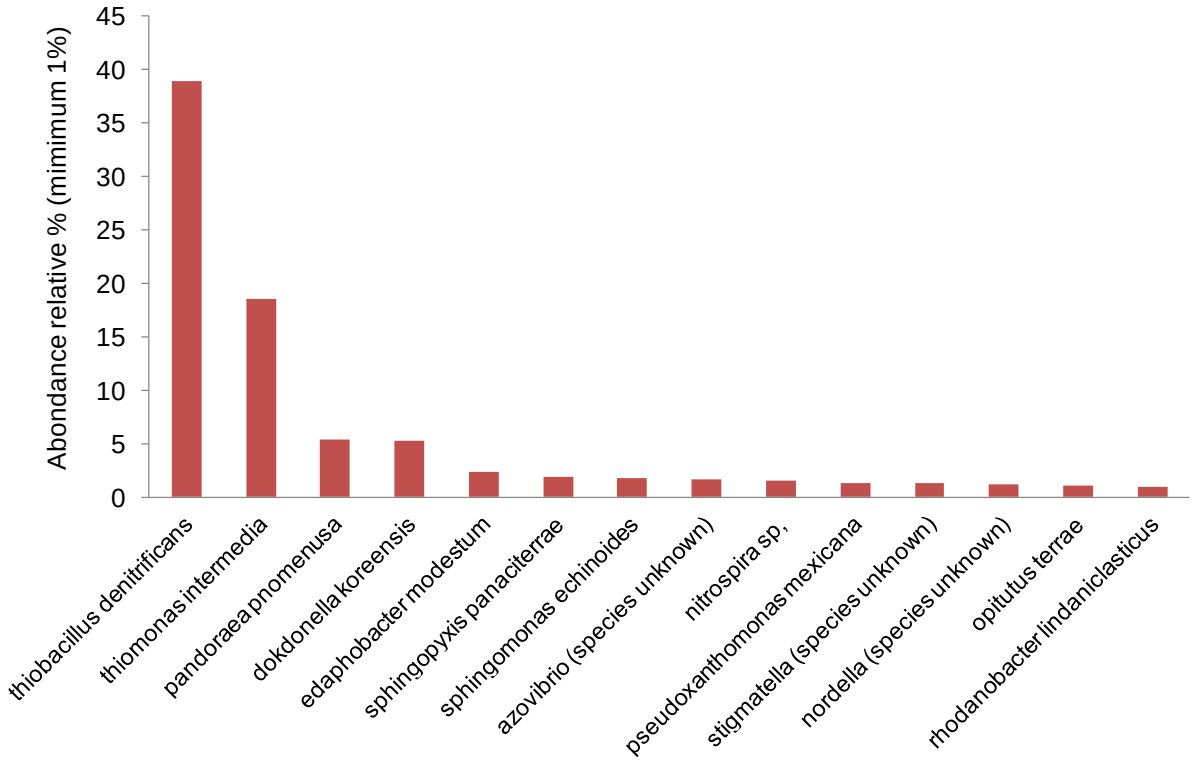

Figure 124: bacteria population selected at the end of the fed-culture (after 65 days from an initial activated sludge consortium). Analyses by16S rRNA tag-encoded pyrosequencing. Only the population with a relative abundance above 1% were represented.

At the end of the fed-batch culture, more than 50% of the clones identified were sulfur-oxidizing bacteria. *Thiobacillus denitrificans* was the major population encountered, making up 38.9% of the total clones (figure 124). According to (Kelly and Wood, 2000), it is a facultative aerobic/anoxic bacterium able to grow with oxygen or nitrogen oxide as terminal respiratory oxidants and having an optimum culture pH range between 6.8 and 7.4. The present study indicates the capacity of *Thiobacillus denitrificans* to live in acidic environment at pH values around 2. *Thiomonas intermedia* (= *Thiobacillus intermedius*) was also identified in the fed-batch culture, and made up 18.5% of the total clones. *Thiomonas intermedia* (strain K12) is an aerobic, moderately acidophilic, sulfur-oxidizing bacterium, which was isolated from a sewage pipe in Hamburg, Germany (Wentzien and Sand, 2004).

The identified population, selected at the end of the fed-batch culture confirmed the sulfur-oxidizing activity recorded and analyzed by the measurements of the thiosulfate consumption and the S(VI)-oxides production.

Edaphobacter modestum is a member of the Acidobacteriaceae family. Its identification confirmed the global acidification of the medium in the biotic pipe-reactor (Koch et al., 2008).

Dokdonella koreensis takes the form of Gram-negative, strictly aerobic rods (Yoon et al., 2006). Heterotrophic growth occurs between 10 and 39°C with an optimum temperature of 30°C. Optimal pH for growth is between 5 and 6. Growth is observed at pH between 5 and 9, but not at pH 4.5 or 9.5. However, in the fed-batch culture, with a pH value of the culture medium around 2, sequencing analyses showed that *Dokdonella koreensis* (5.3% of the total clones) was able to live in an acidic environment (figure 124).

2. The fed-batch culture: Conclusions

The fed-batch culture showed the interest of thiosulfate as sulfur substrate for the selection of sulfur-oxidizing activity and the fast creation of an acidic environment. The global signal analyses indicate some possible secondary pass way for the conversion of thiosulfate.

The dynamical model, describing the abiotic thiosulfate disproportionate reaction, is an interesting tool for a deeper understanding of the different way of conversion of the sulfur compounds, and highlighted by difference interferential precipitation phenomenon and great adaptability of the consortium to the conversion of thiosulfate.

Because the culture was realized in the closed reactor, the accumulation of product as S(VI)-oxides associated to the need of mineral compounds for biological activity led to the precipitation of mineral compounds, causing some biological disturbance.

The next paragraph presents sequenced-batch culture adapted from the experimental set-up used during the fed-batch culture describes here. The operating conditions were defined to limit precipitation phenomenon and ensure (i) new selection of acidophilic sulfur-oxidizing activity, (ii) deeper analyzes of the thiosulfate conversion by an open respirometry system.

II. Arrhenius constant evaluation for *A. thioxidans*

Acidithiobacillus thiooxidans is often considered as the last specie involved in the microbially induced concrete corrosion and was used as representativ specie to simulate the last step of the acidification phenomenon. In 1942, Vogler studied *Acidithiobacillus thiooxidans* and quantified the rate of oxygen consumption in function of the temperature culture (Vogler et al., 1942). The figure 125 presents the results obtained by Volger for the oxygen uptake for different temperature. The results are presented as percentage of oxygen uptake for the operating temperature per the oxygen uptake measured at 28°C.

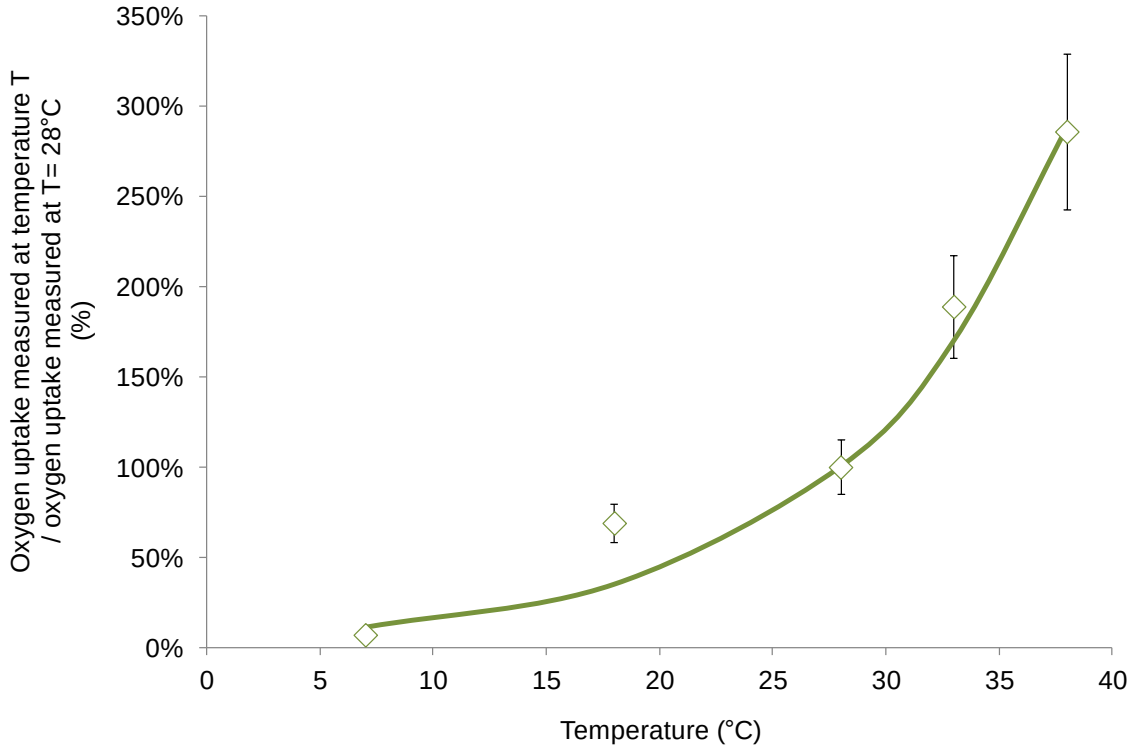

Figure 125: Oxygen uptake measurements at different temperature compared to the oxygen uptake measurement realized at 28°C for Acidithiobacillus thiooxidans (adapted from Volger, 1942), and the Arrhenius function determined to represent the temperature dependency of the specific growth rate. ◇: experimental data from Volger 1942; ——: theoretical definition by Arrhenius function.

The evolution of the oxygen uptake showed clear temperature dependency for *Acidithiobacillus thiooxidans* activity between 5°C and 40°C. Because for initial identical biomass concentration the oxygen uptake is only affected by the specific growth rate, the results obtained by Vogler could be adapted to evaluate an Arrhenius function describing the temperature dependency of the specific growth rate.

The Arrhenius function was defined by the equation (Eq 165).

Eq 165: Arrhenius function = $exp^{(Arr.(T°-T))}$

where *Arr* is the Arrhenius constant; *T°* is a reference temperature (here 28°C) and *T* is the operating temperature (in °C).

In that case, the ratio between the oxygen uptake at an operating temperature and the oxygen uptake measured at a reference temperature defined the Arrehnius function by the equation (Eq 166).

Eq 166: $\frac{OU^{(T)}}{OU°} = exp^{(Arr.(T°-T))}$

where $\frac{OU^{(T)}}{OU°}$ is the ratio between the oxygen uptake at an operating temperature and the oxygen uptake measured at a reference temperature.

The Arrhenius constant (*Arr*) was estimated using least square method with the excel solver to minimize the deviation between calculated values and experimental data. By this method the Arrehnius constant was estimated to 0.106. The exponential definition of the temperature dependency of the oxygen uptake by Arrhenius function was presented in the figure 125. The Arrhenius function could be applied for the evaluation of the specific growth at different temperature for *Acidithiobacillus thiooxidans*. For example, Mason in 1987 at 30°C and pH = 2.5 fixed for *Acidithiobacillus thiooxidans* a specific growth rate in chemostat culture to 0.025 h^{-1}. If this specific growth rate was the maximum available for this strain at these operating conditions, at 20°C, corrected by the Arrhenius function determined here, the specific growth rate will be equal to 0.0086 h^{-1}.

III. Evaluation of the maximum biomass yield by free Gibbs energy calculations

1. Fructose as theoretical compounds for biomass production by chemolithotrophic autotrophic bacteria

Chemolithotrophic autotrophic bacteria as sulfur-oxidizing bacteria use energy produced by chemical oxidation of reduced sulfur compounds to fixed dissolved carbon dioxide and produce cells. Several pathways for carbon dioxide fixation exist (Berg, 2011). Concerning chemolithotrophic sulfur bacteria, Kelly in 1999 used the Calvin-cycle (reductive pentose-phosphate cycle) to evaluate the energy conservation (Kelly, 1999), and proposed the equation (Eq 167) to summarized the overall process to produced fructose ($C_6H_{12}O_6$) form carbon dioxide.

Eq 167: $6\,CO_2 + 18\,ATP + 12\,NADH + 12\,H^+ + 12\,H_2O \rightarrow C_6H_{12}O_6 + 18\,ADP + 12\,NAD^+ + 18\,H_3PO_4$

(mean ΔG^0_f = 113 kJ/molCO_2)

For the first pathway described in the chapter VI for the biological thiosulfate the direct conversion of thiosulfate to sulfate is described by the equation (Eq 168).

Eq 168: $S_2O_3^{2-} + 2O_2 + H_2O \rightarrow 2SO_4^{2-} + 2H^+$ with mean ΔG^0_{R1} = -750.1 kJ/mol$S_2O_3^{2-}$ from Kelly (1999) and ΔG^0_{R1} = -795.52 kJ/ mol$S_2O_3^{2-}$ from McCarty (1975) and Sawyer et al., (1994). To conserve coherent values, $\Delta G°_{R1}$ equal to -750.1 kJ/mol$S_2O_3^{2-}$ was chosen by Kelly.

The maximum carbon dioxide fixation yield is defined by the equation (Eq 169).

Eq 169: $Y_{CO_2 / S_2O_3^{2-}} = \frac{\Delta G^0_{R1}}{\Delta G^0_f}$

In the case of total thiosulfate oxidation to sulfate, Kelly method (1999) evaluated $Y_{CO_2 / S_2O_3^{2-}}$ = 6.54 molCO_2/ mol$S_2O_3^{2-}$, equivalent to 147.8 gVSS/ mol$S_2O_3^{2-}$ (compared to 12.43 gVSS/ mol$S_2O_3^{2-}$ experimentally measured, corresponding to 8.3% of apparent efficiency of energy conservation).

For the second pathway with tetrathionate as intermediate, the total conversion of thiosulfate could be described by two consecutives reactions defined by the equation (Eq 170) and the equation (Eq 171).

Eq 170: $S_2O_3^{2-} + 0.25\,O_2 + 0.5H_2O \rightarrow 0.5\,S_4O_6^{2-} + OH^- \Delta G^0_{R2a}$ = ?

Eq 171: $S_4O_6^{2-} + 3.5\,O_2 + 3\,H_2O \rightarrow 4\,SO_4^{2-} + 6\,H^+$ ΔG^0_{R2b} = -1244.6 kJ/mol$S_4O_6^{2-}$

Concerning the first step of this pathway the free Gibbs energy could be determined by the following expression $\Delta G^0_{R2a} = \Delta G^0_{R1} - \Delta G^0_{R2b}/2$ = -127.8 kJ/mol$S_2O_3^{2-}$.

Using the method proposed by Kelly in 1999, the maximum carbon dioxide yields are $Y_{CO_2 / S_2O_3^{2-} \rightarrow S_4O_6^{2-}}$ = 1.13 molCO_2/ mol$S_2O_3^{2-}$ and $Y_{CO_2 / S_4O_6^{2-}}$ = 11.01 molCO_2/ mol$S_4O_6^{2-}$ (equivalent to $Y_{CO_2 / S_4O_6^{2-}}$ = 5.505 molCO_2/ moleq$S_2O_3^{2-}$). Kelly in 1999 showed that the apparent efficiency of energy conservation for tetrathionate as sulfur substrate was 9.4% for *Thiobacillus tepidarus*, quiet similar of the apparent efficiency of energy conservation for the total oxidation of thiosulfate (8.3%). Thus in real conditions, for growth by the oxidation of thiosulfate in two biological step theoretically 17% of the biomass was produced during the oxidation of thiosulfate to tetrathionate, and 83% of the biomass was produced during the oxidation of tetrathionate to sulfate.